OIL SPILL REMEDIATION

COLLOID CHEMISTRY-BASED PRINCIPLES AND SOLUTIONS

EDITED BY

PONISSERIL SOMASUNDARAN
PARTHA PATRA
RAYMOND S. FARINATO
KYRIAKOS PAPADOPOULOS

WITH A FOREWORD BY **LISA PEREZ JACKSON,**
ENVIRONMENTAL PROTECTION AGENCY ADMINISTRATOR, USA (2009-2013)

WILEY

OIL SPILL REMEDIATION

OIL SPILL REMEDIATION

Colloid Chemistry-Based Principles and Solutions

Edited by

PONISSERIL SOMASUNDARAN
PARTHA PATRA
RAYMOND S. FARINATO
KYRIAKOS PAPADOPOULOS

WILEY

Published by John Wiley & Sons, Inc., Hoboken, New Jersey
Published simultaneously in Canada

Library of Congress Cataloging-in-Publication Data:

Oil spill remediation : colloid chemistry-based principles and solutions / edited by Ponisseril Somasundaran, Partha Patra, Raymond S. Farinato, Kyriakos Papadopoulos.
pages cm
Includes bibliographical references and index.
ISBN 978-1-118-20670-6 (cloth : alk. paper) 1. Oil spills–Cleanup. 2. Oil pollution of water. 3. Oil pollution of the sea. 4. Emulsions. I. Somasundaran, P., 1939– editor of compilation. II. Patra, Partha, editor of compilation. III. Farinato, Raymond S., editor of compilation. IV. Papadopoulos, Kyriakos, 1956-editor of compilation.
TD427.P4O3872 2014
628.1′6833–dc23

2013049558

Printed in the United States of America

ISBN: 9781118206706

10 9 8 7 6 5 4 3 2 1

CONTENTS

FOREWORD

The 2010 Deepwater Horizon oil spill in the Gulf of Mexico ranks among the worst environmental disasters in our history. It claimed 11 lives and interfered with ecological balance, sustainability efforts, and the overall way of life for millions of people. Massive, multipronged, and technologically advanced oil cleanup efforts were launched immediately, and they achieved a remarkable degree of success. But the spill and the cleanup efforts that followed also underscored the scope of the potential for ecological disaster. We still have a great need for technological innovations in this field not only to develop strategies that will prevent another calamity like the Deepwater Horizon spill from occurring but also to strengthen our ability to respond swiftly if that time ever comes.

This issue was the main focus of a symposium organized under the leadership of Professor Somasundaran for the Society for Mining, Metallurgy, and Exploration. The symposium, which I had the privilege of addressing, presented diverse perspectives on the potential use of existing, but as yet unexploited, fundamental scientific principles for developing more effective oil spill remediation technology. The presentations that came out of the conference have been compiled into a monograph titled *Oil Spill Remediation: Colloid Chemistry-Based Principles and Solutions*. They outline the scientific methods, approaches, and plausible routes for the effective and rapid cleanup of spilled oil from sea surfaces, oil-soaked sands, and deep sea, from the perspective of colloid chemistry.

As a former administrator of the U.S. Environmental Protection Agency and a scientist by training, I am delighted to be a part of this endeavor. I am inspired by the dedication that scientists from all over the world have shown in promoting the development of advanced, environmentally safe technology for the quick and effective remediation of spilled oils. I extend my gratitude and appreciation to the authors, editors, and publishers of this important monograph.

Environmental Protection Agency Administrator, USA 2009–2013

LISA PEREZ JACKSON

PREFACE

Major environmental tragedies generate a host of different alarm responses from different communities. Such events trigger a cascade of actions that include immediate response, long-term remediation, and strategies for preventing similar mishaps in the future. Examples of such tragedies include many oil spills the world over. One such recent major incident was the Deepwater Horizon accident in April 2010 in which massive amounts of subsea crude oil escaped into the marine and nearshore environments due to a drilling rig explosion and blowout in the Macondo Prospect in the Gulf of Mexico. While heroic efforts on the part of first-responders and remediation crews lessened the impact of the spill, it was clear that the technologies available for remediation should be improved. Many science and engineering communities applied their expertise and knowledgebase through the lens of a crude oil spill in an effort to contribute to improve future remediation options. A symposium and subsequently this book arose out of one such effort.

The special symposium entitled "Mineral & Metallurgical Processing: Separation Techniques to Meet Oil Spill Challenges" was run at the 2011 annual meeting of the Society for Mining, Metallurgy, and Exploration (SME) in Denver, Colorado. The intent was to draw upon the expertise of scientists, engineers, and policy makers with an aim to advancing oil spill remediation technology and its use. Both the petroleum and mining industries operate on scales that affect the environment. Sharing expertise related to environmental stewardship seemed both prudent and beneficial. Talks presented during this symposium formed the core of, and provided a platform for, additional contributions that were molded into this book. The various chapters present views from a variety of vantage points—regulatory, first-responder, toxicology, and physicochemical and colloid science. We hope that holding such a diverse collection of perspectives in a single purposeful constellation will provide some light along the path to better remediation technologies.

The chapters address the deeper scientific problems associated with the currently used technologies that have either become evident only in hindsight or were initially thought to be too insignificant for consideration. For example, while skimming booms are used, the possibility of improving absorbing efficiency by manipulating surface rugosity is a new direction that can be potentially pursued. Also, how dispersants can be improved for bettering their performance on the sea surface, under deep sea high pressure and at high-temperature conditions is addressed in this book. Novel methods that will enhance our understanding of oil-dispersant microstructure are explored here via molecular dynamic simulation. How fundamental properties such as surface tension, droplet film stability and coalescence, and accessibility of microbes to oil/sand/water are the key to enhancing the efficiency of many remediation applications is discussed in the context of the usage of dispersants and the physicochemical complexity of sand–water–air–oil systems. A few of the authors have combined insights gained from studies on oil dispersion in microscopic environments with the scaled-up technologies that are used in mineral processing to arrive at solutions for the efficient removal of oil from beach sands. The urgency of the need for better remediation technologies is highlighted in some of the chapters, which outline the environmental impact of the various steps that are typically adopted in oil spill remediation currently. Though all the separation techniques may not have been discussed in detail here, we hope that this treatise will prove valuable for scientists and practitioners as well as for researchers and students venturing into this area, in their quests to understand, design, and develop new and more efficient remediation techniques. We thank D. R. Nagaraj for guiding the development of the symposium and Derek D. Kim, Chi Lo, Yang Shen, and S. Murthy Khandrika for their help with formatting. We express our gratitude toward Lisa Jackson, Administrator of the EPA (2009–2013), for the inspiration and encouragement she unstintingly provided.

SOMASUNDARAN
PATRA
FARINATO
PAPADOPOULOS

CONTRIBUTORS

Mohamed A. Abdelrahim, Shell Exploration & Development Co., New Orleans, LA, USA

Edgar J. Acosta, Department of Chemical Engineering, University of Toronto, Toronto, Ontario, Canada

Richard Ambrose, Department of Environmental Health Sciences, University of California, Los Angeles, CA, USA

Paul T. Anastas, Department of Chemistry, Yale University, New Haven, CT, USA

Sean S. Anderson, California State University Channel Islands, Camarillo, CA, USA

Shelly Anghera, Anchor QEA, CA, USA

Thomas Azwell, Department of Environmental Science, Policy & Management, University of California, Berkeley, Berkeley, CA, USA

Mace G. Barron, Office of Research and Development, U.S. Environmental Protection Agency, Gulf Breeze, FL, USA

Steve Bay, Southern California Coastal Water Research Project, Costa Mesa, CA, USA

Pi Belobrov, Molecular Architecture Group, Institute for Biophysics, Siberian Federal University, Krasnoyarsk, Russia

Brittany M. Bernik, Department of Ecology & Evolutionary Biology, Tulane University, New Orleans, LA, USA

Michael J. Blum, Department of Ecology & Evolutionary Biology, Tulane University, New Orleans, LA, USA

Mangesh I. Chaudhari, Department of Chemical and Biomolecular Engineering, Tulane University, New Orleans, LA, USA

Gary Cherr, Bodega Marine Laboratory, University of California, Davis, CA, USA

Rob Condon, Center for Marine Science, University of North Carolina, Wilmington, NC, USA

Robyn N. Conmy, Office of Research and Development, U.S. Environmental Protection Agency, Cincinnati, OH, USA

Meghan Curran, Department of Chemical and Materials Engineering, University of Alberta, Edmonton, Alberta, Canada

Thomas Dean, Coastal Resources Associates, Inc., Carlsbad, CA, USA

Meijiao Deng, Department of Chemical and Materials Engineering, University of Alberta, Edmonton, Alberta, Canada

Raymond S. Farinato, Cytec Industries Inc., Stamford, CT, USA

S. E. Friberg, Ugelstad Laboratory, Department of Chemical Engineering, Norwegian, University of Science and Technology, Trondheim, Norway

William (Monty) Graham, University of Southern Mississippi, MS, USA

Marc S. Greenberg, Office of Solid Waste and Emergency Response, U.S. Environmental Protection Agency, Washington, DC, USA

Michael Guzy, Department of Biological & Ecological Engineering, Oregon State University, OR, USA

Stephanie Hampton, Center for Environmental Research, Education & Outreach (CEREO), Washington State University, WA, USA

Hida Hasinovic, Ashland Consumer Markets, Lexington, KY, USA, USA

Eric M.V. Hoek, Department of Civil and Environmental Engineering, University of California, Los Angeles, Los Angeles, CA, USA

Yuly A. Jaimes-Lizcano, Department of Chemical & Biomolecular Engineering, Tulane University, New Orleans, LA, USA

Graeme J. Jameson, Center for Multiphase Processes, University of Newcastle, Newcastle, New South Wales, Australia

Samantha Joye, Department of Marine Sciences, University of Georgia, Athens, GA, USA

John Lambrinos, Department of Horticulture, Oregon State University, OR, USA

Qingxia Liu, Department of Chemical and Materials Engineering, University of Alberta, Edmonton, Alberta, Canada

Jacob Masliyah, Department of Chemical and Materials Engineering, University of Alberta, Edmonton, Alberta, Canada

Bruce Mate, Marine Mammal Institute, Oregon State University, OR, USA

Douglas Meffert, National Audubon Society, Baton Rouge, LA, USA

K. Nandakumar, Cain Department of Chemical Engineering, Louisiana State University, Baton Rouge, LA, USA

Alex Nikolov, Department of Chemical and Biological Engineering, Illinois Institute of Technology, Chicago, IL, USA

Kyriakos Papadopoulos, Department of Chemical & Biomolecular Engineering, Tulane University, New Orleans, LA, USA

Partha Patra, Department of Earth and Environmental Engineering, Columbia University, New York, NY, USA

Charles H. Peterson, Institute of Marine Sciences, University of North Carolina at Chapel Hill, NC, USA

Sean Powers, Dauphin Island Sea Lab, University of South Alabama, AL, USA

Lawrence R. Pratt, Department of Chemical and Biomolecular Engineering, Tulane University, New Orleans, LA, USA

Suniya Quraishi, Department of Chemical Engineering, University of Toronto, Toronto, Ontario, Canada

A. Rao, Cain Department of Chemical Engineering, Louisiana State University, Baton Rouge, LA, USA

Dandina N. Rao, Department of Petroleum Engineering, Louisiana State University, Baton Rouge, LA, USA

Rupesh K. Reddy, Cain Department of Chemical Engineering, Louisiana State University, Baton Rouge, LA, USA

Kazutami Sakamoto, Professor, Department of Pharmaceutical Sciences, Graduate School of Pharmacy, Chiba Institute of Science, Chiba, Japan

Gopi Sethumadhavan, Department of Chemical and Biological Engineering, Illinois Institute of Technology, Chicago, IL, USA

Sébastien Simon, Ugelstad Laboratory, Department of Chemical Engineering, Norwegian University of Science and Technology, Trondheim, Norway

Johan Sjöblom, Ugelstad Laboratory, Department of Chemical Engineering, Norwegian University of Science and Technology, Trondheim, Norway

Ponisserril Somasundaran, Center for Colloids and Interfaces, Columbia University, New York, NY, USA

Robert Spies, Applied Marine Science, CA, USA

Caz Taylor, Department of Ecology & Evolutionary Biology, Tulane University, New Orleans, LA, USA

L. Thibodeaux, Cain Department of Chemical Engineering, Louisiana State University, Baton Rouge, LA, USA

Ronald Tjeerdema, Environmental Toxicology Department, University of California, Davis, CA, USA

Kalliat T. Valsaraj, Cain Department of Chemical Engineering, Louisiana State University, Baton Rouge, LA, USA

Albert D. Venosa, Land Remediation and Pollution Control Division, National Risk Management Research Laboratory, U.S. Environmental Protection Agency, Office of Research and Development, Cincinnati, OH, USA

Louxiang Wang, Department of Chemical and Materials Engineering, University of Alberta, Edmonton, Alberta, Canada

Qing Wang, Department of Chemical & Biomolecular Engineering, Tulane University, New Orleans, LA, USA

Darsh Wasan, Department of Chemical and Biological Engineering, Illinois Institute of Technology, Chicago, IL, USA

Gregory J. Wilson, Office of Solid Waste and Emergency Response, U.S. Environmental Protection Agency, Washington, DC, USA

C. Wu, Cain Department of Chemical Engineering, Louisiana State University, Baton Rouge, LA, USA

Zhenghe Xu, Department of Chemical and Materials Engineering, University of Alberta, Edmonton, Alberta, Canada

Z. Yu, Cain Department of Chemical Engineering, Louisiana State University, Baton Rouge, LA, USA

Peixi Zhu, Department of Chemical & Biomolecular Engineering, Tulane University, New Orleans, LA, USA

1

SCIENCE-BASED DECISION MAKING ON THE USE OF DISPERSANTS IN THE DEEPWATER HORIZON OIL SPILL

Albert D. Venosa, Paul T. Anastas, Mace G. Barron, Robyn N. Conmy, Marc S. Greenberg, and Gregory J. Wilson

1.1 INTRODUCTION

The explosion of the Deepwater Horizon (DWH) oil rig in the Gulf of Mexico on April 20, 2010, led to the tragic loss of 11 human lives. It also unleashed the largest oil-related environmental disaster in U.S. history and the second largest in recorded history.

A failed blowout preventer below the DWH drilling rig caused an unprecedented amount of oil and associated gas to discharge continuously over a period of 3 months. Spill response capabilities were tested to their limits by the continuous and rapid flow of crude oil from the seafloor. Responders turned to information from previous incidents and all available scientific literature to help formulate effective response approaches and deal with unprecedented circumstances.

Lessons learned from the 1989 Exxon Valdez incident in Alaska and other major oil spills have taught us that conventional mitigation techniques such as booming, skimming, and mechanical recovery cannot be fully relied upon to prevent oil from reaching shorelines and damaging sensitive ecosystems during a large-scale spill. They also offer insights into the conditions and circumstances in which dispersant application may be more or less effective. Early in the Exxon Valdez spill, for example, alternative response techniques including the use of dispersants and *in situ*

Oil Spill Remediation: Colloid Chemistry-Based Principles and Solutions, First Edition.
Edited by Ponisseril Somasundaran, Partha Patra, Raymond S. Farinato, and Kyriakos Papadopoulos.

burning were attempted to minimize spread of the surface slick. Four attempts to apply dispersants over the course of 4 days were deemed ineffective due to circumstantial and operational challenges such as equipment failure and lack of sufficient wave action at sea to adequately mix the dispersant with the oil. As a result, dispersant application was discontinued (NRC, 2005).

While all oil spill cleanup techniques have associated environmental trade-offs, those related to the decision to use dispersants may be especially complex. Unlike mechanical recovery, which physically removes oil from the environment, dispersant application drives oil from the surface into the water column. This keeps oil away from shore and transfers exposure risk from water fowl and shoreline species to planktonic and pelagic species. But at the same time, this technique delays eventual removal of oil fractions that are amenable to natural biodegradation processes. In 2005, the U.S. National Research Council acknowledged that, indeed, "one of the most difficult decisions that oil spill responders and natural resources managers face during a spill is evaluating the environmental trade-offs associated with dispersant use" (NRC, 2005).

The depth at sea and continuous flow of oil from the DWH well also posed entirely new challenges for oil spill responders and decision-makers. The point source of discharge was situated approximately 1500 m below the water surface, and oil rising to the surface continued to spread over an ever-increasing area. Subsea dispersant application was raised as a potential response option to overcome these unprecedented circumstances (Kintisch, 2010). There are several practical advantages associated with the application of dispersant directly at the point source of discharge. First, dispersant can be applied directly to fresh oil, before lighter oil fractions are lost and before oil has time to significantly weather and emulsify with water as a result of naturally present surface active agents. Second, direct injection at the point source increases the probability that applied dispersant will encounter all or most of the released oil. This significantly increases efficiency of treatment and decreases the amount of chemical added to the environment. In contrast, a slick on the water surface may be fragmented and stringy, resulting in wasted chemicals in unnecessary quantities when applied from overhead.

Prior to the DWH incident, most (if not all) existing oil spill response knowledge was based on surface spills and surface applications of dispersant. The behavior of dispersants subsea was (and still is) less understood, and previous research had not focused on the duration or quantity of dispersant used during the DWH incident. Recognizing the unique nature of this challenge and response, the U.S. Environmental Protection Agency (EPA) and the U.S. Coast Guard issued a directive requiring BP to implement a monitoring and assessment plan for both subsurface and surface applications of dispersants as part of the BP oil spill response. The goal of the monitoring program was to evaluate daily the effects of dispersant application at the source of discharge. This required an understanding of the fate and transport of dispersed oil. As a result, monitoring efforts were extensive and multifaceted. Coordinated efforts included dissolved oxygen monitoring to ensure hypoxia was not taking place, fluorometric measurements to track the oil plume, laser *in situ* scattering and transmissometry (LISST) sensor measurements to assess particle size distribution,

oil chemistry analysis of collected samples, monitoring of currents and advective movement of the plume, conductivity/temperature/depth (CTD) profile data collection, and Rototox analyses to estimate acute toxicity from the dispersed plume.

Several government agencies and stakeholders were involved in this monitoring effort, including the National Oceanic and Atmospheric Administration (NOAA), the U.S. Geological Survey (USGS), the Department of Fisheries and Oceans (DFO) Canada, academic researchers funded by the National Science Foundation (NSF), BP response contractors, and the states bordering the Gulf of Mexico. As a result of this collaborative effort, the response community has learned a great deal about subsea dispersion, the behavior of dispersed oil plumes as they advect, how best to monitor oil plumes, and the acute toxicity of certain dispersants. But only those questions immediately relevant to the spill response were able to be addressed in the midst of the crisis and its immediate aftermath. Many more important scientific questions remain. This paper provides the authors' perspective on deep-sea dispersant injection and identifies what research must be undertaken to answer the questions raised by the DWH oil spill tragedy.

1.2 BRIEF HISTORY AND EVOLUTION OF DISPERSANTS FOR OIL

1.2.1 Spill Mitigation

According to Etkin, 367 of the 408 oil spills that occurred globally in the period 1966–1969 were treated with dispersants (Etkin, 1998). The first recorded use was on an offshore tanker spill in Germany in 1966 (Lewis et al., 1985). Of those, the most well-known major spill where dispersants were used for treatment occurred in 1967 during the Torrey Canyon incident, which spilled approximately 1 million barrels (bbl) of crude oil (144 million l) off the western coast of Cornwall, England. Over 10,000 bbl (1.6 million l) of surfactants (alkylphenols) and solvents (aromatic hydrocarbons) were sprayed onto the slick for 14 days following the release. This resulted in extreme toxicity to marine life due to the toxic nature of the chemicals comprising the dispersant. The toxicity of the dispersant was deemed mostly due to the toxicity of the solvents in the mixture, not the surfactants (NRC, 1985). However, alkylphenols today are known to be endocrine disruptors, which exert their effects chronically rather than acutely and at low concentrations. The Torrey Canyon incident spurred European, American, and Canadian governments to sponsor research programs to develop more effective and less ecologically harmful dispersants and application equipment.

One infamous spill incident where dispersants were used for mitigation was the Ixtoc well blowout off the Gulf of Mexico in 1979, where over 3.3 million bbl of crude oil spewed into the sea over a period of 10 months (for perspective, the DWH spill reportedly spewed 4.9 million bbl into the Gulf over an 87-day period before accounting for containment and recovery (http://www.doi.gov/deepwaterhorizon/loader.cfm?csModule=security/getfile&PageID=237763)). Dispersant use by Mexican officials was reported to be successful, but dispersants were not used in U.S. waters

because the oil was too weathered to expect success (Etkin, 1998). The second-generation dispersants produced in the 1970s were less toxic but also considerably less effective. One of the first of the third generation of dispersants that emerged in the 1980s was Corexit 9527, a product then manufactured by Exxon. Its toxicity was substantially reduced, while its efficacy in dispersing oil into the water column was significantly greater. This was followed by Corexit® 9500 in the mid-1990s, and this dispersant is still the predominant one in supply in much of the United States, being the one most used in the DWH spill. Other dispersants were produced in the 1990s and 2000s, leading to the products currently listed on the National Contingency Plan Product Schedule (NCPPS) (http://www.epa.gov/emergencies/content/ncp/tox_tables.htm# dispersants).

1.3 DISPERSANT EFFICACY AND DISPERSION EFFECTIVENESS

The term "efficacy" is generally defined as the capacity to produce a specific effect under highly controlled conditions. "Effectiveness" describes an effect produced under noncontrolled conditions. In the latter sense, the researcher cannot create a control to use as a comparative baseline. So, when we describe how well a product disperses oil, we use efficacy to describe oil dispersion in a controlled laboratory setting such as a flask containing oil, water, and a dispersant, compared to a control flask containing oil and water but without dispersant. In the field, there can be no control. We describe how effective a chemical disperses oil in the field by taking measurements that may indirectly indicate effectiveness such as particle size distribution, buoyancy, analytical measurements, and fluorescence and then comparing these data to measurements from historical, controlled laboratory experiments.

To be considered for use in the United States as an efficacious oil spill mitigation agent, a dispersant product must be listed on the NCPPS. Listing on the NCPPS is obtained by passing test protocols identified by EPA: the manufacturer must provide data on the swirling flask test (SFT) and standard aquatic toxicity assays. These tests are described in Appendix C, Subpart J of 40 CFR part 300, series 900 (U.S. Environmental Protection Agency, 2003). Listing of a dispersant on the product schedule has been contingent on the dispersant being at least 45% effective in dispersing Prudhoe Bay and South Louisiana crude oils in the SFT laboratory test.

After promulgation of the SFT in 1994, unexpectedly large discrepancies were discovered between the data submitted by product vendors and data generated by EPA contractors (Clayton et al., 1993). The EPA's Office of Research and Development (ORD) conducted an in-depth laboratory study to determine the cause of this anomaly. The results indicated that a baffled flask provided substantially superior results both in terms of the degree of dispersion and variability among replicates, mainly due to the over-and-under type of mixing induced by the flask's baffles. Hence, the baffled flask test (BFT) was concluded to be the superior protocol for testing and listing dispersant products on the NCPPS (Sorial et al., 2004a, b). Soon after, ORD began to work with EPA's Office of Emergency Management to develop a proposed rule that incorporated changes to the existing protocol.

A follow-on study was conducted to develop a pass–fail decision rule. The approach is based on calculating the lower 95% confidence limit from the mean of all replicate measurements that must be greater than a set efficacy level. The higher the variance, the lower is the probability of passing the criterion. This approach ensures that only the most effective dispersants will be selected for inclusion on the product schedule and that a high degree of confidence will accrue in making these decisions. When all the results were in, a more stringent threshold was proposed (Venosa et al., 2002), although ongoing research may suggest that the ultimate threshold may be slightly changed to account for physically dispersed oil.

Although other laboratory testing procedures are available in the literature, the BFT is the only one that has undergone quantitative mixing energy calibration. A hot wire anemometer was used to quantify and compare the turbulence in the baffled flask (BF) and the swirling flask (SF). The velocity gradient and energy dissipation rate were computed based on these measurements. Mixing in the BF was found to be much more uniformly distributed than in the SF. The BF average energy dissipation rate was about two orders of magnitude higher than in the SF. Also, in the BF, the size of the microscales approached the size of oil droplets observed at sea, which means that the turbulence in the BF closely resembles the turbulence occurring at sea during breaking waves (i.e., a moderately energetic sea state). Hence, the BF was deemed preferable for dispersant efficacy (DE) testing in the laboratory (Kaku et al., 2006).

In an effort to better understand the effectiveness of the eight dispersants on the NCPPS that at the time were readily available in the U.S. market, EPA conducted efficacy tests in a laboratory using the BFT in a controlled situation using reference S. Louisiana crude (SLC) oil. Testing was conducted at the two temperatures in the Gulf: 5°C to represent temperature conditions for the deep-sea dispersant injection and 25°C to represent the temperature in the top 5 m where surface application was performed. The BFT was modified to test performance only on SLC oil at the two temperatures and to expand the number of replicates from four to six to increase the statistical power. This modification was designed because only one oil was being tested rather than two. Based on the laboratory findings presented earlier, it appears that only three of the eight dispersants would have provided satisfactory SLC dispersion effectiveness (at a volumetric DOR of 1:25) (Venosa and Holder, 2013). Corexit 9500 was one of the three dispersants giving satisfactory results. This conclusion assumes that the BFT is moderately predictive of field results, which may not be an accurate assumption since other factors (e.g., advection, dilution, and current flow) not testable in a closed flask may play a major role in determining performance in the field.

Dispersion effectiveness is ultimately determined by the dispersed oil droplet size distribution (Darling et al., 1990; Lewis et al., 1985). Droplets $< 100\,\mu m$ in diameter have small rise velocities and tend to remain suspended in the water column. They also become widely dispersed in the water column by turbulent diffusion and are more rapidly biodegraded due to the high surface-area-to-volume ratio (Li and Garrett, 1998). In addition, the oil droplets get surrounded by surfactant molecules, forming swollen micelles or microemulsions, which tend to repel each other, further

reducing the probability of recoalescence. Conversely, large oil droplets with diameters in the hundreds of μm tend to recoalesce and resurface unless strong mixing energy exists to overcome their buoyancy. Therefore, smaller droplets are much more favorable from the perspective of oil spill mitigation. Laboratory and field measurements suggest that for effective dispersion of oil in which the dispersed oil droplets remain suspended in the water column, average droplet sizes have to be less than 50–70 μm (Lunel, 1993, 1995).

Unpublished LISST measurements of the dispersed oil plume in the deep sea during the DWH spill at 1100–1300 m below the surface showed that most of the plume consisted of particle sizes ranging from 2.5 to 70 μm in diameter. Furthermore, light scattering measurements of water samples collected from that plume displayed the characteristic bimodal distribution typical of chemically—as opposed to physically—dispersed oil (Li et al., 2008a, 2009). This suggests, but does not scientifically prove, that the oil in the deep zone was likely chemically dispersed due to the injection of dispersant into the oil exiting from the riser tube. Although it is plausible that the extreme turbulence of the oil as it exited the well may have caused extensive physical dispersion without the need for chemical dispersant use, review of reported data and information in the literature leads us to determine that it is less likely and that the application of dispersants in the deep sea was successful in dispersing the oil at the source.

1.4 TOXICITY OF DISPERSANTS

1.4.1 Laboratory Testing

The EPA performed two phases of laboratory dispersant toxicity testing during the DWH spill to supplement existing data available on the NCP product schedule. Phase 1 involved testing of eight dispersants using both standard toxicity bioassays with a fish and an aquatic invertebrate and *in vitro* mammalian cell line assays. Phase 2 of EPA's testing determined the acute toxicity of the eight dispersants mixed with SLC to two Gulf of Mexico estuarine species. *In vitro* testing was focused on determining if any of the eight commercial dispersants had estrogenic or androgenic activity, as well as any activity in other biological pathways using a large battery of cell line assays. Overall, no activity was observed in any androgenic assay, two dispersants showed a weak estrogenic signal in one assay, and all dispersants showed minimal cytotoxicity (Judson et al., 2010).

The ecotoxicity testing approach used consistent test methodologies within a single laboratory in assessing the relative acute toxicity of the eight dispersants, including Corexit 9500A (identical to Corexit 9500), the predominant dispersant applied during the DWH spill. Static acute toxicity tests were performed using the mysid shrimp (*Americamysis bahia*) and the inland silversides (*Menidia beryllina*). For all eight dispersants in both test species, the dispersants alone were less toxic (LC50s, 3 to >5600 ppm) than the dispersant–SLC mixtures (0.4–13 mg TPH/l). SLC alone was in general similarly toxic to mysids (LC50, 2.7 mg/l) and

Menidia (LC50, 3.5 mg/l) as the dispersant–SLC mixtures. The results were consistent with data available on the NCPPS and indicated that the toxicity of Corexit 9500A was generally similar to other available dispersants when tested alone and as a mixture with SLC (Hemmer et al., 2011). The results of EPA's dispersant toxicity testing were made publicly available on the EPA Internet site (http://www.epa.gov/bpspill) and facilitated the EPA administrator's advice and support to the incident commander of the decision regarding dispersant use during the DWH spill response.

1.4.2 In-Field Monitoring

The EPA conducted extensive monitoring of the nearshore environment and communities during the emergency response to the DWH spill that included sampling and testing of marine surface water and sediments. Because EPA recognized early that dispersant usage was an environmental trade-off not to be taken lightly, this monitoring was important because it provided relevant data for detecting any measurable environmental impacts from this usage. Markers of dispersants such as dipropylene glycol butyl ether (DPBE) and dioctyl sulfosuccinate (sodium salt) (DOSS) were included in the chemical analysis, and few detections of these compounds were found in water and sediment samples. All such detections were below aquatic life benchmarks for water that were based on biological effects data (http://www.epa.gov/bpspill; OSAT, 2010). Toxicity testing associated with samples collected in Alabama, Mississippi, and Florida using estuarine and marine organisms (mysid shrimp (*A. bahia*), inland silversides (*M. beryllina*), sea urchin (*Arbacia punctulata*), polychaete worms (*Neanthes arenaceodentata*), and amphipods (*Leptocheirus plumulosus*)) resulted in observed toxicity in one surface water and three sediment samples. However, these findings could not be attributed to the DWH spill because, among many factors, the analytical results did not exceed the ecological screening values, the water samples were negative for petroleum and dispersant analytes, and the observed sediment toxicity was inconsistent across test species and likely due to effects from grain size (Integrated Laboratory Systems, Inc., 2010).

In addition, as a part of the directive issued by the USCG and EPA to BP to implement monitoring and assessment of the subsurface and surface applications of dispersants, daily 24-h acute toxicity testing of rotifers was conducted. Rotifers were exposed to offshore water samples collected near the wellhead and response operations. A critical variable for monitoring the long-term effects of the spill was daily measurements of dissolved oxygen, which would indicate consumption of oil by microbial activity. If DO approached 2 mg/l, which was considered hypoxic in the deep sea, considerations would be made by the Unified Command to suspend dispersant injection at the wellhead. Fortunately, this never occurred. The results from over 1000 sample test results conducted on samples taken from May 29 to August 26, 2010, indicated limited observations of toxicity. Approximately 89% of the samples were not toxic (survival $>90\%$), 10% were marginally toxic (survival range <90 to $\geq 75\%$), and 1% showed survival $<75\%$. Collectively, these monitoring results were

helpful for daily decisions on the use of dispersants during the spill, including the reduction in dispersant application rate as the response unfolded.

1.5 MONITORING OF DISPERSANTS ON THE SURFACE AND IN THE DEEP SEA

1.5.1 Monitoring in Surface Waters

Dispersion effectiveness during an oil spill is most commonly monitored using guidance set forth by the nonregulatory Special Monitoring of Applied Response Technologies (SMART) protocols (Barnea and Laferriere, 1999; U.S. Coast Guard, National Oceanic and Atmospheric Administration, U.S. Environmental Protection Agency, Centers for Disease Control and Prevention, and Minerals Management Service, 2003). The protocols establish a monitoring system for rapid collection of real-time, scientifically based information to assist decision-making during dispersant and *in situ* burning operations. Its primary focus determines if dispersant application is relatively effective or ineffective, where the degree of effectiveness is a secondary focus but is often difficult to address quantitatively in the field. The ultimate objective of SMART is to determine whether or not further chemical dispersion should be carried out during an oil spill.

To meet this objective, relative effectiveness (RE) must be defined. According to the SMART protocol, RE describes the amount of oil that the dispersant puts into the water column relative to the amount of oil that remains in the surface slick. A dispersant is considered "relatively effective" if half the oil is dispersed. Extensive laboratory tests have been conducted to determine the extent of chemical dispersion on various oils, but these studies do not represent real-world conditions for reasons already mentioned. An inherent problem occurs when attempting to calculate this in the field, as plumes and slicks are heterogeneous and patchy and no reliable way exists to accurately measure thickness of either. An added complication is apparent when oil is not from a spill of known volume but from a leak and/or continuous spewing source, making a mass balance of oil challenging (Fingas, 2000). Environmental factors such as conductivity or salinity, water temperature, pressure, sea state, and weathering also influence extent of both physical and chemical dispersion. The extent of these influences is poorly understood in real world situations.

The SMART lays out a tiered, structured approach, where Tier I is reliant on visual criteria from aircraft or ships to confirm the formation of dispersed oil (generally as a yellow- or coffee-colored plume below the water's surface). This is followed by the Tier II, which calls for real-time fluorometric monitoring of the underwater plume and discrete sample analysis of oil concentrations at 1 m depth. Tier III expands on this and uses additional fluorometers to monitor multiple depths between 1 and 10 m and collection of ancillary environmental data on water temperature, conductivity or salinity, pH, dissolved oxygen, and turbidity. These monitoring techniques are sufficient for the majority of spills although false positives and negatives may occur, affecting confirmation of dispersion effectiveness (Fingas, 2003). Since the establishment of SMART, reviews have highlighted the limitations of the methods (Goodman, 2003) and subsequent updates to the protocols in 2006 and 2008.

1.5.2 Monitoring in the Deep Sea

In the case of the DWH oil spill, the existing SMART protocols, as written, provided insufficient guidance for examining dispersant effectiveness. This was due to the unprecedented nature of the spill, given the extreme depth of the wellhead leak within the ocean. This posed unique challenges to the monitoring efforts, where oil that remained in the subsurface plume (between 1000 and 1500 m) could not be tracked via common methods such as aerial surveys or shallow-towed fluorometers. Tracking during the DWH emergency response effort, therefore, required a modified monitoring approach using vertical profiling packages to extend fluorometric measurements and water sample collection to the deep-ocean floor. Sampling was conducted in a radial pattern to initially confirm the existence and location of a subsurface plume resulting from dispersant application at depth. Added to the measurement suite was a LISST sensor to measure suspended particle or droplet size to indicate degree of dispersion (Li et al., 2007). Since the LISST cannot differentiate between chemical and physical dispersion, multiwavelength fluorescence analyses of discrete samples to calculate fluorescence intensity ratios (FIR) were used (Bugden et al., 2008). Discrete and *in situ* fluorescence analyses both revealed the presence of what was termed the "fluorescence anomaly" due to elevated values above background natural organic matter in the deep ocean. Although there has been much debate over which fluorometer is best equipped (wavelengths, sensitivity, calibration) to measure dispersed oil, all sensors used during the response efforts were capable of measuring some portion of the oil. Validation of any anomalies was confirmed with chemical analyses (PAHs, TPH, BTEX) during the response effort.

The DWH oil spill possessed both surface and subsurface plume components (Fig. 1.1). The response efforts at the surface were informed by the SMART monitoring program, along with hydrodynamic ocean circulation models and innovative remote sensing techniques (Hu, 2011). At depth, the response effort used various indicators to detect and track the subsurface plume, where assessment was conducted by a collaborative team of scientists from federal, academic, and industrial organizations who were tasked with providing rapid response analysis of data (Joint Analysis Group membership at http://ecowatch.ncddc.noaa.gov/jag). The multipronged approach required by the unique demands of the spill calls to light the need for further research in monitoring technologies and the need for updating the living guidance documents that make up SMART.

1.6 FATE AND TRANSPORT OF DISPERSANTS AND DISPERSED OIL

Understanding the transport and subsequent fate of oil and dispersed oil is important in aiding the decision-making process for response to an oil spill of any magnitude. These processes have a direct influence on the concentration and, therefore, the effects exerted on the ecosystem. The whole strategy behind use of dispersants is predicated on creating tiny droplets of oil, driving them into the water column where exposure of water fowl to the toxic and smothering slick is limited, and rendering the

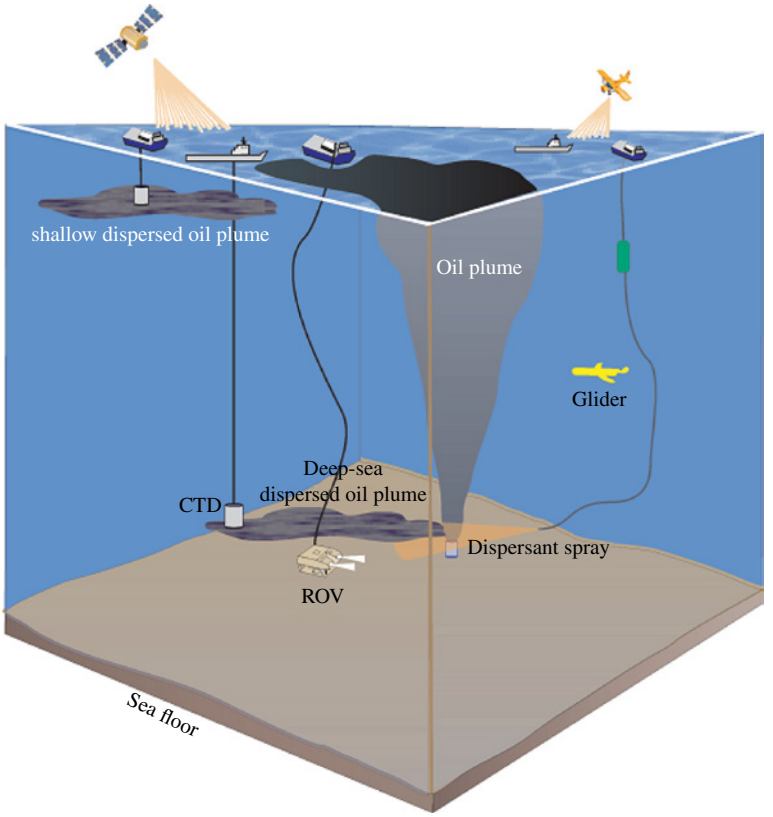

FIGURE 1.1 Conceptual diagram of monitoring efforts on the surface and in the deep sea. *(See insert for color representation of the figure.)*

droplets amenable to more rapid biodegradation due to the high surface area imparted by the dispersant treatment. The use of chemical dispersants also changes the behavioral variation of entrained oil droplets compared to natural dispersion. As pointed out by NRC (NRC, 2005), the movement of oil in the environment involves surface transport (mostly spreading, which determines the shape, thickness, and location of the slick, all of which affect decisions on using dispersants), vertical transport into the water column (which is responsible for the initial dilution after dispersant application), and horizontal transport or advection (which is responsible for the ultimate dilution of the oil mitigating the effect on fish and enhancing its biodegradation).

The EPA in concert with DFO Canada has conducted substantial research in the recent past on the importance of mixing energy in achieving the small particle size distribution needed for permanent dispersion in the bulk-water column (Li et al., 2008a, b). This work was conducted at the wave tank co-owned by EPA and DFO and located at DFO's Bedford Institute of Oceanography in Dartmouth, Nova Scotia (Li et al., 2008a). In this study, the wave tank was operated in flow-through mode to simulate advective dilution of the dispersed oil plume in the sea. This led to the

development of the term "dynamic dispersion effectiveness" (DDE), which reflects both dispersion of oil into the water column and transport and dilution of the dispersed oil droplets through the water column. Dynamic dispersion effectiveness differs from the DE obtained in bench-scale flask tests, where only the contact efficiency between oil and dispersant is measured in small enclosed surroundings during which unlimited collision frequency between oil droplets and eddies may occur. The flow pattern was clearly different when the wave tank was operated in flow-through mode compared to batch mode. In particular, the backflow near the bottom of the wave tank during batch operation was overcome by the forward current in the flow-through system, which purged the smaller dispersed oil droplets that were suspended in the water column out of the wave tank. This reduced the interdrop collision frequency that would cause recoalescence and resurfacing of the smaller dispersed oil droplets while retaining the larger oil droplets floating at the surface to maintain high droplet–eddy collision frequency for the breakage of droplets into small particles (Tsouris and Tavlarides, 1994).

Figure 1.2 summarizes the effect of dispersant type and wave energy on the average dispersed oil droplet volume mean diameter (VMD) for Alaska North Slope crude oil. In the absence of chemical dispersant (Fig. 1.2a), the oil droplet sizes remained large and highly variable (VMD ~ 150–400 μm) under the coherent, nonbreaking wave condition but were rapidly reduced in size and variability (VMD ~ 150–200 μm) under breaking wave conditions. In the presence of the chemical dispersant Corexit 9500 (Fig. 1.2b), the dispersed oil droplet sizes remained large but considerably reduced in variability (VMD ~ 300 μm) under coherent wave conditions. These sizes were dramatically reduced (VMD ~ 50 μm) under breaking wave conditions within 10 min and maintained at this small size for the rest of the experiment (Li et al., 2008a). In the presence of Dispersit SPC1000 (Fig. 1.2c), the droplet sizes of the dispersed oil achieved the same low VMD even under nonbreaking waves, although they began recoalescing after 20–30 min, while the chemically dispersed oil droplets remained stable. Once the small particle size is achieved, especially in the deep sea as observed in the Gulf oil spill, the droplets are in effect neutrally buoyant, do not recoalesce, and remain at depth as advection continues to dilute the plume and biodegradation ensues.

1.7 FUTURE OIL SPILL RESEARCH AS A RESULT OF LESSONS LEARNED

It is critical that EPA strengthen its knowledge base and expertise in oil spill response and prevention. As with all environmental protection issues, agency decisions related to oil spill prevention, preparedness, and response must be informed by sound science and research of the highest caliber. The agency ORD has developed a comprehensive oil spill research strategy to fill knowledge gaps, focusing on potential human and environmental risks from oil spills and the application of dispersants, surface washing agents, bioremediation agents, and other mitigation measures. The goal of this strategy is to identify research that would provide environmental managers with the tools, models, and methods needed to mitigate the effects of oil spills in all

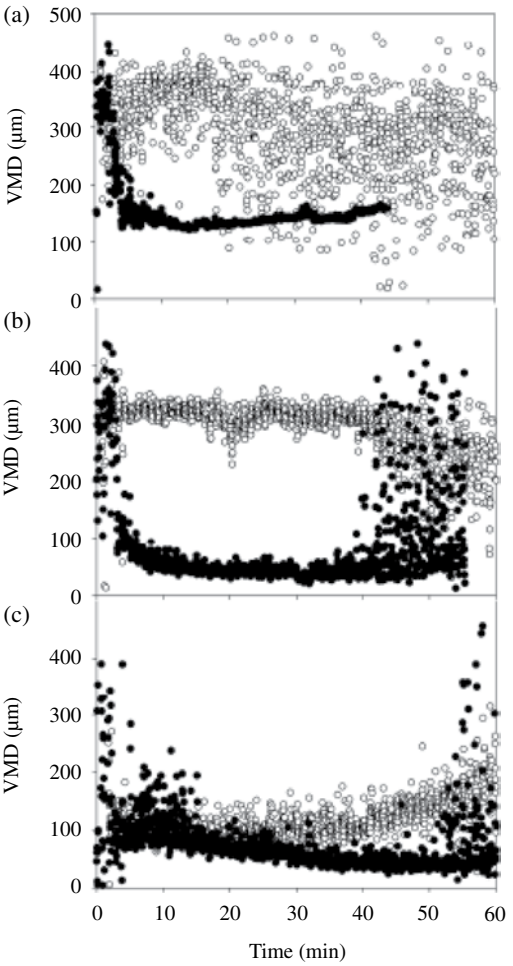

FIGURE 1.2 Dispersed Alaska North Slope crude oil droplet size subjected to (**a**) physical dispersion, (**b**) dispersion by Corexit 9500, and (**c**) dispersion by Dispersit SPC 1000. Open circles are for droplets dispersed under regular nonbreaking waves, and solid circles are under breaking wave conditions (from Li et al., 2009).

environments, emphasizing the coastal and inland environments as summarized in Table 1.1. The research needs identified will fill knowledge gaps in four areas to:

- Develop a better understanding of the impacts of oil spills and dispersant application on the environment
- Develop a better understanding of the shoreline, coastal, and inland environment impacts of oil spills, including nonpetroleum oils
- Develop innovative technologies to mitigate the impact of oil spills
- Address the technical needs of the communities impacted by the DWH oil spill

TABLE 1.1 Decision context, key science questions, and anticipated outcomes from EPA's research strategy

Decision context: What question is the decision-maker asking?	Key science questions: What research will answer that question?	Anticipated outcomes: How will this research inform the overall decision?
Which dispersants are the most efficacious for particular situations?	When is the use of dispersants most effective and what are the key parameters under which spilled oil is dispersible, such as temperature, mixing energy?	Inform Subpart J regulatory actions. Inform selection of the most effective dispersant on a spill-by-spill basis
What regulatory actions under Subpart J are needed for dispersants?	What alternative dispersants are available? How effective are they? How toxic are they?	Inform Subpart J regulatory actions
Do dispersants bioaccumulate in aquatic organisms?	What data are available on dispersant bioaccumulation? Are more studies needed on dispersant bioaccumulation?	Research will provide information about whether dispersants can bioaccumulate through a food chain
How long do dispersed oil and dispersants from surface, subsurface, and deepwater applications remain in the environment?	What is the environmental fate and transport of dispersed oil and dispersants from surface, subsurface, and deepwater scenarios?	Research will provide information on the environmental persistence of dispersants and dispersed oil, which will inform an evaluation of long-term human health and ecological impacts
What happens to dispersants and dispersed oil when used on deep-sea applications?	What are the key variables needed to better understand the coalescence and resurfacing of dispersed oil droplets to develop models for tracking the movement of dispersed oil plumes at the surface, in the subsurface, and in the deep sea?	Research will provide information to decision-makers on how much oil is dispersed chemically versus physically. If extreme turbulence is all that is needed, then chemical dispersants may not be required
What methods are available to track dispersed oil in the deep sea?	How can EPA collaborate to improve the SMART protocol for monitoring dispersed oil in the environment, especially the use of innovative and advanced fluorometric techniques?	Improved methods will allow managers to better track dispersed oil plumes and inform remediation decisions
Are oil dispersant products or chemically dispersed oil chronically toxic to aquatic flora and fauna?	What are the ecotoxicological effects of oil dispersant products and chemically dispersed oil?	Research will be used in ecological risk assessments to inform management decisions on the best products for dispersing oil into the water column

(*Continued*)

TABLE 1.1 (*Cont'd*)

Decision context: What question is the decision-maker asking?	Key science questions: What research will answer that question?	Anticipated outcomes: How will this research inform the overall decision?
Will oil dispersant products be toxic to aquatic species when injected at the surface or underwater to mitigate spill impacts from deep-sea blowouts?	What are the ecotoxicological effects of dispersants in surface and deep-sea injection exposures?	Research will be used in ecological risk assessments to inform management decisions for deploying the least toxic dispersants for mitigating oil spills
Will the effective use of dispersants reduce the impacts of the spill to shoreline and water surface resources without significantly increasing impacts to water-column and benthic resources? (NRC, 2005)	What are the comparative ecotoxicological effects of dispersants in surface and deep-sea injection exposures versus shoreline?	The dispersant ecological risks will be compared to coastal ecological risks from oil spills in a variety of scenarios. This comparative assessment will address key questions on dispersant use and provide information needed to conduct a net environmental benefit analysis
What green chemistry methods are available to use as effective dispersants?	What dispersants can be produced that have a "lighter" environmental footprint than petroleum-based products?	Dispersants will be proposed that have reduced life cycle assessment (LCA) ecological impacts to make available "green" options to decision-makers

Such research would provide a greater understanding of the short- and long-term impacts on the environment and human health associated with the DWH oil spill. Research is proposed to develop innovative technologies to increase the use of green or more benign approaches to mitigate surface and subsurface oil spills and restore environments impacted by oil spills. The strategy informs not only specific decisional endpoints necessary to address the effects and impacts of oil spills, including the DWH oil spill, but also identifies research to inform future scenarios involving oil spills that would potentially impact areas vital to a community's well-being. This includes all environments that are critical to a region's economy, commerce, personal livelihood, ecological sustainability, and the overall welfare of an area's inhabitants.

The research outlined in the strategy can inform agencies and academia of the knowledge gaps and needs associated with oil spill remediation and should take on the same integrated transdisciplinary approach as all of EPA's research programs by

engaging scientists across a spectrum of disciplines, including engineering, health sciences, ecology and ecotoxicity, chemistry, microbiology, and more. The strategy calls for close interaction between scientists across agencies, coordinated leveraging of resources, and ensuring no duplication of efforts.

1.8 SUMMARY

To effectively pursue its mission of protecting human health and the environment, EPA must base all of its decisions and actions on sound science. At the same time, during an environmental disaster, the ability to rapidly respond and make decisions is critical. Given the unprecedented nature of the DWH oil spill, the magnitude and ongoing nature of the event, and the continuous and rapid flow of crude oil from the seafloor, the coordinated federal DWH oil spill response faced significant challenges. Seeking to continuously base all decisions on sound science, responders and decision-makers turned to scientists for guidance on the use of dispersants and the interpretation of field monitoring information. Scientific experts provided input based on years of research and experience and also identified needs, gaps, and outstanding questions. Many lessons were learned through this event. These lessons have been thoroughly captured, with steps towards improvement already under way.

The EPA has developed a comprehensive oil spill research strategy to highlight knowledge gaps and research needs. The goal of the strategy is to encourage relevant research in advance of such events to improve the response by providing credible, applicable information to responders and decisions-makers. This information would help inform effective response approaches in both the planning and operational stages, improve the overall body of scientific knowledge, and inform new and innovative approaches to environmental protection and disaster response.

REFERENCES

Barnea N, Laferriere R. (1999). SMART: Scientific Monitoring of Advanced Response Technologies. International Oil Spill Conference Proceedings: March 1999, Vol. 1999, No. 1, pp. 1265–1267.

Bugden, JBC, Yeung CW, Kepkay PE, Lee K. Application of ultraviolet fluorometry and Excitation–Emission Matrix Spectroscopy (EEMS) to fingerprint oil and chemically dispersed oil in seawater. Mar Pollut Bull 2008;56:677–685.

Clayton JR, Payne JR, Farlow JS, Sarwar C. *Oil Spill Dispersants Mechanisms of Action and Laboratory Tests*. Boca Raton, FL: CRC Press; 1993. p 103.

Darling PS, Mackay D, Mackay N, Brandvik PJ. Droplet size distributions in chemical dispersion of oil spills: toward a mathematical model. Oil Chem Pollut 1990;7(3):173–198.

Etkin DS. Factors in the dispersant use decision-making process: historical overview and look to the future. In: Proceedings of the 21st Arctic and Marine Oilspill Program Technical Seminar; Ottawa: Environment Canada; 1998. p 281–304.

Fingas MF. In: Schramm LL, editor. *Use of Surfactants for Environmental Applications Surfactants: Fundamentals and Applications to the Petroleum Industry*. Cambridge, UK: Cambridge University Press; 2000. p 461–539.

Fingas MF. *Review of Monitoring Protocols for Dispersant Effectiveness*. Anchorage, AL: Report for Prince William Sound Regional Citizens' Advisory Council; 2003. p 33.

Goodman RH. Is SMART really that smart? In: Proceedings of the Twenty-Sixth Arctic and Marine Oilspill Program Technical Seminar; Ottawa: Environment Canada; 2003. p 779–786.

Hemmer M, Barron MG, Greene R. Comparative toxicity of eight oil dispersants, Louisiana Sweet Crude Oil (LSC) and chemically dispersed LSC to two aquatic test species. Environ Toxicol Chem 2011;30(10):2244–2252.

Hu C. An empirical approach to derive MODIS ocean color patterns under severe sun glint. Geophys Res Lett 2011;38(1):L01603.

Integrated Laboratory Systems, Inc. (ILSI). 2010b. Toxicity assessment of surface water and sediments from the Deepwater Horizon Response from the coasts of Florida, Mississippi, and Alabama. Prepared for U.S. Environmental Protection Agency Region 4, Science and Ecosystem Support Divison, Athens, GA. EPA Project ID 10–0607.

Judson RS, Martin MT, Reif DM, Houck KA, Knudsen TB, Rotroff DM, Xia M, Sakamuru S, Huang R, Shinn P, Austin CP, Kavlock RJ, Dix DJ. Analysis of eight oil spill dispersants using rapid, in vitro tests for endocrine and other biological activity. Environ Sci Technol 2010;44(15):5971–5978.

Kaku VJ, Boufadel MC, Venosa AD. Evaluation of mixing energy in laboratory flasks used for dispersant effectiveness testing. J Environ Eng 2006;132(1):93–101.

Kintisch E. An audacious decision in crisis gets cautious praise. Science 2010;329(5993):735–736.

Lewis A, Aurand D. Putting dispersants to work: overcoming obstacles. In: Proceedings of the International Oil Spill Conference, American Petroleum Institute Technical Report IOSC-004; 1997. p 78. Washington, D.C.

Lewis A, Byford DC, Laskey PR. The significance of dispersed oil droplet size in determining dispersant effectiveness under various conditions. In: Proceedings of the International Oil Spill Conference; Washington, DC: American Petroleum Institute; 1985.

Li M, Garrett C. The relationship between oil droplet size and upper ocean turbulence. Mar Pollut Bull 1998;36(12):961–970.

Li Z, Kepkay P, Lee K, King T, Boufadel MC, Venosa AD. Effects of chemical dispersants and mineral fines on crude oil dispersion in a wave tank under breaking waves. Mar Pollut Bull 2007;54(7):983–993.

Li Z, Lee K, King T, Boufadel MC, Venosa AD. Assessment of chemical dispersant effectiveness in a wave tank under regular nonbreaking and breaking wave conditions. Mar Pollut Bull 2008;56(5):903–912.

Li Z, Lee K, King T, Boufadel MC, Venosa AD. Oil droplet size distribution as a function of energy dissipation rate in an experimental wave tank. In: 2008 International Oil Spill Conference; Washington, DC: American Petroleum Institute; 2008b. p 621–626.

Li Z, Lee K, King T, Boufadel MC, Venosa AD. Evaluating chemical dispersant efficacy in an experimental wave tank: 2, significant factors determining in-situ oil droplet size distribution. Environ Eng Sci 2009;26(9):1407–1418.

Lunel, T. 1993. Dispersion: oil droplet size measurements at sea. In Proceedings: 1993 International Oil Spill Conference (Prevention, Preparedness, Response): March 29–April 1, 1993, Tampa, Florida. Washington, D.C.: American Petroleum Institute. pp. 794–795.

Lunel T. In: Lane P, editor. *The Use of Chemicals in Oil Spill Response*. Philadelphia, PA: American Society for Testing and Materials; 1995. p 240.

NRC. *Oil in the Sea: Inputs, Fates, and Effects*. Washington, DC: National Academies Press; 1985. p 601.

NRC. *Oil Spill Dispersants: Efficacy and Effects*. Washington, DC: National Academies Press; 2005.

Operational Science Advisory Team (OSAT), December 2010. "Summary report for sub-sea and sub-surface oil and dispersant detection: sampling and monitoring. Unified Area Command.

Sorial GA, Venosa AD, Koran KM, Holder E, King DW. Oil spill dispersant effectiveness protocol. Part I. Impact of operational variables. J Environ Eng 2004a;130(10):1073–1084.

Sorial GA, Venosa AD, Miller KM, Holder E, King DW. Oil spill dispersant effectiveness protocol. Part II. Performance of the revised protocol. J Environ Eng 2004b;130 (10):1085–1093.

Tsouris C, Tavlarides LL. Breakage and coalescence models for drops in turbulent dispersions. AIChE J 1994;40(3):395–406.

U.S. Coast Guard, National Oceanic and Atmospheric Administration, U.S. Environmental Protection Agency, Centers for Disease Control and Prevention, and Minerals Management Service. 2003. Special monitoring of applied response technologies. Available at http://docs.lib.noaa.gov/noaa_documents/648_SMART.pdf. Accessed October 1, 2013.

U.S. Environmental Protection Agency. 2003. Swirling Flask Dispersant Effectiveness Test, Revised Standard Dispersant Toxicity Test, and Bioremediation Agent Effectiveness Test. In *Appendix C, Part 300, Series 900, 40 CFR Ch. I*, p 224–246.

Venosa A.D, and E.L. Holder, 2013, Determining the dispersibility of South Louisiana crude oil by eight dispersant products listed on the NCP product schedule. Marine Pollution Bulletin 66(1–2):73–77.

Venosa AD, King DW, Sorial GA. The baffled flask test for dispersant effectiveness: a round robin evaluation of reproducibility and repeatability. Spill Sci Technol Bull 2002;7 (5–6):299–308.

2

UNDERSTANDING AND PROPERLY INTERPRETING THE 2010 DEEPWATER HORIZON BLOWOUT

Sean S. Anderson, Charles H. Peterson, Gary Cherr, Richard Ambrose, Shelly Anghera, Steve Bay, Michael J. Blum, Rob Condon, Thomas Dean, William (Monty) Graham, Michael Guzy, Stephanie Hampton, Samantha Joye, John Lambrinos, Bruce Mate, Douglas Meffert, Sean Powers, Ponisseril Somasundaran, Robert Spies, Caz Taylor, and Ronald Tjeerdema
by NCEAS Gulf Oil Spill EcoTox Working Group

2.1 INTRODUCTION

The Gulf of Mexico Deepwater Horizon (DWH) Oil Blowout[1] initiated a previously unknown category of marine pollution. The massive spatial and temporal scales of this release, combined with the ultra-deepwater[2] location of the wellhead, yielded a pollution event dramatically more complex than our prior understanding of the toxicology of oil spills suggested.

[1]Note that the DWH event is properly characterized as a wellhead "blowout" and not a "spill." An oil *spill* refers to the release of a contained volume of oil such as from the rupturing of a tanker's hold or breaking open of a storage tank. A *blowout* occurs when a tapped subsurface reservoir of unknown volume freely

Oil Spill Remediation: Colloid Chemistry-Based Principles and Solutions, First Edition.
Edited by Ponisseril Somasundaran, Partha Patra, Raymond S. Farinato, and Kyriakos Papadopoulos.

Piecemeal deconstruction of this complex, large-scale event has fostered an incorrect understanding of the mechanisms of exposure, the patterns of oil dispersal, the persistence of oil, and ultimately the acute and chronic effects of this spill upon the populations and communities of the Gulf of Mexico. Complete understanding of the ecotoxicology of this and any similar future blowouts requires both a new conceptual model of deep-sea hydrocarbon release, fate, and transport and ultimately a new interdisciplinary approach to quantifying the impacts of such exposure upon marine and coastal ecosystems across all depths and realms.

While a complete understanding of the impacts of this disaster is years or decades away, this chapter serves as an initial orientation to the DWH event and an introduction to the subsequent chapters in this volume.

2.2 BACKGROUND

2.2.1 Significant Past Marine Oil Spills

Free petroleum has been a component of the world's oceans for hundreds of millions of years, primarily entering into the marine environment through slow-release seeps in coastal shelf regions with fractured or discontinuous stratigraphies. Oil spills have gone hand in hand with human oil extraction and posed significant health and environmental risks for well over a century. For example, the largest accidental oil spill to date, the Lakeview Gusher (near Bakersfield, California), occurred a century before the DWH near the dawn of our petroleum age when bores were drilled manually. That 1910 terrestrial blowout ultimately released an estimated 1.5 million m^3 (9.4 million barrels, or 190% of the release of the DWH) over 544 days, creating a series of oil lakes as deep as 30 m before the majority of the oil volatized or seeped into the underlying sediments (West Kern County Oil Museum, 2011). Hundreds of oil spills occur each year in the U.S. waters, with most of these relatively small in both spatial extent and duration (National Research Council, 2003). While large spills from both extraction and transportation occur on a relatively frequent basis, some spills have had a disproportionate influence upon our conceptualization of the nature of oil spills, our resulting management responses to these events, and the aggregate ecological impacts. As such, these have had a direct bearing on our subsequent management and expectations of the DWH blowout.

---

and uncontrollably releases those hydrocarbons. It is important to note the difference, particularly from a policy and management perspective. As evidenced by the DWH event, the management of a *spill* is initially focused on containment only, whereas the management of a *blowout* must initially have dual foci of capping and containment. A *blowout* is therefore a much more difficult beast to deal with, given that the scale of the catastrophe is unknown and ever expanding.

Acknowledging this important semantic distinction, we will use both terms in this chapter. While *blowout* is the preferred term, we have found most audiences prefer the colloquial *spill* moniker and so have accepted its use in even technical writings about this disaster.

[2] The drilling industry and regulatory agencies have revised their depth classifications over time, reflecting technical advances. In 2010, the former Minerals Management Service defined depths below 400 m (1,312 ft) as *deep water* and depths below 1,600 m (5249 ft) as *ultra-deep water* (Nixon et al., 2009).

We briefly review some of the spills that we feel have most influenced our thinking about marine spill ecotoxicology (Table 2.1). These spills have shaped our understanding of spilled oil, transport and fate, and aggregate impact. Hydrocarbon release and dispersants applied are reported. Please note that there are often wide discrepancies between estimates of oil and dispersant released, even within a single agency. These reported volumes are the result of extensive exploration of sources and represent what we believe to be the most accurate accounting of volumes. The single exception to this extensive tracking down of numerous candidate sources here is the estimates for the Kuwaiti oil field releases. Here, the fog of war, active combat, and lack of a functioning government during this spill made estimates for this spill an incredibly subjective endeavor.

2.2.2 1967 Torrey Canyon Spill

The world's first supertanker *Torrey Canyon* ran aground upon the Seven Stones offshore reef on March 18, 1967, as Captain Pastrengo Rugiati attempted to shorten the ship's arrival time in Wales via a shortcut (BBC Newswire, 1967b; Petrow, 1969). Within 12 h of the grounding, the British Navy and local firefighters began spraying dispersants (more appropriately described as detergents, mainly BP1002) upon the expanding slick, applying approximately 75 m^3 over the first 3 days (9,500 m^3 would ultimately be used at sea and upon intertidal shores) onto the accumulating surface slick then comprised of an estimated 30,000 m^3 of oil (Smith, 1968). By day 6, the hull broke apart after refloating attempts had both failed and claimed the life of a Dutch salvage team leader (Axford, 2012). Prime Minister Harold Wilson ordered the military to bomb the fractured hull to sink it and burn the surface slick as the Cornish coast was becoming heavily oiled (BBC Newswire, 1967a; Lewis, 1967). This proved difficult and was complicated by both roughening seas and the fact that a quarter of the 161 bombs and 16 rockets dropped over 3 days by British warplanes missed their conspicuous, stationary target (Barkham, 2010). Ultimately, the military resorted to directly dumping 1,500 m^3 of napalm and 44.5 m^3 of aviation fuel over the wreck site to get that localized slick to ignite and burn consistently (Staff, 1978). Fourteen thousand cubic meters of oil was ultimately released and comprised a surface slick covering 700 km^2 at its peak, which killed an estimated 15,000 seabirds (Smith, 1968) and 90% of the sardine (*Sardina pilchardus*) eggs in the region (Spooner, 1969). As with the DWH four decades later, unseasonable offshore winds kept the majority of the oil off of British shores such that only about 15% of the spilled oil grounded across roughly 240 km (although only about 80 km were heavily oiled) of British coastline (Smith, 1968). The French coastal zone received more of the released oil. Both coastlines were covered with mixtures of weathered and emulsified crude. The French interdictions were more successful at minimizing oil upon their famous tourist beaches by applying 3000 tons of powdered Craie de Champagne (naturally occurring chalk containing stearic acid) onto the surface slick as it reached their nearshore waters (Smith, 1968).

In response to the heavy coastal oiling, the British deployed even more dispersant, ultimately applying the majority of the 9500 m^3 used in the overall response within

TABLE 2.1 Significant marine oil spills[a]

Significant marine oil spills		Oil released						
Year	Event	Release duration	Depth	Distance offshore	% of DWH	U.S. barrels (bbl)	U.S. gallons (gal)	Cubic meters (m^3)
1967	*Torrey Canyon* spill	12 days	Surface	25 km	2	86,000	3.6 million	14,000
1969	Santa Barbara blowout	11 days, reduced flows >1 year	57 m	9.5 km	2	80,000–100,000	3.4–4.2 million	13,000–16,000
1979–1980	*Ixtoc I* blowout	10 months	50 m	80 km	75	3.7 million	150 million	580,000
1989	*Exxon Valdez* spill	<1 day	Surface	2 km	5–16	260,000–760,000	11–32 million	42,000–120,000
1991	Kuwait oilfield sabotage	9 months	Surface	Shoreline	120–170	6–8.2 million	250–350 million	0.95–1.3 million
2010	DWH blowout	87 days	1,544 m	73 km	100	4.9 million	210 million	780,000

TABLE 2.1 (*Cont'd*)

Significant marine oil spills		Dispersant released			
Year	Event	Dispersant used	Cubic meters (m^3)	Spilled oil references	Dispersant references
1967	*Torrey Canyon* spill	At sea and on the UK beaches: BP1002 plus 11 unk others	9,500	Smith (1968)	On Cornish Coast 10,000 tons of detergents to treat 14,000 tons of oil; 12 detergents including BP1002; Chapter 18 in Straughan (1971) gives 2.5 million gallons which was converted
1969	Santa Barbara blowout	At sea Polycomplex A and unk Corexit	294	Nicholson and Cimberg ref is on p. 343 of Straughan (1971), Allen, (1969),	Ara Chemical, Polycomplex A-11, and Corexit 7664, and Unico at sea (Case History)
1979–1980	*Ixtoc I* blowout	At sea Corexit 9527	5,600	Anderson et al. (1982)	Coast Guard says Corexit 9527, Lindblom et al. (1981) (no soild number: 493 flights with approximately 3000 gallons per flight but no totals)
1989	*Exxon Valdez* spill	At sea Corexit 9580 (possibly 9527); on beaches Corexit 7664, 9580, and BP1100X	15	Exxon Valdez Oil Spill Trustee Council (1994)	At sea Corexit 9580 or 9527, says NOAA, 4000 gallons (EPA website: http://www.epa.gov/oem/content/learning/exxon.htm); limited experiments on beaches Corexit 7664, 9580, and BP1100X (Cleaveland and Saundry: http://www.eoearth.org/article/Exxon_Valdez_oil_spill)
1991	Kuwait oilfield sabotage	None	None	UNEP (1993); Readman et al. (1996) and references therein	None
2010	DWH blowout	At sea	7,000	McNutt (2011)	1,843,786 gallons (58% used at surface) USGS, personal communication

Note: An additional 1.6 billion barrels ignited or pooled into terrestrial lakes. 1 barrel = 42 U.S. gallons = 1591 = 0.15899 m^3 = 0.1364 metric tons.

[a]BP (2012), based on worldwide average crude oil specific gravity.

the coastal zone (Smith, 1968). This coastal application utilized often famously ineffectual techniques such as burying drums of dispersant, pouring dispersants directly onto beach sands en masse, or dropping whole dispersant barrels over cliffs (Barkham, 2010; M'Gonigle and Zacher, 1979). These first-generation "dispersants" were essentially engine degreasers, created and applied with little or no concern for any toxicological impacts upon natural systems. In the prescient words of the Guardian's science reporter Anthony Tucker in 1967, "There may be little point in spending many millions of pounds simply to convert an unpleasant but visible marine poison into another kind of poison that is insidious and entirely unknown in its effects" (quoted in Barkham, 2010). The 1968 post spill report by the Marine Biological Association of the United Kingdom (Smith, 1968) found the use of such dispersants magnified the toxicity by making spilled oil more bioavailable than untreated oil, rendering the management decision to use dispersant "largely ineffective, uneconomic, and wasteful of effort," suggesting that a safer route would have been to follow the French lead. Local intertidal populations bore the brunt of the spill impacts, with the highest mortality among sessile invertebrates, mobile herbivores, and macroalgae in areas where dispersants were most heavily applied (O'Sullivan and Richardson, 1967; Smith, 1968). While recolonization by opportunistic algae began in the months following the initial impact, significant differences in intertidal community composition, elevational distributions, and reduced species richness persisted for more than a decade, with the greatest differences in detergent-treated regions (Southward and Southward, 1978). The *Torrey Canyon* spill provided our first modern case study of the effects spilled oil has on the marine ecosystem (see Hawkins, 2012; Hawkins and Hartnoll, 1983; Hawkins and Southward, 1992; Raffaelli and Hawkins, 1999; Southward and Southward, 1978, 1988).

Salvaged coastal oil was deposited directly into an open-air pit approximately 100 m from the shoreline of Guernsey (now known locally as the Torrey Canyon quarry) where the pooled oil continues to kill alighting birds and wildlife to this day (Barkham, 2010). Throughout the immediate spill response, the government and responders were soon painted as either bumbling or (at best) ineffectual (M'Gonigle and Zacher, 1979). In the wake of the immediate impact, the drawn-out legal attempts to deflect responsibility by all potentially responsible parties spurred major reforms of international maritime libel statutes (Okidi, 2010). The *Torrey Canyon* spill marked the advent of long-term monitoring with robust modern statistical approaches on impacted communities (e.g., Schmitt and Osenberg, 1996). It was also the first marine spill wherein researchers and managers would conclude the proposed management was worse than the "baseline" oiling and was therefore directly responsible for stimulating development of second-generation dispersants wherein the ecotoxicology of the dispersants themselves was explored prior to use in a real-world management situation.

2.2.3 1969 Santa Barbara Blowout

One of the most influential oil spills occurred on January 29, 1969, approximately 10 km off of the coast of Summerland (just south of the city of Santa Barbara), California. While nearing the completion of drilling a fifth well, Union Oil's Platform

A suffered a catastrophic failure (National Oceanic and Atmospheric Administration, 1992). Insufficient borehole casings led to multiple ruptures along the adjacent seafloor. This fostered an unrestricted release of oil and gas into the Santa Barbara Channel for 11 days, with subsequent fissures opening up and oil ultimately leaking into the marine environment from associated seafloor cracks for at least a year (albeit at a much reduced flow rate). Somewhere between 13,000 and 16,000 m^3 of oil was released, making it the then-largest marine oil spill in the U.S. waters (Nicholson, 1972; Straughan, 1971a; Table 2.1).

The importance of the Santa Barbara blowout to our conceptualization of spilled marine oil cannot be underestimated. Climactic and oceanic conditions for most of the first 3 days of the spill kept the primary slick offshore, but a large winter storm then brought the oil onto mainland beaches (Kolpack, 1971). The high visibility and popularity of the beaches in the area, disingenuous industry claims of successfully curtailing the spill despite ample evidence to the contrary across newspaper front pages and on evening newscasts, continual reoiling of previously cleaned shoreline, proximity to the nation's film and broadcast epicenter, an eventual visit by the president of the United States, and deep-seated public outrage over the growing disaster set the stage for this oil spill to write the iconic story line of all future oil spills (Corwin, 1989; Easton, 1972; Nash, 1989, 2001). Included in this narrative that now dominates perceptions are conspicuously oiled marine vertebrates that volunteers from the public valiantly strive to clean, rudimentary industry and governmental technologies to sop up oil deposited along the coastline, fishery closures that idled fishing fleets, decimation of the regional coastal-dependent economies, a general inability of regulators and industry to correctly predict or characterize the fate and transport of the oil, and nonexistent processes to robustly characterize the impacts of the spill or offer up effective mitigation for the associated impacts. This was the first test of the recently passed National Pollution Contingency Plan and effectively put the federal government in the driver's seat of response coordination. Numerous regulatory responses to this spill greatly improved our capacity to respond to future spills (e.g., Clean Seas), exert greater regulatory controls over such offshore production (e.g., the California Coastal Commission), and mandate improved contingency plans, which include conceptually modeling such oil spills to help think through what a future spill might look like and who might be affected (e.g., Environmental Impact Reviews). No new oil leases in California state waters have been granted since this spill. The Santa Barbara oil spill was a major influence upon the nascent environmental movement and helped usher in our foundational federal laws of modern ecological protection (i.e., NEPA, Clean Water Act, Clean Air Act (Nash, 1989, 2001)).

Much effort has been devoted to understanding why the Santa Barbara oil did not cause larger impacts. While oil roamed over roughly the same amount of coastline (about 200 km, from Pismo Beach to Ventura) as *Torrey Canyon* oil 2 years before, oil groundings were most concentrated close to the well (Kolpack, 1971; Straughan, 1971a). Oil was coming ashore onto the campus of the University of California Santa Barbara and therefore stimulated a rapid, initially ad hoc inventorying and assessment of the biological impacts of this event by a wide cross section of local marine

researchers and amounted to our first assessment of oil fate and effects post-*Torrey Canyon* (Kolpack, 1971; Straughan, 1971a). Given the high-profile nature of the spill and the relative intensity of post spill biological monitoring, many were therefore surprised by the findings of minimal apparent acute impacts from the blowout. As a group, only several thousand seabirds and very localized populations of sessile intertidal invertebrates appeared to show consistent signs of acute mortality (Straughan, 1971b). To explain this apparent lack of impact, the Straughan (1971a) report set up a series of hypotheses that have generally guided our thinking since.

Straughan (1971b) reasoned that the aspects of the physical environment ameliorated potential impacts. First and foremost were the winter storms that helped break up and degrade oil but also created stresses of their own (that winter had the highest rainfall in two decades), making it difficult to distinguish oil effects from other effects such as low salinity. Secondly, those storms created conditions where oil was constantly moving over and through the coastal environment, in effect reducing site-attached organisms' exposure time to oil. Next, this hypothesis postulates that many species in the Santa Barbara Channel had an inherent physiological (chiefly prokaryotes) or behavioral (mobile animals) protection from hydrocarbon exposure/toxicity owing to their evolution in this oil seep-rich region wherein some level of background oiling has been occurring for millions of years. Lastly and perhaps most importantly was the rather cautious nature of the interpretation of data and the benefit of the doubt that was given. As virtually no baseline monitoring data existed pre spill, Straughan and her colleagues were hard pressed to even document any post spill differences in ecological conditions and were reluctant to attribute any apparent observed differences to the spill (Fauchald, 1972; Straughan, 1971a). This lack of pre spill ecological data and robust statistical methods to interpret impact led to the conclusion that little acute (and by extension chronic) toxicity occurred. The frequent caveats and qualitative statements throughout the report about the lack of tools to conduct a robust analysis (insuring what we might now term statistical power) were largely ignored. It was widely concluded that the Santa Barbara oil spill had little ecological impact (e.g., Epstein, 2010; Squire, 1992). In light of the DWH blowout, it is also important to note that in this and other concurrent explorations of the effects of the Santa Barbara spill, subtidal benthic and pelagic communities were largely ignored (save for offshore fish trawls, some grab sampling of benthic infauna that proved problematic, and limited nearshore kelp bed surveys) and having oil sink out of surface waters was generally considered an improvement from an ecotoxicological perspective. All aspects of this oil spill model have been directly applied to our initial interpretations of the DWH, although this Straughan model has become so deeply engrained into our ecotoxicologist assumptions that few cite her work as the ultimate source.

2.2.4 1979 Ixtoc I Blowout

In June 3, 1979, in Caribbean Mexico's Bay of Campeche, the Pemex semisubmersible exploratory drilling rig Sedco 135 F experienced a drilling mud failure while drilling an exploratory well 80 km offshore (National Oceanic and Atmospheric

Administration, 1992). Diminishing drill mud pressure allowed a methane kick to proceed up the bore and blow out the well. A complete failure of an in-place blowout preventer left the company with no ability to stem the flow and oil flowed for more than 10 months, releasing approximately 580,000 m^3 of oil into the Gulf of Mexico before a new relief well could intercept and cut off the original wellbore (Anderson et al., 1982). A variety of surface-lowered and diver-deployed containment structures failed to stem the flow. Nearly 493 sorties of aerial tankers applied about 5,600 m^3 of dispersants (Corexit 9527) across a wide area of the sea surface in Mexican waters but were disallowed in the U.S. territorial waters (Lindblom et al., 1981).

Despite the relatively shallow and nearshore location of this well, few readily apparent impacts were seen on local shores as most of the slick was transported northward away from the Mexican shore and into the Gulf of Mexico (Jernelöv and Olof, 1981). The application of dispersants to the sea surface soon commenced and became widely viewed as an effective tool with which to attack such spills (e.g., Lindblom et al., 1981; Walker and Henne, 1991; Walker et al., 1999). No dispersants were used in the U.S. territorial waters as federal managers deemed their value limited, given the highly weatherized state of most oil (weeks at sea) by the time it had reached the American shores (National Oceanic and Atmospheric Administration, 1992). The general lack of robust marine science–environmental monitoring capacity (Hooper, 1981), the apparent lack of interest in impact assessment by Mexican authorities (with the possible exception of interest in impacts to local fisherfolks; Editorial Board, 1980; Vargas, 2010), and the fact that the vast majority of the oil went "out of sight, out of mind" led to only limited documentation of the long-term consequences of this spill and any unintended impacts of the dispersant (Energy Resources Co. Inc., 1982; Lewbel, 1985). For example, in a representative description of minimal ecological impact from released hydrocarbons, Jernelöv and Olof (1981) simply note that "…[t]he rest of the oil, about 120,000 metric tons or 25 percent, sank to the bottom of the Gulf" with no other comment or research to support a noneffective impact assessment. The most sustained and robust investigations were conducted upon coastlines and coastal-dwelling species (i.e., birds and infauna) along the Texas shoreline (Kindinger, 1981; Tunnell and Chapman, 1980; Tunnell and Dokken, 1980, Tunnell et al., 1981, 1982), an area that received but a small fraction (perhaps 1%; Jernelöv and Olof, 1981) of the overall released hydrocarbons. DWH response efforts largely paralleled those for *Ixtoc I*, particularly in the initial weeks of the spill (Vargas, 2010).

In addition to little of evidence of any negative (or positive) impacts of sustained dispersant use and implicit acceptance of the Straughan model for oil spills, another notable outcomes of the *Ixtoc I* spill emerged from the time lag preceding surface oiling of the Texas coast. As nearly two months elapsed between the onset of the blowout and landfall (National Oceanic and Atmospheric Administration, 1992) of the weatherized oil upon the American coastline, federal responders realized the importance of coastline mapping relative to oil sensitivity. The resulting mapping/classification project produced the first Environmental Sensitivity Index (ESI) for coastal oiling. Proximately, this helped optimize the deployment of oil-containing booms. For longer term, it helped cement the notion that littoral communities are the

most vulnerable ecological communities and that future spill mitigation planning should de-emphasize concern for pelagic–benthic communities (e.g., Cooper and McLaughlin, 1998; Pincinato et al., 2009).

2.2.5 1989 Exxon Valdez Oil Spill

By early 1989, the Trans-Alaska Pipeline System had been bringing oil from Alaska's North Slope and Prudhoe Bay down to the marine shipping terminal at Valdez for more than 12 years. So routine had the shipping of oil from this facility become that an inebriated Captain Jeffrey Hazelwood abandoned the bridge of the *Exxon Valdez* supertanker soon after leaving port and allowed the autopilot to run the vessel aground on Bligh Reef on the early morning of March 24, 1989, in Alaska's Prince William Sound (Alaska Oil Spill Commission, 1990). Over the course of the next 3 days, the vast majority of the tanker's hold spilled between 42,000 and 120,000 m^3 of crude oil into the sound, with perhaps 25% of that oil subsequently escaping into the northern Gulf of Alaska (Exxon Valdez Oil Spill Trustee Council, 1994).

The oil largely disappeared from the surface of the ocean within a matter of weeks, but the crenulated shoreline of Prince William Sound and the Gulf of Alaska, dominated by cobble and boulders, received large amounts of oil that persisted on the intertidal surfaces for several years and for up to 20 years or more below that surface where protected from surface wave energy (Bodkin et al., 2012). Little of the oil reached the bottom of Prince William Sound, except in the shallow subtidal areas immediately off oiled beaches.

Major impacts of the spill occurred to birds and mammals on the surface of the ocean (e.g., common murres and sea otters) and to plants and animals living in or utilizing the intertidal areas for spawning (De Vogelaere and Foster, 1994; Houghton et al., 1997; van Tamelen et al., 1997). Little damage was documented to midwater animals, and little or none of the oil was found below 20 m depths (Rice et al., 2003). Work done after the spill documented the sublethal effects of low parts-per-billion exposure to polynuclear aromatic hydrocarbons (PAHs) to the young stages of pink salmon (Rice et al., 2001) and herring (Carls et al., 2002) and revised our expectations of toxicity of these compounds following oil spills. Research more than two decades post spill is still illuminating which species and populations have recovered (e.g., Harlequin Ducks; Esler and Iverson, 2010) and which still manifest sublethal impacts (e.g., otters (Bodkin et al., 2012)). Consequently, *Exxon Valdez* has become the world's best studied oil spill. The *Exxon Valdez* Trustee Council, which oversees and authorizes most of this work, has emphasized peer review at all stages and has importantly funded work that has focused on understanding the totality of the coastal ecosystem, thus allowing insights that would not have been possible under the previous, traditional approaches to impact assessment. Without this body of work, we would have been unable to understand the unexpected persistence of subsurface oil and the degree to which sublethal chronic exposures have continued to affect populations and communities (Peterson et al., 2003b).

Without this body of work, we would have been unable to understand, for example, the causal relationship between the 1989 spill and the subsequent reductions of pink

salmon and herring stocks years later (Carls et al., 2002; Rice et al., 2001). As long-term impacts continue to unfold, the *Exxon Valdez* has become a new model for ecotoxicological assessment. It also represents the model upon which the 1990 Oil Pollution Act was based and which now guides the present Natural Resource Damage Assessment process following oil spills (Johnson, 2011).

2.3 BRIEF SUMMARY OF GULF OF MEXICO MARINE ECOSYSTEMS

The Gulf of Mexico basin is effectively a bowl with the southeastern lip of that bowl notched to allow water and material exchange with the Atlantic Ocean. An extensive shallow continental shelf (a third of the overall Gulf) encircles most the perimeter. The northern, western, and southern terrigenous shelves are comparatively restricted with the expansive Floridian and Yucatan shelves of carbonate origin (Rezak and Edwards, 1972). Approximately 40% is continual slope (200–3,000 m), and the remaining quarter is abyssal plain (>3,750 m) with the deepest region (>3,750 m; Pequegnat, 1983) occurring within the Sigsbee Deep. Subtropical and tropical climates and oceanic regimes dominate with physical processes strongly structuring the nearshore, shallow-water communities. This includes significant riverine inputs from 33 major rivers spanning five countries (the United States, Canada, Mexico, Guatemala, and Cuba; Fautin et al., 2010). More than two-thirds of the continental United States drains into the Gulf with the Mississippi River dominating drainage into the north. The Grijalva–Usumacinta River System dominates hydrological inputs into the south. Two hundred and seven estuaries and lagoons are found along the Gulf coastline (Fautin et al., 2010). Northern Gulf shallow waters are warm temperate (Carolinian Province), and south reaches are tropical; Caribbean Province (Briggs, 1974).

Oyster reefs and salt marshes dominate low-salinity estuaries in the northern Gulf with seagrass beds more common in clearer, more saline bays. Notably, seagrass beds, a system of particular importance and concern, have shown rapid and widespread declines in extent (12–66%) in recent years across the entirety of the northern Gulf of Mexico (U.S. Geological Survey, 2000). In the southern Gulf, mangroves dominate bays and lagoons with oyster reefs, salt marshes, and seagrass beds distributed similarly as in the northern Gulf. In the western Gulf, the Laguna Madre of Texas and Tamaulipas is a noted example of a hypersaline lagoon (Tunnell and Judd, 2001), where salinity historically ranged between 51 and 295 ppt, although the dredging of the Gulf Intracoastal Waterway in Texas (late 1940s), barrier island passes, and inlets in Texas and Mexico have moderated that salinity swing to roughly 40 ppt. This highly productive lagoon has extensive wind–tidal flats and shallow seagrass beds in a semiarid region. Offshore, coral reefs are common in the Florida Keys, Cuba, and the southern Gulf off the Mexican state of Veracruz and on the Campeche Bank (Tunnell et al., 2007). Other hard-bottom topographic relief is sporadic on the normally smooth, homogeneous soft substratum of the continental shelves (Hu et al., 2011; Rezak and Edwards, 1972; Rezak et al., 1983, 1985). Unique, recently discovered, and quite diverse habitats in deeper Gulf waters include

chemosynthetic communities and communities of deepwater corals (*Lophelia* reefs; Brooks et al., 2008; Cordes et al., 2008; CSA International, 2007). One of the Gulf's most unique communities is floating *Sargassum* (a Fucalid alga) aggregates. These highly productive stocks of floating *Sargassum* populate the northern Gulf of Mexico, affording ubiquitous nursery habitat for a wide array of larval and juvenile vertebrates and invertebrates in the Gulf (Hoffmayer et al., 2005; Wells and Rooker, 2009) and in turn inoculating northern Atlantic *Sargassum* stocks with approximately 1 million tons of *Sargassum* each year (Gower and King, 2011).

Gulf fisheries are some of the most productive in the world. Important commercial stocks include shrimp (white, pink, and brown), crab (blue, Gulf stone, and stone), oyster, snapper (mutton, grey, red, dog, lane, and yellowtail), grouper (goliath, red, gag, and yellowfin), amberjack (lesser and greater), tuna (yellowfin and bluefin), and billfish (blue marlin and sailfish (Gulf of Mexico Sea Grant Programs, 2010)). In 2010, the commercial fish and shellfish harvest from the five U.S. Gulf states was 583,166 metric tons, 15.6% of the total domestic landings in the overall United States that year (NMFS Fisheries Statistics Division, 2011). Commercial catches in the Gulf comprised 15% of the total U.S. domestic commercial fishing revenue, valued at $639 million (NMFS Fisheries Statistics Division, 2011). The Gulf also supports a productive and economically valuable recreational fishery, principally targeting spotted sea trout, red drum, sand sea trout, Atlantic croaker, and Spanish mackerel in nearshore waters and red grouper, red snapper, white grunt, gag, and yellowtail snapper further offshore. Excluding Texas (which does not report such data), the U.S. Gulf states accounted for 38.6% (34,478 metric tons) of the U.S. recreational landings in 2010 (Lowther, 2011).

2.4 BRIEF DEEPWATER HORIZON OIL SPILL OVERVIEW

2.4.1 Before the Deepwater Horizon: An Overview of Offshore Petroleum Extraction

Global offshore oil production began more than a century ago as intrepid drillers extended piers out over the waters of the Santa Barbara coast in California to capture extremely shallow subtidal reservoirs. Oceanic drilling expanded across the globe in the ensuing decades, reaching about 14% of world oil supply in 1974 and about one-third today (Austin et al., 2004). By the mid-1990s, worldwide natural gas production had risen to around 228 billion cubic feet per day, 20–25% of this total accounted for by offshore gas (Bureau of Ocean Energy Management 2010).

An estimated $0.2–1.1 \times 10^8\,m^3$ of petroleum and $4.4–22.3 \times 10^{10}\,m^3$ of natural gas are believed to be present beneath the seafloor in the northern Gulf (Darnell and Defenbaugh, 1990; Defenbaugh, 1990). According to the Bureau of Ocean Energy Management, Regulation and Enforcement (then known as Minerals Management Service), offshore operations in the Gulf produce a quarter of the U.S. domestic natural gas and one-eighth of its oil. In addition, the offshore petroleum industry

employs over 55,000 U.S. workers in the Gulf (Minerals Management Service, 2002). In Mexico, the Secretariat of Energy (Secretaria de Energia—SENER) estimated that the daily crude oil and natural gas production from Gulf of Mexico offshore operations in the years 2000–2005 ranged from 365,000 to 451,000 m^3 and 41.4 to 44.8 million m^3, respectively (Secretaria de Energia, 2008).

Wells now cover the majority of nearshore, shallow-water lease regions of the continental shelf. By 2011, then-named Bureau of Ocean Energy Management, Regulation and Enforcement recognized 24,486 "permanently" abandoned, 3953 "temporarily" abandoned, and more 4,000 active offshore wells (Bureau of Ocean Energy Management, Regulation and Enforcement, 2011; Skytruth, 2011). Beginning in the mid-1990s, this drove an ever-increasing proportion of new wells into ever-deeper waters. Deepwater drilling and ultra-deepwater drilling are now the focus of current and future production plans (Nixon et al., 2009). Into this mix, the Marshall Islands-flagged mobile, semisubmersible ultra-deepwater drilling platforms DWH and *Deepwater Nautilus* were constructed in 2001 for R&B Falcon (since purchased by Transocean) to meet the demand for drilling in such extremely difficult to get to depths in the Gulf of Mexico. The equipment and logistics of such deepwater drilling make production of oil from such depths two to three times more expensive than more traditional, shallow-water efforts (Rigzone, 2012). As these margins have tightened, we have seen an increasing emphasis on minimizing costs and tightening project management to maintain profitability.

2.4.2 2010 Deepwater Horizon Spill

On April 20, 2010, the ultra-deepwater ocean drilling rig DWH 76 km southeast of the Louisiana coastline experienced a catastrophic wellhead failure, explosion, and fire while drilling an exploratory well (Deepwater Horizon Study Group, 2011). Eleven rig operators were killed outright, with the entire rig subsequently lost on April 22, coming to rest on the seafloor some 400 m from the wellhead (Robertson and Robbins, 2010). Shortly after the rig sank, the U.S. Coast Guard formally announced the leaking of oil from the broken riser pipe on the seafloor (Resnick-Ault and Klimasinska, 2010), 1,544 m below the surface of the Gulf of Mexico. Additional leaks from kinks in the now-broken pipe were observed over the next several days by a suite of remotely operated vehicles (Staff, 2010).

The extreme depth, lax safety protocols (Lustgarten, 2010b), and poor pre spill contingency planning (CBS/Associated Press, 2010) have combined (Graham et al., 2011) to create a situation in which the oil spilled freely for 84 days (although the formal recognition of the complete cessation of the flow came with the static condition declaration on day 87; National Oil Spill Commission, 2011). The inability of industry and government managers to quickly stanch the flow motivated an unprecedented use of dispersants at depth and across the region. Large-scale aerial application of dispersants from heavy lift aerial tankers began on May 1 (AFP Staff, 2010). Three small-scale *in situ* efficacy trials at the wellhead itself followed and paved the way for the large-scale and continuous use of direct injection of dispersant

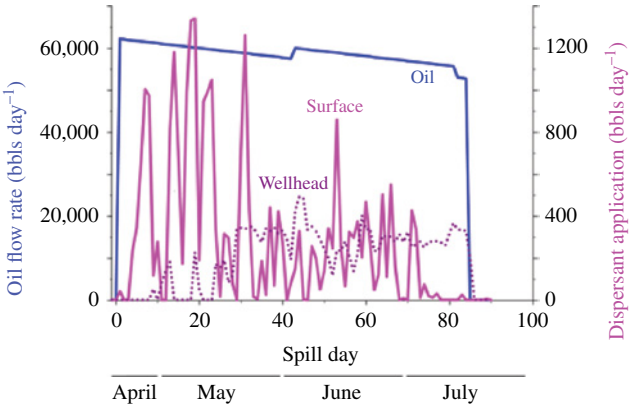

FIGURE 2.1 DWH Macondo blowout daily hydrocarbon release and applied aerial and subsurface dispersant application rates from April to July 2010. This data was used to parameterize the much-discussed Oil Budget Calculator (Oil Budget Calculator Science and Engineering Team, 2010). Daily dispersant application data were compiled from the National Incident Command by USGS and kindly provided by the S. Bristol and the USGS. Records do not clearly distinguish between Corexit 9,500A and 9,527A, and so dispersant data here are combined. Oil release rates decline overtime in responses to lessening pressures inside the Macondo formation. Changes in oil flow correspond to the following: day 1 riser falling to the seabed, day 43 riser cut to facilitate recovery efforts boosting flow by approximately 4%, and day 82 stacking cap installed. All hydrocarbon flow into the Gulf ceased on day 84, but a static condition was not declared until day 87. Subsurface dispersant application near the wellhead began on day 9 and then was stopped until day 14 but still not continuously applied until day 25.

into the oil plume at depth proximate to the riser break beginning on May 14 (Environmental Protection Agency, 2010).

Ultimately, an estimated 780,000 m^3 of hydrocarbon (FRTG; McNutt et al., 2011) flowed into the Gulf (42.8–41% of which were methane and related natural gases; Reddy et al., 2011), of which approximately 127,000 m^3 was recovered (Fig. 2.1; McNutt et al., 2011) Nearly 7,000 m^3 of dispersants, roughly one-third of the existing global supply by one estimate (Lustgarten, 2010a), was released into the northern Gulf of Mexico. The surface extent of the spill exceeded 50,000 km^2 and ranged from central Louisiana to the Florida Panhandle. Subsurface spill extent has been equivocal, but reports of heterogeneous subsea plumes extended as far as 142 km (Helguero, 2010) of often highly emulsified or fractionated, diffuse hydrocarbons (Valentine et al., 2012).

As of this writing, much remains unknown regarding the amount, character, fate, and ultimate impacts of the oil–dispersant–methane brew, but only a subset of these toxicants (i.e., methane and drilling mud) are likely to have been highly localized. Characterizing the ecotoxicological endpoints of this aggregation of toxicants is exceedingly difficult given the inadequate data collection/reporting early on (Wang, 2010a), lack of transparency (Wang, 2010b), and logistical difficulties inherent with a disaster of this magnitude. Nonhuman toxicological endpoints are often poorly characterized (Rand, 1995). Extrapolating such impacts to population and

community levels is made even more complicated in regions such as the northern Gulf of Mexico with poor or absent long-term, sentinel monitoring programs (Paine et al., 1996; Rabalais et al., 1993), a problem little changed from the days when Straughan and her colleagues grappled with this issue in the wake of the 1969 Santa Barbara blowout.

Most efforts to date have focused on documenting acute potential toxicity (e.g., EPA's air quality monitoring in the coastal zone, BP's dispersant toxicity trials). Initially, only the National Science Foundation (via their RAPID program; NSF, 2008) funded any work that began to look beyond immediate toxicity, with most of these funded projects being extensions or modifications of existing (nonspill-related) projects/capacities or descriptions of the abiotic characteristics of the spill. All early indicators suggested a lack of a broad-based overview of the potential ecotoxicological effects of the disaster (Peterson et al., 2012). Happily, most funders have now recognized the need to cast a wider net. More studies are being funded exploring the chronic nature of the spill and its impacts upon a broader range of organisms and communities, aspects that are necessary to fully understand this event.

2.5 EXISTING MARINE OIL SPILL PARADIGM

2.5.1 Old Oil Spill Scenario: The Vast Majority of Oil and Gas Rises to the Sea Surface and No Dispersants Are Used (for a Shallow-Water, Nearshore Spill)

The following is our effort to explicitly layout the spill paradigm that prevailed prior to the DWH blowout, derived from our experience with the processes resulting from shallow-water oil spills near the coast.

2.5.1.1 Offshore Systems

Oil would be expected to form large and thick mats, floating on the sea surface, and be transported via prevailing winds and surface currents. If the crude oil originated from a well blowout, it would be accompanied by release of natural gas, which would also surface readily and disperse into the atmosphere. While at sea, the floating oil would rapidly lose lighter volatile components into the atmosphere. Organisms such as turtles, marine mammals, and seabirds that necessarily make regular and prolonged use of the sea surface run the highest risks of mortality as they come to the surface to breathe or forage and encounter this accumulating crude. Volatile hydrocarbons pose a threat to marine mammals and sea turtles that must breathe in these highly toxic compounds right at the sea surface where concentrations are highest, running risks of death from brain and lung lesions. Direct contact with the fur of marine mammals presents a high risk of ingestion through preening and loss of thermal regulatory capacity, especially for sea otters, which can lead to death. Whales and dolphins are not much impacted by surface contact with oil (Geraci and St. Aubin, 1988), although breathing through dorsally located blowholes can lead to inadvertent uptake of oil into their lungs. The highest inhalation risk of volatile PAHs is close to the spill

source as PAHs dissipate fairly soon after reaching the surface. Sea turtles also run a risk of ingestion of surface oil and consequent mortality from toxic hydrocarbons. Seabirds that float on the sea surface, like those that are rafting, or conduct surface dives to forage for prey, such as grebes and cormorants, run the highest risk of contact with floating oil because they spend more time on the sea surface than seabirds that make aerial dives, such as pelicans (*Pelecanus* spp.), gannets (*Morus* spp.), and gulls (Laridae). For both groups, oiling of feathers leads to ingestion by preening and disables the thermoregulatory function of the feathers, even interfering with flight. High mortality of seabirds is expected when crude oil floats on the sea surface in productive coastal waters. In addition to direct mortality from oil exposure, survivors among these exposed vertebrates likely suffer loss of fitness through behavioral abnormalities and loss of reproductive capacity.

The sea surface is also a biologically significant physical boundary between the atmosphere and water that facilitates many other processes critical to living resources and is consequently occupied by many organisms at risk to floating oil. Along the Gulf and southeast Atlantic coasts, floating *Sargassum* provides structural habitat, sustaining associated communities of coevolved invertebrates and fishes, as well as transient life stages of newly hatched sea turtles, and eggs, postlarvae, and juvenile pelagic fishes, many of which (e.g., billfishes) valuable fishing targets of. *Sargassum* and surfaced oil are transported by the same forces of winds and surface water circulation, thereby leading to almost certain comingling after any oil release in a coastal or open ocean region with floating *Sargassum*. The associated organisms have high probability of encounter with released oil, which can cause direct mortality from toxic ingestion and from physical smothering and indirect impacts through sublethal effects that influence fitness. Many adult vertebrate organisms at higher trophic levels, such as great sharks, petrels, and other pelagic seabirds, are attracted to feed on *Sargassum*-associated prey, thereby exposing them too to oil and to lethal and sublethal injuries.

Even away from any floating biogenic habitat, the sea surface is a critical physical interface between media that is disproportionately biologically active and rich. Many eggs, larvae, and postlarvae of fish and crustaceans (notably including the commercially important blue crabs, *Callinectes sapidus*) occupy the sea surface seasonally, where risk of oil exposure and mortality from acute toxicity (especially for fish and crustacean eggs), smothering, and subsequent developmental abnormalities is high. Notably, the Gulf of Mexico is also the breeding grounds (where eggs, larvae, and postlarvae develop at or near the sea surface) for the western Atlantic stock of the fabled, valuable, and threatened bluefin tuna (*Thunnus thynnus*). Flying fish (Exocoetidae) are also at high risk because of their unique behavior that allows them to use both fluid media, air and water, at the sea surface.

The more prosaic but vital base of the ocean's food chain is dependent on the near-surface layer of the sea from a few centimeters to around 30 m. Light penetration is progressively limited by water depth, and thus, primary production of the phytoplankton and other photonivores is necessarily reduced by floating oil that shades the sea below. The zooplankton that connect the primary producers to higher trophic levels suffer from locally suppressed food supply and are composed largely of

crustaceans, a taxon that is generally sensitive to hydrocarbon pollutants. Jellyfish, especially the purple float-equipped and surface-restricted Portuguese man o' war (*Physalia physalis*), similarly tend towards preferential occupation of the surface ocean, where oil exposure risk is high and where oil-induced suppression of forage items can induce sublethal impacts of reduced growth and reproductive capacity. Higher-level consumers (predatory fish, crustaceans) in this shallow near-surface layer run the risks of ingestion of oil-contaminated prey with sublethal impacts on growth and reproduction, which may ultimately progress to population-level impacts. In the coastal ocean, densely schooling planktivorous fishes, such as menhaden (*Brevoortia patronus*), anchovies (Engraulidae), silversides (Atherinopsidae), and threadfin herring (*Opisthonema oglinum*) in the Gulf of Mexico, face a high risk of population decline from a variety of mechanisms including reduced food supply, egg mortality and larval developmental abnormalities, high dissolved oxygen sensitivity (because of their comparative hyperactivity to oxygen depletion from high microbial demands during biologically mediated oil degradation in waters already stressed by eutrophication), and potentially enhanced induction of disease outbreaks.

Suppressing primary production and breaking the food chain by disabling and killing the necessary zooplankton link to higher trophic levels lead to propagating loss of production throughout the entire water column and down to the seafloor, overwhelmingly dependent on the thin photic zone skin of the sea for sustenance. Consequently, most impacts on the pelagic ecosystem below about 30 m in depth and on the benthic seafloor communities would be connected to reduced primary production in the surface layer and reduced transport of zooplankton fecal pellets to depth, the major vehicle of movement of surface organic production to the deeper ocean. What is transported from the ocean under a surface layer of floating oil will carry oil contamination to the deep sea and seafloor, but perhaps not in amounts that threaten to induce population-level impacts on the animals of this deeper water column or benthos. Little or no impact would be expected in fishes and crustaceans of the deeper ocean. Offshore hard-bottom communities of corals and associated fauna, cold-water seep communities, and the most widespread soft-sediment benthos should persist essentially unaltered under this scenario. A slight increase in microbial activity associated with organic carbon in the petroleum may balance the loss of organic rain of zooplankton feces (i.e., marine snow), distinguishing biogeochemical sources made possible only through functional molecular approaches.

2.5.1.2 Onshore Systems

Floating crude oil released near the coast has a high probability of being transported to shore (e.g., Wolfe et al., 1994) where it can ground and have substantial negative impacts on valuable and sensitive habitats, important organisms, and human uses. In addition, the potential for lingering oil and malingering impacts over long periods of time, exceeding decades, is greater in shoreline systems (Boufadel et al., 2010; Culbertson et al., 2007, 2008; Short et al., 2003). The toxicity of the oil that ultimately grounds on and in shoreline communities will decline as time at sea increases (although some compounds such as PAHs may persist for decades, inducing important, often sublethal impacts to exposed organisms), but many of the environmental

and ecological impacts of grounded oil occur via smothering processes unrelated to the toxicity. Consequently, grounding of oil along shorelines poses the most serious set of concerns associated with a near-coast crude oil release (such as we have seen with the *Exxon Valdez* spill). Under this scenario of floating oil discharged near shore without treatment by dispersants, the risk of shoreline grounding and injury is greater than for all other communities/regions.

The first shoreline habitat likely to be encountered by floating crude oil as it moves onto shore is the relatively high-energy coast: bedrock and boulder–cobble beaches in higher latitudes such as Alaska or sandy beaches along the Gulf and south and mid-Atlantic coasts. Oil spill injury assessments are rarely conducted on high-energy ocean beaches, in part out of a tradition of ignoring them; in part out of recognition of the dynamics of substantial transport of sediments, which disperses and buries oil, complicating Natural Resource Damage Assessments by also dispersing the impacts; and in part out of poor appreciation of the ecosystem services provided by sandy ocean beaches. Warm-temperate ocean sandy beaches are characterized by an astoundingly high diversity of small invertebrates, the so-called meiofauna living among interstitial spaces between the sand grains. Deposition of crude oil on the surface of the low intertidal and swash zones has high potential to clog flows of water, which would otherwise irrigate these interstitial spaces, oxygenate the habitat, and feed many of the meiofaunal invertebrates. Wave action transports water up onto the beach, and much of it percolates as subsurface flow through the sand grains. The impacts of this diverse assemblage of flatworms (Platyhelminthes), nematodes (Nematoda), tardigrades (Tardigrada), and other phyla are largely unstudied but predictably serious where oil has been deposited. The recovery of abundances of the meiofauna of sandy ocean beaches is likely to appear to occur rapidly because of high-energy transport of sediments and organisms replenishing an oiled beach, but such a recovery could be illusory and reflect dispersion of the impact over a much broader area, making its detection and quantification difficult.

The macrofaunal invertebrates of these ocean beaches include bean clams (*Donax*) and mole crabs (*Emerita*), which are highly productive because of the energy subsidy of breaking waves that sustain surf-zone diatom blooms and transport these microalgal foods to these dominant suspension feeders. Dense assemblages of bean clams and crabs feed shorebirds such as sandpipers (*Calidris* spp.) and willets (*Tringa semipalmata*), crabs, and demersal surf fishes, such as pompano (*Trachinotus* spp.), Gulf kingfish (*Menticirrhus littoralis*), and red drum (*Sciaenops ocellatus*). Oiling of intertidal beaches is likely to interfere with the ability of vertically migrating invertebrates such as mole crabs and bean clams, which conduct continuous vertical migrations up and down the shore face tracking each rising and falling tide. Feeding appendages of the mole crab and other suspension feeders are finely articulated and susceptible to fouling by oil, incapacitating feeding. Impacted invertebrates may exhibit acute narcosis when directly exposed to unweathered crude oil. Such macrofaunal invertebrates will be widely affected by even a narrow band of beached oil as they migrate across the entirety of the intertidal with each tide. Mole crabs and bean clams can require a year or more to recover following routine beach nourishment, although an oiled beach in a truly high-energy environment with high longshore

transport of sediments may appear to recover by infaunal emigration from unaffected areas and dispersing the negative impact. Shorebird feeding on ocean beaches where mole crabs and bean clams were depleted by beach nourishment demonstrated substantial reduction that lasted as long as the prey abundance remained depressed (Peterson et al., 2006), demonstrating a functional linkage to an important ecosystem service of the sandy ocean beach and one likely to apply to the surf fishes as well, which consume similar prey.

Oil deposition on ocean beaches occurs most readily at the tide lines where other floating objects also come to rest as the water level falls. Much of the oil is transported with the tides, becoming remobilized so that beaches become reoiled readily and the presence of oil on an ocean beach at any given low tide does not reveal the full extent of beach exposure. This complicates any quantitative damage assessment. Furthermore, because of substantial sediment transport on ocean beaches, oil lenses can be created that extend to depth in the intertidal sediments by its seepage into the sediments and by its burial by newly deposited sediments. Reexposure of this oil will occur when erosion of the overlying sediments occurs, further expanding the spatial scope of exposure and impact. Because smothering and fouling of suspension-feeding apparatus is the dominant mechanism of ocean beach macrofaunal injury, even weathered oil can continue to cause natural resource damages. The oil that is deposited at the drift line on ocean beaches is commingled with any algal or vascular plant wrack also deposited. Wrack helps feed shorebirds by providing the habitat and food source for insects and small crustaceans, which serve to feed some shorebirds, especially plovers (Charadriinae)—a group with many threatened and endangered species. These wrack-associated arthropods are likely to suffer acute mortality and also become fouled by the oil. In addition, shorebirds accustomed to feeding along the wrack line will suffer high risk of contact with the beached oil. This process leads to fouling of feathers and subsequent direct ingestion through preening. Furthermore, oil is transported by externally fouled feathers and legs back to nests with incubating eggs, a life stage that is very vulnerable to mortality by oil, which passes readily through the lipophilic egg membrane (Bowman et al., 1995). If oil remains deposited on the beach surface when sea turtle (Chelonioidea) hatchlings are emerging from their nests, they risk exposure and potential mortality from the fouling and perhaps via ingestion of toxic hydrocarbons. Oil on the beach surface also endangers the iconic ghost crab (*Ocypode* spp.), a proposed indicator of sandy beach health: it is nocturnal and emerges from its burrows high on shore, especially in the dunes, and moves to the swash zone to prey on mole crabs, bean clams, and sea turtle hatchlings during their rush to the sea. The drift lines on beaches also tend to receive deposited tar balls of varying sizes. Tar balls or "cookies" are usually composed of weathered oil with reduced residual toxicity. These generally pose more risk to human uses than to wildlife and so usually compel removal, which if done by mechanical methods can have significant ecological impacts from the physical disturbance (i.e., direct killing and maiming of soft-bodied benthic invertebrates).

Mud and sand flats on low-energy shorelines on the backsides of coastal barriers and on the shores of estuaries, bayous, bays, and coastal lagoons are subject to direct oiling in intertidal areas as waters recede and leave behind the bands of crude oil

(e.g., Elmgren et al., 1983). This process can smother resident benthic invertebrates like amphipods, polychaete worms, bivalve mollusks, and other taxa. Bivalves can survive several days of oxygen depletion under the cover of oil by closing up their shells. As on the ocean sandy beaches, intertidal flats experience oil deposition, remobilization, and reoiling, and so (dependent on the duration of oil cover) bivalves may survive initial oiling. Suspension-feeding bivalves that do survive take up PAHs and heavy metals. In addition to the associated toxicity of this exposure, there markers can serve as an index of exposure of the locale in which they are found (e.g., California Academy of Sciences, 2012). Benthic invertebrates on tidal flats serve an important ecosystem service as a major conduit of energy flow between the high estuarine primary production and predatory crabs, fishes, and birds. The bivalves on these intertidal flats are largely buried beneath the sediments such that the shorebirds like oystercatchers (*Haematopus* spp.) that consume smaller bivalves, diving ducks like scoters (*Melanitta* spp.), and fishes like rays (Batoidea) can ingest oil during their foraging into the sediments and excavation of the buried bivalves. Such ingestion of toxic hydrocarbons provides a mechanism by which sublethal impacts on the vertebrate consumers (lower growth as energy is diverted to detoxification, reproductive impairment, etc.) can lead to population-level consequences. Oil that becomes buried in fine sediments can become sequestered where anoxic conditions inhibit chemical or biological degradation. This can lead to persistent contamination of the sediments and shells of bivalve prey, which may last for years after the oil spill and inhibit the recovery of injured bivalve predators. Soft-sediment amphipods are particularly sensitive to toxic fractions of petroleum hydrocarbons. In subtidal muddy and sandy bottoms, amphipod recovery from oil-induced population declines can be suppressed for decades (Dauvin and Gentil, 1990). The shallow subtidal portions of tidal sand and mud flats are also directly exposed to floating oil through suspension feeding and occasionally through direct deposition of oil and resultant suffocation when wind forcing or special astronomical conditions result in unusually low water levels. Shallow subtidal bivalves, even in the absence of such low water stands, serve to demonstrate this exposure to oil by accumulation of PAHs through their filtration of overlying waters containing low concentrations of the water-soluble fraction of petroleum (Law et al., 1997).

Another notable shoreline community of great value for its many ecosystem services is the oyster (*Crassostrea virginica*) reef (Grabowski and Peterson, 2007), which can be either intertidal or subtidal. Oyster reefs are biogenic structures made of calcium carbonate created by generations of oysters and rising above the soft sediments that dominate the sedimentary estuarine shores of the Gulf and south and mid-Atlantic coasts. Oysters and the reefs they form provide hard substratum, which is in turn occupied by a high diversity of benthic invertebrates (Wells, 1961); enhance water clarity through high rates of filtration; fertilize seagrass beds via biodeposition of feces and pseudofeces; help induce denitrification and thereby partially counteract eutrophication; and serve as feeding grounds for many valuable crustaceans like blue and stone crabs and fishes like red drum, black drum, and sea trout (Peterson et al., 2003a). Intertidal oysters can be smothered by mats of oil left behind as tides recede, but subtidal oysters are relatively resistant to petroleum toxicity and are rarely

smothered. As filter feeders, oysters do accumulate PAHs in proportion to exposure to oil and so can provide an index of biological exposure of the reef system. Oyster larvae are sensitive to toxins in oil, which forms the basis of a standard EPA bioassay (Chapman and Morgan, 1983). Oyster larvae develop in the water column for about 2 weeks, remaining in the estuarine waters so as to be near suitable habitat. So lingering oil in the estuary could suppress the new year class of oysters. Oyster reefs are occupied by several small crustaceans, which comprise important prey for reef-associated fishes (Lenihan et al., 2001). Crustaceans, especially the amphipods, are sensitive to the toxins in petroleum and likely to suffer extensive mortality from the presence of oil, thereby diminishing the value of the oyster reef as fish habitat. Blue crabs and stone crabs (Lenihan et al., 2001) are large reef-associated crustaceans that are likely sufficiently sensitive to oil pollution to exhibit significant adult and juvenile mortality on oiled reefs. Oysters have also been shown to exhibit reduced growth when exposed to oil, which means that their secondary production is lower, representing one form of natural resource injury even if no oyster mortality occurs. The importance of oyster reefs as foraging grounds for many valued fishes, such as red drum, raises concern about the possibility of transferring toxics through ingestion by fish of contaminated prey from oiled reefs, with potential population-level injuries to the fish by reducing fitness.

Seagrass beds (Hydrocharitaceae and Potamogetonaceae) represent another shoreline habitat of demonstrated and acknowledged importance as a nursery for many juvenile fishes and crustaceans, including groupers (Epinephelinae) and snappers (Lutjanidae) that as adults occupy offshore hard-bottom reefs and are seriously overexploited, and blue crabs, a recognized keystone predator of estuarine habitats and the basis of a valuable fishery. Benthic invertebrates are diverse, abundant, and productive in seagrass beds, providing the prey for juvenile fishes and predatory crabs. Seagrasses themselves are more susceptible to mortality from oiling than oysters. Intertidal seagrass probably suffers more mortality from oil than subtidal grass because of depth-dependent differences in exposure to oil. Even in the absence of seagrass mortality, many of the crustaceans, especially amphipods (e.g., Dauvin and Gentil, 1990), are typically killed by exposure to oil. If oil is incorporated into the sediments, the recovery of these amphipods and other crustaceans can require years. Juvenile blue crabs within the seagrass habitat can be killed by exposure to oil. In addition, gravid female blue crabs migrate to seagrass beds near the mouth of the estuary to gain some structural protection from predators while they wait for nocturnal spring high tides to release their eggs for transport to the coastal ocean for early life-history development. While carrying eggs, these adult females bury into the surface sediments. The high mortality of salmon eggs deposited in oiled sediments after the *Exxon Valdez* oil spill (Rice et al., 2001) raises the prospect that blue crab egg mortality may ensue from oiling of shallow sediments in seagrass beds and other estuarine environments. Consequently, multiple life stages of blue crabs (eggs while carried by adult females, larvae and postlarvae in the surface layer of the coastal ocean, juveniles in seagrass and oyster reef habitats, and adults in multiple habitats) suffer the risk of mortality with potentially catastrophic multiplicative consequences to the population. Large herbivores consume seagrasses, which

enhances their risk of contact with oil and of ingestion of oil, if the grass is oiled. Green sea turtles (*Chelonia mydas*), a federally threatened species; sea urchins (Echinoidea), which are extremely sensitive to petroleum exposure; and migratory Brant geese (*Branta bernicla*) are Gulf coast macroherbivores that specialize on consuming seagrass.

Coastal salt marshes arguably capture more attention than any other community/region after a crude oil spill that comes ashore. Well-defined and increasingly appreciated salt marsh ecosystem services include high productivity across all trophic levels, high capacity to filter out and/or uptake a wide array of pollutants (nutrients, pathogens, sediments, etc.), its role as structural habitat (for aquatic animals, birds, and mammals), protection of shorelines from erosion and shoreline development from storm damage, and sequestration of carbon (Millennium Ecosystem Assessment, 2005). Cordgrass (*Spartina alterniflora*) and other dominant salt marsh plants are susceptible to complete mortality of above- and belowground components from heavy oil cover, mortality and loss of aboveground components under moderate oiling, and shoot discoloration and suppressed production under less intense oiling. When both above- and belowground plant materials are killed, enhanced erosion of the marsh edge follows (Silliman et al., 2012). Even with the loss of only aboveground plant material, the marsh's capacity to trap sediments and thereby elevate the marsh surface enough to counteract at least some of the effects of subsidence and sea-level rise is lost until regrowth at similar plant density is achieved. Marsh area is directly related to penaeid shrimp and blue crab production along the Gulf coast. Various crustaceans such as penaeid and grass shrimps, fiddler crabs (*Uca*), foraging adult blue crabs, and amphipods make use of flooded salt marsh habitat and are sensitive to oil toxins. Not only can oiling result in direct acute mortality of these crustaceans, but oil that deposits on the marsh surface is not readily remobilized by succeeding high water stands because of the low-energy environment of salt marshes, the oil penetration into the sediments, and the oil's attachment to the sediments. This leads to persistence of sedimentary oiling of salt marsh soils for decades (Culbertson et al., 2007, 2008; Teal and Howarth, 1984). The oil from a spill in Barnstable Harbor marshes in Massachusetts has been shown to still suppress full primary production of *S. alterniflora* and to have chronic impacts on fiddler crab (*Uca pugnax*) fitness 40 years after the spill. The fiddler crabs do not dig their burrows (which aid *Spartina* in gas exchange) to depths below the oil layer in the sediments, and they exhibit suppressed behavioral reaction responses, probably reducing their ability to avoid predators (Culbertson et al., 2007, 2008). So, although the technological capacity for restoration of salt marshes exists, the exceptionally long duration of oil in the marsh sediments and of chronic impacts and the exceptionally valuable ecosystem services of coastal marshes lead to establishing prevention of oiling as a high priority in spill response. Additionally, it is important to note that many of the traditional oil cleanup/restoration techniques can compound and magnify oiling effects.

The higher trophic-level vertebrates that use salt marshes as habitat for foraging, breeding, or shelter also run a high risk of injury from oiling. Salt marshes possess a high number of endemic birds, reptiles, and mammals, many of which are federally or state listed as endangered, threatened, or of concern, and Gulf coast marshes are

home to more of these species than any other place on earth. Dense marsh-dwelling birds such as rails (Rallidae) and wetland obligate species such as mottled ducks (*Anas fulvigula*) restricted to salt marsh habitat are at the highest risk of meaningful losses that could threaten population persistence. These marsh endemics as well as wading birds like egrets and herons (Ardeidae), storks (Ciconiidae), cranes (Gruidae), and ibises (Threskiornithinae) are at high risk of exposure to oil during foraging and nesting, leading to oiled feathers, ingestion via preening, and mortality. Isolated marsh islands have special significance as relatively terrestrial predator-free nesting areas for ground-nesting seabirds, such as terns (Sternidae), gulls (Laridae), pelicans (*Pelecanus* sp.), and black skimmers (*Rynchops niger*). Encounter with oil by incubating adults can lead to oiling of eggs in the nest and their subsequent high mortality. Diamondback terrapins (*Malaclemys terrapin*), a turtle species of conservation concern, spend their complete life history in coastal marshes and are at high risk of mortality from oil encounters. Mammals such as muskrats (*Ondatra zibethicus*), nutria (*Myocastor coypus*), and river otters (*Lontra canadensis*) are marsh inhabitants that regularly move through the water surface, exposing their fur to high risk of oiling with the subsequent cascade of events leading to mortality akin to the impacts seen with sea otters (*Enhydra lutris*) along the Pacific coast of North America.

Mangrove habitats represent the tropical equivalent of temperate salt marshes. With global warming, mangroves have been spreading into the continental United States, and black mangroves (*Avicennia nitida*) are now established in the Gulf coast states of Louisiana and Florida. Mangroves serve the ecosystem through essentially the same suite of processes identified for coastal salt marshes, differing only in relative magnitude and significance. The Panama oil spill near Galeta in the Caribbean provides graphic evidence of the high risk of extensive mortality of mangroves to oiling and of the multiple-decade period of deforestation to be expected after the spill. Mangrove spills are directly analogous (and possibly more problematic for these longer-lived ecosystem engineer species) to the fate of oil in salt marsh sediments, as the anoxic fine-grained soils retain and bury the oil, preventing sunlight and oxygen from reaching it and thereby inhibiting photodegradation and microbially mediated detoxification of the crude oil (Jackson et al., 1989). Mangroves probably provide more storm wave and high wind protection to upland development than salt marshes because of their taller and sturdier stature as trees. They also provide natural hard-substrate habitat beyond what the salt marsh grasses provide because of the extensive prop roots, which are colonized by a high diversity of benthic invertebrates. Like coastal marshes, crustaceans of mangroves are abundant, are ecologically important, and serve as targets of human exploitation. Many fishes use mangroves as a nursery, including several that are characteristic of coral reefs and other hard-bottom habitat offshore as adults. Birds associated with mangroves include overlap with those of salt marshes, such as the wading birds, but mangroves also support more terrestrial insectivorous birds associated with insect prey feeding on mangrove leaves. Mangroves support a similar mammal community to that found in salt marshes, including muskrats and nutria, although worldwide mangroves are home to tigers, monkeys, and other mammals typically considered terrestrial. The loss of mangrove habitat through plant mortality after oiling implies the loss for support for

these associated animals at least on the scale of the loss of mangrove habitat area if not more for species that survive through important connectivity with other habitats. Like coastal marshes, mangrove communities warrant protection from spilled oil because of the potential scope of plant mortality, the duration of injury, and their high habitat value as a key ecosystem service provider.

The final coastal shoreline community that deserves explicit consideration in this general scenario of oil spill impacts is the shallow-water column along quiescent shores formed by one of these aforementioned communities. This water contains the phytoplankton that feeds suspension-feeding invertebrates, zooplankton, and many small forage fishes, especially at low tide when most fish must retreat from intertidal habitats they occupy during periods of inundation. The planktivorous forage fishes of the shallow-water column include menhaden (*B. patronus*), a species that forms the basis of an important fishery and also serves as prey for fishes on higher trophic levels. Larger fish feed in and transit through these protected nearshore waters, especially at night, including red drum (*S. ocellatus*), speckled trout (*Cynoscion nebulosus*), flounders (*Paralichthys* spp.), and bonnethead sharks (*Sphyrna tiburo*) eating blue crabs as they exit the marsh and bull sharks (*Carcharhinus leucas*) consuming fish. Many terns (Sternidae), pelicans (*Pelecanus* spp.), gulls (Laridae), overwintering diving ducks (Aythyinae), cormorants (*Phalacrocorax* spp.), and loons (*Gavia* spp.) are found in these shallow nearshore waters. Ospreys (*Pandion haliaetus*) and bald eagles (*Haliaeetus leucocephalus*) conduct aerial dives to capture and prey upon large fish in these quiescent nearshore waters. One highly specialized water bird, the black skimmer, runs especially high risk of encounter with floating oil and consequent injury including death because of its unique habit of foraging by skimming the water surface with its lower mandible, collecting small bait fishes and zooplankton right where the floating oil is found. These shallow waters harbor seasonally high populations of demersal fishes, like many drums (Sciaenidae), pinfish (*Lagodon rhomboides*), and flounders (*Paralichthys* spp.), and of demersal crabs. Such organisms run some risk of encounter with floating oil but far higher risk if that oil becomes dispersed into the water column by violent storm winds and waves (Giarrusso et al., 2001). These shallow coastal waters extending out to some distance off the coast and into the ocean are typically intensely trawled for shrimp and also some demersal fishes during open fishing seasons.

One indirect effect of an oil spill is closure of fisheries for a substantial period of time, approaching or equaling the entire fishing season, so as to avoid harvest and marketing of tainted product and to avoid depressing the demand for other fish products captured far away from any possible contact with the oil contamination. The consequences of such a closure of bottom trawling on the Gulf and south Atlantic coasts are likely to prevent the seasonally intense mortality of the targeted shrimp and demersal fishes as well as of those species captured and widely killed as inadvertent bycatch (Upton, 2011). In addition, the closing of bottom trawling prevents the extensive bottom disturbance associated with passage of the weighted net, trawl doors, and tickler chain along the seafloor, which likely resets succession of soft-sediment benthic communities to an earlier pioneer stage, with potential consequences for those organisms that prey upon the benthic invertebrates (Enticknap, 2002). The

indirect effects of releasing the coastal ecosystem from impacts of bottom trawling may provide one of the largest ecological impact signals arising from an oil spill.

2.6 A NEW CONCEPTUAL MODEL FOR DEEPWATER MARINE OIL SPILLS

We propose a new conceptual model for the fate, transport, and exposure pathways for ecological effects of a marine oil spill that unifies our previous understanding of historic spills with the still-unfolding understanding of the DWH oil spill across the Gulf of Mexico.

In stark contrast to our previous experience outlined previously, the DWH blowout occurred in deep offshore waters, where the turbulent discharge of hot, pressurized oil and gas entrained cold seawater, producing a variety of dispersed phases including small oil droplets, gas bubbles, oil–gas emulsions, and gas hydrates. The collective buoyancy of the oil and gas created a rising plume, but unlike a continuous-phase (e.g., sewage) plume, much of the oil and gas separated from the entrained seawater as it became trapped by stratification and deflected by ambient currents (Socolofsky et al., 2011). Such oil behavior should have been anticipated from prescient field (Johansen et al., 2003) and laboratory (Socolofsky and Adams, 2002) experiments, yet the occurrence of a deepwater spill of this magnitude and with these characteristics is unprecedented and clearly warrants a new oil spill paradigm (we contract this model with the previous model in Fig. 2). Although some DWH oil did rise to the sea surface and became weathered during ascent, much of the hydrocarbon release was retained in passive intrusions at depths of 800–1,200 m (Camilli et al., 2010; Joye et al., 2011; Valentine et al., 2010), stimulating heterotrophic microbial activity (Kessler et al., 2011; Valentine et al., 2010) and to some unknown degree entering and exposing deep-sea food chains through pelagic primary consumers (as was exhibited by petroleum carbon from DWH oil being incorporated into nearshore mesozooplankton; Graham et al., 2010). Agglomeration of oil particles and marine snow, mediated by adhesive bacterial exudates, triggered oil transport to the seafloor, where deposition of PAH-enriched particulates is associated with mortality of soft- and hard-bottom invertebrates (Hazen et al., 2010; White et al., 2012).

Our existing scientific model of environmental and ecological impacts of oil spills outlined previously was based upon an entirely different scenario of shallow-water spills with a shorter, more discrete discharge (e.g., NRC, 1985, 2003). Because of the extensive body of process-oriented scientific research done on the ecosystem consequences of the *Exxon Valdez* oil spill (e.g., Peterson et al., 2003b; Rice et al., 1996; Wells et al., 1995) and the wide publicity that impacts of this Gulf of Alaska spill have received, most thought turned immediately to that oil spill for predictions of impact of the DWH release. A much more applicable model might have been provided by the *Ixtoc I* well blowout in the southern Gulf of Mexico (discussed previously), which also occurred in nonsurface (albeit shallow) water over a 10-month duration had lessons learned not been hampered by the limited formal scientific study conducted on spill impacts. *Ixtoc I* therefore squandered an opportunity to

kick-start an alternative, more appropriate model. Unlike the process of oiling of the environment and exposure of organisms in the *Torrey Canyon*, *Exxon Valdez*, and previous spills, the oil released from the DWH (i) was discharged from the wellhead with extremely high turbulent energy that entrained cold deep-sea water into forming emulsions of oil and seawater; (ii) was subjected to high pressure that affected its buoyancy and dissolved the methane gas simultaneously released, naturally preventing a substantial fraction of the oil and the large majority of the methane from surfacing; and (iii) continued to be released in very large amounts for months rather than only for days, thereby providing potential for some organisms to experience repeated exposures to relatively unweathered as well as weathered crude oil (Valentine et al., 2012).

Spill response decisions subsequently introduced other factors that had potential to modify the mechanisms of oil impact even further away from the already largely inapplicable *Exxon Valdez* model of a shallow-water spill. Specifically, dispersants were spread by aircraft on visibly concentrated surface patches of oil and then later also introduced directly at the wellhead on the seafloor in large quantities. The dispersants used have some levels of inherent toxicity that posed a risk to some organisms (e.g., EPA, 2010; Southward and Southward, 1978) and potentially greatly increased exposure to organisms in some locations (deep sea, midwater). The intent of these dispersant applications was to disperse the oil into smaller droplets and thereby speed up its degradation and, for bottom injection, also to limit the amount of oil rising to the surface to form surface flows potentially injurious to sea surface organisms and damaging to shoreline habitats (NRC, 2003; Peterson, 2001). Greater dispersion of oil has the effect of greatly enhancing biological exposures, probably with lethal consequences to many particle feeders. Consequently, the DWH oil release demands the development of new scenarios of ecosystem impact to guide research on ecosystem impacts to insure that relevant processes of potentially damaging ecological impacts do not go unexplored. Out of sight cannot also become out of mind if we are to know the consequences of the oil release and the response decisions so as to assess the full ecosystem injury and guide future responses to the next deepwater blowout. We therefore propose a new model for deep-sea oil spills.

2.7 NEW SPILL SCENARIO: OIL IS RELEASED AT SIGNIFICANT DEPTH FROM A HOT, PRESSURIZED RESERVOIR

The intense turbulence of the wellhead release when combined with high pressure produces naturally high atomization of the oil and enhances the capacity of the dispersant, resulting in the production of very small bubbles of gas and droplets of oil that lack positive buoyancy and remain at depth in the sea. Much of this oil remains demersal near the seafloor, while some rises to mid-depths: all submerged oil is then transported with the three-dimensional circulation of the deep sea. By dispersing the oil into such small droplets, their greater proportional surface area enhances simultaneous access of oil-degrading microbes to the oil and to oxygen, producing relatively

high rates of degradation and soon a massive series of microbial blooms that consume and transform the hydrocarbons in this accumulating subsurface plume. However, this dramatic dispersion also greatly enhances biological exposures, especially of particle feeders, which consume particles in the same size classes as the small oil droplets. The oil droplets in the midwater zones gradually experience increased mass and lower buoyancy through aggregation of particulates on the proportionately large surface area, leading to sinking towards the bottom and increased concentrations of oil and dispersant over time near the seafloor and increased deposition onto the seafloor. Dramatically, less oil reaches the ocean's surface under this scenario, with or without dispersant injection at the wellhead, and thus, the suite of environmental and ecological consequences of oil that reaches the sea surface is reduced independent of the use of dispersants, although dispersants will likely still contribute to keeping more crude at depth (but the exact magnitude of that is likely to be dependent upon local conditions). Nevertheless, the costs of this response action are those associated with the introduction of an additional toxicant, the dispersant, and the production and deepwater retention of small oil droplets of a size available to various deep-sea habitats and organisms.

The effects of a deep, pressurized release of oil upon the ecology of the offshore ocean surface and nearshore surface waters are all reduced in proportion to the amount of oil that "fails" to reach the sea surface because of its dispersal, buoyancy, and resultant retention at depth. As a consequence of the large quantity of dispersants injected into the gushing DWH wellhead, the negative effects of floating oil on the sea surface to seabirds, floating *Sargassum*, sea turtles, phytoplankton, fish and crustacean eggs, larvae, and postlarvae, and surface processes are likely all greatly diminished relative to the previous model expectations. Similarly, the impacts of released oil from a deepwater source to near-surface waters are also reduced in proportion to the amount of oil retained at depth. By retaining oil at depth, wellhead injection of dispersants can avoid some of the negative effects of surface dispersant application upon organisms in the surface and near-surface water column (presumably proportional to the reduction of oil treated by surface-applied dispersants). The midwater habitat suffers prolonged exposures to emulsions of oil, seawater, and dispersant mixes wherever the released and dispersed oil stops rising and remains at depth. Deepwater Horizon observations and modeling (Helguero, 2010; MBARI, 2010; Socolofsky and Adams, 2002; Valentine et al., 2012) suggest slight differences in water density create at least partial bounding surfaces for dispersed hydrocarbons (albeit within a dynamic, three-dimensional state space), with much of the midwater plume being retained within these water masses. Similar behavior is observed for some gelatinous zooplankton (Pagès et al., 2001; Sabatès et al., 1989). This may prove to be an at-depth, three-dimensional analog of the *Sargassum* mats and surface oil entanglement. While the midwater hydrocarbon plume persists, we predict that many plankton and possibly even some nekton organisms could suffer high exposures including scyphomedusae, ctenophores, chaetognaths, and cephalopods. In addition, organisms that feed with filtering appendages or mucosal webs will also likely be strongly affected. These doubly impacted pelagic groups include pteropods, siphonophores, salps, and larvaceans.

Major concerns about increased ecological consequences of wellhead dispersant injection involve the deepwater benthic communities and the benthopelagic system above the deep-sea floor. Our historic model would predict virtually no toxic deposition of oil onto the seafloor, yet the DWH blowout induced widespread oiling of the seafloor and consequent mortality of benthic organisms on hard and soft bottoms. A significant fraction of dispersed oil in fine droplets combined with the toxic dispersant remains close to and eventually deposits onto the seafloor after release and/or dispersant mixing at depth. Some subset of dispersed hydrocarbons apparently interact with extant marine snow (via mechanisms currently not well understood) to form agglomerations and in so doing tend to sink out of the water column over time (if they are not otherwise consumed or transformed). The rate of the deposition of this "oiled marine snow" appears to have been enhanced following the capping of the well and halting of free-flowing hydrocarbons into the water column. At this point, these massive microbial populations feeding off of this diffused hydrocarbon plume appear to have rapidly become food stressed. Subsequent increased extracellular exudates may foster increased "oiled marine snow" flocculent agglomerations that speed downward translocation and benthic deposition of degraded hydrocarbons. We now have an increased oil–dispersant pulse to the benthic invertebrate community. These emulsions and repackaging of fine droplets in a flocculent matrix render it biologically available to the benthos and capable of inducing death by acute toxic exposures, fouling of feeding or respiring apparatus, or induction of localized hypoxia as microbial degradation demands and depletes oxygen, consistent with the limited data we have of gorgonian mortality proximate to the wellhead (White et al., 2012). In addition, the long-term nature of the oil release and its potential persistence around the seafloor render likely various impacts of chronic exposure on growth, reproduction, and behavior, which can result indirectly in death by reduced fitness. The most susceptible invertebrates are probably those associated with the most valued habitats and that serve as biogenic habitat engineers, namely, the deepwater corals (e.g., *Lophelia* spp.), gorgonians, and other epibiotic invertebrates on hard-bottom substrata around the wellhead location (Brooks et al., 2008; CSA International, 2007). These organisms are suspension feeders, exposing them to risk of encounter with, ingestion of, and toxicity from petroleum hydrocarbons and dispersants. These emergent colonial invertebrates provide structure that is occupied by many crustaceans and demersal fishes, probably serving as a nursery habitat for early life stages and foraging grounds for larger nektonic predators. The majority of the seafloor around the DWH blowout is comprised of sediments with largely infaunal invertebrate inhabitants. The echinoderms and crustaceans (especially amphipods) among them are highly susceptible to acute mortality from exposure to toxicants. Other taxa like bivalve and gastropod mollusks and polychaete worms are generally more resilient to PAH exposures but as deposit feeders can ingest and concentrate PAHs, potentially passing on toxins to predatory demersal fishes. Enhanced microbial oxygen demand on and around the seafloor where oil is retained and deposited can create hypoxia and induce mortality of sedentary invertebrates, including soft-sediment invertebrates otherwise resilient to toxins. While it is possible that the addition of oil droplets to cold-water seep communities could enhance the production

of benthic invertebrates adapted to provision of energy in the form of hydrocarbon-degrading microbes, we have seen no evidence of this to date in the DWH event. The small sizes of the dispersed oil droplets lead to risks of fouling of feeding and respiratory organs and ingestion of the community of suspension-feeding invertebrates occurring throughout the water column, perhaps more abundantly near the seafloor but extending upward into the midwater depths where dispersed oil droplets are expected to reside until they accumulate sediments and sink to the seafloor. These deepwater benthic, epibenthic, benthopelagic, and midwater pelagic communities are not well described or well known functionally. The need for specialized equipment to conduct studies at such water depths to render assessment of oil release impacts cannot be overemphasized. This is the precise environment where the most unique aspects of the DWH incident are continuing to play out.

The impacts of the DWH oil release on the nearshore shallow waters and shorelines under this scenario of intense use of dispersant at the wellhead will be further reduced beyond what was achieved with only surface application of dispersant. Declines in nearshore and coastal impacts are expected to be proportional to the amount of oil that was prevented from surfacing and retained at depth in the deep sea. Thus, in the short term, the application of dispersants injected directly into the wellhead of the gushing well at the deep location may have some benefits in the form of reduced injuries to abundant and valuable coastal habitats, resources, and services. Nevertheless, there exists potential for pelagically or demersally retained oil to become transported to shore after some time lag, driven by ocean currents and perhaps brought finally to the shore by coastal upwelling induced via offshore winds of winter. Indirect effects of fishery closures are at least as great as in the old model and could potentially be even greater if the demersal–pelagic oil spreads into shallow enough waters to contaminate commercially exploited shrimps and crabs. Demersal oil reaching shallow coastal waters would also result in closures of fisheries and other bivalve shellfish, probably over large areas.

2.8 THE NEED FOR AN INTEGRATIVE, INTERDISCIPLINARY MARINE OIL SPILL OCEANOGRAPHY

Without completion of oil spill oceanography studies of pelagic and benthic impacts in the deep ocean, thereby fleshing out the new paradigm for deep oil releases outlined here, some natural resource impacts of the DWH blowout will remain unknown, and the use of dispersants at depth will likely be concluded to be an effective management tool. With absent adequate knowledge to characterize and quantify impacts from this spill and the use of subsurface dispersants in particular, we will be in a poor position to responsibly respond to any future deep-sea spill. The present gaps in scientific appreciation of the roles of the deep sea in ocean ecosystem functioning and, more narrowly, in our understanding of how microbial processes serve to sustain ocean food webs can lead to a conclusion that the biogeochemical interventions induced by massive injection of oil and gas into the deep sea do not degrade the delivery of ocean ecosystem services of value to humans. Such a

conclusion is presently unjustified. We are aware, for example, of routine deep-ocean use of the spill area by sperm whales as they feed on squid and other prey. How microbial production and toxic contamination may link to these whales and their prey is but one of several related questions whose answers would educate the present and future policymakers on the value of sustaining the integrity of deep-ocean functions. Even if a rapid settlement of damage claims from the parties responsible for the DWH blowout is negotiated, public trust interests can be fully served only if restoration funds include sufficient investigations into the functioning of the deep sea to understand its ecosystem services and allow mitigation where justified.

2.9 CONCLUSIONS

1. Huge amounts of hydrocarbons went into the deep sea and water column following the DWH blowout, entering the pelagic food chain and being retained at depth and in epibenthic environments, where we know virtually nothing. This has motivated our proposed new conceptual model for deepwater oil spills.
2. Changing paradigm. Our previous conception of oil spills simply did not account for the reality of deepwater oil spills, with pressurized, high-energy atomization and dispersant use at depth:
   a. We need a robust research effort throughout the water column and on the seafloor of the deep sea to document what happened and what is happening.
   b. We also need research on the shelf and nearshore because of the potential delayed consequences of migrating oil–ecosystem level impacts.
3. All is likely not well with the Gulf of Mexico. The mass of oil introduced and its impacts via toxicity, physical smothering, and the amount of aggregate carbon input have direct and indirect impacts both short term and long term upon the structure of, functioning of, and services provided by the northern Gulf of Mexico.
4. Managing large-scale spills by definition requires trade-offs that are multi-dimensional (impacts, fates, social costs, time scales), which may not be fully appreciated.
5. Use of dispersants was driven by desire to keep beaches and shorelines clean, which included socioeconomic considerations as well as current ecological understanding (relying heavily on a series of assumptions surrounding dispersant efficacy).
6. Use and efficacy of dispersants in deep water involved novel and poorly understood impacts.
7. There remains a lack of key data about the spill (subsurface extent, fate, etc.). This combined with the novel ecotoxicological impacts has made the interpretation of overall effects difficult and speculative. In addition to manipulative ecotoxicological experiments, we need long-term monitoring of community-level impacts across all coastal, pelagic, and deepwater ecosystems. This

includes a strong need for improved understanding of background Gulf of Mexico ecological conditions.

8. Our existing response and recovery process is not able to apply scientific capacity in a nimble and effective manner to inform the management of quickly unfolding environmental disasters.

2.10 FUTURE RESEARCH

Key questions that are at this point unknown and must be addressed by current and future research:

1. How much oil would remain at depth without the use of dispersants?
2. How much more oil occurred and persisted because of dispersant use?
3. Did use of dispersants increase oil deposition onto the benthos?
4. How well are the existing political and management tools able to address these particular novel spill dynamics and impacts? And how well would these tools function in other settings (such as the Arctic)?
5. Will our current long-term monitoring agenda adequately address the research needs in an integrative, interdisciplinary manner that will promote a holistic understanding of deep-sea oil impacts?
6. Did we shift temporal duration of oil biodegradation by shunting oil to the deep sea?
7. How robust are our emerging conceptual models under various geographic, weather, etc., conditions? For example, would such a spill in the Arctic progress in the same manner?

REFERENCES

AFP Staff. *US oil production, shipping unaffected by spill so far*. Paris: Agence France-Presse Wire Service; 2010.

Alaska Oil Spill Commission. Spill: the wreck of the Exxon Valdez Final Report; 1990.

Anderson S, Boehm P, Fiest D, Howard R, Lewbel C, Pilson D, Wait A. IXTOC Oil Spill Damage Assessment Study. Minerals Management Service; 1982. Final report for the U.S. Department of Interior, Bureau of Land Management, New Orleans, LA, AA851-CTO-71, 447 pp.

Austin D, Carriker B, Priest TMJPT, Pulsipher AG. History of the offshore oil and gas industry in southern Louisiana interim report volume I: Papers on the evolving offshore industry. OCS MMS 2004-049. Baton Rouge, LA: U.S. Department of the Interior; 2004.

Axford DN. The breaking-up of the oil tanker Torrey Canyon; 2012.

Barkham P. Oil spills: legacy of the Torrey Canyon. *The Guardian*, London; 2010.

BBC Newswire. Bombs rain down on Torrey Canyon. *BBC Hourly News Summary*; 1967a.

BBC Newswire. Supertanker Torrey Canyon hits rocks; 1967b.

Bodkin JL, Ballachey BE, Coletti HA, Esslinger GG, Kloecker KA, Rice SD, Reed JA, Monson DH. Long-term effects of the 'Exxon Valdez' oil spill: sea otter foraging in the intertidal as a pathway of exposure to lingering oil. Mar Ecol Prog Ser 2012;447:273–287.

Boufadel MC, Sharifi Y, Van Aken B, Wrenn BA, Lee K. Nutrient and oxygen concentrations within the sediments of an Alaskan beach polluted with the Exxon Valdez oil spill. Environ Sci Technol 2010;44:7418–7424.

Bowman TD, Schempf PF, Bernatowicz JA. Bald eagle survival and population dynamics in Alaska after the "Exxon Valdez" oil spill. J Wildl Manage 1995;59:317–324.

Briggs JC. *Marine Zoogeography*. New York: McGraw Hill; 1974.

Brooks JM, Fisher C, Roberts H, Bernard B, MacDonald I, Carney R, Joye S, Cordes E, Wolff G, Goehring E. Investigations of chemosynthetic communities on the lower continental slope of the Gulf of Mexico: Interim report 1. OCS MMS 2008-009. Department of the Interior; 2008.

Bureau of Ocean Energy Management. Regulation and Enforcement. History of offshore oil and gas development in the Gulf of Mexico. Washington, DC: Bureau of Ocean Energy Management, Regulation and Enforcement; 2010.

Bureau of Ocean Energy Management, Regulation and Enforcement. Well information and data available in ASCII files for downloading. Washington, DC: Bureau of Ocean Energy Management, Regulation and Enforcement; 2011.

California Academy of Sciences. Scientists find higher concentrations of heavy metals in post-spill oysters from Gulf of Mexico. In: California Academy of Sciences, editors. *California Academy of Sciences*. San Francisco, CA: California Academy of Sciences; 2012.

Camilli R, Reddy CM, Yoerger DR, Van Mooy BAS, Jakuba MV, Kinsey JC, McIntyre CP, Sylva SP, Maloney JV. Tracking hydrocarbon plume transport and biodegradation at Deepwater Horizon. Science 2010;330:201–204.

Carls MG, Marty GD, Hose JE. Synthesis of the toxicological impacts of the Exxon Valdez oil spill on Pacific herring (*Clupea pallasi*) in Prince William Sound, Alaska, U.S.A. Can J Fish Aquat Sci 2002;59:153–172.

CBS/Associated Press. BP's spill contingency plans vastly inadequate. *CBS News*. CBS; 2010.

Chapman PM, Morgan JD. Sediment bioassays with oyster larvae. Bull Environ Contam Toxicol 1983;31:438–444.

Cooper JAG, McLaughlin S. Contemporary multidisciplinary approaches to coastal classification and environmental risk analysis. J Coastal Res 1998;14:512–524.

Cordes EE, McGinley MP, Podowski EL, Becker EL, Lessard-Pilon S, Viada ST, Fisher CR. Coral communities of the deep Gulf of Mexico. Deep Sea Research Part I: Oceanographic Research Papers 2008;55:777–787.

Corwin M. The oil spill heard 'Round The Country. *Los Angeles Times*, Los Angeles, CA; 1989. p I23.

CSA International I. Characterization of northern Gulf of Mexico deepwater hard-bottom communities with emphasis on *Lophelia* coral. OCS MMS 2007-044. U.S. Department of the Interior; 2007.

Culbertson JB, Valiela I, Peacock EE, Reddy CM, Carter A, VanderKruik R. Long-term biological effects of petroleum residues on fiddler crabs in salt marshes. Mar Pollut Bull 2007;54:955–962.

Culbertson JB, Valiela I, Pickart M, Peacock EE, Reddy CM. Long-term consequences of residual petroleum on salt marsh grass. J Appl Ecol 2008;45:1284–1292.

Darnell RM, Defenbaugh RE. Gulf of Mexico: environmental overview and history of environmental research. Am Zool 1990;30:3–6.

Dauvin J-C, Gentil F. Conditions of the peracarid populations of subtidal communities in Northern Brittany ten years after the Amoco Cadiz oil spill. Mar Pollut Bull 1990;21:123–130.

De Vogelaere AP, Foster MS. Damage and recovery in Intertidal Fucus Gardneri assemblages following the 'Exxon Valdez' oil spill. Mar Ecol Prog Ser 1994;106:263–271.

Deepwater Horizon Study Group. Final report on the investigation of the Macondo Well blowout. Berkeley, CA: Center for Catastrophic Risk Management, University of California; 2011.

Defenbaugh, RE. The Gulf of Mexico: a management perspective. Am Zool 1990;30:7–13.

Easton, RO. *Black Tide: The Santa Barbara Oil Spill and its Consequences*. New York: Delacorte Press; 1972.

Editorial Board. The lessons of Ixtoc I. *New York Times*, New York; 1980. p 22.

Elmgren R, Hansson S, Larsson U, Sundelin B, Boehm PD. The "Tsesis" oil spill: acute and long-term impact on the benthos. Mar Biol 1983;73:51–65.

Energy Resources Co. Inc. Ixtoc oil spill assessment final report. AA851-CTO-71. Bureau of Land Management; 1982.

Enticknap B. Trawling the North Pacific: understanding the effects of bottom trawl fisheries on Alaska's living seafloor. Anchorage, AK: Alaska Marine Conservation Council; 2002.

Environmental Protection Agency (EPA). EPA and NOAA Press Conference Call on Dispersant Use and Approval; 2010.

Epstein A. Obama Follows Nixon on Oil Spills. *Wall Street Journal*.

Esler D, Iverson SA. Female Harlequin duck winter survival 11 to 14 years after the Exxon Valdez oil spill. J Wildl Manage 2010;74:471–478.

Exxon Valdez Oil Spill Trustee Council. Final environmental impact statement for the Exxon Valdez oil spill restoration plan; 1994.

Fauchald K. A survey of the Benthos off Santa Barbara following the January 1969 Oil Spill. CalCOFI Report; 1972.

Fautin D, Dalton P, Incze LS, Leong J-AC, Pautzke C, Rosenberg A, Sandifer P, Sedberry G, Tunnell Jr, JW, Abbott I, Brainard RE, Brodeur M, Eldredge LG, Feldman M, Moretzsohn F, Vroom PS, Wainstein M, Wolff N. An overview of marine biodiversity in United States waters. PLoS One 2010;5:e11914.

Geraci JR, St. Aubin DJ. *Synthesis of Effects of Oil on Marine Mammals*, OCS MMS 88-0049. Ventura, CA: Minerals Management Service; 1988.

Giarrusso CC, Pugliese Carratelli E, Spulsi G. On the effects of wave drift on the dispersion of floating pollutants. Ocean Eng 2001;28:1339–1348.

Gower JFR, King SA. Distribution of floating Sargassum in the Gulf of Mexico and the Atlantic Ocean mapped using MERIS. Int J Remote Sens 2011;32:1917–1929.

Grabowski JH, Peterson CH. Restoring oyster reefs to recover ecosystem services. In: Cuddington K, Byers JE, Wilson WG, Hastings A, editors. *Ecosystem Engineers*. Amsterdam: Elsevier Academic Press; 2007. p 281–298.

Graham WM, Condon RH, Carmichael RH, D'Ambra I, Patterson HK, Linn LJ, Hernandez Jr, FJ. Oil carbon entered the coastal planktonic food web during the Deepwater Horizon oil spill. Environ Res Lett 2010;5:045301.

Graham B, Reilly WK, Beinecke F, Boesch DF, Garcia TD, Murray CA, Ulmer F. Deep water: the Gulf oil disaster and the future of offshore drilling – report to the President (BP Oil Spill Commission Report). BP Oil Spill Commission; 2011.

Gulf of Mexico Sea Grant Programs. *Fish stocks in the Gulf of Mexico fact sheet*, U. S. Department of Commerce, National Oceanic and Atmospheric Administration; 2010. p 3.

Hawkins SJ. Marine conservation in a rapidly changing world. Aquatic conservation: marine and freshwater. Ecosystems 2012;22:281–287.

Hawkins SJ, Hartnoll RG. Changes in a rocky shore community: an evaluation of monitoring. Mar Environ Res 1983;9:131–181.

Hawkins SJ, Southward AJ. The Torrey Canyon oil spill: recovery of the rocky shore communities. In: Thayer GW, editor. *Restoring the Nation's Marine Environment*. College Park, MD: Maryland Sea Grant; 1992. p 583–631.

Hazen TC, Dubinsky EA, DeSantis TZ, Andersen GL, Piceno YM, Singh N, Jansson JK, Probst A, Borglin SE, Fortney JL, Stringfellow WT, Bill M, Conrad MS, Tom LM, Chavarria KL, Alusi TR, Lamendella R, Joyner DC, Spier C, Baelum J, Auer M, Zemla ML, Chakraborty R, Sonnenthal EL, D'haeseleer P, Holman H-YN, Osman S, Lu Z, Nostrand JDV, Deng Y, Zhou J, Mason OU. Deep-sea oil plume enriches indigenous oil-degrading bacteria. Science 2010;330:204–208.

Helguero G. U.S. confirms underwater oil plume from Deepwater Horizon well. *International Business Times*; 2010.

Hoffmayer ER, Franks JS, Comyns BH, Hendon JR, Waller RS. Larval and juvenile fishes associated with pelagic Sargassum in the northcentral Gulf of Mexico. In: Proceedings of the Gulf and Caribbean Fisheries Institute; 2005. p 259–270.

Hooper CH. IXTOC I oil spill: the federal scientific response. Report. Boulder, CO: National Oceanic and Atmospheric Administration; 1981.

Houghton JP, Gilmour RH, Lees DC, Driskell WB, Lindstrom SC, Mearns A. Prince William Sound intertidal biota seven years later: has it recovered? In: International Oil Spill Conference. Washington, DC: American Petroleum Institute; 1997. p 679–686.

Hu X, Cai W-J, Wang Y, Guo X, Luo S. Geochemical environments of continental shelf-upper slope sediments in the northern Gulf of Mexico. Palaeogeogr, Palaeoclimatol, Palaeoecol 2011;312:265–277.

Jackson JBC, Cubit JD, Keller BD, Batista V, Burns K, Caffey HM, Caldwell RL, Garrity SD, Getter CD, Gonzalez C, Guzman HM, Kaufmann KW, Knap AH, Levings SC, Marshall MJ, Steger R, Thompson RC, Wei E. Ecological effects of a major oil spill on Panamanian coastal marine communities. Science 1989;243:37–44.

Jernelöv A, Olof L. Ixtoc I: a case study of the world's largest oil spill. Ambio 1981;10: 299–306.

Johansen Ø. Rye H, Cooper C. DeepSpill—field study of a simulated oil and gas blowout in deep water. Spill Sci Technol Bull 2003;8:433–443.

Johnson CC. The oil pollution act of 1990: a long time coming. Fordham Environmental Law Review 2011;2:58–77.

Joye S, MacDonald I, Leifer I, Asper V. Magnitude and oxidation potential of hydrocarbon gases released from the BP blowout. Nat Geosci 2011;4:160–164.

Kessler JD, Valentine DL, Redmond MC, Du M, Chan EW, Mendes SD, Quiroz EW, Villanueva CJ, Shusta SS, Werra LM, Yvon-Lewis SA, Weber TC. A persistent oxygen anomaly reveals the fate of spilled methane in the deep Gulf of Mexico. Science 2011;331(6015):312–315.

Kindinger ME. Impact of the Ixtoc I oil spill on the community structure of intertidal and subtidal infauna along south Texas beaches. Master's thesis. Corpus Christi State University; 1981.

Kolpack RL, editor. *Biological and Oceanographical Survey of the Santa Barbara Channel Oil Spill 1969–1970: Volume II. Sea Grant*. Los Angeles, CA: University of Southern California; 1971.

Law RJ, Kelly CA, Graham KL, Woodhead RJ, Dyrynda PEJ, Dyrynda EA. Hydrocarbons and PAH in fish and shellfish from southwest Wales following the Sea Empress oil spill in 1996. In: International Oil Spill Conference, Fort Lauderdale, FL, 1997. p 205–211.

Lenihan HS, Peterson CH, Byers JE, Grabowski JH, Gordon WT, Colby DR. Cascading of habitat degradation: oyster reefs invaded by refugee fishes escaping stress. Ecol Appl 2001;11:764–782.

Lewbel GS. Strengths and weaknesses of damage assessment programs: the IXTOC-I and Burmah Agate oil spills and the benthic macroinfauna of the Texas continental shelf. Texas J Sci 1985;37:269–310.

Lewis A. British jets drop bombs, napalm and rockets on stranded tanker in new effort to burn oil cargo. *New York Times*, New York; 1967.

Lindblom GP, Emery BD, Lara IMAG. Aerial application of dispersants at the Ixtoc I Spill. In: Oil Spill Conference; 1981. p 259–262.

Lowther A. Fisheries of the United States 2010. In: *Current Fishery Statistics No. 2010, National Marine Fisheries Service*. Silver Spring, MD: U.S. Department of Commerce, National Oceanic and Atmospheric Administration, National Marine Fisheries Service; 2011.

Lustgarten A. Chemicals meant to break up BP oil spill present new environmental concerns. *ProPublica*, New York; 2010a.

Lustgarten A. Years of internal BP probes warned that neglect could lead to accidents. *ProPublica*, New York; 2010b.

M'Gonigle RM, Zacher MW. *Pollution, Politics, and International Law: Tankers at Sea*. Berkeley, CA: University of California Press; 1979.

MBARI. Data Report: NOAA Ship Gordon Gunter cruise GU-10-02, Gulf of Mexico June 2–3, 2010 operations of the MBARI AUV Dorado. Moss Landing, CA: Monterey Bay Aquarium Research Institute; 2010.

McNutt M, Camilli R, Guthrie G, Hsieh P, Labson V, Lehr B, Maclay D, Ratzel A, Sogge M. Assessment of flow rate estimates for the Deepwater Horizon/Macondo Well oil spill. Flow rate Technical Group report to the National Incident Command, Interagency Solutions Group, March 10, 2011, p 30.

Millennium Ecosystem Assessment. *Ecosystems and Human Well-Being: Wetlands and Water Synthesis*. Washington, DC: World Resources Institute; 2005.

Minerals Management Service. Summary of offshore petroleum operations in the Gulf of Mexico OCS Region. New Orleans, LA: U.S. Department of the Interior; 2002.

Nash R. Experiencing the Santa Barbara oil spill and energizing effect upon the environmental movement in California, In: S. Anderson, editor. University of California Santa Barbara; 1989.

Nash RF. *Wilderness and the American Mind*. 4th ed. New Haven, CT: Yale University Press; 2001.

National Oceanic and Atmospheric Administration. Oil spill case histories: 1967–1991 Summaries of significant U.S. and international spills. HMRAD 92-11. Seattle, WA: Hazardous Materials Response and Assessment Division; 1992.

National Oil Spill Commission. *Stopping the Spill: The Five-Month Effort to Kill the Macondo Well*. Washington, DC: National Commission on the BP Deepwater Horizon Oil Spill and Offshore Drilling; 2011.

National Research Council (NRC). *Oil in the Sea: Inputs, Fates, and Effects*. Washington, DC: National Academies Press; 1985.

National Research Council (NRC). *Oil in the Sea III: Inputs, Fates, and Effects*. Washington, DC: National Academies Press; 2003.

National Science Foundation (NSF). *Proposal and Award Policies and Procedures Guide: Part I – Proposal Preparation & Submission Guidelines Grant Proposal Guidelines*. Arlington, VA: NSF; 2008.

Nicholson N. The Santa Barbara oil spills in perspective. CalCOFI Report 1972;16:130–149.

Nixon LD, Shepard NK, Bohannon CM, Montgomery TM, Kazanis EG, Gravois MP. Deepwater Gulf of Mexico 2009: interim report of 2008 highlights. New Orleans, LA: Minerals Management Service; 2009. p 87.

NMFS Fisheries Statistics Division. Annual commercial landing statistics. Silver Spring, MD: National Marine Fisheries Service; 2011.

O'Sullivan AJ, Richardson AJ. The Torrey Canyon disaster and intertidal marine life. Nature 1967;214:448–541.

Okidi CO. International legal responses to threats to marine biodiversity from pollution. Presented at the 8th Annual Colloquium of IUCN Academy of Environmental Law, Ghent University, Belgium; 2010. p 1–31.

Pagès, F, González HE, Ramón M, Sobarzo M, Gili JM. Gelatinous zooplankton assemblages associated with water masses in the Humboldt Current System, and potential predatory impact by Bassia bassensis (Siphonophora: Calycophorae). Mar Ecol Prog Ser 2001;210: 13–24.

Paine RT, Ruesink JL, Sun A, Soulanilee EL, Wonham MJ, Harley CDG, Brumbaugh DR. Secord DL. Trouble on oiled waters: lessons from the Exxon Valdez oil spill. Ann Rev Ecol Syst 1996;27:197–235.

Pequegnat WE. The ecological communities of the continental slope and adjacent regimes of the northern Gulf of Mexico. OCS MMS 1983-11, Metairie, LA: Minerals Management Service; 1983.

Peterson CH. The "Exxon Valdez" oil spill in Alaska: acute, indirect and chronic effects on the ecosystem. Adv Mar Biol 2001;39. Academic Press. p 1–103.

Peterson CH, Grabowski JH, Powers SP. Estimated enhancement of fish production resulting from restoring oyster reef habitat: quantitative valuation. Mar Ecol Progr Ser 2003a; 264:249–264.

Peterson CH, Rice SD, Short JW, Esler D, Bodkin JL, Ballachey BE, Irons DB. Long-term ecosystem response to the Exxon Valdez oil spill. Science 2003b;302:2082–2086.

Peterson CH. Anderson SS, Cherr GN, Ambrose RF, Anghera S, Bay S, Blum M, Condon R, Dean TA, Graham M, Guzy M, Hampton S, Joye S, Lambrinos J, Mate B, Meffert D, Powers SP, Somasundaran P, Spies RB, Taylor CM, Tjeerdema R, Adams EE. A tale of two spills: novel science and policy implications of an emerging new oil spill model. BioScience 2012;62:461–469.

Petrow R. What really caused the Torrey Canyon disaster? Popular Mechanics 1969, p 114–119, 226.

Pincinato FL, Riedel PS, Milanelli JCC. Modelling an expert GIS system based on knowledge to evaluate oil spill environmental sensitivity. Ocean Coastal Manage 2009;52:479–486.

Rabalais NN, McKee BA, Reed DJ, Means JC. Fate and effects of produced water discharged in coastal Louisiana, Gulf of Mexico, USA. In: Ray JP. Englehart FR, editors. *Produced Water: Technological/Environmental Issues and Solutions*. New York: Plenum Press; 1993, p 355–369.

Raffaelli D, Hawkins S. *Intertidal Ecology*. 2nd ed. Dordrecht: Kluwer Academic Publishers; 1999.

Rand GM, editor. *Fundamentals of Aquatic Toxicology: Effects, Environmental Fate, and Risk Assessment*. 2nd ed. Washington, DC: Taylor and Francis; 1995.

Reddy CM, Arey JS, Seewald JS, Sylva SP, Lemkau KL, Nelson RK, Carmichael CA, McIntyre CP, Fenwick J, Ventura GT, Van Mooy BAS, Camilli R. Composition and fate of gas and oil released to the water column during the Deepwater Horizon oil spill. Proc Natl Acad Sci USA 2012;109:20229–20234.

Resnick-Ault J, Klimasinska K. Transocean oil-drilling rig sinks in Gulf of Mexico. *Bloomberg*; 2010.

Rezak R, Edwards GS. Carbonate sediments of the Gulf of Mexico. In: Rezak R, Henry VJ, editors. *Contributions on the Geographical and Geophysical Oceanography of the Gulf of Mexico*, Texas A & M University Ocean Studies 1972;3:263–280.

Rezak R, Bright TJ, McGrail DW. Reefs and banks of the Northwestern Gulf of Mexico: their geological, biological, and physical dynamics. 83-1-T, New Orleans, LA: Minerals Management Service; 1983.

Rezak R, Bright TJ, McGrail DW. *Reefs and Banks of the Northwestern Gulf of Mexico*. New York: John Wiley & Sons; 1985.

Rice SD, Spies RB, Wolfe DA, Wright BA., editors. In: Proceedings of the "Exxon Valdez" oil spill symposium. Bethesda, MD: American Fisheries Society; 1996.

Rice SD, Thomas RE, Heintz RA, Wertheimer AC, Murphy ML, Carls MG, Short JW, Moles A. Synthesis of long-term impacts to pink salmon following the Exxon Valdez oil spill: persistence, toxicity, sensitivity, and controversy. 99329, Exxon Valdez Trustee Council; 2001.

Rice SD, Carls MG, Heintz RA, Short JW. Comment on "hydrocarbon composition and toxicity of sediments following the Exxon valdez oil spill in Prince William Sound, Alaska, USA". Environ Toxicol Chem 2003;22:2539–2540.

Rigzone (2012). Offshore Rig Day Rates. Dice Holdings, Inc.

Robertson C, Robbins L. Oil rig sinks in the Gulf of Mexico. *New York Times*, New York; 2010.

Sabatès A, Gili JM, Pagès F. Relationship between zooplankton distribution, geographic characteristics and hydrographic patterns off the Catalan coast (Western Mediterranean). Mar Biol 1989;103:153–159.

Schmitt RJ, Osenberg CW, editors. *Detecting Ecological Impacts: Concepts and Applications in Coastal Habitats*, San Diego, CA: Academic Press; 1996.

Secretaria de Energia. Sistema de Informacion Energetica: Informacion Estadistica. Mexico City: Secretaria de Energia; 2008.

Short JW, Lindeberg MR, Harris PM, Maselko JM, Pella JJ, Rice SD. Estimate of oil persisting on the beaches of Prince William Sound 12 years after the Exxon Valdez oil spill. Environ Sci Technol 2003;38:19–25.

Silliman BR, van de Koppel J, McCoy MW, Diller J, Kasozi GN, Earl K, Adams PN, Zimmerman AR. Degradation and resilience in Louisiana salt marshes after the BP–Deepwater Horizon oil spill. Proc Natl Acad Sci USA 2012.

Skytruth. Over 28,000 abandoned wells in the Gulf of Mexico. Skytruth Blog. Skytruth, FL; 2011.

Smith JE, editor. 'Torrey Canyon' pollution and marine life: a report by the Plymouth Laboratory of the Marine Biological Association of the United Kingdom. Cambridge, UK: Cambridge University Press; 1968.

Socolofsky SA, Adams EE. Multi-phase plumes in uniform and stratified crossflow. J Hydraul Res 2002;40:661–672.

Socolofsky SA, Adams EE, Sherwood CR. Formation dynamics of subsurface hydrocarbon intrusions following the Deepwater Horizon blowout. Geophys Res Lett 2011;38:L09602.

Southward AJ, Southward EC. Recolonization of rocky shores in cornwall after use of toxic dispersants to clean up the *Torrey Canyon* spill. Journal of the Fisheries Research Board of Canada 1978;35:682–706.

Southward AJ, Southward EC. Disappearance of the warm-water hermit crab *Clibanarius erythropus* from south-west Britain. J Mar Biol Assoc UK 1988;68:409–412.

Spooner M. Some ecological effects of marine oil pollution. In: Proceedings of the Joint Conference for Preventing and Controlling Oil Spills; 1969, New York. p 313–316.

Squire Jr, LJ. Effects of the Santa Barbara, Calif., oil spill on the apparent abundance of Pelagic fishery. Mar Fish Rev 1992;54:7.

Staff. The ecological disaster caused by the stricken Torrey Canyon. *Look and Learn*; 1978.

Staff. NOAA confirms USF oil plume research. *Tampa Bay Business Journal*, Tampa Bay, FL; 2010.

Straughan D, editor. *Biological and Oceanographical Survey of the Santa Barbara Channel Oil Spill 1969–1970: Volume I Bacteria and Bacteriology*. Los Angeles, CA: University of Southern California Sea Grant; 1971a.

Straughan D. What has been the effect of the spill on the ecology in the Santa Barbara Channel? In: Straughan D, editor. *Biological and Oceanographical Survey of the Santa Barbara Channel Oil Spill 1969–1970: Volume I Bacteria and Bacteriology*, Sea Grant, University of Southern California; 1971b. p 401–426.

van Tamelen PG, Stekoll MS, Deysher L. Recovery processes of the brown alga *Fucus gardneri* following the 'Exxon Valdez' oil spill: settlement and recruitment. Mar Ecol Prog Ser 1997;160:265–277.

Teal JM. Howarth RW. Oil spill studies: A review of ecological effects. Environ Manag 1984;8:27–43.

Tunnell JWJ, Chapman BR. Environmental effects of Ixtoc I oil spill on south Texas barrier islands. In *Congreso sobre problemas ambientales de Mexico*. Mexico: Instituto Politecnico Nacional; 1980.

Tunnell JWJ, Dokken QR. Observations on Ixtoc I oil impact of southwestern Gulf of Mexico coral reefs. In: *Congreso sobre problemas ambientales de Mexico*; 1980.

Tunnell JWJ. Judd FW, editors. *The Laguna Madre of Texas and Tamaulipas*. College Station, TX: Texas A&M University Press; 2001.

Tunnell JWJ, Dokken QR, Kindinger ME. Effects of the Ixtoc I oil spill on the intertidal and subtidal infaunal populations along lower Texas coast barrier island beaches. In: Oil Spill Conference, Washington, DC: American Petroleum Institute; 1981. p 467–475.

Tunnell JWJ, Chapman BR, Kindinger ME, Dokken QR. In *Environmental Impact of Ixtoc I Oil Spill on South Texas Sandy Beaches: Infauna and Shorebirds*, International Symposium on Ixtoc-I; 1982. p 142.

Tunnell JWJ, Chavez EA, Withers K, editors. *Coral Reefs of the Southern Gulf of Mexico*. College Station, TX: Texas A&M University Press; 2007.

U.S. Geological Survey. Seagrasses in northern Gulf of Mexico: an ecosystem in trouble. Factsheet USGS factsheet FS-017-00. Lafayette, LA: USGS National Wetland Research Center; 2000.

Upton HF. The deepwater horizon oil spill and the Gulf of Mexico fishing industry. CRS 7-5700 R41640. Washington, DC: Congressional Research Service; 2011.

Valentine DL, Kessler JD, Redmond MC, Mendes SD, Heintz MB, Farwell C, Hu L, Kinnaman FS, Yvon-Lewis S, Du M, Chan EW, Tigreros FG, Villanueva CJ. Propane respiration jump-starts microbial response to a deep oil spill. Science 2010;330:208–211.

Valentine DL, Mezic I, Macesic S, Crnjaric-Zic N, Ivic S, Hogan PJ, Fonoberov VA, Loire S. Dynamic autoinoculation and the microbial ecology of a deep water hydrocarbon irruption. Proc Natl Acad Sci USA 2012;109:20286–20291.

Vargas RA. 1979's Ixtoc oil well blowout in Gulf of Mexico has startling parallels to current disaster. *The Times-Picayune*, New Orleans, LA; 2010.

Walker AH, Henne DR. The region III regional response team technical symposium on dispersants: an interactive, educational approach to enlightened decision making. In: Proceedings of the 1991 International Oil Spill Conference. San Diego, CA: American Petroleum Institute; 1991.

Walker AH, Scholz DK, Kucklick JH, Pond RG. Government and industry partnering: nationwide progress in pre-authorization agreements since 1994. In: International Oil Spill Conference. Seattle, WA: American Petroleum Institute; 1999.

Wang M. After 3 weeks, BP handed over samples requested by scientists. *ProPublica*, New York; 2010a.

Wang M. Top BP exec still says spill flow rate doesn't matter. *ProPublica*, New York; 2010b.

Wells HW. The fauna of oyster beds, with special reference to the salinity factor. Ecol Monogr 1961;31:239–266.

Wells RJD, Rooker JR. Feeding ecology of pelagic fish larvae and juveniles in slope waters of the Gulf of Mexico. J Fish Biol 2009;75:1719–1732.

Wells PG, Butler JN, Hughes JS, editors. *Exxon Valdez Oil Spill: Fate and Effects in Alaskan Waters*. Philadelphia, PA: American Society of Testing and Materials; 1995.

West Kern County Oil Museum. The lakeview gusher. Page exhibit, 1168 Wood Street, Taft, CA; 2011.

White HK, Hsing P-Y, Cho W, Shank TM, Cordes EE, Quattrini AM, Nelson RK, Camilli R, Demopoulos AWJ, German CR, Brooks JM, Roberts HH, Shedd W, Reddy CM, Fisher CR. Impact of the Deepwater Horizon oil spill on a deep-water coral community in the Gulf of Mexico. Proc Natl Acad Sci USA 2012;109:20303–20308.

Wolfe DA, Hameedi MJ, Galt JA, Watabayashi G, Short J, O'Claire C, Rice S, Michel J, Payne JR, Braddock J, Hanna S, Sale D. The fate of the oil spilled from the Exxon Valdez. Environ Sci Technol 1994;28:560A–568A.

3

REMEDIATION AND RESTORATION OF NORTHERN GULF OF MEXICO COASTAL ECOSYSTEMS FOLLOWING THE DEEPWATER HORIZON EVENT

Michael J. Blum, Brittany M. Bernik, Thomas Azwell, and Eric M.V. Hoek

3.1 INTRODUCTION

On April 20, 2010, an explosion on the Deepwater Horizon (DWH) drilling platform and blowout of the Macondo well 1500 m below resulted in the worst marine oil spill on record. An estimated 205 million gallons of crude oil and 260,000–520,000 tons of methane (the energy equivalent of 80–155 million gallons of crude oil) were released into the Gulf of Mexico (GoM) over the following 87 days (Camilli et al., 2012; Joye et al., 2011; McNutt et al., 2011). The DWH blowout was unlike all other well-studied crude oil releases into marine environments. The blowout resulted in a massive shore-bound surface spill, but the discharge of oil and gas under high pressure at extreme depth also resulted in unprecedented deep-ocean persistence of highly dispersed hydrocarbons. Addressing both surface and subsurface conditions posed unanticipated challenges to governmental responses shaped by traditional surface spills (Peterson et al., 2012). Response efforts not only identified major gaps in baseline knowledge of vulnerable ecosystems (Peterson et al., 2012) but also demonstrated that advances in deepwater drilling far outpaced advances in spill containment and shoreline remediation.

Oil Spill Remediation: Colloid Chemistry-Based Principles and Solutions, First Edition.
Edited by Ponisseril Somasundaran, Partha Patra, Raymond S. Farinato, and Kyriakos Papadopoulos.

Upon surfacing, oil from the blown Macondo well was transported across the northern GoM, where it grounded on shorelines from Louisiana to Florida. Within 9 days of the explosion on the DWH drilling rig, oil entered Louisiana wetlands at the mouth of the Mississippi River. Within a month, oil had coated shoreline beaches and wetlands throughout the Mississippi River Delta, the largest coastal wetland complex in the continental United States. By the time the disabled well had been capped, oil had grounded on shorelines throughout the northern GoM, including sensitive wildlife refuges like the Chandeleur Islands in Breton Sound, and white sand beaches frequented by tourists in Florida, Alabama, and Mississippi. As of January 20, 2011, surveys of more than 4000 linear miles of the northern GoM coast conducted for the preassessment phase of the Natural Resource Damage Assessment (NRDA) documented 1053 miles of oiled shoreline (http://www.gulfspillrestoration.noaa.gov/oil-spill/gulf-spill-data/). The heaviest accumulations occurred in Louisiana as a consequence of currents and prevailing winds directing much of the oil to the west of the mouth of the Mississippi River. As in other states, oil grounded on to barrier island beaches, but much of the shore-bound oil penetrated into Mississippi River Delta wetland ecosystems. Oil entered marsh and mangrove habitats from the Bird's Foot Delta to Terrebonne Bay, including areas located miles inland from the ocean.

Coastal ecosystems of the northern GoM encompass many of the most productive and biologically important habitats in North America. In addition to supporting sensitive resident species like the brown pelican, these areas shelter the majority of overwintering waterfowl that travel the Mississippi Flyway. Northern GoM coastal ecosystems also provide regulatory services such as storm protection, water filtration, and nutrient capture; provisioning services like finfish and shellfish fisheries; and cultural services including heritage tourism, recreation, and aesthetic value. Coastal habitats (e.g., oyster reefs and marshes) in Louisiana alone support 30% of U.S. fisheries production, and it has been estimated that Mississippi River Delta ecosystems generate at least $12–47 billion in annual benefits (Batker et al., 2010). As an economic asset, the Delta has a minimum value of $330 billion to $1.3 trillion, with 90% of its value attributable to services derived from wetlands (Batker et al., 2010). Oil exposure has placed the ecological and economic well-being of the northern Gulf region at risk by potentially affecting many, if not all, of the valued services provided by these coastal ecosystems.

The federal government, state governments, and the responsible party (British Petroleum (BP) Plc.) mounted a vast and complex response effort soon after oil from the Macondo well was detected in offshore waters. Responders were required to make difficult choices among possible interventions, including what steps to take to prevent oiling of shorelines and removal of oil from sensitive coastal ecosystems. Responders had to decide, for example, whether to contain and recover oil via skimming technologies versus chemically dispersing and burning hydrocarbons from the surface of the water. Experiences during prior oil spills have led to a general understanding that response actions can cause more harm than good. Pressurized hot-water washing of oiled rocky intertidal shorelines during the Exxon Valdez oil spill (EVOS), for example, likely induced greater macroalgal and invertebrate mortality than did exposure to oil (Peterson et al., 2003). Even though consideration is now given to the possibility of unintended outcomes, imperfect knowledge of

trade-offs between potential benefits and risks from interventions nonetheless complicated DWH response efforts (Anastas et al., 2010; Peterson et al., 2012).

As in the EVOS, protection and remediation of oiled northern GoM shoreline ecosystems involved weighing potential benefits against risks that interventions intended to reduce damages from oil exposure will instead lead to further injury. Oil removal from coastal wetlands, for example, can reduce acute and chronic exposure of both resident and migratory species, but many traditional removal approaches can cause immediate and enduring damage to fragile soils and sensitive wetland biota. Simply setting foot into salt marshes can result in soil compaction and loss of foundational plants, which can accelerate erosion and lead to permanent loss of marsh habitat. Surface application of dispersants, as was done across northern GoM waters, can reduce shoreline oil accumulations, but it can add petroleum-based (NRC, 2005) into other areas that serve as nursery habitat. Thus interventions, such as diversions from the Mississippi River, can involve protection of one ecosystem at the expense of another. Freshwater diversions intended to provide counterbalancing flows to prevent oil from entering delta wetlands may have collaterally damaged nearby oyster grounds sensitive to low-salinity conditions. Oyster grounds were exposed to the combined influence of oil and freshwater during peak spawning periods, which may have resulted in greater injury to future harvests (i.e., by elevating larval mortality and depressing adult reproduction) than complications from oil exposure alone. Decisions to intervene must also account for how actions may endanger the socioeconomic well-being of communities including cities like New Orleans that depend on coastal ecosystems for income and security.

Despite the possibility of unintended outcomes, interventions were necessary to prevent acute and chronic oil exposure of sensitive biota to oil. As of April 2011, the consolidated fish and wildlife collection report maintained by the U.S. Fish and Wildlife Service (USFWS), which provided daily updates on the number of injuries and deaths of vertebrate species of concern, listed 3596 injuries and 6918 mortalities associated with the spill. In comparison to similar counts following the EVOS disaster, it appears that the Gulf has sustained relatively low levels of damage from the Macondo well blowout (Tunnel, 2010). Acute damages are far less than what many feared would result from the massive release of oil, but little is known about damages that emerge over time and span long time horizons (Peterson et al., 2003). Population- or species-level responses can lag behind a spill when acute exposure to oil and oil-borne contaminants occurs during sensitive life stages. Exposure can interrupt complex life cycles, which can give rise to delayed responses (Peterson et al., 2003). Additionally, lags can emerge if reproduction is depressed by chronic, sublethal exposure or reduced resource availability due to ecosystem-wide disruption of food webs (Peterson et al., 2003).

The persistence of oil in coastal environments more than a year after the DWH blowout indicates that GoM biota have been susceptible to acute and chronic exposure. At the beginning of 2011, the Shoreline Cleanup Assessment Technique (SCAT) program reported that 336 of 1053 miles of oiled shoreline warranted treatment and that at least 83 miles remained heavily to moderately oiled (Owens et al., 2011). Surveys of Louisiana embayments conducted by independent researchers also found

that oil persisted under heavily matted vegetation in Barataria Bay marshes, especially in areas where surfaces are not exposed to weathering (Macdonald et al., 2011). Impervious rinds formed on some surfaces exposed to weathering, which can slow aeration and inhibit microbial activity (Deocampo et al., 2011). A survey of beaches on the barrier island chain fronting Barataria Bay found evidence of buried oil in cohesive layers ≥20 cm thick covered by 10–80 cm of clean sand above the water table and vertically diffuse 10–50 cm thick bands of oil below the water table (Fitzgerald et al., 2011). Oiled sand reworked by wave action coalesced into subtidal tar mats in surf zone depressions that could extend for miles off of some areas of the coast, such as Perdido Key beach on the Florida panhandle.

It is now widely recognized that many of the most pressing questions about shoreline impacts and recovery remain unanswered. Created by an Executive Order on October 5, 2010, the Gulf Coast Ecosystem Restoration Task Force has been tasked with addressing this concern by promoting the development of more effective shoreline remediation strategies. Two key conditions have been identified for redressing shoreline damage from the DWH blowout. First, approaches must be science based. And second, approaches must address oiling, erosion, and subsidence. Oil from the blown Macondo well grounded on to areas of the Gulf coast that are experiencing high rates of habitat loss as a consequence of erosion and subsidence. Marshes in Barataria Bay and other heavily degraded deltaic wetlands, for example, are hotspots of habitat loss. Estimates suggest that oiling more than doubled the rate of annual shoreline erosion (Silliman et al., 2012), with most of the additional loss concentrated in highly susceptible wetlands that provide valuable ecosystem services. Thus, response strategies that only address oiling likely will not result in permanent gains.

Here, we assess the prospects for achieving and implementing a forward-minded response policy of postspill habitat remediation and restoration. Focusing on Louisiana coastal marshes that received the heaviest accumulations of oil, we first review the formulation and execution of conventional response strategies for shoreline protection and remediation. We then examine how novel approaches were evaluated and implemented, including several controversial interventions undertaken to protect sensitive coastal ecosystems during the DWH spill. We also overview the down-selection process of shoreline cleanup approaches with reference to studies aiming to improve the process and outcomes of shoreline remediation. Finally, we identify steps that could be taken to promote ecosystem recovery by linking shoreline remediation with habitat restoration, placing emphasis on local sourcing and novel approaches that reduce operational trade-offs and maximize efficiencies.

3.2 SHORELINE PROTECTION DURING AND FOLLOWING THE SPILL

3.2.1 Oil Spill Response Administration and Structure

The National Contingency Plan (NCP) serves as the federal government blueprint for responding to oil spills in federal waters. In accordance with the plan for coastal zones, the U.S. Coast Guard (USCG) was charged with overseeing the DWH oil spill

and appointed a National Incident Commander after it was declared a Spill of National Significance. The incident command system (ICS) provided the framework for coordinating the effort of the government agency response organizations (NRT, 2011). The agency organizational structure in the spill response, from top to bottom, included:

- The National Response Team (NRT)—15 federal departments and agencies including the USCG, the National Oceanographic and Atmospheric Administration (NOAA), the Department of Interior (DOI), and the U.S. Environmental Protection Agency (USEPA);
- Regional Response Teams (RRTs) and Rapid Assessment Teams (RATs)—cleanup operation staff led by the USCG and USEPA, which have authority over the use of dispersants; and
- Area Committees (ACs)—local government and environmental agency representatives.

As oil came ashore, RRTs commenced local cleanup operations, guided by preestablished Area Contingency Plans (ACPs). Cleanup proceeded in stages following the SCAT process, using surveys and assessments to create stage-specific Shoreline Treatment Recommendations (STRs) (Santer et al., 2011). RRTs deployed operations task forces to conduct cleanup activities using remediation techniques described by STRs until the segment was judged to require "no further treatment" (NFT) (Santer et al., 2011). Evaluations were made according to group consensus among members of a SCAT team, requiring agreement between representatives from federal, state, and sometimes local government or other shareholders, as well as the team lead and representatives of BP (Santer et al., 2011). The transition from cleanup to long-term recovery follows the Shoreline Cleanup Completion Plan (SCCP) as a framework for providing the final definition of NFT for each shoreline type (DWH UC, 2011a). The SCCP was written collaboratively between the USCG, NOAA, DOI, BP, and the Gulf states except for the State of Louisiana, which refused to sign (Schleifstein, 2011). Having the authority to make response decisions, the USCG federal on-scene coordinator nonetheless enacted the SCCP on November 2, 2011 (DWH UC, 2011a, Schleifstein, 2011).

3.2.2 Limitations of Shoreline Protection through Conventional Offshore Treatment

The chemical and physical composition of oil, as well as ocean and climate conditions, determine the behavior and outcomes of offshore oil spills. The same factors influence the effectiveness of methods for removing oil from the ocean surface (Douglas et al., 1996). Crude oil that rises to the ocean surface is conventionally recovered by response teams with containment boom and skimming technology (Figure 3.1). Surface oil can also be eliminated using fire-resistant containment boom for *in situ* burning or aerial and vessel applications of chemical dispersants. Few feasible options are available for offshore treatment, however, once oil undergoes

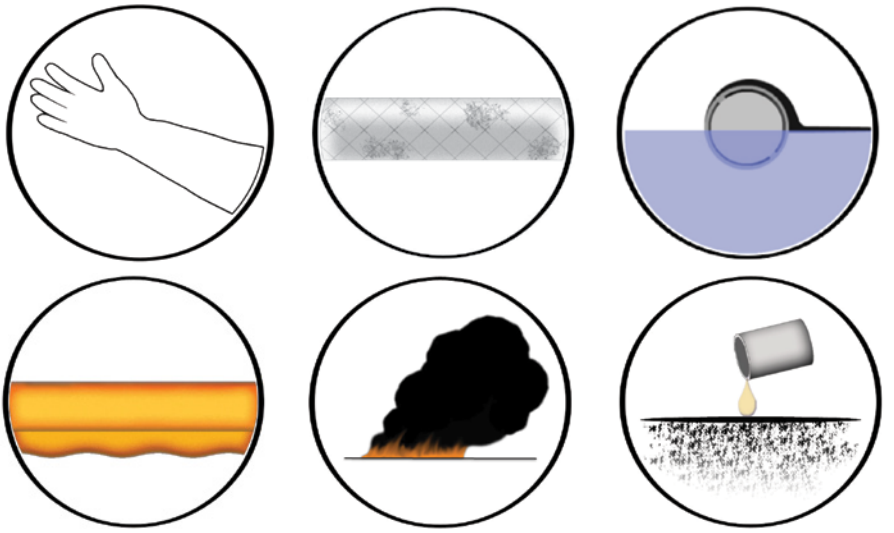

FIGURE 3.1 Conventional oil spill cleanup technology. Top left to right: manual cleanup, polypropylene-filled sorbent boom, and oil skimmer. Bottom left to right: containment boom, *in situ* burning, and chemical dispersant.

weathering through evaporation, dissolution, biodegradation, and photooxidation. Containment, skimming, and burning are not possible as weathered oil loses buoyancy and enters subsurface waters. Surface application of dispersants, which are not designed to break up weathered oil, also becomes unfeasible.

Containment and sorbent boom are often among the first response technologies deployed during offshore surface oil spills. As oil is moved along the surface of the water by current and wind, booming can temporarily hold it in place prior to skimming or burning. Containment boom is either rigid or inflatable, high-strength polyurethane-coated fabric that remains partially submerged below the surface of the water. Containment boom is often outfitted with a vertical skirt that extends below the water surface to improve stability and capture efficiency. White polypropylene-filled sorbent boom works to adsorb oil from the water and is often used in conjunction with containment boom. Boom must be monitored and replaced to keep pace with spill, weather, and tidal conditions. During the DWH event, approximately 4.2 million feet of containment boom and approximately 9.1 million feet of sorbent boom were deployed—considered to be the largest deployment of boom in the history of spill response—to aid in skimming, *in situ* burning, and temporary shoreline protection (British Petroleum, 2010). Eventually, though, monitoring difficulties arising from the magnitude of the deployment, coupled with oil weathering and natural forces (e.g., wind, tide, and currents) overcame the boom, allowing oil to reach sensitive shoreline ecosystems.

Boom is often paired with other technologies to remove oil from the ocean surface. Oil that is contained in rigid boom can be skimmed from the ocean surface into tanks

on board a vessel and transported to shore. Conventional skimmers move the surface water toward a recovery system that transfers surface and near-surface layers of oil–water mixtures into a storage tank. Conventional skimming can prove ineffective under adverse weather conditions that complicate containment and that promote subsurface mixing. Equipment availability and personnel costs are two other major limiting factors to skimming oil from the water. During the DWH event, conventional skimming efficiencies were less than 30% oil to water—a figure not uncommon to offshore oil response (British Petroleum, 2010). Oil that is contained in fire-resistant booms also can be burned from the surface with an incendiary charge to promote ignition. Because of public health concerns, burning is typically considered only when mechanical recovery response methods are incapable of controlling the spill (Team, 1998). In Alaska, for example, burning is necessary when ice prevents skimming operations, but waves must be less than 3 ft high, winds less than 20 knots, and the oil slick thickness must be more than 2 mm for burning to commence. Burns release particulate matter as smoke and soot, polycyclic aromatic hydrocarbons, volatile organic compounds, carbon dioxide, and carbon monoxide into air and water (Aurell and Gullett, 2010). In contrast, burning was implemented over nearly the full course of the DWH event. A total of 411 burns removed an estimated 5% (10.3 million gallons) of oil from the ocean surface (Ramseur, 2010), but concerns remain about acute and persistent exposure of coastal populations and response workers to residual contaminants.

Chemical dispersants are not easily paired with containment or sorbent boom. Chemical dispersants are petroleum solvents that move oil from the water surface to the water column by breaking the surface tension or cohesive capacity of the oil, thus breaking it into smaller droplets. The use of chemical dispersants follows a risk-based paradigm with recognized trade-offs between benefits and harm to the environment (see other chapters herein for more detailed discussions of dispersant properties and use). Chemically dispersed oil is more dilute in the water column, which can reduce acute toxicity. Use of dispersants, however, can increase exposure of marine organisms to contaminants that are more bioavailable or more readily absorbed (Bhattacharyya et al., 2003). The total volume of chemical dispersant used in the GoM during the DWH event was approximately 1.8 million gallons. Dispersants were applied on the ocean surface by plane (“carpet bombing”) or boat. The first subsurface application of dispersants approved by the USEPA also was carried out during the DWH event. Approximately 800,000 gallons (44% of the total used) of dispersants were directly injected into oil flowing from the Macondo wellhead in an effort to prevent oil from reaching the surface near the incident site where crews were working to close the well.

Rapid Assessment Teams provided daily on-site prioritization and identification of oiled areas to the Incident Command Center (British Petroleum, 2010). Because of the sheer scale of the surface spill and the response effort, decisions as to whether to contain, disperse, burn, or skim were sometimes based on the proximity of cleanup teams to surface oil. Vessels are typically equipped with only one response technology, so proximity can sometimes outweigh consideration of net environmental benefits of the response approach available for immediate deployment (Baker, 1995). Disparities between need and availability can reduce the effectiveness of offshore recovery

efforts (Lehr et al., 2010) and consequently contribute to oil grounding on to sensitive shoreline ecosystems where recovery and remediation can be significantly more challenging than in open ocean conditions.

3.2.3 Limitations of Shoreline Protection and Conventional Onshore Treatment

The magnitude of the DWH surface spill and limitations of offshore prevention and containment measures (characterized as "keeping it out" strategies) required implementation of measures to remediate oil contaminated shoreline (characterized as "getting it out" and "getting rid of it" strategies) (USNRT, 2010). Stage I and II shoreline cleanup responses were implemented to treat moderately to heavily oiled shoreline in danger of being repeatedly oiled while the wellhead was leaking (USNRT, 2010). Shoreline Cleanup Assessment Technique teams created general STRs for Stage I and Stage II responses according to whether habitat was sandy shoreline, man-made shoreline, or coastal marshes and mangroves (DWH UC, 2010a). After the Macondo well was capped, SCAT teams shifted to Stage III responses to treat oiled shoreline (Santer et al., 2011). Stage III guidelines were based on SCAT Core Group concerns and Taskforce Working Group recommendations for different habitats (DWH UC, 2010b). Site-specific STRs were also created with the goal of removing enough oil to enable natural attenuation (Santer et al., 2011).

Response methods were selected according to the intensity and form of oiling as well as potential treatment impacts (DWH UC, 2010b). Strategies were guided by concepts underpinning net environmental benefit analysis, where responders clearly recognize what can be achieved before treatment actions become unsafe, become impractical, provide no significant benefit, or become damaging to shoreline habitat (DWH UC, 2010b; Santer et al., 2011). For sand shorelines, which represent perhaps the simplest logistical conditions for shoreline treatment, responses largely involved removal, tilling, and sifting of contaminated sand by crews supplemented with industrial scale equipment like "Sand Sharks" (DWH UC, 2010b). Sand was also cleaned in treatment plants and returned to affected shorelines (DWH UC, 2010b). Coastal marsh habitat presents significantly more challenging conditions for treatment as a consequence of soil and biotic structural complexity (USNRT, 2010). Although oiling mostly occurred along peripheral edges, oil penetrated tens of meters into marsh interiors at some locations, where foundational vegetation was coated to heights ranging from a few centimeters to over one meter due to tidal flux (DWH UC, 2011b; Lin and Mendelssohn, 2012; Silliman et al., 2012; Zengel and Michel, 2013). Thick layers of oil were found trapped in dense stands of vegetation, underneath organic debris (e.g., wrack), and on soil surfaces (DWH UC, 2011b; Lin and Mendelssohn, 2012; Silliman et al., 2012; Zengel and Michel, 2013). Oil also grounded on to root surfaces, which can prevent oil from penetrating deeply into soils. Guidelines for STRs and NFT under the Stage III Shoreline Treatment Plan recognized that treatment of sensitive marsh environments could cause physical harm significantly more detrimental than consequences solely attributable to oiling

(DWH UC, 2010b). The primary response recommended for oiled marshes was natural attenuation, whereby oil would be physically removed by wave action and tides or natural degradation through microbial metabolism and photooxidation (DWH UC, 2010b). Initial plans nonetheless identified a limited set of possible treatment options (depending on site conditions), which included low-pressure or ambient-temperature flushing, contained sorbents, manual removal, vacuuming, and vegetation cutting (DWH UC, 2010b).

Implementation of initial treatment options for coastal marshes proved problematic. Low-pressure, ambient-water flushing, which was permitted from vessels operated from the marsh edge, was not effective against heavy accumulations of fresh and weathered oil (DWH UC, 2010b). Low-pressure flushing techniques were also recommended for use only when tides covered marshes because spray turbulence could suspend sediment and spread contaminants (DWH UC, 2010b). This technique also saw little use because of limited availability in Louisiana; for example, only crews from St. Bernard Parish had access to proper equipment (DWH UC, 2010b). Contained sorbents, typically made of polypropylene, were used on water surfaces to recover oil being released from adjacent shoreline (DWH UC, 2010b). Limited surface area and the adsorbent nature of the boom provided little capacity for use against light sheens. Improperly monitored boom also became stranded in marshes, spreading contaminants, creating debris, and causing physical damage. Manual removal of oil was constrained by limited access and potential damage resulting from foot traffic; even light foot traffic can compact soils and cause significant long-term harm to resident biota in marshes. Consequently, manual oil removal was restricted to areas of marsh with firm sand or shell substrate, where hand tools such as trowels and shovels were used to remove thick accumulations (DWH UC, 2010b). Because of risks to sensitive shoreline, response teams typically only completed partial treatment through manual removal. Similar concerns restricted implementation of portable vacuum treatments to partial removal of oil from marsh shoreline: vacuums could not be operated from an offshore vessel without potentially disturbing and removing soil and sediment (DWH UC, 2010b). Cutting and removing oiled vegetation and organic debris, often with string trimmers and blades, was considered to be too aggressive to serve as a primary response approach. It was permitted on a case-by-case basis, however, for recovering oil trapped in thick stands of *Phragmites australis*. Initial treatment plans prohibited cutting *Spartina* cordgrass and mangrove vegetation (DWH UC, 2010b).

Several treatment methods were identified as being of little potential value because of limited applicability against weathered oil or because oiled materials could not be recovered from the environment. These included deluge flooding, solidifiers, loose sorbent materials, and surface cleaning agents (DWH UC, 2010b). *In situ* burning, where tidal flooding allows for plant regrowth by protecting roots from heat, would have been considered an appropriate remediation tool if the oil had been ignitable and floating freely in marshes (DWH UC, 2010b). Fertilizer additions to promote microbial metabolism and breakdown of oil were also ruled out because northern Gulf coast marshes are not nutrient-limited environments (DWH UC, 2010b). Methods specifically not recommended for vegetated shoreline included mechanical

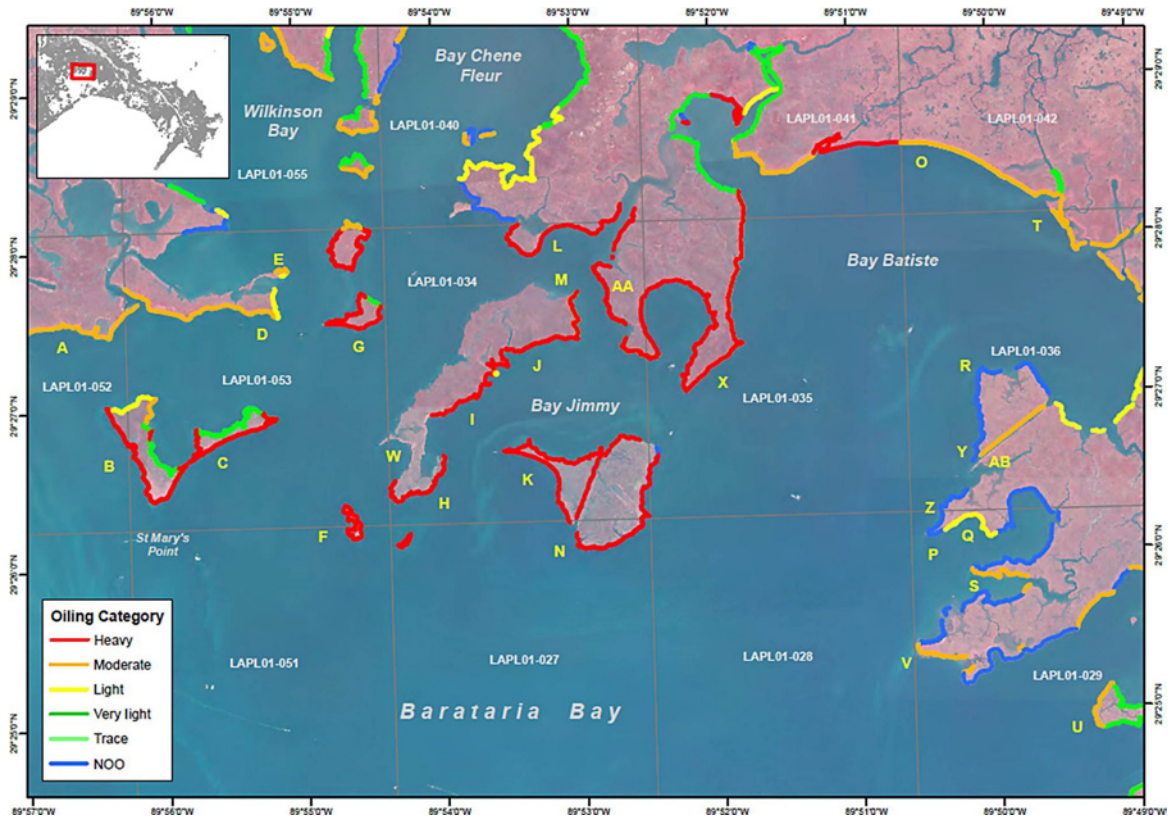

FIGURE 3.2 The distribution and intensity of oiling in northeastern Barataria Bay, Louisiana. Shoreline was categorized and identified for remediation according to the extent of oiling. Shoreline "K" in Bay Jimmy is host to ongoing studies of shoreline remediation and recovery. Map from Zengel and Michel (2013). *(See insert for color representation of the figure.)*

oil removal, sediment reworking/tilling, and any kind of high-pressure or heated water flushing (DWH UC, 2010b). These methods were deemed too destructive because of the likelihood that oil would penetrate further into porous sediment, that substrates would be compacted, or that plants or soil microorganisms would be damaged (DWH UC, 2010b).

The DWH Shoreline Treatment Implementation Framework incorporated guidance and recommendations to minimize potential harm from treatment approaches, citing research literature, agency protocols, and previous oil spill experiences compiled by the SCAT Taskforce Working Groups. The framework outlined appropriate Stage III STRs and NFT goals and was approved by Core Groups made up of stakeholder representatives. Nonetheless, SCAT teams developed STRs that strongly deviated from the Implementation Framework, and the UAC approved the use of aggressive strategies to remove oil from sensitive ecosystems.

The cleanup of marshes in Bay Jimmy (Barataria Bay, Plaquemines Parish, Louisiana), which may have received more oil than any other vegetated shoreline during the DWH event, offers exceptional examples of how cleanup crews implemented aggressive treatment strategies. Across Bay Jimmy (Fig. 3.2), vegetation laid down by waves became trapped under the weight of oil, creating tarry debris mats. Heavily oiled wrack lines subsequently hardened into tarry asphalt. Thick emulsified oil, or mousse, pooled on soil surfaces and became trapped beneath matted vegetation and wrack, preventing degradation. Tidal flushing and compaction nonetheless released buried mousse from exposed marsh. Few options are available to remove heavy accumulations of weathered oil without disrupting vegetated shorelines. The ineffectiveness of conventional treatment approaches, and the threat of additional resources suffering damages from oiling (i.e., contaminants could persist and potentially spread throughout the embayment), prompted consideration of aggressive tactics for remediation of Bay Jimmy shoreline. Following completion of a study to assess potential outcomes (as described in the following text), aggressive measures were implemented to recover oil trapped in marsh soils, vegetation, and debris that would have otherwise remained heavily contaminated (DWH UC, 2011b; Zengel and Michel, 2013).

In Northern Barataria Bay, 11 km of shoreline were treated using aggressive raking and cutting (Zengel and Michel, 2013). Cleanup crews entered marshes, provided that boards were laid down to serve as temporary walkways. Thick mousse was scooped out with shovels, and heavily oiled wrack lines and vegetation mats were raked and removed through manual or mechanical means (Fig. 3.3). Raking and cutting continued until contaminated soil and sediment were excavated, including horizons dominated by organic content. This continued until clean sediment was uncovered, often leaving only plant stubble behind (Zengel and Michel, 2013). When force was required to break through hardened surfaces to reach oiled mats below, tools like hedge trimmer and chain saws were used to penetrate surface tar and remove oiled debris (Zengel and Michel, 2013). A provision was made to allow heavy equipment to be used on a case-by-case basis to scale up treatment and improve response efficiency (Zengel and Michel, 2013). Long hydraulic arms operated from barges or airboats could reach into the marsh with automatic raking, cutting, and

FIGURE 3.3 Aggressive remediation of oiled shoreline in Bay Jimmy (Barataria Bay, Louisiana). Left: cleanup crews manually cutting oiled vegetation (Zengel and Michel, 2013). Right: mechanical removal of oiled material.

excavation attachments, allowing crews to scale up aggressive treatment techniques, but with less precision than manual remediation and increased potential to damage marsh soils. Heavy machinery also enabled debris to be transferred directly from the marsh to offshore disposal containers.

Seasonal conditions prompted shoreline treatment to be expedited (Zengel and Michel, 2013). Access generally improves toward winter months as tides decrease and substrates harden, and removing oil during winter also enables plants to recover the following spring before the beginning of hurricane season. However, shoreline treatment in Bay Jimmy stretched into the summer of 2011, when wet conditions in the marshes increased susceptibility to damage. Nonetheless, the approaching hurricane season raised concerns that unrecovered oil could become resuspended and redistributed, and spurred ambitious STRs for Northern Barataria Bay that prescribed aggressive removal approaches. By the end of September 2011, shoreline remediation crews had manually or mechanically removed over one million pounds of material from Bay Jimmy marshes alone (Zengel and Michel, 2013).

Remediation of vegetated shoreline was further complicated by the nature of on-site reviews of treatment outcomes. Meeting NFT guidelines under the STR for each site requires unanimous agreement between a federal representative (usually NOAA, a NOAA contractor, or USCG), a state representative, and a BP representative on each SCAT team (a landowner might also be involved) (Santer et al., 2011). Representatives sometimes disagree, though, as to what constitutes cleaned shoreline. Variable experience and training can contribute to differing perspectives, including the amount of emphasis placed on risks posed by toxicity and exposure.

Attempts to achieve consensus potentially pushed teams (i.e., particularly those that included determined members) to err on the side of overtreatment, extending well beyond STR guidelines. Yielding to aggressive removal techniques to obtain an immediate measure of remediation arguably reflects the difficulty of quantifying potential impacts of remaining debris or impacts arising from treatment.

3.3 ADVANCEMENT THROUGH FAILURE AND INNOVATION

The 1989 EVOS in Prince William Sound (Alaska) exposed troubling limitations in response technologies and approaches, including the design and implementation of chemical dispersants and shoreline cleaning agents. The EVOS resulted in passage of the Oil Pollution Act (OPA) in 1990, which created an interagency committee responsible for coordinating oil spill response research and technology development. Adopting the principles established by the OPA, some states (including California and Alaska) now explicitly require that oil spill response make use of the best available or "achievable" technologies. Under the OPA, spill response is intended to keep pace with advances in oil and gas exploration through a system of exercise drills, specialized training, and contingency planning (USEPA, 2011). Yet, response improvements have largely been motivated during oil spill events rather than from preparation between spills (Epperson, 2011). The logic of this is simple—interim preparation and planning based on past spill events and potential contingencies will not necessarily reflect novel conditions emerging from unfolding events. Little innovation will come from practice exercises and spill response training limited to a predetermined range of spill scenarios. The frequency and scope of exercises may also reduce the likelihood that innovations to improve deficiencies will emerge from planning and exercises (Epperson, 2011). In any given area of concern, exercises are held once every 3 years and may only involve participation of one "responsible party" (Epperson, 2011), which can prevent interactions among regulatory and industry partners (i.e., a port may have anywhere from 25 to 250 regulated entities) and limit knowledge of ACP. Furthermore, few clear mechanisms exist after exercises for sharing lessons, best practices, or new knowledge (i.e., of corrective actions) gained by agencies and outside partners.

Given the structure of the OPA, it is not surprising that the best available response technologies and approaches did not adequately address the range of conditions that emerged during the DWH event. The experimental use of dispersants is among the most widely recognized outcomes of the limited range of innovations that were achieved prior to the spill. Lisa Jackson, the administrator of the USEPA, described the novel use of dispersants as "somewhat trial and error," with concerns ranging from the potential impact of the volume of dispersants applied, effectiveness of dispersants at depth in low temperatures and high pressure, oil weathering as it rose to the surface, and environmental effects of dispersant in deep-ocean environments. Indeed, the Region 6 RRT Regional Integrated Contingency Plan lists one of the disadvantages of subsurface dispersant use as "lots of unknowns" (USEPA, 2011).

3.3.1 Evaluation of Alternative Response Technologies

Recognizing the need for innovation, the Unified Command implemented the NOAA-led alternative response technology evaluation system (ARTES) as response efforts proceeded during the DWH event. ARTES was developed to help identify viable spill-specific response tools through the evaluation of tools based on technical merit. Traditionally, ARTES only considers chemical and biological

countermeasures, but the program was expanded during the DWH event to include mechanical countermeasures. The ARTES program consequently considered a range of technologies including oil sensors, booms, skimmers, decontamination and waste minimization technology, shoreline cleaning machines, and source containment innovations (Addassi, 2010).

The ARTES was modified during the DWH event to include four primary stages of review. There were four mechanisms for vendors wishing to introduce alternative technologies for use during the spill—Unified Command center walk-ins, website submission (www.horizonedocs.com), community meeting forums, and VIP submissions. VIP submissions were prompted by requests from high-ranking government officials or high-profile individuals or because the candidate technology garnered mass media attention during the course of the spill. Technologies that passed Stage III review were considered for field testing and potential adoption. Of the approximately 123,000 submissions, approximately 100 reached Stage IV field testing, and only 25 technologies were adopted (Addassi et al., 2011). Several of the field tested technologies originated as VIP submissions. These included the following.

3.3.1.1 Human Hair Sorbent Boom

Alternative sorbent technologies, including human hair, were considered for oil adsorption as a consequence of public pressure arising from extensive media exposure of a grassroots effort orchestrated by the nonprofit organization Matter of Trust (www.matteroftrust.org) to introduce the use of natural fiber as a filler material for sorbent boom. Media attention, which included interviews with the director of Matter of Trust by National Public Radio and the British Broadcasting Corporation, resulted in the donation of more than a dozen >10,000 square foot warehouses for storage and fabrication of hair booms across the Gulf coast. Hundreds of pounds of hair were received daily during the height of media coverage, with volunteers working to fabricate sorbent boom. Field tests of the boom, carried out by BP near the Incident Command Center in Mobile, Alabama, revealed that it did not float and therefore did not meet established criteria for sorbent boom.

3.3.1.2 A Whale Skimmer

A Taiwanese-made 1115 foot freighter, built originally as an oil/bulk/ore (OBO) carrier, was modified during the DWH event for oil skimming (Froomkin, 2010). According to maritime reports, the ship was in Rio de Janeiro awaiting orders when it then traveled 4240 nautical miles to a shipyard in Setubal, Portugal, for skimming modification. A series of twelve 16 foot slots were cut in the forward hull of the ship, allowing oil–water mixtures to pass into existing internal tanks where oil would separate from water by gravity. The water would then be returned to the ocean, and the oil would be held on the vessel for transport to a shoreside facility. On July 3, 2010, the BP, the USEPA, and the USCG conducted a test of the vessel's oil skimming ability. The USCG subsequently reported that *A Whale* recovered negligible amounts of oil. Limited to speeds of 2–3 knots, *A Whale* did not efficiently capture oil–water mixtures through its passive intake system (Rioux, 2010). Smaller Vessels of Opportunity were comparably more efficient and considered to be logistically more nimble than the modified freighter.

3.3.1.3 Costner Centrifuge

Blue Planet Water Solutions (BPWS) is a recently formed company founded by actor–director–producer Kevin Costner in collaboration with partners based in New Orleans. The mission of BPWS is to develop advanced oil–water separation technologies for oil spill cleanup. The company's foundation oil separation technology, which was transferred from the Department of Energy to Costner Industries Nevada Corporation (CINC) in 1993, is capable of highly efficient mechanical separation across a range of throughput conditions on board spill response vessels. The BPWS liquid–liquid centrifugal separator unit utilizes the force generated from rotating an object around a central axis. Spinning two fluids of different densities within a rotating container results in the heavier fluid being forced to the exterior walls of the rotor and the lighter fluid being forced to the center. Separation of oil and water can yield water of more than 99.999% purity and oil of more than 99.5% purity, depending on the nature of the crude oil, extent of weathering after the spill, receiving water chemistry, and state of oil emulsification.

With the assistance of Plaquemines Parish President Billy Nungesser, BPWS approached BP about carrying out field tests to evaluate potential applications of the company's centrifugal separation technology. The BPWS Integrated System was tested by BP in April 2010, after which engineers from BP and BPWS worked in concert to optimize the BPWS Integrated System to process recovered oil of various ages and in varying states of emulsification. After roughly a month of ongoing testing and optimization, BP leased 32 of the BPWS Integrated Systems, 8 of which were installed on *Edison Chouest Offshore* platform supply vessels (Fig. 3.4). In addition, two shallow-water barges from D&L Salvage and two deepwater barges from *Hornbeck Offshore Services* were outfitted with the BPWS systems to enhance onboard storage capacity via rapid dewatering of skimmed oil (Fig. 3.4).

During the course of the spill response phase, BPWS and its engineering partners integrated centrifugal oil dewatering with membrane-based water filtration technology.

FIGURE 3.4 Two BPWS Integrated Systems installed on the D&L Salvage spud barge *The Splash* (left) and four BPWS Integrated Systems installed on *Edison Chouest* platform supply vessel *ELLA G* (right).

The "centrifuge plus membrane" approach proved capable of rapid dewatering of skimmed oil followed by purification of effluent water to nondetectable levels of crude oil hydrocarbons. In comparison, the use of nonmembrane-based water filtration technologies (e.g., nutshell, coalescer, or organoclay media) did not significantly reduce crude oil hydrocarbon levels below that achieved by the centrifuge alone. Blue Planet Water Solutions and its engineering partner Water Planet Engineering (WPE) have subsequently designed a new centrifuge and membrane-based sediment–oil–water separator to handle small and large volumes of oil and water at throughputs of up to 400 gallons per minute within a footprint of a standard shipping container. The separator system, which is now referred to as the "*WPE Vorti-SEP™ Advanced Sediment-Oil–Water Separator* designed for BPWS by WPE," can handle changes in liquid ratios from 10:1 oil-in-water to 10:1 water-in-oil mixtures with similar efficiencies. Performance also can be adapted (in real time) to fluctuations in oil rheology, emulsification, flow rate, water quality, and temperature.

The BPWS *WPE Vorti-SEP* system is arguably among the best available oil spill response technologies. The use of technologies like the BPWS system can help to reduce use of conventional technologies and approaches—including chemical dispersants, burning boomed oil, and the use of oil adsorbent media—that can leave troubling environmental footprints. The BPWS system serves as an exceptional example of how the development and adoption of innovative treatment technology can increase the efficiency of oil spill recovery operations (e.g., improving the quantity and quality of recovered oil) while also addressing environmental concerns such as reducing hazardous waste disposal and discharging skimmed water that meets or exceeds clean water standards.

Ensuring that future spill responses make use of the "best available technology" requires that incentives to innovate and technology review programs be maintained on a permanent basis. A collaborative effort between federal and state agencies is now underway to revise the structure of ARTES so that it is available between oil spill events, with the goal of continuously improving spill response technologies. Nonetheless, it remains unclear whether sufficient incentives (e.g., grant programs, tax subsidies, industry safety regulations) will be emerge so that innovation and advancement of spill technologies does not wane.

3.3.2 Shoreline Interventions

Actions taken to keep oil from grounding on northern Gulf coast shorelines extended well beyond technology review and approval through the ARTES program. The demand for novel approaches and solutions to reduce risks of shoreline contamination increased with the growing magnitude of the DWH spill. Media and institutional pressure, sometimes from state and regional authorities, to protect shorelines resulted in major interventions being proposed and executed. The construction of temporary sand berms, restriction of tidal inlets, and diversion of Mississippi River flows were three highly controversial (i.e., of high risk and uncertain outcome) interventions executed to reduce the likelihood of oil entering sensitive coastal ecosystems.

3.3.2.1 Barrier Sand Berms

One month after the DWH rig exploded, the Louisiana Office of Coastal Protection and Restoration (OCPR) applied for a permit to build sand berm barriers to protect shorelines to the east and west of the Mississippi River outlet. The purpose of the project was to move 20 million cubic yards of dredge sediment seaward to the existing barrier island system in an effort to mitigate flow of oily seawater into the Mississippi Delta region. The OCPR application argued that the berm structures could function as geomorphic obstructions capable of protecting sensitive coastal ecosystems far more difficult to remediate than sandy substrate. The Louisiana Barrier Berm Oil Spill Response Project was approved by the Army Corps of Engineers on May 27, 2010 (USACE, 2010), with the USCG instructing BP to provide $360 million for construction of 74 km of sand berms on the Chandeleur Islands and from Scofield Island to Timbalier Island as part of the ongoing oil spill response. By November 22, 2010, however, only 20 km of berm had been completed according to the permitted plan.

Critics of the project—which was largely designed by a dredging company prior to the DWH event to help reduce saltwater intrusion into the delta—expressed concerns reflecting value, logistics, and functional outcomes. At least 1 million m^3 of material would be necessary to build 74 km of berms at the proposed 2 m height (Bahr, 2010). Suitable materials are limited in the areas where the berms were to be constructed (Finkl et al., 2006; Kulp et al., 2005), and much of the material in the areas of concern had already been identified for future barrier island restoration projects. Dredging of material in the targeted areas also could have resulted in displacement or mortality of benthic biota. By reducing seafloor elevations, for example, dredging can potentially reduce areas used by benthic biota as refugia during seasonal periods of anoxia (Erftemeijer and Lewis, 2006; Wilber and Clarke, 2001). Critics also argued against dedicating large amounts of response resources to temporary structures that might not function as expected (Martinez et al., 2011). Sand berms are immediately susceptible to erosion from wave action, especially during hurricane season. Assimilation of the berms into the littoral budget of the protected islands was presented as a potentially positive outcome of the project (Martinez et al., 2011), but critics viewed this as a suboptimal and costly use of limited resources. Noting many of these concerns, the National Commission on the DWH Oil Spill and Offshore Drilling (2011) concluded that the berm project was arguably "the most expensive and perhaps most controversial response measure deployed to fight the Deepwater Horizon spill."

3.3.2.2 Inlet Restrictions

During the DWH event, inlets located between barrier islands or at the mouth of estuaries functioned as potential gateways for oil to cross into inland waterways and ground on to interior shorelines. Recognizing the potential for oil to pass through inlets, state and parish authorities in Louisiana proposed closing the mouth of Barataria Bay with rock and barges. Coastal scientists expressed concern in response to the proposal, indicating that the project could have lasting detrimental consequences. By reducing tidal-driven sediment and water exchange, restriction of inlets

can profoundly alter the physicochemistry of inland waters and ecosystems (Goodwin, 1996; Kraus and Militello, 1999; Martinez et al., 2011). Changes in salinity, oxygen levels, and turbidity of inland waters (Chaibi and Sedrati, 2009) can subsequently result in mass mortality of inland biota (e.g., fish kills). By increasing tidal flow velocity, inlet restriction also can promote scouring and loss of adjacent shoreline (Martinez et al., 2011). Although the permit request for the planned inlet closures for Barataria Bay was denied by the USACE, a similarly minded plan was executed on Dauphin Island at the mouth of Mobile Bay in Alabama. Referred to as the "Katrina Cut" project, geotextile tubes and riprap fill were used to close a gap in the island created by storm surge from Hurricane Katrina in 2005. The Katrina Gap closure was initially intended to be temporary, but it is now likely that the inlet will remain closed (Martinez et al., 2011).

3.3.2.3 Freshwater Diversions

Soon after the oil spill commenced, the State of Louisiana opened two diversions (with maximum discharge rates of 150–200 m^3/s) to allow freshwater from the Mississippi River to flow into Barataria Bay and Breton Sound. Diversions had previously been carried out to regulate salinity conditions and to deliver sediment for coastal restoration, whereas the intended outcome of the diversions during the DWH event was a countervailing force capable of preventing the flow of oil into inland waters and coastal ecosystems. No evidence is available that suggests the freshwater diversions prevented or reduced the flow of oil into inland waters and ecosystems (Martinez et al., 2011). It is becoming clear, however, that the diversions resulted in water quality conditions unfavorable to some of the coastal ecosystems, such as oyster reefs, slated for protection. The productivity of oyster grounds exposed to elevated freshwater conditions is expected to be depressed for a subsequent period of at least 3 years (Greater New Orleans Inc. Regional Economic Alliance, 2010).

Although the decisions to construct sand berms, fill inlets, and divert freshwater may indicate otherwise, innovation in spill response will likely be a defining element of the DWH legacy. The costly and controversial interventions undertaken during the DWH event underscore the importance of basing spill response strategies on sound scientific knowledge so that outcomes do not undermine long-term coastal management plans. Perhaps even more so than the EVOS, the DWH spill has promoted greater awareness and appreciation that logistical and technological challenges must be overcome while being mindful of ecological conditions to effectively recover and sustain valued ecosystem services provided by oiled shoreline habitats.

A growing body of research begun soon after the Macondo well blowout will undoubtedly help advance oil spill response in the GoM and elsewhere. RAPID grant funding from the National Science Foundation (NSF), for example, provided support for a suite of studies on GoM marine and coastal ecosystems. Although the policy of NSF RAPID funding is to provide time-sensitive support for basic science, many of these studies were intended to assess outcomes of oil being released into the Gulf. Studies intended to evaluate the influence of oil on the structure of salt marsh and estuarine food webs, for example, can also provide a basis for assessing whether species interactions and trophic cascades extend the footprint of exposure beyond immediate

contact (Graham et al., 2010). Other studies intended to evaluate biogeochemical outcomes of carbon subsidies from oil degradation can help determine the potential for manipulating resources (e.g., nutrients) to optimize plant and microbial breakdown of oil under recalcitrant conditions. The legacy of advancement will be considerably extended through funding made available by BP for applied research on oil spill dynamics and outcomes. Managed by the Gulf of Mexico Research Initiative (GoMRI), this 10-year $500 million program aims to build comprehensive knowledge of oil spills. The program will undoubtedly offer stronger platforms for innovation in oil spill response, including improved methods for shoreline remediation.

3.3.3 Proving Grounds for Shoreline Remediation and Restoration

Bay Jimmy has become a proving ground for determining how to advance the process and outcomes of shoreline remediation, with the goal of identifying clear pathways toward recovery. Remediating oil from coastal marshes presents technical (i.e., what approach will remove the greatest amount of oil while doing the least harm?) and logistical (i.e., when and how rapidly should oil be removed?) challenges that can involve trade-offs. Without greater understanding of potential outcomes of alternative treatment approaches, decisions to escalate remediation to meet immediate demands could jeopardize long-term ecosystem recovery. It is possible, for example, that reducing environmental exposures to oil may come at the expense of marsh integrity. Wholesale removal of soil, organic debris, and plant cover during treatment also can endanger marshes by reducing elevation via loss of above- and belowground biomass and subsidence through elevated metabolism of subsurface organic soils following exposure to oxygen (Hatton et al., 1983; Nyman et al., 1993, 2006; Turner et al., 2006; Walker et al., 1987). Aggressive remediation that increases inundation and erosion can result in greater rates of marsh loss and conversion of shorelines to open water, especially in areas like Barataria Bay where background rates of loss are among the highest on the Gulf coast (USGAO, 2007). Alternative approaches that leave oil in marshes may not immediately eliminate risks of chronic exposure and toxicity, but marsh platforms remain largely intact as risks of exposure decline over time due to natural attenuation, burial, and weathering.

Recognizing that marsh habitat is difficult to regain once it is lost, the Unified Incident Command approved a plan for conducting tests in Northern Barataria Bay to evaluate outcomes of aggressive treatment approaches. Led by Dr. Scott Zengel, a scientist overseeing shoreline assessment for NOAA, a remediation treatment study was implemented to improve decision-making for ongoing marsh cleanup efforts (Zengel and Michel, 2013). The study was designed to evaluate three primary treatments (vegetation cutting, vegetation raking, and vegetation raking followed by cutting), followed by four secondary treatment techniques (low-pressure flushing, two types of surface washing agents, and vacuuming). Comparisons were drawn to areas that received no treatment (i.e., areas set aside to undergo natural recovery) and uncontaminated areas that served as controls. On shoreline “K” of Bay Jimmy (Fig. 3.2), treatments were randomly assigned across plots measuring 8.5 m along the water’s edge and 10 m toward the marsh interior, including the oiled wrack line

bounding landward contamination. Unexposed control sites were located on nearby shorelines. Treatments were applied adaptively, allowing ineffective techniques to be discarded as tests proceeded. For example, vegetation cutting using a weed trimmer was immediately abandoned after various cutting attachments failed to remove oil mats, even after plots underwent preparatory raking. Instead, raking was used to break up oiled mats until the mousse below was exposed to weathering.

Early observations revealed no difference in oil characterization following the initial treatment tests. Vegetation left standing had subsequently laid down, trapping oil beneath a new tarry mat. Subsequent tests employed more aggressive techniques, including raking down through the oil and cutting vegetation with articulating hedge trimmers on poles. Mousse was raked onto standing vegetation, allowing it to be cut out and removed with exposed plant growth. Raking and cutting were alternated until only clean sediment remained. Responders gathered oiled debris for disposal and then proceeded to test secondary treatment options. Low-pressure washing and each of two surface washing agents (CytoSol and PES-51, both NCP Product Schedule listed) were tested in three different plots. These treatments resulted in scouring upon application and failed to release oil from the marsh beyond sheening. Vacuuming from marsh boards resulted in the recovery of more water and sediment than oil and also promoted subsurface penetration of oil. Further tests of secondary treatment techniques were consequently canceled.

Conditions in the treatment and control plots were monitored on a monthly basis from October 2010 through September 2011 following SCAT protocols to characterize oil, sediment chemistry, vegetation cover, and benthic macroinvertebrates. SCAT assessments measure oiling distribution (length, width, percent cover), oiling type (oiled wrack, oiled vegetation/debris mats, oil on standing vegetation, oil on/in substrate), oil thickness, and oil character (liquid oil, mousse, surface residue, tar, etc.). Cross sections from dominant oiling zones also are used to quantify oil burial, penetration, and mixing into subsurface sediments.

Preliminary findings of the remediation study indicated that aggressive treatment enabled effective recovery of oil without jeopardizing marsh integrity. Aggressive raking and cutting were the only treatment that completely and persistently removed oiled vegetation mats and that left no evidence of increasing oil penetration or mixing in subsurface sediments. Vegetation regrowth appeared to be greater in aggressively treated plots than other treatment plots, which in turn experienced greater regrowth than plots undergoing natural recovery. Preliminary surface sediment chemistry data, however, indicated that total petroleum hydrocarbons and polycyclic aromatic hydrocarbon content did not differ across the treatments, though levels were slightly lower and more weathered in aggressively treated plots.

The treatment study implemented in Bay Jimmy represents an innovative effort to provide standardized, replicated comparisons of treatment options to inform ongoing remediation efforts. Follow-on studies are nonetheless necessary to provide more rigorous understanding of postremediation shoreline recovery. Coastal marsh responses to disturbance can span years to decades. Plant responses, soil oxidation, rates of decomposition, and consequences of compaction, subsidence, and erosion are all important ecosystem characteristics that have not yet been assessed. Continued

monitoring of the treatment plots represents a singular opportunity to track ecosystem recovery following alternative shoreline remediation approaches. Yet, it is unclear whether the treatment plots will remain available for study. Completion of Stage III response requires that all oiled shoreline receive treatment to satisfy NFT guidelines. Petitions have been filed to exempt the study plots from treatment, highlighting how useful continued research would be for future oil spill responses.

Bay Jimmy has also become a proving ground for achieving better integration of remediation and restoration. Undertaking restoration alongside remediation—something that could be referred to as "restorative remediation"—could enhance treatment and recovery of sensitive ecosystems such as coastal marshes in erosional environments (Bergen et al., 2000). Under the current plan, restoration is not part of the NCP and NIMS. Barring a settlement, restoration follows completion of the NRDA process: after data is gathered to determine resource injury, economic and scientific studies are conducted, a restoration plan is developed, and trustees identify restoration projects of interest (NOAA, 2012). Consequently, years can pass between shoreline remediation and restoration. Long delays between remediation and restoration elevate risks of habitat loss and consequent losses in dependent species and valued ecosystem services (Bergen et al., 2000), especially for erosional environments like Bay Jimmy. Restorative remediation (as compared to emergency restoration or restoration following the NRDA process) can potentially reduce responsible party costs and long-term natural resource damages. Restorative remediation might also reduce costs by eliminating redundant logistical expenses, as restoration could be readily implemented via response personnel and equipment marshaled for shoreline treatment. Denuded shorelines in Bay Jimmy, for example, could have been anchored with plants to replace lost vegetation after remediation crews removed oiled material. Although concerns about rates of survivorship of transplants in oiled sediments must be addressed (Bergen et al., 2000), integrating restoration with remediation could alleviate concerns of loss while making better use of available resources.

Studies are being carried out in Bay Jimmy to assess the outcome of alternative restoration approaches in areas where remediation has left behind exposed shoreline at risk of inundation and erosion. A series of test plots were established in July 2011 through academic–industry–agency partnerships (led by Tulane University, WPE, and BPWS) to evaluate the recovery of exposed shorelines planted with native and cultivated smooth cordgrass (*Spartina alterniflora*) genotypes. Smooth cordgrass functions as an "ecosystem engineer" by regulating physical and biological conditions independently of the local environment (Seliskar et al., 2002). The addition of smooth cordgrass to remediated shoreline can prevent marsh loss by trapping mineral sediment, adding organic biomass to substrates, and armoring platforms against tidal erosion. Replanting shorelines may also encourage oil degradation by oxygenating soils, elevating microbial metabolism in soils, and uptake of hydrocarbons from soils (Lytle and Lytle, 1987; Pezeshki et al., 2000; Sandmann and Loos, 1984; Walton and Anderson, 1990). Different smooth cordgrass genotypes, however, exhibit variation in functional performance. Properties known to vary according to *S. alterniflora* genotype range from plant community composition (Proffitt et al., 2005), microbial

activity and diversity (Nie et al., 2010; Seliskar et al., 2002), organic matter distribution, and the presence of fish larvae (Seliskar et al., 2002). Marsh restoration projects in Louisiana nonetheless are now required to use a single smooth cordgrass genotype, referred to as Vermilion, which has been cultivated for maximum aboveground biomass, disease resistance, and transplantation survival at the expense of other traits such as belowground biomass (Utomo et al., 2008). The use of cultivars for marsh restoration can alter local gene pools through replacement or admixture with native genotypes. By extension, conventional restoration can result in unexpected and potentially undesirable ecosystem properties.

The test plots in Bay Jimmy have been planted with arrays of native genotypes, Vermilion, and other cultivar genotypes to first assess how planting contributes to the recovery of remediated shoreline and to also assess how use of different parent stocks can influence ecosystem attributes. For each plot, bare-root stems were hand-planted in four rows perpendicular to the shoreline, spaced on 1 m centers (Fig. 3.5). Planted rows began 5 m from the water's edge, with each row containing 11 stems spaced 0.5 m apart. Baseline characteristics of soil structure and content, surface and subsurface hydrocarbon content, and plant productivity were measured prior to planting. Plot characteristics have subsequently been monitored on a monthly basis, with additional information on accretion rates, soil stabilization, and soil development collected at quarterly intervals. By capturing regular and stochastic disturbances, such as storm events, the study will offer exceptional opportunities to assess shoreline resilience.

Improving restoration technologies to decrease the labor, expense, and risk associated with planting marsh vegetation could further promote recovery of remediated shorelines. Because smooth cordgrass exhibits low seed viability, restoration projects often involve manual installation of plants. Using stems, plugs, or containers costs an average of $9000 per acre in Louisiana CWPPRA projects and requires labor ranging from 25 to 125 h/acre (Leonards, 2008; USGAO, 2007). Besides the costs involved, logistical challenges of manual installation limit the feasibility of large-scale implementation. Salt marshes are often remote environments that are difficult to access. Also, marsh substrates are fragile, so entry and movement within a marsh can result in considerable damage.

Members of the academic–industry–agency partnership are undertaking additional transplant studies in Bay Jimmy to test prefabricated technologies that aim to address some of these concerns. Biodegradable mesh tubes have been designed and built to

FIGURE 3.5 Shoreline restoration studies being conducted in Bay Jimmy; transplant plot (left), propagation tube plot (center), and detail of propagation tube (right).

contain smooth cordgrass rootstock in a bagasse growth medium (Fig. 3.5). Bagasse is a waste product left over from refining sugarcane that is readily available from the Louisiana sugarcane industry. Diverted from processing plants, it can be supplemented with organic substrate to create a mixture that facilitates plant establishment. This design enables plants to be introduced to targeted restoration sites by simply laying out and securing "propagation tubes" on exposed shoreline. Incorporation of plants into the design allows natural root growth to help anchor tubes securely to the marsh. The tubes therefore promote regrowth while armoring shorelines against erosion.

During experimental trials conducted in Bay Jimmy, tubes were established in plots measuring 15 m wide along the shore and 15 m long from shore. The propagation tubes were initially arranged as a comb with four tubes perpendicular to the shoreline (spaced 1 m apart) abutting a fifth tube that was placed on top of the shoreline scarp. The tubes were secured with wooden furring strips at 1 m intervals. This arrangement proved unstable, however, during storm events. In subsequent trials, the comb arrangement faced the water, which minimized stress from wave impacts (Fig. 3.5). This configuration also caused the interior tube to trap debris carried to shore, resulting in the rapid development of organic wrack. Other preliminary observations indicated that the propagation tubes reduce marsh restoration labor and expense while increasing the pace of shoreline development and facilitating lateral growth of the marsh surface. Smooth cordgrass root masses in deployed tubes exhibited nearly 100% survivorship, and the slow deterioration of the tubes appears to be enabling plants to become firmly embedded in the marsh platform as root expansion take place. Further monitoring and additional trials will be necessary to quantify rates of regrowth, shoreline development, and marsh accretion (Bergen et al., 2000).

3.4 CONCLUSIONS

The Macondo well blowout resulted in an environmental disaster of global proportions. In an era of energy production shifting away from coastlines, it has redefined our understanding of risks associated with deepwater wells. It has enhanced our awareness of the intricate complexity of communities whose livelihoods rely as much on the energy sector as on fisheries that are at risk from well blowouts. The disaster has also refocused our attention on Gulf coast ecosystems, including at-risk areas of the Mississippi River Delta that sustain ecological and cultural resources of national importance.

Understanding of ecological and related economic outcomes of the DWH oil spill remains cursory, including potential timelines of recovery (i.e., return to a state comparable to states exhibited by uncontaminated sites). Based on commonly measured ecological parameters (e.g., vegetative cover and structure, species diversity, petroleum hydrocarbon concentrations in soils), recovery times for oiled marshes can range from a few weeks to decades. Recovery times spanning years to decades have been documented for marshes in cold-temperate environments that were heavily exposed to fuel oils such as bunker C or no. 2 fuel and that were damaged by intensive

remediation methods (Hoff, 1995). Under recalcitrant conditions (Baker et al., 1993; Getter et al., 1984; Hambrick et al., 1980), oil persisting in buried sediments can continue to influence the integrity of coastal ecosystems long after a spill. Four decades after the 1969 *Florida* barge spill in Wild Harbor (Massachusetts), oil remaining in marsh sediments continued to stunt belowground growth, with affected areas exhibiting lower marsh elevations and greater bank erosion (Culbertson et al., 2008). Long recovery times were also found following a spill in Buzzards Bay, Massachusetts; the *Miguasha* spill in Canada; the *Metula* in Chile; and the *Amoco Cadiz* in France (Baca et al., 1987; Baker et al., 1993; Hampson and Moul, 1978; Vandermeulen and Jotcham, 1986). Recovery times of less than a year were found for marshes in warm climates that experienced light to moderate oiling with light crude oil and little or no remediation (Hoff, 1995). Several of the spills resulting in short recovery times have occurred in Galveston Bay and other areas of Texas (Hoff, 1995). Similar recovery rates might be expected following the DWH spill (i.e., evidence of natural recolonization and regrowth has been found in some oiled marshes), except that oil from the blown Macondo well grounded on to erosional shorelines and heavily degraded deltaic wetlands–hotspots of habitat loss. Aggressive remediation that strips marshes of plants and sediment could compound injury or fully prevent recovery, given the distinct possibility of accelerated habitat loss (Baca et al., 1987; Bergen et al., 2000; Lin and Mendelssohn, 2012; Mendelssohn et al., 2012; Silliman et al., 2012; Vandermeulen and Jotcham, 1986).

Redressing shoreline damage from the DWH event requires science-based approaches that address the trifecta of oiling, erosion, and subsidence. In the future, embracing a policy of shoreline remediation followed by habitat restoration can promote postspill recovery while preventing habitat loss from erosion or subsidence. Restoration should not be considered a consequent step to remediation, but rather an important remediation technology in its own right, imperative to protecting oiled shoreline from damage and loss. The potential for restoration to promote postspill recovery through revegetation or accelerating natural recolonization has been widely recognized (Baker 1971; Dicks and Levell, 1989; Krebs and Tanner, 1981; Webb and Alexander, 1991). Baker (1971), for example, suggested that faster recovery of marshes might be achieved by planting *Spartina* shoots directly into oil-laden sediments. This suggestion is supported by Lin and Mendelssohn (1998), who showed that *S. alterniflora* can successfully recolonize areas with oil concentrations as high as 250 mg/g so long as the oil is sufficiently weathered. Although little formal work has been done to assess postspill restoration outcomes, Bergen et al. (2000) found that replanting significantly improved marsh recovery after the 1990 *Arthur Kill* oil spill in New Jersey. Oiled salt marshes where smooth cordgrass was replanted exhibited 70% vegetative cover after 3 years, whereas only 5% coverage was achieved at oiled sites that were not replanted (Bergen et al., 2000). The treatment study and follow-on restoration studies in Bay Jimmy represent important steps toward achieving greater understanding for Gulf coast marshes.

Restoring oiled shorelines to conditions comparable to natural ecosystems is a deceptively simple goal. Conventional restoration practices often fail to recover original levels of ecosystem function and structure (Moreno-Mateos et al., 2012).

Understanding the ecological outcomes of practical trade-offs can help minimize undesirable outcomes. Some choices made during project execution, as simple as the spacing of transplanted propagules, can lead to failure. Other choices, such as replanting shorelines with ecosystem engineers (e.g., smooth cordgrass), can modify ecosystem attributes and result in alternative states that will never resemble reference conditions (Moreno-Mateos et al., 2012). Although conventional practices can serve as precautionary measures to ward off the specter of habitat loss, innovative methods for shoreline restoration may prove critical for the recovery of Gulf coast ecosystems.

Shoreline remediation and restoration should be guided by comprehensive coastal restoration plans. It has long been recognized that coastal ecosystems of the northern GoM, and in particular wetlands of the Mississippi River Delta, are in dire need of restoration. Vast areas of the Mississippi River Delta are being lost and will continue to disappear without restoration being undertaken at a grand scale. Many of the challenges of coastal restoration are well recognized and are being addressed in regional and statewide plans (e.g., CPRA, 2010) that have broad support from coastal scientists and stakeholders. These plans can serve as a secure platform for remediation and restoration of oiled shoreline. New challenges may surface, however, as information becomes available from ongoing studies of coastal ecosystem responses to oiling. Accordingly, greater reciprocity between oil spill response efforts and coastal restoration planning will help ensure that progressive measures are taken to secure the future of Gulf coastal ecosystems.

REFERENCES

Addassi YN. Interim operational report. Alternative Response Technologies (ART) Program. MC252 Deepwater Horizon Response; 2010.

Addassi YN, Faurot-Daniels E, Hansen K, Van Haverbeck M, Wilcox M, Hall C. The Deepwater Horizon spill response: standing-up a large-scale alternative response technologies review, testing, and evaluation program within the incident command structure. International Oil Spill Conference Proceedings March 2011; 2011: pp. abs373.

Anastas PT, Sonich-Mullin C, Fried B. Designing Science in a Crisis: The Deepwater Horizon Oil Spill. Environ Sci Technol 2010;44:9250–9251.

ARRT Response Technology Working Group (1998). *ARRT in situ burning guidelines for Alaska*. Alaska Regional Response Team; 1998. 61pp.

Aurell JG, Gullett BK. Aerostat sampling of PCDD/PCDF emissions from the Gulf oil spill in situ burns. Environ Sci Technol 2010;44:9431–9437.

Baca BJ, Lankford TE, Gundlach ER Recovery of brittany coastal marshes in the eight years following the Amoco Cadiz incident. In: Proceedings of the 1987 Oil Spill Conference. Washington, DC: American Petroleum Institute; 1987. p 459–464.

Bahr L. 2010. Like sand through the hour glass, so are the dunes of our lies. Available at http://lacoastpost.com/blog/?p=24268. Accessed March 12, 2012.

Baker JM. The effects of oils on plant physiology. In: Cowell EB, editor. *The Ecological Effects of Oil Pollution on Littoral Communities*. London: Institute of Petroleum; 1971. p 88–98.

Baker JM. Net environmental benefit analysis for oil spill response. In: Proceedings of the 1995 Oil Spill Conference. Washington, DC: American Petroleum Institute; 1995. p 611–614.

Baker JM, Guzman LM, Bartlett PD, Little DI, Wilson CM. Long-term fate and effects of untreated thick oil deposits on salt marshes. In: Proceedings of the 1993 International Oil Spill Conference. Washington, DC: American Petroleum Institute; 1993. p 395–399.

Batker D, de la Torre I, Costanza R, Swedeen P, Day J, Boumans R, Bagstad K. *Gaining Ground Wetlands, Hurricanes and the Economy: The Value of Restoring the Mississippi River Delta*. Tacoma, WA: Earth Economics; 2010. 101pp.

Bergen A, Alderson C, Bergfors R, Aquila C, Matsil MA. Restoration of a *Spartina alterniflora* salt marsh following a fuel oil spill, New York. Wetlands Ecol Manage 2000;8:185–195.

Bhattacharyya S, Klerks PL, Nyman JA. Toxicity to freshwater organisms from oils and oil spill chemical treatments in laboratory microcosms. Environ Pollut 2003;122:205–215.

British Petroleum. 2010. Deepwater Horizon containment and response: harnessing capabilities and lessons learned. Available at http://www.boemre.gov/ooc/PDFs/NarrativeFinal.pdf. Accessed March 8, 2012.

Camilli R, Di Iorio D, Bowen A, Reddy CM, Techet AH, Yoerger DR, Whitcomb LL, Seewald JS, Sylva SP, Fenwick J. Acoustic measurement of the Deepwater Horizon Macondo well flow rate. Proc Natl Acad Sci USA 2012;109:20235–20239.

Chaibi M, Sedrati M. Coastal erosion induced by human activities: the case of two embayed beaches on the Moroccan coast. J Coast Res 2009;56:1184–1188.

Coastal Protection and Restoration Authority (CPRA). Integrated ecosystem restoration and hurricane protection: Louisiana's comprehensive master plan for a sustainable coast. Baton Rouge, LA: CPRA; 2010.

Culbertson JB, Valiela I, Pickart M, Peacock EE, Reddy CM. Long-term consequences of residual petroleum on salt marsh grass. J Appl Ecol 2008;45:1284–1292.

Deocampo D, Perry VR, Chin KJ. Biodegradation of Deepwater Horizon petroleum hydrocarbons in Barataria Bay marshes: geomicrobiology and clay mineral enhancement. Geological Society of America. Abstracts with Programs 2011;43:12.

Dicks B, Levell D. Refinery-effluent discharges into Milford Haven and Southampton water, In: Dicks B, editor. *The Ecological Impacts of the Oil Industry*. New York: John Wiley and Sons; 1989. p 287–316.

Douglas GS, Bence AE, Prince RC, McMillen SJ, Butler EL. Environmental Stability of Selected Petroleum Hydrocarbon Source and Weathering Ratios. Environ Sci Technol 1996; 30:2332–2339.

DWH UC. Mississippi canyon 252 incident, near shore and shoreline stage I and II response plan, Louisiana division, Version 1.0. New Orleans, LA; 2010a. 15pp. plus tables.

DWH UC. *MC-252 stage III, SCAT-shoreline treatment implementation framework for Louisiana*. New Orleans, LA; 2010b. 11pp. plus appendices.

DWH UC. *Deepwater Horizon, Shoreline Clean-Up Completion Plan (SCCP)*. New Orleans, LA; 2011a. 39pp.

DWH UC. *Shoreline treatment recommendation, operational permit to work, north Barataria Bay [STR#: S3-045.r.2]*. New Orleans, LA; 2011b. 17pp.

Epperson CR. A perspective from within Deepwater Horizon unified command post Houma. Published online http://ccrm.berkeley.edu/deepwaterhorizonstudygroup/dhsg_resources.shtml. Deepwater Horizon Study Group Working Paper; 2011.

Erftemeijer PLA, Lewis RRR. Environmental impacts of dredging on seagrasses: A review. Mar Pollut Bull 2006;52:1553–1572.

Finkl CW, Khalil SM, Andrews J, Keehn S, Benedit L. Fluvial sand sources for barrier island restoration in Louisiana: geotechnical investigations in the Mississippi River. J Coast Res 2006;22:773–787.

Fitzgerald D, Kulp M, MacDonald S, Owens E. Oiling of Louisiana's central sandy beaches. Geological Society of America. Abstracts with Programs 2011;43:11.

Froomkin D. 2010. Gulf oil spill: 'A Whale' of a skimmer offers up its services, online, *Huffington Post*. Available at http://www.huffingtonpost.com/2010/06/29/gulf-oil-spill-a-whale-of_n_629575.html. Accessed March 8, 2012.

Getter CD, Cintron G, Dicks B, Lewel RR, Seneca ED. The recovery and restoration of salt marshes and mangroves following an oil spill. In: Cairns Jr, E, Buikema Jr, AL, editors. *Restoration of Habitats Impacted by Oil Spills*. Stoneham, MA: Butterworth; 1984. p 65–114.

Goodwin P. Predicting the stability of tidal inlets for wetland and estuary management. J Coast Res 1996;23:83–101.

Graham WM, Condon RH, Carmichael RH, D'Ambra I, Patterson HK, Linn LJ, Hernandez FJ, Jr. Oil carbon entered the coastal planktonic food web during the Deepwater Horizon oil spill. Environ Res Lett 2010;5(4):045301.

Greater New Orleans Inc. Regional Economic Alliance. 2010. A study on the economic impact of the Deepwater Horizon oil spill. Part one – fisheries. Available at www.uflib.ufl.edu/docs/Economic% 20Impact %20Study,%20Part%20I%20-%20Full%20Report.pdf. Accessed March 12, 2012.

Hambrick GA, DeLaune RD, Patrick Jr, WH. Effect of estuarine sediment pH and oxidation–reduction potential on microbial hydrocarbon degradation. Appl Environ Microbiol 1980;40:365–369.

Hampson GR, Moul ET. No. 2 fuel oil spill in Bourne, Massachusetts: immediate assessment of the effects on marine invertebrates and a 3-year study of growth and recovery of a salt marsh. J Fish Res Board Can 1978;35:731–743.

Hatton RS, Delaune RD, Patrick Jr, WH. Sedimentation, accretion, and subsidence in marshes of Barataria Basin, Louisiana. Limnol Oceanogr 1983;28:494–502.

Hoff RZ. Responding to oil spills in coastal marshes: the fine line between help and hindrance. HAZMAT Report 96–1. Seattle, WA: Hazardous Materials Response and Assessments Division, National Oceanic and Atmospheric Administration; 1995. 23pp.

Joye SB, MacDonald IR, Leifer I, Asper V. Magnitude and oxidation potential of hydrocarbon gases released from the BP oil well blowout. Nat Geosci 2011;4:160–164.

Kraus NC, Militello A. Hydraulic study of multiple inlet system: East Matagorda Bay, Texas. J Hydrol Eng 1999;125:224–232.

Krebs CT, Tanner CE. Restoration of oiled marshes through sediment stripping and *Spartina* propagation. In: Proceedings of 1981 Oil Spill Conference. Washington, DC: American Petroleum Institute; 1981. p 375–385.

Kulp M, Penland S, Williams J, Jenkins C, Flocks J, Kindinger J. Geologic framework, evolution, and sediment resources for restoration of the Louisiana coastal zone. J Coast Res 2005;44:56–71.

Lehr B, Bristol S, Possolo A. Oil budget calculator: Deepwater Horizon. A report to the National Incident Command. Durham, NH: Coastal Response Research Center, University of New Hampshire; 2010.

Leonards B. 2008. Improving technology for coastal wetlands restoration. *LSU AgCenter*. Available at http://text.lsuagcenter.com/en/our_offices/research_stations/Rice/Features/Publications/Improving+Technology+for+Coastal+Wetlands+Restoration.htm. Accessed March 12, 2012.

Lin Q, Mendelssohn IA. The combined effects of phytoremediation and biostimulation in enhancing habitat restoration and oil degradation of petroleum contaminated wetlands. Ecol Eng 1998;10:263–274.

Lin Q, Mendelssohn IA. Impacts and recovery of the Deepwater Horizon oil spill on vegetation structure and function of coastal salt marshes in the northern Gulf of Mexico. Environ Sci Technol 2012;46:3737–3743.

Lytle JS, Lytle TF. The role of *Juncus roemerianus* in cleanup of oil-polluted sediments. In: Proceedings of the 1987 Oil Spill Conference. Washington, DC: American Petroleum Institute; 1987. p 495–501.

Macdonald S, Kulp M, Fitzgerald D, Georgiou I. Oiling inside Barataria Bay. Geological Society of America. Abstracts with Programs 2011;43:12.

Martinez ML, Feagin RA, Yeager KM, Day J, Costanza R, Harris JA, Hobbs RJ, López-Portilloo J, Walker IJ, Higggs E, Moreno-Casasola P, Sheinbaum J, Yáñez-Arancibia A. Artificial modifications of the coast in response to the Deepwater Horizon oil spill: quick solutions or long term liabilities? Front Ecol Environ 2012;10:44–49.

McNutt MK, Camilli R, Guthrie G, Hsieh P, Labson V, Lehr B, Maclay D, Ratzel A, Sogge M. Assessment of flow rate estimates for the Deepwater Horizon/Macondo well oil spill. Flow rate technical group report to the National Incident Command, Interagency Solutions Group. Reston, VA: US Department of Interior; 2011. p 22.

Mendelssohn IA, Andersen GL, Baltz DM, Caffey RH, Carman KR, Fleeger JW, Joye SB, Lin QX, Maltby E, Overton EB, Rozas LP. Oil impacts on coastal wetlands: implications for the Mississippi River delta ecosystem after the Deepwater Horizon oil spill. BioScience 2012;62:562–574.

Moreno-Mateos D, Power ME, Comin FA, Yockteng R. Structural and functional loss in restored wetland ecosystems. PLoS Biol 2012;10:e1001247.

National Commission on the DWH Oil Spill and Offshore Drilling. Deep water: the Gulf oil disaster and the future of offshore drilling. Recommendations. Washington, DC: National Commission on the BP Deepwater Horizon Oil Spill and Offshore Drilling; 2011. 380pp.

Nie M, Gao LX, Yan JH, Fu XH, Xiao M, Yang J, Li B. Population variation of invasive *Spartina alterniflora* can differentiate bacterial diversity in its rhizosphere. Plant Ecol 2010;209:219–226.

NOAA. 2012. Damage assessment. Gulf spill restoration. NOAA Restoration Center. Available at http://www.gulfspillrestoration.noaa.gov/assessment. Accessed March 12, 2012.

NRC. *Understanding Oil Spill Dispersants: Efficacy and Effects*. Washington, DC: National Academies Press; 2005. 377pp.

NRT. Incident Command System/Unified Command (ICS/UC). *Technical Assistance Document*; 2011.

Nyman JA, Delaune RD, Roberts HD, Patrick Jr, WH. Relationship between vegetation and soil formation in a rapidly submerging coastal marsh. Mar Ecol Prog Ser 1993;96:269–279.

Nyman JA, Walters RJ, Delaune RD, Patrick Jr, WH. Marsh vertical accretion via vegetative growth. Est Coastal Shelf Sci 2006;69:370–380.

Owens E, Taylor E, Michael J. The Deepwater Horizon-Macondo 2010 Shoreline Cleanup Assessment Technique (SCAT) program. Geological Society of America. Abstracts with Programs 2011;43:11.

Peterson CH, Rice SD, Short JW, Esler D, Bodkin JL, Ballachey BE, Irons DB. Long-term ecosystem response to the Exxon Valdez oil spill. Science 2003;302:2082–2086.

Peterson CH, Anderson SS, Cherr GN, Ambrose RF, Anghera S, Bay S, Blum M, Condon R, Dean TA, Graham M, Guzy M, Hampton S, Joye S, Lambrinos J, Mate B, Meffert D, Powers SP, Somasundaran P, Spies RB, Taylor CM, Tjeerdema R, Adams EE. A tale of two spills: novel science and policy implications of an emerging new oil spill model. Bioscience 2012;65:461–469.

Pezeshki SR, Hester MW, Lin Q, Nyman JA. The effects of oil spill and clean-up on dominant US Gulf coast marsh macrophytes: a review. Environ Pollut 2000;108:129–139.

Proffitt CE , Chiasson RL, Owens AB, Edwards KR, Travis SE. *Spartina alterniflora* genotype influences facilitation and suppression of high marsh species colonizing an early successional salt marsh. J Ecol 2005;93:404–416.

Ramseur JL. (2010). Deepwater Horizon oil spill: the fate of the oil. Congressional Research Service, 7–5700, R41531, 24pp.

Rioux P. 2010. Giant oil skimmer 'A Whale' deemed a bust for the Gulf of Mexico spill, *The Times-Picayune*. Available at http://www.nola.com/news/gulf-oil-spill/index.ssf/2010/07/giant_oil_skimmer_a_whale_deem.html. Accessed March 12, 2012.

Sandmann ERIC, Loos MA. Enumeration of 2,4-D-degrading microorganisms in soil and crop plant rhizospheres using indicator media: high population associated with sugarcane (*Saccharum officinarum*). Chemosphere 1984;13:1073–1083.

Santer R, Cocklan-Vendl M, Strong B, Michel J, Owens EH, Taylor E. The Deepwater Horizon MC252-Macondo Shoreline Cleanup Assessment Technique (SCAT) Program. International Oil Spill Conference Proceedings March 2011; 2011: pp. abs270.

Schleifstein M. 2011. Louisiana refuses to sign BP-coast guard oil spill cleanup transition plan. *The Times-Picayune*. Available at http://www.nola.com/news/gulf-oil-spill/index.ssf/2011/11/louisiana_refuses_to_sign_bp-c.html. Accessed March 12, 2012.

Seliskar DM, Gallagher JL, Burdick DM, Mutz LA. The regulation of ecosystem functions by ecotypic variation in the dominant plant: a *Spartina alterniflora* salt-marsh case study. J Ecol 2002;90:1–11.

Silliman BR, van de Koppel J, McCoy MW, Diller J, Kasozi GN, Earl K, Adams PN, Zimmerman AR. Degradation and resilience in Louisiana salt marshes after the BP–Deepwater Horizon oil spill. Proc Natl Acad Sci USA 2012;109:11234–11239.

Tunnel JW, Jr. An expert opinion on when the Gulf of Mexico will return to pre-spill harvest status following the BP Deepwater Horizon MC 252 oil spill. Gulf Coast Claims Facility, Feinberg Rozen, LLP; 2010. 55pp.

Turner RE, Milan CS, Swenson EM. Recent volumetric changes in salt marsh soils. Est Coast Shelf Sci 2006;69:352–359.

USACE. (2010). Team New Orleans. Deepwater Horizon emergency permit request. Project MVN-2010-01066-ETT and Project MVN-2010-01271-EOO. Available at www.mvn.usace.army.mil/pao/mvnoilspill.asp. Accessed March 12, 2012.

USEPA. Office of Inspector General. Revisions needed to national contingency plan based on Deepwater Horizon oil spill. Report No. 11-P-0534; 2011.

USGAO. Report to Congressional Addressees, Coastal Wetlands, Lessons Learned from Past Efforts in Louisiana Could Help Guide Future Restoration and Protection [GAO-08-130]. Washington, DC: USGAO; 2007. 57pp.

USNRT. 2010. Oil spill response strategies for coastal marshes during the Deepwater Horizon MC252 spill. Available at http://www.nrt.org/Production/NRT/NRTWeb.nsf/AllAttachmentsByTitle/SA1061NRT_Marsh_Cleanup_Options_DWH.06032010.pdf/$File/NRT_marsh_cleanup_overview_6-15.pdf?OpenElement. Accessed March 12, 2012.

Utomo HS, Wenefrida I, Meche M, Nash J. Synthetic seed as a potential direct delivery system of mass produced somatic embryos in the coastal marsh plant smooth cordgrass (*Spartina alterniflora*). Plant Cell Tissue and Organ Culture Plant Cell Tiss Org 2008;92:281–291.

Vandermeulen JH, Jotcham JR. Long-term persistence of bunker C fuel oil and re-vegetation of a north-temperate salt marsh: Miguasha 1974–1985. In: Proceedings of the Ninth Annual Arctic and Marine Oil spill Program Technical Seminar, June 10–12, 1986, Ottawa: Environment Canada; 1986. p 151–178.

Walker HJ, Coleman JM, Roberts HH. Tye RS. Wetland loss in Louisiana. Geogr Ann Ser A—Phys Geogr 1987;69:189–200.

Walton BT, Anderson TD. Microbial degradation of trichloroethylene in the rhizosphere: potential application to biological remediation of waste sites. Appl Environ Microbiol 1990;56:1012–1016.

Webb JW, Alexander SK. No. 2 fuel oil effects on *Spartina alterniflora* in a Texas salt marsh. Contrib Mar Sci 1991;32:9–19.

Wilber DH, Clarke DG. Biological Effects of Suspended Sediments: A Review of Suspended Sediment Impacts on Fish and Shellfish with Relation to Dredging Activities in Estuaries. N Am J Fish Manage 2001;21:855–875.

Zengel S, Michel J. Deepwater Horizon oil spill: salt marsh oiling conditions, treatment testing, and treatment history in northern Barataria Bay, Louisiana (Interim Report, October 2011). U.S. Department of Commerce, NOAA Technical Memorandum NOS OR&R 42. Seattle, WA: Emergency Response Division, NOAA; 2013.

4

CHALLENGES IN AND APPROACHES TO MODELING THE COMPLEXITIES OF DEEPWATER OIL AND GAS RELEASE

Rupesh K. Reddy, A. Rao, Z. Yu, C. Wu, K. Nandakumar, L. Thibodeaux, and Kalliat T. Valsaraj

4.1 INTRODUCTION

The recent (April 2010) Deepwater Horizon (DWH) oil spill due to the Macondo well blowout in the Gulf of Mexico (GoM) has been a serious accident that has drawn wide attention (see Burns, 2010) for various reasons. Obviously, the concerns of public health and safety, which is addressed in detail in the report by Burns (2010); its impact on the economic way of life of the residents; and its longer-term effect on the marine environment are all concerns that need to be addressed. The mechanisms of interaction of such deepwater hydrocarbon spills with the environment span a broad range and are not well understood. Exxon Valdez (see Guterman, 2009) was a similarly well-known example of a *surface spill*. In both cases, a priori knowledge of their consequences and hence the predictive capability to anticipate the extent of the spread of oil and its effect on the environment was almost nonexistent. In the case of Exxon Valdez accident, significant surveillance and research have been conducted subsequent to the spill. The article in *Science* by Guterman (2009) and the one by Payne et al. (2008) survey the aftermath of Exxon Valdez event after nearly 20 years.

The DWH spill is not the first one to occur, nor is it likely to be the last one, although it has attracted the most attention in recent years. A number of other spills that occurred between 1967 and 1991 are documented in a report published by the

Oil Spill Remediation: Colloid Chemistry-Based Principles and Solutions, First Edition.
Edited by Ponisseril Somasundaran, Partha Patra, Raymond S. Farinato, and Kyriakos Papadopoulos.

National Oceanic and Atmospheric Administration (NOAA) (see Curl et al., 1992, Report# HMRAD 92–11). Considering the frequency of past occurrences and the likelihood of another occurrence, the dearth of understanding and the inability to predict the outcome of such spills are surprising. There have been significant developments in the general area of Simulation-Based Science and Engineering, made possible by advances in hardware and in algorithms that in turn make possible detailed examination of a variety of engineering design problems. However, deepwater spill appears to have been an exception. Even the discharge rate could not be assessed accurately during the early stage of the blowout. The state of model prediction for *surface* spills is perhaps a bit more advanced by the availability of such simulation tools as ADCIRC (Luettich and Westerink, 2004). This model uses depth-averaged equations of motion that takes into account the dominant wave interactions on the ocean surface. There have also been many individual studies devoted to specific aspects of deepwater oil spills. Yapa and Li (1997a) provide a review of such efforts for modeling the oil and gas releases from deep water. Other significant efforts on various aspects of deepwater oil spill studies are listed in the following:

1. Studies on *Lagrangian models* (i.e., dispersed phase tracking) for various aspects of the oil spill: Yapa and Li (1997b), Zheng and Yapa (1998), Johansen (2000), Yapa et al. (2001), Zheng et al. (2002), Chen and Yapa (2003), Johansen (2003), and Dasanayaka and Yapa (2009)
2. Studies on *hydrate formation* in deepwater spills: Chen and Yapa (2001) and Yapa et al. (2008, 2010)
3. Studies on *droplet size distribution* in deep-sea discharge: Chen and Yapa (2007)
4. Studies on the effect of ocean *crosscurrents* on the plume trajectory: Masutani and Adams (2001) and Socolofsky and Adams (2002)
5. Studies on surface *wave interaction* with the oil spill: Luettich and Westerink (2004) and Agrawal and Dakshinamoorthy (2011)
6. Studies on *weathering* of spilled oil: Short and Heintz (1997), Comerma et al. (2002), and Brandvik and Faksness (2009)

While there are some similarities between the deepwater and surface spills in terms of the effect of hydrocarbons on the marine environment, there are clearly differences in the hydrodynamic interactions between a deepwater blowout, a shallow-water blowout, and a surface oil spill (Johansen, 2000). Deepwater blowouts from a producing well often contain a mix of oil and gas (e.g., methane) that interacts with the ocean at various depths in complex ways, while a surface spill from a ship as a source contains essentially crude oil that is already processed to some extent in separating the gas, water, etc., at the source. The surface spill creates a dramatic visual impact, while the deepwater spill remains largely unseen particularly when treated with dispersants, the primary use of which appears to be to keep the oil out of sight, while its environmental impact remains largely unknown.

In this assessment, we focus on the following: (i) document scantily available data on the DWH oil spill and the sources of such data, (ii) identify the various mechanisms for transport and physicochemical change of the oil–gas mixture as it interacts with the seawater, (iii) summarize the mechanistic models available in the literature for each individual process, (iv) identify the knowledge gaps, and (v) finally present a framework towards a global, integrated computational transport phenomena model that could be used in future spills to predict possible scenarios.

While the mechanisms can be identified and a computational model built, the uncertainties in the input parameters to the model are often quite significant. Hence, the precise prediction of the fate of such spill will remain a formidable challenge, one as challenging as the weather prediction. Yet possible scenarios and their impact can be investigated with such tools (see, e.g., Nagheeby and Kolahdoozan, 2010; Peishi et al., 2011; Sotillo et al., 2008; Verma et al., 2008; Vethamony et al., 2007). The time scale of interest for such predictive tools will be what we call as *near term* (of the order of days to months) that focuses on transport of oil and gas plume from the source to its destination on either the ocean–air interface or the ocean floor. While some may be trapped in neutrally buoyant zones temporarily, they must eventually either sink or float as they continue to lose lighter material by dissolution or gain heavier marine particulate material and continue their journey up or down or be consumed by biological organisms. The latter types of interactions and fate involving interaction with biological material, while extremely important, are beyond the scope of the present review and the expertise of the present authors (see, e.g., Gin et al., 2001; Kessler et al., 2011a, 2011b; Valentine et al., 2010; Zhang et al., 2011).

4.2 SURVEY OF AVAILABLE DATA

The extent of the uncertainty in the immediate aftermath of this accident is clear when we recognize that even the discharge rate of the oil and gas was not known precisely for weeks after the accident. The initial estimates of flow rates of 1000–5000 barrels per day by British Petroleum (BP) were unrealistically low and were not based on any scientific measurement principles. At the extreme conditions encountered near an accident site, it is indeed a difficult challenge to estimate the oil and gas flow rates with any degree of certainty. Since then, several government and corporate websites such as the Department of Energy (DOE) (2010a and 2010b), the Environmental Protection Agency (EPA) (2010), and the BP website (2010) have gathered data pertaining to the BP accident and made them publically available. The data gleaned from these sources are discussed in this section in the hope that it will be a starting point for an effort at model building and validation. Table 4.1 provides a summary of such data for easy reference.

From the day the TopHat recovery procedure was successfully installed, the flow of oil and gas and the wellhead pressure and temperature were monitored on a daily basis. The data are available as a downloadable spreadsheet (DOE, 2010a).

TABLE 4.1 BP spill-related data from various sources

Quantity	Value	Source of data
Depth of sea at the wellhead	5053 ft	DOE (2010)
Static pressure at wellhead (May 25, 2010)	4400 psia	DOE (2010)
Total oil recovered after TopHat was installed between June 4, 2010, and July 16, 2010	804,000 barrels	DOE (2010)
The GOR defined as cubic feet of gas to a barrel of oil	2380	DOE (2010)
Oil density	38 API	DOE (2010)
In situ density of oil (kg/m^3)	858	Socolofsky et al. (2011)
Gas gravity	0.7	DOE (2010)
In situ density of gas (kg/m^3)	99.2	Socolofsky et al. (2011)
Wellhead oil pressure range from June 3, 2010, to July 9, 2010	1800–900 psia	DOE (2010)
Wellhead oil temperature range from June 3, 2010, to July 9, 2010	106–81 °F	DOE (2010)
Typical current speed (m/s)	0.078	Socolofsky et al. (2011)
Gas effective droplet diameter (m)	0.02	Socolofsky et al. (2011)

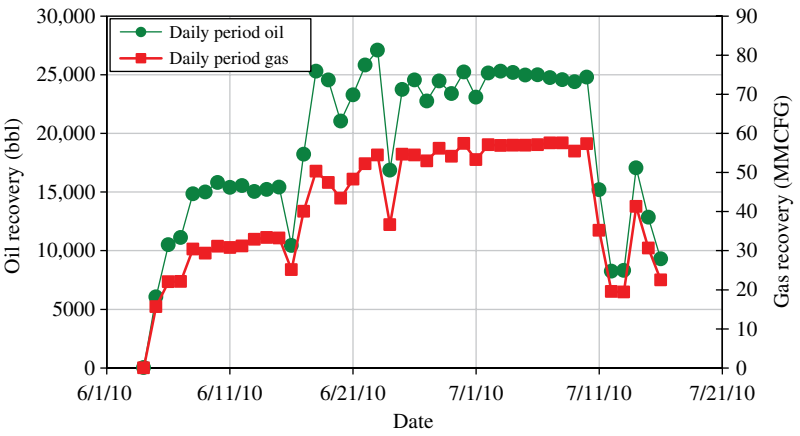

FIGURE 4.1 Flow rates of oil and gas from Macondo well (DOE, 2010).

Figure 4.1 shows the daily oil and gas flow rate. The daily production reached as high as 25,000 bbl/day of oil and over 50 million standard cubic feet per day (MMSCFD) of gas.

While the data in Figure 4.1 are based on actual physical measurements published by the DOE on the amount of oil and gas collected from the well, it would be fair to assume that the discharge rates were similar in magnitude prior to the TopHat

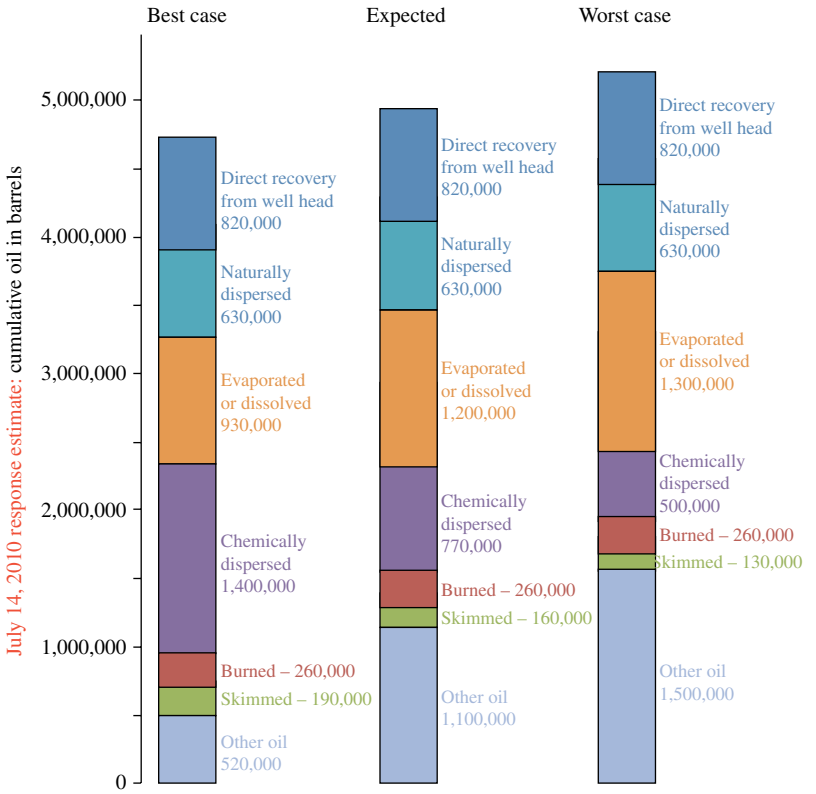

FIGURE 4.2 The results of estimates from the Oil Budget Calculator, a model used to estimate where the discharged oil ended up (Lehr et al., 2010).

collection device was in place. The fate of those discharges could only be estimated, and the oil budget published by the Federal Interagency Solutions Group consisting of lead researchers from NOAA, U.S. Geological Survey (USGS), and NIST (Lehr et al., 2010) was based on empirical models and best estimates of rate parameters to identify where all of the oil and gas could have dispersed.

Figure 4.2 shows the summary findings from this group. Here, *direct recovery* refers to oil and gas collected once the TopHat recovery system was in place, and this number is consistent with the DOE data shown in Table 4.1. It accounts for about 17% of the estimated release. The *naturally dispersed* components are those small droplets that remain suspended in the water column for an extended period of time, which is estimated to be 13%. There is a significant uncertainty in estimating this amount as it depends on knowing the droplet size distribution, which in turn depends on turbulent energy dissipation rates as the jet comes out of the well. The *evaporated–dissolved* amount is estimated to be about 23%. While in surface spills evaporation is a major mechanism, in deepwater spills of raw crude containing a larger portion of lighter material, dissolution is an equally important mechanism although solubility

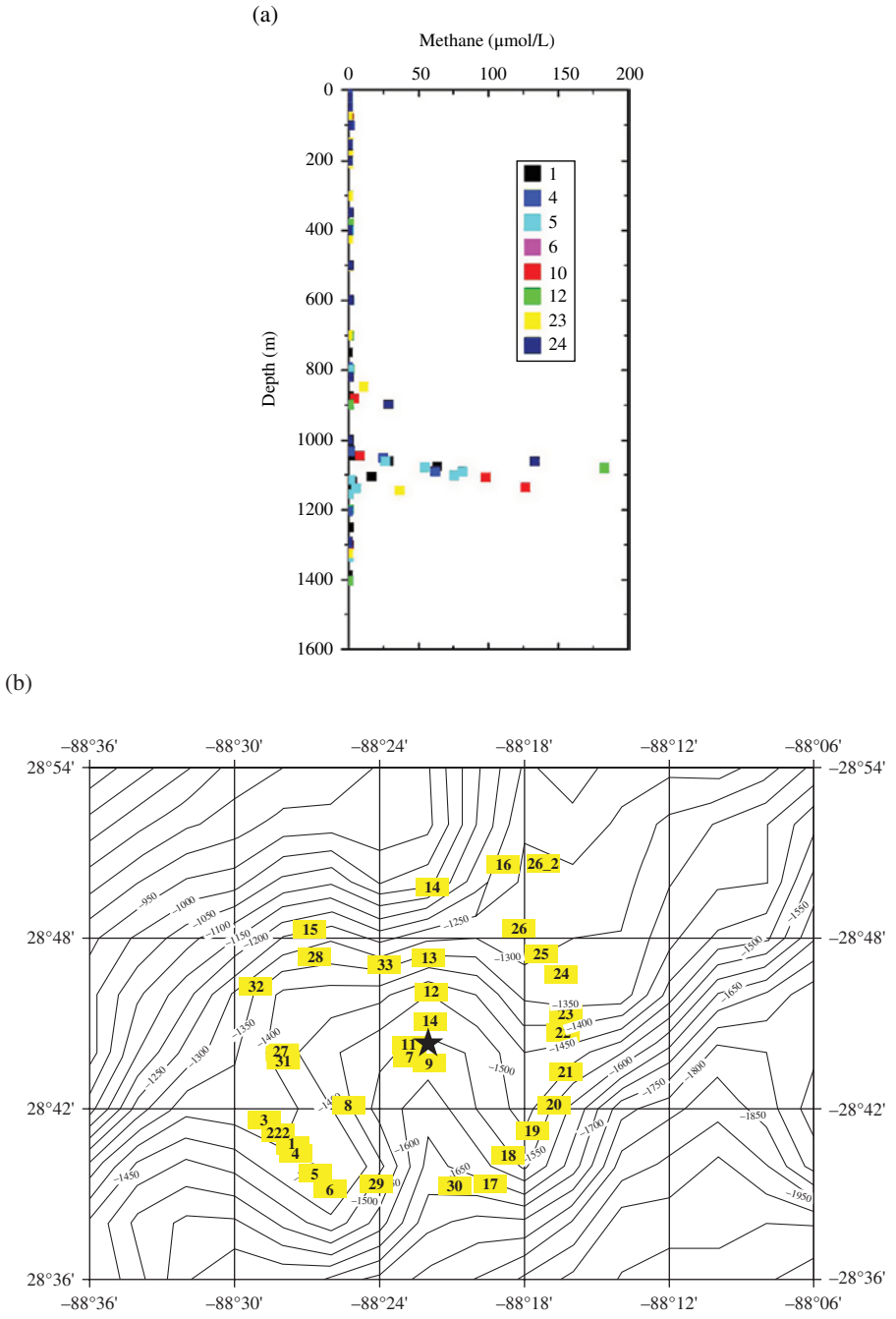

FIGURE 4.3 Methane concentration with depth at various areal locations around the wellhead (Yvon-Lewis et al., 2011). Notice that near a depth of 1100 m, there is an unusual increase in the concentration of methane.

may be small. Continuous extraction of the hydrocarbons into an infinitely large reservoir of seawater would suggest that equilibration is not important, but accurate mass transfer models and droplet size estimates (which determine the mass transfer surface area) are important factors. The *chemically dispersed* amount is estimated to be 16%. The complexity of assessing the effectiveness of the dispersants under field conditions, which are discussed in the report (Lehr et al., 2010), points to further needs for laboratory-scale and field-scale experimental and modeling studies to predict the droplet size in the presence of surfactants. In addition, the mass transfer (dissolution) from surfactant-coated droplets could be different from untreated droplets, pointing to the coupled nature of these mechanisms (Haghdoost et al., 2011; Saien and Rezabeigy, 2011). The amounts that are *burned* and *skimmed* are estimated to be 5 and 3%, respectively. The amount unaccounted by any of the aforementioned estimates is still 23%, which is labeled as *other oil* in the report.

The mass balance approach is admittedly a simple one with a number of rate constants to be estimated from other physical and mechanistic considerations. Nevertheless, it does offer guidance and a focus for further investigations on a problem that was originally fraught with simple guesswork.

In another recent field study, Yvon-Lewis et al. (2011) monitored the hydrocarbons (particularly methane), concentrations with reasonable spatial and temporal resolution near the spill region. The results of their monitoring showed very low flux of methane to the atmosphere (0.024 μmol/m^2/d). Their measurements indicate that over a region of up to 17 km from the wellhead, hydrocarbon concentration in the atmosphere averaged 1.86 ppm (and not significantly elevated from the norm), while that in the surface of the ocean showed only a slightly elevated average of 2.85 ppm. They suggest that most of the methane from the wellhead (which they estimate to consist of 30.2% of methane by weight) was dissolved in the deep ocean. Any attempt to estimate the mass transfer rates requires a good estimate of the size distribution of the bubbles since the mass transfer rate is directly proportional to the interfacial area.

Figure 4.3 is reproduced from Yvon-Lewis et al. (2011), which shows the concentration of methane at various depths in the ocean at points surrounding the wellhead identified in Figure 4.3b. This data is very interesting because it shows a distinct structural behavior in measured concentrations at depths of 1050 m and a secondary intrusion at 900 m, where there has been an increase in methane concentration. Pure dissolution and dispersion from the rising plume alone could not explain such a behavior since the concentration above that intrusion level is very low; nor could any crosscurrent flow at that elevation explain it as it will not result in nearly axisymmetric spread. But this field-scale observation is consistent with the earlier laboratory-scale studies of McDougall (1978) and Socolofsky and Adams (2005). The earliest study on such likelihood was noted in a study by McDougall (1978) who investigated the dynamics of gas plumes and showed that such horizontal spreads are feasible in a stratified environment. Subsequently, in another study, Socolofsky and Adams (2005) also observed the formation of such horizontal intrusions as sketched by them and reproduced here in Figure 4.4. More recently, Socolofsky et al. (2011) have reexamined their earlier models in light of

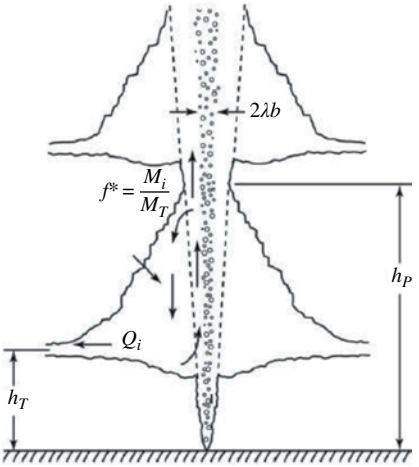

FIGURE 4.4 Plume structure that shows a possible horizontal intrusion. Source: Socolofsky and Adams, 2005. Reproduced with permission of the American Society of Civil Engineers.

the additional data that have been measured specifically for the DWH blowout. While their earlier study used linear density stratification, the data pertaining to the DWH site showed a quadratic variation. In the interest of assembling as much of data pertaining to the modeling efforts for the DWH spill, we reproduce the density variation and the quadratic fit in Figure 4.5. Revising their earlier study to account for the quadratic density variation, Socolofsky et al. (2011) showed that the present field observations are consistent with their model of intrusion layer formation.

In the case of the GoM DWH oil spill, the hydrocarbon audit does not appear to be closed in the sense that a lot of the oil that is produced from the well does not appear to be accounted for. The use of surfactants may have had the effect of producing tiny oil droplets with a very slow rise velocity and hence may interact by dissolution of lighter hydrocarbon into the water or attachment of suspended particles thus making it heavier and find their way to the bottom of the ocean floor often many miles away from the source that is influenced in part by any ocean currents.

As a part of emergency response to such massive oil spills, the scientific community has been challenged in understanding, predicting, and minimizing the negative effects to any extent possible. An important component of such emergency response should be to build some *predictive capability* using mathematical models to answer a variety of questions such as (i) likely areal extent of the dispersion of oil, (ii) maximum likely concentration of hydrocarbons in the seawater, and (iii) long-term fate of hydrocarbons in the ocean and its effect on the marine life, arising out of such an uncontrollable deepwater discharge of hydrocarbons. A recent article by Thibodeaux et al. (2011) offers a perspective of knowledge gaps and the basic research that needs to be undertaken

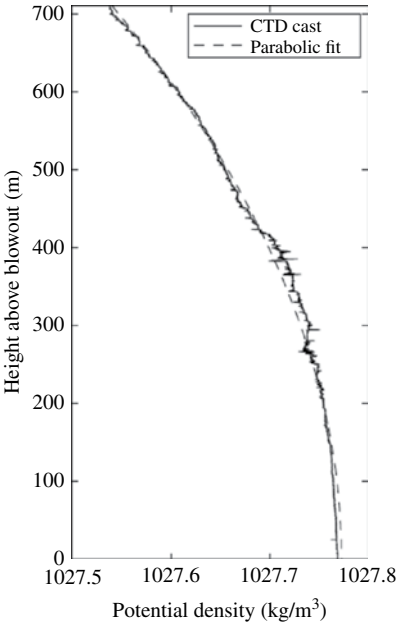

FIGURE 4.5 Density profile measured at Station B54 (28°43.945′N, 88°22.607′W; May 20, 2010). The solid line is the measured density. Dashed line is the parabolic fit given by $\rho(z) = 1027.77 - 4.60434 \times 10^{-7}\, z^2$. Z is in meters above the blowout, and the density is in kg/m^3 (Socolofsky et al., 2011).

to fill these knowledge gaps. They raise a fundamental question, *Is it wise to do deepwater O&G extraction in the Gulf, and if so, under what conditions?* They identify the following knowledge gaps for our inability to answer that question: *(1) the science/engineering community knows too little about the massive deep-sea O&G release processes, (2) where does all the material released in the deep go?, and (3) its impact on the Gulf biota.*

Based on this quick survey, it is clear that there has been a significant work on understanding deepwater oil and gas releases, but this has not evolved into a comprehensive model that can be used to analyze the data and answer the question, *Where does all the material released in the deepwater go?* While the Oil Budget Calculator (Lehr et al., 2010) is a first step, it is not clear that the rate constants estimated will remain invariant and applicable to other oil spills. Here, we will review the science of submerged jets and plumes and their dynamics, followed by work done on modeling the trajectories of oil and gas two-phase plumes, studies on hydrate formation, and studies on droplet breakup and coalescence in such an environment. Finally, the interaction of such plumes with the prevailing cross flow in the ocean will determine the answer to the question, *Where does all the material released in the deepwater go?* This will be followed by a hierarchical class of coupled multiphase flow models that could be used to predict the trajectory and the eventual fate of the hydrocarbons released in deepwater conditions.

4.3 DESCRIPTIONS OF PHYSICAL MECHANISMS

4.3.1 Qualitative Dynamics of Two-Phase Plume

In deepwater blowouts, consisting of a mixture of oil and gas, the volume ratio of these two fluids depends on the characteristics of the producing reservoir fluids. The natural gas, being a compressible fluid under pressure at reservoir conditions, provides the driving force for an uncontrolled blowout. As the plume travels upward in water column, the decreasing pressure causes gas to expand, and it ultimately exits the wellhead at very high velocities. At this location, oil makes up only a fraction of the total volumetric flow rate. In the absence of cross flow, the oil and gas released from a subsea blowout can be thought to pass through three zones as they move to the sea surface. A schematic of the plume dynamics taken from S.L. Ross Environmental Research Ltd. (1997) along with the simulation of such a plume taken from Cloete et al. (2009) is shown in Figure 4.6.

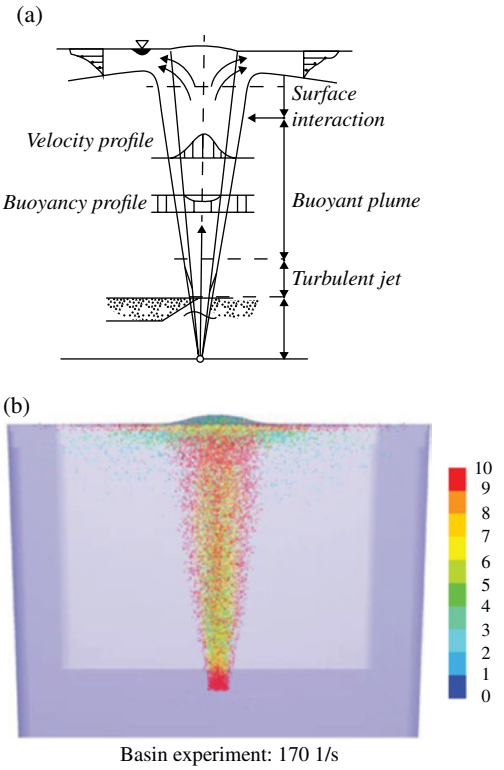

FIGURE 4.6 (**a**) A schematic taken from S.L. Ross Environmental Research Ltd. (1997) that shows the three zones of a gas plume, namely, the turbulent jet zone, buoyant plume zone, and surface interaction zone. (**b**) shows the results from a CFD-based simulation of bubbles tracked in the Lagrangian framework. The color map indicates the bubble size in millimeters. Source: Cloete et al., 2009. Reproduced with permission of Elsevier.

The initial high momentum prevailing at the exit well head gives rise to a turbulent jet zone, which disintegrates larger droplets into smaller ones of diameters ranging from 0.5 to 2.0 mm (Dickins and Buist,1981). The bubble and droplet size in this region has profound effects on the fate of the injected material. In fact, the purpose of using surfactants is to minimize the size so that their rise velocity could be reduced and hence their residence time in the water column increased.

It is not easy to predict the size distribution without careful experimentation and modeling, particularly in the presence of surfactants. The surrounding bulk water is entrained with the jet flowing upward, robbing it of its initial momentum, and the dispersed phase enters a *buoyant plume zone* where buoyancy provides the main driving force for the remainder of its journey. The terminal rise velocity of a gas bubble in stationary water is lower than the velocities in the center of blowout plumes due to the pumping effect (buoyancy) of rising gas in the bulk liquid, which essentially implies that water surrounding the upward-moving gas is entrained and imparts an upward velocity. When the plume becomes fully developed, a considerable quantity of water containing the oil droplets is pumped to the surface. The velocity profile reaches a self-similar pattern, for a certain distance before the instability of the gas plume sets in (see Topham, 1984), particularly at large depths when the transit time of the plume is large. In the "surface interaction zone," the upward flow of water moves in a horizontal layer away from the center of plume. The influence of the surface water current results in a radial flow and results in the spreading of oil over the surface up to the point where this flow no longer influences the surface water movement. The gas exits finally from the center of plume and causes a disturbance at the water surface.

Subsea oil well blowout in deep water is different from that in shallow water in other respects as the high pressure and low temperatures prevailing at these depths may cause the natural gas to combine with water to form *solid hydrates*. *Dissolution* is another process that can bring about reduction in gas volume. The rising plume may completely lose its driving buoyancy due to considerable loss of gas through either or both of these processes, which will result in the oil droplets rising slowly under gravity forces alone. The movement of the oil droplets will at this stage be affected by the crosscurrents during the rise. This will result in the separation of oil droplets. The large diameter oil droplets reach the surface earlier compared to smaller droplets (the turbulent zone created at the release point causes the oil to fragment into droplets of various sizes). The sketch in Figure 4.7 is taken from Socolofsky and Adam (2002), and it shows the schematic of the separation process in the presence of cross flow.

Gas bubble separation can be considered to be a self-reinforcing process, as deflection caused by the crosscurrent will increase when buoyancy in the plume is reduced. The aforementioned process drastically reduces buoyancy in the plume at an early stage. As a result, the plume will cease to rise, when it meets a neutrally buoyant zone, while gas bubbles will continue their ascent to the surface as individual bubbles. The leak of gas bubbles from an inclined plume can be visualized as the deviation of bubble trajectory from the plume trajectory due to the extra vertical velocity component (slip velocity) of the bubbles.

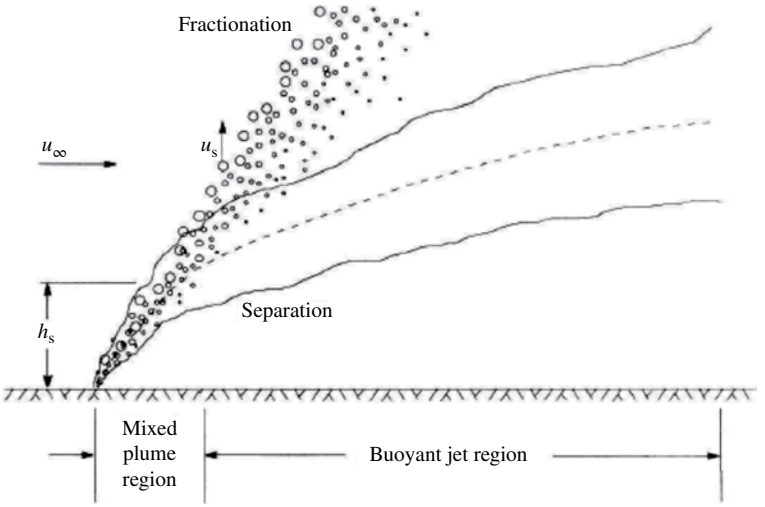

FIGURE 4.7 Definition sketch for a two-phase plume in a cross flow. Source: Socolofsky and Adam, 2002. Reproduced with permission of Taylor and Francis.

For oil droplet diameters in the range of 5–10 mm, the maximum rise velocity is about 12–15 cm/s (depending on the density of the oil), while for gas bubbles with 3–4 mm diameters, it is around 30 cm/s (Johansen, 2000). The size of droplets emanating from the oil well depends on the conditions at the discharge point (exit velocity U_0 and diameter d_0) and on the physical properties of the oil (density, interfacial tension, viscosity). The oil droplet size and its distribution are important factors, which not only dictate the leakage of oil droplets from the plume but also determine the surface appearance of the released oil, which defines slick formation.

4.3.2 Review of Studies on Submerged Jets and Plumes

Numerous fundamental studies have appeared on the dynamics of submerged jets and plumes. As the pressurized, *high-temperature* oil (relative to the surrounding seawater) is released from a ruptured wellhead at the bottom of the sea into the *cold seawater*, a significant pressure drop occurs from the reservoir conditions to the ambient seabed conditions, which is also at *elevated pressure* but at a *low temperature*. The flow processes are determined by the dynamics of jets and plumes (Chen and Rodi, 1980; Chen and Yapa, 2004a, b; Cloete et al., 2009; Kotsovinos and Angelidis, 1991; List, 1982; Rogers and Morris, 2009; So and Aksoy, 1993; Yapa et al., 1999). A jet is defined as one driven by the momentum flux at the source with significant pressure decrease across an orifice that results in an increase in the kinetic energy of the ejected fluid, while a plume is driven by body forces (buoyancy) derived from *inhomogeneities in density* that can be caused by differences in *temperature* or *concentration* between miscible fluids (often small in magnitude) or larger differences

in densities between an immiscible source fluid and ambient fluids (such as oil/gas in seawater). In the case of the oil discharge, depending on the reservoir pressure, the momentum source at the wellhead could be significant, yet, because it is discharged into an infinite body of water, the jet momentum will be reduced quickly in accelerating and entraining the ambient fluid, and the longer time scale dynamics is then governed by the buoyancy force. The density difference between the ejected fluid and the ambient seawater is due to many factors: (i) there are density differences due to differences in the material composition between the seawater and the oil; (ii) because of the pressure drop experienced by the oil across the wellhead, dissolved lighter gases are released from the oil creating a new phase and causing yet another source of density difference; (iii) there are also temperature differences between the ejected fluid and the seawater that will give rise to thermally induced buoyancy; and (iv) in addition, the lighter components so produced can also form hydrates because of the low temperature of the seawater at those depths. Thus, a complex process can result in the formation of a solid (hydrate), liquid (oil), and gas mixture that will be broken up into smaller bubbles, droplets, or particles by the *shear interaction* between the jet/plume and the ambient fluid. Predicting the size distribution of these bubbles, droplets, and particles is a challenging task (Clift et al., 2005; Gennes et al., 2010). To complicate the situation further, surfactants are injected directly at the emerging jet/plume, with the purpose of breaking up the size of the dispersed phases into smaller units. The eventual fate of these dispersed phase materials will critically depend on the *initial size distribution*, because the rise velocity and hence the residence time depend critically on the diameter of these dispersed phases. During their upward motion, these dispersed phases are not inactive, but continue to eject gas due to lowering of the hydrostatic head and continue to exchange mass with the environment due to dissolution of the lighter material and may even become heavier and sink to the bottom of the ocean floor or be consumed by living organic matter in the environment. Detailed auditing of the hydrocarbons taking into account all of these mechanism will remain a challenging task. But systematic application of the *computational transport phenomena* that can account for each of these physical mechanisms can begin to address some of these issues and reduce the uncertainties in the prediction to the uncertainties in the initial and boundary conditions alone.

4.3.2.1 Fine Structures of Single-Phase Jets and Plumes

If one examines the finer fluid mechanical structures near the wellhead, the high-speed single-phase jet causes an unstable shear layer in the neighborhood of the ruptured well, forming vortices that break up as shown in Becker and Massaro (1968). Figure 4.8 shows the vertical structures that form at the interface between the jet and the ambient fluid. An immiscible two-phase jet is likely to inherit some of the dynamical features at high velocities in forming such vertical structures. In such flows, the turbulence intensity levels at the two-phase boundary between the jet and the ambient fluid will strongly influence the droplet sizes that form.

An excellent review of the turbulent jets and plumes is presented by List (1982). Experimental data on $\sqrt{u'^2}/U_m$, a measure of intensity of fluctuations, in axisymmetric

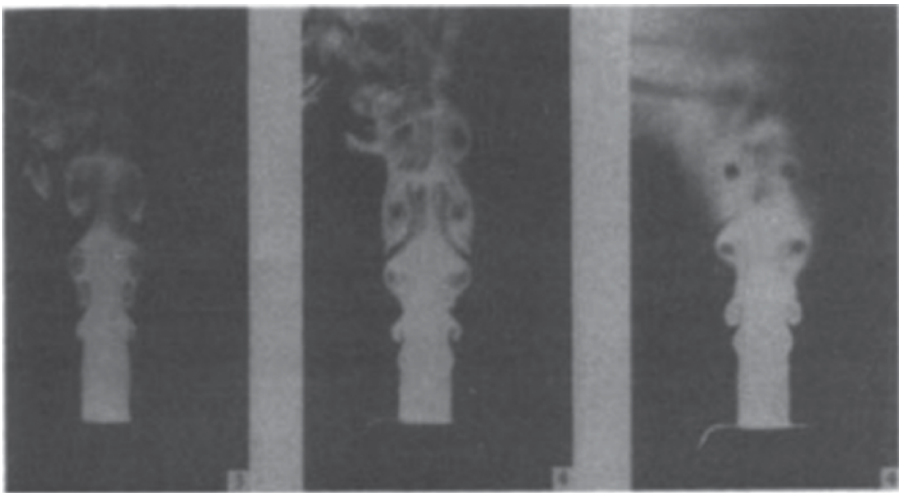

FIGURE 4.8 Formation and breakdown of vortical structures in single-phase turbulent jets. Source: Becker and Massaro, 1968. Reproduced with permission of the Cambridge University Press.

jets at downstream distances of up to 40 jet diameters show that the turbulent jet remains self-similar and has the following form:

$$\overline{u} = U_{\mathrm{m}} e^{-(r/b_{\mathrm{u}})^2} \tag{4.1}$$

where $(U_{\mathrm{m}}(x), b_{\mathrm{u}}(x))$ are functions of downstream distance from the jet inlet. Additional details on the evaluation of $(U_{\mathrm{m}}(x), b_{\mathrm{u}}(x))$ can be found in List (1982).

In the case of laminar buoyant plumes, buoyancy plays a key role in determining the structure of the plume. The driving force could be from either a thermal or a mass source. In the case of thermal plumes, a buoyancy flux is defined as (List, 1982)

$$B = \frac{g\beta H_0}{\rho C_{\mathrm{p}}} \tag{4.2a}$$

where β is the volumetric coefficient of thermal expansion, H_0 is the heat flux, and C_{p} is the heat capacity. For the case of a mass source, with a mass flux of $\rho_0 Q$, a similar term is defined as

$$B = \frac{g\left(\rho_{\mathrm{s}} - \rho_0\right)Q}{\rho_0} \tag{4.2b}$$

where ρ_0 is the source fluid density and ρ_{s} is the ambient fluid density. If the buoyancy source is not sustained (e.g., a pulse created by nuclear explosion or volcanic

eruption), a typical mushroom cloud forms. When the source is sustained (as in the case of prolonged rupture of an oil well), an initial starting cap advances with a displacement proportional to $B^{1/4}t^{3/4}$ (see Turner, 1973). If the initial, transient dynamics of the plume is neglected, then the mean properties of a steady plume are given by the following expression from dimensional analysis (see List, 1982):

$$U_{\mathrm{m}} = \left(\frac{B}{x}\right)^{1/3} f\left(\frac{B^{1/3}x^{2/3}}{\nu}, \frac{\nu}{\kappa}\right) \tag{4.3}$$

where $(B^{1/3}x^{2/3})/\nu$ is a local Reynolds number. The self-similarity is lost due to the instability of the plume beyond a certain critical value of the dynamical parameter, $(B^{1/3}x^{2/3})/\nu$, which was investigated by Mollendrof and Gebhart (1973). Bill and Gebhart (1975) found the transition from laminar to turbulent planar plume to occur at a Grashof number $[\mathrm{Gr} = g\,x^3\beta(T_{\mathrm{m}} - T_{\infty})/\nu^2]$ of 3×10^8.

4.3.2.2 Flow Transitions

There is very little study on the dynamics of transitions from jets to plumes. Kotsovinos (1975) is the only experimental study to examine the dynamics when a jet evolves into a plume. In the jet regime, there is a kinetic energy production from the mean flow and loss by viscous dissipation. In the plumes, there is an increase in the mean momentum flux and a direct transfer from potential energy into turbulent kinetic energy. List (1982) argues that the equilibrium turbulence intensities should be significantly higher in the plumes than in the jets. The other kinds of transitions that occur with either jet regime or plume regime are due to hydrodynamic instability of the respective flows. As pointed out earlier, Bill and Gebhart (1975) have studied such transitions for single-phase plumes.

4.3.2.3 Density Stratifications

The next level of complication that can arise is in density stratification in the environment (as documented, e.g., in Figure 4.5 based on the GoM data). A positively buoyant jet or plume will rise in regions of denser fluid until carried to a less dense environment. Due to the momentum of the jet, it may actually carry dense fluid beyond a level of neutral stability so as to fall back to its neutral zone. In linear density stratification, the important parameter is the Brunt–Väisälä frequency defined as

$$N^2 = -\left(\frac{g}{\rho}\right)\frac{\partial \rho}{\partial z}. \tag{4.4}$$

The terminal height of a jet or plume is proportional to $(M/N^2)^{1/4}$ or $(B/N^3)^{1/4}$ where, as before, M is the momentum flux and B is the buoyancy flux. In cases where the fluid in the plume is lighter than the lightest zones in the stratified environment, the plume will break through at the top. If there are soluble species in the plume that can dissolve in the ambient fluid, then there is evidence that they can form intrusion

layers (see Socolofsky et al., 2011). The trap height of a single-phase fluid plume is given by Turner (1986) and Crawford and Leonard (1962):

$$h_{\mathrm{T}} = 2.8\left(\frac{B}{N^3}\right)^{1/4}. \tag{4.5}$$

Socolofsky (2001) found that for two-phase plumes in stratified environment, the single-phase value of h_{T} is reduced because of progressive weakening of buoyancy as the bubbles separate, causing the intrusion to form deeper in the profile. Trap height in this case is given by

$$\frac{h_{\mathrm{T}}}{(B/N^3)^{1/4}} = 2.8 - 0.27\left[\frac{u_{\mathrm{s}}}{(BN)^{1/4}}\right] \tag{4.6}$$

where u_{s} is the slip velocity of the bubble.

4.3.2.4 Effect of Cross Flows

The next level of complication that can occur is the superposition of the jet or plume dynamics with a cross flow. The dynamics can be complex indeed, and few experimental works are available (see Chassaing et al., 1974; Crabb et al., 1981; Moussa et al., 1977). The two basic variables are the jet momentum flux, *M*, and the mean cross flow velocity, *U*. List (1982) summarizes the analysis of trajectories of the jet and plume in cross flow. Additional details of the similarity theory can be found in Fischer et al. (1979). The analysis becomes much more complex when cross flow and stratification are present simultaneously for jets and plumes that are rising. The aforementioned summary is drawn from the excellent review article on turbulent jets and plumes by List (1982). It is, however, focused on single-phase jets and plumes, driven by both thermal and momentum gradients.

4.3.2.5 Multiphase Flows

In the case of multiphase plumes, the dispersed phase dynamics and size distribution are controlled by both its own characteristics and that of the entrained continuous phase. This recognition is all the more important in the case of stratification and cross flows. In the presence of cross flows, there can be a separation between the dispersed phases (liquid and gas) and the entrained phase, resulting in qualitatively different behavior from single-phase plumes.

The released gas can undergo any of the following processes: (i) under high pressure and low temperatures, and in the presence of water, the natural gas can convert to a solid hydrate; (ii) the free gas may dissolve into the surrounding ambient water body; (iii) the gas that rises will experience lower pressures and expand; and (iv) the buoyancy of gas bubbles can create a pumping action that results in the development of a rising oil plume, gas, and water to the surface at velocities that can dominate the effects of the prevailing water currents.

The gas can be converted to hydrates in case of releases occurring at depths greater than 900 m. No hydrate formation takes place for releases in water shallower than 300 m (because of prevailing temperature and pressure conditions at those depths). Oil and gas, being released at the depths between 900 and 300 m, can witness both the processes of dissolution and hydrate formation. Often, there exists a competition between the conversion of gas to hydrate film around gas bubble–oil droplet and the loss of gas through dissolution to the water (Maini and Bishnoi, 1981; Vysniauskas and Bishnoi, 1980, 1983). As hydrates rise above the 300 m depth, they will decompose to gas and again assist in powering the bubble plume due to increase in buoyancy.

Extensive experimental study on the dynamics of the multiphase plumes was carried out by Socolofsky (2001). The modeling of the phase separation was accomplished by Chen and Yapa (2004a, b). Einarsrud and Brevik (2009) present an analysis of dissolving, axisymmetric, multiphase plume, the features of which would be important in the BP spill case as the lighter hydrocarbons that are released as gas can dissolve into the seawater. They develop a phenomenological kinetic energy theory coupled with mass transfer to study the fully developed, self-similar profiles of dispersed gas phase in a liquid. The rate of mass transfer from the dispersed phase to the ambient fluid is modeled by

$$\frac{dm_{\mathrm{b}}}{dt} = -4\pi r_{\mathrm{b}}^2 K\left(c_{\mathrm{s}} - c_{\infty}\right) \tag{4.7}$$

where m_{b} is the mass of one spherical bubble of radius r_{b}, c_{s} is the solubility of the species in the dispersed phase into the continuous phase, and c_{∞} is the concentration in the ambient fluid. K is the mass transfer coefficient that depends on the local flow conditions (or Reynolds number) as discussed by Zheng and Yapa (2002), who present the following relation:

$$K = 0.0113\sqrt{\frac{u_{\mathrm{s}}\mathcal{D}}{\left(r_0 + 0.1 r_{\mathrm{b}}\right)}} \tag{4.8}$$

where $r_0 = 0.45$ cm, r_{b} is the radius of the bubble, u_{s} is the bubble slip velocity, and $\mathcal{D}$ is the molecular diffusivity of the gas in the liquid. Combining Equation (4.6) with the ideal gas law, the following equation is derived to estimate the change of bubble radius with height

$$\frac{dr_{\mathrm{b}}}{dz} = \frac{K\ P_{atm}\left(c_{\mathrm{s}} - c_{\infty}\right)}{u_{zb}\rho_{gs}\left(P_{atm} + D - z\right)} + \frac{r_{\mathrm{b}}}{3\left(P_{atm} + D - z\right)} \tag{4.9}$$

where u_{zb} is the vertical velocity of the bubble, D is the depth of the source, and ρ_{gs} is the gas density at the surface. The slip velocity of the bubble is often

assumed to be the terminal velocity, and one set of correlations proposed by Wüest et al. (1992) is

$$\begin{aligned} u_s(r_b) &= 4474\, r_b^{1.357} \quad if \;\; r_b < 7\times10^{-4} \\ u_s(r_b) &= 0.23 \quad\quad\quad\;\; if \;\; 7\times10^{-4} < r_b < 5.1\times10^{-3} \\ u_s(r_b) &= 4.202\, r_b^{0.547} \quad if \;\; r_b > 5.1\times10^{-3} \end{aligned}.$$

One must exercise caution in using these equations as their general applicability is not clear. Ishii and Zuber (1979) have also developed correlations for slip velocities of bubble flows, and Onda et al. (1959) have developed correlations for liquid-side mass transfer coefficients.

4.3.2.6 Formation of Droplets at the Source

It is clear that in order to solve the aforementioned differential equation (4.8) from the source at the bottom to the surface at the top, the initial bubble size distribution is needed, which in the case of oil spill depends on a series of complex processes occurring near the wellhead. The oil breakup is influenced by interfacial forces, viscous forces, and inertial forces acting at jet–ambient fluid interface. The competition between cohesive and disruptive forces is responsible for various types of instabilities, shear layer interactions, and entrainment mechanisms that are ultimately responsible for it to break into small dispersed droplets. Instabilities resulting in the deformation of jet surface can be either amplified or damped (see Masutani and Adams, 2001).

A number of distinct flow regimes have been identified to explain the process of jet breakup. Each regime can be associated with a different mechanism by which droplet formations take place. A sound knowledge about the boundaries of these regimes is essential for predicting the type of droplets (mono- or polydispersed) in different oil spill scenarios.

Figure 4.9 shows the evolution of "jet breakup length" observed with a gradual increase in the jet discharge velocity. "Breakup length" is defined as the distance from the discharge location (oil wellhead) to the point where discrete droplets are first observed. The jet is continuous and is able to maintain its integrity, until the breakup point. When oil exits the well at very low velocities, large droplets are produced (drip flow). Further increase in velocity results in the formation of a laminar jet (point C), and breakup length increases linearly until it reaches a maximum. This flow regime is called "Rayleigh instability regime," in which the growth in amplitude of axisymmetric disturbances on the jet surface results in the generation of a stream of essentially *monodispersed* droplets. As indicated in Figure 4.9, breakup length decreases after reaching a maximum value. It has been observed that breakup is accelerated in the presence of shear layers and entrainment originating from the relative velocities of the jet and ambient fluid. Beyond point F on the curve, the relative influence of surface tension decreases, and breakup is mainly dictated by hydrodynamic forces. The "sinuous instability" causes breakup in this regime, and

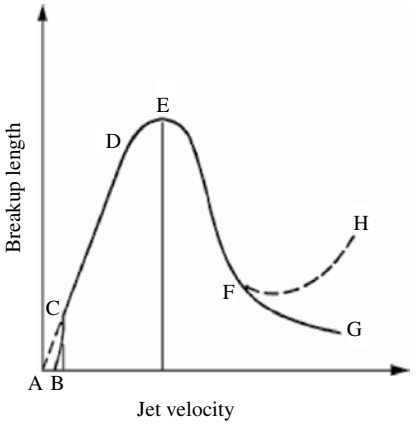

FIGURE 4.9 Variation of jet breakup length with velocity (Grant and Middleman, 1966).

the resulting droplets are smaller in size and are irregular (polydispersed). With further increase in velocity, instability starts on the jet surface and results in a polydispersed spray of fine droplets immediately downstream of the discharge point; however, the core of the jet may still keep its shape intact for some distance before disintegrating into fine droplets. Nondimensional numbers that characterize the jet flow are as follows: (i) Reynolds No, $\mathrm{Re}_D = U_j D/\nu_j$; (ii) Weber No, $\mathrm{We} = \rho_j U_j^2 D/\sigma$; (iii) Ohnesorge No, $Z = \sqrt{We}/\mathrm{Re}_D = \mu_j/\sqrt{\rho_j \sigma D}$; and (iv) Bond No, $\mathrm{Bo} = g\Delta\rho D^2/\sigma$. The subscript j denotes the properties of the jet fluid, and D is jet diameter. Many of these mechanistic models based on an integral approach provide proper scaling laws but leave a number of parameters to be determined from few experimental observations. A different strategy to study multiphase plume and jet would be the *volume average two-fluid model* (TFM), which requires closure relations to capture the dynamical interactions between the dispersed and continuous phase, for interphase momentum, heat, and mass transfer. Such attempts have been made by Buscaglia et al. (2002), Bravo et al. (2007), and Bombardelli et al. (2007) in studying the dynamics of multiphase jets and plumes.

4.3.2.7 Models for Gas Hydrate Formation

Hydrates are crystalline solid-phase compounds that form due to physical forces of attraction between hydrocarbon and water molecules under the right conditions. Such conditions exit near the wellbore of submerged deepwater spills. A number of researchers (e.g., Ng and Robinson, 1977) have investigated the thermodynamics of hydrate formation to identify the pressure and temperature at which hydrates can form. Even the thermodynamics is fairly complicated in the sense that three- (L_1L_2H = liquid – liquid – hydrate) and four-phase (L_1L_2HG = liquid – liquid – hydrate – gas) equilibria are involved. An example of the phase equilibrium is reproduced from Ng and Robinson (1977) in Figure 4.10.

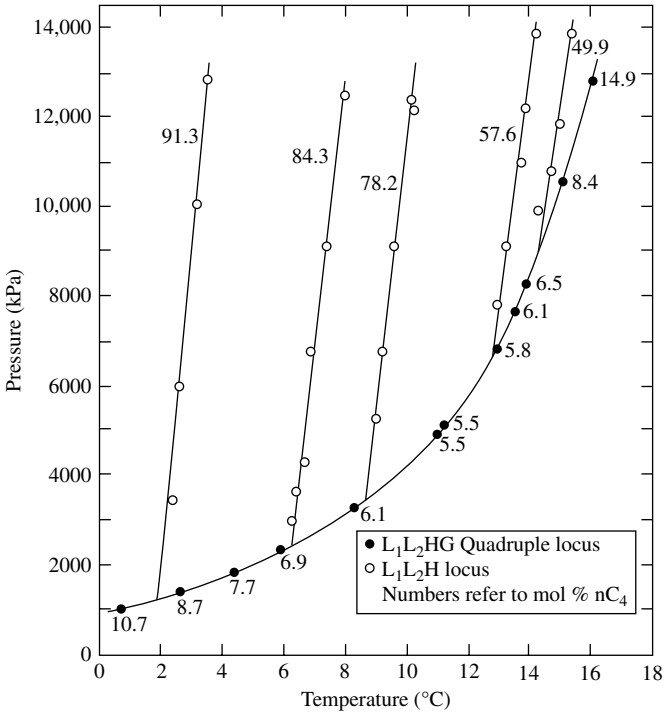

FIGURE 4.10 Three- and four-phase equilibrium in the water, methane, and n-butane system (Ng and Robinson, 1977).

It is clear from the extensive literature that the liquid–liquid–hydrate loci for many of these systems indicate almost linear behavior with a very high positive slope of the order of 1000–10,000 kPa/C. Thermodynamic models to predict such behavior are now well developed. However, hydrate formation under extreme conditions is governed by other rate processes, and the kinetics of methane hydrate formation was investigated, for example, by Vysniauskas and Bishnoi (1983) and others. Topham (1984) has combined the kinetic model for hydrate formation with the integral, self-similar, plume dynamic model of McDougall (1978). The rate expression for the hydrate formation is taken from Vysniauskas and Bishnoi (1983) as

$$r = p^{\alpha} A \exp\left(-\frac{\Delta E}{\mathrm{RT}}\right) \exp\left(-\frac{a}{\Delta T^{\mathrm{b}}}\right) \tag{4.10}$$

where r is the volumetric rate of conversion of gas per unit gas–liquid interfacial area when reduced to normal temperature and pressure (NTP). ΔT is the subcooling below the phase equilibrium temperature at the pressure p, and ΔE is the apparent activation energy of the formation. The exponent α has a value of about 3.0. Topham

(1984) applies his model to a modest hypothetical blowout of 18,000 barrels per day with a gas–oil ratio (GOR) for 150:1. For depths below 800 m, the conversion of gas into hydrates results in the loss of buoyancy of the gas phase, and he concludes that under certain conditions the gas will be lost before the plume reaches the surface. He also cautions that the actual rate of conversion of gas to hydrate depends, among other things, on the bubble surface area that in turn depends on the plume dynamics.

Experimental investigation of hydrate formation under simulated deep-sea environment was conducted by Maini and Bishnoi (1981) using a novel, high-pressure device, in which the bubble of up to 3 cm diameter was held stationary by a downward-flowing water column. They present qualitative observations of the process of hydrate formation with increasing pressures at a temperature of 3°C. Although the equilibrium pressure for hydrate formation was 862 kPa, no hydrates were observed for pressures as high as 2758 kPa. At 4826 kPa, hydrates formed on the surface of the bubble, which were shed as small particles. At higher pressures of 7791 kPa, hydrates formed rapidly and the bubble collapsed, a feature discussed by Topham (1984) in his model causing loss of buoyancy. Other mechanistic models of the hydrate formation under deep-sea conditions have been developed by Yapa et al. (2010) and Chen and Yapa (2001). Both the formation and decomposition of hydrates as the bubble travels up the water column are considered by Chen and Yapa (2001). Once again, the estimation of the initial bubble size is of great importance as the ultimate fate of the bubble depends sensitively on this size. Such mechanistic studies explore the dynamics under controlled conditions, isolating one mechanism at a time, often in the asymptotic limits to yield scaling laws, analytical expressions, and deep insight into the dynamics. On the other hand, the real world, such as those encountered in the oil spill case, is much more complicated, where density gradients caused by salinity, temperature, and phase change coexist and the momentum source is also strong near the well and momentum jet turns into a plume as it evolves over time and with height. Additional factors such as simultaneous dissolution of the hydrocarbons into the aqueous phase, gas release from the oil with decreasing pressures, and the formation of hydrates from both gas- and liquid-phase hydrocarbons cause dynamic changes in the density and size distribution of droplets, bubbles, and solids as dispersed phases. These in turn have profound effect on the dynamics of the plume. The complexities of such processes have been captured in cartoons such as the one shown in Figure 4.11 taken from Thibodeaux et al. (2011). The mathematical equivalent of this conceptual representation is not yet available, although multiphase modeling framework using computational fluid dynamics (CFD), coupled with other transport processes and kinetics of droplet coalescence and breakup through population dynamics, could provide such a general framework.

To be able to capture all of these interactions and transitions in a dynamically evolving scenario should be the goal of a comprehensive computational model in the framework of a CFD model. Nevertheless, such analytical results and experimental data offer opportunities for model validation for studies using the general framework of CFD models. Next, we review the current status of this approach as applied to oil spill scenarios and present some preliminary results based on our recent work.

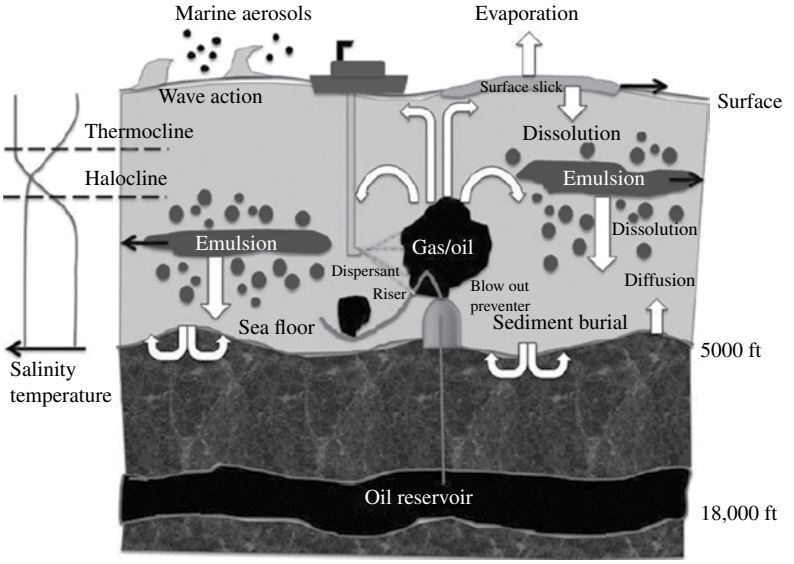

FIGURE 4.11 Illustration of mechanisms in deepwater oil spill process (Thibodeaux et al., 2011).

4.4 GENERIC APPROACHES FOR MULTIPHASE FLOW MODELS

Depending on the fidelity of the mathematical model and the level of details required from the model, a variety of alternate formulations are available for studying multiphase transport processes that permit coupling between various mechanisms. The common ones are the Mixture–Eulerian (M–E) framework, the Eulerian–Lagrangian (E–L) framework, and the Eulerian–Eulerian (E–E). Other methods such as the direct numerical simulations (DNS), both for turbulence and for multiphase flows, and level-set or volume-of-fluid formulations to study the dynamics of immiscible fluids are not suitable for field-scale applications, although they can offer insight into transport process between dispersed phases under small scales and assist in developing closure models that are needed in the field-scale applications using E–E and E–L frameworks. Recent books devoted to the theoretical treatment of this subject are Brennen (2009), Tryggvason et al. (2011), and Prosperetti and Tryggvason (2007).

The idea of interpenetrating continua is illustrated in Figure 4.12. The inset shows the representative elemental volume over which we average all of the field quantities. As with any averaging operation, there is a progressive loss of information that must be provided by closure relations. Commercially available CFD simulators such as FLUENT offer such modeling framework with a set of predefined closure models as options. The success of using such models depends on the appropriateness of the closure models to capture the interphase transport processes. First, we discuss the M-E model, which is based on this concept of interpenetrating continua.

FIGURE 4.12 Concept of interpenetrating continua. In averaging over a sample volume that remains large enough compared to dispersed phase but small enough to vessel dimensions, interphase transport of momentum, heat, and mass are not resolved, but must be modeled by closure relations. Volume-averaged quantities such as velocities and volume fractions of each phase are treated as continuous variables of space.

The continuity equation is

$$\frac{\partial \rho_{\mathrm{m}}}{\partial t} + \nabla \cdot \left(\rho_{\mathrm{m}} \boldsymbol{v}_{\mathrm{m}} \right) = 0 \tag{4.11}$$

where $v_{\mathrm{m}} = \sum_{\mathrm{k}} \alpha_{\mathrm{k}} \rho_{\mathrm{k}} v_{\mathrm{k}} / \rho_{\mathrm{m}}$ is the mass-averaged velocity of the mixture of all phases k, $\rho_{\mathrm{m}} = \sum_{\mathrm{k}} \alpha_{\mathrm{k}} \rho_{\mathrm{k}}$ is the mixture density, and α_{k} is the volume fraction of the phase k.

Similarly, the momentum equation for the mixture is given by

$$\begin{aligned} \frac{\partial \rho_{\mathrm{m}} \boldsymbol{v}_{\mathrm{m}}}{\partial t} + \nabla \cdot \left(\rho_{\mathrm{m}} \boldsymbol{v}_{\mathrm{m}} \boldsymbol{v}_{\mathrm{m}} \right) = -\nabla p + \nabla \cdot \left[\mu_{\mathrm{m}} \left(\nabla \boldsymbol{v}_{\mathrm{m}} + \nabla \boldsymbol{v}_{\mathrm{m}}^{\mathrm{T}} \right) \right] \\ + \rho_{\mathrm{m}} \boldsymbol{g} + \boldsymbol{F} + \nabla \cdot \left(\sum_{\mathrm{k}} \alpha_{\mathrm{k}} \rho_{\mathrm{k}} \boldsymbol{v}_{\mathrm{dr,k}} \boldsymbol{v}_{\mathrm{dr,k}} \right) \end{aligned} \tag{4.12}$$

where $\boldsymbol{F}$ is the body force and $\boldsymbol{v}_{\mathrm{dr,k}} = \boldsymbol{v}_{\mathrm{k}} - \boldsymbol{v}_{\mathrm{m}}$ is the drift velocity for phase k. If the drift velocity is assumed to be 0, then it is equivalent to all phases moving with the same velocity as in a homogeneous flow model, which is not suitable for bubble plume dynamics. The drift flux model requires the drift flux to be specified by an external model. In this approach, we solve for mean velocity from (4.11) and (4.12) and the volume fraction from the continuity equation for each phase, p, given by

$$\frac{\partial \alpha_{\mathrm{p}} \rho_{\mathrm{p}}}{\partial t} + \nabla \cdot (\alpha_{\mathrm{p}} \rho_{\mathrm{p}} \boldsymbol{v}_{\mathrm{m}}) = -\nabla \cdot (\alpha_{\mathrm{p}} \rho_{\mathrm{p}} \boldsymbol{v}_{\mathrm{dr,p}}) + \sum_{\mathrm{q}=1}^{n} (\dot{m}_{\mathrm{qp}} - \dot{m}_{\mathrm{pq}}), \tag{4.13}$$

where $\dot{m}_{\mathrm{qp}}$ is the interphase mass transfer between phases q and p. This represents the total mass transfer between the phases due to evaporation, condensation, etc.

Next, in the E-L framework, the dispersed phases, namely, oil and gas, are tracked in the Lagrangian framework, while the ambient fluid, namely, the seawater in this case, is solved in the Eulerian framework. Since the interaction of the *rise velocity* of

the oil and gas with the *crosscurrent velocity* of the seawater determines the time and location of the plume to reach its terminal state either on the ocean surface or floor, a representative sample of the dispersed phase droplets/bubbles could be tracked to identify the location and time to reach it. The rise velocity however depends *critically* on the size of the dispersed phase, and often, there is a distribution of sizes that must be dealt with. In addition, interface mass transfer from the dispersed phase to the continuous phase can also be modeled to determine if the initially light oil droplets will lose all of the lighter material and end up heavier and as a result sink to the bottom of the floor. Models based on purely Lagrangian framework have been developed and validated for oil spill by several researchers (see Yapa and Li, 1997b; Zheng and Yapa, 1998; Zheng et al., 2002; Johansen, 2000, 2003; Johansen et al., 2003).

Examples of such studies in the E-L framework as applied to subsea gas release are by Cloete et al. (2009), Johansen (2000), and Johansen et al. (2003). The single-phase *continuity* and momentum equations are given by

$$\frac{\partial(\rho)}{\partial t} + \nabla \cdot (\rho \boldsymbol{u}) = 0 \tag{4.14}$$

$$\frac{\partial(\rho \boldsymbol{u})}{\partial t} + \nabla \cdot (\rho \boldsymbol{u}\boldsymbol{u}) = -\nabla P + \nabla \cdot \left[\mu \left(\nabla \boldsymbol{u} + \nabla \boldsymbol{u}^{\mathrm{T}} \right) \right] + \rho \boldsymbol{g} + \boldsymbol{F}. \tag{4.15}$$

These are the standard single-phase Navier–Stokes equations for the continuous phase. If the flow is turbulent, then a turbulence model is added and the effective viscosity used is $\mu = \mu_{\mathrm{M}} + \mu_{\mathrm{T}}$, the sum of molecular and turbulent viscosities. For trajectory tracking of the dispersed phase, the net momentum transfer to the continuous phase, $\boldsymbol{F}$, could be neglected if the volume fraction of the dispersed phases is low. If the volume fraction is large, then $\boldsymbol{F}$ could be determined and added to the aforementioned equation. The dispersed phases are modeled in the Lagrangian framework using the following equation:

$$m_{\mathrm{p}} \frac{d\boldsymbol{u}_{\mathrm{p}}}{dt} = F_{\mathrm{D}}(\boldsymbol{u} - \boldsymbol{u}_{\mathrm{p}}) + \frac{\boldsymbol{g}(\rho_{\mathrm{p}} - \rho)}{\rho_{\mathrm{p}}} + \boldsymbol{F}_{\mathrm{p}}; \qquad \frac{d\boldsymbol{x}_{\mathrm{p}}}{dt} = \boldsymbol{u}_{\mathrm{p}}. \tag{4.16}$$

Here, the first term on the right-hand side represents the drag force exerted by the fluid on the dispersed phase, the second term represents the buoyancy force, and the third term could represent additional forces like the added mass force and turbulent dispersion forces. $\boldsymbol{u}_{\mathrm{p}}$ is the dispersed phase velocity, and $\boldsymbol{u}$ is the continuous phase velocity given by the Navier–Stokes equation. While Cloete et al. (2009) treat these as *point particles* released at a rate of 10 bubbles every 2 ms to track the trajectory of a representative volume of the dispersed phase that are subject to realistic external forces from the continuous fluid, more recent progress (Wu et al., 2009, 2010) permits the dynamics of millions of *finite size* particles/droplets to be simulated taking into account the two-way coupling between the dispersed phase and the continuous phase. Furthermore, in the case of gas bubbles, as it rises through

a column of water, it will undergo size changes not only due to coalescence and breakup, which can be included using a population balance model (see Farzpourmachiani et al., 2011), but will also expand due to decreasing hydrostatic pressure or contract due to the loss of lighter material by dissolution. Cloete et al. (2009) track the bubble diameter in the Lagrangian framework using

$$\frac{\partial \rho_b d_b}{\partial t} = \rho_b \frac{d_b^{eq} - d_b}{\tau_{rel}} \tag{4.17}$$

where $\rho_b = \alpha_b \hat{\rho}_b$ is the bulk density, τ_{rel} is the relaxation time, and d_b^{eq} is the mean equilibrium diameter given by

$$d_v^{eq} = C_1 \alpha_1^{0.5} \frac{(\sigma/\rho)^{0.6}}{\varepsilon^{0.4}} \left(\frac{\mu_b}{\mu} \right)^{0.25} + C_2 \tag{4.18}$$

where σ is the surface tension, ρ is the density of the continuous phase, ϵ is the turbulent dissipation energy, and $\mu$is the viscosities of the bubble and continuous phases, respectively. C_1, C_2 are taken as tuning constants in the model. Although detailed heat and mass transfer in such plumes have not been modeled in the literature, recent evidence in the DWH spill suggests that these processes are indeed important.

Finally, we present the details of the E-E framework and in fact present some simulation results using this model for the actual oil spill scenario. This framework is used to track the dynamics of a submerged oil–gas plume using a three-phase model under controlled laboratory conditions for which experimental data are available in the literature (Masutani and Adams, 2001). The unsteady-state equations of continuity for ambient liquid, oil, and gas phases are given by (see, e.g., Ranade, 2002)

$$\frac{\partial(\rho_q \alpha_q)}{\partial t} + \nabla \cdot (\rho_q \alpha_q \langle \boldsymbol{u}_q \rangle) = 0 \tag{4.19}$$

where α stands for volume fraction, ρ stands for density, $\boldsymbol{u}$ stands for the volume-averaged velocity, and the subscript q stands for (L, O, G) the continuous liquid phase, oil phase, and gas phase, respectively. Note that in the aforementioned model, no mass transfer rate from phase p to phase q through dissolution or evaporation is accounted for, since the experimental data that we are validating using this model considers only hydrodynamic factors. In the actual case, this mechanism is important, and it could be easily included in our model. The momentum balance equations for each of the phases is given by

$$\begin{aligned} \frac{\left(\partial \rho_L \alpha_L \boldsymbol{u}_L\right)}{\partial t} + \nabla \cdot \left(\rho_L \alpha_L \left\langle \boldsymbol{u}_L \right\rangle \left\langle \boldsymbol{u}_L \right\rangle \right) &= -\alpha_L \nabla \langle P \rangle \\ &+ \nabla \cdot \left(\alpha_L \mu_{eff,L} \left(\nabla \left\langle \boldsymbol{u}_L \right\rangle + \left(\nabla \left\langle \boldsymbol{u}_L \right\rangle \right)^T \right) \right) \\ &+ \rho_L \alpha_L \boldsymbol{g} + \boldsymbol{K}_{LO} + \boldsymbol{K}_{Lg} + \boldsymbol{F}_{lg} + \boldsymbol{F}_{vg} \end{aligned} \tag{4.20a}$$

$$\frac{\partial\left(\rho_{\mathrm{O}}\alpha_{\mathrm{O}}\left\langle \boldsymbol{u}_{\mathrm{O}}\right\rangle\right)}{\partial t}+\nabla\cdot\left(\rho_{\mathrm{O}}\alpha_{\mathrm{O}}\left\langle \boldsymbol{u}_{\mathrm{O}}\right\rangle\left\langle \boldsymbol{u}_{\mathrm{O}}\right\rangle\right)=-\alpha_{\mathrm{O}}\nabla P$$
$$+\nabla\cdot\left(\alpha_{\mathrm{O}}\mu_{\mathrm{eff,O}}\left(\nabla\left\langle \boldsymbol{u}_{\mathrm{O}}\right\rangle+\left(\nabla\left\langle \boldsymbol{u}_{\mathrm{O}}\right\rangle\right)^{\mathrm{T}}\right)\right)$$
$$+\rho_{\mathrm{O}}\boldsymbol{\alpha}_{\mathrm{O}}\boldsymbol{g}-\boldsymbol{K}_{\mathrm{LO}} \tag{4.20b}$$

$$\frac{\partial\left(\rho_{\mathrm{g}}\alpha_{\mathrm{g}}\left\langle \boldsymbol{u}_{\mathrm{g}}\right\rangle\right)}{\partial t}+\nabla\cdot\left(\rho_{\mathrm{g}}\alpha_{\mathrm{g}}\left\langle \boldsymbol{u}_{\mathrm{g}}\right\rangle\left\langle \boldsymbol{u}_{\mathrm{g}}\right\rangle\right)=-\alpha_{\mathrm{g}}\nabla P$$
$$+\nabla\cdot\left(\alpha_{\mathrm{g}}\mu_{\mathrm{eff,g}}\left(\nabla\left\langle \boldsymbol{u}_{\mathrm{g}}\right\rangle+\left(\nabla\left\langle \boldsymbol{u}_{\mathrm{g}}\right\rangle\right)^{T}\right)\right)$$
$$+\rho_{\mathrm{g}}\alpha_{\mathrm{g}}\boldsymbol{g}-\boldsymbol{K}_{\mathrm{Lg}}-\boldsymbol{F}_{\mathrm{lg}}-\boldsymbol{F}_{\mathrm{vg}} \tag{4.20c}$$

where $\boldsymbol{g}$ is the gravitational acceleration, $\boldsymbol{K}_{\mathrm{LO}}$ and $\boldsymbol{K}_{\mathrm{Lg}}$ are the interphase momentum transfer terms with the oil and gas phases being treated as the dispersed phases, and μ_{eff} is the effective viscosity. $\boldsymbol{F}_{\mathrm{lg}}$ and $\boldsymbol{F}_{\mathrm{vg}}$ are the lift and virtual mass forces for the gas phase (in the present model, the lift and virtual mass forces on the oil droplets are neglected due to the small density difference between seawater and the oil). The phase volume fractions satisfy the following condition:

$$\alpha_{\mathrm{L}}+\alpha_{\mathrm{O}}+\alpha_{\mathrm{g}}=1. \tag{4.21}$$

Constitutive equations are required to close these governing equations. Interactions between the phases involve various momentum exchange mechanisms such as the drag, the lift, and the added mass force.

For drag law,

$$\boldsymbol{K}_{\mathrm{LO}}=\frac{3}{4}\rho_{\mathrm{L}}\alpha_{\mathrm{L}}\alpha_{\mathrm{O}}\frac{C_{\mathrm{D}}}{d_{\mathrm{o}}}\left(\boldsymbol{u}_{\mathrm{L}}-\boldsymbol{u}_{\mathrm{o}}\right) \tag{4.22a}$$

$$\boldsymbol{K}_{\mathrm{Lg}}=\frac{3}{4}\rho_{\mathrm{L}}\alpha_{\mathrm{L}}\alpha_{\mathrm{g}}\frac{C_{\mathrm{D}}}{d_{\mathrm{g}}}\left(\boldsymbol{u}_{\mathrm{L}}-\boldsymbol{u}_{\mathrm{o}}\right), \tag{4.22b}$$

where C_{D} is the drag coefficient, and the correlation proposed by Schiller and Naumann (1933) was used:

$$C_{\mathrm{D}}=\frac{24}{\mathrm{Re}}\left(1+0.15\,\mathrm{Re}^{0.687}\right)\quad \mathrm{Re}\le 1000$$
$$=0.44\quad \mathrm{Re}>1000$$

where Re is the Reynolds number for either the oil droplet $(d_{\mathrm{o}}|u_{\mathrm{L}}-u_{\mathrm{o}}|\rho_{\mathrm{L}})/\mu_{\mathrm{L}}$ or the gas bubble $(d_{\mathrm{g}}|u_{\mathrm{L}}-u_{\mathrm{g}}|\rho_{\mathrm{L}})/\mu_{\mathrm{L}}$. Note that the *bubble and droplet diameters* $(d_{\mathrm{g}},d_{\mathrm{o}})$ are key input parameters, which unfortunately depend dynamically on the flow conditions

with perhaps a distribution of sizes in each phase (see Masutani and Adams, 2001). A population balance model can be coupled with the CFD model that will give greater flexibility to the modeler to track size distributions of these dispersed phases based on the coalescence and breakup models. Recent study on bubble columns exploits this framework, and a similar approach could be readily applied to oil–gas discharge under submerged jets, provided controlled experiments are available on bubble/droplet size distribution to tune the parameters in the coalescence–breakup models. This is beyond the scope of the present discussions; the reader is referred to Farzpourmachiani et al. (2011) for further details. But generic codes such as FLUENT do offer such ability to solve flow models coupled with population balance models.

Lift force (F_{lg}) for gas bubbles is modeled by

$$\boldsymbol{F}_{\mathrm{lg}} = -0.5\rho_{\mathrm{L}}\alpha_{\mathrm{g}}(\boldsymbol{u}_{\mathrm{L}} - \boldsymbol{u}_{\mathrm{g}}) \times (\nabla \times \boldsymbol{u}_{\mathrm{L}}). \tag{4.23}$$

Virtual mass force (F_{vg}) for gas bubbles is modeled by

$$\boldsymbol{F}_{\mathrm{vg}} = 0.5\frac{\rho_{\mathrm{L}}}{\rho_{\mathrm{o}}}\frac{d}{dt}(\boldsymbol{u}_{\mathrm{L}} - \boldsymbol{u}_{\mathrm{g}}). \tag{4.24}$$

It is proposed to use the most common k–ε model for turbulence closure. The standard k–ε model for single-phase flows has been extended in an ad hoc manner for the three-phase flows with extra terms that include interphase turbulent momentum transfer to take into account the effects of turbulence. The governing equations for the turbulent kinetic energy (k) and the energy dissipation rate (ε) for the ambient liquid phase are given by

$$\frac{\partial\left(\rho_{\mathrm{L}}\alpha_{\mathrm{L}}k_{\mathrm{L}}\right)}{\partial t} + \langle u_{\mathrm{L}}\rangle\nabla\cdot\left(\rho_{\mathrm{L}}\alpha_{\mathrm{L}}k_{\mathrm{L}}\right) = \nabla\cdot\left(\alpha_{\mathrm{L}}\left(\mu_{\mathrm{L}} + \frac{\mu_{\mathrm{T}}}{\sigma_{\mathrm{k}}}\right)\nabla k_{\mathrm{L}}\right) + \rho_{\mathrm{L}}\alpha_{\mathrm{L}}\left(P_{kL} - \varepsilon_{\mathrm{L}}\right) \tag{4.25}$$

$$\begin{aligned}\frac{\partial\left(\rho_{\mathrm{L}}\alpha_{\mathrm{L}}\varepsilon_{\mathrm{L}}\right)}{\partial t} + \langle u_{\mathrm{L}}\rangle\nabla\cdot\left(\rho_{\mathrm{L}}\alpha_{\mathrm{L}}\varepsilon_{\mathrm{L}}\right) &= \nabla\cdot\left(\alpha_{\mathrm{L}}\left(\mu_{\mathrm{L}} + \frac{\mu_{\mathrm{T}}}{\sigma_{\varepsilon}}\right)\nabla\varepsilon_{\mathrm{L}}\right) \\ &\quad + \rho_{\mathrm{L}}\alpha_{\mathrm{L}}\frac{\varepsilon_{\mathrm{L}}}{k_{\mathrm{L}}}\left(C_{\varepsilon 1}P_{\mathrm{kL}} - C_{\varepsilon 2}\varepsilon_{\mathrm{L}}\right).\end{aligned} \tag{4.26}$$

The solution of these field equations can be accomplished routinely with CFD software tools such as FLUENT. These are highly nonlinear, coupled partial differential equations, requiring access to high-performance computing (HPC) facilities at LSU, the Louisiana Optical Network Initiative (LONI) supercomputers.

Future work will couple species transfer model using the convective-diffusion equation for lighter hydrocarbons to track dissolution and evaporation of species from one phase to the other. At present, we restrict ourselves to the hydrodynamics of underwater transportation of the spilled oil/gas and effect of crosscurrents using the experimental data of Masutani and Adams (2001) for validation.

4.5 SAMPLE MODEL RESULTS

The present mathematical model has been validated for a submerged jet/plume in confined boundaries by different researchers under different flow scenarios (Gulawani et al., 2008; Karvinen and Ahlstedt, 2005; Patwardhan, 2002). However, there is little information about the applicability of this model for a three-phase plume (oil, gas, and water) and the separation of oil and gas plumes in the presence of the ambient currents. Therefore, we first validated the present model with the small-scale laboratory experiments of Masutani and Adams (2001). These controlled experiments have been performed with a mixture of oil and gas plume with uniform ambient cross flow along the height.

Simulations have been performed in a 2-D domain with a height of 0.8 m and width of 1.2 m. A uniform cross flow boundary condition has been implemented. The diameter of the oil–gas plume inlet is 10 mm. In all simulations, the oil to gas flow rate ratio was kept at unity. The oil and gas inlet flow rate is 250 ml/min. The geometrical details and the physical properties of the oil and gas used in the simulations are given in Table 4.2.

The contour plots of the volume fraction of the oil and gas phase have been shown along with the snapshot of the experiment in Figure 4.13. In order to show the volume fractions of each phase and their trajectories, the oil and the gas volume fraction contour plots are shown separately. It can be observed that at an ambient crosscurrent of 2 cm/s, the oil and gas plumes remain close to each other and rise to the surface as a single plume. As the ambient crosscurrent strength increases, it is expected the plumes will separate. At a crosscurrent strength of 10 cm/s, the separation of the two plumes is more pronounced. It can be observed that the trajectories of the experiments and simulations are in good agreement.

In the next step, we applied the validated CFD model to a few realistic scenarios of a deepwater oil spill corresponding to the conditions experienced in the DWH oil spill in the GoM at a water depth of approximately 5000 ft (1524 m) and 41 miles of

TABLE 4.2 Simulation details of oil–gas plume separation in a laboratory-scale experiment

Contents	Values
Domain size	1.2 m × 0.8 m × 0.7 m
Number of controlled volumes	Around 1.1 million
Oil/gas inlet diameter	0.02 m
Water density	1000 kg/m^3
Oil density	870 kg/m^3
Oil droplet average size	1 mm
Flow rate of oil	600 cc/min
Viscosity of the oil	28 cP
Gas density	1.25 kg/m^3
Gas bubble average size	2.4 mm
Flow rate of gas	600 cc/min

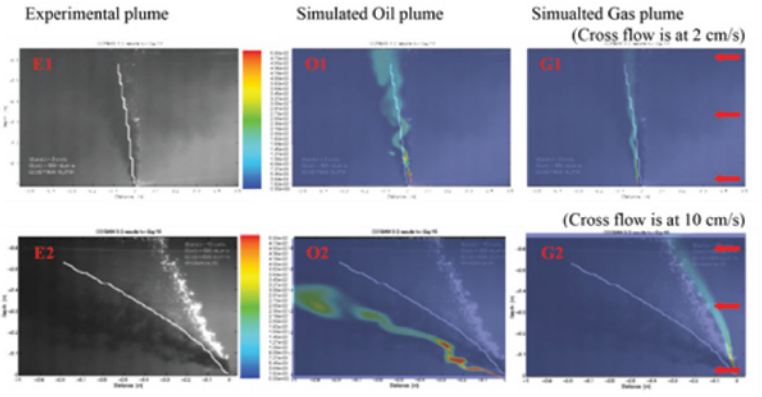

FIGURE 4.13 Oil and gas plume trajectories. (E1, E2) are experimental trajectories at cross flow of 2 and 10 cm/s, and (O1, O2) show the oil trajectories at the same cross flows. (G1, G2) show the gas trajectories at the same cross flows. The separation of trajectories is small at low cross flow velocities.

TABLE 4.3 Large-scale oil/gas simulation details

Contents	Values
Domain size	1500 m × 1500 m × 1500 m
Number of controlled volumes	Around 650,000
Oil/gas inlet diameter	1 m
Water density	1025 kg/m^3
Oil density	870 kg/m^3
Oil droplet average size	3 mm
Inlet velocity of oil	1 m/s
Viscosity of the oil	30 cP
Methane gas density	0.665 kg/m^3
Methane gas bubble average size	3 mm
Inlet velocity of methane gas	1 m/s

the Louisiana coast. For this, the domain having dimensions of 1500 m × 1500 m × 1500 m has been selected.

The total numbers of control volumes are around 650,000. The details of the physical properties of the oil and gas used in the simulations are given in Table 4.3. The trajectories of the oil plume at ocean currents of 0.2 m/s (starting at a height of 300 m from seabed and remaining uniform up to 1500 m) are shown in Figure 4.14 at various instants of time. The cross flow intensity and domain of depth are arbitrarily chosen to show the correct cause and effect relationships. It can be seen that due to ocean currents, the oil remains in the subsurface for an extended period of time and appears at the surface many miles above the well site. Such behavior provides a longer residence time for the more soluble oil and gas (e.g., methane) fractions to dissolve. Occasional high ocean current regimes in their path may carry the

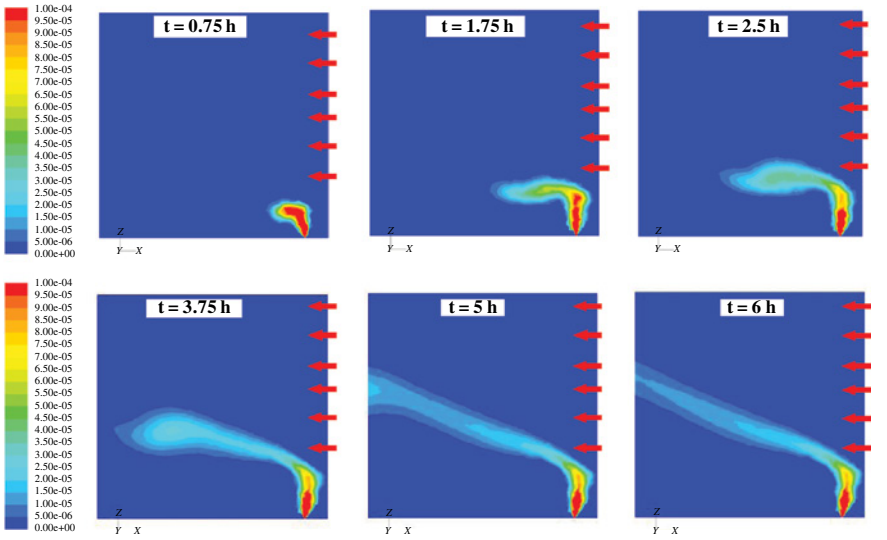

FIGURE 4.14 Contour plots of volume fraction of oil plume (cross flow velocity is 0.2 m/s and starts from 300 m above seabed).

hydrocarbons even wider and far. It is obviously interesting to conduct a parametric study of the oil and gas injection velocity from the well, their relative volume fraction, and their droplet and bubble size on the trajectory.

Figure 4.15 shows the trajectory in the likely event of a cross flow occurring only from 300 to 700 m from the bed height at two cross flow intensity values of 0.2 and 0.4 m/s. The trajectories show a consistent behavior that one would expect, with the correct causal relationship. The impact of the limited cross flow region is to shift the trajectory to the left only in that zone; otherwise, the plume travels vertically upward both below and above the cross flow regime.

In the presence of a density gradient and dissolution of lighter hydrocarbon in the water, a methane intrusion layer has been documented in field measurements by Yvon-Lewis et al. (2011). In order to simulate those features, a species transport equation must be added to the aforementioned model together with the mass transfer and dissolution model to couple the plume dynamics with the stratification and dissolution in order to capture the intrusion layer feature. It is such detailed validation of every documented feature on the large scale that will instill confidence in the predictive capabilities of such modeling approaches. Our current work is continuing along those lines of inquiry.

4.6 CONCLUDING REMARKS

Validated model development is the key to reliability of any future predictions for a deepwater oil spill. Coupling of various mechanisms that we have reviewed here and for which isolated models are available is another key feature that must be

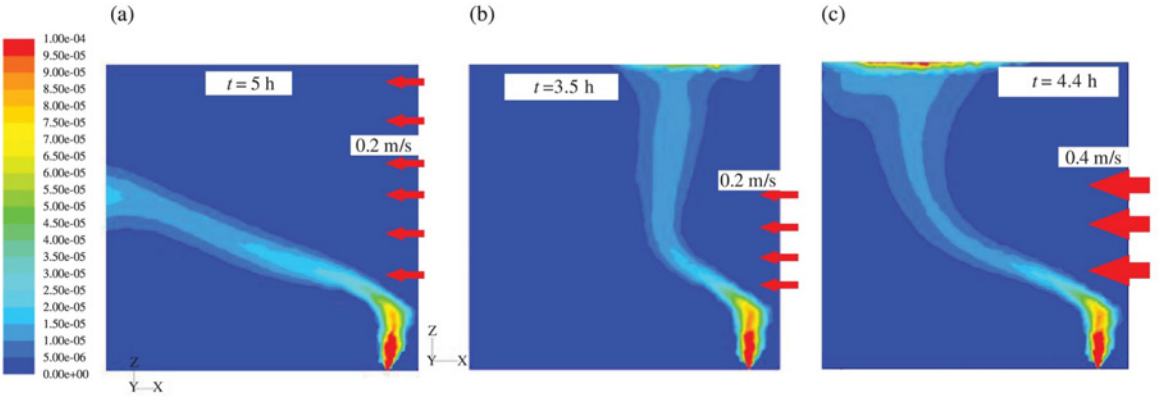

FIGURE 4.15 Contour plots of volume fraction of oil plume. Cross flow velocity is (**a**) 0.2 m/s and starts from 300 m above seabed to 1500 m, (**b**) 0.2 m/s and starts from 300 m above seabed to 700 m, and (**c**) 0.4 m/s and starts from 300 m above seabed to 700 m.

accomplished in the next generation of oil spill models. Coupling of deepwater process with the surface spill models remains another elusive goal as once the oil breaks through to the surface, weathering and ocean wave dynamics will determine the fate of the oil that continues to age on the surface. While it is feasible to develop a comprehensive model with all of the coupled mechanisms, we still need three-dimensional data on the prevailing ocean currents. The output of such models is only as good as the input data to the model. In that sense, the development of a comprehensive model for predicting the oil spill fate requires sustained effort to develop modular toolboxes that can be integrated into a general modeling framework for versatile applications.

ACRONYMS

API	The American Petroleum Institute gravity, or *API gravity*, is a measure of how heavy or light a petroleum liquid is compared to water. If its API gravity is greater than 10, it is lighter and floats on water; if less than 10, it is heavier and sinks.
BP	British Petroleum
DWH	Deepwater Horizon
DOE	Department of Energy
EPA	Environmental Protection Agency
MMSCFD	Million standard cubic feet per day of gas
NOAA	National Oceanic and Atmospheric Administration
NTP	Normal temperature and pressure
TFM	Two-fluid model
USGS	U.S. Geological Survey

NOTATION

b_u	Jet lateral dimension where velocity is 37% of maximum mean
B	Specific buoyancy flux
$b(x)$	Jet lateral dimension at boundary
C_s	Solubility of species in dispersed phase into continuous phase
C_∞	Concentration in ambient fluid
C_D	Drag coefficient
D	Molecular diffusivity
ΔE	Apparent activation energy of formation
h_T	Trap height
K	Mass transfer coefficient
M	Momentum flux
m_b	Mass of the bubble of radius r_b
N	Brunt–Väisälä frequency
r	Radial velocity
r_b	Radius of the bubble
T_m	Maximum mean temperature on the jet axis

T_∞ Temperature in the environment
ΔT Subcooling below phase equilibrium temperature at pressure "p"
u_{zb} Vertical velocity of bubble
u, v, w Velocity components along x, y, and z coordinates
u' Local velocity fluctuation from mean in x-direction
$\overline{u}$ Mean velocity in axial direction on jet or plume
u_s Slip velocity of bubble
U_m Maximum mean velocity on jet axis
v_m Mass-averaged velocity

GREEK LETTERS

α_k Volume fraction of phase "k"
β Volumetric coefficient of thermal expansion
ν Kinematic viscosity
ϵ Turbulent dissipation energy
K Thermal diffusivity
ρ_{gs} Gas density at surface
ρ_0 Source fluid density
ρ_s Ambient fluid density
ρ_g Gas-phase density
ρ_L Liquid-phase density
ρ_m Mixture density
ρ_b Bulk fluid density
τ_{rel} Relaxation time
σ Surface tension
ϵ Turbulent dissipation energy

ACKNOWLEDGMENTS

The authors (KN and KTV) would like to acknowledge the financial support from the Gulf of Mexico Research Initiative (GoMRI) to the CMEDS consortium. Access to the computational resources from HPC, LONI and XSEDE are also gratefully acknowledged.

REFERENCES

Agrawal M, Dakshinamoorthy D. Computational analysis of oil spill in shallow water due to wave and tidal motion. In: Offshore Technology Conference, Houston, TX; 2–5 May 2011.

Becker HA, Massaro TA. Vortex evolution in a round jet. J Fluid Mech 1968;31(3):435–448.

Bill RG, Gebhart B. The transition of plane plumes. Int J Heat Mass Transfer 1975;18(4):513–526.

Bombardelli FA, Buscaglia GC, Rehmann CR, Rincón LE, García MH. Modeling and scaling of aeration bubble plumes: a two-phase flow analysis. J Hydraul Res 2007;45(5):617–630.

Brandvik PJ, Faksness LG. Weathering processes in Arctic oil spills: meso-scale experiments with different ice conditions. Cold Reg Sci Technol 2009;55(1):160–166.

Bravo HR, Gulliver JS, Hondzo M. Development of a commercial code-based two-fluid model for bubble plumes. Environ Model Softw 2007;22:536–547.

Brennen CE. *Fundamentals of Multiphase Flow*. Cambridge, UK: Cambridge University Press; 2009.

British Petroleum. 2010. Deepwater Horizon accident. Available at http://www.bp.com/sectiongenericarticle800.do?categoryId=9036575&contentId=7067541. Accessed October 16, 2002.

Burns K. Gulf oil spill health hazards. Public report. Lexington, MA: Sciencecorps; 2010. Ver 1.0: 51.

Buscaglia GC, Bombardelli FA, García M. Numerical modeling of large-scale bubble plumes accounting for mass transfer effects. Int J Multiph Flow 2002;28(11):1763–1785.

Chassaing P, George J, Claria A, Sananes F. Physical characteristics of subsonic jets in a cross stream. J Fluid Mech 1974;62:41–64.

Chen CJ, Rodi W. *Vertical Turbulent Buoyant Jets: A Review of Experimental Data*. London/New York: Pergamon; 1980.

Chen FH, Yapa PD. Estimating hydrate formation and decomposition of gases released in a deepwater ocean plume. J Mar Syst 2001;30(1–2):21–32.

Chen F, Yapa PD. A model for simulating deep water oil and gas blowouts – Part II: Comparison of numerical simulations with "Deepspill" field experiments. J Hydraul Res 2003;41(4):353–365.

Chen FH, Yapa PD. Modeling gas separation from a bent deepwater oil and gas jet/plume. J Mar Syst 2004a;45(3–4):189–203.

Chen FH, Yapa PD. Three-dimensional visualization of multi-phase (oil/gas/hydrate) plumes. Environ Model Softw 2004b;19(7–8):751–760.

Chen FH, Yapa PD. Estimating the oil droplet size distributions in deepwater oil spills. J Hydraul Eng 2007;133(2):197–207.

Clift R, Grace JR, Weber ME. *Bubbles, Drops, and Particles*. Mineola, NY: Dover Publications; 2005.

Cloete S, Olsen JE, Skjetne P. CFD modeling of plume and free surface behavior resulting from a sub-sea gas release. Appl Ocean Res 2009;31(3):220–225.

Comerma E, Espino M, Daniel P, Doré A, Cabioch F. An update of an oil spill model and its application in the Bay of Biscay: the weathering processes. In: Brebbia CA. Oil and Hydrocarbon Spills III: Modelling, Analysis and Control, 2002;11:13–22.

Crabb D, Durao DFG, Whitelaw JH. A round jet normal to a crossflow.J Fluids Eng—Trans ASME 1981;103(1):42–53.

Crawford TV, Leonard AS. Observations of buoyant plumes in calm stably stratified air. J Appl Meteorol 1962;1(2):251–256.

Curl HC , Barton K, et al. (1992). Oil spill case histories, 1967–1991 summaries of significant U.S. and international spills. NOAA, Hazardous Materials Response and Assessment Division. Seattle, WA.

Dasanayaka LK, Yapa PD. Role of plume dynamics phase in a deepwater oil and gas release model. J Hydro-Environ Res 2009;2(4):243–253.

Department of Energy (DOE). 2010, Updated through 12:00 AM on July 16, 2010. Combined total amount of oil and gas recovered daily from the Top Hat and choke line oil recovery systems. Available at http://www.energy.gov/open/documents/5_2_Item_84_Recovery_Volumes_16_July_0000.xls. Accessed October 16, 2013.

Dickins, D.F. and Buist, I.A. (1981). Oil and Gas Under Sea Ice. Prepared by Dome Petroleum Ltd. for COOSRA, Report CV-1, Volumes I and II, Calgary, Alberta, Canada.

DOE. 2010. Department of Energy actions on BP oil spill. Available at http://www.energy.gov/open/oil_spill_updates.htm. Accessed October 16, 2013.

Einarsrud KE, Brevik I. Kinetic energy approach to dissolving axisymmetric multiphase plumes. J Hydraul Eng 2009;135(12):1041–1051.

Environmental Protection Agency. 2010. EPA response to BP spill in the Gulf of Mexico. Available at http://www.epa.gov/bpspill/. Accessed October 16, 2013.

Farzpourmachiani A, Shams M, Shadaram A, Azidehak F. Eulerian–Lagrangian 3-D simulations of unsteady two-phase gas–liquid flow in a rectangular column by considering bubble interactions. Int J Non-Linear Mech 2011;46(8):1049–1056.

Fischer HB, List EJ, Koh RCY, Imberger J, Brooks NH. *Mixing in Inland and Coastal Waters*. New York: Academic Press; 1979.

Gennes P-Gd, Brochard-Wyart F, Quéré D. *Capillarity and Wetting Phenomena: Drops, Bubbles, Pearls, Waves*. New York: Springer; 2010.

Gin KYH, Huda K, Lim WK, Tkalich P. An oil spill-food chain interaction model for coastal waters. Mar Pollut Bull 2001;42(7):590–597.

Grant RP, Middlema S. Newtonian jet stability. AIChE J 1966;12(4):669–678.

Gulawani SS, Dahikar SK, Joshi JB, Shah MS, RamaPrasad CS, Shukla DS. CFD simulation of flow pattern and plume dimensions in submerged condensation and reactive gas jets into a liquid bath. Chem Eng Sci 2008;63(9):2420–2435.

Guterman L. Conservation biology: Exxon Valdez turns 20. Science 2009;323(5921): 1558–1559.

Haghdoost A, Dehkordi AM, Darbandi M, Shahalami M, Saien J. Combined model of mass-transfer coefficients for clean and contaminated liquid-liquid systems. Ind Eng Chem Res 2011;50(8):4608–4617.

Ishii M, Zuber N. Drag coefficient and relative velocity in bubbly, droplet or particulate flows. AIChE J 1979;25(5):843–855.

Johansen Ø. DeepBlow – a Lagrangian plume model for deep water blowouts. Spill Sci Technol Bull 2000;6(2):103–111.

Johansen Ø. Development and verification of deep-water blowout models. Mar Pollut Bull 2003;47(9–12):360–368.

Johansen Ø, Rye H, Cooper C. DeepSpill – field study of a simulated oil and gas blowout in deep water. Spill Sci Technol Bull 2003;8(5–6):433–443.

Karvinen A, Ahlstedt H. Comparison of turbulence models in case of jet in crossflow using commercial CFD code. Eng Turbulence Modelling and Exp-International Symposium Eng Turbulence Model Exp 2005;6:399–408. Amsterdam.

Kessler JD, Valentine DL, Redmond MC, Du M. Response to comment on "A Persistent Oxygen Anomaly Reveals the Fate of Spilled Methane in the Deep Gulf of Mexico". Science 2011a;332(6033):1033.

Kessler JD, Valentine DL, Redmond MC, Du M, Chan EW, Mendes SD, Quiroz EW, Villanueva CJ, Shusta SS, Werra LM, Yvon-Lewis SA, Weber TC. A persistent oxygen anomaly reveals the fate of spilled methane in the Deep Gulf of Mexico. Science 2011b;331(6015):312–315.

Kotsovinos NE. A study of the entrainment and turbulence in a plane buoyant jet [PhD dissertation]. Pasadena, CA: California Institute of Technology; 1975.

Kotsovinos NE, Angelidis PB. The momentum flux in turbulent submerged jets. J Fluid Mech 1991;229:453–470.

Lehr B, Bristol S, Antonio P. et al. (2010). Oil Budget Calculator, Deep water Horizon, The Federal Interagency Solutions Group, Oil Budget Calculator Science and Engineering Team. A Report to the National Incident Command. http://www.restorethegulf.gov/sites/default/files/documents/pdf/OilBudgetCalc_Full_HQ-Print_111110.pdf

List EJ. Turbulent jets and plumes. Annu Rev Fluid Mech 1982;14:189–212.
Luettich R, Westerink J. Formulation and numerical implementation of the 2D/3D ADCIRC finite element model Version 44.XX, Internal report; 2004.
Maini BB, Bishnoi PR. Experimental investigation of hydrate formation behavior of a natural-gas bubble in a simulated deep-sea environment. Chem Eng Sci 1981;36(1):183–189.
Masutani SM, Adams EE. Experimental study of multi-phase plumes with application to deep ocean oil spills. Final report to the MMS U.S. Department of the Interior Minerals Management Service by University of Hawaii; 2001. Honolulu, Hawaii.
McDougall TJ. Bubble plumes in stratified environments. J Fluid Mech 1978;85(4):655–672.
Mollendorf JC, Gebhart B. An experimental and numerical study of the viscous stability of a round laminar vertical jet with and without thermal buoyancy for symmetric and asymmetric disturbances. J Fluid Mech 1973;61:367–399.
Moussa ZM, Trischka JW, Eskinazi S. The near field in the mixing of a round jet with a cross stream. J Fluid Mech 1977;80(1):49–80.
Nagheeby M Kolahdoozan M. Numerical modeling of two-phase fluid flow and oil slick transport in estuarine water. Int J Environ Sci Technol 2010;7(4):771–784.
Ng HJ, Robinson DB. Prediction of hydrate formation in condensed systems. AIChE J 1977;23(4):477–482.
Onda K, Sada E, Murase Y. Liquid-side mass transfer coefficients in packed towers. AIChE J 1959;5(2):235–239.
Patwardhan AW. CFD modeling of jet mixed tanks. Chem Eng Sci 2002;57(8):1307–1318.
Payne JR, Driskell WB, Short JW, Larsen ML. Long term monitoring for oil in the Exxon Valdez spill region. Mar Pollut Bull 2008;56(12):2067–2081.
Peishi Q, Zhiguo S, Yunzhi L. Mathematical simulation on the oil slick spreading and dispersion in nonuniform flow fields. Int J Environ Sci Technol 2011;8(2):339–350.
Prosperetti A, Tryggvason G. *Computational Methods for Multiphase Flow*. Cambridge, UK: Cambridge University Press; 2007.
Ranade VV. *Computational Flow Modeling for Chemical Reactor Engineering*. San Diego, CA: Academic Press; 2002.
Rogers MC, Morris SW. Natural versus forced convection in laminar starting plumes. Phys Fluids 2009;21(8):083601.
Saien J, Rezabeigy S. Alternative influence of binary surfactant mixtures on the rate of mass transfer in a liquid-liquid extraction process. Ind Eng Chem Res 2011;50(11): 6925–6932.
Schiller L, Naumann A. Fundamental calculations in gravitational processing. Zeitschrift Des Vereines Deutscher Ingenieure 1933;77:318–320.
Short JW. Heintz RA. Identification of Exxon Valdez oil in sediments and tissues from Prince William Sound and the northwestern Gulf of Alaska based on a PAH weathering model. Environ Sci Technol 1997;31(8):2375–2384.
S.L.Ross Environmental Research Ltd . Fate and behavior of Deepwater Subsea Oil Well blowouts in the Gulf of Mexico. Minerals Management Service; 1997. Ottawa (Ontario).
So RMC, Aksoy H. On vertical turbulent buoyant jets. Int J Heat Mass Transf 1993;36(13): 3187–3200.
Socolofsky SA. Laboratory experiments of multi-phase plumes in stratification and crossflow [PhD dissertation]. Cambridge, MA: Massachusetts Institute of Technology, 1987; 2001.
Socolofsky SA, Adams EE. Multi-phase plumes in uniform and stratified crossflow. J Hydraul Res 2002;40(6):661–672.
Socolofsky SA, Adams EE. Role of slip velocity in the behavior of stratified multiphase plumes. J Hydraul Eng 2005;131(4)":273–282.

Socolofsky SA, Adams EE, Sherwood CR. Formation dynamics of subsurface hydrocarbon intrusions following the Deepwater Horizon blowout. Geophys Res Lett 2011;38:L09602.

Sotillo MG, Fanjul EA, Castanedo S, Abascal AJ, Menendez J, Emelianov M, Olivella R, García-Ladona E, Ruiz-Villarreal M, Conde J, Gómez M, Conde P, Gutierrez AD, Medina R. Towards an operational system for oil spill forecast over Spanish waters: initial developments and implementation test. Mar Pollut Bull 2008;56(4):686–703.

Thibodeaux, L.J., K.T., Valsaraj, et al (2011). Marine Oil Fate: Knowledge Gaps, Basic Research, and Development Needs; A Perspective Based on the Deepwater Horizon Spill. Environmental Engineering Science. 2011, 28(2): 87–93.

Topham DR. The modelling of hydrocarbon bubble plumes to include gas hydrate formation. Chem Eng Sci 1984;39(11):1613–1622.

Tryggvason G, Scardovelli R, Zaleski S. *Direct Numerical Simulations of Gas–Liquid Multiphase Flows*. Cambridge, UK: Cambridge University Press; 2011.

Turner JS. *Buoyancy Effects of Fluids*. Cambridge, UK: Cambridge University Press; 1973.

Turner JS. Turbulent entrainment – the development of the entrainment assumption, and its application to geophysical flows. J Fluid Mech 1986;173:431–471.

Valentine DL, Kessler JD, Redmond MC, Mendes SD, Heintz MB, Farwell C, Hu L, Kinnaman FS, Yvon-Lewis S, Du M, Chan ER, Tigreros FG, Villanueva CJ. Propane respiration jump-starts microbial response to a deep oil spill. Science 2010;330(6001):208–211.

Verma P, Wate SR, Devotta S. Simulation of impact of oil spill in the ocean – a case study of Arabian Gulf. Environ Monit Assess 2008;146(1–3):191–201.

Vethamony P, Sudheesh K, Babu MT, Jayakumar S, Manimurali R, Saran AK, Sharma LH, Rajan B, Srivastava M. Trajectory of an oil spill off Goa, eastern Arabian Sea: field observations and simulations. Environ Pollut 2007;148(2):438–444.

Vysniauskas T, Bishnoi PR. Thermodynamics and kinetics of gas hydrate formation. Abstr Pap Am Chem Soc 1980;180(Aug):6-GEOC.

Vysniauskas A, Bishnoi PR. A kinetic-study of methane hydrate formation. Chem Eng Sci 1983;38(7):1061–1072.

Wu CL, Berrouk AS, Nandakumar K. Three-dimensional discrete particle model for gas-solid fluidized beds on unstructured mesh. Chem Eng J 2009;152(2–3):514–529.

Wu CL, Berrouk AS, Nandakumar K. An efficient chained-hash-table strategy for collision handling in hard-sphere discrete particle modeling. Powder Technol 2010;197(1–2): 58–67.

Wüest A, Brooks NH, Imboden DM. Bubble plume modeling for lake restoration. Water Resour Res 1992;28(12):3235–3250.

Yapa PD, Li Z. Modelling oil and gas releases from deep water: a review. Spill Sci Technol Bull 1997a;4(4):189–198.

Yapa PD, Li Z. Simulation of oil spills from underwater accidents I: Model development. J Hydraul Res 1997b;35(5):673–688.

Yapa PD, Zheng L, Nakata K. Modeling underwater oil/gas jets and plumes. J Hydraul Eng 1999;125(5):481–491.

Yapa PD, Zheng L, Chen F. A model for deep water oil/gas blowouts. Mar Pollut Bull 2001;43(7–12):234–241.

Yapa PD, Nakata K, Dasanayaka LK, Bandara UC, Sukizaki S, Suzuki S. A model for gas and hydrates plumes in deep ocean. Oceans 2008 – Mts/Ieee Kobe Techno-Ocean 2008;1–3:82–89.

Yapa PD, Dasanayaka LK, Bandara UC, Nakata K. A model to simulate the transport and fate of gas and hydrates released in deepwater. J Hydraul Res 2010;48(5):559–572.

Yvon-Lewis SA, Hu L, Kessler J. Methane flux to the atmosphere from the Deepwater Horizon oil disaster. Geophys Res Lett 2011;38:L01602.

Zhang ZZ, Hou ZW, Yang C, Ma C, Tao F, Xu P. Degradation of *n*-alkanes and polycyclic aromatic hydrocarbons in petroleum by a newly isolated *Pseudomonas aeruginosa* DQ8. Bioresour Technol 2011;102(5):4111–4116.

Zheng L, Yapa PD. Simulation of oil spills from underwater accidents II: Model verification. J Hydraul Res 1998;36(1):117–134.

Zheng L, Yapa PD. Modeling of gas dissolution in deepwater oil/gas spills. J Mar Syst 2002;31(4):299–309.

Zheng L, Yapa PD, Chen F. A model for simulating deepwater oil and gas blowouts – Part I: Theory and model formulation. J Hydraul Res 2002;41(4):339–351.

5

OIL FILMS: SOME BASIC CONCEPTS

JOHAN SJÖBLOM AND SÉBASTIEN SIMON

5.1 INTRODUCTION

From time to time, the oil production and transportation is the subject of dramatic accidents resulting in the spillage of oil. These oil spills can involve tankers like the Torrey Canyon in 1967 or the Amoco Cadiz in 1979, oil platforms like the Ixtoc 1 in 1979 and the recent Deep Water Horizon accident and war time sequels like the immediate aftermath of the *Gulf War*. As a result of these events, up to hundred thousands of tonnes of oil has been released to the environment (Rogowska and Namieśnik, 2010).

In most accidents at sea (ship accidents or blowout situations from platforms), the result is the formation of a sticky crude oil layer at the aqueous surface. Obviously, this film material is of significant interest from both compositional as well as functionality aspects. In this chapter, we try to analyze processes in crude oils that will result in the unwanted sticky material. There are several processes of interest that will contribute to the final state (Rogowska and Namieśnik, 2010). When crude oil is exposed to air, the composition will undergo changes. This is mainly due to the evaporation process that will take place. The evaporation will have some drastic consequences for the film material. First of all, mainly the short-chain aromatic and aliphatic components will be extracted from the film due to this process (Díez et al., 2007; Fingas, 1999). This will influence several properties like density and viscosity of the remaining film. With lower molecular compounds evaporated, the density and viscosity will increase. The change in molecular composition will also influence the state of the heavier components like the asphaltenes. Asphaltenes are molecules built up by polyaromatic cores, aliphatic hydrocarbon chains, and polar groups (Mullins,

Oil Spill Remediation: Colloid Chemistry-Based Principles and Solutions, First Edition.
Edited by Ponisseril Somasundaran, Partha Patra, Raymond S. Farinato, and Kyriakos Papadopoulos.

2010; Sjöblom et al., 2003). Their solubility is very much dependent on the solvency (Spiecker et al., 2003a, b). Normally, asphaltenes will precipitate in solutions of aliphatic hydrocarbons like *n*-pentanes and *n*-heptanes, while solutions of toluene and xylene will dissolve the asphaltenes. However, due to the evaporation process of the aromatics, the asphaltene molecules will aggregate and build up large agglomerates. Normally, these aggregates will diffuse to interfaces and build up layers here. In this way, one can foresee a buildup of a concentration gradient inside the film.

In addition to processes inside the oil film affecting its composition, another process that seriously will change the behavior of the film is the uptake of water. When water is incorporated in the film, a water-in-oil emulsion will form (Fingas and Fieldhouse, 2009, 2012; Rogowska and Namieśnik, 2010). This state constitutes water droplet dispersed in the oil phase. The size of these droplets is dependent on the mixing energy (in this case the combination of the waves and wind). The most significant issue is however the stability of the emulsion state. This stability is due to the existence of indigenous stabilizers, which should be molecules (or aggregates) with a clear attraction for the water–oil interface. In our case, this role will be covered by asphaltene monomers and aggregates (McLean and Kilpatrick, 1997a, 1997b) together with naphthenic acids (NA) (Arla et al., 2007). The viscosity of the oil film will increase exponentially with the water content (Fingas and Fieldhouse, 2009; Keleşoğlu et al., 2011; Pal, 2001; Pal and Rhodes, 1989), which is the central reason for the formation of the highly viscous film that sticks to most materials.

In this chapter, we present different crude oil components, their basic chemistry, and different techniques to determine them. Further, we present water-in-oil emulsions, their formation, and their stability mechanisms. Finally, we discuss recent research in the area of thin films and how these differ from bulk conditions.

5.2 CRUDE OIL COMPOSITION

Crude oils are continuums of tens of thousands of different hydrocarbon molecules. However, the proportions of the elements in crude oils vary over fairly narrow limits despite the wide variation found in properties from the lightest crude oils to highly asphaltenic crudes. The carbon content normally is in the range 83–87 wt% and the hydrogen content varies between 10 and 14 wt%. In addition, varying small amounts of nitrogen, oxygen, sulfur, and metals (Ni and V) are found in crude oils (Speight, 2007).

5.2.1 SARA (Saturates, Aromatics, Resins, Asphaltenes)

Due to the complex composition of crude oils, characterization by the individual molecular types is not possible. Instead, hydrocarbon group type analysis is commonly employed (Ali and Nofal, 1994; Bollet et al., 1981; Dark, 1982; Grizzle and Sablotny, 1986; Lundanes and Greibrokk, 1994; Radke et al., 1980; Suatoni and Swab, 1975). The SARA-separation is an example of such group type analysis, separating the crude oils in four main chemical classes based on differences in solubility and polarity. Although the SARA fractionation method is a rough sorting of the crude oil constituents, it can provide an important classification of crude oils. Figure 5.1 demonstrates

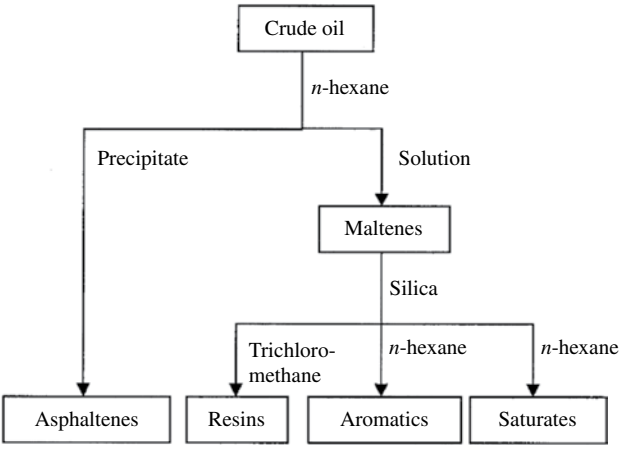

FIGURE 5.1 SARA-separation scheme. Reprinted from Sjöblom et al. (2003), © 2003, with permission from Elsevier.

the SARA-separation scheme used by Aske et al. (2001) and Hannisdal et al. (2005). It must be mentioned that most of the acids and bases present in crude oils are part of the resin fraction (Simon et al., 2010).

5.2.2 Asphaltenes

5.2.2.1 Presentation

Asphaltenes are components present in petroleum crude oils in concentration varying from zero to tens of percents (Hemmingsen et al., 2005). They have been studied extensively since they are responsible for different problems in oil industry. One problem is that asphaltenes can precipitate in reservoir, well, or downstream (in pipeline or refinery) by change of pressure (Shokrlu et al., 2011) or mixing incompatible fluids (Deo and Parra, 2011; Wiehe and Kennedy, 1999). Another problem of asphaltenes is that they are responsible for formation of stable emulsions (Sjöblom et al., 2003) created at different points in the oil production chain or during oil spillage. As these emulsions must be broken to get specified values of product quality, as a consequence emulsion stabilization properties of asphaltenes have been thoroughly studied.

5.2.2.2 Structure

Asphaltenes are typically defined as the fraction of petroleum insoluble in *n*-alkanes (typically heptane, but also hexane or pentane) but soluble in toluene (Speight, 2004, 2007). From this definition, they are not a pure material but a mixture of molecules. These molecules whose molecular weight is around 500–1000 g/mol (Groenzin and Mullins, 1999; Groenzin et al., 2003; Hortal et al., 2006) are aromatics. They concentrate the major part of the heteroatoms (nitrogen, oxygen, and sulfur) and metal atoms (nickel, vanadium) present in a crude oil. Currently, it exists two different models aiming to depict an average asphaltene molecule. These are the "continental" (also known as "like your hand" or "island") and archipelago models (Murgich, 2003). The former represents asphaltenes as composed of a single polyaromatic part surrounded by aliphatic chains

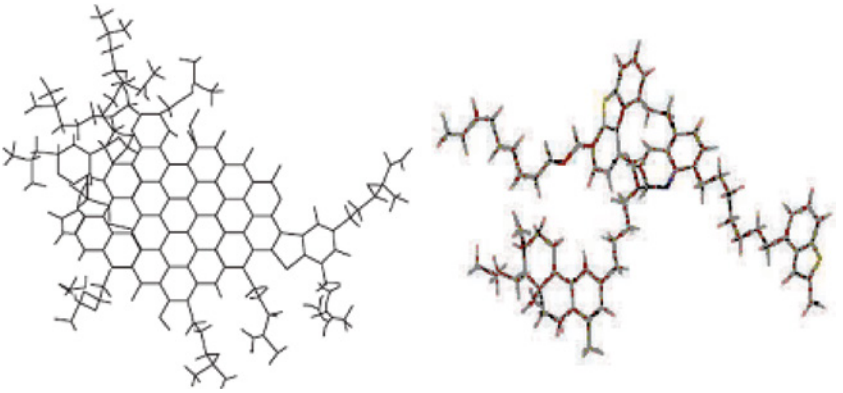

FIGURE 5.2 Examples of continental (**left**) and archipelago (**right**) type asphaltenes. Please note the double bonds and the heteroatoms are not represented. Reprinted from Murgich (2003), © 2003, with permission from Taylor & Francis Ltd.

while the latter shows asphaltenes as being composed of several polyaromatic parts linked by aliphatic or naphthenic moieties (Fig. 5.2) (Mullins, 2010).

Asphaltene molecules can associate in solution (in crude oils or in model solvents). Above a concentration known as the critical nanoaggregate concentration (~100 mg/l in toluene) (Andreatta et al., 2005; Goncalves et al., 2004; Mostowfi et al., 2008; Zeng et al., 2009), they start to self-associate to form aggregates with an average molar mass which can vary depending on thermodynamic conditions such as solvent nature, temperature, or pressure in both model solvents (such as toluene) and crude oil (Espinat et al., 2004; Fenistein and Barre, 2001; Simon et al., 2009; Spiecker et al., 2003a, b). It is commonly known that the asphaltenes precipitate when the crude oil is treated with a light aliphatic hydrocarbon.

5.2.3 Naphthenic Acids and Bases

5.2.3.1 Bases

Nitrogen is present in petroleum crude oils at concentration varying from 0.05% to 0.9% w/w (Thompson, 1994). Despite this low concentration, its presence is associated to problems in some processes: for instance, they are known to be responsible for the poisoning of cracking catalysts (Speight, 2007) and also contribute to gum formation in fuel oil (Dahlin et al., 1981). They are generally classified into basic and nonbasic, that is, respectively titrable and nontitrable by a mineral acid (Speight, 2007). The basic components are mainly represented by derivatives of pyridines and its benzologs (Arkenov et al., 1979).

Bases present some interfacial properties. Indeed, Nenningsland et al. (2010) have measured the interfacial tension (IFT) between different oil fractions and water as function of pH (Fig. 5.3). The results indicated that the interfacial activity is governed by the bases in the lower pH range (pH ≤5) and by the nonbases at higher pH values. The results do not imply any interactions between the two separated fractions, but rather that the activity of the crude oil is a combination of the individual components.

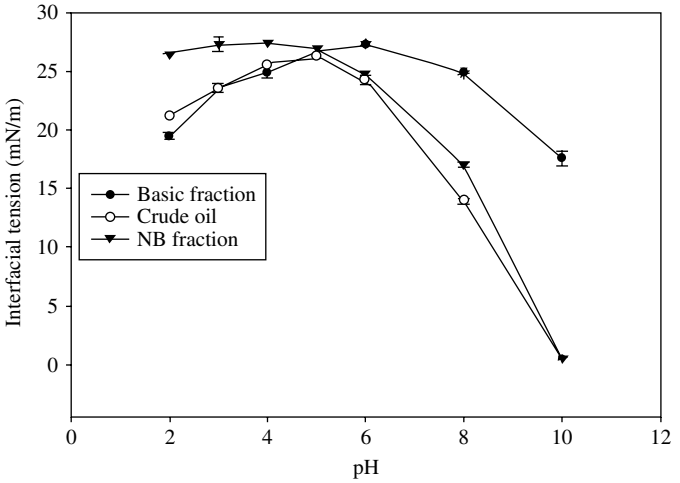

FIGURE 5.3 The interfacial tension between different oil fractions and water as a function of pH. The oil fractions are the entire crude oil (a heavy acidic one), the bases extracted from it and dissolved in xylene, and the crude oil whose bases have been removed (NB fraction). The IFT for both the crude oil and the NB fraction at pH 10 were below the detection limit for the instrument (<0.5 mN/m). Reprinted with permission from Nenningsland et al. (2010). © American Chemical Society.

Different methods have been developed to extract basic components from crude oil. They can be ranked in liquid/liquid (L/L), solid/liquid (S/L), and precipitation as hydrochloride salt methods.

The L/L methods consist in putting crude oil into contact with an acidic water solution. The bases are protonated and as a result their solubility in water increases. Like that the aqueous phase containing protonated bases initially present in crude oil is recovered (Barth et al., 2005; Merdrignac et al., 1998). It is worth noticing that some special devices must be applied to avoid formation of emulsions detrimental to the method.

The S/L methods are based on the use of cation-exchange column. The packing material can be either cation-exchanger macroreticulated resins (generally, the Amberlyst-15) (Conceição Oliveira et al., 2004; McKay et al., 1976; Rosset et al., 1978) or acid-modified silica (Laredo et al., 2002; Merdrignac et al., 1998; Schmitter et al., 1983; Simon et al., 2010). Using this methodology, Simon et al. (2010) have developed an easy-to-implement S/L extraction method to extract the basic molecules from petroleum crude oil in significant amounts (700–800 mg). The basic molecules are first extracted from crude oil using a propylsulfonic acid–modified silica sorbent, then recovered using methylamine. This method is nearly quantitative (extraction of 80–90% of bases) and repeatable (repeatability of 5% on the extracted mass). However, the extraction yield is significantly lower (around 70%) for the heaviest crude oil sample tested.

More anecdotal, the precipitation method consists to pass gaseous hydrogen chloride to the sample to precipitate the base hydrochlorides which are filtered off and washed with benzene. To our knowledge, this method has only been applied to asphaltenes (Wallace et al., 1986). From the results published in the literature,

it seems that the S/L extraction method provides the highest basic component extraction yield among the three methods (Merdrignac et al., 1998; Wallace et al., 1986). The lower extraction yield for the L/L method is due to poor solubility of high molecular weight compounds in water.

5.2.3.2 Naphthenic Acids

Crude oils are considered as acidic if their total acid number (TAN) exceeds a value of 0.5 mg KOH /g crude oil. This acidity is mainly, but not only (Tomczyk et al., 2001), due to the presence of NA which are complex mixtures of cylic, acyclic, and aromatic carboxylic acids (Hemmingsen et al., 2006; Meredith et al., 2000; Qian et al., 2001). Their presence is associated with several problems in oil production, such as corrosion in refineries (Slavcheva et al., 1999), pollution in refinery wastewaters and in oil sands extraction waters (Clemente and Fedorak, 2005), formation of emulsion (Arla et al., 2007; Brocart and Hurtevent, 2008; Gallup et al., 2007; Havre and Sjöblom, 2003; Sjöblom et al., 2003), and calcium naphthenate deposits (Brocart and Hurtevent, 2008; Hurtevent et al., 2006; Shepherd et al., 2006).

Many different methods and analytical techniques have been used for analyzing these acids in the past (Acevedo et al., 1999; Fan, 1991; Headley et al., 2002; Hsu et al., 2000; Koike et al., 1992; Tomczyk et al., 2001; Qian et al., 2001). An overview shows that the majority of the NA are C_{10}–C_{50} compounds with 0–6 fused saturated rings and with the carboxylic acid group apparently attached to a ring with a short side chain (Robbins, 1998). The distribution of carbon number and ring content varies with crude oil source and distillate fraction. NA with similar TAN and average molecular weight can exhibit significantly different profiles (Brient, 1998).

The properties of NA are dependent on the pH due to the acid–base equilibrium since the features of the naphthenates (surface activities, solubility in oil and water, etc.) are different from the NA ones:

$$\mathrm{RCOOH} \rightleftarrows \mathrm{RCOO^-} + \mathrm{H^+}$$

Consequently, the following properties of NA solutions vary with pH:

- Interfacial tension at oil–water interface (Arla et al., 2007; Havre et al., 2003)
- Emulsion type formation (water-in-oil vs. oil-in-water) (Ese and Kilpatrick, 2004),
- Emulsion stability (Ese and Kilpatrick, 2004)
- Partition coefficient (repartition of NA in oil and water) (see Section 5.3.3) (Havre et al., 2003; Nordgård et al., 2012).

Similarly to bases, there are two main methods to extract NA from crude oils. The main one is to extract NA using an anion exchange column like quaternary ammonium-bonded silica column (Jones et al., 2001; Meredith et al., 2000; Merlin et al., 2007; Saab et al., 2005; Simon et al., 2008). The other method, the L/L extraction method, consists in putting crude oil into contact with a basic solution. The acids are ionized and as a result their solubility in water increases. Like that the aqueous phase containing naphthenates initially present in crude oil is recovered (Hemmingsen et al., 2006).

5.3 OIL FILMS

5.3.1 Introduction

In connection with an oil spill, the oil will normally leak out over a large area. Regardless of the constitution and the dimensions of the initial layer, the outer conditions (wind, waves, temperature) will reduce the spill to an oil film with a different composition than the original crude oil. The final composition of the film will be dependent on evaporation of light components and partitioning of polar–ionic components to the water phase. Water can also be incorporated onto the film by emulsification.

5.3.2 Evaporation

Evaporation is a very important process in oil spill in which lighter components of the oil will evaporate to the atmosphere. As a result, the density and the viscosity of the spilled oil will increase with time (Ahamad and Barker 2011; Betancourt et al., 2005). Blumer et al. (1973) have studied stranded crude oils and noticed they lose its lower boiling point components after the spills. Above the boiling point of $C_{23}H_{48}$ to $C_{24}H_{50}$ alkanes, the hydrocarbons are hardly affected by evaporation even after time periods exceeding 1 year.

Several models have been proposed to model the evaporation of petroleum crude oils. According to Fingas (1999, 2011, 2012), the models can be classified into two groups as a function of the mechanism that regulates evaporation: the air-boundary layer and the diffusion-regulated mechanisms.

In the air-boundary layer, the molecules evaporate from the surface into a thin layer of air known as the air-boundary layer. It is this layer that regulates the evaporation. One of the properties of this regulation mechanism is the evaporation rate increases with wind or turbulence because the molecular motion is faster in the air-boundary layer.

In the diffusion-controlled regulation mechanism, the limiting factor for evaporation is the diffusion of molecules through the evaporating liquid. As a result, the evaporation rate is not increased or little by wind or turbulence in the air above the oil as shown by laboratory-controlled experiments (Fingas, 1999, 2012). According to the experiences carried out by Fingas (1999, 2012), air-boundary layer mechanism is valid for fast-evaporating molecules like water whereas the diffusion-controlled regulation mechanism is valid to model the evaporation of crude oils.

By performing laboratory-controlled experiences, Fingas has shown that the variation of mass evaporated for crude oil can follow either a logarithmic or a square root equation whose parameters are linked to the weight percentage of crude oils distilled at 180°C (%D) (Fingas, 1997, 2004). The square root type equation is valid for compounds that have a narrow range of compounds that evaporate at a similar rate like diesel fuel, while the logarithmic type equation is more valid for "classical" crude oils. The equations are:

- For oils that follow a logarithmic equation

$$\text{Percentage\_evaporated} = \left[0.165 \times \%\text{D} + 0.045(T - 15)\right] \times \text{Ln}(t)$$

- For oils that follow a square root equation:

$$\text{Percentage\_evaporated} = \left[0.0254 \times \%\text{D} + 0.01(T - 15)\right] \times \sqrt{t}$$

with T the temperature in degree celsius and t the time in minutes

5.3.3 Partitioning

Polar or ionic molecules present in petroleum crude oil can partition between oil and water phases that means be present in these two phases in variable amounts. The most significant and studied compounds that can partition are NA (Bitsch-Larsen and Andersen, 2008; Havre et al., 2003; Nordgård et al., 2012).

Several thermodynamic equilibria rule the NA partition. First, the partition coefficient, K_{wo}, which is defined for the fully protonated acid as how it is distributed between the two immiscible phases at equilibrium. Second, the acid dissociation constant, K_a, of the NA/naphthenates (A^-) in the aqueous phase which means that the NA partition depends on aqueous phase pH. These equilibria are summarized in Figure 5.4. Several other equilibria could, a priori, play a role in the partition such as the dimerization of acids in the oil phase (Goodman, 1958; Suzuki et al., 1973) and the micellization process in the aqueous phase.

As an example, we present the recently published partition behavior (Nordgård et al., 2012) of a molecule named BP-10 (Nordgård and Sjöblom, 2008; Nordgård et al., 2009), which has been designed to mimic the properties of a NA discovered in 2004 in calcium naphthenate deposits: the Arn or C_{80}-tetraacid (Baugh et al., 2004, 2005). As shown in Figure 5.5, this molecule is composed of four carboxylic functions at the end of each of four interconnected hydrocarbon chains onto an aromatic core.

The classical method to study partition of NA is to dissolve a constant concentration of NA in oil phase and then put this oil phase into contact with water phases at different pH. After reaching equilibrium, the concentration of NA is determined in both phases.

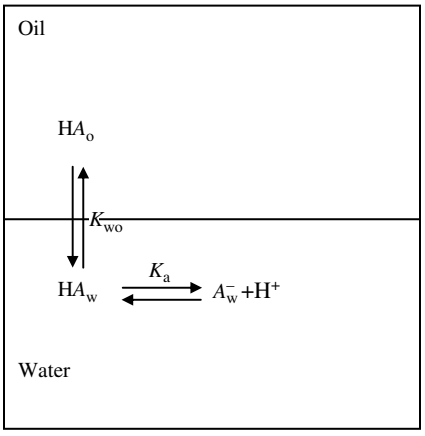

FIGURE 5.4 Equilibria in oil/oil/NA systems.

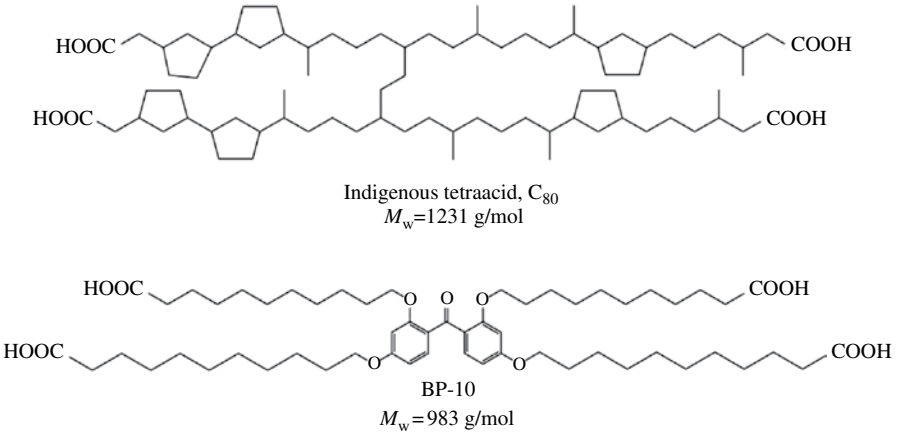

FIGURE 5.5 Formula of BP-10 (**bottom**), molecules developed to mimic the properties of C_{80}-TA (**top**) by Nordgård and Sjöblom (2008).

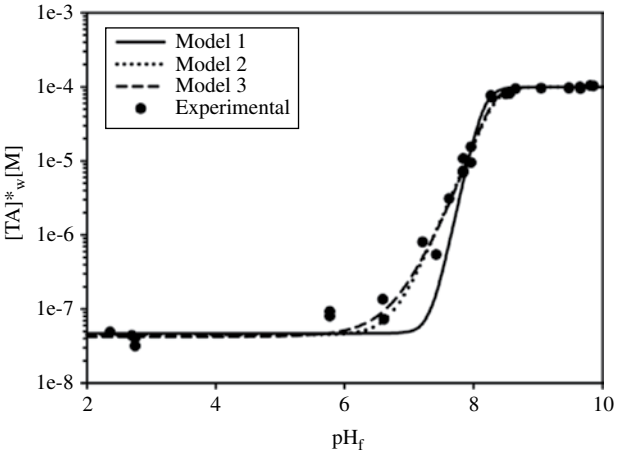

FIGURE 5.6 Partitioning of BP-10 between $CHCl_3$ and buffer solutions at 184 mM K^+ as a: The total concentration of BP-10 in water $[TA]^*_w$ as a function of final pH with an initial concentration of BP-10 in the oil phase of 0.1 mM. The solid, dotted, and long dashed lines represent the best fit by the sum of least square method with $K_{wo} = 4.7 \times 10^{-4}$, $pK_a = 7.3$ for Model 1 (assuming equal acid constant for all the 4 BP-10's acid functions), $K_{wo} = 4.5 \times 10^{-4}$ and $pK_a = 6.7$ and 8.3 for Model 2 (model assuming two acid dissociation constants), $K_{wo} = 4.3 \times 10^{-4}$ and $pK_a = 6.7$, 6.8, 8.0, and 8.3 for Model 3 (assuming four acid dissociation constants). Reprinted from Nordgård et al. (2012). © 2012, with permission from Taylor & Francis Ltd.

Figure 5.6 presents an example of such a determination depicting the variation of the concentration of BP-10 in the water phase as a function of its pH for an initial concentration in oil of 0.1 mM (Nordgård et al., 2012). At low pH, the concentration in water is low and constant while from a pH of ≈7, the concentration of water increases

due to the ionization of the NA. A model based on equilibrium constants K_a and K_{wo} allows to obtain a good fit of experimental data. The p*K*a of BP-10 fitted with this method is quite high (7–8) compared with classical values for carboxylic acids (≈5). The apparently lower acidity of BP-10 must be influenced by other equilibriums other than only partitioning and dissociation, most likely micellization of NA in the aqueous phase. In a recent paper, the acid–base behavior of BP-10 was studied with high-precision potentiometric titration above the CMC, showing the same shift to unusual high apparent p*K*a values in the range 8–9 (Sundman et al., 2010). The apparent lower acidity was explained by the formation of micelles and protonation/deprotonation from the negatively charged micellar surface.

The aqueous phase ionic strength has some influence on the BP-10 partition coefficient K_{wo}. It was shown that this coefficient decreases with salinity. This decrease can be explained by a salting out effect of the added cations, reducing the solubility of BP-10 (or its partially dissociated species) in the water phase (Nordgård et al., 2012).

5.3.4 Crude Oil Emulsion

5.3.4.1 Introduction

During oil spillage, water can be incorporated into the oil phase as droplets thereby forming water-in-oil emulsions. This occurs by physical mixing due to turbulences at the water surface (Rogowska and Namieśnik, 2010). As a consequence, the volume of the oil phase will increase as well as its viscosity (Fingas and Fieldhouse, 2009, 2012). These increases make the understanding the formation of emulsion is important in order to be able to predict the fate of oil spills. Study of crude oil emulsion stability is also important to improve the oil–water separation during crude oil production. Indeed, water and crude oil are generally coproduced and they must be separated to get specified values of content of oil-in-the-water phase and water-in-the-oil phase.

5.3.4.2 Crude Oil Emulsion Stabilization

The stability of crude oil emulsions is extremely variable, depending on the field (Aske et al., 2002), and it is generally recognized that it is due to the presence of crude oil indigenous surfactants, mainly asphaltenes (Grutters et al., 2007; McLean and Kilpatrick, 1997a, b; Sjöblom et al., 2003), NA (Arla et al., 2007; Czarnecki and Moran, 2005; Wu, 2003), and particles such as clay covered with asphaltene-like compounds (Hannisdal et al., 2006; Kotlyar et al., 1999; Sullivan and Kilpatrick, 2002; Sztukowski and Yarranton, 2005). In this part, we will present properties of asphaltene-stabilized emulsions. When asphaltenes stabilize emulsions, it has been shown that

- Water–oil emulsions, that is, water droplets dispersed in oil phase, are preferentially formed in respect with the Bancroft's rule (asphaltenes are oil-soluble).
- The stability of asphaltene-stabilized emulsions is governed by the solvation state of asphaltenes and therefore their aggregation/flocculation (Kilpatrick and Spiecker, 2001; McLean and Kilpatrick, 1997a, b).

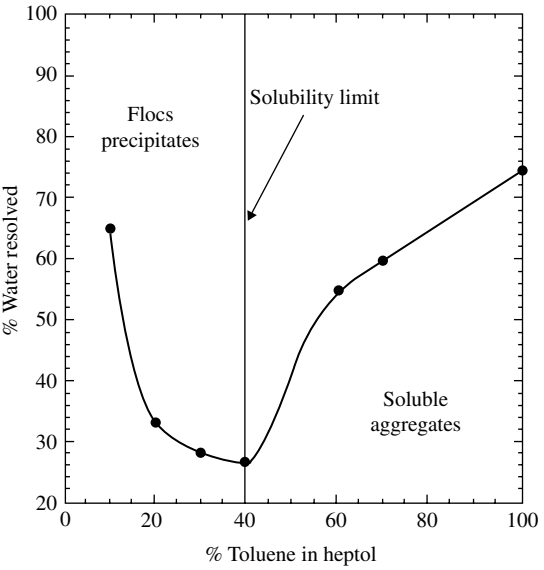

FIGURE 5.7 Emulsion stability as gauged by % water resolved following centrifugation versus % (v/v) toluene in heptane for 0.5% asphaltenes dissolved in oleic phase and mixed with water in a 40:60 (v/v) proportion. The studied asphaltenes are partially precipitated below 40% toluene. Republished with permission of Taylor and Francis Ltd. from Kilpatrick and Spiecker (2001).

About the effect of solvation state, Kilpatrick et al. (Kilpatrick and Spiecker, 2001; McLean and Kilpatrick, 1997a; Singh et al., 1999), by using oil phase composed of asphaltenes in toluene + heptane solvents, have studied the influence of level of aggregation of asphaltene onto the stability of water–oil emulsions. They have showed that asphaltenes are the most effective in stabilizing emulsions when they are near the point of incipient precipitation: for higher heptane proportions in the solvent asphaltenes are precipitated and therefore cannot "go" to the interface, whereas for higher toluene proportions asphaltenes are well solubilized and their solubilization in the bulk is favored (Fig. 5.7). They also have studied the effect of resins, the second most polar fraction of a crude oil. As presence of resins increases the solvency of asphaltenes, the resins have a similar effect to the aromaticity of organic solvent (Spiecker et al., 2003a, b).

The pH of the aqueous phase has an influence on the stability of emulsions. Indeed, asphaltenes being amphoteres, their ionization state and therefore their affinity toward interface vary with the pH of the aqueous phase (Nenningsland et al., 2011; Poteau et al., 2005). For instance, Nenningsland et al. have measured the stability of asphaltene-stabilized emulsions at different pH (Fig. 5.8). The figures show that the emulsion has a minimum stability at intermediate pH (around pH 6), while the stability is higher at lower and higher pH. At lower pH values, it is reasonable to suggest that the increasing stability could be attributed to the protonation of the basic functionalities, which are known to be present in crude oil and to influence the oil–water interface

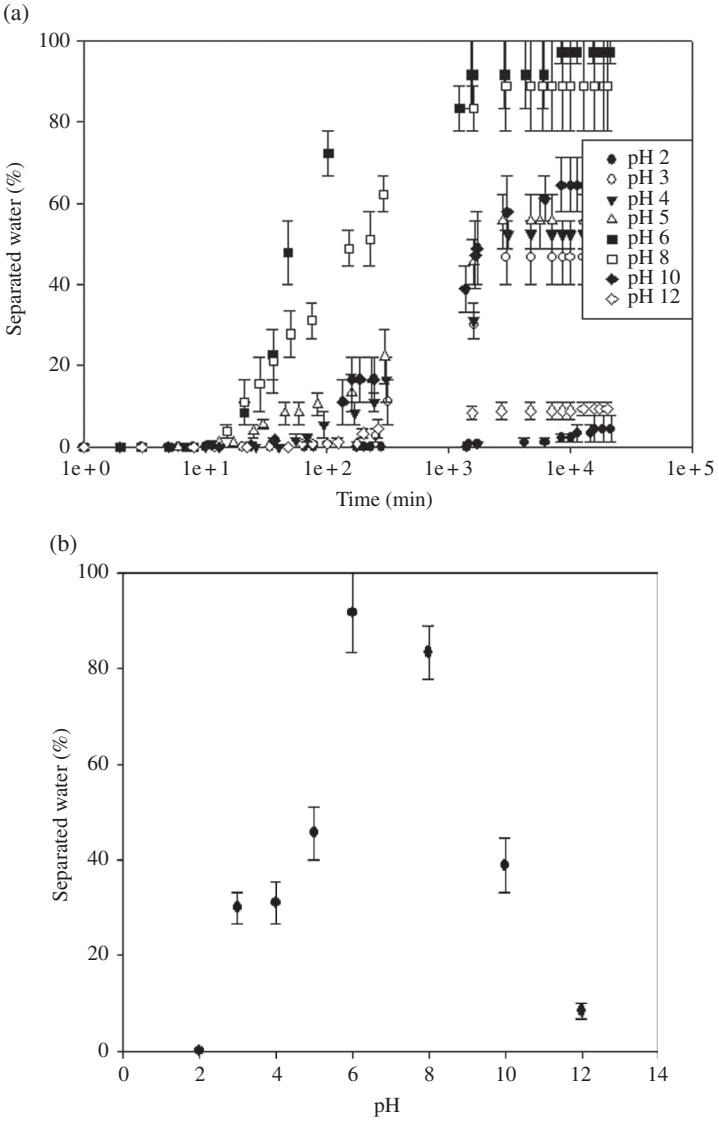

FIGURE 5.8 Separated water as a function of (**a**) time and (**b**) pH for emulsions stabilized by asphaltenes in xylene (w/o), with a constant asphaltene concentration of 0.5 g/l. The water cut of the emulsions is 20%v/v. Reprinted with permission from Nenningsland et al. (2011). © American Chemical Society.

(Nenningsland et al., 2010). At pH 6 the emulsion had the lowest stability, where over 90% of the emulsified water was separated. The change observed from pH 6 and upward is attributed to the ionization of acid functions present in the asphaltene fraction. The amphoteric nature of asphaltenes has been shown on a prior occasion by Poteau et al. (2005). The variation of stability with pH is correlated with the IFT variations.

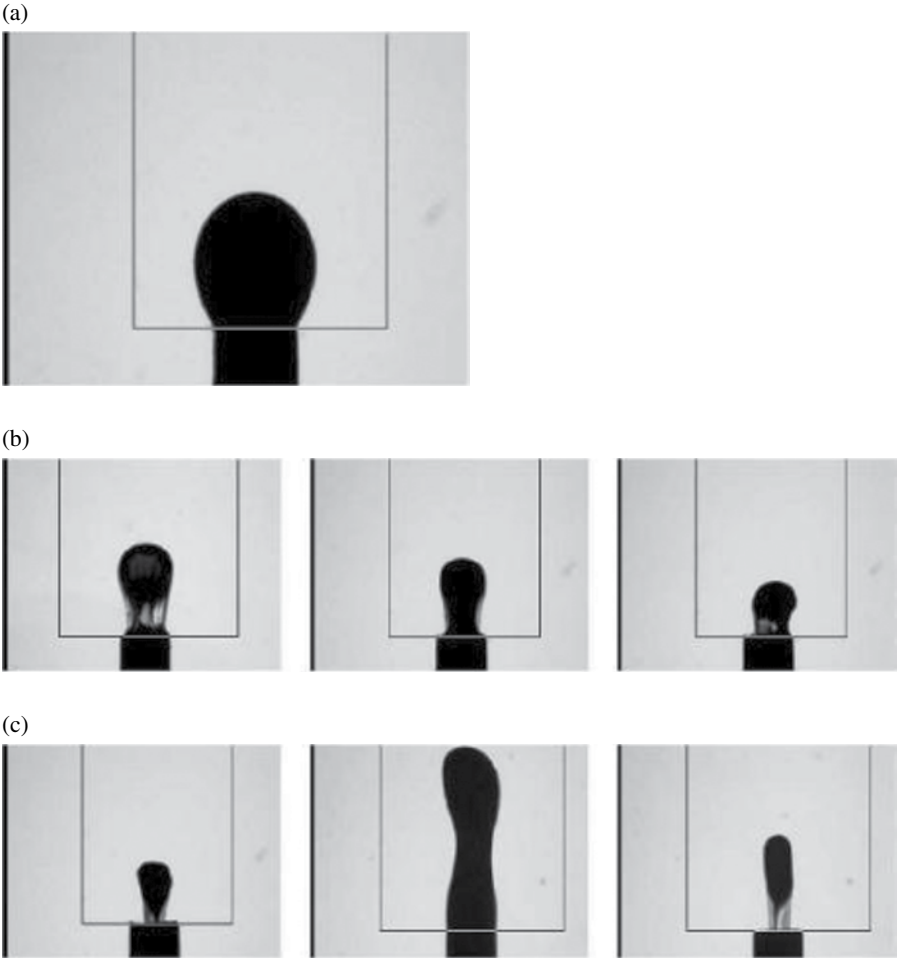

FIGURE 5.9 Drops of an asphaltene solution in toluene held by the tip of a syringe and immersed in water: (**a**) regular shape; (**b**) examples of shapes obtained at long times and large asphaltene concentration; (**c**) shapes obtained during a rapid expansion/contraction cycle (time is increasing from left to right). Reprinted from Jeribi et al. (2002). © 2002, with permission from Elsevier.

The reasons behind the stability of asphaltene emulsions are generally considered to be searched in the structure formed by asphaltenes at the L/L interface. One of their most striking properties is the formation of a "skin" around droplets. Indeed, if we form a water drop into an asphaltene-containing oil phase, we can notice that the surface become extremely rigid after aging. This rigidity is easily observed by contracting the water droplet (Fig. 5.9) (Hannisdal et al., 2007a; Jeribi et al., 2002). It is thought that it is the formation of this skin or in other word the rigidity of the asphaltene layer that explains the stability of asphaltene-stabilized emulsions. In order to characterize the building up of the "skin," interfacial rheology is a technique of choice.

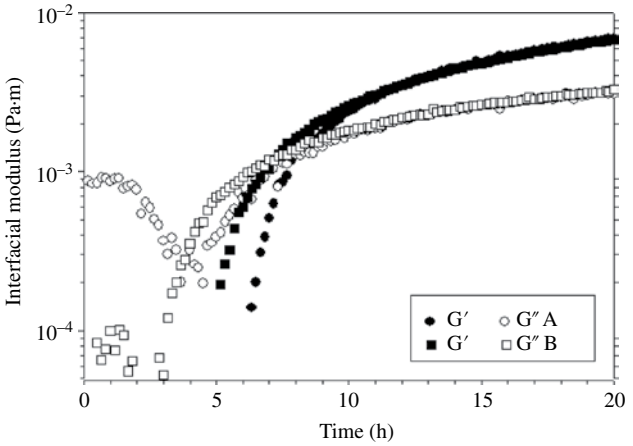

FIGURE 5.10 Time-dependent variations of G′ and G″ at oil–brine interface for 5 g/l asphaltene (toluene–heptane volume ratio 6:4, frequency: 1 Hz, strain: 0.1%). The reproducibility is shown with the presentation of two tests A and B. Reprinted from Fan et al. (2010b). © 2010, with permission from Elsevier.

5.3.4.3 Interfacial Rheology Properties of Oil–Water Interfaces

Some Experimental Techniques. Interfacial rheology is more or less similar to the classical bulk rheology in the sense that the focus is on the response shown by interfaces against deformations (Miller et al., 2010). Within interfacial rheology, the main two types of deformation are dilational and shear. Dilational involves changing the area of the interface by expansion or compression, while keeping the shape intact. Shear, on the other hand, involves to change the shape of the interface without any variations in the area (Bos and van Vliet, 2001; Miller et al., 2010). In the following, we present some studies carried out on asphaltene/water and diluted crude oil–water interfaces.

Shear Rheology Experiments. This technique has been, for instance, used by Fan et al. (2010b) and Kilpatrick et al. (Kilpatrick and Spiecker, 2001; Spiecker and Kilpatrick, 2004) to characterize asphaltenic interface. Figure 5.10 presents the time variation of elastic and viscous modulus G′ and G′′ measured in the linear viscoelastic range at the asphaltene-contained oil–brine interface. We can notice that it takes nearly 5 h before G′ value is high enough to be detected by the rheometer, then it keeps increasing and even after 20 h the equilibrium value is not attained since both moduli are still increasing. We can also notice that the interface is predominantly viscous at short times (lower to 7–8 h) and predominantly elastic for longer time. This time variation is classically attributed to a combination of diffusion, adsorption, rearrangement, physical gelation (cross-linking) and so on, but it is not possible to determine their relative importance with only interfacial rheology data.

To probe the structure of the interfacial film, frequency sweep was carried out after aging for 20 h. Figure 5.11 presents the variations of G′ and G″ with the frequency for systems having oil phase composed of toluene and heptane in different ratio. For pure

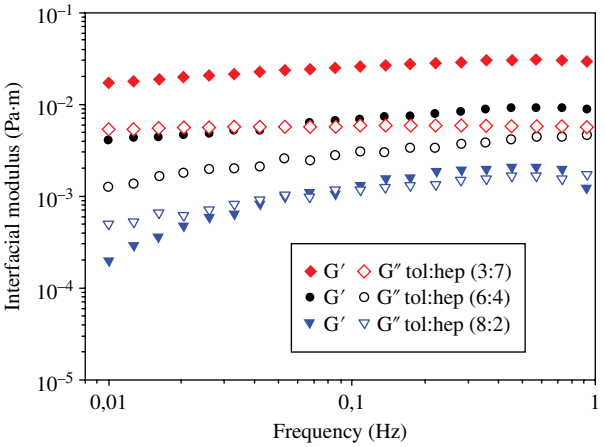

FIGURE 5.11 Effect of toluene–heptane volume ratio on frequency sweep at 0.1% strain after aging for 20 h (5 g/l asphaltene). Reprinted from Fan et al. (2010b). © 2010, with permission from Elsevier.

toluene (not shown), no G′ value is detected after 20 h. For a toluene–heptane ratio of 8:2, a crossover point of G′ and G″ characteristic of a viscoelastic interface is visible. For higher heptane proportion, no crossover point between G′ and G″ extending to frequency as low as 0.01 Hz is detected, and G′ and G″ slightly increase with frequency. Furthermore, G′ is significantly larger than G″. These features have been identified as phenomenological characteristics of a typical gel in the bulk phase by Almdal et al. (1993). This means that for the two systems investigated having the highest heptane proportion, we have formation of a network structure at interface. For lower heptane proportion, there is not enough interaction between asphaltenes at the interface to create a cross-linking network and therefore a gel.

The effect at higher aromaticity on the interfacial film properties is consistent with the macroscopic stability of emulsions presented section 5.3.4.2. When the solvent is predominantly aromatic, most asphaltenes prefer to stay in the bulk oil phase instead of becoming interfacially active. It also indicates that the network formation is directly related to the aggregation state of asphaltenes.

Dilational Rheology Experiments. Dilational rheology (variation of the area of the interfaces with time) using an oscillating pendant–sessile drop tensiometer was used by Bouriat et al. (2004), Hannisdal et al. (2007a, b), and Yarranton et al. (Yarranton et al., 2007a, b) to characterize crude oil and asphaltenic interfaces. In the following, we will present the results by Hannisdal et al. on diluted crude oil systems (Hannisdal et al., 2007a, b).

The oscillating pendant drop method was used to study the rheology of diluted crude oil–water interfaces and the effect of altering aromaticity of the diluent and the concentration of crude oil (Hannisdal et al., 2007a). The storage E′ and loss E″ moduli of one of the crude oil–water systems studied is presented in Figure 5.12. The measurements were carried out with a constant applied frequency $f = 0.1$ Hz. It can be noticed that the modulus E′ is superior to E″ for all the experiments indicating "solid

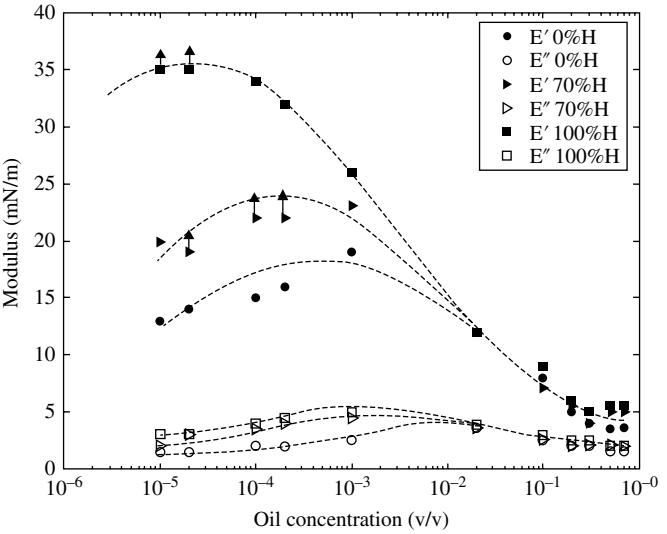

FIGURE 5.12 Near-equilibrium (2.5 h after preparation) of the storage E′ and loss E″ moduli determined by dilational rheology at a diluted crude oil/brine (3.5% NaCl solution) interface as a function of the bulk crude oil concentration and the aromaticity of the solvent. The crude oil was diluted to different extents in heptane–toluene mixtures as indicated in the legend (vol% H). The measurements were carried out with a constant applied frequency (0.1 Hz). The characteristics of the crude oil are reported in Hannisdal et al. Reprinted from Hannisdal et al. (2007a). © 2007, with permission from Taylor & Francis Ltd.

like" properties of the interface. The interfaces were apparently more viscoelastic with low aromaticity of the solvent. Finally, the equilibrium storage and loss moduli passed through distinct maxima as a function of bulk concentration. The apparently low viscoelasticity of the interfaces in systems with high bulk concentration was at least partly caused by high diffusion flux of interfacially active components from bulk.

In the continuation of this work, interfacial rheology properties of 30 crude oils, undiluted and diluted in 30 vol% toluene, were analyzed using the oscillating drop technique in the frequency range from 0.01 to 1 Hz (Hannisdal et al., 2007b). As expected in this low-frequency range, molecular exchange from bulk strongly affected the measured dilational parameters. For the diluted crude oils, the frequency dependence of the dilational modulus increased with its magnitude as expected for diffusion-controlled relaxation of soluble films. For this reason, the systems which exhibited particularly low magnitude of the dilational modulus were the heaviest crude oils in the sample set, whereas the systems with the greatest dilational modulus were among the lightest crude oils. The frequency dependence of the dilational modulus increased with its magnitude as expected for diffusion-controlled relaxation of soluble films. Overall, the undiluted crude oil–water interfaces had similar relaxation characteristics as the diluted samples except for slightly reduced magnitude of the dilational modulus.

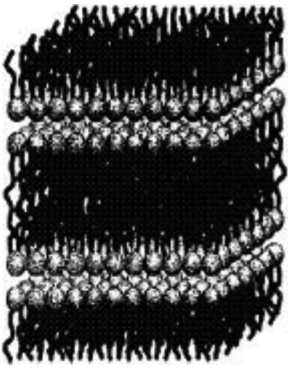

FIGURE 5.13 Structural element of a lamellar liquid crystal.

5.3.4.4 Other Emulsion Stabilization Mechanism: Liquid Crystal Stabilization (D Phase)

5.3.4.4.1 Introduction

In this section, we introduce the stabilization of emulsion by liquid crystals which can stabilize water-in-oil emulsions. In the first part, we will present generalities about this stabilization mechanism before presenting results of its effects on stability of water–oil emulsions.

Generalities About Liquid Crystal Stabilization. The traditional definition (II.1) of water–oil and oil–water emulsions consisting of two liquids with one liquid dispersed in form of droplets (Sherman, 1968) has been modified by the IUPAC Committee for Nomenclature (International Union of Pure and Applied Chemistry, 1972) to include a third phase, that is, a lyotropic liquid crystalline phase (see Fig. 5.13 for a structural element). The background of this remarkable decision was a scientific breakthrough in fundamental research together with a technical breakthrough in understanding of commercially available emulsion-based products in field like foods, pharmaceutics, personal care, etc.

A central aspect of the definition is to distinguish emulsified systems and optimized surfactant systems, that is, microemulsions. The latter contains small droplets in a monophasic fluid, and in contrast to emulsions are thermodynamically stable, not kinetically stabilized as emulions. An elegant way to study emulsions, as opened up by the IUPAC definition, is through equilibrium studies of phase equilibria in three or four component systems.

The pioneer in connecting phase equilibria of surfactant systems and enhanced stability of both oil–water and water–oil systems is Professor Stig Friberg (Sjöblom, 1997). In a series of publications from 1970s, Friberg et al. (Friberg, 1971; Friberg et al., 1969, 1976; Krog, 1975) show that the lamellar lyotropic liquid crystalline phase D (in some literature also denoted L_α or neat phase) has an enhanced effect on the stability of the corresponding emulsions. The surfactant multilayer arrangement (Fig. 5.13) will obviously enhance the interfacial rigidity and delay–prevent coalescence. The degree of flocculation is not influenced to the same extent by the occurrence of a third phase. Professor Friberg verified the multilayer mechanism for

enhanced stability in a variety of model systems including three (water–oil–surfactant) or four component (water–oil–surfactant mixture) systems. Later on, several schools have extended the correlations to other similar systems (Fontell et al., 1986; Selle et al., 1991; Skurtveit et al., 1992).

Stabilization of Water–Oil Emulsions by Liquid Crystals. Oil-continuous emulsions can be stabilized by multiple layers of surfactant (Havre and Sjöblom, 2003). In an equilibrium situation, this corresponds to a sample location in a three-phase area where two solution phases (L1 and L2) are in equilibrium with a lamellar liquid crystalline phase D phase. The D phase might act as an efficient emulsifier. When present in a three-phase system, it will cover the emulsion droplets and lead to reduced interfacial mobility and bending ability.

Knowledge about phase behavior in an oil–surfactant–water system is of crucial importance when studying the mechanisms behind emulsion formation and stability in such a system. Häger and coworkers (2005), using model NA, proved that increasing pH decreases the lipophilicity of the acid species and may induce an inversion from water–oil emulsion to an oil–water emulsion. They observe strong competition between salinity effect and pH effect especially in case of systems with anionic surfactant included fatty acids. Stable water–oil emulsions were found at a pH close to 8. All emulsions were shown to be stabilized by a liquid gel phase consisting of a lamellar structure.

Many ternary systems based on a fatty acid (C_nCOOH) and long-chain alcohol (C_nOH) have been thoroughly investigated in past years. However, there are only a few reports where the phase behavior has been studied in systems based on polar aromatic acids or alcohols. Horvath-Szabo and coworkers (Horváth-Szabó et al., 2002, 2003) have studied the phase equilibria in a sodium naphthenate–water system and sodium naphthenate–water–hydrocarbon systems. The influence on phase diagrams of model compounds for NA and phenols when mixed with water was studied based on the compounds 5-phenylvaleric acid, 5-phenylvalerate, 1-decanol, and 4-pentylphenol (Häger and Sjöblom, 2006). Figure 5.14 illustrates that an extended isotropic oil–water micellar (L1) phase exists up to approximately 45 wt% surfactant along the binary surfactant–water axis. In the dilute aqueous regime only monomer exists. Addition of more alcohol leads to a turbid lamellar liquid crystalline (D) phase, which was identified by microscopic investigation (Fig. 5.15a and b). The typical texture of Maltese crosses and oily streaks is an indication of the lamellar structure. The reason for this transformation is that the alcohol gives the aggregates a more hydrophobic character and reduces the charge density of the polar surface layer, which will favor the formation of the lamellar bilayer structure. This D phase has a very high swelling capacity, that is, it has a large extension toward the water apex. The swelling of a lamellar phase can be explained by the difference in chemical potential of pure water and water incorporated into the intervening layers of the lamellae. A lamellar phase in the produced water of a crude oil may have a large impact of the elements that contaminate the water stream. That the lamellar phase is formed at low concentrations is important information when treating production water. In the alcohol-rich corner of the phase diagram, a reverse water–oil micellar (L2) phase exists. In addition, a reverse hexagonal (F, also denoted H_2 or M_2) structure

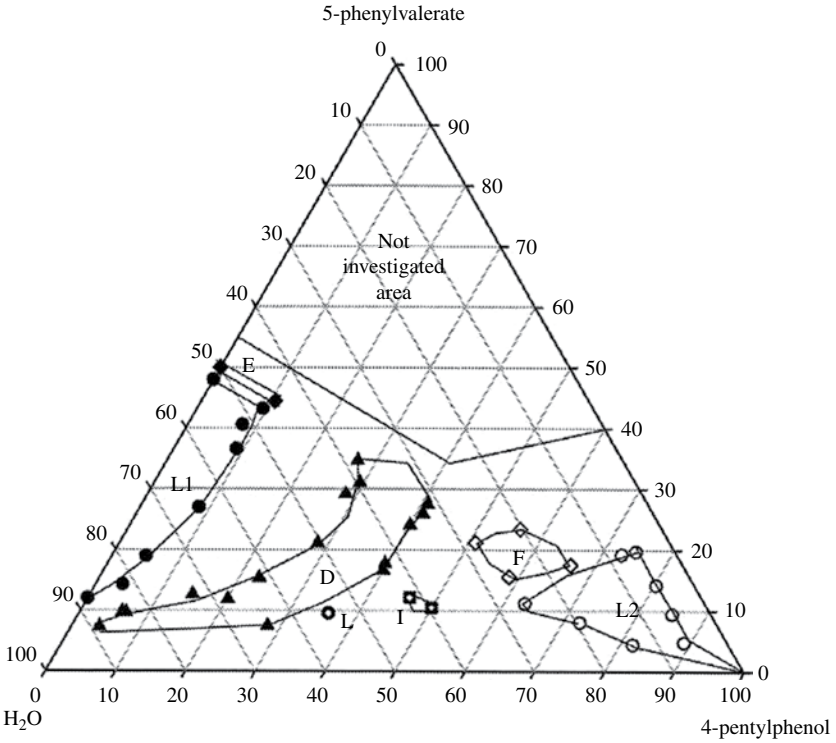

FIGURE 5.14 Partial phase diagram based on weight fraction of the ternary system based on 5-phenylvalerate, 4-pentylphenol, and water at 25°C. Reprinted from Häger and Sjöblom (2006), with permission from Taylor & Francis Ltd.

is formed between the D and the L2 phase. This phase is found at the surfactant content around 20 wt%. Microscopic investigation identified the anisotropic phase on the basis of the characteristic optical fan-like texture (Fig. 5.15c). The two-phase region between the D and the F phase was also recorded by polarizing microscopy (Fig. 5.15d).

The phase behavior was found to depend on salinity of the system. The system in the presence of salt was shown to significantly change the character of the lamellar phase. Its region of existence was much smaller than that of the system in the absence of salt, that is, its swelling capacity was obviously reduced. Häger et al. (Häger and Sjöblom, 2006) also investigated the effect of the ratio between the undissociated (RCOOH) and the dissociated (RCOO~) acid. A solubilization limit of the acid around 10 wt% is observed. Increasing the concentration of the surfactant leads to formation of the hexagonal (E) phase. Addition of more acid leads to a transition to a D phase region above 40 wt% surfactant. This means that replacing the surfactant by the acid gives only normal micellar and hexagonal structures. The poor phase behavior of the system can be explained in terms of a low ability of the acid to solubilize into the different self-assembly structures.

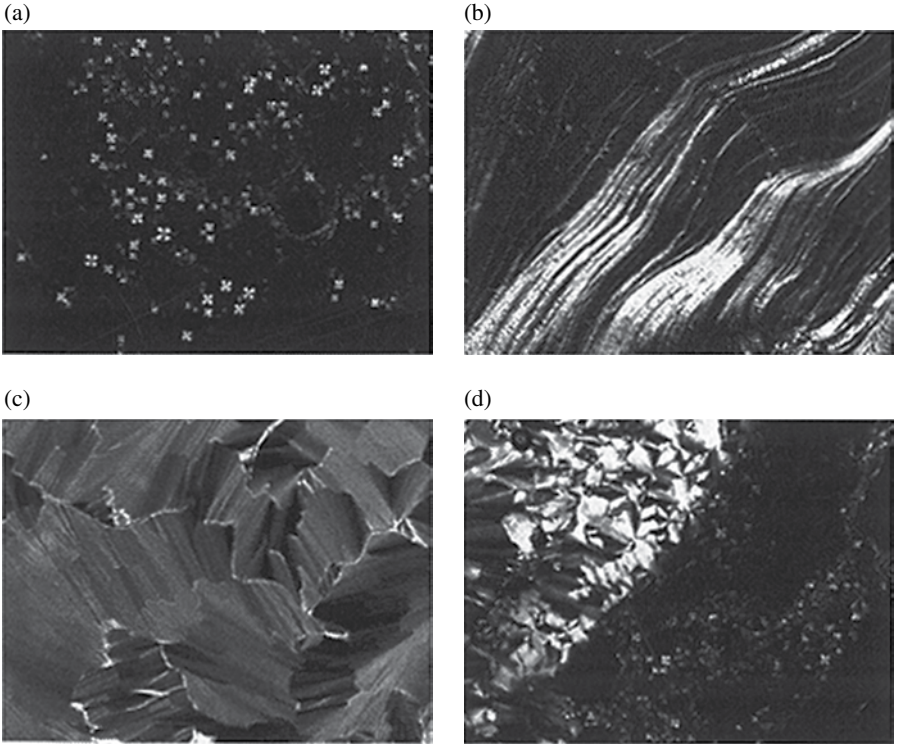

FIGURE 5.15 Light microscopy micrographs showing the (**a**) Maltese cross and (**b**) oily streak textures of the lamellar liquid crystalline (D) phase based on 5-phenylvalerate, 4-pentylphenol, and water at 25°C. The fan-like texture in (**c**) is an indication of the hexagonal liquid crystalline (E or F) phase. The two-phase region (**d**) consisted of a lamellar and hexagonal phase; both Maltese cross and fan-like textures were observed, respectively. Reprinted from Häger and Sjöblom (2006). © 2006, with permission from Taylor & Francis Ltd.

5.3.5 Thin Films

Thin film research is highly relevant in colloid chemistry. Most colloidal states dealing with dispersions, emulsions, or foams where one state is dispersed in another one include thin liquid films (or even monolayers) as stabilizing unit. Hence, a lot of work has been directed toward monolayers, interfaces (with miscellaneous compositions), and thin films.

5.3.5.1 Monolayers

Most of the research directed toward monolayers (at a liquid–air interface) is focused on research applied with Langmuir troughs or Langmuir-Blodgett films deposited on a solid substrate.

The classical approach to explain the behavior of surface-active monolayers was given by Langmuir. He conducted experiments with a trough monitoring the surface

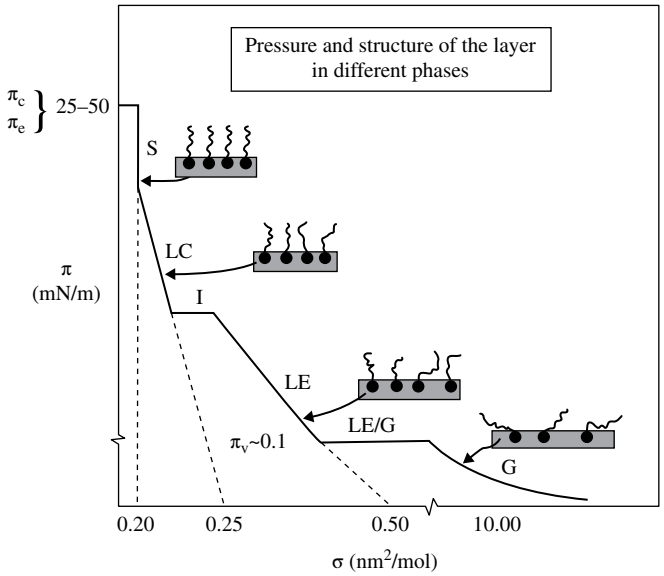

FIGURE 5.16 Composite two-dimensional pressure π versus area σ isotherm, which includes a wide assortment of monolayer phenomena. Note that the scale of the figure is not uniform so that all features may be included on one set of coordinates. The sketches of the surfactants show the orientations of the molecules in each phase at various phases of compression. Adapted from Hiemenz and Rajagopalan (1997).

pressure ($\pi = \gamma_0 - \gamma$) as a function of molecular area on the surface, a so-called π-A isotherm. When the total area available for the molecules is reduced due to the position of the barriers, one observes a transition from a gaseous state (G) to a liquid-like state (L) to a solid–liquid state (S). The change between these states lies within the interaction between the molecules. In the gaseous state, the molecules have large available surfaces and practically no interaction between the species. The molecules have an ideal behavior with no interaction profiles. When the distance between the molecules is reduced, a condensation will take place indicating a stronger intermolecular interaction. Finally, when the packing of the molecules is optimal, the hydrocarbon chains are in hexagonal array characteristic for a solid state. Between the gaseous, liquid, and solid states, there are equilibrium states, for instance, G+L, L+S, and so on, where the surface pressure is constant (Fig. 5.16).

A Langmuir film is obviously a two-dimensional version of a three-dimensional PV case for gas molecules. The difference is that we have lost one dimension since the components in a monolayer have the ionic–polar head anchored in the aqueous phase. Hence, the mobility and thermodynamics are restricted to two dimensions.

However, this is the idealized picture of a Langmuir film. Brewster angle microscopy has revealed that some surface-active molecules are not homogeneously spread, but form patches with higher local interactions interaction parameters (see an example in Fig. 5.17). When the area is reduced, the patches will coalesce/integrate into a homogeneous film.

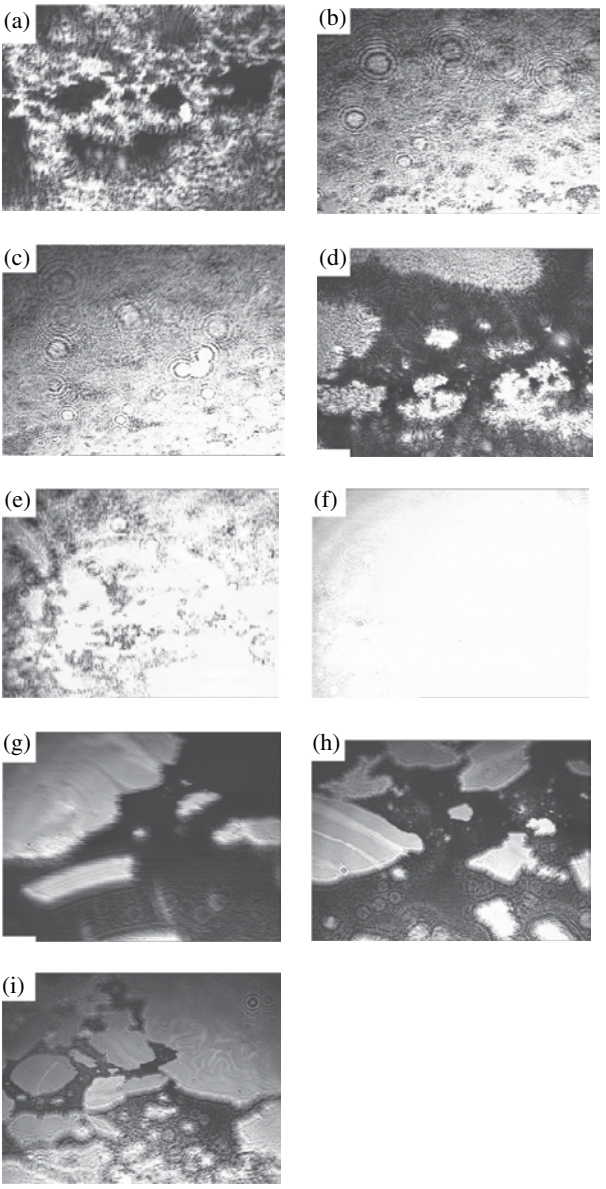

FIGURE 5.17 Effect of surface pressure on BAM images of asphaltenes spread on an aqueous subphase with identical spreading amount of 0.02 mg and varying spreading concentrations. (**a–c**) 50 mg/l 400 µl: before compression, 4 mN/m, 11 mN/m. (**d–f**) 200 mg/l 100 µl: before compression, 4 mN/m, 11 mN/m. (**g–i**) 1000 mg/l 20 µl: before compression, 4 mN/m, 11mN/m. The image size is 400 × 300 µm except B and C (320 × 240 µm). Reprinted from Fan et al. (2010a). © 2010, with permission from the American Chemical Society.

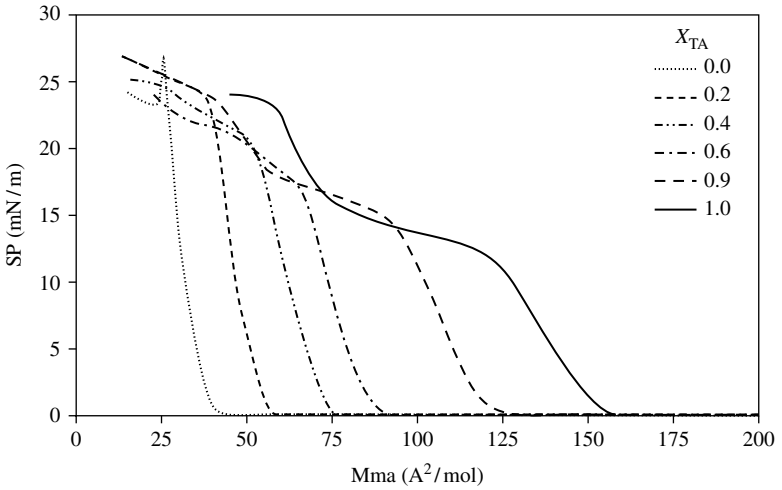

FIGURE 5.18 Surface pressure area isotherms for mixed monolayers of C_{80}-TA and MA at pH 5.6. Reprinted from Brandal et al. (2007). © 2007, with permission from Taylor & Francis Ltd.

5.3.5.2 Mixed Monolayers

The determination of Langmuir isotherm can successfully be used to study mixed films formed of two or several components. The interactions and miscibility between components can therefore be studied. To illustrate this part, an example of interest is presented below.

Using the Langmuir trough and BAM microscopy, Brandal et al. (2007) have studied the interactions between C_{80}-TA (presented in Fig. 5.5) and C_{18} monoacid (stearic acid), hereafter noted MA. Figure 5.18 shows compression isotherms for mixed monolayers of C_{80}-TA and MA on pure water at different C_{80}-TA molar ratio X_{TA}. The isotherms to the very left and right are those of pure MA and C_{80}-TA, respectively. For pure MA, the rise in pressure starts at around 40 Å^2/molecule and no phase transition area is visible before the collapse. For C_{80}-TA, the pressure starts to rise at around 160 Å^2/molecule, then the isotherm gradually flattens out and reaches a nonhorizontal plateau before the pressure continues to increase until the collapse. This plateau is attributed to a transition of conformation: at low surface pressure the C_{80}-TA adopts a flat conformation with all the carboxylic groups in contact with the water surface, while when the plateau-like region is reached, two of the carboxylic groups are expelled from the surface.

The isotherms of the mixed monolayers are located between those of the pure components. The miscibility of two components in a monolayer can be examined by calculation of the excess area (A_{ex}) of the mixed monolayer at the water surface. The excess area is determined by comparing the average area per molecule at a given value of surface pressure of a mixed monolayer consisting of components 1 and 2 (A_{12}) with that of an ideally mixed monolayer (A_{id}):

$$A_{ex} = A_{12} - A_{id} = A_{12} - \left(X_1 A_1 + X_2 A_2\right)$$

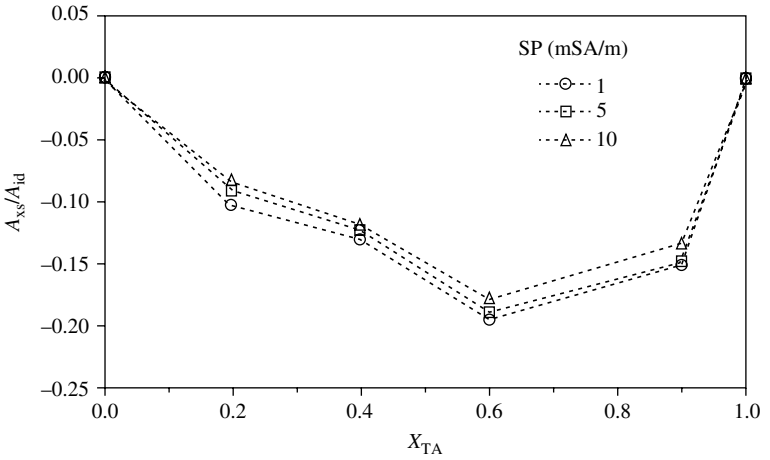

FIGURE 5.19 Excess area/ideal area versus mole fraction of C_{80}-TA of mixed monolayers of C_{80}-TA and MA. Reprinted from Brandal et al. (2007). © 2007, with permission from Taylor & Francis Ltd.

where A_{12} is the measured area and A_{id} is the ideal area (when no interactions occur). A_i and x_i are the area and fraction of pure component i. For an ideally mixed monolayer or when the components are immiscible, the excess area will be 0 and A_{12} will increase in proportion to X_1.

In Figure 5.19, the ratio excess area/ideal area is plotted as a function of the composition. Although all the mixtures of TA and MA exhibit a negative deviation, which implies interactions between the components in the entire concentration range, the most negative deviation appears at 60% TA, which suggests stronger interactions for that composition.

5.3.5.3 Thin Films

Thin liquid oil films composed of bitumen have been studied in detail and with success by the groups in Edmonton, Canada (Khristov et al., 2000; Taylor et al., 2002; Tchoukov et al., 2010). It is obvious that the properties of such films separating two water (aqueous) domains will be crucial for the stability of whole dispersed systems as water-in-oil emulsions. In order to draw correct conclusions about the properties and mechanisms inside the film, the preparation protocol is also important. The experimental procedure is described in Figure 5.20.

One of the parameters affecting the oil film stability is the composition of the solvent, especially the level of the aromaticity. Tchoukov et al. (2010) investigated the oil film behavior for different ratios of heptane to toluene (50:50 and 80:20) and several bitumen concentrations. The authors found a critical S/B (solvent-to-bitumen ratio) value at which the film behavior changed dramatically. For low solvent contents (lower

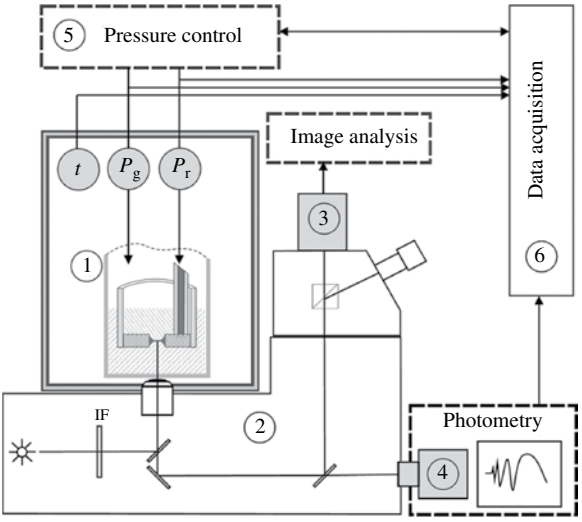

FIGURE 5.20 Experimental setup (Scheludko-Exerowa) used in the thin film experiments by Tchoukov et al.: ①, measuring cell; ②, inverted microscope Carl Zeiss axio observer; ③, CCD camera—Leica DFC500; ④, Hamamatsu Si photodiode; ⑤, Hamilton syringe drive—PSD/2, pressure transducer omega PX143; ⑥, NI data acquisition with LabVIEW. Reprinted from Tchoukov et al. (2010). © 2010, with permission from Elsevier.

than the critical S/B) the films showed a behavior of diluted bitumen films with a time evolution and drainage into a uniform film thickness. High aliphatic concentrations led to film rupture. The authors used the Reynold equation to estimate the time evolution of the film thickness:

$$V_{\mathrm{Re}} = \frac{dh}{dt} = \frac{2h^3 \Delta P}{3\eta R^2} \; with \; \Delta P = P_\gamma - \pi(h)$$

where h is the film thickness, η is the bulk viscosity of the film liquid, R is the film radius, P_γ is the capillary pressure due to the curvature of the film meniscus, and $\pi(h)$ is the disjoining pressure. There was surprisingly good agreement between experimental values and predicted ones by Reynold equation below than the critical S/B. When the solvent (either pure heptane or mixture of heptane and toluene) amount exceeds the critical value, the film properties change drastically. Now the film shows signs of thickness gradients due to drainage together with a formation of a rigid interface, longlasting dimples, and sensitivity toward ageing. An interesting observation is the formation of distinct asphaltene aggregates upon ageing (Fig. 5.21). This phenomenon is attributed to the buildup of a multilayer of asphaltenes at the water–oil interface due to their poor solubility above the critical S/B ratio.

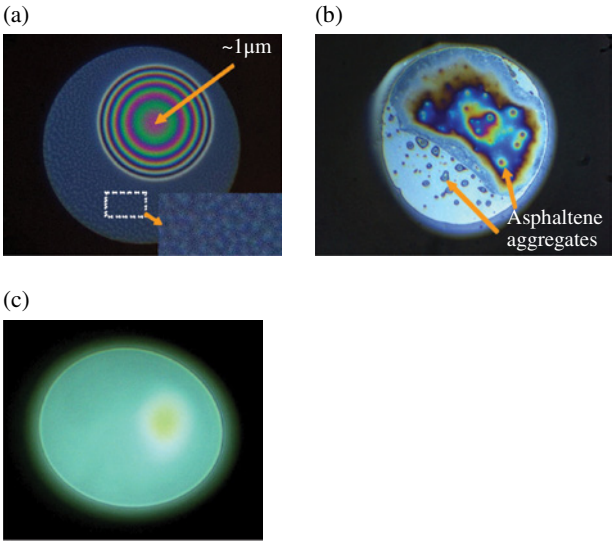

FIGURE 5.21 Film of 10 wt% bitumen in heptol 80:20 (above the critical S/B) for different age of the water–oil interface: (**a**) 15 min water–oil interface age—dimple formation and network structure in film; (**b**) 2.5 h water–oil interface age—skin formation and secondary precipitates; (**c**) after one night and additional centrifugation—very stable, thick, homogeneous film. Reprinted from Tchoukov et al. (2010), with permission from Elsevier.

ACKNOWLEDGMENTS

This work has been supported by grants to the industrial consortium JIP-1 "Increased Energy Savings in Water–Oil Separation through Advanced Fundamental Emulsion Paradigms" and JIP-2 "Prediction of Ca-naphthenate deposition in water–oil systems" by The Norwegian Research Council and the following industrial partners: AkzoNobel, BP, Champion Technologies, Clariant, ConocoPhillips, ENI, Hamworthy, Kemira, Petrobras, REP (Recherche, Exploitation, Produits), Saudi Aramco, Shell Global Solutions, Statoil, Talisman Energy and Total.

REFERENCES

Acevedo S, Escobar G, Ranaudo MA, Khazen J, Borges B, Pereira JC, Méndez B. Isolation and characterization of low and high molecular weight acidic compounds from cerro negro extraheavy crude oil. Role of these acids in the interfacial properties of the crude oil emulsions. Energy Fuels 1999;13(2):333–335.

Ahamad AR, Barker C. Role of evaporation in degrading the "oil lakes." Am J Environ Sci 2011;7(3):219–223.

Ali MA, Nofal WA. Application of high performance liquid chromatography for hydrocarbon group type analysis of crude oils. Fuel Sci Technol Int 1994;12(1):21–33.

Almdal K, Dyre J, Hvidt S, Kramer O. Towards a phenomenological definition of the term 'gel.' Polym Gels Netw 1993;1(1):5–17.

Andreatta G, Goncalves CC, Buffin G, Bostrom N, Quintella CM, Arteaga-Larios F, Pérez E, Mullins OC. Nanoaggregates and structure-function relations in asphaltenes. Energy Fuels 2005;19(4):1282–1289.

Arkenov VS, Titov VI, Kam'yanov VF. Nitrogen compounds of petroleum oils. Chem Heterocycl Compd 1979;15(2):119–135.

Arla D, Sinquin A, Palermo T, Hurtevent C, Graciaa A, Dicharry C. Influence of pH and water content on the type and stability of acidic crude oil emulsions. Energy Fuels 2007;21(3):1337–1342.

Aske N, Kallevik H, Sjöblom J. Determination of saturate, aromatic, resin, and asphaltenic (SARA) components in crude oils by means of infrared and near-infrared spectroscopy. Energy Fuels 2001;15(5):1304–1312.

Aske N, Kallevik H, Sjöblom J. Water-in-crude oil emulsion stability studied by critical electric field measurements. Correlation to physico-chemical parameters and near-infrared spectroscopy. J Petrol Sci Eng 2002;36(1–2):1–17.

Barth T, Hoiland S, Fotland P, Magne Askvik K, Myklebust R, Erstad K. Relationship between the content of asphaltenes and bases in some crude oils. Energy Fuels 2005;19(4):1624–1630.

Baugh TD, Wolf NO, Mediaas H, Vindstad JE, Grande K. Characterization of a calcium naphthanate deposit - the arn acid discovery. Am Chem Soc 2004;49(3):274–276.

Baugh TD, Grande KV, Mediaas H, Vindstad JE, Wolf NO. In: The discovery of high molecular weight naphthenic acids (ARN acid) responsible for calcium naphthenate deposits; 2005 May 11–12; Aberdeen, United Kingdom. SPE International Symposium on Oilfield Scale, SPE 93011, Aberdeen, United Kingdom; 2005.

Betancourt F, Palacio A, Rodriguez A. Effects of the mass transfer process in oil spill. Am J Appl Sci 2005;2(5):939–946.

Bitsch-Larsen A, Andersen SI. Simple method to determine the partition coefficient of naphthenic acid in oil/water. J Chem Eng Data 2008;53(10):2272–2274.

Blumer M, Ehrhardt M, Jones JH. The environmental fate of stranded crude oil. Deep Sea Res Oceanogr Abstr 1973;20(3):239–259.

Bollet C, Escalier JC, Souteyrand C, Caude M, Rosset R. Rapid separation of heavy petroleum products by high-performance liquid chromatography. J Chromatogr A 1981;206(2):289–300.

Bos MA, van Vliet T. Interfacial rheological properties of adsorbed protein layers and surfactants: a review. Adv Colloid Interf Sci 2001;91(3):437–471.

Bouriat P, El Kerri N, Graciaa A, Lachaise J. Properties of a two-dimensional asphaltene network at the water/cyclohexane interface deduced from dynamic tensiometry. Langmuir 2004;20(18):7459–7464.

Brandal Ø, Viitala T, Sjöblom J. Compression isotherms and morphological characteristics of pure and mixed langmuir monolayers of C80 isoprenoid tetraacids and a C18 monoacid. J Disper Sci Technol 2007;28(1):95–106.

Brient JA. Commercial utility of naphthenic acids recovered from petroleum distillates. Am Chem Soc 1998;43(1):131–133.

Brocart B, Hurtevent C. Flow assurance issues and control with naphthenic oils. J Disper Sci Technol 2008;29(10):1496–1504.

Clemente JS, Fedorak PM. A review of the occurrence, analyses, toxicity, and biodegradation of naphthenic acids. Chemosphere 2005;60(5):585–600.

Conceição Oliveira E, Vaz de Campos MC, Sant'Ana Lopes A, Rodrigres MG, Bastos Caramão E. Ion-exchange resins in the isolation of nitrogen compounds from petroleum residues. J Chromatogr A 2004;1027(1–2):171–177.

Czarnecki J, Moran K. On the stabilization mechanism of water-in-oil emulsions in petroleum systems. Energy Fuels 2005;19(5):2074–2079.

Díez S, Jover E, Bayona JM, Albaigés J. Prestige oil spill. III. Fate of a heavy oil in the marine environment. Environ Sci Technol 2007;41(9):3075–3082.

Dahlin KE, Daniel SR, Worstell JH. Deposit formation in liquid fuels. 1. Effect of coal-derived Lewis bases on storage stability of Jet A turbine fuel. Fuel 1981;60(6):477–480.

Dark WA. Crude oil hydrocarbon group separation quantitation. J Liquid Chromatogr 1982; 5(9):1645–1652.

Deo M, Parra M. Characterization of carbon-dioxide-induced asphaltene precipitation. Energy Fuels 2011;26(5):2672–2679.

Ese MH, Kilpatrick PK. Stabilization of water-in-oil emulsions by naphthenic acids and their salts: model compounds, role of pH, and soap: acid ratio. J Disper Sci Technol 2004;25:253.

Espinat D, Fenistein D, Barré L, Frot D, Briolant Y. Effects of temperature and pressure on asphaltenes agglomeration in toluene. A light, x-ray, and neutron scattering investigation. Energy Fuels 2004;18(5):1243–1249.

Fan TP. Characterization of naphthenic acids in petroleum by fast atom bombardment mass spectrometry. Energy Fuels 1991;5(3):371–375.

Fan Y, Simon S, Sjöblom J. Influence of nonionic surfactants on the surface and interfacial film properties of asphaltenes investigated by langmuir balance and brewster angle microscopy. Langmuir 2010a;26(13):10497–10505.

Fan Y, Simon S, Sjöblom J. Interfacial shear rheology of asphaltenes at oil–water interface and its relation to emulsion stability: influence of concentration, solvent aromaticity and nonionic surfactant. Colloid Surf A 2010b;366(1–3):120–128.

Fenistein D, Barre L. Experimental measurement of the mass distribution of petroleum asphaltene aggregates using ultracentrifugation and small-angle X-ray scattering. Fuel 2001;80(2): 283–287.

Fingas MF. Studies on the evaporation of crude oil and petroleum products: I. the relationship between evaporation rate and time. J Hazard Mater 1997;56(3):227–236.

Fingas MF. *The evaporation of oil spills: development and implementation of new prediction methodology, 1999 International Oil Spill Conference*, Seattle, WA; 1999.

Fingas MF. Modeling evaporation using models that are not boundary-layer regulated. J Hazard Mater, 2004;107(1–2):27–36.

Fingas M. Evaporation modeling. In: Mervin F, editor. *Oil Spill Science and Technology*. Boston, MA: Gulf Professional Publishing; 2011. p 201–242.

Fingas MF. Studies on the evaporation regulation mechanisms of crude oil and petroleum products. Adv Chem Eng Sci 2012;2(2):246–256.

Fingas M, Fieldhouse B. Studies on crude oil and petroleum product emulsions: water resolution and rheology. Colloid Surf A 2009;333(1–3):67–81.

Fingas M, Fieldhouse B. Studies on water-in-oil products from crude oils and petroleum products. Mar Pollut Bull 2012;64(2):272–283.

Fontell K, Ceglie A, Lindman B, Ninham B. Some observations on phase diagrams and structure in binary and ternary systems of didodecyldimethylammonium bromide. Acta Chem Scand 1986;40A:247–256.

Friberg S. Liquid crystalline phases in emulsions. J Colloid Interf Sci 1971;37(2):291–295.

Friberg S, Mandell L, Larsson M. Mesomorphous phases, a factor of importance for the properties of emulsions. J Colloid Interf Sci 1969;29(1):155–156.

Friberg S, Jansson PO, Cederberg E. Surfactant association structure and emulsion stability. J Colloid Interf Sci 1976;55(3):614–623.

Gallup DL, Curiale JA, Colin Smith P. Characterization of sodium emulsion soaps formed from production fluids of Kutei Basin, Indonesia. Energy Fuels 2007;21(3):1741–1759.

Goncalves S, Castillo J, Fernández A, Hung J. Absorbance and fluorescence spectroscopy on the aggregation behavior of asphaltene-toluene solutions. Fuel 2004;83(13):1823–1828.

Goodman DS. Distribution of fatty acids between heptane and aqueous phosphate buffer. J Am Chem Soc 1958;80:3887–3892.

Grizzle PL, Sablotny DM. Automated liquid chromatographic compound class group-type separation of crude oils and bitumens using chemically bonded silica-NH_2. Anal Chem 1986;58(12):2389–2396.

Groenzin H, Mullins OC. Asphaltene molecular size and structure. J Phys Chem A 1999; 103(50):11237–11245.

Groenzin H, Mullins OC, Eser S, Mathews J, Yang MG, Jones D. Molecular size of asphaltene solubility fractions. Energy Fuels 2003;17(2):498–503.

Grutters M, van Dijk M, Dubey S, Adamski R, Gelin F, Cornelisse P. Asphaltene induced w/o emusilon: false or true? J Disper Sci Technol 2007;28(3):357–360.

Häger M, Sjöblom J. Phase equilibria in systems of water, naphthenic acids, and phenols. J Disper Sci Technol 2006;27(3):399–406.

Häger M, Ese M-H, Sjöblom J. Emulsion inversion in an oil-surfactant-water system based on model naphthenic acids under alkaline conditions. J Disper Sci Technol 2005;26(6): 673–682.

Hannisdal A, Hemmingsen PV, Sjöblom J. Group-type analysis of heavy crude oils using vibrational spectroscopy in combination with multivariate analysis. Ind Eng Chem Res 2005; 44(5):1349–1357.

Hannisdal A, Ese M-H, Hemmingsen PV, Sjöblom J. Particle-stabilized emulsions: Effect of heavy crude oil components pre-adsorbed onto stabilizing solids. Colloids Surf A 2006; 276(1–3):45–58.

Hannisdal A, Orr R, Sjöblom J. Viscoelastic properties of crude oil components at oil/water interfaces. 1. The effect of dilution. J Disper Sci Technol 2007a;28(1):81–93.

Hannisdal A, Orr R, Sjöblom J. Viscoelastic properties of crude oil components at oil/water interfaces. 2: comparison of 30 oils. J Disper Sci Technol 2007b;28(3):361–369.

Havre TE, Sjöblom J. Emulsion stabilization by means of combined surfactant multilayer (D-phase) and asphaltene particles. Colloids Surf A 2003;228(1–3):131–142.

Havre TE, Sjöblom J, Vindstad JE. Oil/water-partitioning and interfacial behavior of naphthenic acids. J Disper Sci Technol 2003;24(6):789–801.

Headley JV, Peru KM, McMartin DW, Winkler M. Determination of dissolved naphthenic acids in natural waters by using negative-ion electrospray mass spectrometry. J AOAC Int 2002;85(1):182–187.

Hemmingsen PV, Silset A, Hannisdal A, Sjöblom J. Emulsions of heavy crude oils I: influence of viscosity, temperature and dilution. J Disper Sci Technol 2005;26(5):615–627.

Hemmingsen PV, Kim S, Pettersen HE, Rodgers RP, Sjöblom J, Marshall AG. Structural characterization and interfacial behavior of acidic compounds extracted from a North Sea Oil. Energy Fuels 2006;20(5):1980–1987.

Hiemenz PC, Rajagopalan R. *Adsorption from Solution and Monolayer Formation. Principles of Colloid and Surface Chemistry*. 3rd ed. Boca Raton, FL: CRC Press; 1997, p 297–354.

Hortal AR, Martínez-Haya B, Lobatao MD, Pedrosa JM, Lagoet S. On the determination of molecular weight distributions of asphaltenes and their aggregates in laser desorption ionization experiments. J Mass Spectrom 2006;41(7):960–968.

Horváth-Szabó G, Czarnecki J, Masliyah JH. Sandwich structures at oil–water interfaces under alkaline conditions. J Colloid Interf Sci 2002;253(2):427–434.

Horváth-Szabó G, Masliyah JH, Czarnecki J. Emulsion stability based on phase behavior in sodium naphthenates containing systems: gels with a high organic solvent content. J Colloid Interf Sci 2003;257(2):299–309.

Hsu CS, Dechert GJ, Robbins WK, Fukudaet EK. Naphthenic acids in crude oils characterized by mass spectrometry. Energy Fuels 2000;14(1):217–223.

Hurtevent C, Rousseau G, Bourrel M, Brocart B. Production issues of acidic petroleum crude oils. In: Sjöblom J, editor. *Emulsions and Emulsion Stability*. 2nd ed. Surfactant Science Series 132. Boca Raton, FL: CRC Press LLC; 2006. p 477–516.

International Union of Pure and Applied Chemistry. *Manual on Colloid and Surface Science*. London: Butterworths; 1972.

Jeribi M, Almir-Assad B, Langevin D, Hénaut I, Argillier JF. Adsorption kinetics of asphaltenes at liquid interfaces. J Colloid Interf Sci 2002;256(2):268–272.

Jones DM, Watson JS, Meredith W, Chen M, Bennettet B. Determination of naphthenic acids in crude oils using nonaqueous ion exchange solid-phase extraction. Anal Chem 2001;73(3):703–707.

Keleşoğlu S, Pettersen BH, Sjöblom J. Characterization of water-in-North Sea acidic crude oil emulsions by means of rheology, droplet size, and laminar flow in pipeline. J Disper Sci Technol 2011;33(4):536–548.

Khristov K, Taylor SD, Czarnecki J, Masliyah J. Thin liquid film technique—application to water–oil–water bitumen emulsion films. Colloids Surf A 2000;174(1–2):183–196.

Kilpatrick PK, Spiecker PM. Asphaltene emulsions. In: Sjöblom J, editor. *Encyclopedic Handbook of Emulsion Technology*. New York: Marcel Dekker, Inc; 2001.

Koike L, Rebouças LMC, Reis FDAM, Marsaioli AJ, Richnow HH, Michaelis W. Naphthenic acids from crude oils of Campos Basin. Org Geochem 1992;18(6):851–860.

Kotlyar LS, Sparks BD, Woods JR. Solids associated with the asphaltene fraction of oil sands bitumen. Energy Fuels 1999;13(2):346–350.

Krog N. Structures of emulsifier-water mesophases related to emulsion stability. Fette, Seifen, Anstrichmittel 1975;77(7):267–271.

Laredo GC, Leyva S, Alvarez R, Mares MT, Castillo J, Cano JL. Nitrogen compounds characterization in atmospheric gas oil and light cycle oil from a blend of Mexican crudes. Fuel 2002;81(10):1341–1350.

Lundanes E, Greibrokk T. Separation of fuels, heavy fractions, and crude oils into compound classes: a review. J High Resolut Chromatogr 1994;17(4):197–202.

McKay JF, Weber JH, Lathamet DR. Characterization of nitrogen bases in high-boiling petroleum distillates. Anal Chem 1976;48(6):891–898.

McLean JD, Kilpatrick PK. Effects of asphaltene aggregation in model heptane-toluene mixtures on stability of water-in-oil emulsions. J Colloid Interf Sci 1997a; 196(1):23–34.

McLean JD, Kilpatrick PK. Effects of asphaltene solvency on stability of water-in-crude-oil emulsions. J Colloid Interf Sci 1997b;189(2):242–253.

Merdrignac I, Behar F, Albrecht P, Briot P, Vandenbroucke M. Quantitative extraction of nitrogen compounds in oils: atomic balance and molecular composition. Energy Fuels 1998; 12(6):1342–1355.

Meredith W, Kelland SJ, Jones DM. Influence of biodegradation on crude oil acidity and carboxylic acid composition. Org Geochem 2000;31(11):1059–1073.

Merlin M, Guigard SE, Fedorak PM. Detecting naphthenic acids in waters by gas chromatography–mass spectrometry. J Chromatogr A 2007;1140(1–2):225–229.

Miller R, Ferri JK, Javadi A, Krägel J, Mucic N, Wüstneck R. Rheology of interfacial layers. Colloid Polym Sci 2010;288(9):937–950.

Mostowfi F, Indo K, Mullins OC, McFarlane R. Asphaltene nanoaggregates studied by centrifugation. Energy Fuels 2008;23(3):1194–1200.

Mullins OC. The modified yen model. Energy Fuels 2010;24(4):2179–2207.

Murgich J. Molecular simulation and the aggregation of the heavy fractions in crude oils. Mol Simul 2003;29(6–7):451–461.

Nenningsland AL, Simon S, Sjöblom J. Surface properties of basic components extracted from petroleum crude oil. Energy Fuels 2010;24(12):6501–6505.

Nenningsland AL, Gao B, Simon S, Sjöblom J. Comparative study of stabilizing agents for water-in-oil emulsions. Energy Fuels 2011;25(12):5746–5754.

Nordgård EL, Sjöblom J. Model compounds for asphaltenes and c80 isoprenoid tetraacids. Part I: synthesis and interfacial activities. J Disper Sci Technol 2008;29(8):1114–1122.

Nordgård EL, Magnusson H, Hanneseth AMD, Sjöblom J. Model compounds for C80 isoprenoid tetraacids: part II. Interfacial reactions, physicochemical properties and comparison with indigenous tetraacids. Colloid Surf A 2009;340(1–3):99–108.

Nordgård EL, Ahmad J, Simon S, Sjöblom J. Oil–water partitioning of a synthetic tetracarboxylic acid as a function of pH. J Disper Sci Technol 2012;33(6):871–880.

Pal R. Novel viscosity equations for emulsions of two immiscible liquids. J Rheol 2001;45(2): 509–520.

Pal R, Rhodes E. Viscosity/concentration relationships for emulsion. J Rheol 1989;33(7): 1021–1045.

Poteau S, Argillier JF, Langevin D, Pincent F, Perez E. Influence of pH on stability and dynamic properties of asphaltenes and other amphiphilic molecules at the oil–water interface. Energy Fuels 2005;19(4):1337–1341.

Qian K, Robbins WK, Hughey CA, Cooper HJ, Rodgers RP, Marshall AG. Resolution and identification of elemental compositions for more than 3000 crude acids in heavy petroleum by negative-ion microelectrospray high-field fourier transform ion cyclotron resonance mass spectrometry. Energy Fuels 2001;15(6):1505–1511.

Radke M, Willsch H, Welte DH. Preparative hydrocarbon group type determination by automated medium pressure liquid chromatography. Anal Chem 1980;52(3):406–411.

Robbins WK. Challenges in the characterization of naphthenic acids in petroleum. Am Chem Soc 1998;43(1):137–140.

Rogowska J, Namieśnik J. Environmental implications of oil spills from shipping accidents. In: Whitacre DM, editor. *Reviews of Environmental Contamination and Toxicology*. New York: Springer; 2010. p 95–114.

Rosset R, Caude M, Escalier JC, Bollet C. Analysis of nitrogen compounds in light petroleum products by ion exchange followed by gas chromatography with a hall detector and mass spectrometry. J Chromatogr 1978;167:125–131.

Saab J, Mokbel I, Razzouk AC, Ainous N, Zydowicz N, Jose J. Quantitative extraction procedure of naphthenic acids contained in crude oils. Characterization with different spectroscopic methods. Energy Fuels 2005;19(2):525–531.

Schmitter JM, Ignatiadis I, Arpino P, Guiochon G. Selective isolation of nitrogen bases from petroleum. Anal Chem 1983;55(11):1685–1688.

Selle MH, Sjöblom J, Høiland H. Emulsions under elevated pressure and temperature conditions: II. The model system water (electrolyte)–octanoic acid–sodium octanoate–*n*-heptane at 20 C. J Colloid Interf Sci 1991;144(1):36–44.

Shepherd AG, Thomson GB, Westacott R, Sorbie KS, Turner M, Smith PC. *In: Analysis of organic field deposits: new types of calcium naphthenate scale or the effect of chemical*

treatment? SPE International Oilfield Scale Symposium, SPE 100517, May 30 to June 1 2006, Aberdeen, United Kingdom; 2006.

Sherman P. *Emulsion Science*. New York: Academic Press, Inc., Ltd; 1968.

Shokrlu YH, Kharrat R, Ghazanfari MH, Saraji S. Modified screening criteria of potential asphaltene precipitation in oil reservoirs. Petrol Sci Technol 2011;29(13):1407–1418.

Simon S, Nordgård E, Bruheim P, Sjöblom J. Determination of C80 tetra-acid content in calcium naphthenate deposits. J Chromatogr A, 2008;1200(2):136–143.

Simon S, Jestin J, Palermo T, Barré L. Relation between solution and interfacial properties of asphaltene aggregates. Energy Fuels 2009;23(1):306–313.

Simon S, Nenningstand AL, Herschbach E, Sjöblom J. Extraction of basic components from petroleum crude oil. Energy Fuels 2010;24:1043–1050.

Singh S, McLean JD, Kilpatrick PK. Fused ring aromatic solvency in destabilizing water-in-asphaltene-heptane-toluene emulsions. J Disper Sci Technol 1999;20(1–2):279–293.

Sjöblom J. Professor Stig Erik Friberg 65 years. Colloids Surf A 1997;123–124(0):1–2.

Sjöblom J, Aske N, Auflem IH, Brandal Ø, Havre TE, Sæther Ø, Westvik A, Johnsen EE, Kallevik H. Our current understanding of water-in-crude oil emulsions.: recent characterization techniques and high pressure performance. Adv Colloid Interf Sci 2003;100–102: 399–473.

Skurtveit R, Sjöblom J, Bouwstra J, Gooris G, Selle MH. Effect of electrolyte on the phase behavior and emulsion stability in the system didodecyldimethylammonium bromide (DDAB)/dodecane/water. J Colloid Interf Sci 1992;152(1):205–217.

Slavcheva E, Shone B, Turnbull A. Review of naphthenic acid corrosion in oil refining. Br Corros J 1999;34:125–131.

Speight JG. Petroleum asphaltenes – Part 1: Asphaltenes, resins and the structure of petroleum. Oil Gas Sci Technol 2004;59(5):467–477.

Speight JG. *The Chemistry and Technology of Petroleum*. 4th ed. Boca Raton, FL: CRC Press; 2007.

Spiecker PM, Kilpatrick PK. Interfacial rheology of petroleum asphaltenes at the oil–water interface. Langmuir 2004;20(10):4022–4032.

Spiecker PM, Gawrys KL, Kilpatrick PK. Aggregation and solubility behavior of asphaltenes and their subfractions. J Colloid Interf Sci 2003a;267(1):178–193.

Spiecker PM, Gawrys KL, Trail CB, Kilpatrick PK. Effects of petroleum resins on asphaltene aggregation and water-in-oil emulsion formation. Colloids Surf A 2003b;220(1–3):9–27.

Suatoni JC, Swab RE. Rapid hydrocarbon group-type analysis by high performance liquid chromatography. J Chromatogr Sci 1975;13(8):361–366.

Sullivan AP, Kilpatrick PK. The effects of inorganic solid particles on water and crude oil emulsion stability. Ind Eng Chem Res 2002;41(14):3389–3404.

Sundman O, Nordgård EL, Grimes B, Sjöblom J. Potentiometric titrations of five synthetic tetraacids as models for indigenous C80 tetraacids. Langmuir 2010;26(3):1619–1629.

Suzuki K, Taniguchi Y, Watanabe T. Effect of pressure on the dimerization of carboxylic acids in aqueous solution. J Phys Chem 1973;77(15):1918–1922.

Sztukowski DM, Yarranton HW. Oilfield solids and water-in-oil emulsion stability. J Colloid Interf Sci 2005;285(2):821–833.

Taylor SD, Czarnecki J, Masliyah J. Disjoining pressure isotherms of water-in-bitumen emulsion films. J Colloid Interf Sci 2002;252(1):149–160.

Tchoukov P, Czarnecki J, Dabros T. Study of water-in-oil thin liquid films: Implications for the stability of petroleum emulsions. Colloid Surf A 2010;372(1–3):15–21.

Thompson KFM. A classification of petroleum on the basis of the ratio of sulfur to nitrogen. Org Geochem 1994;21(8–9):877–890.

Tomczyk NA, Winans RE, Shinn JH, Robinson RC. On the nature and origin of acidic species in petroleum. 1. Detailed acid type distribution in a California crude oil. Energy Fuels 2001; 15(6):1498–1504.

Wallace S, Crook MJ, Bartle KD, Pappin AJ. Isolation of nitrogen bases from coal-derived asphaltenes and preasphaltenes. Fuel 1986;65(1):138–139.

Wiehe IA, Kennedy RJ. The oil compatibility model and crude oil incompatibility. Energy Fuels 1999;14(1):56–59.

Wu X. Investigating the stability mechanism of water-in-diluted bitumen emulsions through isolation and characterization of the stabilizing materials at the interface. Energy Fuels 2003;17(1):179–190.

Yarranton HW, Sztukowski DM, Urrutia P. Effect of interfacial rheology on model emulsion coalescence: I. Interfacial rheology. J Colloid Interf Sci 2007a;310(1):246–252.

Yarranton HW, Urrutia P, Sztukowski DM. Effect of interfacial rheology on model emulsion coalescence: II. Emulsion coalescence. J Colloid Interf Sci 2007b;310(1):253–259.

Zeng H, Song Y-Q, Johnson DL, Mullins OC. Critical nanoaggregate concentration of asphaltenes by direct-current (DC) electrical conductivity. Energy Fuels 2009;23(3):1201–1208.

6

REMEDIATING OILFIELD WASTE AND SPILLS

Raymond S. Farinato

6.1 INTRODUCTION

The massive seafloor release of crude oil resulting from the Deepwater Horizon drilling rig explosion and blowout in the Macondo Prospect in the Gulf of Mexico beginning in April 2010 and lasting for 3 months spawned responses from governmental agencies, corporations, and technical communities. Events of this magnitude give us immediate and serious cause to reevaluate with heightened focus the available preventative, response, and remediation options. We conclude in almost all such situations that we should improve our options before the next occurrence. While the petroleum and mining industries operate somewhat separately, they both create situations and develop technologies and systems that can have enormous environmental impact as they turn natural resources into valuable reserves and finally into useful products. Indeed, the technical portions of these enterprises have similar goals (benign, sustainable, and efficient separation of valuable components from natural mixtures), comparable problems (acceptable collateral effects on all resources involved including water and energy usage, waste management, and human safety), and overlapping scientific and technological underpinnings.

The skills and technologies from mineral processing that may be appropriately marshaled to deal with oil spills may be roughly divided into three categories depending on their relationship to the spill event: prior to, during, or after the fact. To state the obvious, risk analysis and mitigation schemes and engineering designs and controls should be employed as effectively as possible to avoid a spill. Large-scale logistics, cooperation

Oil Spill Remediation: Colloid Chemistry-Based Principles and Solutions, First Edition.
Edited by Ponisseril Somasundaran, Partha Patra, Raymond S. Farinato, and Kyriakos Papadopoulos.

between companies and agencies, and dispersion suppression and mitigation methods are necessary in response to a spill event. After the fact, we are left with data collection and analysis, solid–liquid–liquid separation, education and regulatory action as primary activities.

6.2 PARTICLE-STABILIZED INTERFACES

One set of common problems in several petroleum and mineral processing operations arises from the need to control the stability of oil–water interfaces especially in the presence of biwettable solids, that is, solids that have some affinity for both aqueous and (predominantly nonpolar) organic phases and that readily locate at these interfaces.

6.2.1 Solvent Extraction Crud

One example of particle-stabilized interfacial problems from the mineral processing realm may be found in solvent extraction operations that are often part of hydrometallurgical processing in the production of copper, nickel, molybdenum, etc. Such separation operations are designed to result in the efficient transfer of specific metal ions from aqueous pregnant liquors into immiscible ligand-bearing organic phases or from the metal complex-laden organic phases into clean aqueous solutions. These schemes are used to isolate and purify specific metal ions in solutions, which then form the feed to electrowinning operations for the fabrication of metal monoliths. These solvent extraction processes are essentially interfacial transfer processes and thus require a large organic–aqueous interfacial area to be effective. However, once the ion transfer has taken place, the organic–aqueous emulsion must be broken quickly and cleanly in order to separate bulk phases for further processing. The efficiency and speed of solvent extraction processes are greatly impacted by phase disengagement kinetics, that is, the rate at which any dispersed organic or aqueous phase coalesces back into separate single phases. Producing an unstable emulsion satisfies these requirements. However, the presence of biwettable solids, which collect at aqueous–organic interfaces, often frustrates the speed if not the completeness of the disengagement of those two phases since these solid particles stabilize the aqueous–organic interface. The problematic mass of poorly disengaged oil, water, and solids is commonly referred to as “crud” in those applications (Evans and Hughes, 1995; Hughes and Forsyth, 1996; Hughes et al., 1996; Mover and Mc Dowell, 1981; Ritcey, 1980; Taghizadeh et al., 2009; Wang, 2001).

The nature of the solids located at the aqueous–organic interface in solvent extraction cruds ranges from organic compounds to precipitated minerals. The aqueous phase is typically characterized by high ionic strength and low pH. Approaches to treat and separate stable crud, mainly for the purpose of recovering the organic phase, are constrained by a requirement to maintain an uncontaminated organic phase. This motivates efforts to modify upstream operations in order to mitigate the presence of a solid phase during the phase disengagement step of solvent extraction whenever possible (Fletcher and Gage, 1985; Ning et al., 2009; Ritcey, 1992). Failing this, mechanical schemes for gathering and excising crud from the operation are used (Allen and Berry, 1981; Dorlac

and Sudderth, 2002). Most of the separation schemes used to recover the organic phase are gravity driven (i.e., settling or flotation) since the corrosive nature of the aqueous phase and the combustible nature of the organic phase make the use of conventional centrifuges unappealing. Chemical treatments to enhance gravity-driven separation have been developed (Gillaspie et al., 2010; Goren, 1966; Groh, 1958). These treatments are mainly based on aggregating the solids that stabilize the crud emulsion rather than altering their wettability. The aggregating agent is typically a soluble polymer that flocculates the interfacial solids. Such a strategy works better under circumstances where the solid content is low, thereby avoiding the creation of a flocculated network that might entrap liquid phases.

6.2.2 Oilfield Waste Management

The petroleum processing industry can also provide numerous examples of similar behavior arising from the presence of finely divided biwettable solids in drilling, production, refining, and waste management operations (Angle, 2001; Angle et al., 2007; Donaldson and Alam, 2008; Sjöblom, 2001). The ternary diagram in Figure 6.1 indicates composition ranges of oilfield mixtures whose separations are both integral to their processing and often hampered by the presence of biwettable solids. This includes the materials resulting from an oil spill. Two specific examples discussed in this chapter are the separation of used oil-based drilling muds (Adams et al., 2008a, b; Ivan and Browne, 2008) and the separation of oilfield slops into recyclable phases.

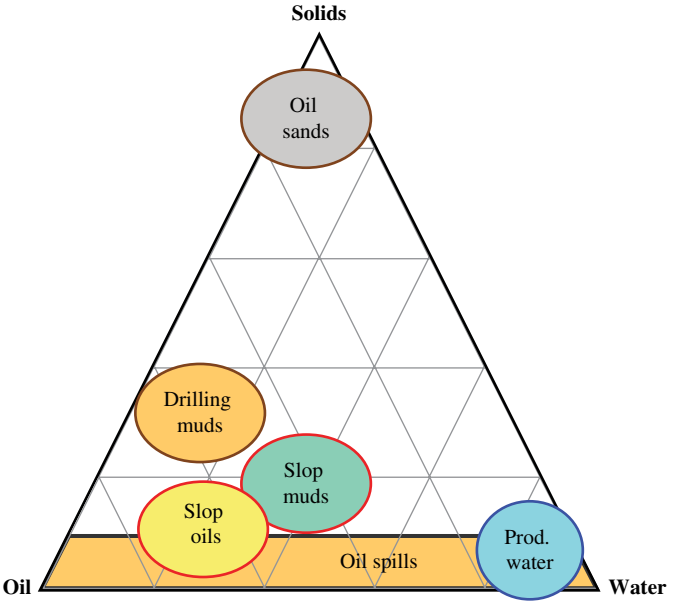

FIGURE 6.1 Oilfield mixtures whose separations are made difficult by the presence of biwettable solids and the oil–water–solid networks they form.

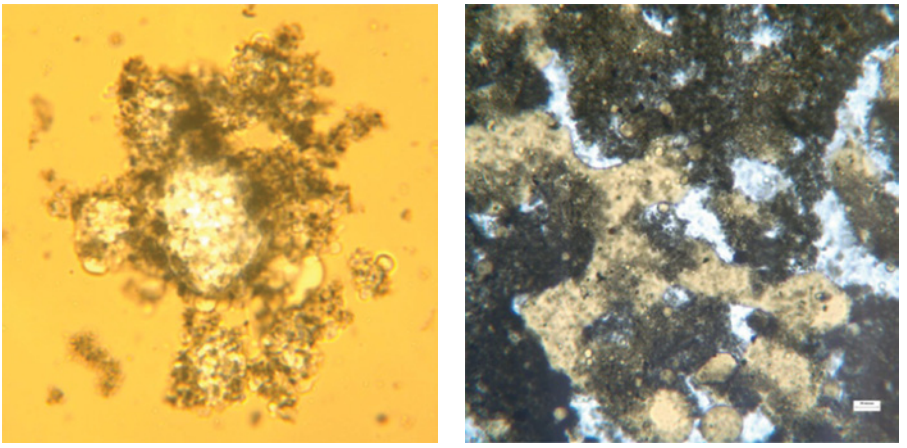

FIGURE 6.2 Photomicrographs of oil–water systems stabilized by biwettable particles located at the oil–water interface. Cluster of water droplets in oil prevented from coalescence by solids adsorbed at the oil–water interface. Scale bar is 20 μm (left). Crud phase from poorly separated slop oil. Light blue regions are aqueous, tan regions are oil, and black material is composed of bi-wettable solids. Scale bar is 20 μm (right). *See insert for color representation of the figure.*

There are two general ways in which biwettable solids located at oil–water interfaces cause separation problems. Stabilization of independent or small clusters of emulsified droplets due to particles located at the oil–water interface results in what are referred to as Pickering emulsions (Aveyard and Clint, 2003; Binks, 2002; Leal-Calderon and Schmitt, 2008; Menon and Wasan, 1988; Pickering, 1907; Poindexter et al., 2005; Sztukowski and Yarranton, 2004; Thompson et al., 1985; Yan et al., 2001). An example of aqueous droplets stabilized in oil by such a mechanism is shown in the photomicrograph in Figure 6.2 (left side). Aqueous droplets in close proximity are kept from coalescing due to the particles located at oil–water interfaces. There is insufficient force, even in well-mixed systems, to displace the particles located at the oil–water interface and allow droplet coalescence.

Another class of problems arising from biwettable solids lodged at the oil–water interface is the formation of mechanical barriers to gravity-driven separation. Structural oil–water–solid networks with sufficient mechanical integrity to block or impede droplets rising or falling can form over a sufficiently large expanse to virtually halt or at least greatly slow down gravity-driven separations in settling tanks. It is most problematic when these networks locate at a level between oil and aqueous phases that have collected as a result of a partially successful coalescence of individual droplets. The yield stresses and elastic moduli of the solid-stabilized network are large enough such that the network can resist deformation by the forces available. Capillary pressures within the system of solid-stabilized, interdigitated oil and aqueous pools are large enough to reduce counterflow of the two immiscible liquid phases to a glacial pace. Liquid movement is confined to narrow channels, some of which are not even connected to the larger macroscopic reservoirs. Such a formation greatly increases resistance to flow resulting in arrested separation. Even when the networks locate on the top or bottom of a mixture, they can

sequester significant volumes of the aqueous and oil phases, with consequences for process economics and regulatory compliance in disposal of these dispersions. Masses of these networked dispersions are commonly referred to in the petroleum industry as crud, slop, rag layers, or a variety of other terms revealing the nuisance they produce. A photomicrograph of one such network is shown in Figure 6.2 (right side).

The conditions found in stable oil spill emulsions can be quite similar to those in some oilfield wastes, so it is worth considering the treatment methods employed there to enhance separation even though the compositions of the solid phases responsible for emulsion stability may differ somewhat. Crude oil released into aquatic environments from spills can readily form particle-stabilized dispersions. Particulate matter susceptible to locating at the oil–water interface can come from aquatic biota, finely divided minerals, organic compounds from the crude oil that are insoluble under the prevailing conditions, or insoluble reaction products.

6.3 CHEMICAL TREATMENT TO ENHANCE SOLID-STABILIZED OIL–WATER SEPARATION

While centrifugation or thermal treatment could in general be applied to separate oil, water, and solid phases, this approach may be neither economical nor achievable on the scale required to be practical for oil spill mixtures. Dismantling the structure of particle-stabilized networks via chemical means is often more pragmatic. Materials and methods used for this purpose in oilfield and mineral processing applications are potentially useful or may at least provide some guidance in dealing with related problems from oil spills.

Many of the particle-stabilized mixtures found in mineral processing or oilfield drilling, production, and refining operations can be treated under controlled conditions, that is, confined to vessels or containers that keep the contents reasonably well isolated from the environment. Such a situation allows one to employ a wider range of treatment chemicals since their release into the environment can be controlled if necessary. The typical list of industrial chemicals available in the arsenal to enhance oil–water separation under those conditions includes surfactants, organic coagulants (e.g., cationic polymers), inorganic coagulants (e.g., Fe or Al salts), mineral- and plant-based adsorbents (e.g., clays, silica, cellulosics), dispersants (e.g., low-molecular-weight anionic polymers), flocculants (e.g., high-molecular-weight water-soluble polymers), and diluents. However, oil spill scenarios usually imply a definite and poorly uncontrolled contact with the natural environment. Therefore, the chemicals used should be as environmentally benign as possible or at least not raise the environmental risk beyond what the spill produced in the first place. Development of these more benign treatment materials then becomes a very worthwhile and important endeavor.

The following two sections discuss examples of strategies and methods developed to enhance separation of oilfield wastes in which networks stabilized by solids had to be overcome. The first one involves separating oil from dispersions having high solid content, that is, a used oil-based drilling mud. The second section discusses recovering both oil and clean water from an oilfield waste dispersion having lower solid content, that is, a slop mud. Both of these examples show how three-phase separations can be

improved by adjusting colloid stability in a controlled manner. The principles underlying these approaches are also applicable to the three-phase systems generated in an oil spill, for example, particle-stabilized oil-in-water or water-in-oil emulsions.

6.3.1 Separating Oil from Used Oil-Based Drilling Fluids

Oil-based drilling fluids, although typically more expensive than water-based drilling fluids, have characteristics that make them superior in comparison to the water-based fluids in some circumstances (Darley and Gray, 1988). As prepared, oil-based drilling fluids (muds) are typically inverse emulsions (i.e., oil-continuous with discrete brine droplets) containing certain solids by design. A typical oil-based drilling fluid might comprise the following components: oil (diesel or synthetic), emulsifiers and wetting agents, brine (for osmotic control), thixotropic agents (e.g., organophilic clay), weighting agent (e.g., barite), and fluid loss control agents (e.g., lignins). In many instances, drilling mud formulations also contain lime to counteract H_2S formation, with the consequence that many of these drilling fluids have a high pH. Therefore, treatment materials must have adequate chemical stability under those conditions.

These drilling fluids serve multiple functions including lubricating and cooling the drill bit, removing suspended cuttings, controlling fluid loss to the formation, and preventing borehole fracture or collapse by balancing hydrostatic pressures against formation pressures. During drilling operations, the larger cuttings entrained in the drilling mud are mechanically removed with screens and shakers so that the fluid remains functional and can be recirculated or reused. Fine cuttings however eventually accumulate in the drilling mud, along with other liquids from the formation, ultimately degrading the drilling mud's properties to the point where it is no longer useable. An optical micrograph of a used oil-based drilling fluid is shown in Figure 6.3. Colors in the micrograph are mainly due to the use of polarization optics in combination with a quarter-wave plate. The solid content in this example was approximately 20 wt%.

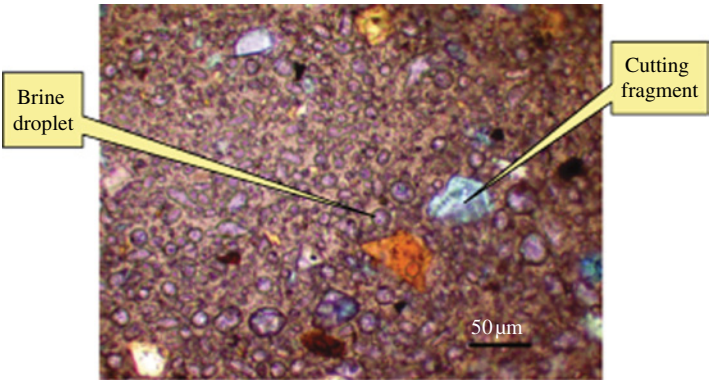

FIGURE 6.3 Optical micrograph of used oil-based drilling mud; polarized light with quarter-wave plate; scale bar is 50 µm. *See insert for color representation of the figure.*

The congested nature of this dispersion is quite obvious. The continuous phase was synthetic oil, and the aqueous brine droplets were stabilized by a combination of emulsifying surfactants and biwettable solids. Recovery of the oil phase from such a used fluid would allow that oil to be recycled instead of being disposed. However, the types of centrifuges commonly employed in oilfield operations often do not produce adequate separation of the oil, aqueous, and solid components by direct centrifugation of such a used drilling fluid. The oil may alternatively be recovered in a thermal process that essentially distills off the oil. However, this approach is not energy efficient and adds to atmospheric carbon emissions. Instead, a chemical approach to destabilizing the system, thereby allowing a more complete separation with the mechanical means available, was developed, as described in the succeeding text. A general description of this approach and examples may be found in several patents (Adams et al., 2008a, b; Ivan and Browne, 2008).

The goal is to aggregate the hydrophilic components in the mixture in a manner that allows easier egress of oil from the destabilized dispersion into a macroscopic phase. Centrifugal separation of the oil then becomes more complete. This enhanced separation may be accomplished by using an inverse polymeric emulsion as the aggregating agent. Inverse polymeric emulsions comprise a microscopic discrete phase containing a water-soluble polymer and water, dispersed in an oil-continuous medium. The discrete phase is colloidally stable by virtue of emulsifying surfactants present at the droplet surface. Inverse polymeric emulsions are a common formulation format in the production of high-molecular-weight water-soluble polymers used as flocculants in water purification and wastewater treatment. In water treatment, the flocculants must first dissolve in water before they can adsorb to multiple particulates in the water, thereby causing them to aggregate. In the present example of aggregating particulates in an oil-continuous medium (i.e., the used drilling fluid), the high-molecular-weight water-soluble polymers in the droplet remain undissolved and in the form of a microscopic (~ micron diameter) hydrophilic droplet whose material constitution is that of a semisolid. That is, even though the polymer molecules are not chemically cross-linked, they are of sufficient concentration in the droplet to be entangled and give the droplet semisolid material properties. When an inverse polymeric emulsion is diluted into a compatible oil phase, the physically bound emulsifier molecules are diluted off the polymeric droplet surfaces, and those droplets then lose their colloidal stability. The destabilized polymeric droplets then readily adhere to other hydrophilic materials, for example, drill cuttings, in the mixture. In some drilling mud systems, the addition of only an inverse polymeric emulsion is insufficient to cause the necessary extent of aggregation. Adding a high-HLB surfactant along with the polymeric emulsion to the drilling mud can often rectify this situation.

Since many used oil-based drilling fluids are very congested dispersions, a network of the aggregated hydrophilic components tends to form as a result of the treatment described earlier. These networks must be crafted in a manner that allows pathways for the oil to be extracted, by centrifugation in the present case. Such networks are of course metastable structures, so mixing (intensity and duration), sequencing of chemical addition, contact time, and particle concentration (sometimes adjusted by dilution with oil) can all be factors in achieving an acceptable

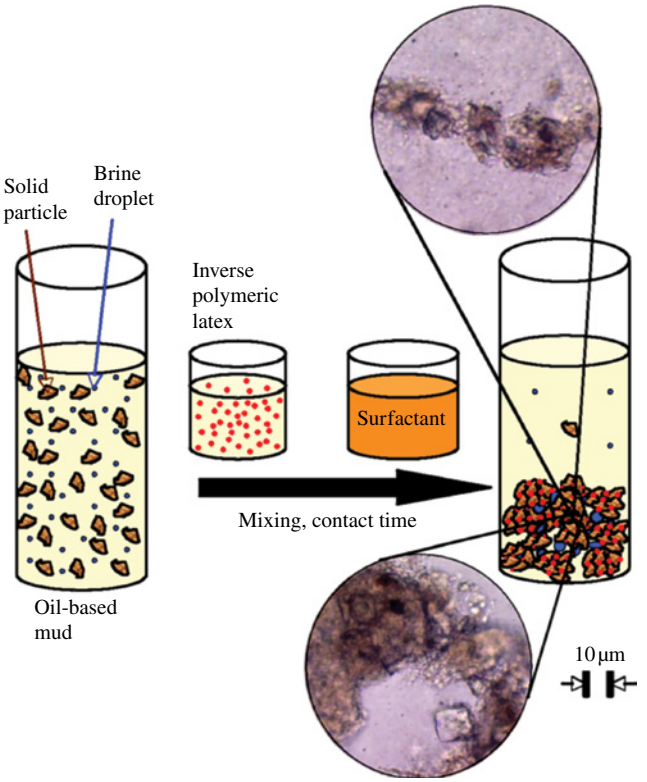

FIGURE 6.4 Direct use of polymeric inverse emulsions to aggregate hydrophilic solids in a used oil-based drilling mud in order to recover oil phase. Bright-field optical micrograph scale bar is 10 µm. *See insert for color representation of the figure.*

aggregation network with the desired oil recovery. A schematic illustrating the essential features of this process is shown in Figure 6.4.

The optical micrographs in Figure 6.4 show the open network of aggregated solids (mainly silicates and clays in this case) that forms after treatment with hydrophilic polymer droplets, the open spaces being an oil-continuous phase that more easily drains from the network under centrifugal force. In many cases, the addition of a high-HLB surfactant is necessary for good aggregation of the mineral particles and separation of the oil phase. Our observations suggest that at least partial demulsification of the aqueous drops and water wetting of the dispersed solids in the used drilling mud (either brine droplets added by design or inadvertent aqueous phase collected during use) is necessary for the solid aggregation to be effective. While this hypothesis remains to be completely tested, we find it to be straightforward to empirically identify combinations of high-HLB surfactants and polymeric emulsions that may be used to enhance the separation of oil from used oil-based drilling muds. An example of such an identification exercise is shown in the Figure 6.5. The inverse

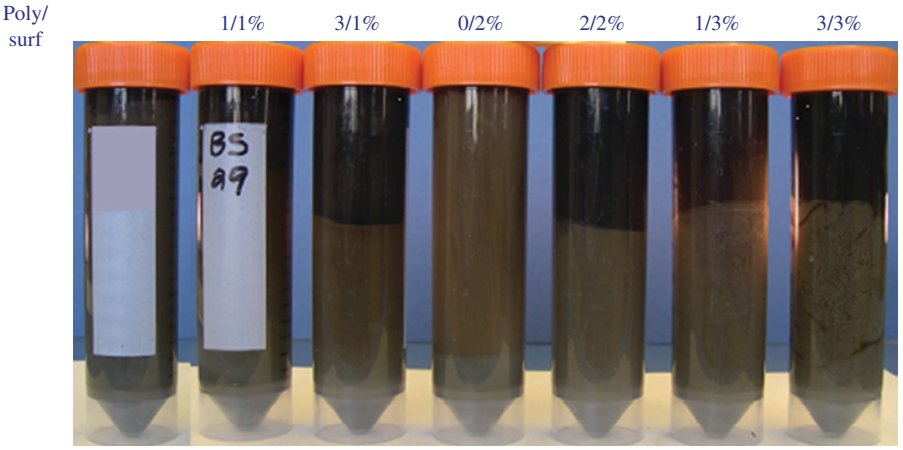

FIGURE 6.5 Lab testing of chemical treatment of used oil-based drilling fluid; samples shown after centrifugation. *See insert for color representation of the figure.*

polymeric emulsion droplets contained a high-molecular-weight copolymer of acrylamide and a cationic ester similar to the one previously described (Adams et al., 2008b). A high-HLB surfactant similar to the one also previously described (Adams et al., 2008b) was employed in combination with the polymer emulsion. The used oil-based drilling mud was based on a synthetic oil. Chemicals were mixed vigorously into the used mud for 1 min; then, the mixtures were centrifuged for 10 min (2000 rpm) to evaluate their potential for separation in a field operation. Since the test substrate was a used drilling mud, the recovered oil phase (upper layers in Fig. 6.5) was quite dark due to dissolved organic material. However, the solid and water contents of the recovered oil in the best case were essentially nil. Doses are quoted on a product volume per drilling fluid volume basis.

There are several benefits to using this approach of hydrophilic polymer droplets as aggregating agents in oil-continuous media when compared to other chemical treatments that have been tried on used oil-based drilling fluids. Other approaches reported include the use of sodium silicates (Dawson, 1949), carboxylic acids (Van Slyke, 1992), organic solvents (Mondshine, 1977), neutralization plus dissolved flocculant (Malhis, 2003; Shiver, 1984), and surfactants (Duke, 1983; Ezell and Harvey, 2008; Hamill, 1992). Separation efficiencies reported for these methods tended to be less than we have achieved using a combination of surfactant and undissolved polymeric emulsion droplets. Also, there was very little residual from the treatment that ended up in the oil phase. The high-HLB surfactant and polymer droplets tended to go with the aqueous–solid mixture, and the low-HLB surfactant from the polymer emulsion formulation (present in small concentrations as emulsifier) tended to go with the oil phase. We believe that this approach of aggregating suspended particles in oil-continuous media using inverse polymeric emulsions would be applicable to solid-stabilized oil-continuous dispersions of the sort resulting from oil spills.

6.3.2 Separating Oilfield "Slops"

There are a host of other waste fluids that arise from oilfield operations that are oil–water–solid mixtures in which the solid concentrations are substantially less than in drilling muds yet separating the phases is made difficult by solids that stabilize oil–water interfaces. We'll refer to these complex mixtures simply as "slops," although there are a number of other common terms that reflect the problems they cause in oilfield operations. Dispersions of this sort range from oil-continuous to water-continuous and even bicontinuous compositions. Incomplete separations of these dispersions reduce the economic value of phases recovered and can create environmental problems. Figure 6.6 shows an optical micrograph of one such slop. The spherical droplets are water and the oil phase has been dyed red.

The presence of particles collecting at oil–water interfaces is readily apparent. These particles certainly interfere with droplet coalescence even when the water droplets are forced against one another. In the example that follows, the strategy described earlier using a combination of inverse polymeric emulsion and a high-HLB surfactant nearly simultaneously to improve oil separation had to be modified to account for the greater concentration of water and lesser concentration of solids in this particular slop fluid. A high-HLB surfactant similar to the one previously described (Adams et al., 2008a) was first mixed into the slop, followed by a quiescent period during which much of the water droplets coalesced and formed a retrievable phase that was removed. The residual dispersion was similar in composition and properties to the used drilling mud discussed earlier. This fluid was then chemically treated as mentioned earlier

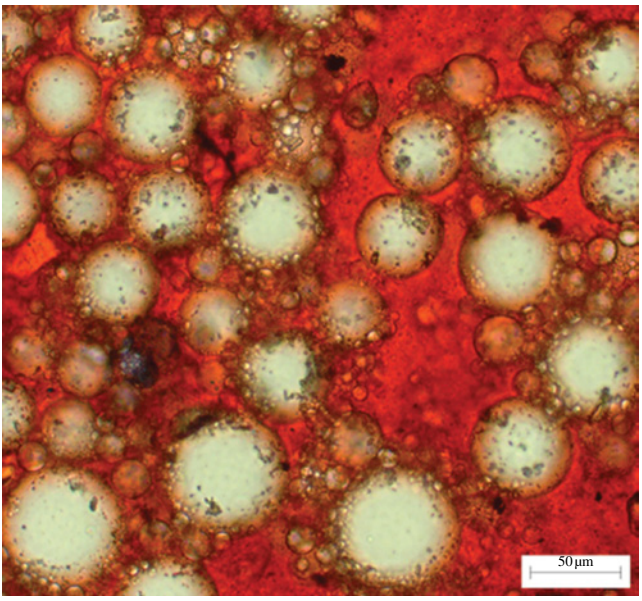

FIGURE 6.6 Optical micrograph of oil-continuous slop; scale bar is 50 µm. *See insert for color representation of the figure.*

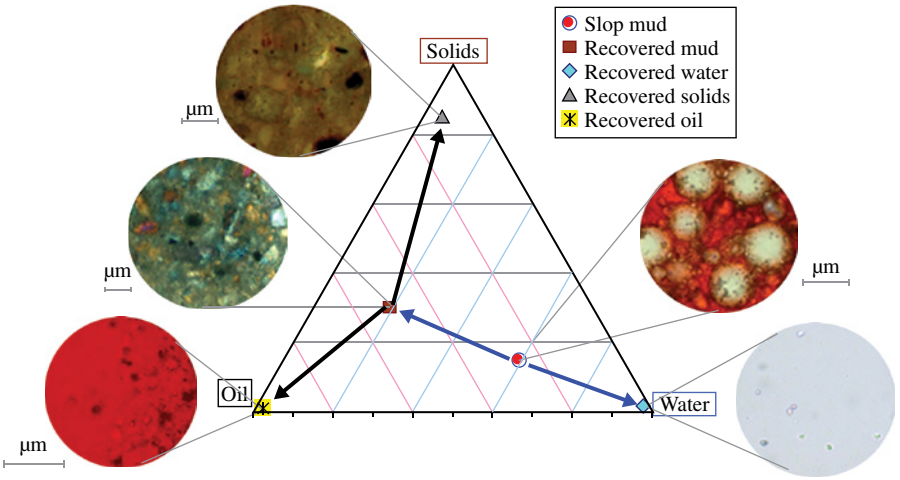

FIGURE 6.7 Two-stage slop mud separation. "Slop mud" is first treated with a high-HLB surfactant resulting in "recovered water" and "recovered mud." The "recovered mud" is then treated with an inverse polymeric emulsion and a high-HLB surfactant resulting in "recovered solids" and "recovered oil." Optical micrographs show the structure of each phase; scale bars are 50 μm. Oil phase was dyed red.

with good recovery of the oil phase. This double separation process is shown diagrammatically in Figure 6.7 as a trajectory on a ternary phase diagram. The starting composition (slop mud) is denoted by the red circle. Fluid compositions were determined using a retort ramped from room temperature to 900°F. Optical micrographs of the various phases are included to demonstrate the separation process.

This example highlights the importance of chemical treatment sequencing and mixing history on separation efficacy, in addition to the actual chemicals used. These principles are often useful in designing a scheme for separating complex mixtures. We expect that oilfield examples such as these can add to the knowledgebase drawn upon when having to remediate oil spills.

6.4 SUMMARY AND CONCLUSIONS

We have described several chemically enhanced methods used in mineral processing and oilfield waste management to separate oil from water when biwettable solids located at the oil–water interface severely retard their natural separation tendency. A judicious aggregation of the offending solid particulates in a manner that allows formation of an open network with sufficient permeability to permit drainage and recovery of the fluid phases from the original mixture is critical to success. The use of hydrophilic polymeric droplets for this purpose, even in congested dispersions, was demonstrated. Such an approach may be applicable in treating stable oil–water–solid dispersions resulting from crude oil spills. All that we might do as responsible scientists to develop understanding and technology to deal with oil spills once they occur is of course only secondary to preventing their occurrence in the first place.

DISCLAIMER

Cytec Industries Inc. in its own name and on behalf of its affiliated companies (collectively, "Cytec") decline any liability with respect to the use made by anyone of the information contained herein. The information contained herein represents Cytec's best knowledge thereon without constituting any express or implied guarantee or warranty of any kind (including, but not limited to, regarding the accuracy, the completeness or relevance of the data set out herein). Nothing contained herein shall be construed as conferring any license or right under any patent or other intellectual property rights of Cytec or of any third party. The information relating to the roducts is given for information purposes only. No guarantee or warranty is provided that the product and/or information is adapted for any specific use, performance or result and that product and/or information do not infringe any Cytec and/or third party intellectual property rights. The user should perform its own tests to determine the suitability for a particular purpose. The final choice of use of a product and/or information as well as the investigation of any possible violation of intellectual property rights of Cytec and/or third parties remains the sole responsibility of the user.

REFERENCES

Adams J, Masias H, Huang S-Y, Farinato R. Solid-liquid separation of oil-based muds. US patent 7,381,332 (B2). June 2008a.

Adams J, Masias H, Huang S-Y, Farinato R. Solid-liquid separation of oil-based muds. US patent 7,338,608 (B2). March 2008b.

Allen HL, Berry WW. Solvent extraction of metallic mineral values from acidic solutions. US patent 4,278,640A. July 1981.

Angle CW. Chemical demulsification of stable crude oil and bitumen emulsions in petroleum recovery – a review. In: Sjöblom J, editor. *Encyclopedic Handbook of Emulsion Technology*. Boca Raton, FL: CRC Press; 2001. p 541–594.

Angle CW, Dabros T, Hamza HA. Demulsifier effectiveness in treating heavy oil emulsion in the presence of fine sands in the production fluids. Energy Fuels 2007;21(2):912–919.

Aveyard R, Clint JH. Solid particles at liquid interfaces, including their effects on emulsion and foam stability. In: Mittal KL, Shah DO, editors. *Adsorption and Aggregation of Surfactants in Solution*. Surfactant Science Series 109. New York: Marcel Dekker; 2003. p 61–90.

Binks BP. Particles as surfactants – similarities and differences. Curr Opin Colloid Interf Sci 2002;7(1–2):21–41.

Darley HCH, Gray GR. *Composition and Properties of Drilling and Completion Fluids*. 5th ed. Woburn, MA: Butterworth-Heinemann; 1988, p 63.

Dawson RD. Reclamation of waste oil-base drilling fluid. US patent 2,476,846. July 1949.

Donaldson EC, Alam W. *Wettability*. Houston, TX: Gulf Publishing Company; 2008.

Dorlac JP, Sudderth RB. Crud removal system and method for solvent extraction. WO 2002/013939 (A1). February 2002.

Duke RB. Mineral acid demulsification of surfactant-containing emulsion. US patent 4,396,530. August 1983.

Evans HA, Hughes CA. Investigation of crud formation in solvent extraction. Australas Inst Min Metal 1995;8/95:30–34.

Ezell R, Harvey T. Separation and reuse of invert emulsion fluids. In: American Association of Drilling Engineers (AADE) Houston Chapter Fluids Technical Conference & Exhibition; Apr 9; AADE-08-DF-HO-33; 2008.

Fletcher AW, Gage RC. Dealing with a siliceous crud problem in solvent extraction. Hydrometallurgy 1985;15(1):5–9.

Gillaspie JD, Baughman DR, Gertenbach DD, Hazen WW, Owusu G, Wilmot JC. Silica removal from pregnant leach solutions. US patent 7,691,347 (B2). April 2010.

Goren MB. Process for absorbing solubilized silica from acidic aqueous media with an organic compound containing a poly(alkylene oxide) structure. US patent 3,266,888. August 1966.

Groh HJ. Removal of silica from solutions of nuclear fuels. DOE Report # DP-293. Washington, DC: United States Atomic Energy Commission. 1958.

Hamill J. Water wash/oil wash cyclonic column tank separation system. US patent 5,090,498. February 1992.

Hughes KC, Forsyth MT. Phase disengagement problems in solvent extraction. In: Value adding through solvent extraction, Papers presented at ISEC'96; 1996 Mar 19–23; Melbourne: University of Melbourne: Department of Chemical Engineering, 1996.

Hughes CA, Evans HA, Warren LJ. Investigation of the role of silica in the formation of cruds in a hydroxyoxime/sulfuric acid solvent extraction system. In: Value adding through solvent extraction, Papers presented at ISEC'96; 1996 Mar 19–23; Melbourne: University of Melbourne, Department of Chemical Engineering; 1996.

Ivan C, Browne N. Apparatus and method for recovering oil-based drilling mud. US 2008/0236896 (A1). October 2008.

Leal-Calderon F, Schmitt V. Solid-stabilized emulsions. Curr Opin Colloid Interf Sci 2008; 13(4):217–227.

Malhis S. Conversion of oil well drilling waste to fuel. US patent 6,689,925. February 2004.

Menon VB, Wasan DT. Characterization of oil–water interfaces containing finely divided solids with applications to the coalescence of water-in-oil emulsions: a review. Colloids Surf 1988;29(1),7–27.

Mondshine TC. Laundering of oil-base mud from cuttings. US patent 4,040,866. August 1977.

Mover BA, Mc Dowell WJ. Factors influencing phase disengagement rates in solvent extraction systems employing tertiary amine extractants. Separ Sci Technol 1981;16(9): 1261–1289.

Ning P, Cao H, Liu C, Li Y, Zhang Y. Characterization and prevention of interfacial crud produced during the extraction of vanadium and chromium by primary amine. Hydrometallurgy 2009;97(1–2):131–136.

Pickering SU. Emulsions. J Chem Soc Trans 1907;91:2001–2021.

Poindexter MK, Chuai S, Marble RA, Marsh SC. Solid content dominates emulsion stability predictions. Energy Fuels 2005;19(4):1346–1352.

Ritcey GM. Crud in solvent extraction processing – a review of causes and treatment. Hydrometallurgy 1980;5(2–3):97–107.

Ritcey GM. Development of industrial solvent extraction processes. In: Rydberg J, Cox M, Musikas C, Choppin GR, editors. *Solvent Extraction Principles and Practice*. New York: Marcel Dekker; 1992. p 277–337.

Shiver C. Continuous process for the reclamation of waste drilling fluids. US patent 4,482,459. November 1984.

Sjöblom J. Demulsifiers in the oil industry. In: Sjöblom J, editor. *Encyclopedic Handbook of Emulsion Technology*. Boca Raton, FL: CRC Press; 2001. p 595–620.

Sztukowski DM, Yarranton HW. Characterization and interfacial behavior of oil sands solids implicated in emulsion stability. J Dispers Sci Technol 2004;25(3):299–310.

Taghizadeh M, Ghasemzade R, Ghanadi Maragheh M, Ashrafizadeh SN. Crud formation in the solvent extraction system Zr (IV), HNO_3-D2EHPA. Miner Process Extract Metall Rev 2009;30(3):260–268.

Thompson DG, Taylor AS, Graham DE. Emulsification and demulsification related to crude oil production. Colloids Surf 1985;15:175–189.

Van Slyke DC. Separation of oils from solids. US patent 5,156,686. October 1992.

Wang C-Y. Formation and control of crud in SX-EW process. Kuangye (Beijing), 2001;10: 68–71.

Yan N, Gray MR, Masliyah JH. On water-in-oil emulsions stabilized by fine solids. Colloids Surf A 2001;193(1–3):97–107.

7

MULTIPRONGED APPROACH FOR OIL SPILL REMEDIATION

Partha Patra and Ponisseril Somasundaran

7.1 INTRODUCTION

Historically, millions of tons of oil have been accidentally spilled into oceans, and the remediation of the polluted areas poses unique scientific and technological challenges. Approaches used in the past in oil cleanup have employed booms, skimmers, dispersants, sorbents, etc. Booms and skimmers can be ineffective and unsafe in currents of more than 1 knot and waves exceeding 1.5 m (http://www.popularmechanics.com/science/energy/coal-oil-gas/state-of-oil-cleaning-tech). Thus, Extreme Spill Technology's "high speed" skimming vessel's mechanical cleanup technology tends to work only in placid waters. Furthermore, major limitations of some of these techniques are their high cost and inefficient trace level adsorption (http://www.epa.gov/oem/docs/oil/edu/oilspill_book/chap2.pdf; http://www.popularmechanics.com/science/energy/coal-oil-gas/state-of-oil-cleaning-tech; National Research Council, 1989; Schatzberg, 1971; Schatzberg and Jackson, 1972; The International Tanker Owner Pollution Federation Limited, 1980; Wardley-Smith, 1983).

Sorbents are of three basic categories: natural organic, natural inorganic, and synthetic types. Relatively inexpensive and readily available natural organic sorbents include peat moss, straw, hay, sawdust, ground corncobs, feathers, and other carbon-based products. Organic sorbents can typically absorb oil up to 3–15 times their weight. However, some organic sorbents tend to soak up water as well, causing them to sink. Organic sorbents such as sawdust pose difficulty in their collection after use. Synthetic sorbents include plastics, such as polyurethane, polyethylene, and nylon fibers. Most synthetic sorbents

Oil Spill Remediation: Colloid Chemistry-Based Principles and Solutions, First Edition.
Edited by Ponisseril Somasundaran, Partha Patra, Raymond S. Farinato, and Kyriakos Papadopoulos.

can absorb as much as 70 times their weight in oil, and a few can be reused (Chol, 1992). It is to be noted that since many of the oil types are biodegradable, it could be disposed of by composting, and in this regard, biodegradable material with excellent absorption properties would be advantageous (Johnson et al., 1973).

Dispersion of floating oil into the form of oil droplets is a more appropriate approach in high-wave seawater with currents more than 1 knot and waves exceeding 1 m. Such an approach however has its own limitations due to the toxicity of both the dispersant and oil on marine habitats and the stability of the dispersion. It is clear that nontoxic biodispersants are preferred over synthetic ones.

In this chapter, three different aspects are presented:

1. Scientific basis for the role of rugosity and fiber aspect ratio on oil recovery
2. Use of a hybrid approach that includes absorption of oil by hydrophobic nylon followed by froth flotation
3. Application of bacteria derived biosurfactants

7.2 MICROFIBROUS SORBENTS FOR OIL REMOVAL AND RECOVERY

Selection of sorbents is based on their hydrophobicity and oleophilicity. Their effectiveness is dependent on parameters defining retention of oil over time, recovery of oil from them, the amount of oil sorbed per unit weight of sorbent, and the reusability and biodegradability of the sorbent (Chol, 1992; http://www.epa.gov/oem/docs/oil/edu/oilspill_book/chap2.pdf; National Research Council, 1989; Schatzberg, 1971; Schatzberg and Jackson, 1972; The International Tanker Owner Pollution Federation Limited, 1980; Wardley-Smith, 1983). One way to categorize oil-sorbent materials is based on their origin: natural or synthetic. Natural sorbents can be considered as inorganic mineral products, organic synthetic products, or organic vegetable products. These natural sorbents are not as effective as oil absorbers, and some of these are poor in buoyancy (Halligan et al., 1976; Johnson et al., 1973; Melvold et al., 1988). Fibrous materials are preferred, mostly due to their high oil-absorbing capability. In this regard, the role of cotton has been explored (Choi and Moreau, 1993; Suni et al., 2004).

The important determining factors are fiber aspect ratios and rugosity. The mechanism of sorbing oil by fibers is via entrapment of oil in the three-dimensional networks formed by the entangled fiber structures. In this regard, nylon fibers are attractive as they are effective sorbent material for oil removal from sea surface. An additional benefit with nylon is that soaked oil can be squeezed for recovery of oil. Figure 7.1 shows a series of snapshots demonstrating entrapment and recovery of oil using nylon fibers. One-centimeter-long (15–20 μm thickness) nylon fibers were used, which resulted in nearly complete removal of oil. In addition, 90% of the removed oil could subsequently be recovered as filtered fluid. In the tests reported here, nylon fibers were subjected to size reductions from 1 cm to 700–900 μm. Clusters/aggregates made up of relatively smaller fibers (~700–900 μm) showed much better recovery of oil. Interestingly, the absorption efficiency of the smaller (700–900 μm) nylon fiber-based clusters was increased by 30–40% compared to longer (1 cm) fibers.

In order to determine the role of surface rugosity on oil recovery, tests were done with fibers with surface roughness altered by various techniques. In one of

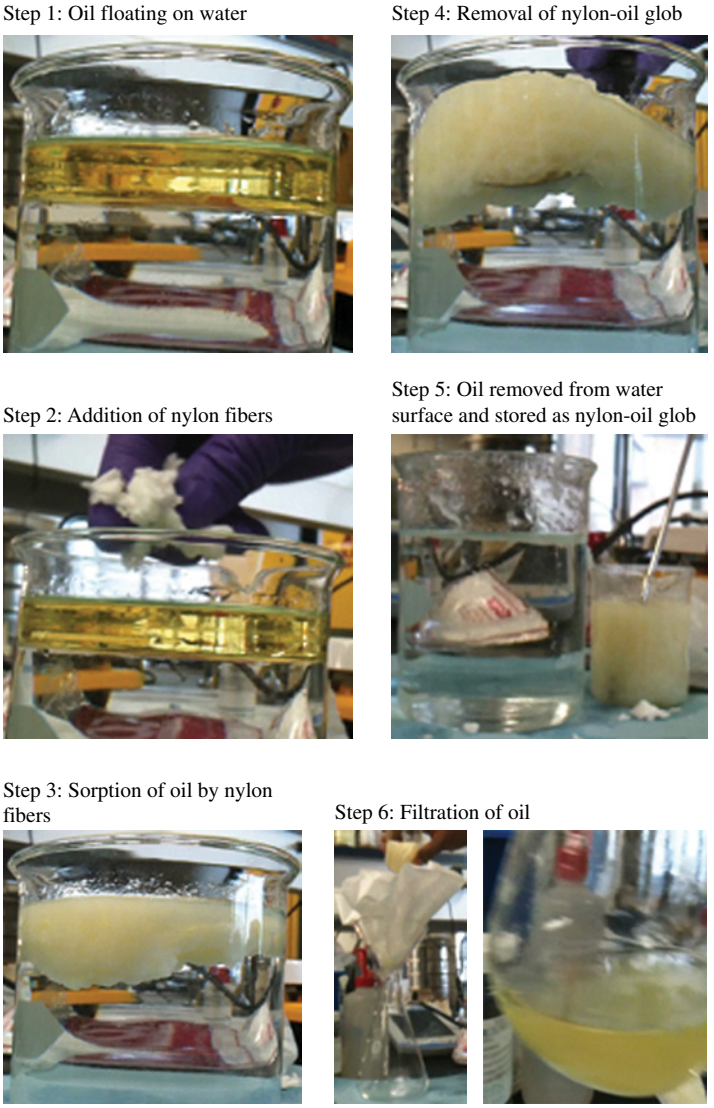

FIGURE 7.1 Snapshots of a demonstration of oil removal and recovery from water surface using nylon microfibers.

the techniques, fibers were impacted with mineral particles during grinding in a rod mill with a copper ore. It can be observed from Figure 7.2 that beating with minerals made the nylon surface relatively less smooth. Interestingly, the oil recovery improved by 10–15% as compared to 1 cm fibers. This indicated that besides the entrapment of oil in the nylon fiber interstices, other factors such as pore size owing to reduction in fiber aspect ratios of the nylon fiber network and surface rugosity play an important role in oil removal.

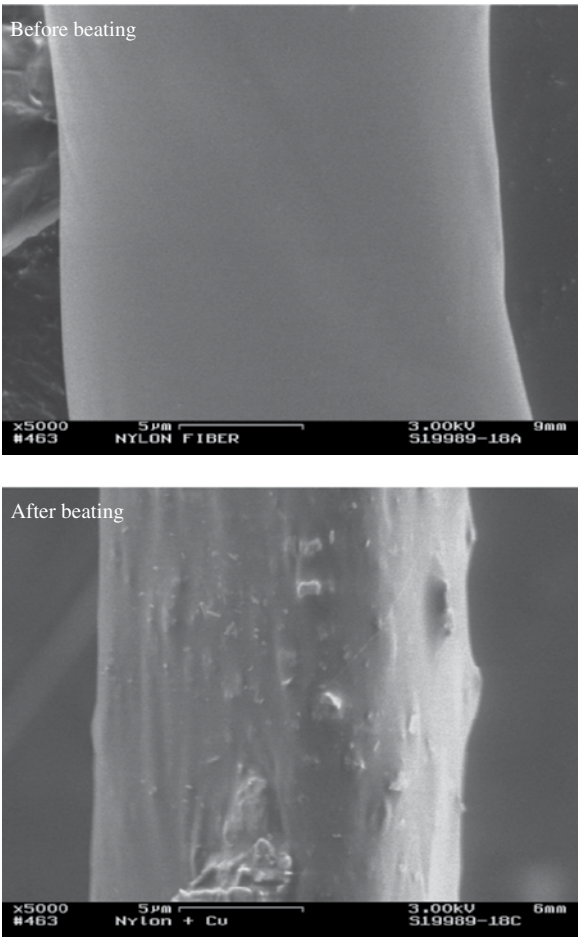

FIGURE 7.2 Surface of nylon fiber before and after beating with copper ore in rod mill.

7.3 OIL REMOVAL USING FROTH FLOTATION TECHNIQUE

Froth flotation is possibly the most widely used technique for mineral separation. Using this technique, desired minerals are separated from others by rendering the surface of one or more of the desired minerals selectively hydrophobic.

Subsequently, hydrophobic minerals attach to the air bubbles, rise to the surface, and form a froth. However, a major hurdle often encountered is that undesired gangue minerals report to the froth phase. There are various ways gangue minerals report to the froth phase, such as entrainment and floc flotation. Among these ways, it was recently found that transport of any fibrous gangue network by bubble flux can take place in flotation. Fibrous particles entangle in suspension and form a large network

with a pore size much smaller than the bubble sizes. This mechanism can be applied for recovery of oil droplets, where oil droplets can be trapped in the intricate mesh of the fibrous network.

Oil is dispersed along the various depths of the sea and results in the formation of submicron-sized oil droplets. Though there are various reagent-based methods to deal with the dispersed oil, a relatively greener approach would be to develop a reagent-less "greener" technique. In this regard, our approach includes the usage of the nylon fiber network that is used to sweep across the depth of seawater and scavenge micron-sized oil droplets. In our experiments, nylon fibers were suspended in water, followed by purging of the air at the bottom of the suspension. It was observed that most of the nylon fibers were removed from the suspension by the bubble flux to the top. A series of snapshots that illustrates the transport of a nylon fiber network by bubble flux from the suspension to the surface of a suspension is shown in Figure 7.3 (Patra et al., 2012). This experiment did not include oil in the suspension. However, as explained earlier, the aggregate-based network of nylon fiber can entrap oil (Fig. 7.4). An optical microscopy picture of the fibers at the end of the experiment (demonstration, Fig. 7.3) was taken using a stereomicroscope (Fig. 7.4). It was observed that the fibers from clusters entrapped water inside in its voids. The fibers entangle in suspension as floc-like structures with pore sizes as small as 20–30 μm. Such pore-size networks are ideal for entrapment of oil similarly to other sorbents.

7.4 USE OF GREENER BIO DISPERSANTS

Greener surfactants derived from bacteria are used for applications in food industries, pharmaceuticals, personal and home care, and many other sectors. The majority of the surfactants used today are petroleum based, and their toxicity impact is of considerable concern. Besides the toxicity impact, the synthesizing routes of surfactants can contribute to an increase in the carbon footprint and the emission of greenhouse gases. The development of environmentally benign reagents and processes requires surfactants that are biocompatible, biodegradable, nontoxic, and, most importantly, produced by a greener route.

Potential biosurfactants include hydroxylated and cross-linked fatty acids, glycolipids, polysaccharide–lipid complexes, lipoproteins–lipopeptides, phospholipids, and even the complete cell surface itself. The following are some of the common biosurfactants (Van Dyke et al., 1991).

7.4.1 Emulsan

Emulsan (Fig. 7.5) is an anionic polysaccharide produced by the gram-negative bacterium *Acinetobacter calcoaceticus* strain RAG-1 from a variety of hydrocarbon feed sources including crude oil. Emulsan causes little reduction in surface tension at an oil–water interface (10 dynes/cm) but binds tightly to oil surfaces and protects oil droplets from coalescence (Hong et al., 2002; Schippers et al., 2000).

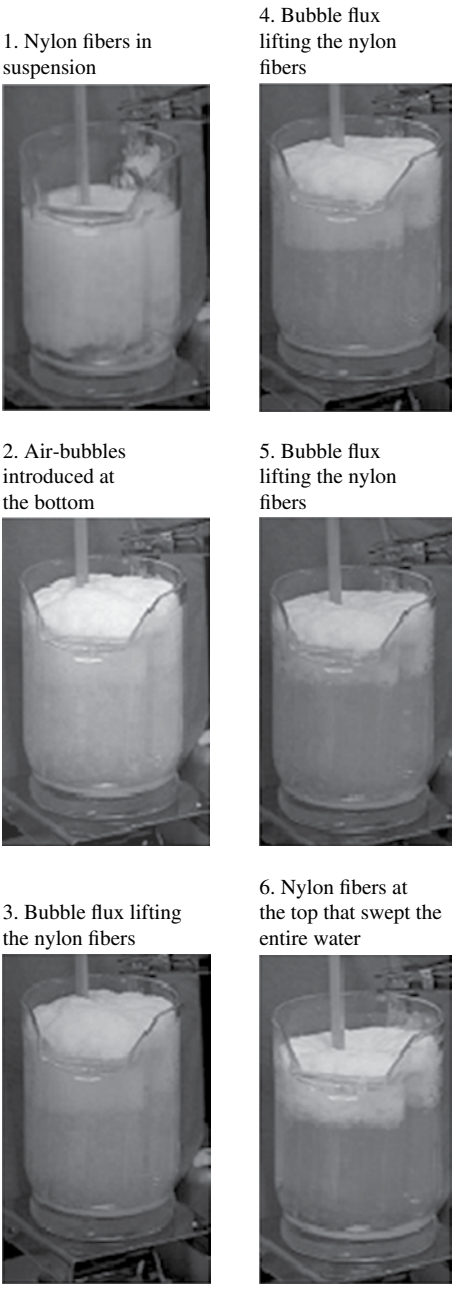

FIGURE 7.3 Snapshots of demonstration of nylon fiber network sweeping the entire volume of water.

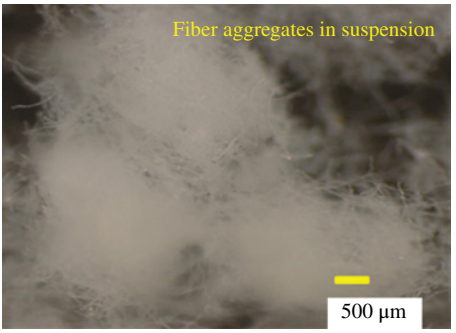

FIGURE 7.4 Network of nylon fibers.

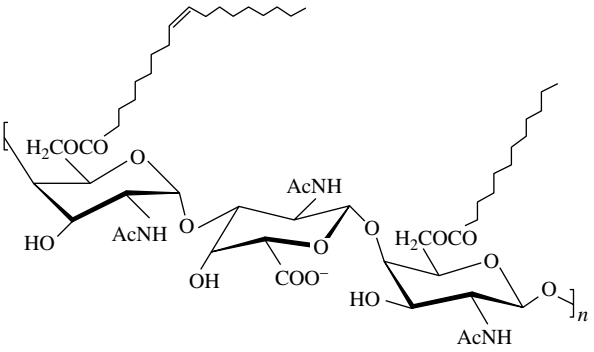

FIGURE 7.5 Structure of emulsan.

7.4.2 Sophorolipids

Sophorolipids (Fig. 7.6) are extracellular glycolipids produced mainly by the *Candida bombicola* species during their stationary phase. There has been a considerable amount of interest in the physiology of sophorolipid biosynthesis by yeast strains of the Candida genus. It is very likely that the physiological role of sophorolipid production is related to the regulation of energy metabolism (Garti, 1999; Kitamoto et al., 1993; Royal et al., 2003; Uchida et al., 1989).

7.4.3 Rhamnolipids

Rhamnolipids, in which one or two molecules of rhamnose are linked to one or two molecules of β-hydroxydecanoic acid, are a family of microbial glycolipids that have thus far received the most attention. *Pseudomonas aeruginosa* produces rhamnolipids in two forms: L-rhamnosyl-L-rhamnosyl-β-hydroxydecanoyl-β-hydroxydecanoate and L-rhamnosyl-β-hydroxydecanoyl-β-hydroxydecanoate (Fig. 7.7). Fermentative production of rhamnolipids having one β-hydroxydecanoic acid with one or two rhamnose lipids, methyl ester derivatives, and rhamnolipids with alternative fatty acid chains has also been reported. Several types of rhamnolipids produced by *P. aeruginosa* have been characterized (Healy et al., 1996; Mager et al., 1986).

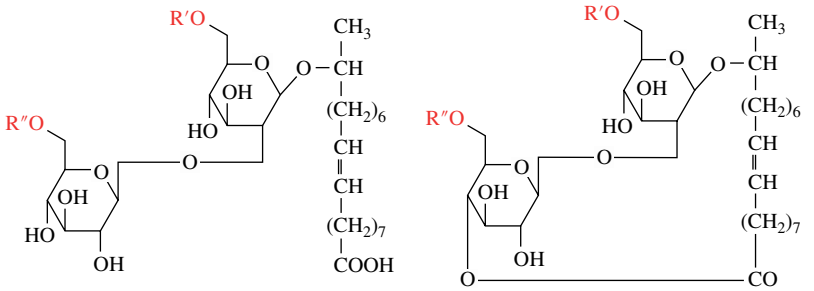

5. R′ = R″ = Ac or H
6. R′ = Ac; R″ = H
7. R′ = H; R″ = Ac
8. R′ = R″ = H

1. R′ = R″ = Ac or H
2. R′ = Ac; R″ = H
3. R′ = H; R″ = Ac
4. R′ = R″ = H

FIGURE 7.6 Natural sophorolipids are composed of a mixture that contains the lactonic and ring-opened forms, as well as various degrees of acetylation at the primary positions.

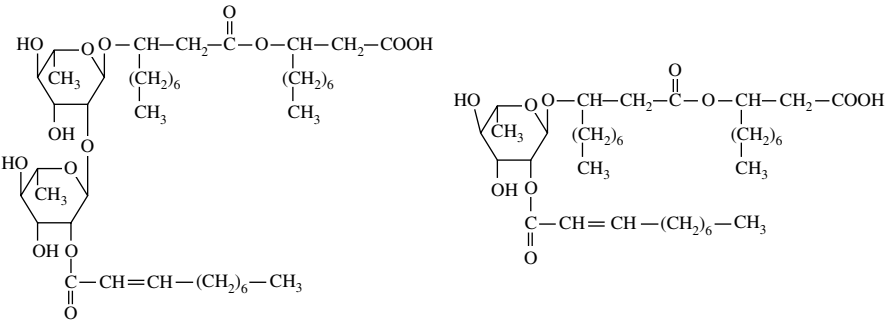

FIGURE 7.7 Structure of rhamnolipid from *P. aeruginosa*.

7.5 LIPOPEPTIDE: *BACILLUS SUBTILIS* BIOSURFACTANTS AND LIPOPEPTIDES

Modular Genetics, Inc. (Modular), has developed an automated system for designing and generating modified microorganisms of *Bacillus subtilis* strains. Those modifications can include anything from changing a single base pair to deleting large regions of the chromosome or building large sets of "heterologous genes." This technology is used to produce engineered strains that synthesize novel lipopeptides.

Each of these lipopeptides is a variant of the naturally occurring molecule surfactin, which is known to act as a powerful surfactant and oil dispersant (Gutnick et al., 1991). Surfactin is synthesized by a peptide-synthetase enzyme. The three genes that encode these three synthetase subunits are shown in Figure 7.8. The integration of computer design tools with robotic manipulation enables the use of cellular and molecular biology to produce new chemicals and materials. The lipopeptide is highly water soluble and has excellent biophysical properties that are important for its effective use (such as a low critical micelle concentration (CMC), 1.3 mM).

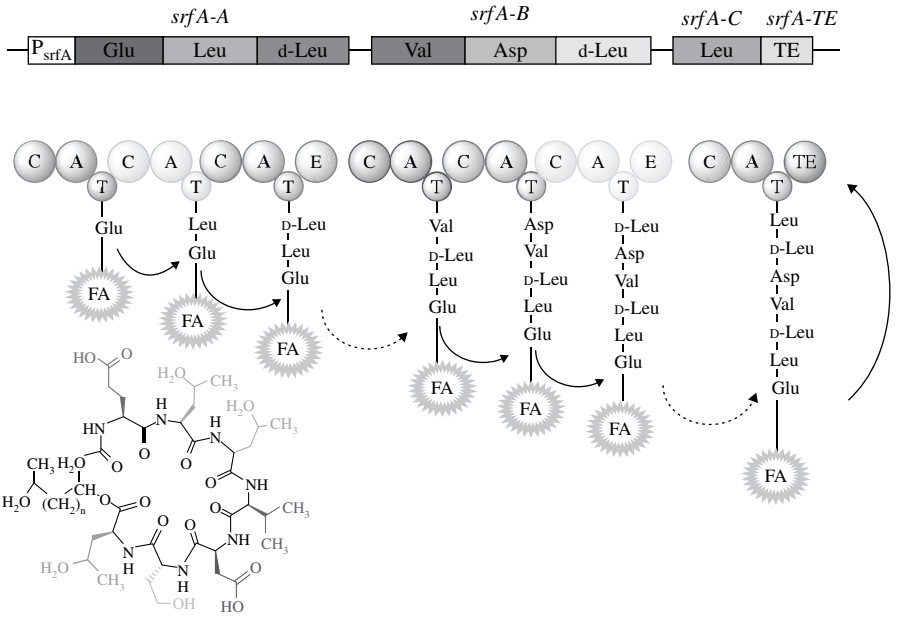

FIGURE 7.8 Surfactin is a lipopeptide that is produced naturally by *B. subtilis*. It is composed of a fatty acid chain that is 12–17 carbons in length and a seven-amino-acid cyclic peptide.

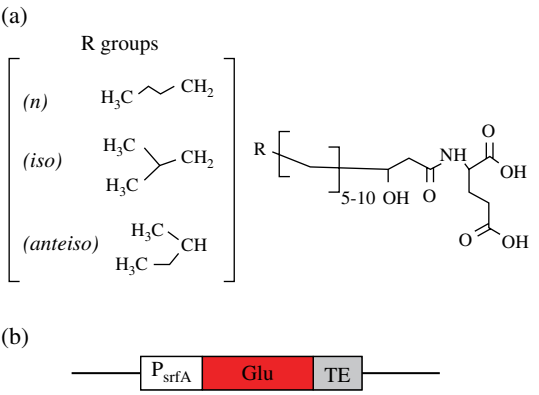

FIGURE 7.9 Modular's acyl amino acid: (**a**) chemical structure of the acyl amino acid with glutamate attached to a lipid moiety and (**b**) modular structure of the modified surfactin synthetase operon.

It is well established that surfactin is an effective oil dispersant (Gutnick and Shabtai, 1987). Figure 7.9 and Figure 7.10 show a few of the novel lipopeptides that have been generated using modified automated, microbial strain. In this particular case, all of the variant molecules have amino acid substitutions at position 2 of the amino acid component of surfactin. By testing this set of compounds, along with sets

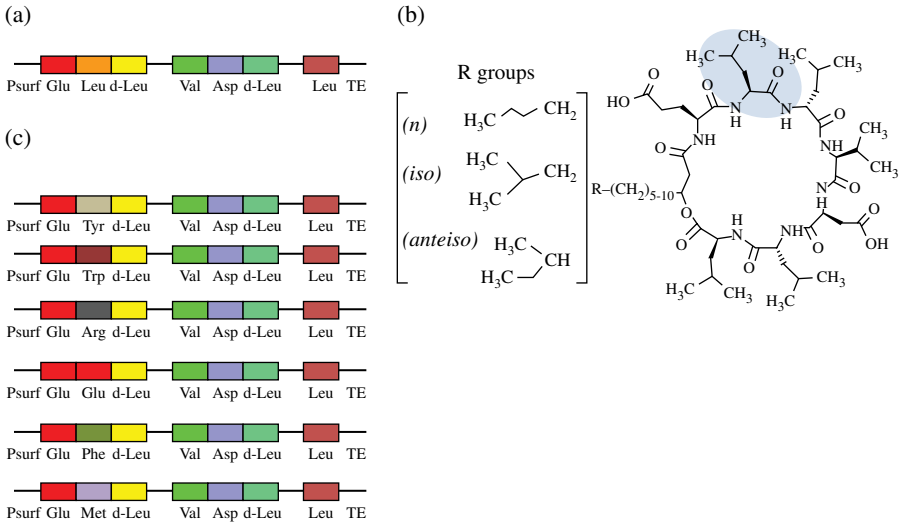

FIGURE 7.10 (**a**) Wild-type surfactin synthetase operon. (**b**) Chemical structure of wild-type surfactin. (**c**) Six of the surfactin analogs in Modular's collection have substitutions at position 2 of the cyclic amino acid. *(See insert for color representation of the figure.)*

of compounds with specific amino acid substitutions at other positions, it is expected to identify amino acid positions (and particular amino acids at those positions) that are critical for it to function as a biodispersant.

7.6 STRUCTURE–PROPERTY RELATIONSHIPS OF BIOSURFACTANTS

7.6.1 Interfacial Properties of Sophorolipids

Research with biosurfactants has led to a good understanding of the relationship between the alkyl ester chain length attached to the carboxyl of the sophorolipid lipid moiety and their interfacial properties (Fig. 7.11). The *n*-alkyl chain length variation investigated includes C1, C2, C3, C4, and C6. Relatively high activity of butyl and hexyl reagents can be observed from Figure 7.11. Critical micelle concentration and minimum surface tension exhibited a normal inverse relationship with the alkyl ester chain length; and, as usual, the CMC decreased to 1/2 per additional CH_2 group for the methyl, ethyl, and propyl series of chain lengths.

The surface tension results have been corroborated by fluorescence experiments. It can be seen from Figure 7.12 that all the esters are capable of forming hydrophobic domains (higher I3/I1), which have the potential to solubilize oleophilic materials.

Adsorption of sophorolipid alkyl esters on hydrophilic solids was studied in order to determine the extent of lateral association in the adsorbed film. During the investigation of the surface activity of these compounds, surprisingly, the

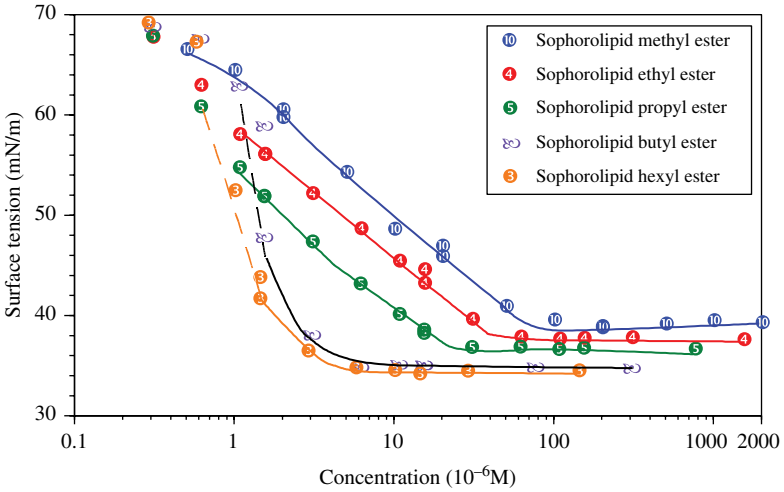

FIGURE 7.11 Surface tension of esters of sophorolipids. Reproduced with permission from Somasundaran et al. (2004). © Elsevier. *(See insert for color representation of the figure.)*

adsorption of these surfactants was found to be better on alumina than on silica (Fig. 7.13). In addition, it was also observed from Figure 7.13 that an increase in the *n*-alkyl ester chain length of the sophorolipids makes it more surface active and causes a shift of the adsorption isotherms to lower concentrations with the magnitude of the shift corresponding to the change in CMC of these surfactants.

This selective adsorption behavior on hydrophilic solids is similar to that of sugar-based nonionic surfactants. Interestingly, it does not bear any similarity to that of nonionic ethoxylated surfactants. While the mechanism of adsorption on solids is not understood, it has been proposed that hydrogen bonding is the primary driving force for adsorption of the sophorolipids on alumina.

7.6.2 Role of FA-Glu and Surfactin in Oil Dispersion

The CMC of both FA-Glu and surfactin were determined to obtain insight into the potential of these molecules for oil dispersion. It was observed that the CMC values of FA-Glu and surfactin were 0.01 and 0.02 g/l, respectively. These values are comparable to some of the commercially available surfactants and enzymes used for oil dispersion today.

7.7 SUMMARY AND CONCLUSIONS

Technologically, numerous options exist that are relatively safer and are on the laboratory scale with regard to addressing various scientific needs for oil spill remediation. In this chapter, three potential approaches for oil spill remediation are presented in the laboratory scale, including:

1. Suitable berms for removal of oil from the floating surface—smaller and rough-surfaced nylon fibers are more effective than longer and smoother nylon fibers.

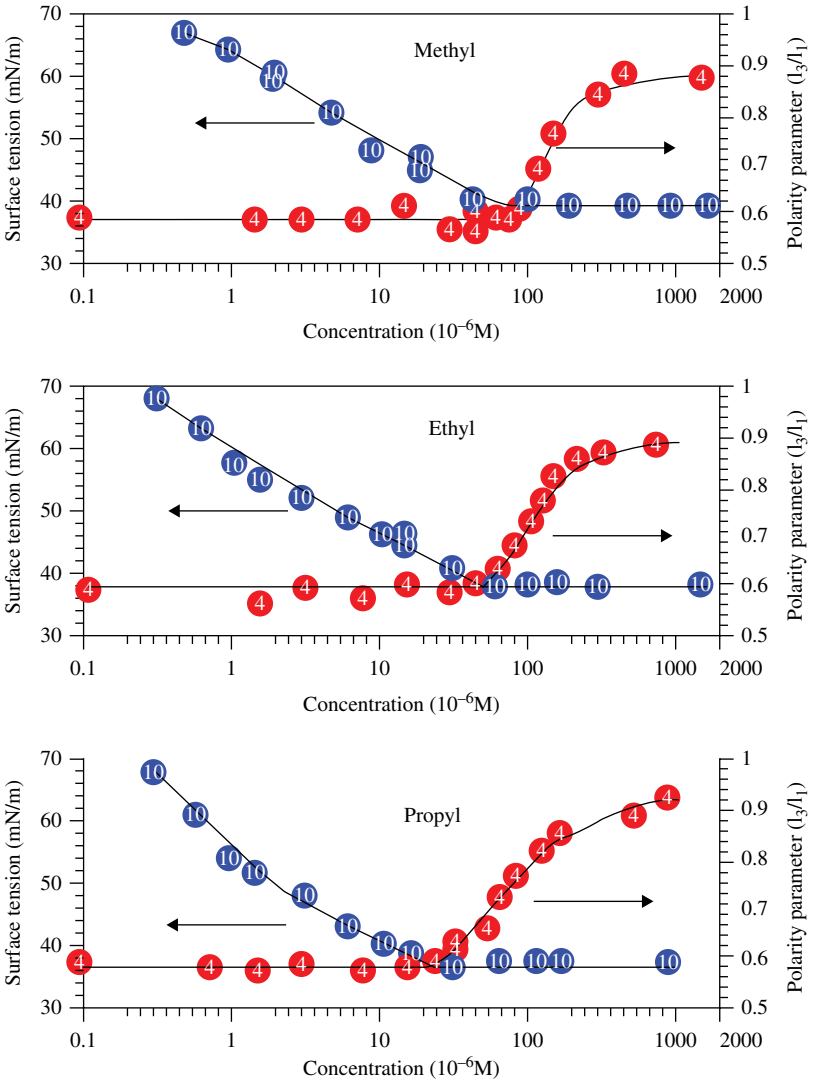

FIGURE 7.12 Surface tension and polarity parameters of sophorolipid methyl, ethyl, and propyl esters in solutions. Reproduced with permission from Somasundaran et al. (2004). © Elsevier. *(See insert for color representation of the figure.)*

2. Oil droplets dispersed in the sea can be trapped in nylon fiber networks followed by removal using flotation technique as similar to a technique used in mineral separation.
3. Usage of microbially and plant-derived reagents for oil dispersion such as rhamnolipids, surfactin, FA-Glu, sophorolipids, and emulsans.

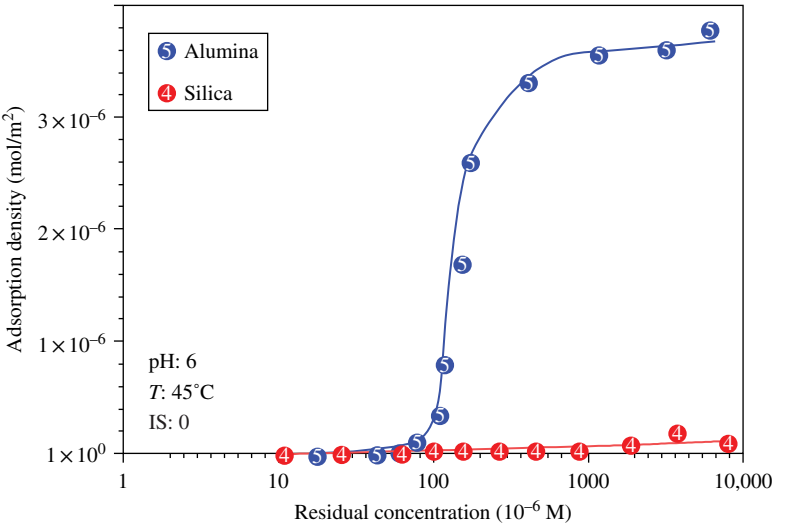

FIGURE 7.13 Adsorption isotherms of sophorolipid methyl ester on alumina and silica. Reproduced with permission from Somasundaran et al. (2004). © Elsevier. *(See insert for color representation of the figure.)*

Transformations of these techniques from laboratory scale are associated with benefits as well as limitations. Benefits include biodegradability of bioreagents that are also relatively nontoxic compared to synthetic ones. Limitations lie in the cost associated with regard to the cost of material and, in particular with the bio-based reagent, the complicated routes that are adopted to purify them. However, with advances in the colloid and science in industries and especially with rapid progress in the development of state-of-the-art synthetic biology protocols in purification strategies, it is envisaged here that in the future a multipronged approach as outlined in this chapter will be adopted towards oil spill remediation.

ACKNOWLEDGMENTS

The authors acknowledge the support of the National Science Foundation, researchers, and industrial members of the IUCRC.

REFERENCES

Choi H-M, Moreau JP. Oil sorption behavior of various sorbents studied by sorption capacity measurement and environmental scanning electron microscopy. Microsc Res Techniq 1993; 25(5–6):447–455.

Chol H-M. Natural sorbents in oil spill cleanup. Environ Sci Technol 1992;26(4):772–776.

Garti N. What can nature offer from an emulsifier point of view: trends and progress? Colloids Surf A: Physicochem Eng Asp 1999;152(1–2):125–146.

Gutnick DL, Shabtai Y. Exopolysaccharide bioemulsifiers. In: Kosaric N, Cairns WL, Gray NCC, editors. *Biosurfactants and Biotechnology*. Surfactant Science Series 25. New York: Marcel Dekker, Inc.; 1987. p 211.

Gutnick DL, Allon R, Levy C, Petter R, Minas W. Applications of *Acinetobacter* as an industrial microorganism. In: Towner KJ, Bergogne-Berezin E, Fewson CA, editors. *The Biology of Acinetobacter*. New York: Plenum Press; 1991. p 411–441.

Halligan JE, Ball AA, Meenaghan GF. U.S. Coast Guard Report No. CG-D-63-76. Washington, DC: U.S. Coast Guard Headquarters; 1976.

Healy MG, Devine CM, Murphy R. Microbial production of biosurfactants. Resourc Conserv Recycl 1996;18(1–4):41–57.

Hong K-J, Tokunaga S, Kajiuchi T. Evaluation of remediation process with plant-derived biosurfactant for recovery of heavy metals from contaminated soils. Chemosphere 2002;49(4):379–387.

Johnson RF, Manjrekar TG, Halligan JE. Removal of oil from water surfaces by sorption on structured fibers. Environ Sci Technol 1973;7(5):439–443.

Kitamoto D, Yanagishita H, Shinbo T, Nakane T, Nakahara T, Kamisawa C. Surface active properties and antimicrobial activities of mannnosylerythritol lipids as biosurfactants produced by *Candida antarctica*. J Biotechnol 1993;29(1–2):91–96.

Mager H, Roetlisberger R, Wagner F, to Wella Aktiengesellschaft. European Patent 0 209 783. 1/1987.

Melvold RW, Gibson SC, Scarberry R. *Sorbents for Liquid Hazardous Substance Cleanup and Control*. Park Ridge, NJ: Noyes Data Corporation; 1988.

National Research Council (NRC). *Using Oil Spill Dispersants on the Sea*. Washington, DC: National Academy Press; 1989. p 265–306.

Patra P, Bhambhani T, Vasudevan M, Nagaraj DR, Somasundaran P. Transport of fibrous gangue mineral networks to froth by bubbles in flotation separation. Int J Miner Process 2012;104–105:45–48.

Royal CL, Preston DR, Sekelsky AM, Shreve GS. Reductive dechlorination of polychlorinated biphenyls in landfill leachate. Int Biodeter Biodegr 2003;51(1):61–66.

Schatzberg P. U.S. Coast Guard Report No. 724110.1/2/1. Washington, DC: U.S. Coast Guard Headquarters; 1971.

Schatzberg P, Jackson DF. U.S. Coast Guard Report No. 734209.9. Washington, DC: U.S. Coast Guard Headquarters; 1972.

Schippers C, Geßner K, Muller T, Scheper T. Microbial degradation of phenanthrene by addition of a sophorolipid mixture. J Biotechnol 2000;83(3):189–198.

Suni S, Kosunen AL, Hautala M, Pasila A, Romantschuk M. Use of a by-product of peat excavation, cotton grass fibre, as a sorbent for oil-spills. Mar Pollut Bull 2004;49(11–12):916–921.

The International Tanker Owner Pollution Federation Limited. *Measures to Combat Oil Pollution*. London: Graham & Trotman Limited.

Uchida Y, Misava S, Nakahara T, Tabuchi T. Factors affecting the production of succinoltrehalose lipids by *Rhodococcus erythropolis* SD-74 grown on *n*-alkanes. Agric Biol Chem 1989; 53:765–769.

Van Dyke MI, Lee H, Trevors JT. Applications of microbial surfactants. Biotech Adv 1991;9(2): 241–252.

Wardley-Smith J. *The Control of Oil Pollution*. London: Graham & Trotman Publication.

Zhang L, Somasundaran P, Singh SK, Felse AP, Gross R (2004) Synthesis and interfacial properties of sophorolipid derivatives. Colloid Surf A-Physicochem Eng Asp 240:75–82.

8

PACKED-BED CAPILLARY MICROSCOPY ON BP-OIL-SPILL OIL IN POROUS MEDIA

Peixi Zhu, Qing Wang, Yuly A. Jaimes-Lizcano, and Kyriakos Papadopoulos

8.1 INTRODUCTION

While there may be varying findings and opinions on the fate of the oil spill's oil in the bulk waters of the Gulf of Mexico, a good part of oil that entered porous media, that is, beach sands, wetland soils, and marine sediments, is still there (Tansel et al., 2011; Voosen, 2011). More importantly, judging from the experience of previous oil spills (Table 8.1), the oil trapped in porous media can persist for years or even decades (Guterman, 2009; Peacock et al., 2005; Sale et al., 1989; Short et al., 2004, 2007). The oil in bulk water is subjected to fluid flows that bring it to the sea's surface where it weathers by evaporation and where it may be contained by boons and skimmed by cleanup crews. Fluid flows, and perhaps dispersants, also break the bulk-water oil into small drops that migrate away from a spill's oil source, thus diluting its presence in a given area, while at the same time increase significantly the interfacial area that becomes available for oil-eating bacteria to access it. On the other hand, the oil that is trapped in porous media, as depicted in Figure 8.1, is "protected" from fluid flows and shares a large interface with the granular solid substrate of the porous medium, which makes it difficult to be mobilized. While over time light components, for example, *n*-alkanes, may be degraded in oxygen-rich pores (Frysinger et al., 2003), heavy compounds tend to remain, which further compounds the oil's immobility. It has been reported that oil

Oil Spill Remediation: Colloid Chemistry-Based Principles and Solutions, First Edition.
Edited by Ponisseril Somasundaran, Partha Patra, Raymond S. Farinato, and Kyriakos Papadopoulos.

TABLE 8.1 Historical oil spill with oil persisting for 5 years or longer[a]

Name of vessel	Date of spill	Location	Type of coastline	Type of oil	Size of spill (l)	What is left
Florida	09/1969	Buzzards Bay, MA	Salt marsh	No. 2 fuel oil	0.7 million	After 30 years, TPH values are similar to values observed in mid 1970s. Only *n*-alkanes completely degraded
Arrow	02/1970	Chedabucto Bay	Beach with sand and cobbles	Bunker C	2 million	After 22 years, *n*-alkanes were mostly lost, and target PAHs were degraded
Metula	08/1974	Strait of Magellan, Chile	Marsh and beach	Light Arabian crude	52 million	After 24 years, lightly weathered oil in one marsh and heavily weathered in one marsh and one beach, with most compounds including biomarkers showing some degradation
Bouchard	10/1974	Buzzards Bay, MA	Salt marsh	No. 2 fuel oil	42,000–140,000	After 30 years, partially weathered diesel fuel remains with moderate biodegradation

Amoco Cadiz	03/1978	Ile Grande Salt Marsh, North Coast of Brittany, France	Salt marsh, rocky and sandy beaches	Crude Iranian and Arabian Light	223 million	After 13 years, hydrocarbon levels were generally low, with localized areas of highly weathered oil in the marsh
Ruptured storage tank	04/1986	East Coast of Panama, near Galeta	Mangroves, seagrasses, and coral reefs	Medium-weight crude oil	12–16 million	Exposed oil weathered rapidly, while oil protected under sediments retained most compounds after 5 years
Exxon Valdez	03/1989	Prince William Sound, Alaska	Wide variety of beaches	Alaskan North Slope crude oil	42 million	Boulders and cobbles continue to protect oil in the intertidal zone, inhibiting disturbance and weathering

[a]Reproduced from Peacock et al. (2005) with permission of Taylor & Francis.

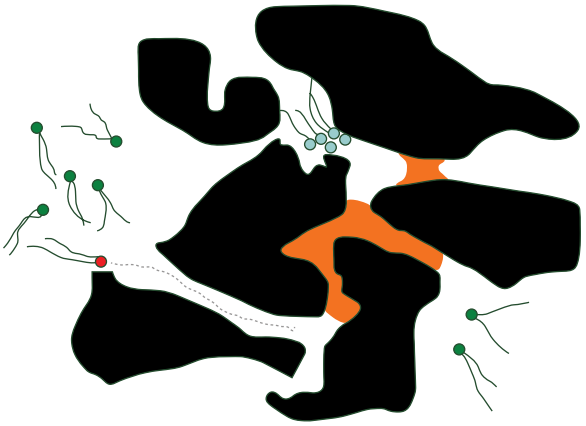

FIGURE 8.1 Schematic of trapped oil (orange) in porous media (black). *(See insert for color representation of the figure.)*

can persist longer in sheltered salt marsh areas (Baker, 1999), due to the temperate and anoxic nature of marsh subsurface. Considering the large dimensions of such a sensitive ecosystem that exists in Louisiana's coastal region, the cleaning is a difficult task.

The long-term-persisting oil trapped in sediments can be physically mobilized in the presence of flow, which can be created by water precipitation, flow of ground water, tides, waves, etc. Depending on the nature of a certain geological sediment, mobilization of persisted oil can either facilitate the cleanup or further contaminate the ecosystem. For example, groundwater can be polluted by the soluble components of the oil. On the other hand, persisting oil can be degraded if transported to an oxygen-rich or a nutrient-rich environment where oil-eating bacteria can have their access. Flow conditions in geological sediments vary widely depending on the physical force of the flow and porous-media permeability. For swash upon breakup of sea waves and entering beach subsurface, water velocity is generally the order of 10^{-1} to 1 m/s (Steenhauer et al., 2011), while for groundwater, it can be as low as 1 m per day or even per year. In addition, sediments in some geological conditions can be mixtures of different types of soils. For example, in a silty sand environment, the pore space between sand grains can be filled by silt grains, the sizes of which are a few microns to tens of microns. The transport of oil and water in a single pore that is filled with even smaller particles is apparently different from macroscale porous media, for example, low porosity, low permeability, and short oil travel distance (Fig. 8.2). When being carried by aqueous flow, oil phase behaves as a nonwetting phase. Understanding transport of nonwetting phase in geological porous media from macroscale to pore scale is essential in predicting oil fate in subsurface sediments.

Addressing some key phenomena affecting oil trapped in porous media, in this chapter, the following issues will be addressed: (i) up-to-date experimental visualization and study of nonwetting phase transport in the presence of water or aqueous solution, including microcapillary packed bed and other larger-scale porous-media models, and (ii) direct visualization of bacterial transport through porous media

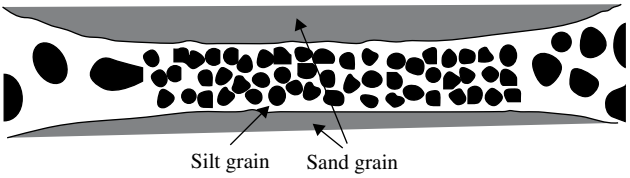

FIGURE 8.2 A schematic of pore-scale packed bed composed of silt grains (black) between sand grain (grey) pores. The size of silt grains is tens of microns, while sand grain pores are about 100 μm. Reproduced with permission from Papadopoulos et al. (2012). © American Physical Society.

achieved from different methods, including three-dimensional (3-D) tracking microscopy (Berg and Brown, 1972), confocal microscopy (Chen and Jin, 2011), and packed-bed-capillary video microscopy.

The main methodology, known as microcapillary video microscopy, was developed and has been intensively used in Papadopoulos' lab since the early 1990s. It has been utilized to study interfacial phenomena (e.g., coalescence in single and double emulsions, mass transport in dispersed systems, interfacial reaction and crystallization). The premise of the technique is that conducting optical–fluorescent microscopy inside narrow capillaries provides micromanipulation of observed microscopic objects to extents that are not possible without steric restriction such as that imposed by the capillary's geometry. The reason is a simple one: observable objects with dimensions comparable to a host capillary's diameter are stripped of two degrees of freedom in their movement, while the third degree can be manipulated by flow and the movement of microneedles. Phenomena that have been studied include (i) bacterial motility and *chemotaxis* in the confined space of a cylindrical channel (Liu and Papadopoulos, 1995, 1996; Liu et al., 1997); (ii) electrokinetic transport of solid particles (Kuo and Papadopoulos, 1996) and motile bacteria (Liu et al., 1999); (iii) drop–drop coalescence and drop–solid particle aggregation (Deshiikan and Papadopoulos, 1995a, b, 1997); (iv) double-emulsion stability, swelling, and transport (Cheng et al., 2007; Hou and Papadopoulos, 1996, 1997; Lawson and Papadopoulos, 2004; Rojas et al., 2006; Villa et al., 2003; Wang et al., 2010; Wen and Papadopoulos 2000a, b, 2001); and (v) the interfacial neutralization of acids by "overbased" lubricants in marine engines (Fu et al., 2005, 2006a, b, 2007; Wu et al., 1999, 2000a, b). Precise high-temperature manipulation was also achieved by coating the capillary outer surface with a thin indium tin oxide (ITO) (Fu et al., 2005). Once placed vertically, such device could also be used for study of droplet reaction/dissolution in levitating flow (Garcia-Bermudes et al., 2011).

8.2 WATER–OIL TWO-PHASE TRANSPORT IN POROUS MEDIA

For immiscible two-phase transport in porous media, when one of the phases is water, usually the wetting phase is the aqueous fluid, while the nonwetting phase is oil or air. For an oil–air system, air is usually the nonwetting phase and oil is the wetting phase. Here, the terms wetting and nonwetting referred to the wettability of

the porous material. When fluid of one phase initially occupying the pore is squeezed out by another immiscible phase, the process is termed displacement. If the invading fluid is a nonwetting phase, then it is called drainage displacement. The other way around is called imbibition. In macroscale, based on the assumption of a linear interface, steady-state two-phase immiscible flow can be described for simplicity by Darcy's law, an analogy to Fick's law of diffusion. In many cases, however, the displacement interface shows fractal structures, as observed from experimental measurement and simulation modeling. The patterns of these structures are subjected to capillary number N_c and viscosity ratio. Here, capillary number is defined as:

$$N_c = \frac{v\mu}{\gamma},$$

where v is the superficial flow rate, μ the viscosity of the more viscous fluid, and γ the interfacial tension between wetting and nonwetting phase. For convenience, viscosity of the invading fluid and defending fluid are denoted as μ_I and μ_D, respectively. Two extreme flow conditions are discussed later. If the capillary number is large, the flow mechanism is dominated by viscous force. The interface is stable if $\mu_I/\mu_D > 1$. If $\mu_I/\mu_D < 1$, viscous fingering is observed. It is a pattern formed by the invading fluid with small size of trapped defending fluid clusters left behind. For near-zero N_c, for example, flow velocity $v \to 0$, the viscous force of the defending fluid is negligible and capillary forces dominate. The mechanism for drainage and imbibition are quite different. For imbibition, the invading fluid first occupies pores that have the narrowest size since such pores have the lowest resistance. For drainage, defending fluid is invaded only if the pressure exceeds the critical value, which is given by the Laplace equation:

$$P_{\text{critical}} = \frac{2\gamma \cos\theta}{r},$$

where P_{critical} is the critical capillary pressure, r is the narrowest radius of the pore, and θ is the contact angle. Mobility of oil is manifested by discontinuous pistonlike motion, known as Haines jump, sometimes termed avalanche, with various sizes of trapped defending fluid clusters left behind.

Several types of model porous media have been constructed for visualization of two-phase flow. The most simplified design is along the lines of a two-dimensional (2-D) mesh grid flow cell (Cottin et al., 2010; Crandall et al., 2008, 2009; Ferer et al., 2004, 2011) composed of variable sizes of perpendicular flow channels to imitate natural porous media. The cell can be made of glass or resin from photolithography. An example of such flow cell is shown in Figure 8.3. Tsakiroglou et al. (2007) adopted a different approach by using a crossed-linked-network flow cell. The channels of the network are 45° to the direction of the inlet flow (Fig. 8.4).

Pseudorandom porous media could be made of uniform-size spherical glass beads (Fig. 8.5). This approach was adopted by Tallakstad et al. (2009) to make a much larger dimension porous media. Immiscible displacement in a larger size scale could be clearly seen in such porous medium, which consists of many single-layer 1 mm

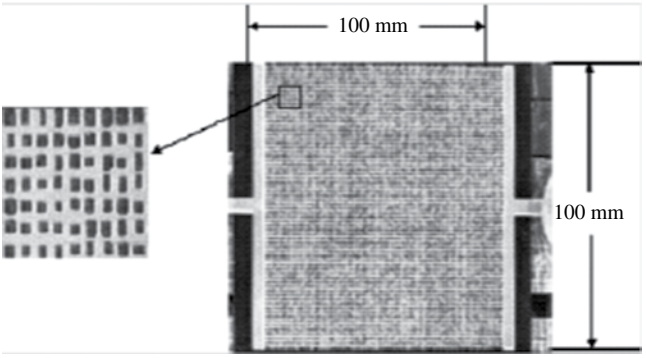

FIGURE 8.3 Snapshots of mesh grid flow cell. Cell dimension is $100 \times 100\,\text{mm}^2$ with etched channels that are 410 μm width and 67 μm depth on average. Reproduced from Ferer et al. (2004) with permission of the American Physical Society.

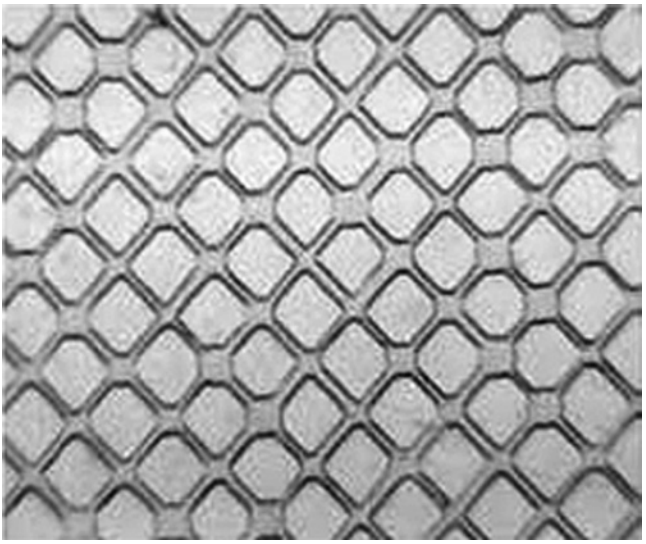

FIGURE 8.4 A cross-linked network flow cell made by Tsakiroglou et al. Cell size is $160 \times 110\,\text{mm}^2$. Throat sizes are not uniform, with a mean of 167.5 μm in width and 116.6 μm in depth. Reproduced from Tsakiroglou et al. (2007) with permission from Elsevier.

beads. For microscopic visualization of two-phase flow in porous media, however, glass beads are not a good choice because of the occurrence of refraction, which can darken the solid–liquid interface and reduce visibility. To solve such problem while at the same time creating a truly random porous medium, Zhu et al. (2012) use cryolite particles as grain material for the preparation of random porous media inside microcapillaries. When water-wet, the refractive index of cryolite matches that of water, so mobilization of oil phase can be observed clearly (Fig. 8.6). To further ensure visibility, the capillary was fit into a glass jacket, and the defending fluid was filled in between to cancel out refraction effect.

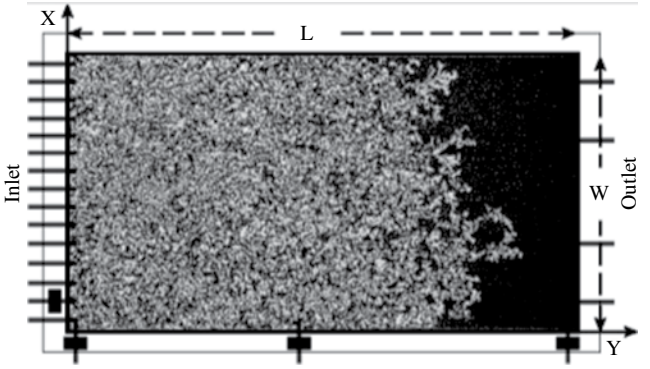

FIGURE 8.5 A 2-D porous media packed bed made by Tallakstad et al. Overall size of the packed bed is $85 \times 42\,cm^2$. To ensure transparency, porous media are made of randomly packed glass spheres of 1 mm in diameter. Reproduced from Tallakstad et al. (2009) with permission of the American Physical Society.

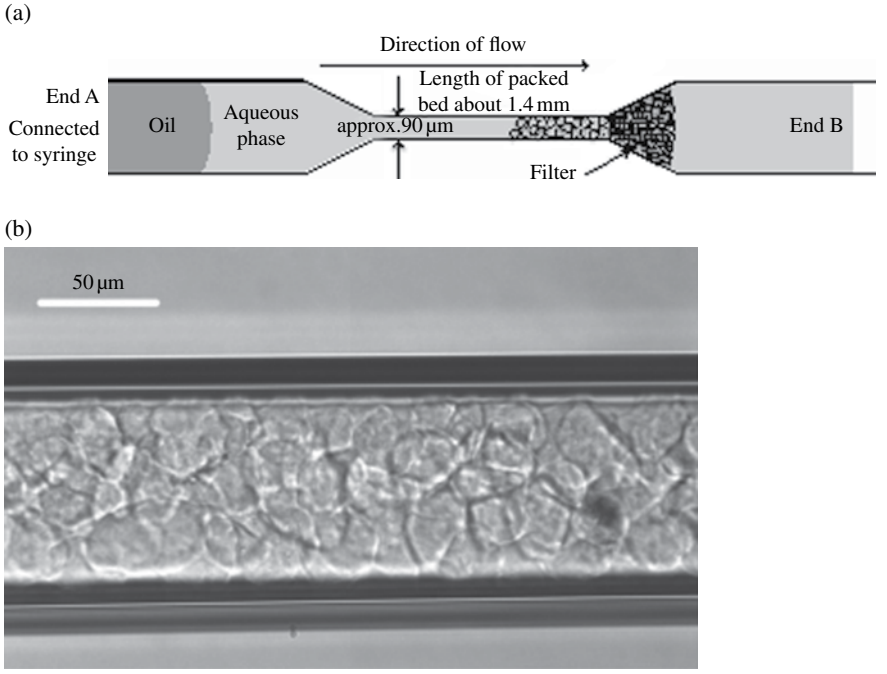

FIGURE 8.6 (**a**) Scheme of a microcapillary porous media made by Papadopoulos et al.. Flow was generated from a syringe pump connected to the capillary. Dimension of the porous media was about 90 μm in diameter and 1.4 mm in length. Such small-scale porous media was made with the attempt to imitate a practical situation as depicted in Figure 8.2. (**b**) Microscopy image of the microcapillary porous media. Cryolite particles were randomly packed inside capillary and immersed by aqueous phase. Particles have various sizes and shapes to ensure random packing. Average grain size is 30–40 μm. The edge of the particles can be clearly seen because the refractive index is close to water. Reproduced with permission from Papadopoulos et al. (2012). © American Physical Society.

8.2.1 Experimental Observation

8.2.1.1 Visualization of Flow Patterns

An example of visualization of drainage invasion is shown in Figure 8.7. Experiments were conducted by Cottin et al. (2010) on a 2-D mesh grid flow cell. The details of the system are given in Table 8.2, and Figure 8.7 shows the occurrence of capillary fingering when capillary number is extremely small.

Quantification of capillary fingering structure can be obtained through image analysis for 2-D structured porous media. A correlation between saturation interfacial width w_s and N_c has been found to be

$$w_s \propto N_c^{-\alpha},$$

with $\alpha = 0.6 \pm 0.2$ (Frette et al., 1997). The physical definition of w_s in 2-D porous media is equivalent to front interfacial area in three dimensions. A 3-D interfacial area,

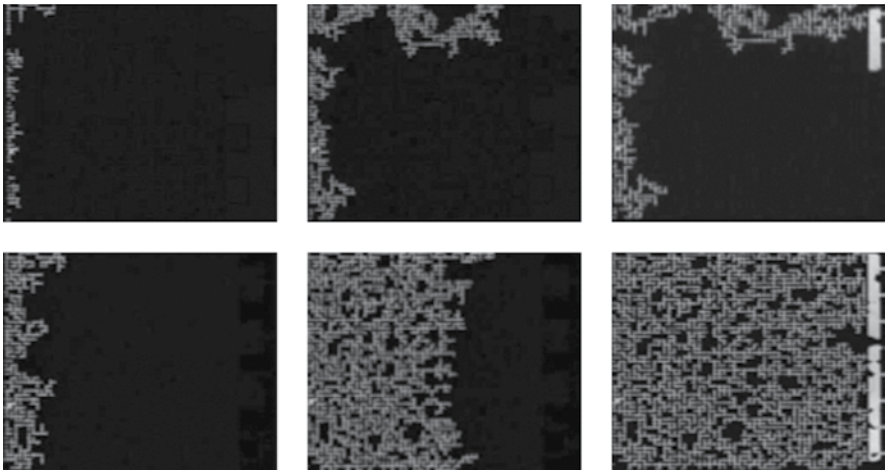

FIGURE 8.7 Snapshots of drainage process as taken from Cottin et al. at two different capillary numbers. Experiment parameters are given in Table 8.2. Reproduced from Cottin et al. (2010) with permission of the American Physical Society.

TABLE 8.2 System parameters for displacement experiments conducted by Cottin et al. (2010)

Cell size	$1.3 \times 1.3\,\text{cm}^2$
Invading fluid	Dodecane (nonwetting phase)
Defending fluid	Water (wetting phase)
Displacement type	Drainage
Grid channel width	$90 \pm 0.1\,\mu\text{m}$
μ_I/μ_D	1.43
Interfacial tension	25 mN/m
Capillary number (Fig. 8.6, top/bottom)	$9 \times 10^{-7}/1.85 \times 10^{-5}$
Saturation of water after breakthrough (top/bottom)	Approximately 80% or less than 20%

however, is impractical to measure experimentally. Therefore, simulation is needed in order to obtain such information. For stable displacement, which has $\mu_I/\mu_D > 1$, as N_c is increased, for example, by increasing the flow rate, a more compact nonwetting phase pattern is manifested, which corresponds to viscous flow (second row of Fig. 8.7). It should be noted that such "crossover" could also occur even for $N_c \to 0$, given enough time for the flow to reach a steady state. Such evidence is shown by Ferer et al. (2007) through simulation. The transparent porous medium inside a cylindrical microcapillary environment, which was designed in Papadopoulos' laboratory (Zhu et al. 2012), is theoretically 3-D; however, the radial direction of fluid movement is restricted by the small capillary diameter, and therefore, fingering events are suppressed by the geometry of the capillary. Fingering still was observed for low N_c, and as N_c was increased, the flow became viscous with constant interfacial width (Fig. 8.8).

The compact flow pattern at high N_c could only be observed for stable displacement, that is, $\mu_I/\mu_D > 1$. If the nonwetting invading fluid has a smaller viscosity, for example, air as displacing and water as invading fluid, viscous fingering will be observed. In such case, increase of capillary number will result in increase of finger size (Lovoll et al., 2011).

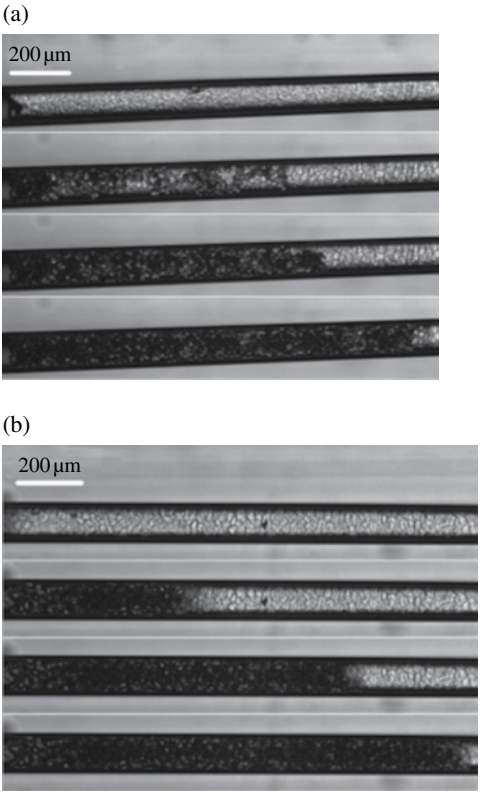

FIGURE 8.8 Snapshots of oil displacing aqueous phase in microcapillary porous media. Capillary numbers are 5.67×10^{-5} (**a**) and 5.06×10^{-3} (**b**). Reproduced from Papadopoulos et al. (2012). © American Physical Society.

8.2.1.2 Saturation of Porous Media

Saturation is defined as the volume fraction of pore space that is occupied by a fluid phase. For biphasic flow, saturations of nonwetting phase and wetting phase should satisfy:

$$S_{nw} + S_w = 1.$$

Saturation can be determined by measuring the volume of wetting–nonwetting fluid entering the porous media and subtracting the amount exiting the system. For 2-D visualization, saturation can also be obtained from image analysis provided there is substantial contrast between wetting and nonwetting fluid. Intuitively, for drainage of stable displacement, the saturation of nonwetting phase should be an increasing function of capillary number. The reason is that fingering structures result in early breakthrough of nonwetting phase and increase trapped clusters of defending fluid (Frette et al., 1997). Such clusters are stable regions disconnected from the main body of invading fluid. To displace them, larger pressures are required in order to overcome the threshold pressure, which cannot be obtained unless N_c is increased to overcome the local advancing capillary pressure. A schematic of trapped clusters in soil grains with the presence of flow is shown in Figure 8.9. A theoretical interest for drainage in well-structured porous media is how the size of trapped clusters and saturation correlates with N_c. Surprisingly, such systems have rarely been investigated (Cottin et al., 2010) and remain to be explored.

8.2.1.3 Quantitative Measurement of Displacing Phase Travel Distance

Measuring travel distance of nonwetting phase as a function of time gives an idea of how fast oil could travel in porous media under different flow conditions. In a well-structured porous medium, for example, Ferer et al.'s (2011) mesh grid model, travel

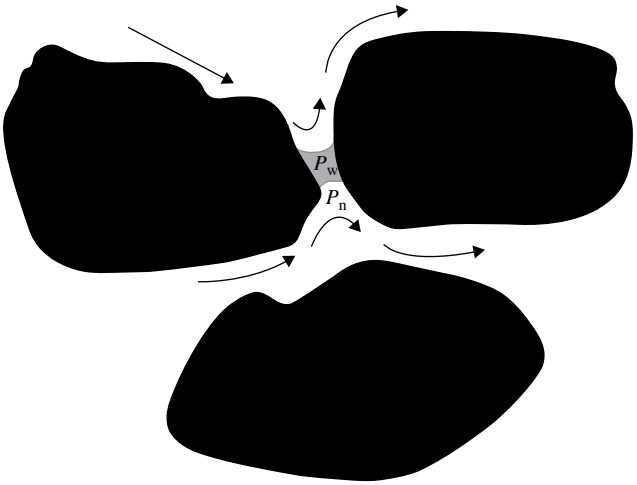

FIGURE 8.9 Trapped cluster of defending fluid (wetting phase) between soil grains (black). The pressure difference between nonwetting phase P_{nw} and wetting phase P_w gives the capillary pressure as $P_c = P_{nw} - P_w$. Arrows indicate direction of the oil flow.

distance can be defined according to the position of the center of mass of invading phase. By comparing data from different capillary number, a generalized correlation for all capillary number N_c was discovered:

$$x(t) \propto (N_c t)^e,$$

with $x(t)$ as the average center of mass of the invading fluid. Such correlation turns out to match the results of simulation very well (Ferer et al., 2004).

For the random packing porous medium in a microcapillary made in Papadopoulos' laboratory (2012), instead of the center of mass of invading phase, the front of the oil phase was used to determine travel distance and measure the

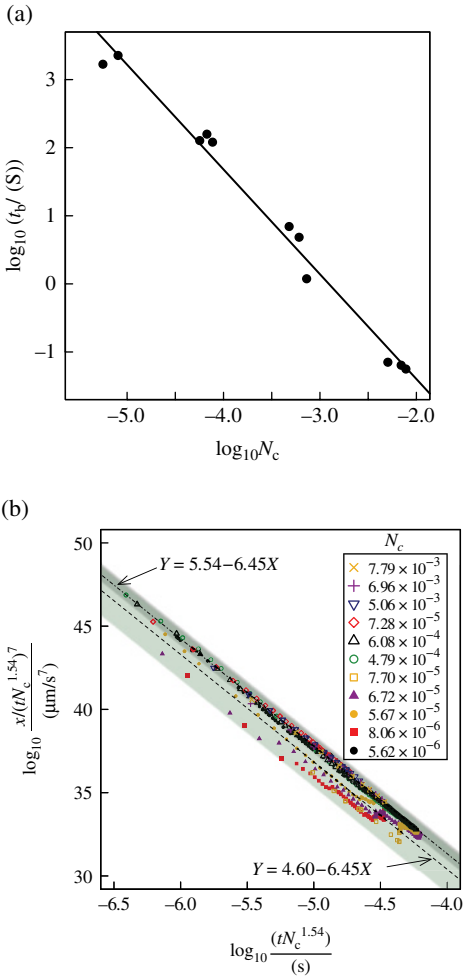

FIGURE 8.10 (**a**) Breakthrough time t_b as a function of capillary number N_c. (**b**) Correlation of flow history x with time t for different capillary numbers N_c. Reproduced from Papadopoulos et al. (2012). © American Physical Society.

breakthrough time as a function of N_c. The relationship between breakthrough time t_b and N_c is shown in Figure 8.10. The slope of the line is −1.54 rather than −1. It indicates that residue saturation of the defending phase upon breakthrough may vary as a function N_c.

Furthermore, an empirical correlation $\log_{10}(x / tN_c^{1.547})$ versus $\log_{10} tN_c^{1.54}$ was found, with x as the position of the oil phase front. Presenting all experimental results on a log–log plot in Figure 8.10b, it can be seen that the reduced $x \sim t$ data fall onto the green-shaded linear region, the center line of which is $Y = 4.60 - 6.45X$. For $N_c > 10^{-4}$, all data collapse onto a linear curve $Y = 5.54 - 6.45X$. For $N_c < 10^{-4}$, the curves show a zigzag shape due to burst motion but also collapse at final stage. According to Figure 8.10b, oil travel distance x for $N_c > 10^{-4}$, as well as for $N_c < 10^{-4}$ at large time scale, can be expressed as

$$x \propto t^{0.55} N_c^{0.847}.$$

Such relationship gives a general sense of how oil displaces water in pore-scale channels, for example, pores that are composed by sand grains, in between which silt particles form a micron dimension porous medium. It should be noted that the empirical relationship was derived from packed beds of very narrow size distribution and may not apply to systems of different size. Further investigation is needed to discover how packed-bed geometry and size may affect flow behavior. Furthermore, the size of such packed bed indicates that wettability of glass wall and cryolite particles are both essential to the flow, especially for small capillary numbers. Therefore, for practical application as well as theoretical study, it will be interesting to investigate how the $x \sim t$ correlation changes if wettability varies, for example, by modifying the surface properties of the glass wall.

8.3 HOW BACTERIA MAY ACCESS POROUS-ENTRAPPED OIL

Mobilizing the oil that is trapped in porous media helps facilitate the oil cleanup; however, ultimately the degradation of petroleum hydrocarbons and restoration of oil-polluted environments are mainly achieved through the oil-eating action of bacteria. For the oil that remains entrapped in porous media, successful bioremediation requires access of the oil to bacteria, and such access is attained through the movement of bacteria through the water-filled pores of soils, sands, and sediments and toward the oil. Therefore, knowledge of bacterial transport/swimming in porous media is necessary for the development of effective *in situ* bioremediation strategies.

Over the span of over two decades, bacterial transport in porous media has been extensively investigated (Barton and Ford, 1995; Becker et al., 2003; Camesano and Logan, 1998; Camper et al., 1993; Duffy and Ford, 1997; Duffy et al., 1995; Ford and Harvey, 2007; Gannon et al., 1991; Hornberger et al., 1992; Kinoshita et al., 1993; Kusy and Ford, 2007; Lutterodt et al., 2009; Oates et al., 2005; Olson et al., 2004; Reynolds et al., 1989; Sharma and McInerney, 1994; Sherwood et al., 2003). The effects of bacterial properties, such as cell size, hydrophobicity, net surface electrostatic charge, and the presence of capsules and flagella, on their retention by soil were

studied based on 19 strains of bacteria, suggesting that these properties have synergetic effects on the occurrence and extent of bacterial transport through soil (Gannon et al., 1991). Regarding fluid flow effects, Camesano and Logan (1998) indicated that for motile bacteria, low flow velocities facilitate transport of bacteria through soil, whereas higher velocities hinder it by causing bacteria to adhere on the pores' surface and aggregate, thus decreasing permeability. Ford and Harvey (2007) summarized how the concentration gradients of chemicals can stimulate *chemotaxis* in saturated porous media and quantified chemotactic responses in different kinds of porous media.

At an individual-cell level, cell motility, interactions, and transport in geometrically restrictive environments were first addressed experimentally in the 1990s by Papadopoulos and coworkers and showed some motility behaviors which were very different than those exhibited in unconfined environments (Berg and Brown, 1972; Frymier et al., 1995; Phillips et al., 1994; Turner et al., 2000), mainly due to restrictions imposed on the cell flagella by confining walls (Liu and Papadopoulos, 1995) and the "crowded swimming space" that forced interactions among cells (Liu et al., 1997). Since then, several other factors on the swimming behavior of individual bacterial cells in restrictive geometries have been addressed, such as *chemotaxis* (Chen and Jin, 2011; Kusy and Ford, 2009), electric fields (Liu et al., 1999), and the size of microchannels and their complexity (Binz et al., 2010; Biondi et al. 1998; Galajda et al., 2007). In the following subsections, we summarize some pertinent investigations of bacterial transport in confined spaces and porous media.

8.3.1 Bacterial Motility in Restrictive Capillaries

A technique, capillary video microscopy, developed by Papadopoulos and coworkers in the 1990s offered the capability of visualizing and quantitating the swimming behavior of *Escherichia coli* (*E. coli*) in restrictive microcapillaries (Liu and Papadopoulos, 1995, 1996; Liu et al., 1997, 1999). In this technique, a microcapillary with the desired inside diameter was made by pulling the center of a micropipette with an original inside diameter of 0.275 mm and a length of 78 mm using a micropipette puller. The pulled microcapillary, secured on a capillary holder, was then placed on the stage of an optical microscope. *E. coli* were injected inside the microcapillaries by injection micropipettes and using a micromanipulator. After all convection flows had vanished, the swimming behavior of bacteria was monitored and analyzed. The effects of the inside diameter of the capillary (Liu and Papadopoulos, 1995; Liu et al., 1997), *chemotaxis* (Liu and Papadopoulos, 1996), and electric field (Liu et al., 1999) on bacterial movement in restrictive capillaries were studied, which provided the background for our recent and ongoing studies of bacterial transport through oil spill-contaminated porous media.

In the study of Liu and Papadopoulos (1995), the size of the capillary inside diameter shows a significant effect on the swimming behavior of *E. coli* in a motility buffer. When the host cylindrical capillary had an inside diameter of 50 μm, the motile bacteria swam in a random motion, similar to that in the unrestricted bulk medium. However, for capillaries with much smaller inside diameter, for example, 6 or 10 μm, the pattern of bacterial swimming varied significantly. It was observed that bacteria not only swam with reduced randomness along the capillary but also were

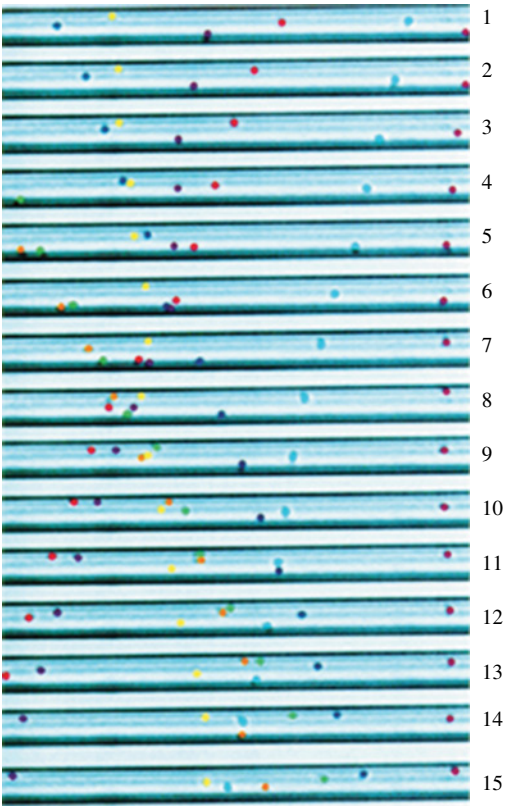

FIGURE 8.11 Sequence of 15 photographic stills shows the swimming of eight *E. coli* cells in a 6 μm capillary. Each still is taken at the time interval of 0.33 s. Bacteria were artificially colored so as to track their path in time. Reprinted from Liu and Papadopoulos (1995) with permission of the American Society of Microbiology. *(See insert for color representation of the figure.)*

unable to reverse their swimming direction. Figure 8.11 shows a typical sequence of bacterial swimming in a very fine pore, where the swimming of eight cells in a 6 μm capillary was tracked. Occasionally, bacteria swimming in a certain direction were temporarily pushed back by groups of cells swimming in the opposite direction. This is seen in stills 6–8, where a series of interactions of the "yellow cell" with other cells caused it to have a net backward movement of 1.6 μm for the period of about 0.6 s. Nevertheless, even in such crossing-path cases, bacteria did not reverse their swimming direction; instead, after a temporary backward displacement or pause, they resumed their previous swimming direction and speed.

The unidirectional motility of bacteria in restrictive capillaries was attributed to their flagellar dimensions being longer than the host capillary's diameter, which prevented them from turning back as explained in the following. *E. coli* is a peritrichously flagellated bacterium with a cell body of approximately 0.5–1.0 μm in diameter and approximately

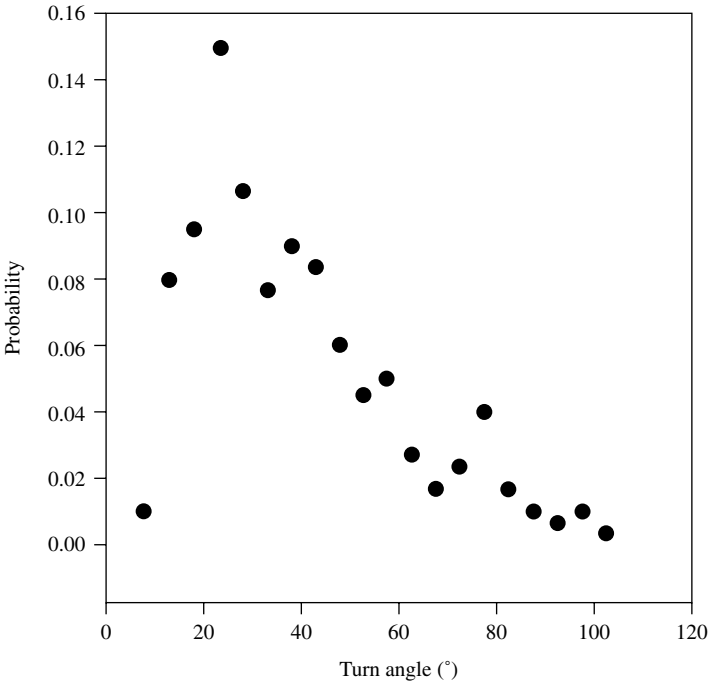

FIGURE 8.12 Turn angle distribution of *E. coli* in a 6 μm capillary. Reprinted from Liu and Papadopoulos (1995) with permission of the American Society of Microbiology.

1.0–3.0 μm in length and with flagella of approximately 5–10 μm in length. For motile *E. coli*, there are two types of locomotion, smooth swimming and tumbling, which are caused by counterclockwise and clockwise rotation of flagella, respectively (Larsen et al., 1974). Therefore, when *E. coli* start to tumble or turn around in a narrow capillary whose dimension is smaller than the length of the cells' flagella, reorientation of the flagella and body is restricted, and the bacteria, not being able to reverse their direction, perform unidirectional swimming. However, tumbling did occur inside the restrictive capillaries, but the turn angle, as shown in Figure 8.12, was rarely larger than 90°.

Several other phenomena, including capillary-induced bacterial aggregation, motility of bacterial aggregates, and the pushing of weakly swimming bacteria by stronger ones, were observed when bacteria swam in an extremely narrow capillary with an inside diameter of 3 μm (Liu et al., 1997). An example of the formation of bacterial aggregates followed by a breakup is shown in Figure 8.13. Initially, there were four cells, three moving from left to right and one adhering to the capillary wall. Since the leftmost one swam faster than the one ahead of it, they met each other (still 4), aggregated (still 5), swam together as a doublet (still 6–25), broke up (still 26), and subsequently resumed their individual swimming. More interestingly, when cells had the head-on collision as a result of which they formed an aggregate, the weaker cell was pushed by the stronger swimming cell or aggregate, thus reversing its swimming direction (image not shown).

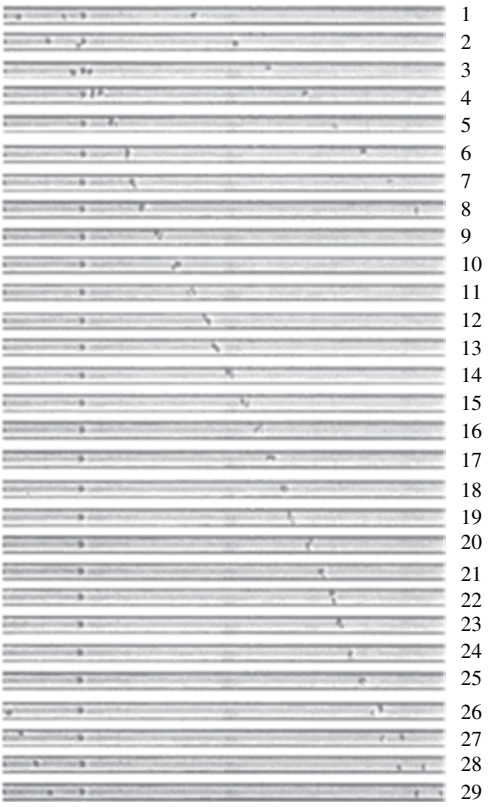

FIGURE 8.13 Sequence of photographic stills showing the aggregation of two cells followed by a later breakup. Each still is taken at the time internal of 0.33 s. Reprinted from Liu et al. (1997) with permission of Wiley.

8.3.2 Visualization of Bacterial Transport in a Porous Medium Using Magnetic Resonance Imaging and Immunomagnetic Labeling

To facilitate the measurement of bacterial density distributions as a function of time in a water-saturated porous medium, Ford and coworkers utilized an approach of magnetic resonance imaging (MRI) in conjunction with the immunomagnetic labeling (Sherwood et al., 2003). Via a monoclonal antibody, magnetite nanoparticles (50–60 nm diameter), composed of a quasispherical crystalline magnetite core coated with a monolayer of derivatized bovine serum albumin, were attached to the surface of *E. coli*. Such method enhances the sensitivity of MRI, so that bacteria can be detected at a relatively low concentration.

Experiments were preformed in an adjusted-bed borosilicate glass chromatography column with an inside diameter of 1.5 cm. As depicted in Figure 8.14, in order to allow the impinging flow, four evenly spaced holes, located at the midpoint of the bed, were drilled around the surface of the column. A piece of nylon fabric with a plastic tubing connector was placed at each hole to retain the porous medium.

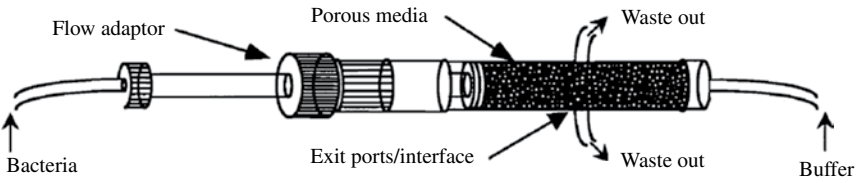

FIGURE 8.14 Schematic illustration of the packed column apparatus. Reprinted from Sherwood et al. (2003) with permission of the American Chemical Society.

Glass-coated polystyrene microbeads with a size distribution of 250–300 μm, as the model porous medium, were packed in the column. A flow adapter with a 40 μm glass frit was used to keep the bed in place and to maintain the incoming flow evenly across the cross section of the bed.

The impinging flow was created by loading buffer and labeled motile bacteria from two sides of the column simultaneously. After the impinging flow was maintained at a steady flow rate, an interface was created at the center of the packed bed because no mixing took place between the two halves of the column. After stopping the flow, bacteria freely migrated to the other half of the column, and magnetic resonance images were collected under no-flow conditions. Since the changes in spin–spin relaxation time (T_2) are related to the changes in the concentration of labeled motile bacteria, the concentration of labeled bacteria c can be given as

$$c = \frac{1}{\mathrm{R}}\left(\frac{1}{T_2} - \frac{1}{T_{2,0}}\right),$$

where R is the relaxivity constant and $T_{2,0}$ is the T_2 value for pure water (Sherwood et al., 2003). When compared to nonmotile bacteria (Fig. 8.15a), a significant amount of penetration for motile bacteria (Fig. 8.15b) was observed. An agreement of theoretical predictions with experimental data indicated that bacterial migration within the porous medium was successfully monitored.

Ford's group also studied bacterial *chemotaxis* in porous media using MRI and firstly reported bacterial chemotactic parameters within the porous-medium-packed column (Olson et al., 2004). This powerful technique provides a noninvasive visualization of changes in bacterial density distributions and shows the importance for studying bacterial transport in porous media.

8.3.3 Motility of Bacteria in Glass-Bead-Packed Porous Medium as Affected by Chemoattractant

In the presence of chemical attractants or repellents, bacteria swim preferentially toward the direction of high attractant concentration and away from the repellents. This phenomenon, known as *chemotaxis*, is believed to play a great role in bioremediation and biorestoration by bringing bacteria to the proximity of the contaminants, since many soil bacteria that degrade chemical pollutants are chemotactic (Pandey

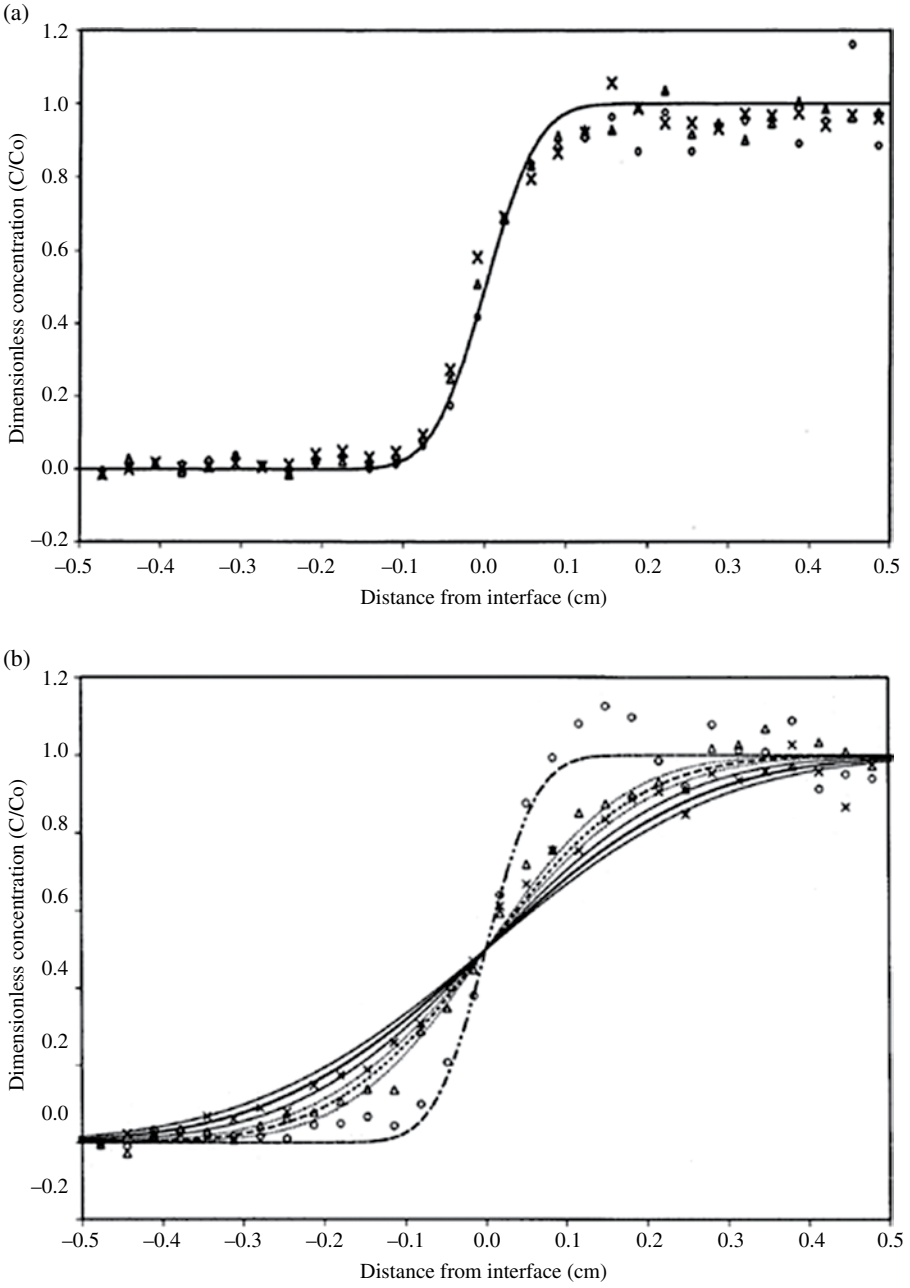

FIGURE 8.15 Dimensionless concentration profiles for nonmotile *E. coli* (**a**) and motile *E. coli* (**b**) in the packed column at 23 min (o), 376 min (Δ), and 736 min (×) after stopping the impinging flow. Reprinted from Sherwood et al. (2003) with permission of the American Chemical Society.

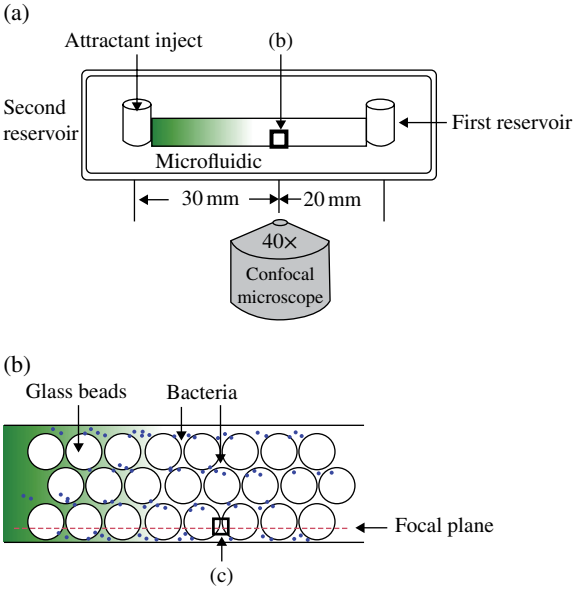

FIGURE 8.16 (**a**) The microfluidic showing the gradient of chemoattractant. (**b**) The profile of the microchannel filled with three layers of glass beads and the focal plane where the bacterial swimming was recorded. Reprinted from Chen and Jin (2011) with permission of Elsevier.

and Jain, 2002). The effect of *chemotaxis* on bacterial transport in porous media has been investigated extensively (Barton and Ford, 1995; Chen and Jin, 2011; Ford and Harvey, 2007; Ford et al., 1991; Olson et al., 2004; Reynolds et al., 1989).

An example of *chemotaxis* assay setup is shown in Figure 8.16. By using microfluidic channels and a high-speed confocal microscopy, the swimming behavior of *Pseudomonas aeruginosa* in the glass-bead-packed porous medium and in the presence of a chemoattractant was visualized directly (Chen and Jin, 2011). The microchannel in Figure 8.16a was made of an optical plastic with a 100 µl volume capacity. To create a chemoattractant gradient, 40 µl bacterial suspension with 1 mM serine as attractant was added to the microchannel containing 100 µl bacterial suspension from one reservoir, followed by aspirating the same volume of bacterial suspension from the other reservoir. The glass-bead-packed microchannel, in Figure 8.16b, was prepared by loading dry glass beads (88–125 µm diameter) into the microchannel with one end clogged, resulting in a compact-packing mode with a pore space of 55%.

Consistent with documented behavior of *P. aeruginosa* (Harwood et al., 1989), tumbles between runs and turns were not observed either in aqueous medium (Fig. 8.17a and b) or in saturated glass beads (Fig. 8.17c and d).

After colliding with glass beads, bacteria did one of the following: (i) 80% of the cells made sharp turns and rebounded instantly (A in Fig. 8.17c and d); (ii) 15% of the cells glided over the glass-bead surface for a few seconds before swimming back to the aqueous phase (B in Fig. 8.17c and d); and (iii) 5% of the cells escaped from

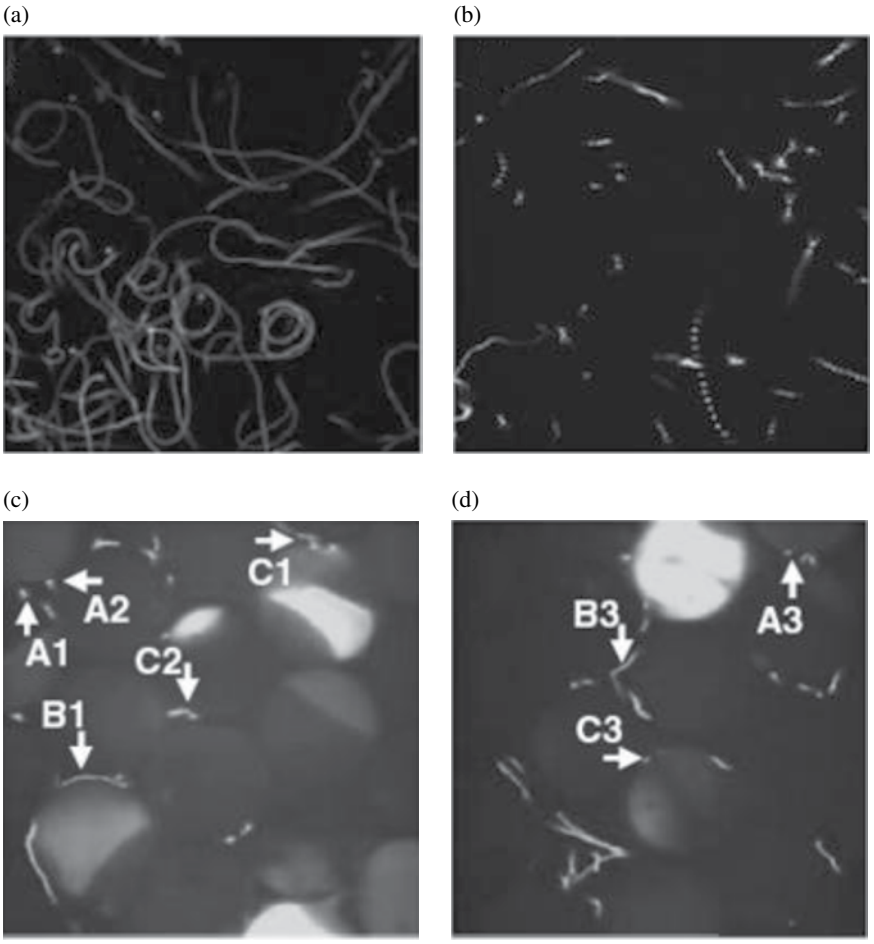

FIGURE 8.17 Bacterial trajectories in aqueous medium (**a**) and (**b**). The focal plane was near the bottom (**a**) and in the middle (**b**) of the microchannel. Bacterial movement in the glass-bead-packed porous medium (**c**) and (**d**). Reprinted from Chen and Jin (2011) with permission of Elsevier.

the glass-bead surface after rotating or vibrating on the surface for several seconds (C in Fig. 8.17c and d). Although the trajectories of bacteria were intricate, it is evident that bacteria can transport from low to high serine concentration in the glass-bead-packed porous medium.

8.3.4 Visualization of Bacterial Transport in Cryolite-Packed Porous Medium

In most studies, the model porous media used are soils, glass spheres, or quartz sands, which might limit direct observation of bacterial movement due to opacity of the porous media. To solve this problem, cryolite mineral particles with the mean size

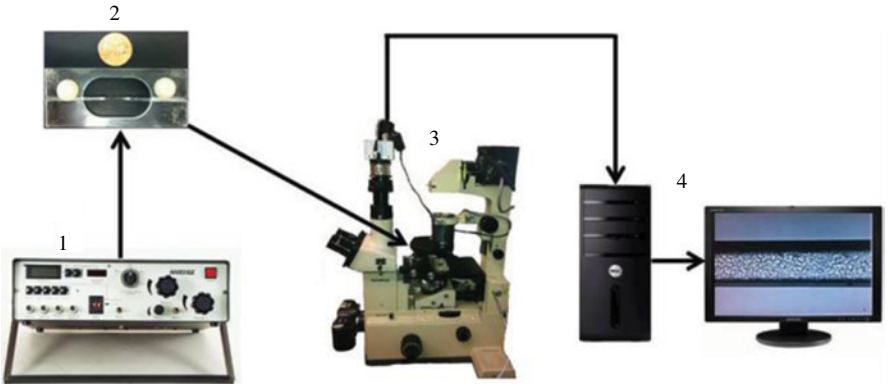

FIGURE 8.18 Setup of the packed-bed-capillary video microscopy. The legend for this figure is as the following: (1) microinjection system, (2) a capillary holder carrying a cryolite-packed-bed capillary, (3) optical microscope equipped with a high performance CCD camera, (4) PC with image processing software.

of 29.46 ± 2.17 μm were selected to pack the random porous medium by Papadopoulos and coworkers, since they have the unique property of becoming transparent upon wetting by water. By use of packed-bed-capillary video microscopy (Fig. 8.18), as earlier described in this chapter, the movement of motile flagellated *Bacillus subtilis* (*B. subtilis*) through random pores and the effects of irregularly confined space on their swimming behavior were observed and analyzed.

Figure 8.19 shows the characteristic trajectories of bacteria in a capillary with bulk growth medium (a) and cryolite-packed porous medium (b). In bulk unrestricted growth medium (Fig. 8.19a), bacteria swam in long runs with few tumbles, which can be explained by the fact that bacteria swam in a nutrient-rich environment. Instead of linear-like long runs seen in the growth medium, more cell tumbles and turns were seen in the cryolite-packed porous medium (Fig. 8.19b). Once the cells collided with the walls of the cryolite grain, they slowed down on the solid surfaces and performed one of the following: (i) most cells reoriented their bodies gradually before they resumed their swimming toward new directions; (ii) some cells tethered onto the cryolites and became stuck for a period of time; and (iii) in rare cases, it was observed that bacteria's forward end became their backward end, as well as by possible orientation reversal of their flagella, which allowed them to move away from the cryolites. The rarity of such reversal of bacterial movement is possibly due to the cell spatial constraint caused by packed cryolites. Even though bacterial pathways in the random porous media were complicated, most bacteria were able to perform long-distance migration according to our visual observation.

In 1997, Papadopoulos and coworkers (Nguyen, Liu and Papadopoulos, unpublished) observed that when *E. coli* swam in a tapered glass microcapillary whose diameter is comparable to the length of flagella, they exhibited a tactical movement toward the narrower segment of the capillary, thus causing a net bacterial transport in

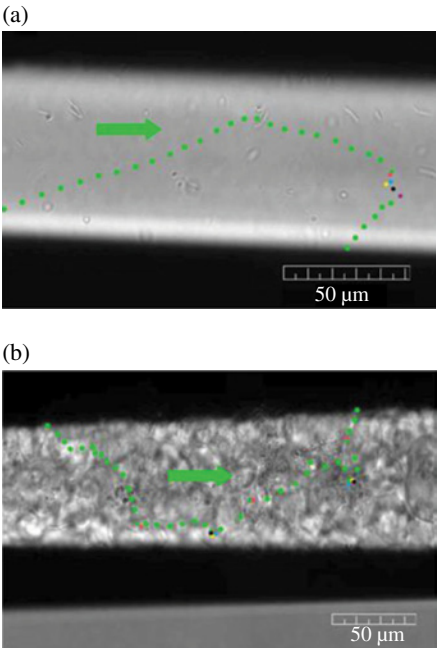

FIGURE 8.19 The movement pathways of *B. subtilis* in bulk growth medium (**a**) and random porous medium (**b**), which are shown by dots drawn at time increment of 0.4 s. Green arrows indicate the swimming direction of the bacterium followed. In the case of tumbles, they are indicated by a dot-color change from green to one or more different colors and by resuming the use of green dots once the tumbling has ceased. *(See insert for color representation of the figure.)*

that direction. This phenomenon is explained by the comparable size of the bacteria's flagella and capillary's diameter, which is also the origin of unidirectional motility inside cylindrical capillaries. For a conical (tapered) capillary, Figure 8.20a shows a section with diameter from 50 to 43 μm, where the swimming of bacteria was random, similar to that in unrestricted bulk. As the diameter of capillary decreased, bacteria were observed to reduce their randomness and perform preferential swimming toward the narrower region of the capillary. In Figure 8.20b, most bacteria swam toward the decreasing diameter; however, very few were able to turn around and switch their swimming to the opposite direction. In Figure 8.20c, with the diameter of the capillary at about 8 μm, bacteria swam unidirectionally, being unable to turn back. As a result, a bacterial cluster was formed in the thinnest region, due to the formation of bacterial aggregates (Fig. 20d). Research along the lines of the 1997 experiment described earlier was not continued in Papadopoulos' lab until recently, and in ongoing research using *B. subtilis*, we are confirming it in conical (tapered) capillaries by eliminating chemotactic factors that may interfere with the phenomenon. It should be noted however that this phenomenon does **not** imply actual "sensing" by the bacteria that there is a progressive constriction of the confining space they find themselves in and that they "respond" by swimming preferentially toward increased

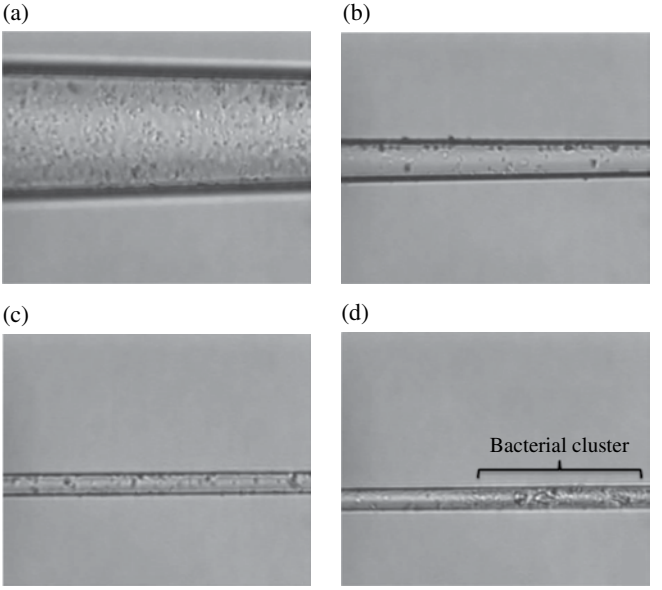

FIGURE 8.20 *E. coli* swimming through a tapered capillary. In image (**a**), diameter is varying from 50 to 43 μm; in image (**b**), diameter is varying from 15 to 13 μm; in image (**c**) and (**d**), diameter is about 8 μm (Nguyen, Liu and Papadopoulos, unpublished).

confinement (or decreased available swimming volume). In this sense, this biased bacterial migration does not indicate a tactical response of bacteria because they actually sense a stimulus; instead, it describes the resulting preferential bacterial movement, simply due to sterically restricting their choices for swimming directions.

In line with observations in a single conical capillary, the fact that *B. subtilis* is capable of long-distance migration in the cryolite-packed porous medium may also be attributed to this phenomenon. In the confining pores of the porous medium, any reversal of cell body or change in swimming direction is difficult since the lengths of cell bodies and flagella can be comparable or larger than the pore size of the cryolite beds. Therefore, due to this same phenomenon, we believe that populations of flagellated cells can perform directional travel toward very fine pores of the porous media, where crude oil may get trapped, as depicted in Figure 8.21.

An example of how bacteria reached the crude oil in cryolite-packed capillary is shown in Figure 8.22. *B. subtilis* were slowly introduced on the left side of the capillary via a micropipette, at a location approximately 5.10 mm away from the oil droplet (Fig. 8.22a). After approximately 21 min, some very active bacteria that traveled through pore channels reached the oil droplet and swam around at the interface, as shown in Figure 8.22b. At approximately 9.5 h, more bacteria accumulated around the oil droplet (Fig. 8.22c). A bacterial colony was formed on the surface of the oil droplet, pointed out by a white rectangle, consisting of active (moving) bacteria that seemed to be swarming onto the BP oil drop's surface. An interesting observation relates to cells that traveled beyond the BP oil drop, all the way to the end of the

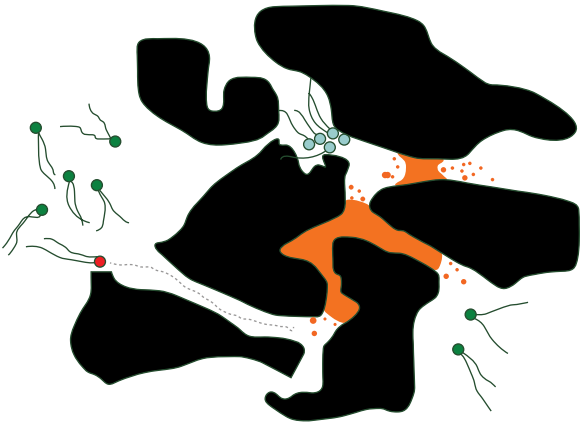

FIGURE 8.21 A schematic of how bacteria get access to oil (orange) trapped in the porous medium (black). The steric hindrance of pore space can assist bacteria (red) to travel through pore channels unidirectionally. *(See insert for color representation of the figure.)*

microscopic packed bed, that is, to distances up to approximately 9.15 mm from the point of injection and up to approximately 4.05 mm from the location of the drop. Almost all these bacteria were long-shaped sessile cells, and the ones shown in Figure 8.22d have an average length of 26.51 ± 5.60 μm. As proposed by Kearns and Losick (2005) due to "bet hedging" strategy, two states of cells, motile and long-shaped sessile, are produced during their growth, which allow *B. subtilis* both to explore new environments and to survive at their old location. It should be pointed out that oxygen depletion, certain gradients caused by bacterial metabolism, as well as possible chemotactic response toward the BP oil drop may also have been factors in the experiment described earlier. For this reason, it will be necessary to confirm these results on nonchemotactic bacterial strains in our continuing studies.

8.4 SUMMARY

In this chapter, the fate of oil as it enters geological sediments is discussed, with focus on drainage displacement, that is, occupation of pores that are initially filled with aqueous phase by oil phase and *vice versa*, as well as bacterial transport in restrictive geometries, such as microcapillaries and porous media. The transport of oil phase in porous media can be affected by many geological and physical reasons, including flow conditions, type of sediments, and packing and homogeneity.

Various types of experimental model porous media have been made for visualization of drainage phenomena, from well-structured networks to randomly packed microcapillaries. Efforts were made to correlate flow patterns with capillary number. The results indicate occurrence of capillary fingering at low N_c, and for such flow condition, capillary force is the main resistance dominating the flow. Interfacial width decreases with increasing N_c, which is consistent with the finding of capillary

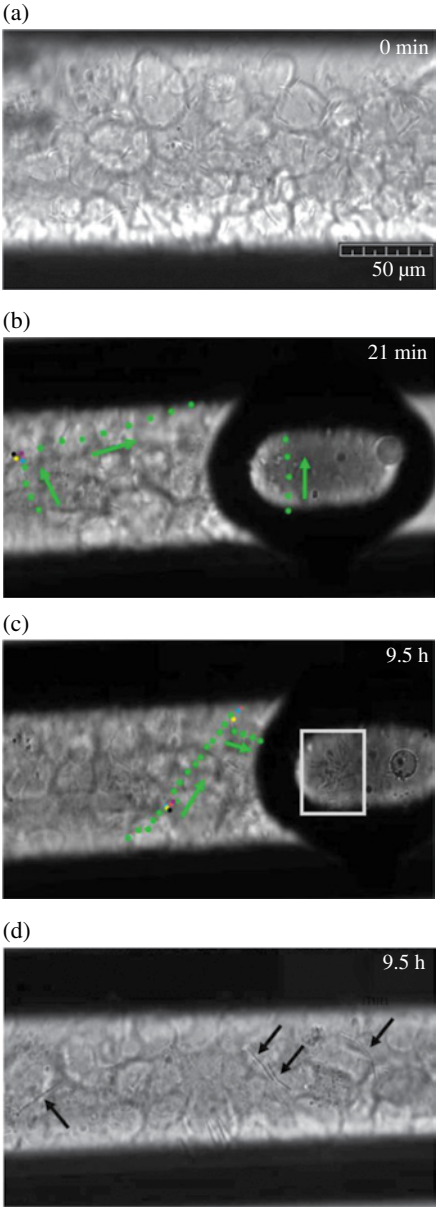

FIGURE 8.22 The movement of *B. subtilis* in the random porous medium with the presence of a Horizon-BP-crude oil droplet. (**a**) Initial injection of *B. subtilis*; (**b**) bacteria reaching the oil droplet after approximately 21 min; (**c**) bacteria have formed a colony around oil droplet at approximately 9.5 h; (**d**) the porous medium at a location of approximately 7.35 mm from the point of injection (~9.5 h). In (**b**) and (**c**), the trajectories of *B. subtilis* are indicated by dots separated by time increments of 0.4 s; green arrows indicate the swimming direction of the bacterium followed. To facilitate the observation of bacterial movement, instances of tumbling are indicated by a dot-color change from green to different colors with the order of red, blue, yellow, black, and purple and by resuming the use of green dots once the tumbling has ceased. The scale bar in (**a**) is applicable for all other images. *(See insert for color representation of the figure.)*

fingering. As N_c is increased, the flow is turned to a viscous dominated one, and capillary fingering diminishes. In a microcapillary geometry that was made to imitate microchannel porous media in certain areas of natural inhomogeneous geological sediments, flow history was correlated with time. The results indicate that movement of the invading (nonwetting) phase increases with the increase of N_c, but not at a constant rate.

Packed-bed-capillary video microscopy was also used to explore how bacteria transport themselves through porous media. Prior to this study, this unique technique was utilized to investigate bacterial swimming in a tapered glass microcapillary, in which a phenomenon according to which bacteria swim preferentially toward the narrower segment of the capillary was proposed. The results of all the studies to date are providing insight into bacterial transport through porous media. Due to the effect of biased bacterial migration in the direction of increasing constriction, population of bacteria may perform directional travel toward very fine pores of the porous media, where contaminants may get trapped. In natural or augmented bioremediation, this phenomenon may be a determining and perhaps controllable mechanism, which can facilitate the access of flagellated bacteria to contaminants.

ACKNOWLEDGMENTS

We acknowledge the partial support from NSF CBET (Award No. 1052697) and from the Gulf of Mexico Research Initiative.

REFERENCES

Baker JM. Ecological effectiveness of oil spill countermeasures: how clean is clean? Pure Appl Chem 1999;71(1):135–151.

Barton JW, Ford RM. Determination of effective transport coefficients for bacterial migration in sand columns. Appl Environ Microbiol 1995;61(9):3329–3335.

Becker MW, Metge DW, Collins SA, Shapiro AM, Harvey RW. Bacterial transport experiments in fractured crystalline bedrock. Ground Water 2003;41(5):682–689.

Berg HC, Brown DA. Chemotaxis in *Escherichia coli* analysed by three-dimensional tracking. Nature 1972;239(5374):500–504.

Binz M, Lee AP, Edwards C, Nicolau DV. Motility of bacteria in microfluidic structures. Microelectron Eng 2010;87(5–8):810–813.

Biondi SA, Quinn JA, Goldfine H. Random motility of swimming bacteria in restricted geometries AIChE J 1998;44:1923–1929.

Camesano TA, Logan BE. Influence of fluid velocity and cell concentration on the transport of motile and nonmotile bacteria in porous media. Environ Sci Technol 1998;32(11): 1699–1708.

Camper AK, Hayes JT, Sturman PJ, Jones WL, Cunningham AB. Effects of motility and adsorption rate coefficient on transport of bacteria through saturated porous media. Appl Environ Microbiol 1993;59(10):3455–3462.

Chen J, Jin Y. Motility of *Pseudomonas aeruginosa* in saturated granular media as affected by chemoattractant. J Contam Hydrol 2011;126:113–120.

Cheng J, Chen JF, Zhao M, Luo Q, Wen LX, Papadopoulos KD. Transport of ions through the oil phase of W-1/O/W-2 double emulsions. J Colloid Interface Sci 2007;305(1):175–182.

Cottin C, Bodiguel H, Colin A. Drainage in two-dimensional porous media: from capillary fingering to viscous flow. Phys Rev E 2010;82(4):046315.

Crandall D, Ahmadi G, Leonard D, Ferer M, Smith DH. A new stereolithography experimental porous flow device. Rev Sci Instrum 2008;79(4):044501.

Crandall D, Ahmadi G, Ferer M, Smith DH. Distribution and occurrence of localized-bursts in two-phase flow through porous media. Phys A Stat Mech Appl 2009;388(5):574–584.

Deshiikan SR, Papadopoulos KD. London-van der Waals and EDL effects in the coalescence of oil drops: II. Ionic strength and pH effects. J Colloid Interface Sci 1995a;174(2):313–318.

Deshiikan SR, Papadopoulos KD. London-vdW and EDL effects in the coalescence of oil drops. J Colloid Interface Sci 1995b;174(2):302–312.

Deshiikan SR, Papadopoulos KD. Visual microscopic studies on hetero-aggregation and selective aggregation. Colloid Polym Sci 1997;275(5):440–448.

Duffy KJ, Ford RM. Turn angle and run time distributions characterize swimming behavior for *Pseudomonas putida*. J Bacteriol 1997;179(4):1428–1430.

Duffy KJ, Cummings PT, Ford RM. Random walk calculations for bacterial migration in porous media. Biophys J 1995;68(3):800–806.

Ferer M, Ji C, Bromhal GS, Cook J, Ahmadi G, Smith DH. Crossover from capillary fingering to viscous fingering for immiscible unstable flow: experiment and modeling. Phys Rev E 2004;70:016303.

Ferer M, Bromhal GS, Smith DH. Crossover from capillary fingering to compact invasion for two-phase drainage with stable viscosity ratios. Adv Water Resour 2007;30(2):284–299.

Ferer M, Anna SL, Tortora P, Kadambi JR, Oliver M, Bromhal GS, Smith DH. Two-phase flow in porous media: predicting its dependence on capillary number and viscosity ratio. Transport Porous Med 2011;86(1):273–289.

Ford RM, Harvey RW. Role of *chemotaxis* in the transport of bacteria through saturated porous media. Adv Water Resour 2007;30(6–7):1608–1617.

Ford RM, Phillips BR, Quinn JA, Lauffenburger DA. Measurement of bacterial random motility and chemotaxis coefficients: I. Stopped-flow diffusion chamber assay. Biotechnol Bioeng 1991;37(7):647–660.

Frette OI, Måløy KJ, Schmittbuhl J. Immiscible displacement of viscosity-matched fluids in two-dimensional porous media. Phys Rev E 1997;55(3):2969–2975.

Frymier PD, Ford RM, Berg HC, Cummings PT. Three-dimensional tracking of motile bacteria near a solid planar surface. Proc Natl Acad Sci 1995;92(13):6195–6199.

Frysinger GS, Gaines RB, Xu L, Reddy CM. Resolving the unresolved complex mixture in petroleum-contaminated sediments. Environ Sci Technol 2003;37(8):1653–1662.

Fu J, Lu Y, Campbell CB, Papadopoulos KD. Optical microscopy inside a heating capillary. Ind Eng Chem Res 2005;44(5):1199–1203.

Fu J, Lu Y, Campbell CB, Papadopoulos KD. Acid neutralization by marine cylinder lubricants inside a heating capillary: strong/weak-stick collision mechanisms. Ind Eng Chem Res 2006a;45(16):5619–5627.

Fu JZ, Lu YF, Campbell CB, Papadopoulos KD. Temperature and acid droplet size effects in acid neutralization of marine cylinder lubricants. Tribol Lett 2006b;22(3):221–225.

Fu J, Papadopoulos K, Lu Y, Campbell C. Ostwald ripening: a decisive cause of cylinder corrosive wear. Tribol Lett 2007;27(1):21–24.

Galajda P, Keymer J, Chaikin P, Austin R. A wall of funnels concentrates swimming bacteria. J Bacteriol 2007;189(23):8704–8707.

Gannon, JT, Manilal VB, Alexander M. Relationship between cell surface properties and transport of bacteria through soil. Appl Environ Microbiol 1991;57(1):190–193.

Garcia-Bermudes M, Rausa R, Papadopoulos K. Vertically-oriented-capillary video-microscopy: drops levitated by a (reacting) fluid. Ind Eng Chem Res 2011;50(24):14142–14147.

Guterman L. Conservation biology Exxon Valdez turns 20. Science 2009;323(5921): 1558–1559.

Harwood CS, Fosnaugh K, Dispensa M. Flagellation of *Pseudomonas putida* and analysis of its motile behavior. J Bacteriol 1989;171(7):4063–4066.

Hornberger GM, Mills AL, Herman JS. Bacterial transport in porous media: evaluation of a model using laboratory observations. Water Resour Res 1992;28:915–923.

Hou W, Papadopoulos KD. Stability of water-in-oil-in-water type globules. Chem Eng Sci 1996;51(22):5043–5051.

Hou W, Papadopoulos KD. W1/O/W2 and O1/W/O2 globules stabilized with Span 80 and Tween 80. Colloids Surf A 1997;125(2–3):181–187.

Kearns DB, Losick R. Cell population heterogeneity during growth of *Bacillus subtilis*. Gene Dev 2005;19(24):3083–3094.

Kinoshita T, Bales RC, Yahya MT, Gerba CP. Bacteria transport in a porous medium: Retention of *bacillus* and *pseudomonas* on silica surfaces. Water Res 1993;27(8):1295–1301.

Kuo C-C, Papadopoulos KD. Electrokinetic movement of settled spherical particles in fine capillaries. Environ Sci Technol 1996;30(4):1176–1179.

Kusy K, Ford RM. Monte Carlo simulations derived from direct observations of individual bacteria inform macroscopic migration models at granular porous media interfaces. Environ Sci Technol 2007;41(18):6403–6409.

Kusy K, Ford RM. Surface association of motile bacteria at granular porous media interfaces. Environ Sci Technol 2009;43(10):3712–3719.

Larsen SH, Reader RW, Kort EN, Tso W-W, Adler J. Change in direction of flagellar rotation is the basis of the chemotactic response in *Escherichia coli*. Nature 1974;249(5452):74–77.

Lawson LB, Papadopoulos KD. Effects of a phospholipid cosurfactant on external coalescence in water-in-oil-in-water double-emulsion globules. Colloids Surf A 2004;250(1–3):337–342.

Liu Z, Papadopoulos KD. Unidirectional motility of *Escherichia coli* in restrictive capillaries. Appl Environ Microbiol 1995;61(10):3567–3572.

Liu Z, Papadopoulos KD. A method for measuring bacterial chemotaxis parameters in a microcapillary. Biotechnol Bioeng 1996;51(1):120–125.

Liu Z, Chen W, Papadopoulos KD. Bacterial motility, collisions, and aggregation in a 3-μm-diameter capillary. Biotechnol Bioeng 1997;53(2):238–241.

Liu Z, Chen W, Papadopoulos KD. Electrokinetic movement of *Escherichia coli* in capillaries. Environ Microbiol 1999;1(1):99–102.

Løvoll G, Jankov M, Måløy KJ, Toussaint R, Schmittbuhl J, Schäfer G, Méheust Y. Influence of viscous fingering on dynamic saturation-pressure curves in porous media. Transport Porous Med 2011;86(1):335–354.

Lutterodt G, Basnet M, Foppen JW, Uhlenbrook S. The effect of surface characteristics on the transport of multiple *Escherichia coli* isolates in large scale columns of quartz sand. Water Res 2009;43(3):595–604.

Oates, PM, Castenson C, Harvey CF, Polz M, Culligan P. Illuminating reactive microbial transport in saturated porous media: demonstration of a visualization method and conceptual transport model. J Contam Hydrol 2005;77(4):233–245.

Olson MS,, Ford RM, Smith JA, Fernandez EJ. Quantification of bacterial *chemotaxis* in porous media using magnetic resonance imaging. Environ Sci Technol 2004;38(14):3864–3870.

Pandey G, Jain RK. Bacterial chemotaxis toward environmental pollutants: role in bioremediation. Appl Environ Microbiol 2002;68(12):5789–5795.

Peacock EE, Nelson RK, Solow AR, Warren JD, Baker JL, Reddy CM. The West Falmouth oil spill: similar to 100 kg of oil found to persist decades later. Environ Forensics 2005;6(3):273–281.

Phillips BR, Quinn JA, Goldfine H. Random motility of swimming bacteria: single cells compared to cell populations. AIChE J 1994;40(2):334–348.

Reynolds PJ, Sharma P, Jenneman GE, McInerney MJ. Mechanisms of microbial movement in subsurface materials. Appl Environ Microbiol 1989;55(9):2280–2286.

Rojas EC, Sahiner N, Lawson LB, John VT, Papadopoulos KD. Controlled release from a nanocarrier entrapped within a microcarrier. J Colloid Interface Sci 2006;301(2):617–623.

Sharma PK, McInerney MJ. Effect of grain size on bacterial penetration, reproduction, and metabolic activity in porous glass bead chambers. Appl Environ Microbiol 1994; 60(5):1481–1486.

Sherwood JL, Sung JC, Ford RM, Fernandez EJ, Maneval JE, Smith JA. Analysis of bacterial random motility in a porous medium using magnetic resonance imaging and immunomagnetic labeling. Environ Sci Technol 2003;37(4):781–785.

Short JW, Lindeberg MR, Harris PM, Maselko JM, Pella JJ, Rice SD. Estimate of oil persisting on the beaches of Prince William Sound 12 years after the Exxon Valdez oil spill. Environ Sci Technol 2004;38(1):19–25.

Short JW, Irvine GV, Mann DH, Maselko JM, Pella JJ, Lindeberg MR, Payne JR, Driskell WB, Rice SD. Slightly weathered Exxon Valdez oil persists in Gulf of Alaska beach sediments after 16 years. Environ Sci Technol 2007;41(4):1245–1250.

Steenhauer K, Pokrajac D, O'Donoghue T, Kikkert GA. Subsurface processes generated by bore-driven swash on coarse-grained beaches. J Geophys Res Oceans 2011;116:C04013.

Tallakstad KT, Knudsen HA, Ramstad T, Løvoll G, Måløy KJ, Toussaint R, Flekkøy EG. Steady-state two-phase flow in porous media: statistics and transport properties. Phys Rev Lett 2009;102(7):074502.

Tansel B, Fuentes C, Sanchez M, Predoi K, Acevedo M. Persistence profile of polyaromatic hydrocarbons in shallow and deep Gulf waters and sediments: effect of water temperature and sediment-water partitioning characteristics. Mar Pollut Bull 2011;62(12):2659–2665.

Tsakiroglou CD, Avraam DG, Payatakes AC. Transient and steady-state relative permeabilities from two-phase flow experiments in planar pore networks. Adv Water Resour 2007;30(9): 1981–1992.

Turner L, Ryu WS, Berg HC. Real-time imaging of fluorescent flagellar filaments. J Bacteriol 2000;182(10):2793–2801.

Villa CH, Lawson LB, Li Y, Papadopoulos KD. Internal coalescence as a mechanism of instability in water-in-oil-in-water double-emulsion globules. Langmuir 2003;19(2):244–249.

Voosen P. The oil's story, from wellhead to beach. *The New York Times*; April 29 2011.

Wang Q, Tan G, Lawson LB, John VT, Papadopoulos KD. Liposomes in double-emulsion globules. Langmuir 2010;26(5):3225–3231.

Wen LX, Papadopoulos KD. Effects of surfactants on water transport in W-1/O/W-2 emulsions. Langmuir 2000a;16(20):7612–7617.

Wen LX, Papadopoulos KD. Visualization of water transport in W-1/O/W-2 emulsions. Coll Surf A 2000b;174(1–2):159–167.

Wen LX, Papadopoulos KD. Effects of osmotic pressure on water transport in W-1/O/W-2 emulsions. J Colloid Interface Sci 2001;235(2):398–404.

Wu RC, Papadopoulos KD, Campbell CB. Visualization test for neutralization of acids by marine cylinder lubricants. AIChE J 1999;45(9):2011–2017.

Wu RC, Campbell CB, Papadopoulos KD. Acid-neutralizing of marine cylinder lubricants: effects of nonionic surfactants. Ind Eng Chem Res 2000a;39(10):3926–3931.

Wu RC, Papadopoulos KD, Campbell CB. Acid-neutralizing of marine cylinder lubricants: measurements and effects of dispersants. AIChE J 2000b;46(7):1471–1477.

Zhu P, Papadopoulos KD. Visualization and quantification of two-phase flow in transparent miniature packed beds. Phys Rev E 2012;86(4):046313.

9

JAMESON CELL TECHNOLOGY FOR ORGANICS RECOVERY

GRAEME J. JAMESON

9.1 INTRODUCTION

When a major oil spill occurs at sea, the amount of oil that reaches nearby shores, the time it takes to reach land, and the length of coastline affected will depend on numerous factors. The nature of the oil and debris that have to be remediated is similarly contingent on a variety of influences. Nevertheless, it can be said that the pollution will take various forms, including oil and oily wastes, seaweed, plastics, wood, and dead birds and animals. Oily waste that has been washed ashore could also affect the sand and soil, the pebbles and gravel, and the rocks on the beach. Furthermore, materials that have been used to adsorb and collect the spilled oil, such as straw, plastic foam, and porous beads, must also be removed and treated.

If the oily waste is collected and concentrated, it is inevitable that seawater will be associated with it. The oil will probably be emulsified to some extent, through the action of natural surfactants in the sea and dispersing agents that could be used to break up oil slicks. Thus, one of the tasks that could be necessary is the separation of oil with a wide range of boiling points, emulsified or otherwise dispersed, from the associated seawater.

The mineral industry is accustomed to handling large volumes of aqueous suspensions and separating particles from them. Apart from gravity separations, the process most commonly used is froth flotation, in which the particles to be recovered are rendered water repellant (hydrophobic) and then introduced into a tank with air bubbles. The bubbles attach themselves to the hydrophobic particles and carry them to the top

Oil Spill Remediation: Colloid Chemistry-Based Principles and Solutions, First Edition.
Edited by Ponisseril Somasundaran, Partha Patra, Raymond S. Farinato, and Kyriakos Papadopoulos.

of the vessel to form a froth layer, which then flows out of the cell. Examples where organic species are recovered include the solvent extraction process for recovering metal ions from solution by sequestration into hydrocarbon solvents and subsequent elution back into an acid solution prior to electrolysis and the recovery of hydrocarbons in the extraction of hydrocarbons from oil sands. The challenges faced in these processes include the following:

- Large volumes of feed to be processed, up to 3000 m^3/h (792,000 US gallons/h)
- Ionic species in the feed, such as salt in seawater, or metallic ions in acid solutions
- Sand and silt in suspension
- Highly variable feed conditions, relating to flow rate and organic content

All these have their counterparts in oil spill cleanup.

The Jameson Cell (Jameson, 1988) was developed initially for the recovery of ultrafine coal particles from waste streams in the coal industry and has also been applied for the recovery of hydrocarbons. Here, several examples of the use of the Jameson Cell for the recovery of hydrocarbons is described, including in the solvent extraction and electrowinning (SX-EW) process for copper refining, and the recovery of middlings in the primary separation of oil from oil sands.

9.2 FLOTATION AND WATER TREATMENT

There are two major types of flotation: dissolved air flotation (DAF) and induced air flotation (IAF). In the former, part of the tails from the flotation vessel is aerated under pressure, becoming saturated with air. The recycle stream is returned to the flotation vessel through a small orifice. When the pressure is released, the gas comes out of solution in the form of very small bubbles that are highly effective for capturing floatable particles. The DAF process is characterized by the formation of small bubbles of order 50 μm in diameter; low air flows that are limited by the solubility of air in the liquid; high pressures in the recycle line, typically 60 psig; and long residence times in the flotation vessel.

In the IAF process, air is dispersed into the liquid to be treated by a mechanical means such as an impeller or a plunging jet. The bubbles are not so large as those found in the DAF process, being typically in the range 0.3–2 mm. Consequently, these bubbles are not so difficult to disengage from the liquid in the cell, so the residence times are shorter. The air comes from the atmosphere, and the ratio of the air flow rate to the flow rate of liquid can be much higher than found in the DAF process. Induced air flotation machines include mechanical flotation cells, pneumatic cells, and the Jameson Cell.

9.3 THE JAMESON CELL FOR OIL FLOTATION

Figure 9.1 shows the principles of operation of a Jameson Cell. Feed is pressurized to 15–20 psi and introduced to the head of a vertical pipe in the form of a high-speed jet. Air is entrained from the atmosphere and is dispersed into fine bubbles by the shearing action of the jet, which also serves to bring the feed particles into close

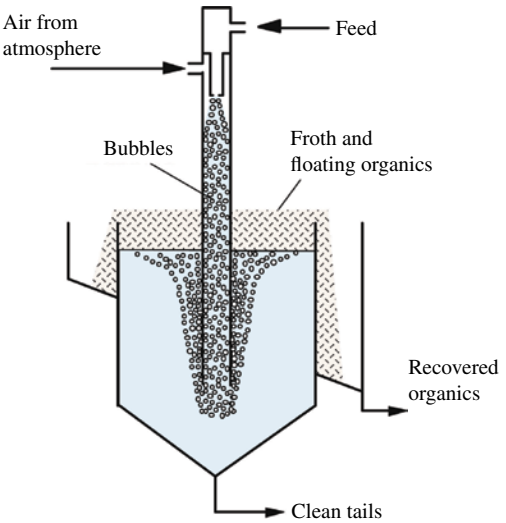

FIGURE 9.1 Schematic of a Jameson Cell.

contact with the bubbles. The aerated mix discharges into the cell, which acts as a disengagement vessel. Thus, the bubbles rise to the top of the vessel to form a froth layer carrying the floatable particles, and the cleaned liquid discharges out of the base of the vessel as the tailings.

The design of the feed nozzle is important to minimize wear. Figure 9.2 shows the design currently in use, which has evolved over many years of testing and operation.

A full-scale version of a Jameson Cell is shown in Figure 9.3. The figure shows only two downcomers, as the vertical injection tubes are known, for simplicity. For mineral and coal processing, versions are available with up to 24 standard 280 mm downcomers, with a total capacity of 1920 m^3/h (510,000 US gallons/h). Larger downcomers are also available, with three times the capacity, reducing the number required proportionately. In the version shown in Figure 9.3, two launders are used to collect the froth product—one external to the cell and the other internal. The largest cells currently in operation have a diameter of 6.5 m (21 ft).

9.4 JAMESON CELLS IN SOLVENT EXTRACTION TREATMENT

Figure 9.4 shows a typical circuit for the recovery of organic extractant from copper-loaded electrolyte. The organic is a hydrocarbon with properties similar to kerosene. It is used as a carrier for copper ions, removing them selectively from an impure leach liquor that may contain many other ions and carrying them to another part of the circuit where they are transported back into an aqueous acidic solution, from which they can be deposited electrolytically in the form of metallic copper. The hydrocarbon is valuable because it contains special reagents that can facilitate the transfer of copper ions in and out of the organic phase. During transfer, the organic is vigorously mixed with the aqueous solution, and it is inevitable that some of the hydrocarbon forms an emulsion,

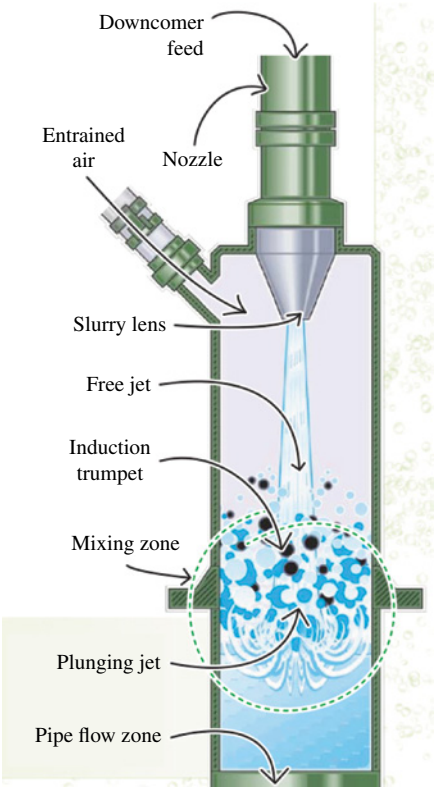

FIGURE 9.2 Expanded view of the injection nozzle and slurry lens. *(See insert for color representation of the figure.)*

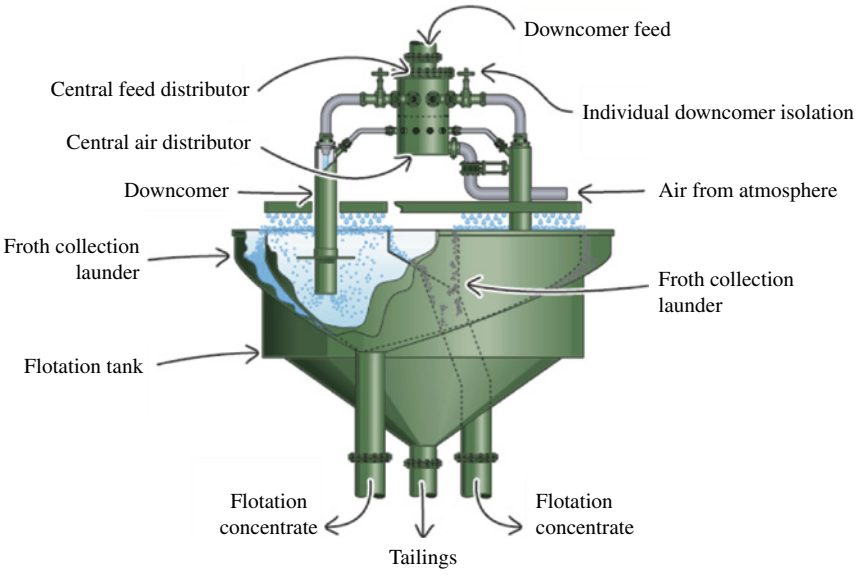

FIGURE 9.3 A full-size Jameson Cell. *(See insert for color representation of the figure.)*

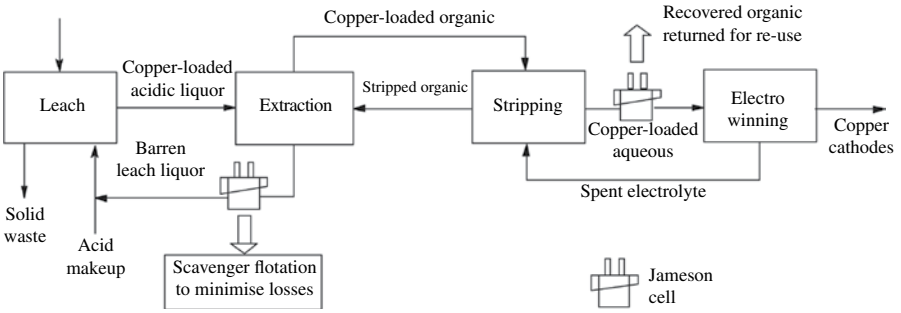

FIGURE 9.4 A typical circuit for removal of emulsified hydrocarbon during the electrolytic extraction of copper from leach liquor.

FIGURE 9.5 Patches of recovered oil are seen floating on top of the blue copper sulfate solution prior to electrolysis. *(See insert for color representation of the figure.)*

with deleterious consequences. If the organic remains in the electrolyte, it tends to disfigure the copper as it deposits on the cathode in the electrolytic cell, spoiling the bright-red appearance. Also, the reagent and the hydrocarbon are expensive, and it is desirable to be able to recover them both, to be recycled to the head of the circuit, and to be used again. For this function, the Jameson Cell has been found to be very useful. In the circuit shown in Figure 9.4, the Cell is used in two places, firstly to float the hydrocarbon emulsion from the copper-loaded aqueous solution prior to electrolysis and, in a scavenging function, to remove as much as possible of the hydrocarbon from the recycle stream prior to entering the leach process with makeup acid.

The photographs of Jameson Cells in use for recovery of organics from solvent extraction liquors are shown in Figure 9.5 and Figure 9.6. In the installation shown in Figure 9.5, the liquor contains a relatively small concentration of oil, up to 1000 ppm, so the volume of oil recovered is not great. Oil attached to bubbles rises into the froth

FIGURE 9.6 A large Jameson Cell for treatment of solvent extraction liquor, at Cananea, Mexico. This cell has a rated capacity of 2800 m^3/h (740,000 US gallons/h).

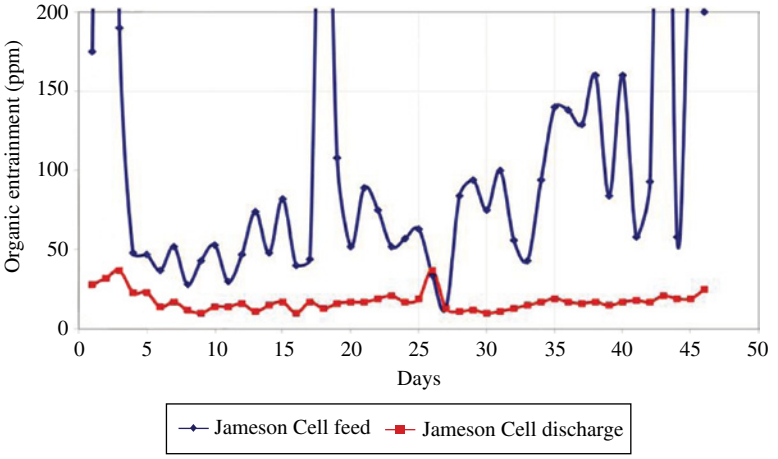

FIGURE 9.7 Measured value of the hydrocarbon before and after flotation. *(See insert for color representation of the figure.)*

layer, where it aggregates into brown islands. There is insufficient oil to warrant the withdrawal of a continuous stream of the froth layer, so the oil is allowed to build up for removal once a day or as required. Figure 9.6 shows a single cell with large downcomers of capacity 240 m^3/h each. The installation draws its air from the atmosphere, giving a considerable saving in operating cost compared with a dissolved air system, where a compressor is needed to dissolve the air at a pressure of typically 300 kPa (60 psig).

The operating data over a 6-week period are shown in Figure 9.7. The concentrations of oil in the feed and the treated liquor were monitored on a daily basis for a period of 2 months. Although the feed was highly variable, the oil concentrations in the treated effluent were generally on the order of 20 ppm.

9.5 OIL SAND FLOTATION

The recovery of useful oil from the extensive sand deposits in Alberta, Canada, poses problems that are similar in many ways to the recovery of hydrocarbons from oil spills. In the oil sands, the oil is commingled with fine wet sand particles. To separate the oil from the sand, an aggressive chemical regime is used, working at high temperatures on the order of 85°C, in a high-shear environment. The resulting product passes to a gravity separation vessel. Here, a layer of mainly free oil is formed above an aqueous phase. Solids settle to the bottom of the vessel. However, there are some particles that are a mixture of oil and sand in such proportions that their density is close to that of water, so they form an intermediate or middlings layer in the settling tank. The middlings layer contains valuable oil that will not separate by long-term standing, so an alternative process that does not depend on density, such as flotation, is required.

Figure 9.8 shows a flow sheet in which conventional mechanical cells are used for recovery of oil from a preconditioned feed. The majority of oil droplets are free from the sand solids and can be recovered by a simple gravity separation. However, a substantial amount of oil remains in the middlings layer in the center of the primary separation vessel (PSV). This stream flows to a flotation circuit not unlike that found in a base metal concentrator.

In the mechanical cell flow sheet, a bank of cells is required, each of three or four units. The cells have large volumes, typically 150–300 m^3 (5300–10,600 ft^3). The

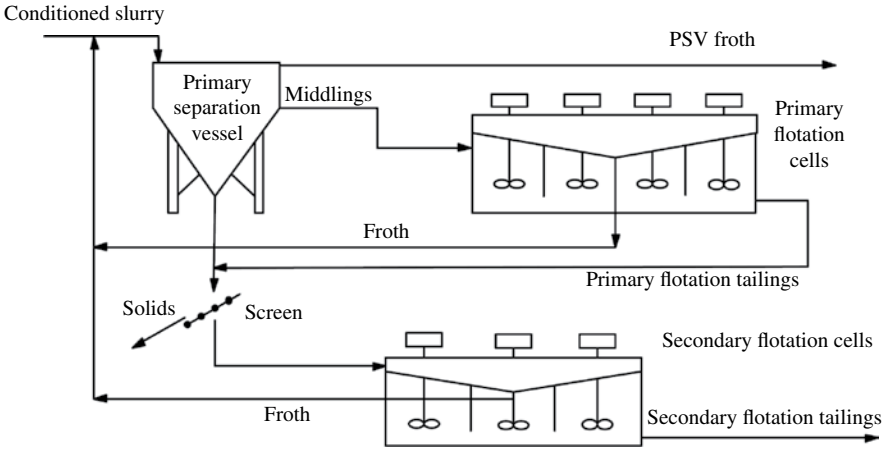

FIGURE 9.8 Flow sheet for recovery of oil from a preconditioned feed, using conventional mechanical cells.

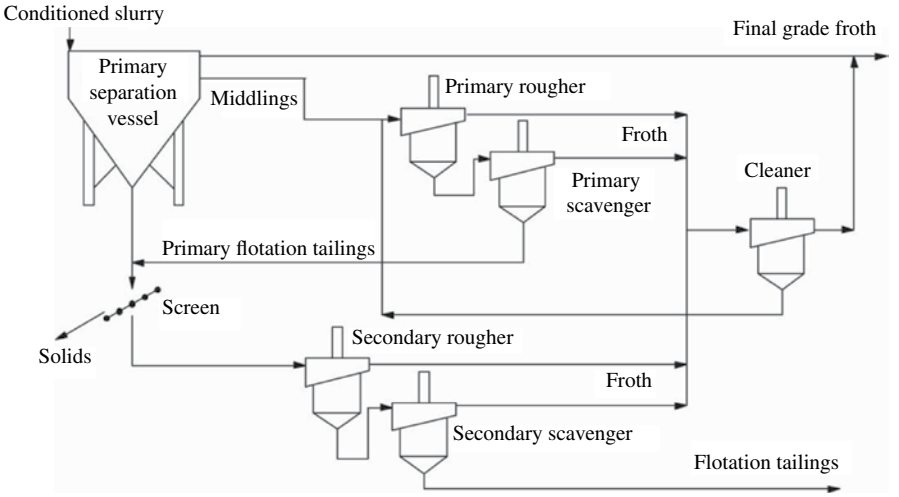

FIGURE 9.9 Flow sheet for treatment of the middlings stream in an oil sand recovery process, using the Jameson Cell.

circuit is configured for recovery rather than grade or product purity. Mechanical cells are not particularly efficient for recovering fine particles and emulsions, so large residence times are needed.

Figure 9.9 shows an alternative flow sheet using the Jameson Cell. The purpose of the circuit is to recover as much oil as possible, with the least contamination by siliceous matter. This is achieved by a primary rougher–scavenger combination, followed by a secondary combination that also treats the fine solids from the base of the gravity separator. The froth products from the four rougher–scavenger cells are diluted with clean water and given a final polish in the cleaner cell. Because of the intense mixing that takes place in the downcomer, the Jameson Cell is highly efficient. Thus, the contact time in the downcomer is typically on the order of 10 s, while in the cell as a whole, it is 1.5–2 min.

The primary rougher alone achieves a grade of 20–40% bitumen, at a recovery of 60–80%, while the primary scavenger product has a grade of 10–20% at a recovery of 40–70%, depending on the air supply rate. The primary circuit alone achieves recoveries in the range 80–90%. The primary tailing grade is 0.1–0.2% bitumen. Additional recovery is achieved in the secondary treatment circuit.

9.6 SUMMARY

The management of oil and associated debris resulting from spills at sea poses particular problems ranging from the collection and segregation of the oil itself while still floating to the treatment of beached oil that will be mixed with sand, pebbles, plastic waste, and dead birds, fish, and mammals. Part of the treatment chain will involve the separation of oils of a range of boiling points and viscosities, from

contaminated seawater. The volumes of liquid to be treated can be quite large. There are similarities with the mining industry, where huge tonnages of crushed and ground rock must be processed in suspension in water, to recover relatively small amounts of valuable mineral. Over the past 100 years, the flotation process has been successfully applied to the recovery of base metal particles, and flotation has also been applied to the recovery of organics.

In this chapter, the use of a particular device, the Jameson Cell, for the separation of emulsified oil droplets and bitumen from process streams is described. One example is the removal of a kerosene-like hydrocarbon from pregnant liquor in the solvent extraction process for recovery of copper from acid solutions. The concentrations of organics are generally low, perhaps 100–1000 ppm, but the flow rates of liquor to be treated are high. The hydrocarbon is recovered because it interferes with the electrolytic process and also because it is a high-value reagent. In one installation in a solvent extraction plant, a single Jameson Cell is in use for treatment of 2800 m^3/h (740,000 US gallons/h).

Another example is in the recovery of bitumen and other hydrocarbons, in the Canadian oil sand industry. The hydrocarbons as-mined are mixed intimately with water and siliceous rock particles, from which they are liberated by a combination of chemical treatment at high temperature and high-shear mixing. The resulting oily water is first separated in a simple gravity treatment tank, in which a middlings layer is formed that has the same density as water, so it will not respond to gravity. The Jameson Cell has been used successfully to treat this middlings stream, to produce a high-grade hydrocarbon product, and siliceous particles that are sent to waste.

ACKNOWLEDGMENTS

The Jameson Cell is licensed to Xstrata Technology, of Brisbane, Australia, with offices in Vancouver, Santiago, Johannesburg and London. Assistance from Le Huynh of Xstrata Technology in the preparation of this chapter is gratefully acknowledged.

REFERENCE

Jameson GJ. New concept in flotation column design. Miner Metall Process 1988;5(1): 44–47.

10

DEVELOPMENT OF GELLING AGENT FOR SPILLED OILS

KAZUTAMI SAKAMOTO

10.1 INTRODUCTION

In Santa Barbara right off the UCSB campus, there is a shore called the Coal Oil Point. As the name explains, we could smell oil as though we were at a gas station. This is a place where oils come up from the offshore seabeds as the Marin Hydrocarbon Seeps Oil Point near Santa Barbara, California lie the worlds most active and most studied marine hydrocarbon (oiland gas) seeps (Leifer, 2004) and the sand is slightly sticky with oil slicks.

Although the oil-soaked shore has been there long before human civilization, its effects are small, and the beautiful coast of Santa Barbara makes it one of the most attractive places to live in and to visit. Along the coastline, one can find offshore oil rigs that pump up crude oil, which is why I made a visit during the late 1980s a few years after the Exxon Valdez oil spill in Alaska.

I went to Valdez, Alaska, right after the accident with the delegation team from Japan, which intended to introduce an oil-gelling agent approved in Japan for the treatment of the spilled oil. The team was guided by Leonard Walde (Len), president of Sigma Environment Engineering, a start-up company for environmental protection. We had nothing to do at Alaska at that time as we were unable to reach the EPA, local government agent, or Exxon representatives to show our experiences in Japan. Valdez, a small town remote from Anchorage, was filled with recreational vehicles (RVs) even at the curve side though it was still very cold and too early for vacation.

Oil Spill Remediation: Colloid Chemistry-Based Principles and Solutions, First Edition.
Edited by Ponisseril Somasundaran, Partha Patra, Raymond S. Farinato, and Kyriakos Papadopoulos.

It was filled with people who drove all the way from Anchorage to work on cleaning the affected area or to offer some help in the aftermath of the disaster.

After a year or so, Len and I drove down to Santa Barbara from San Francisco in his pickup truck filled with experimental gear to do a demonstration of the oil-gelling agent for the people at the oil company responsible for the treatment of spilled oil. Although, I don't remember the details of the event, we failed to get a positive response.

This chapter is prepared to introduce an episode of the discovery and the development of the gelling agent for the treatment of spilled oils so as to minimize environmental damage. I believe there are some lessons we can learn for the development of a green and sustainable way for the treatment of oil spills.

10.2 DISCOVERY OF CHIRAL SELF-ASSEMBLY OF AMPHIPHILES DERIVED FROM OPTICALLY ACTIVE AMINO ACID

Sometime in 1972, at the Central Research Laboratories of Ajinomoto Co., Inc., I was trying to purify a crude material I had synthesized from glutamic acid and fatty acid as a promising new surfactant mild to skin and gentle to the environment. A problem I faced was that the material became an organic gel instead of a solid crystal. Namely, acylglutamic acid (LGA) treated in benzene turned to a gel with an iridescent color. Eventually, I found this gel to be an early example of lyotropic cholesteric liquid crystal as a self-assembly of chiral surfactant L-LGA (Sakamoto, 1980; Sakamoto et al., 1978).

It was a time when Ajinomoto, as a leading manufacturer of amino acids in the world, was conducting projects to develop functional materials from amino acids for industrial applications (Sakamoto, 2011) and coincidently my colleague in a different team found a similar property but even stronger gel formation for the molecule abbreviated as LGDB as a derivative of L-LGA (Fig. 10.1). In Section 10.3 the development of the gelling agent based on LGDB will be introduced, and here we continue the exploration of the mechanism of how these molecules make oil gel.

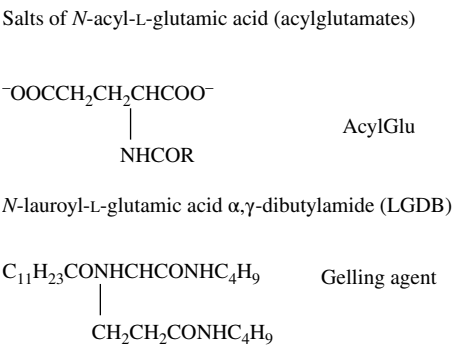

FIGURE 10.1 Chemical structure of *N*-acyl-L-glutamic acid (LGA) and gelling agent (LGDB).

As shown in Table 10.1, L-LGA (*N*-lauroyl-L-glutamic acid) is derived from L-glutamic acid, one of the natural amino acids, with lauroyl chloride. Prior to the discovery of this organic gel, we found the formation of chiral micelles for the series of optically active acyl amino acid salts, including L-LGA salts in aqueous solution (Fig. 10.2) (Sakamoto, 2005; Yoshida et al., 1975).

Bearing this chiral self-assembly in mind, I continued the analysis of the organic iridescent gel made by LGA and benzene or toluene and found a strong wide range of circular dichroism (CD) spectra which polarity depends on the molecular chirality (Sakamoto et al., 1978) as shown in Figure 10.3.

TABLE 10.1 Synthesis of *N*-acyl-L-amino acids by Schotten–Baumann method[a]

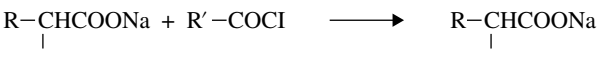

R			R′			
	H	Gly		$C_{11}H_{23}$	Lauroyl	L
	CH_3	Ala		$C_{13}H_{27}$	Mytlstoyl	M
	$CH(CH_3)_2$	Val		$C_{15}H_{31}$	Palmitoyl	P
	CH_2Ph	Phe		$C_{17}H_{35}$	Stearoyl	S
	$(CH_2)_4COOH$	Glu				

[a]Reproduced with kind permission from the Japan Oil Chemists' Society.

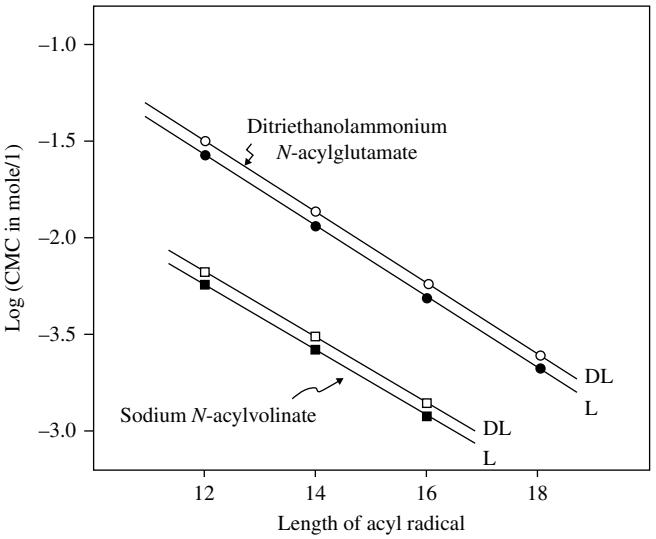

FIGURE 10.2 Relationship between log(cmc) and number of carbon atoms for *N*-acyl amino acids at 40°C: ○, triethanolammnonium *N*-lauroyl-L-glutamate; ●, triethanolammnonium *N*-lauroyl-DL-glutamate; □, sodium *N*-acyl-L-valinate; ▲, sodium *N*-acyl-DL-valinate. Reproduced with kind permission from Japan Oil Chemists' Society.

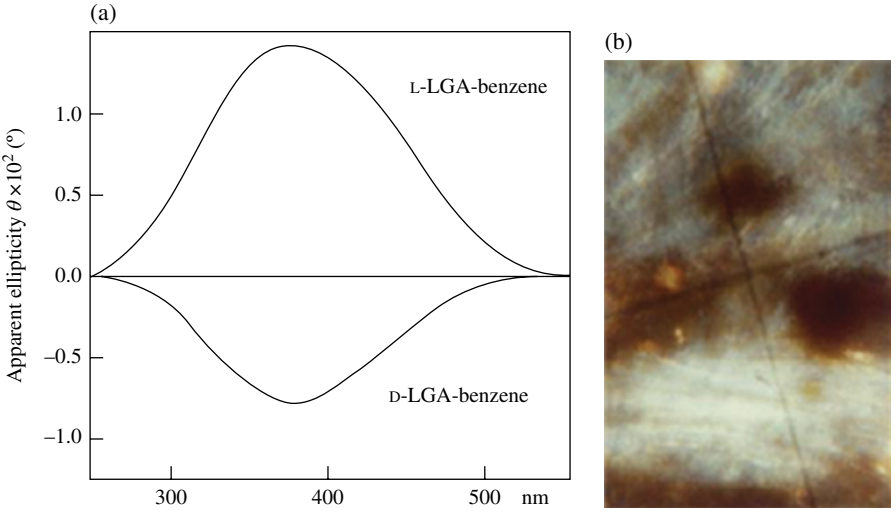

FIGURE 10.3 Properties of iridescent gel composed of *N*-lauroyl-L or D-glutamic acid (L- or D-LGA): (**a**) circular dichroism (CD) spectrum of L- or D-LGA as a lyotropic liquid crystal and (**b**) texture of iridescent gel (L-LGA and benzene) under polarized microscope. Reproduced with kind permission from the Japan Oil Chemists' Society.

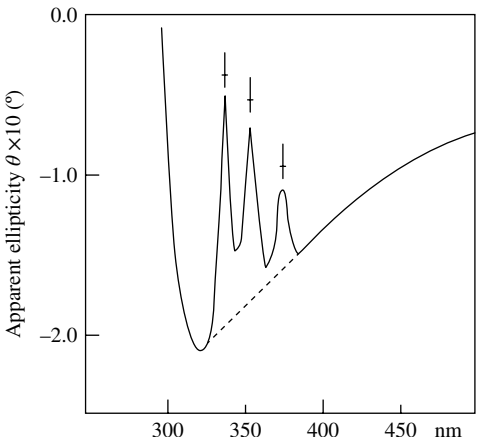

FIGURE 10.4 Induced circular dichroism (ICD) for anthracene (2×10^{-3} M) solved in the L-LGA/benzene system as a cholesteric liquid crystal. Reproduced with kind permission from the Japan Oil Chemists' Society.

Achiral molecules—such as anthracene—dissolved in the iridescent gel showed an induced CD (ICD) spectrum (Fig. 10.4) (Sakamoto, 2006). As a result, these gels are assigned to be a lyotropic cholesteric liquid crystal that has a hierarchical chiral structure induced by LGA's molecular chirality. On the other hand, racemic LGA (DL-LGA) neither formed a gel nor showed CD spectra.

Eventually, I developed a general hypothesis of three elemental requirements to construct hierarchical chiral self-assemblies. At first, the molecule as a unit of chiral self-assembly must be optically active or, in other words, must have an asymmetric structure. Second, the molecule must bear donors and acceptors to form intermolecular hydrogen bonds through an optically active center so that the resulting hydrogen bond expands the asymmetric geometry to the assembled molecules. The third requirement is that the molecule should be amphiphilic so that it has an affinity to accommodate the organic molecule to be gelatinized (Fig. 10.5) (Sakamoto, 2006).

All acyl amino acids fulfill these basic requirements and acylglutamic acid and acyl lysine are optimal as they have extra carboxylic or amino group as a point to make an extra hydrogen bond. Further to this hypothesis, LGBD has additional amide bonds to provide three-dimensional chiral hydrogen bond networks. By fulfilling all these features for the general hypothesis, a molecule such as LGBD can turn nonpolar oils to a stiff gel. As an evidence of LGBD oil gel as a lyotropic cholesteric liquid crystal, the CD spectra of L- or D-LGBD gel in benzene are shown in Figure 10.6 (Sakamoto, 2005, 2006). The formation of the hydrogen bond was confirmed for L-LGBD gel with tetrachrolomethane by IR spectra (Fig. 10.7). As shown in Figure 10.8, racemic isomer (DL-LGBD) could not form stiff gel in tridecane, which provides further evidence for the necessity of molecular asymmetry to form oil gel.

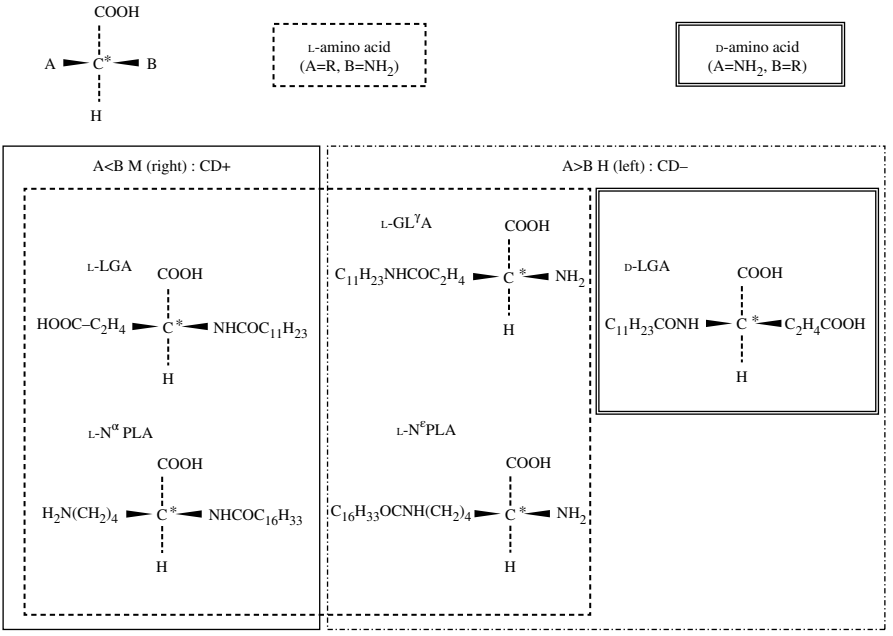

FIGURE 10.5 Schematic description of the configuration of amino acid-based amphotelics and signs of CD spectra of lyotropic cholesteric liquid crystal with nonpolar solvents (Sakamoto, 2006). Reproduced with kind permission from the Japan Oil Chemists' Society (2006).

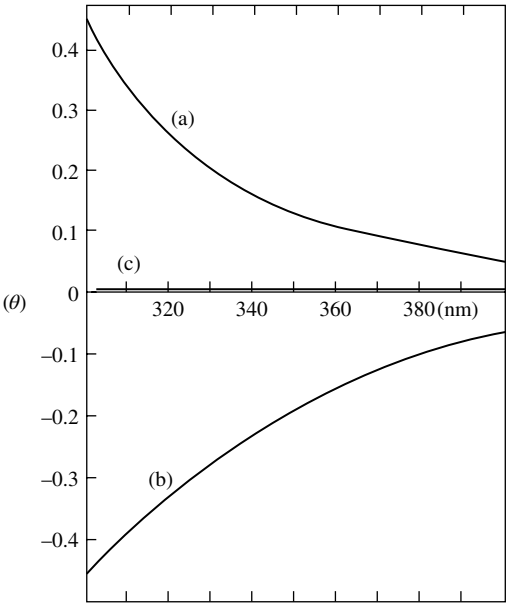

FIGURE 10.6 CD spectra of LGBD/benzene gel (25°C): (**a**) D-LGDB/benzene gel (25°C), (**b**) L-LGDB/benzene gel (25°C), and (**c**) L-LGDB/benzene solution (60°C). Reproduced with kind permission from the Japan Oil Chemists' Society.

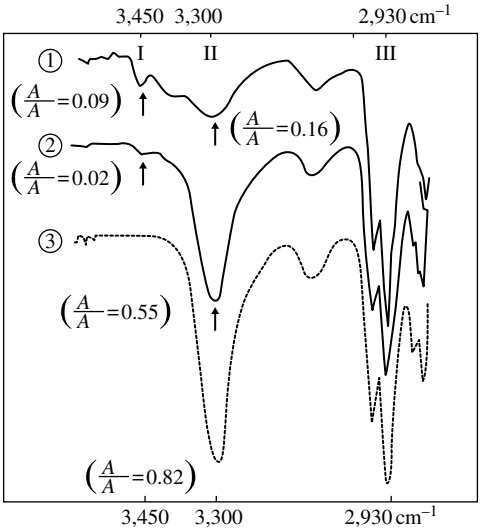

	I/III	II/III
① 0.044 g/dl	0.09	0.16
② 0.22 g/dl	0.02	0.55
③ 2.0 g/dl	–	0.82

I (λ_{3450}) : NH free (Streching)
II (λ_{3300}) : NH hydrogen bond (Streching)
III (λ_{2930}) : CH_2 (Streching)

FIGURE 10.7 IR spectra of L-LGDB/CCl4: ① 0.044 g/dL (solution), ② 0.22 g/dL (oil gel), and ③ 2.0 g/dL (oil gel). Formation of intermolecular hydrogen bond (amide II) was confirmed for oil gel. Reproduced with kind permission from the Japan Oil Chemists' Society.

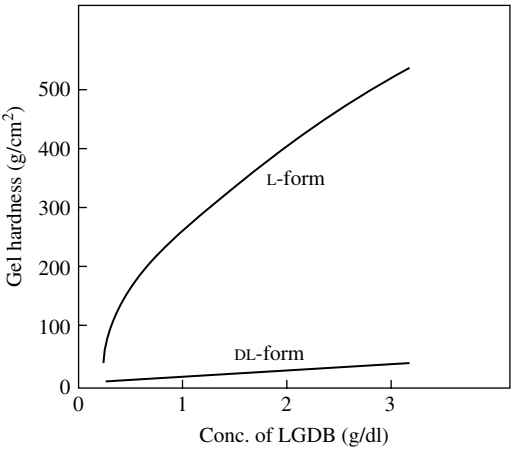

FIGURE 10.8 Difference of the gel hardness for L- and DL-LGDB in tridecane optically active LGDB formed stiff gel in tridecane, while racemic (DL) isomer could not get enough hardness for gel application. Reproduced with kind permission from the Japan Oil Chemists' Society.

10.3 DEVELOPMENT OF OIL GELLING AGENT TO TREAT SPILLED OIL

Research on the application of L-LGBD was conducted extensively at the Central Research Laboratories of Ajinomoto from the late 1970s to the early 1980s. The drawbacks of L-LGBD are its high melting point and high sol–gel transition temperature of gelled oils as shown in Table 10.2 and Table 10.3. These cause difficulties in dissolving L-LGDB into the oils to be gelatinized. A key breakthrough to make L-LGBD a practical gelling agent is the discovery of a solvent system to make L-LGBD a stable solution (Esaki, 2005).

The drawbacks pointed out are due to the strong intermolecular hydrogen bond between L-LGBD molecules, so that the solvents for the gelling agents are designed to have a hydrogen bond breaker such as calcium chloride in alcohol as a good solvent, both for L-LGBD and a hydrogen bond breaker. When this gelling agent is applied to oil spilled in water, L-LGBD dissolves into oil and makes the gel while the hydrogen bond breaker and most of the alcohol dissolves into water, which will not be a pollutant to the extent used in the gelling agent. Thus, the development of the gelling agent based on L-LGBD has succeeded (Fig. 10.9).

10.3.1 Laboratory Scale Test and Field Demonstration of the Agent to Treat Spilled Oil

As shown in Figure 10.10, heavy crude oil floating on the water can be easily gelatinized by adding the agent under gentle agitation. The resulting gel can easily be collected by a net. Gasoline can also be gelatinized, and flammability is dramatically

TABLE 10.2 Gel properties with L-LGDB and types of oils versus gel hardness and pour point[a]

Type of oil	Oil	Gel hardness	Pour point (°C)
Aliphatics	Heavy oil (A type)	149 (g/cm^2)	105 (°C)
	Kerosene	206	106
	Liquid paraffin	52	123
Aromatics	Benzene	156	40
	Toluene	218	59
Halogenated	CCl_4	74	58
hydrocarbon	CCl_2=CCl_2	95	63
Ester	Butyl acetate	71	57
	Dibutylphtharate	100	79
Triglyceride	Olive oil	93	108
	Soy oil	353	109

[a]Reproduced with kind permission from Ajinomoto Co., Inc.

TABLE 10.3 Solubility of L-LGDB to organic oils[a]

Solvent	Solubility g/100 ml	
	at 20°C	at 90°C
Acetic acid	17	NA
$CHCl_3$	15	NA
N-methylpyrrolidone	2.3	>10
Dimethyformamide	0.5	>10
MeOH	1.4	c. 20
n-BuOH	1.4	>10
Cyclohexane	<1	>10
Dioxane	<1	>10

[a]Reproduced with kind permission from Ajinomoto Co., Inc.

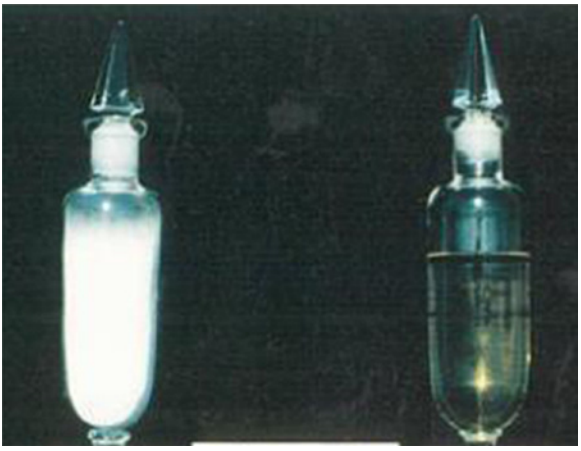

FIGURE 10.9 The oil gelling agent (the Agent). Left: *N*-lauroyl-L-glutamic acid α,γ-dibutylamide (LGDB). Base material for gelling agent, Right: gelling agent (the Agent). Reprinted with permission from Ajinomoto Co., Inc.

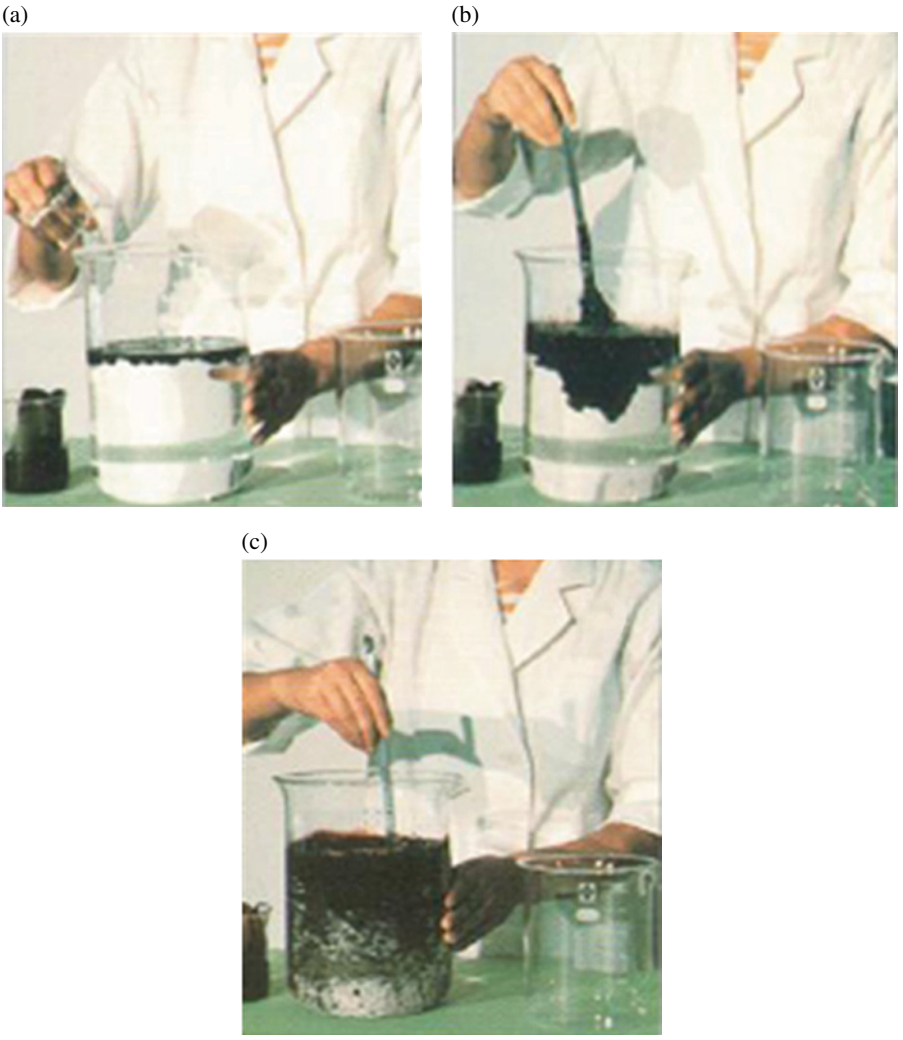

FIGURE 10.10 A method to gelatinize spilled oil. (**a**) Pour the Agent. (**b**) Stir and mix. (**c**) The oil starts to gelatinize after 2–3 min. Gelatinized oil can be easily picked up by the net and drains well. Reproduced with kind permission from Ajinomoto Co. Inc. © Ajinomoto Co., Inc.

reduced as shown in Figure 10.11. As such, the gelling agent would reduce the risk of accidental explosion of spilled gasoline.

10.3.2 System Development for the Spilled Oil Treatment with the Agent

Figure 10.12 shows the design of the system for the tank test. The dimension of the water tank was 4 m wide × 6 m long and the water depth was 0.6 m, which

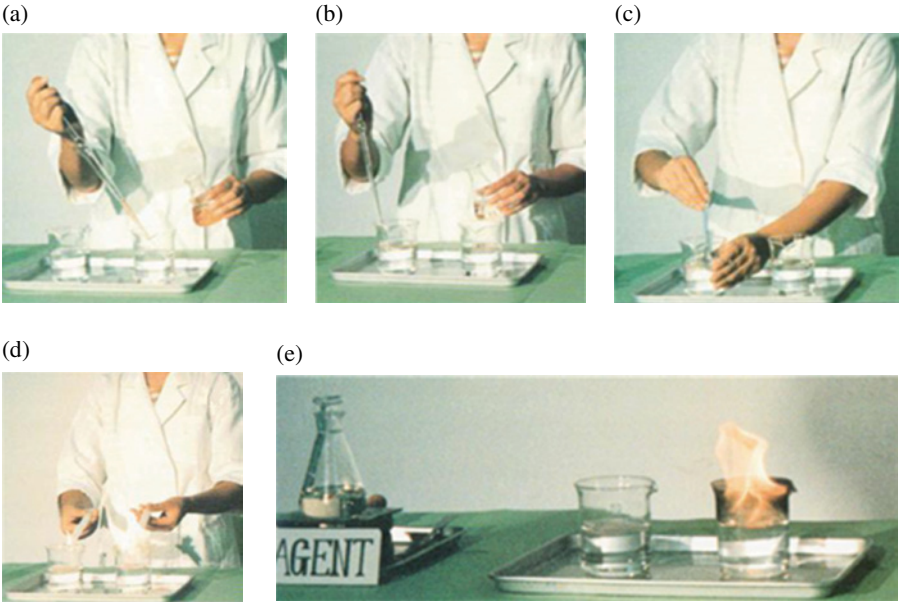

FIGURE 10.11 Flash inhibition for spilled volatile oil by gelling agent (the Agent). (**a**) Pour gasoline into beakers. (**b**) Add the Agent to the left baker. (**c**) Stir and mix to gelatinize the gasoline. (**d**) Hold flames near the surface to flash the gasoline. (**e**) The gelatinized gasoline at the left would not catch the fire. Reproduced with kind permission from Ajinomoto Co. Inc. © Ajinomoto Co., Inc.

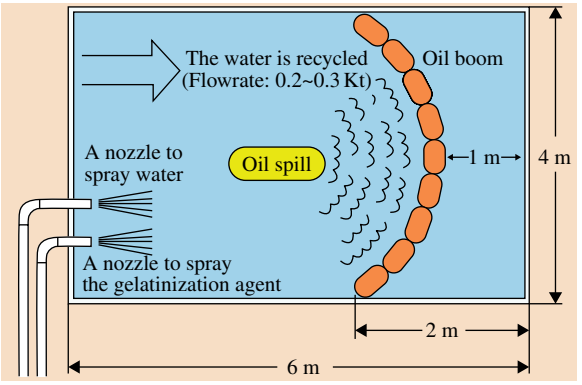

FIGURE 10.12 Outline of the tank used for the experiment (depth of water, about 0.6 m). Reproduced with kind permission from Ajinomoto Co. Inc. © Ajinomoto Co., Inc.

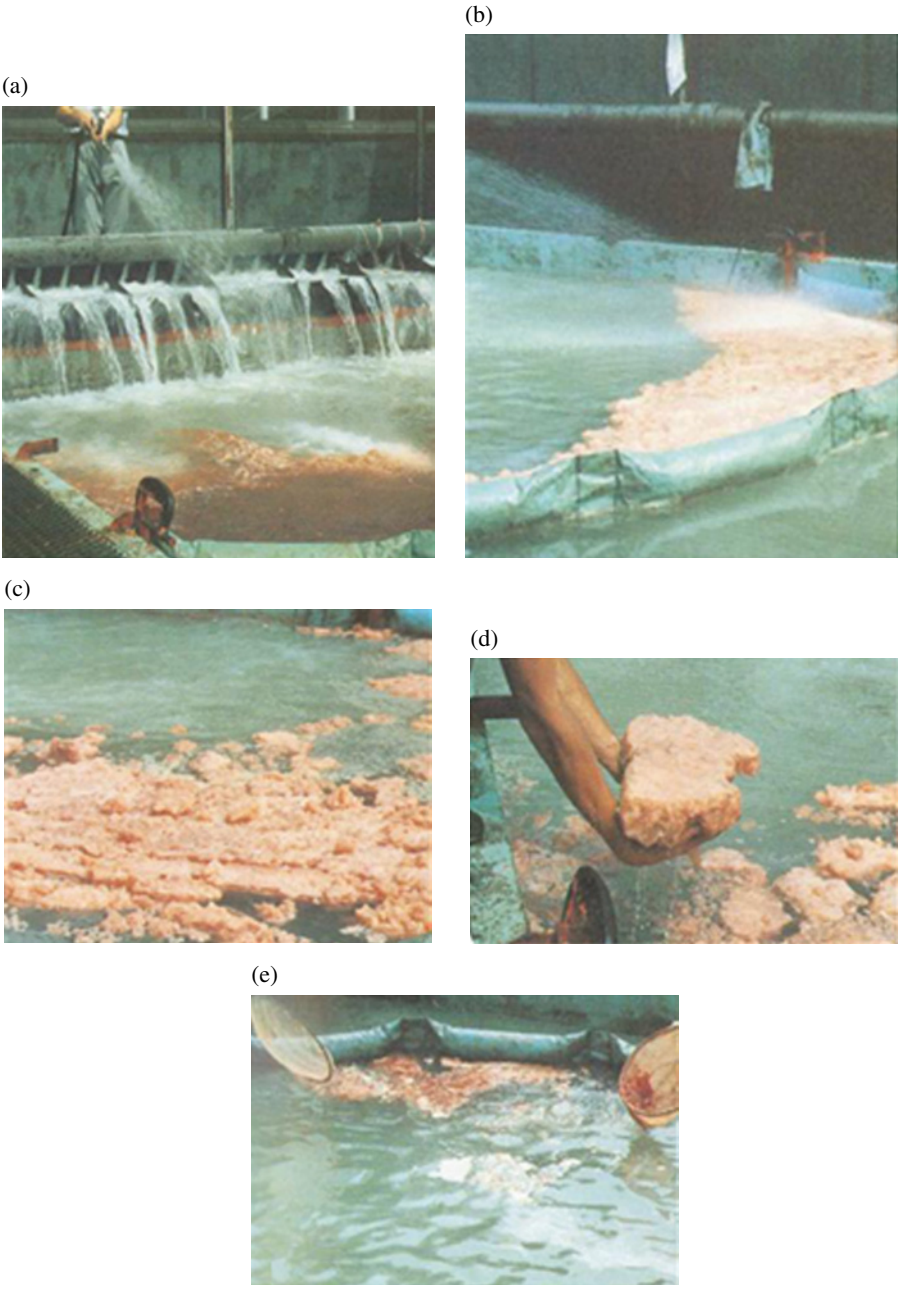

FIGURE 10.13 (**a**) Gelatinization of oils and recovery with a hand net spraying the Agent. (**b**) Spraying water to mix oil with the Agent. (**c**) The gelatinized oil (oil became gel instantaneously by spraying water). (**d** and **e**) Recovery of gelled oil with hand or net. Reproduced with kind permission from Ajinomoto Co. Inc. © Ajinomoto Co., Inc.

was circulated at the flow rate of 200–300 L/h. There were two sprays equipped, one for the agent and the other for water. To treat the oil, the agent was first sprayed uniformly with high pressure in the case of heavy viscous oil and at low pressure for light and fluid oil. Then, water was sprayed along the oil and water boundary towards the oil boom. Figure 10.13 shows the pool test of the system for kerosene. As shown in the picture, oils are effectively gelatinized and collected. Thus, a new treatment system for spilled oil has been established, and this system with the agent based on L-LGDB has been commercialized and endorsed by the Japanese Marine Conservation Agent as one of the systems to be equipped to the ships.

10.3.3 Application of the Agent to the Actual Oil Recovery in Open Sea

For the treatment of spilled oil on open water, a new cleanup system with gelling agent (the Agent) was developed as shown in Figure 10.14. Following are examples of the recovery operation with these systems.

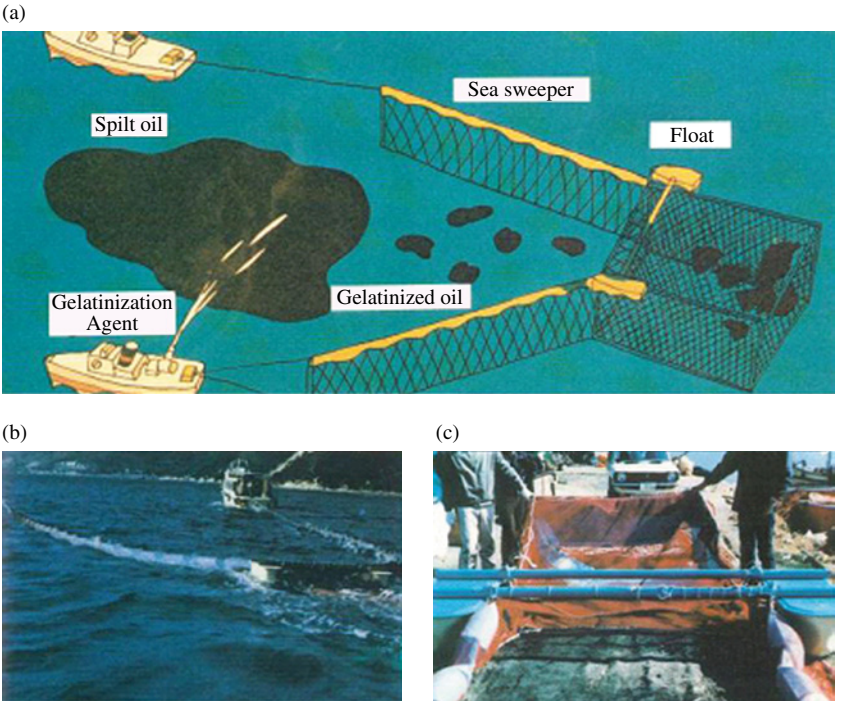

FIGURE 10.14 A new oil cleanup method by the Agent: (**a**) an example of a gelatinization and recovery system, (**b**) towing of Sea Sweeper, and (**c**) floats and the recovery net bag of Sea Sweeper. Reproduced with kind permission from Ajinomoto Co. Inc. © Ajinomoto Co., Inc.

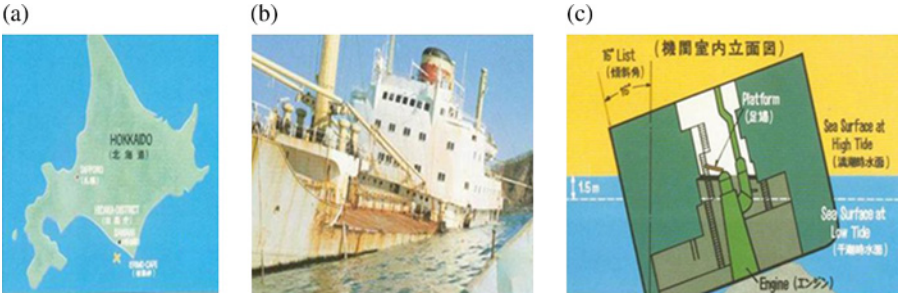

FIGURE 10.15 Recovery operation of oil spill in aground freighter with the Agent. Place: about 500 m off shore from Samani Town, Hokkaido, Japan. Cause: a large ship was run aground on October 19, 1979 during typhoon No. 20. Date of the recovery operation: from April 16 to 25, 1980. (**a**) The place of the accident, (**b**) Chinese freighter "YINGSHAN" 8000 ton, and (**c**) sectional view of the engine room. Reproduced with kind permission from the Ajinomoto Co. Inc. © Ajinomoto Co., Inc.

10.3.3.1 Case 1

In 1979, a large ship was grounded in the midst of fishing beds with marine creatures such as sea urchins in Hokkaido, Japan. Oil had leaked in the engine room, and there was anxiety that oil might flow out of the ship (Fig. 10.15). The oil was gelatinized with the agent within the engine room, collected with a hand net, packed into corrugated cardboard boxes, and carried out to a safe place. The total amount of oil collected was about 14,000 L. No glittering oil film was recognized on the water's surface after the recovery operation. Although there were many negative factors that exacerbated the recovery operation, the recovery was completed by seven persons after 36 h.

Conditions: The water temperature was 1–2°C. The atmospheric temperature was 1–5°C. The ship was under 16 degree list. The oil covered an area of 160 m^2 over the complex engine room plant. And the oil layer rose and fell about 1.5 m according to the tide. Tools used for the operation were small pumps, hand nets, and oil fence. No specially designed or large machines were needed.

The agent effectively gelatinized the spilled oil that had been adhering to inaccessible locations, such as the bottom or the back of machinery as well as pipes and other narrow spaces. The oil stopped oozing and after recovering the oil gel, the water surface was clean and free of any oil film.

10.3.3.2 Case 2

A large ship was grounded at the outer part of the Rumoi harbor in Hokkaido, which continues to the fishing ground and also a seashore resort. Oil had leaked from the double-bottom tank about 6 m under the sea surface, and there was concern that oil might flow out of the fence and soil the fishing ground and the resort. The spilled oil (Heavy oil ASTM No. 6) was gelatinized with the agent as shown in Figure 10.16. After the following process, 6.4 ton of oil was successfully corrected: (i) injection of the agent into the double-bottom tank under the sea surface and the gelatinized oil

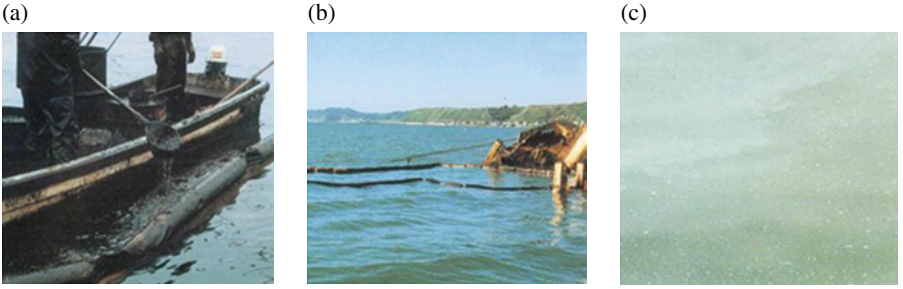

FIGURE 10.16 Recovery of oil spill from aground freighter using the Agent: (**a**) collection of the gelatinized oil with a hand net and (**b** and **c**) the water surface after the treatment. Reproduced with kind permission from the Ajinomoto Co. Inc. © Ajinomoto Co., Inc.

that prevented the liquid oil to floating up to the sea surface, (ii) gelatinization of oil in the vicinity of the oil fence to prevent overflow out of the fence, (iii) spraying of the agent to the thin oil film on the surface for cleaning up, and (iv) spraying of the agent to the oil fence to clean up the fence.

These cases were conducted as trials to validate if the agent and the system were effective for the treatment of spilled oil; the effectiveness of the agent was proven as long as the condition and scale of the spilled oil were appropriate. In reality, there were not many cases reported afterwards, possibly because the cost of the agent was not competitive with the other methods for the cleaning up of spilled oil. In the future, we could expect green chemicals to be developed, which would fulfill the mechanism mentioned in 10.2 and would be economically feasible given the increasing concern for environmental sustainability. Extensive research reported by Hanabusa et al. shows a wide variety of potential molecules in this regard (Hanabusa et al., 1992, 1993). Further, as an example of a derivative from nature's feedstock, the gelling performance of rosin derivatives has been reported (Esaki, 2005).

10.4 CONCLUSIONS

Although the agent was not successful practically for the treatment of spilled oil, L-LGBD and its mechanism of gel formation found applications in the field of cosmetics and household products. L-LGBD has been utilized as a gelling agent for stick-type antiperspirant and is expanding further in cosmetic formulations together with other derivatives. The gelling mechanism of L-LGDB, by the formation of intermolecular chiral hydrogen bonding to construct hierarchical chiral self-assembly, was applied to 12-hydroxystearic acid (Tachibana et al., 1979, 1981), a natural chiral fatty acid from castor oil, and it has been used as a popular household gelling agent to treat wasted fry oil in Japan (Esaki, 2005). As such, we could expect many natural feedstocks as precursors of oil gelling agents, because most elemental molecules in nature such as amino acids, sugars, and even lipids are optically active.

ACKNOWLEDGMENTS

The author gratefully acknowledges Ajinomoto Co., Inc. for approving and providing all the data relating to the development of the gelling agent for the treatment of spilled oil to make this chapter possible.

REFERENCES

Esaki Y. Technical development on rosin type gelling agents for oils. JETI 2005;53(7):77–79.

Hanabusa K, Okui K, Koyama T, Shirai H. A small molecular gelling agent for organic liquids: N-benzyloxycarbonyl-L-alanine 4-hexadecanoyl-2-nitrophenyl ester. J Chem Soc, Chem Commun 1992;(18):1371–1373.

Hanabusa K, Tange J, Taguchi Y, Koyama T. Small molecular gelling agents to harden organic liquids: alkylamide of N-benzyloxycarbonyl-L-valyl-L-valine. J Chem Soc, Chem Commun 1993;(4):390–392.

Leifer I, Boles J, Clark JF, Luyendyk BP. The dynamic nature of marine hydrocarbon seepage. Environ Geol 2004;46(8):1038–1052.

Sakamoto K. Liquid-crystals composed of N-acylamino acids. 2. Influence of crystalline-structure of N-acyl-L-glutamic acid on the formation of liquid-crystals. Mol Cryst Liquid Cryst 1980;59(1–2):59–71.

Sakamoto K. Self organization of amino acid based chiral surfactants: evaluation of organized structures and interaction with biological system. J Oleo Sci 2005;5(12):573–587.

Sakamoto K. N-acylamino acids as chiral surfactant: formation of chiral liquid crystal as soft self-assembly and imprinting of the structure to mesoporous silica as hard material. Liq Cryst (Ekisho) 2006;10(3):284–295.

Sakamoto K. Protein based surfactants. In: Xia and Nnann, editors. *Amino Acid Surfactants: Chemistry, Synthesis and Properties*. Surfactant Science Series Vol 101. New York: Marcel Dekker, Inc, p 75–122, Chapter 4; Sakamoto, K. Current market development and trend in amino acid and protein based surfactants. In: Xia and Nnann, editors. *Amino Acid Surfactants: Chemistry, Synthesis and Properties*. Surfactant Science Series Vol 101. New York: Marcel Dekker, Inc; 2011, p 261–280, Chapter 10.

Sakamoto K, Yoshida R, Hatano M, Tachibana T. Liquid-crystals composed of N-acylamino acids. 1. Circular-dichroism and selective light transmission in cholesteric liquid-crystals composed of N-acylamino acids and organic-solvents. J Am Chem Soc 1978;100(22):6898–6902.

Tachibana T, Mori T, Hori K. New type of twisted mesophase in jellies and solid films of chiral 12-hydroxyoctadecanoic acid. Nature 1979;278(5704):578–579.

Tachibana T, Mori T, Hori K. Chiral mesophases of 12-hydroxyoctadecanoic acid in jelly and in the solid-state.2. A new type of mesomorphic solid-state. Bull Chem Soc Jpn 1981;54(1):73–80.

Yoshida R, Takehara M, Sakamoto K. Surfactants derived from amino acids I. Critical micelle concentrations of the salts of optically active and racemic N-acylamino acids. J Jpn Oil Chem Soc 1975;24(8):538–541.

11

MICROSTRUCTURES OF CAPPED ETHYLENE OXIDE OLIGOMERS IN WATER AND *N*-HEXANE

Mangesh I. Chaudhari and Lawrence R. Pratt

11.1 INTRODUCTION

Dispersant materials used in response to oil spills (Ocean Studies Board (OSD), 2005) undergo a demanding effectiveness approval process, and approved dispersants are stockpiled near drilling activity and possible spill locations. These factors inhibit continuous improvement of dispersants. Rigorous laboratory studies of the molecular–thermodynamic interactions at play in dispersant systems are, therefore, particularly welcome. In addition, effective thermophysical modeling for these systems should improve the fidelity of laboratory-scale simulations of field-scale and ocean-scale oil spill dispersion. A typical prerequisite for development of effective molecularly specific thermophysical models is computational simulation of these solutions on a molecular basis.

Arguably, the most important water-soluble synthetic polymers (Alessi et al., 2005; Norman et al., 2007), $(-CH_2-CH_2-O-)_n$ chain molecules, are also soluble in common organic solvents and are intrinsic to the dispersant materials in use (OSB, 2005). This report establishes molecular-scale microstructures of PEO oligomers in aqueous solutions, information preparatory to molecular-scale theories of the structure and function of these species in solution.

The molecular versatility of PEO/PEG polymers in solution makes them a challenge for molecularly specific statistical thermodynamic theory. For example,

Oil Spill Remediation: Colloid Chemistry-Based Principles and Solutions, First Edition.
Edited by Ponisseril Somasundaran, Partha Patra, Raymond S. Farinato, and Kyriakos Papadopoulos.

their conformations respond sensitively to the solution environment (Alessi et al., 2005; Norman et al., 2007). Common-sized PEO molecules are distinctly helical in *n*-propanoic, isobutyric, and isopentanoic acid solutions coexisting with liquid water (Norman et al., 2007). That helicity emphasizes the contrasting behavior that these chains exhibit generic coil structures in aqueous solutions. Though the helices are not evident in bulk liquid water and indeed also not in acetic acid nor in isobutanol nor in *n*-butanol, helix formation does seem to require at least a trace of water (Norman et al., 2007).

The solvent plays an intrinsic role in solution thermodynamics also. The conformational sensitivity noted earlier is associated with a polymer size fractionation between those coexisting solutions (Alessi et al., 2005; Norman et al., 2007). Experimental evaluation of a Flory–Huggins interaction parameter for PEO/PEG in either water or methanol shows compositional dependence that is substantially different in these two cases (Bae et al., 1993; Zafarani-Moattar and Tohidifar, 2006).

In many applications (Lin and Rubtsov, 2012) and specifically for dispersants used on oil spills (OSB, 2005), the PEO/PEG chains are decorated with junction, head, or capping groups. The work in the succeeding text anticipates those molecular designs but treats explicitly only the simplest capping group, CH_3 (methyl). Correlations associated with capping groups serve to focus structural analyses, and the following work focuses on the radial distributions of capping groups. Alternatively, spatial extensions of chain molecules in solution are often characterized by a mean square radius of gyration $<R_g^2>$, and that information is addressed later for the cases treated. A conclusion we draw from the recent exhaustive treatment of longer alkanes in water (Ferguson et al., 2009, 2010) is that distributions of $<R_g^2>$ are less informative of molecular structure than spatial correlations between chemical groups such as capping groups. The results in the succeeding text should provide further clarification of that issue. We note that single-molecule pulling experiments (Gunari et al., 2007; Li and Walker, 2010, 2011, 2012; Liu et al., 2011; Oesterhelt et al., 1999) are becoming a new source of microstructural information, though not yet at the molecular resolution of interest in the present work. Those important experiments do not track the radius of gyration specifically, but instead manipulate lengths between tethered chemical groups.

Numerous traditional statistical thermodynamic theories of aqueous PEO/PEG solutions have been suggested; some representatives were noted in our initial report (Chaudhari et al., 2010), and we do not attempt a review here. An alternative nontraditional procedure for theory development accepts that simulations are necessary for evaluation of molecular theories of liquids and that simulations will always be carried out in any case, and so the simulation work might as well contribute to formulation of physical theories. Of course, analyses for those purposes must express the natural physical concepts underpinning molecular theories, and those analyses must be sufficiently general. We have elsewhere argued (Chempath and Pratt, 2009) that the recently developed molecular quasichemical theory does achieve those requirements. That molecular quasichemical theory has led over that past decade to resolution of the most basic puzzles of hydrophobic effects (Ashbaugh and Pratt, 2006; Pratt, 2002). It is our intention to establish, for the interesting and important aqueous

solutions considered here, some of the groundwork required for fully defensible molecular theory.

As noted already, direct high-resolution molecular simulations are necessary for the theory development that is sought. Because these systems are of practical

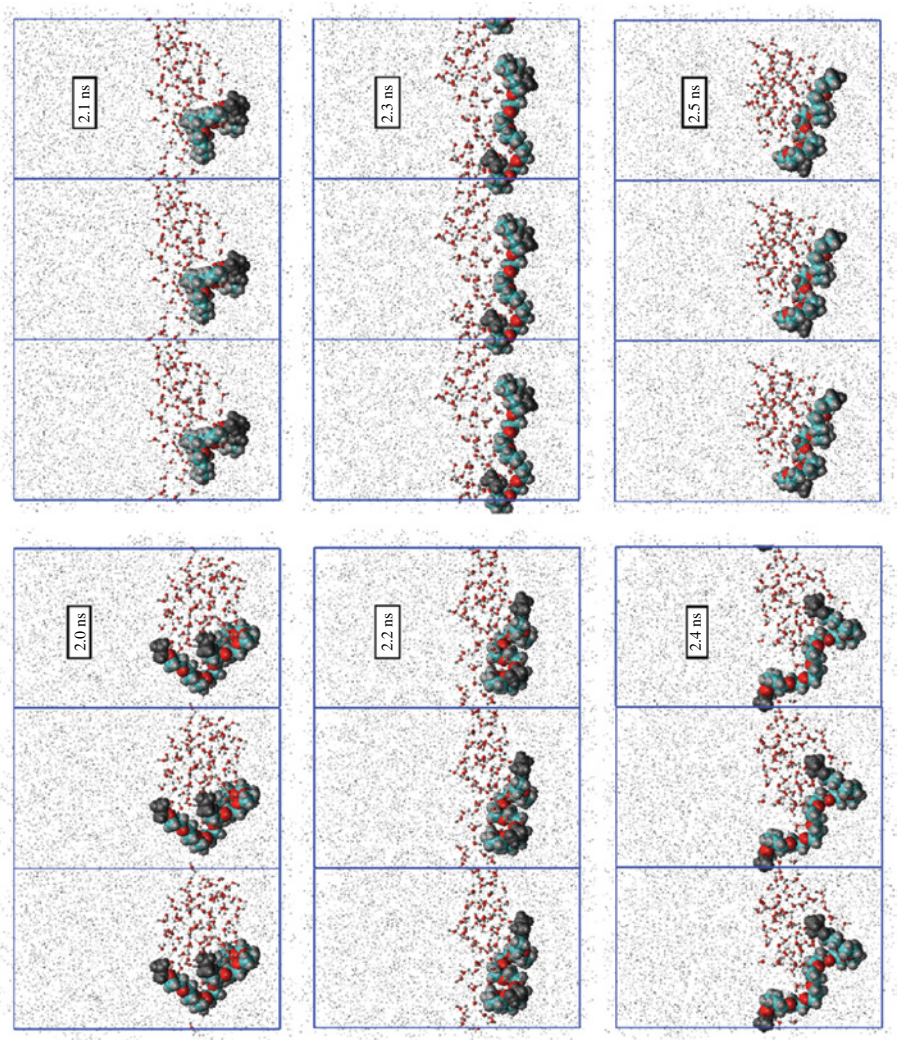

FIGURE 11.1 Formation and then breakup of a fluid column by reconnection across periodic boundary conditions. For visual convenience, three images are shown laterally in each frame. In this case, the droplet/column structure is composed of water with one $CH_3(CH_2–O–CH_2)_mCH_3$ (m = 11) chain molecule (in VDW representation) that here resides near the interface. The majority material in the background is n-hexane. *(See insert for color representation of the figure.)*

importance, a wide range of simulation calculations have been carried out. Again, we do not attempt a review here, but merely note a recent contribution (Starovoytov et al., 2011) that gives access to that substantial available literature. The results here were obtained by combination of standard molecular simulation procedures appropriate for the sampling requirements of different configurational aspects of $CH_3(CH_2–O–CH_2)_mCH_3$ chain molecules in water and *n*-hexane solutions (Chaudhari et al., 2010). Further specific details are provided in the Appendix. We note here that the combined results support comparisons over a range of molecule extensions, between different chain molecule lengths, between different-sized simulation systems, and between water and *n*-hexane solvents.

A curiosity of this simulation work is that with the typical time scales and length scales, it is easy to observe (Fig. 11.1) molecular-scale breakup of a fluid column to produce droplets and then reformation of a fluid column. We hope in subsequent work to return to these observations with further analysis.

11.2 RESULTS AND DISCUSSION

From small to large end-to-end lengths, the observed probability density (Fig. 11.2) displays three distinct behaviors, loop-closure, globule, and high-extension (elastic) regions (Chaudhari et al., 2010). The loop-closure feature is a realization of a primitive hydrophobic bond (Chaudhari et al., 2010), which has been extensively studied by simulation but not yet susceptible to experimental measurement due to solubility limitations (Asthagiri et al., 2008). In contrast (Fig. 11.3), distributions of $<R_g^2>$ are less distinctive of these microstructural features.

For liquid water, the loop-closure feature is largely independent of oligomer size (Fig. 11.4). This feature in liquid water is different from what is observed in *n*-hexane and for nonsolvated chains (Fig. 11.5). These points support the identification of the loop-closure feature as an experimentally realizable hydrophobic bond.

The globule region is clear for the hydrated chains, but not for the case of *n*-hexane solvent (Fig. 11.6). Thus, in the more benign organic solvent, the chains are collapsed relative to the more swollen hydrated oligomers. This also supports the interpretation of intrachain interactions from the perspective of simple aqueous solution examples.

The profiles of the density of chain C-atoms, measured relative to the chain centroid, are different (Fig. 11.7) for the two solvents. For *n*-hexane, the density profiles are similar for the different chain lengths when the distances are scaled by the observed $<R_g^2>^{1/2}$. This similarity does not obtain for the case for water. In water and for the smaller chains studied, the carbon material exhibits a distinctive enhanced concentration in the middle of the distribution, a concentration that is not evident for the case of *n*-hexane. This interesting internal condensation is characterized by a length scale smaller than $<R_g^2>^{1/2}$. Thus, the overall density profiles show less similarity on the $<R_g^2>^{1/2}$ scale, and the internal condensation feature is not evident for the largest $m = 31$ chain.

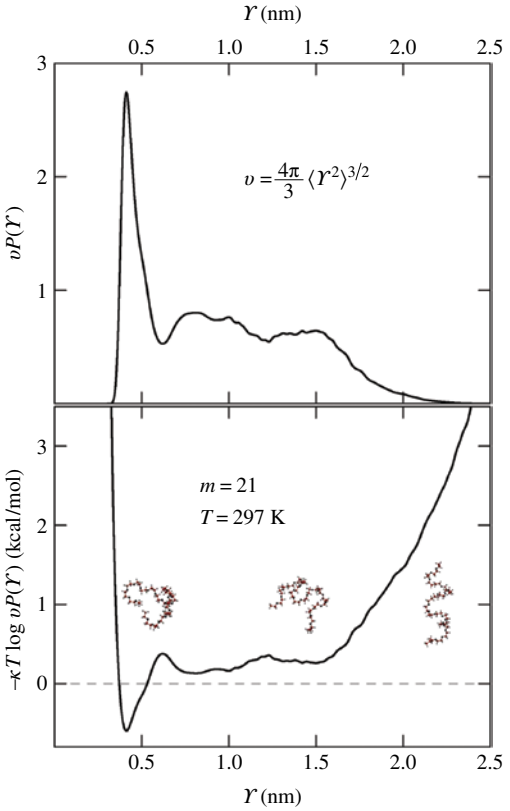

FIGURE 11.2 (Upper) Probability density $P(r)$ for end-to-end (methyl–methyl) length for $[CH_3(CH_2–O–CH_2)_mCH_3](aq)$ with $m = 21$. The normalization of this graph is chosen to suggest the analogy with conventional atom–atom radial distribution function in liquids. (Lower) Potential of the average end-to-end forces showing distinct loop-closure, globule, and high-extension regions. The choice of normalization for the upper panel sets the origin of the y-axis of the lower panel, and the same convention is followed in both cases. Results here for $r < 1.0$ nm were obtained utilizing the WHAM procedure. Those high-resolution results were matched to overall observation of $P(r)$ from molecular simulations with parallel tempering.

11.3 CONCLUSIONS

The probability density for end-to-end distance (and the associated pmf) for $CH_3(CH_2–O–CH_2)_mCH_3$ is more revealing of chain microstructures than are the corresponding results for the radii of gyration. For water, the pmf identifies three distinct regions: loop-closure, globule, and high-extension regions. In water, the loop-closure feature is similar to a primitive hydrophobic bond and is insensitive to chain length. The globule region exposes a water-swollen chain and is not evident in the *n*-hexane results. Chain C-atom density profiles from the chain centroid are different in the water and *n*-hexane cases. For *n*-hexane (but not water), the density profiles are

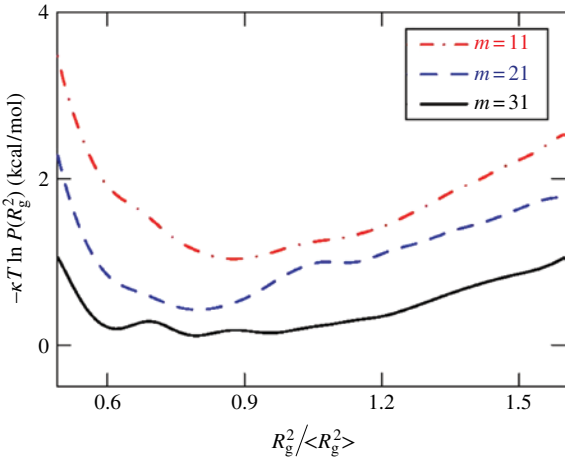

FIGURE 11.3 For $[CH_3(CH_2–O–CH_2)_mCH_3](aq)$, distributions of square radius of gyration displaced vertically for visual convenience, extracted utilizing GROMACS analysis tools. Scaling of the abscissa brings the results for different lengths into a similar range: $\langle R_g^2 \rangle^{1/2} = 0.61, 0.84,$ and 1.22 nm for $m = 11$, 21, and 31, respectively. These values are larger than the ideal $(1/\sqrt{6})$ proportion of the observed $\langle r^2 \rangle^{1/2}$.

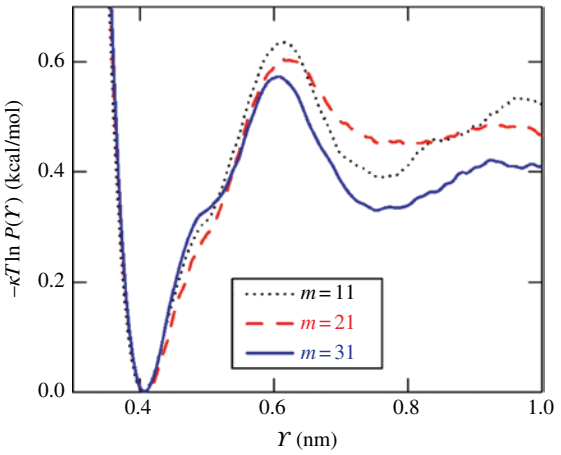

FIGURE 11.4 High-resolution results for $r < 1$ nm for several chain lengths from windowing/WHAM calculations.

similar for the different chain lengths when the distances are scaled by the observed $\langle R_g^2 \rangle^{1/2}$. For water (but not *n*-hexane) and the smaller chains considered, the carbon material exhibits a distinctive, enhanced concentration, or internal condensation, at the centroid core of the structure.

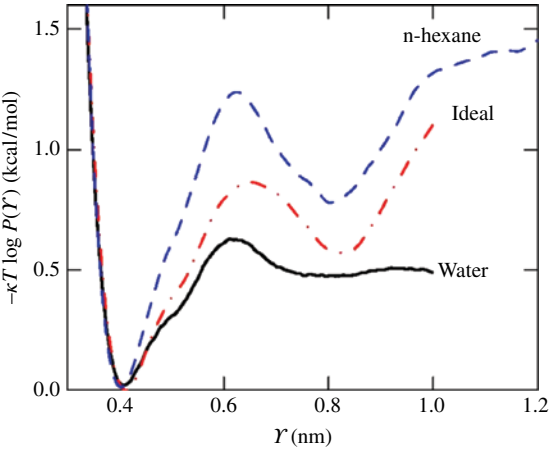

FIGURE 11.5 In the loop-closure region, the $[CH_3(CH_2–O–CH_2)_mCH_3]$ (m = 21) oligomer behaves differently in n-hexane and water, and the results for n-hexane are similar to those obtained with no solvent (ideal gas case). The temperature variation here is small, T = 297 K (water), 302 K (ideal), and 297 K (n-hexane).

APPENDIX: SIMULATION SPECIFICS

Two different simulation techniques were used for the molecular dynamic calculations. The first class of calculations used parallel tempering (Earl and Deem, 2005) to achieve enhanced sampling of the mixing characteristics with water or n-hexane solvent and of $CH_3(CH_2–O–CH_2)_mCH_3$ chain conformations. The chain molecules were represented by a generalized amber force field (GAFF) (Wang et al., 2004), the SPC/E model for water (Berendsen et al., 1987), and optimized potentials for liquid simulations (OPLS-AA) were used to describe n-hexane in those simulations (Jorgensen et al., 1996). GROMACS 4.5.3 molecular dynamic simulation package (Van Der Spoel et al., 2005) was used for all parallel tempering simulations spanning the 256–550 K temperature range with 32 replicas (for m = 11, and 21, cases) and 40 replicas (for m = 31). Long-range electrostatic interactions were treated in standard periodic boundary conditions using the particle mesh Ewald method with a cutoff of 0.9 nm. The Nosé–Hoover thermostat maintained the constant temperature, and chemical bonds involving hydrogen atoms were constrained by the LINCS algorithm. Energy minimization and constant pressure density equilibration was performed at 300 K to set the constant volume conditions, and then, production calculations for each replica set were extended to 10 ns. Parallel tempering swaps were attempted at a rate of 100/ns, and the temperature grid chosen resulted in a success rate of 15–25%.

The second class of simulations obtained higher spatial resolution in the loop-closure region using the windowing stratification method (Shell et al., 2007). In these simulations, a harmonic interaction between the capping atoms of the $CH_3(CH_2–O–CH_2)_mCH_3$

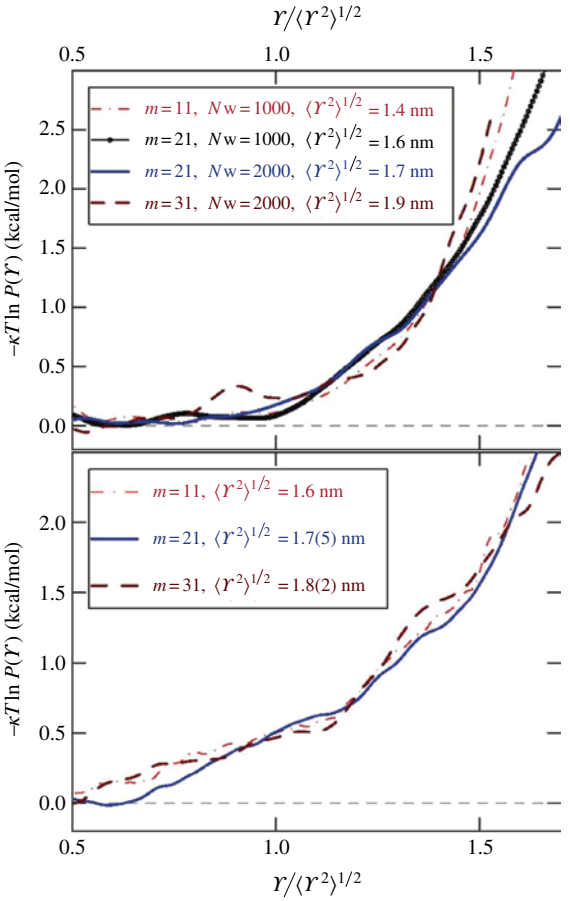

FIGURE 11.6 (Upper) For $CH_3(CH_2–O–CH_2)_mCH_3$ (aq) chains, at constant density corresponding to 300 K and p = 1 atm: parallel tempering results for different chain lengths and system sizes overlap each other on normalized end-to-end distance. Globule and high-extension regions are separated at $r \approx \langle r^2\rangle^{1/2}$ for these chain lengths and system sizes. (Lower) Corresponding results for *n*-hexane at constant density (T = 300 K and p = 1 atm): separation of a globule region and a high-extension region is indistinct here. A Gaussian (parabola) model satisfactorily fits the data in this high-extension regime.

chain was exploited to concentrate the sampling of the end-to-end distance to each particular window. For a $CH_3(CH_2–O–CH_2)_mCH_3$ chain in water or *n*-hexane, we performed simulations with radial displacement coordinate covering the range from 3.0 to 10.0 Å uniformly with 15 windows. Trajectories were recorded for 10 ns/window at the temperature of 297.1 K. $P(r)$ was then reconstructed over the whole range using the weighted histogram analysis method (WHAM) (Shell et al., 2007).

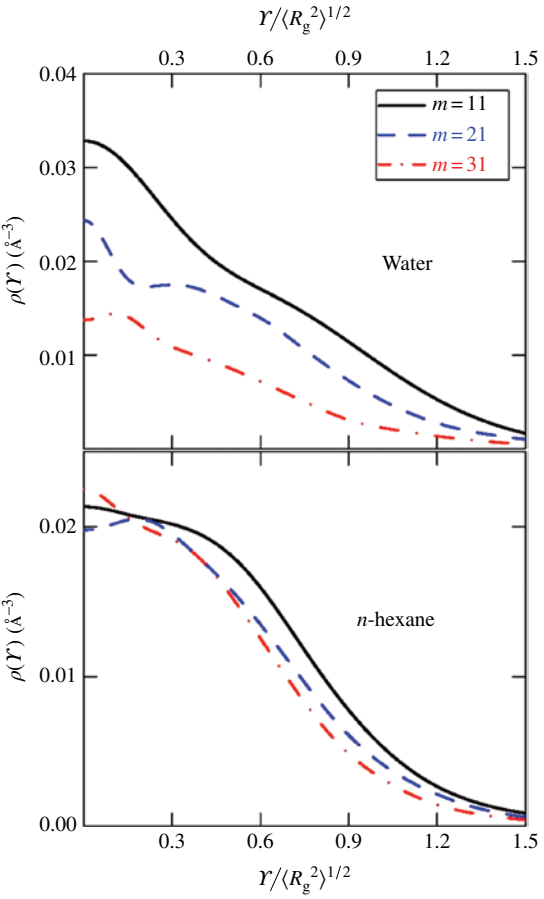

FIGURE 11.7 $CH_3(CH_2–O–CH_2)_mCH_3$ chain C-atom density profiles from the chain centroid shows higher concentrations of polymer C-atoms in water the middle of distribution for the aqueous solutions. That feature is absent for *n*-hexane solvated polymer.

REFERENCES

Alessi ML, Norman AI, Knowlton SE, Ho DL, Greer SC. Helical and coil conformations of poly(ethylene glycol) in isobutyric acid and water. Macromolecules 2005;38(22): 9333–9340.

Ashbaugh HS, Pratt LR. Colloquium: scaled particle theory and the length scales of hydrophobicity. Rev Mod Phys 2006;78(1):159–178.

Asthagiri D, Merchant S, Pratt LR. Role of attractive methane–water interactions in the potential of mean force between methane molecules in water. J Chem Phys 2008; 128(24):244512.

Bae YC, Shim JJ, Soane DS, Prausnitz JM. Representation of vapor–liquid and liquid–liquid equilibria for binary systems containing polymers: applicability of an extended Flory–Huggins equation. J Appl Polym Sci 1993;47(7):1193–1206.

Berendsen HJC, Grigera JR, Straatsma TP. The missing term in effective pair potentials. J Phys Chem 1987;91(24):6269–6271.

Chaudhari MI, Pratt LR, Paulaitis ME. Communication: direct observation of a hydrophobic bond in loop closure of a capped $(-OCH_2CH_2-)_n$ oligomer in water. J Chem Phys 2010;133(23):231102.

Chempath S, Pratt LR. Distribution of binding energies of a water molecule in the water liquid–vapor interface. J Phys Chem B 2009;113(13):4147–4151.

Earl DJ, Deem MW. Markov chains of infinite order and asymptotic satisfaction of balance: application to the adaptive integration method. J Phys Chem B 2005;109(14): 6701–6704.

Ferguson AL, Debenedetti PG, Panagiotopoulos AZ. Solubility and molecular conformations of *n*-alkane chains in water. J Phys Chem B 2009;113(18):6405–6414.

Ferguson AL, Panagiotopoulos AZ, Debenedetti PG, Kevrekidis IG. Systematic determination of order parameters for chain dynamics using diffusion maps. Proc Natl Acad Sci USA 2010;107(31):13597–13602.

Gunari N, Balazs AC, Walker GC. Force-induced globule-coil transition in single polystyrene chains in water. J Am Chem Soc 2007;129(33):10046–10047.

Jorgensen WL, Maxwell DS, Tirado-Rives J. Development and testing of the OPLS all-atom force field on conformational energetics and properties of organic liquids. J Am Chem Soc 1996;118(45):11225–11236.

Li IT, Walker GC. Interfacial free energy governs single polystyrene chain collapse in water and aqueous solutions. J Am Chem Soc 2010;132(18):6530–6540.

Li IT, Walker GC. Signature of hydrophobic hydration in a single polymer. Proc Natl Acad Sci USA 2011;108(40):16527–16532.

Li IT, Walker GC. Single polymer studies of hydrophobic hydration. Acc Chem Res 2012;45(11):2011–2021.

Lin Z, Rubtsov IV. Constant-speed vibrational signaling along polyethylene glycol chain up to 60-Å distance. Proc Natl Acad Sci USA 2012;109(5):1413–1418.

Liu K, Song Y, Feng W, Liu N, Zhang W, Zhang X. Extracting a single polyethylene oxide chain from a single crystal by a combination of atomic force microscopy imaging and single-molecule force spectroscopy: toward the investigation of molecular interactions in their condensed states. J Am Chem Soc 2011;133(10):3226–3229.

Norman AI, Fei Y, Ho DL, Greer SC. Folding and unfolding of polymer helices in solution. Macromolecules 2007;40(7):2559–2567.

Ocean Studies Board (OSB). *Understanding Oil Spill Dispersants: Efficacy and Effects*. Washington, DC: National Academies Press; 2005.

Oesterhelt F, Rief M, Gaub HE. Single molecule force spectroscopy by AFM indicates helical structure of poly(ethylene-glycol) in water. New J Phys 1999;1(1999):6.1–6.11.

Pratt LR. Molecular theory of hydrophobic effects: “she is too mean to have her name repeated”. Annu Rev Phys Chem 2002;53:409–436.

Shell MS, Panagiotopoulos A, Pohorille A. Calculating free energy differences using perturbation theory. In: Chipot C, Pohorille A, editors. *Free Energy Calculations*. New York: Springer; 2007.

Starovoytov ON, Borodin O, Bedrov D, Smith GD. Development of a polarizable force field for molecular dynamics simulations of poly (ethylene oxide) in aqueous solution. J Chem Theory Comput 2011;7(6):1902–1915.

Van Der Spoel D, Lindahl E, Hess B, Groenhof G, Mark AE, Berendsen HJ. GROMACS: fast, flexible, and free. J Comput Chem 2005;26(16):1701–1718.

Wang J, Wolf RM, Caldwell JW, Kollman PA, Case DA. Development and testing of a general amber force field. J Comput Chem 2004;25(9):1157–1174.

Zafarani-Moattar MT, Tohidifar NJ. Vapor–liquid equilibria, density, and speed of sound for the system poly(ethylene glycol) 400 + methanol at different temperatures. J Chem Eng Data 2006;51(5):1769–1774.

12

SOME COLLOIDAL FUNDAMENTALS IN OIL SPILL REMEDIATION: THE WATER/SURFACTANT/HYDROCARBON COMBINATION

S. E. Friberg, H. Hasinovic, and Pi Belobrov

12.1 INTRODUCTION

Oil is by far the main energy resource of the world and it is transported in huge amounts in supertankers, each of which may carry millions of gallons of crude oil adding up to billions of gallons per day over the sea. With this constant transport, the potential for accidents with huge amounts of oil spill is significant. In addition to these transport-oriented calamities, misfortunes at the deep water oil rigs may lead to severe environmental problems.

In the actual spill situation, several factors are at play. The oil spreads on water; parts of it are dissolved, while other parts of it evaporate, and parts are even emulsified due to the movement of waves and wind. These factors are treated in several chapters in the book; this chapter is limited to some more fundamental factors in hydrocarbon–water dispersions. The introduction, a brief account of different structures encountered in such systems, is followed by a description of some essentials of spontaneous emulsification and finished by a definition of the optimal fundamentals of a surfactant to disperse the oil.

Oil Spill Remediation: Colloid Chemistry-Based Principles and Solutions, First Edition.
Edited by Ponisseril Somasundaran, Partha Patra, Raymond S. Farinato, and Kyriakos Papadopoulos.

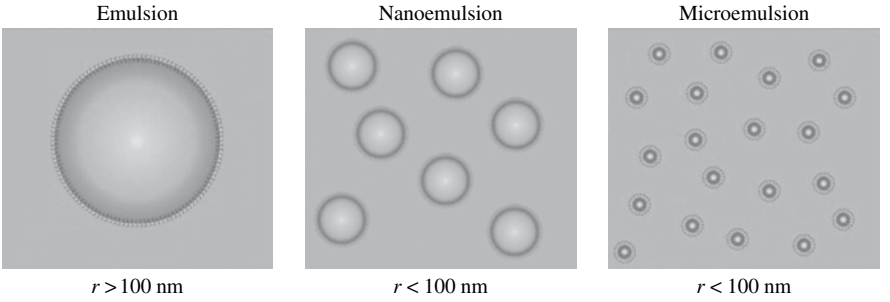

FIGURE 12.1 An illustration of the relative sizes of different emulsions.

12.2 SIZE AND HYDROCARBON–WATER DISPERSIONS

The most basic condition in the water–oil systems is the fact that the mutual solubility is extremely small. This is because the main interaction between water molecules is by polar forces, while in hydrocarbons the interaction is virtually limited to nonpolar dispersion forces. As a result, water and hydrocarbon in general do not form but the most dilute molecular solutions; instead, dispersions of one liquid in the other are in the form of drops, the name of which depends on the size of the drops. With decreasing drop size, one finds macroemulsions with micron-sized drops (Binks, 1998; Leaf-Calderon et al., 2010; McClements, 2004; Sjöblom, 2006), nanoemulsions with drops in the range of 10–50 nm (Forgiarini et al., 2001; Mason et al., 2006; Solans et al., 2005; Tadros et al., 2004), microemulsions (Fanum, 2008; Lindman et al., 1980; Lindman and Friberg, 1999) with drops usually in the range less than 10 nm, and micellar solutions with usually even smaller drops than the microemulsions; there is no defined structural difference between the latter two. This difference is instead found between nanoemulsions and microemulsions. For these two, the drop size may actually overlap, but they are, in fact, fundamentally different species. A nanoemulsion is an emulsion and hence not thermodynamically stable, while the microemulsion is a thermodynamically stable colloidal solution. The numbers of the drop size per se are better illustrated directly, as in Figure 12.1.

12.3 EMULSIONS

The systems in the first category, the emulsions, are thermodynamically unstable because of a positive interfacial free energy. As a consequence, minimization of the interface size gives the morphology of spherical emulsion drops, unless too crowded. Secondly, long-term destabilization leads to separation into two layers. Emulsions are, in fact, extremely unstable if not stabilized. According to flocculation theory, the half-life, the time for the original drops to be reduced to one half, is on the order of seconds for an emulsion with no stabilizers present. The half-life is increased by surface-active compounds or aggregates, which adsorb at the interface. This adsorption

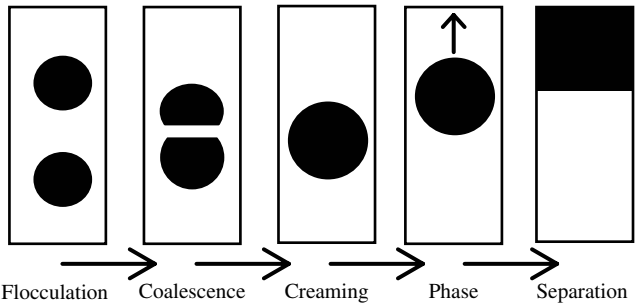

FIGURE 12.2 An emulsion is thermodynamically unstable. The drops in it first aggregate, called flocculation, followed by uniting to larger drops, called coalescence. In parallel, they cream if they are less dense than the continuous phase. Finally, these combined processes result in two separate layers, called phase separation.

also reduces the interfacial free energy, and it is tempting to refer the stabilization to this factor, but this approach is not based on reality. The colloidal stability of emulsions, that is, the reduction of the destabilization rate, depends on forces acting *between* the drops. The reduced free energy operates only by a small increase of the temperature: less than 2°C for a completely insulated emulsion.

The instability causes the emulsion to flocculate and coalesce the drops until the emulsion forms two layers as shown in Figure 12.2. The stabilization of emulsions is commercially of crucial importance, and the literature on the stabilization of emulsions is vast (Binks, 1998; Leaf-Calderon et al., 2010; McClements, 2004; Sjöblom, 2006), but its direct relevance for cleaning of an oil spill in water is not as pronounced. Instead, the energy and mechanism for the formation of structures becomes the vital factor.

12.4 ASSOCIATION STRUCTURES AND EMULSIONS

In the simplest systems, such as aqueous solutions of surfactants, the relation between the surface tension of water and the surfactant concentration, Figure 12.3a, provides information about the potential structures. In a solution of low concentration, surfactants exist as individual molecules, but in excess of a certain value they associate to micelles (a) for the "water-soluble" kind, while the other kind gives rise to lamellar liquid crystal, which separates as a distinct phase (b) (Ekwall and Brown, 1975). The former remain soluble in the aqueous solution and may solubilize hydrocarbons as shown by the dashed line in Figure 12.3a. This difference is crucial for the application in remediation of oil spills, and the fact that the association to liquid crystal takes place at a much lower surfactant concentration (b) should be observed. A suspension of the liquid crystal in water forms vesicles if energy is added, shown in Figure 12.4a, or a sponge phase, Figure 12.4b (Granek and Cates, 1992; Le et al., 2002; Maldonado et al., 1996).

The final item is the formation of association structures in the hydrocarbon. In contrast to the conditions in aqueous solutions, the association now takes place more

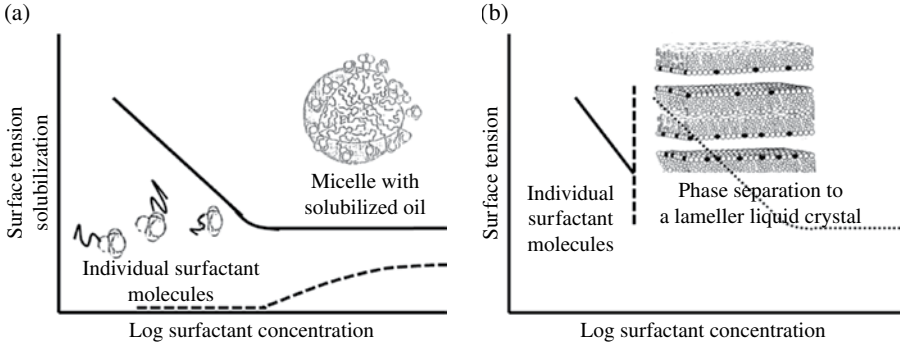

FIGURE 12.3 Relation between surface tension (solid line) and surfactant association structures in water for "water-soluble" (**a**) and "water-insoluble" (**b**) surfactants. The dotted line in the (**b**) part is the surface tension from (**a**), illustrating the fact that the critical association concentration (**b**) is significantly less than the critical micellization concentration (**a**).

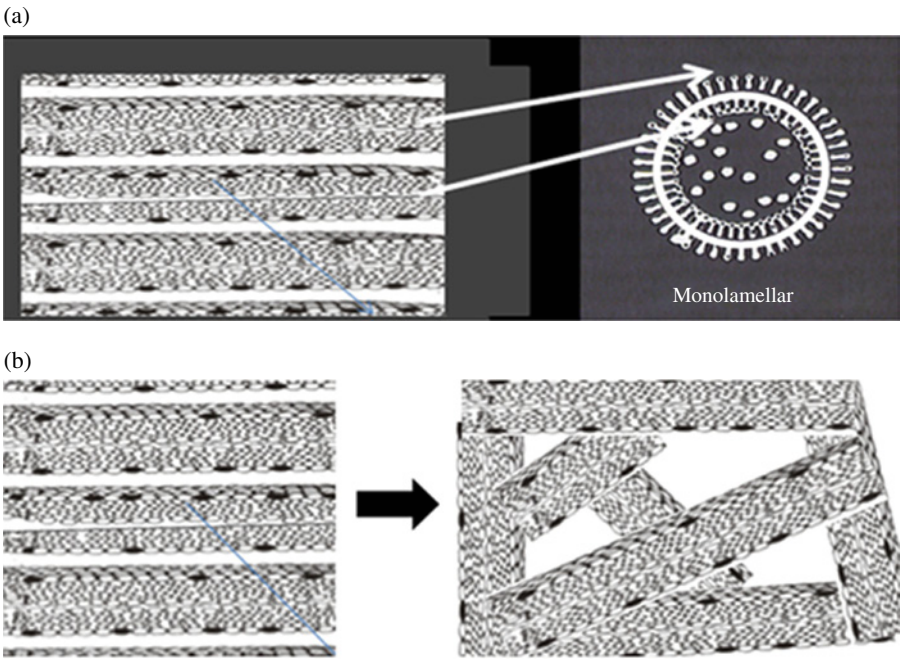

FIGURE 12.4 The bilayer in the lamellar liquid crystal (left) forms the shell of a vesicle (**a**, right) or a sponge phase (**b**, right).

gradually (Schelly, 1997), and the number of premicellar aggregates is significant. Figure 12.5 indicates the gradual development. With increased hydrocarbon content in the aqueous micelles or increased water content in the inverse micelles, bicontinuous microemulsions are formed in some systems (Scriven, 1976; Talmon and Prager, 1977).

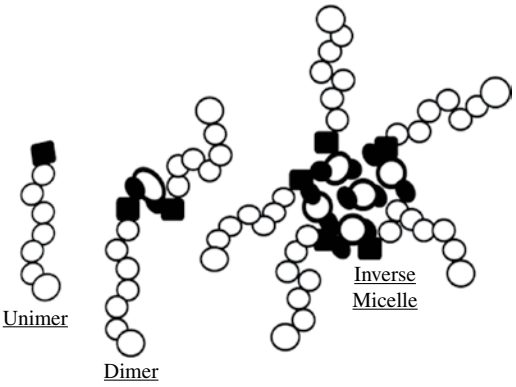

FIGURE 12.5 The gradual association with increased water content from unimers to premicellar aggregates to inverse micelles.

FIGURE 12.6 The change from aqueous micelles to inverse micelles over a bicontinuous microemulsion.

With these different morphologies briefly introduced, some specific features will be discussed. The discussion is focused on the fundamentals of the systems per se to establish a basis for evaluation of the usefulness for oil spill remediation (Fig. 12.6).

12.5 SPONTANEOUS EMULSIFICATION

Although the stability of emulsions is a fascinating subject and has been the focus of a huge volume of research over the years, it does not occupy the same level of importance for the remediation of oil spills. Instead, the formation process of emulsions is the vital concept. Most of the literature in that area is concerned with methods requiring high energy input, but the situation of an oil spill renders such methods less practicable. Hence, in this discussion, the low-energy emulsification approach is emphasized, and in this group, the most essential one is the spontaneous emulsification. The earliest publication on spontaneous emulsification was by Johannes Gad (1878),

and extensive and competent review articles are available (Davies and Rideal, 1963; Lopez-Montilla et al., 2002; Miller, 1988; Salager et al., 2004).

A systematic overview of the phenomenon was later given by Salager et al. (2004) who listed three main reactions: surfactant mass transfer, spontaneous emulsification, and transitional or/and catastrophic phase inversion. This also reflects the early attempts to fundamental understanding of the process concentrating on subtle changes in interfacial properties for instability mechanisms in low-tension systems, and the first contribution in the area (Gad, 1878) serves as a useful illustration of interfacial instability due to added energy. Gad brought a hydrocarbon–fatty acid solution in contact with an aqueous sodium hydroxide solution, and the neutralization reaction caused spontaneous emulsification. The energy of the reaction (a combination of neutralization energy, ≈56 kJ/mol, and the coulombic energy gain from the majority of the sodium ions being close to the interface, several joules per molecule) is sufficient to form an interface. The morphology of the O/W emulsion is aided by the spontaneous curvature of the interface being convex toward the water.

The application of this mechanism to the film on the sea surface or to an ejection of a massive bulk stream of oil is straightforward. Injection of a readily hydrolyzable, oil-soluble compound into the oil would lead to the formation of a surface-active substance at the interface, and the energy of hydrolysis would compensate for the energy of forming the interface. However, as the continued analysis will show, emulsification per se may not be satisfactory, and the structures formed are a factor of essence. For a successful treatment, the morphology enters as a second factor of equal importance as will be demonstrated in the detailed analysis following.

The fundamentals of spontaneous emulsification were given a new direction away from interfacial properties by Miller (Miller, 1988; Ruschak and Miller, 1972), who introduced the concept of the diffusion path and spontaneous emulsification as shown in Figure 12.7. When water and a solution of alcohol and hydrocarbon are contacted (Fig. 12.7), the mutual diffusion of water and the two organic compounds changes

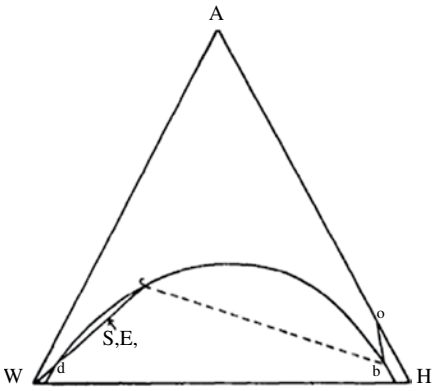

FIGURE 12.7 An example of the diffusion path leading the system through a two-phase range with subsequent spontaneous emulsification; W = water, H = hydrocarbon, and A = alcohol. Reproduced from Miller (1988) with permission of Elsevier.

the composition along the line reaching b. Assuming *local* equilibrium at the interface, this b phase will be in equilibrium with the aqueous phase at the other end of the tie line, c. The c phase is in contact with the water saturated by ethanol and benzene, phase d. The new phases formed by the diffusion (Fig. 12.7) give rise to spontaneous emulsification. As emphasized by Miller, the diffusion approach predicts not only if spontaneous emulsification occurs but actually in which phase the process will take place, in the cited example in the aqueous solution. This approach was successfully applied to detergency (Miller and Raney, 1993) and has direct bearing on the remediation of oil spills on land, an area outside this chapter.

These contributions emphasize the effect of diffusion on spontaneous emulsification. Evidently, there is no doubt that the diffusion process per se is the decisive element in the spontaneous emulsification process, but an analysis of the phase equilibria is also useful, providing information about less instantaneous events. In the following, some features will be evaluated of the role of phase equilibria in spontaneous emulsification and some preliminary aspects on oil spill remediation.

12.6 PHASE DIAGRAMS AND SPONTANEOUS EMULSIFICATION

In the following, the relationship between phase diagram features and spontaneous emulsification is analyzed, beginning with the simplest systems to illustrate the capability of the algebraic system (Friberg and Al-Bawab, 2005; Friberg, 2006). The primary emulsion system, water (W), ethanol (E), and benzene (B) (Fig. 12.8), is utilized to outline the procedure and illustrate the information to be gathered from the approach. This analysis is purely fundamental, but the potential for guiding the relevant choice of surfactants in the oil spill remediation field is not insignificant and will be illustrated later.

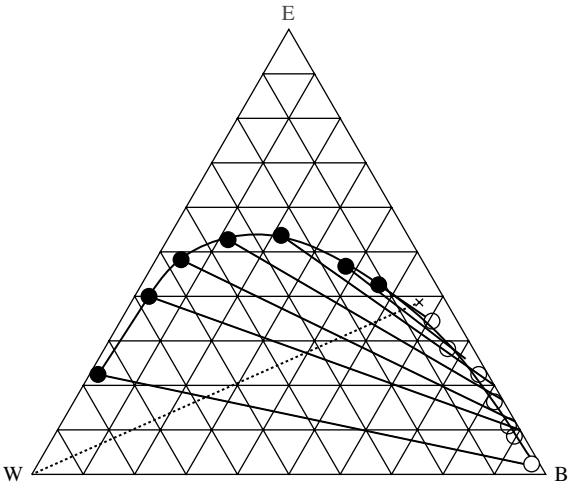

FIGURE 12.8 The system, water (W), ethanol (E), and benzene (B), based on Lee and Peters (2004), Lee (2010) and A. Bozeya (personal information).

The analysis is patterned on a realistic situation in an oil spill; the surfactant is added to the oil, which is in contact with an infinite amount of water. As the water and the oil–surfactant solution interact, the spontaneous emulsification leads to a sequential increase of the total water content in the equilibrium emulsion system, reflected in the dashed arrow from the oil solution toward the water corner, Figure 12.8. The system offers extensive information about the process (Friberg and Al-Bawab, 2005; Friberg, 2006). In the following, some examples are offered that have some relevance for oil spill remediation.

The diagram offers direct information on the weight fractions of the phases in the equilibrium system, but the crucial factor for the potential application in the oil spill remediation is the interfacial transfer of individual compounds, which are calculated using the algebraic approach (Friberg and Al-Bawab, 2005; Friberg, 2006) to interpret phase diagrams. In the primary example, the composition of the former is chosen as weight fractions (X_W, X_E, X_B) equal to (0.1, 0.36, 0.54), Figure 12.8, and water is added to different amounts. According to the phase diagram, two solutions will form: one mostly of water and ethanol, Aq, and the second mostly benzene, BE.

To calculate the essential factors, the algebra is established with the equation for the water dilution line

$$^{DL}X_W = 1 + {}^{DL}Y_W\,(\,{}^{O}X_W - 1)\,/\,{}^{O}Y_W \tag{12.1}$$

in which superscript DL stands for dilution line.

For the tie lines,

$$^{TL}X_W = {}^{Aq}X_W + \left({}^{TL}X_B - {}^{B}X_B\right)\left({}^{B}X_W - {}^{Aq}X_W\right)/\left({}^{B}X_B - {}^{Aq}X_B\right) \tag{12.2}$$

in which the superscripts Aq and BE stand for the coordinates on the aqueous and benzene branches of the emulsions, respectively, and TL stands for tie line.

The intersection ${}^{I}X_B$ of the tie lines with the dilution line (as indicated by the superscript I) expressed as a function of the coordinates of the emulsion compositions

$$\begin{aligned} {}^{I}X_W = \Big(\big(1 - {}^{Aq}X_W + {}^{BE}X_B\big)\left({}^{BE}X_W - {}^{Aq}X_W\right)/\left({}^{BE}X_B - {}^{Aq}X_B\right)\Big)\,/ \\ {}^{TL}X_W\,/\Big(5/3 + \left({}^{BE}X_W - {}^{Aq}X_W\right)/\left({}^{BE}X_B - {}^{Aq}X_B\right)\Big). \end{aligned} \tag{12.3}$$

The weight fraction of the Aq fraction of the emulsion is

$$X_{Aq} = \frac{{}^{BE}X_B - {}^{BE}X_B}{{}^{BE}X_B - {}^{Aq}X_B} \tag{12.4}$$

and the corresponding value for the B is $X_{BE} = 1 - X_{Aq}$.

These equations primarily provide information about the relative changes in the system, and the weight fractions of the two phases are presented in Figure 12.9.

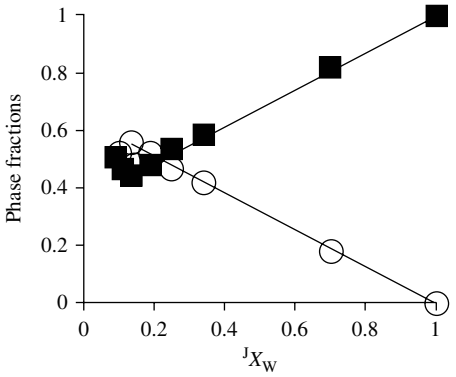

FIGURE 12.9 The weight fractions of the two phases during dilution along the dashed line in Figure 12.8. ■, aqueous phase; ○, benzene phase.

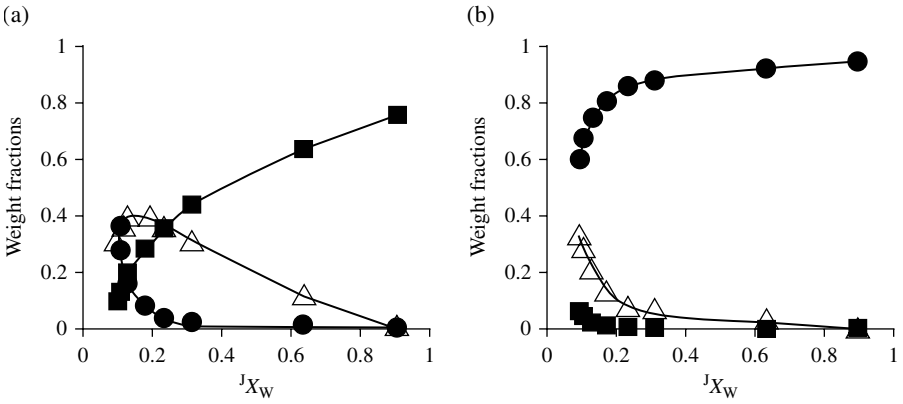

FIGURE 12.10 The weight fractions of the individual compounds in the two phases versus the weight fraction of water, $^{J}X_{W}$. A, aqueous phase; B, benzene phase. ■, water; ●, benzene; Δ, ethanol.

It illustrates the continuous addition of water to cause an increase in the fraction of the aqueous phase and a corresponding reduction of the fraction benzene phase.

The calculations also offer the weight fractions of the individual compounds in the two phases, Figure 12.10. The curves illustrate the fact that the water is concentrated into the aqueous phase, while the benzene remains in the benzene phase. The initial increase in the ethanol fraction is a reflection of the features of the phase diagram. The initial change of total water weight fraction from 0.1 to 0.15 results in an increase in the ethanol weight fraction in the aqueous phase from 0.4 to 0.55, corresponding to the maximum in the ethanol curve in Figure 12.10a.

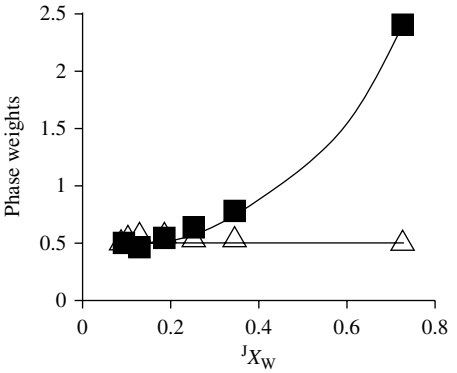

FIGURE 12.11 The weights of the phases versus the weight fraction of the total water, $^{I}X_{W}$. ■, BE phase; Δ, aqueous phase.

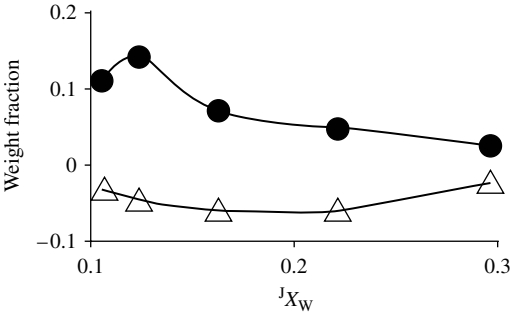

FIGURE 12.12 The weight fractions of individual compounds transferred from the aqueous to the benzene phase. Δ, ethanol; ●, benzene.

However, these variations reflect only the relative changes in the phases. From the perspective of oil spill remediation, the absolute weights are more informative. Figure 12.11 gives the weights of the two phases versus the weight fraction of total water in the system, $^{I}X_{W}$.

The pronounced increase in the weight of the aqueous phase is a reflection of the water preferentially being added to that phase. A presentation versus the total weight of the emulsion would show a close to linear weight curve. The weight of the benzene phase has a direct relevance for the oil spill remediation; it shows the preservation of the benzene in the oil phase. In fact, it demonstrates that adding a water-soluble surfactant to the oil does not affect the situation. The oil may be emulsified but remains unchanged, and the advantage of it being dispersed lasts only as long as the drops do not coalesce to bulk oil.

For the spontaneous emulsification *per se*, the transfer of compounds between the phases is a contributing factor, and the algebraic system (Friberg, 2006; Friberg and Al-Bawab, 2005) allows calculation of the amounts. Figure 12.12 offers an example of

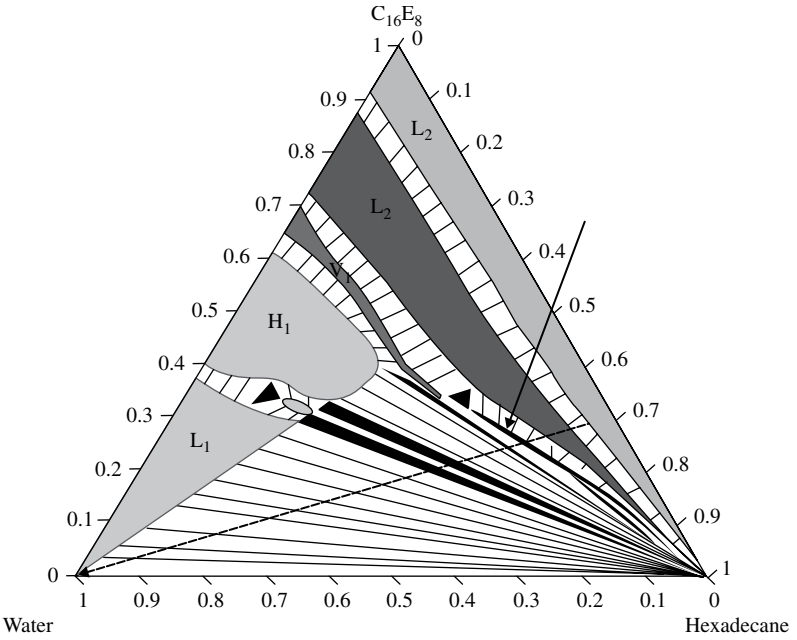

FIGURE 12.13 The phase diagram for water, hexadecane, and octaethylene glycol monohexadecyl ether, $C_{16}E8$. Reproduced from Roger et al. (2011) with permisson of the American Chemical Society.

the amounts of benzene and ethanol transferred to the benzene phase as a fraction of its weight. The numbers show a modest transfer of compounds from the aqueous phase to the BE solution; it is not at a magnitude to cause much perturbation of the interface.

The summary of the results in Figure 12.9 and Figure 12.10 shows the process to lead a final configuration of a two-phase emulsion, of which one phase is pure benzene and the other an aqueous phase with negligible fraction of ethanol. In spite of the simplicity, not to say artificiality of the system, the vital information is the fact that a water-soluble surfactant will inevitably be partitioned into the aqueous phase, leaving pure oil. This is also true for surfactants of a structure similar to that of commercial varieties, Figure 12.13.

The dashed arrow in Figure 12.13 shows the dilution line, when water is added to a 30 wt% hexadecane solution of the surfactant. In the early stages of water addition, the hydrocarbon phase contains surfactant and water, but after addition of 0.25 weight of water, bringing its weight fraction to 0.2 (arrow in the figure), the hydrocarbon in equilibrium with the aqueous structures contains no water or surfactant. Infinite dilution will lead to an extremely dilute solution of surfactant in the aqueous phase and pure oil. Obviously, water-soluble surfactants may not be the most useful choice in the oil spill remediation process. Instead, the phase diagram solution to the condition for a successful surfactant to emulsify the oil is given by Figure 12.14.

Figure 12.14 reveals the essential feature of a surfactant for oil spill remediation in aqueous environment. The surfactant is not soluble in water; instead, it forms a

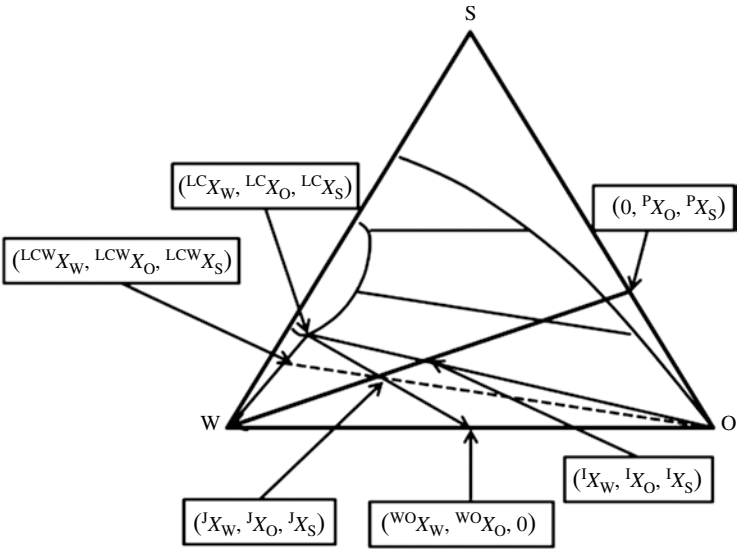

FIGURE 12.14 Essential features for a surfactant in oil spill remediation in an aqueous environment.

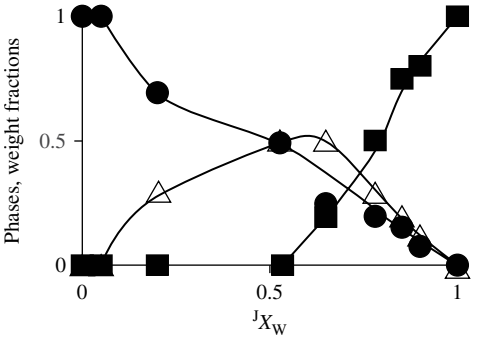

FIGURE 12.15 Approximate weight fractions of the phases during dilution by water. ■, aqueous phase; Δ, liquid crystal phase; ●, oil phase.

liquid crystal when in contact with water, Figure 12.3. Contrary to the conditions for a water-soluble surfactant, Figure 12.2, when high fractions of water lead to the oil separating as such, now a combination of the liquid crystal and the oil forms. Such a combination results in stable emulsions, as was previously discovered (Friberg et al., 1969).

The phase diagram, Figure 12.13, and the algebraic system (Friberg and Al-Bawab, 2005; Friberg, 2006) were used to calculate the equilibrium weight fractions of the aqueous phase, the oil phase, and the liquid crystal phase versus the total water weight fraction, Figure 12.15, for the dilution of a 30 wt% solution of the surfactant, S, in the oil, O.

Figure 12.15 shows the strong increase in the weight fraction of aqueous phase reaching a fraction of 1 for infinite dilution, but contrary to the case for a water-soluble surfactant, the aqueous phase is not in equilibrium with the pure oil. Instead, the oil is accompanied by liquid crystalline phase. The ratio between the two depends on the features of the phase diagram, Figure 12.14, and the calculation of this ratio is critical to judge the system. A glance at the phase diagram, Figure 12.13, makes it obvious that there are two factors that are decisive for the weight ratio between the two phases: the fraction of surfactant in the initial oil phase (0, ${}^{P}X_{O}$, ${}^{P}X_{S}$) and the amount of oil solubilized in the liquid crystal (${}^{LC}X_{W}$, ${}^{LC}X_{O}$, ${}^{LC}X_{S}$). The algebraic approach (Friberg and Al-Bawab, 2005; Friberg, 2006) was utilized to evaluate the effect of these two key aspects of the system. The calculations were limited to water fractions in excess of ${}^{I}X_{W}$, Figure 12.13, because the relevance for oil spill in aqueous environment is limited to extremely high water contents.

The system is described with the equations for different lines given first

$$\left(0,{}^{P}X_{O}\,{}^{P}X_{S}\right) \text{ to } (1,0,0)$$

$$X_{O} = {}^{P}X_{O}\left(1-X_{W}\right) \tag{12.5}$$

$$\left({}^{LC}X_{W},\,{}^{LC}X_{O}\,{}^{LC}X_{S}\right) \text{ to } \left({}^{WO}X_{W},\,{}^{WO}X_{O}\,{}^{WO}X_{S}\right)$$

$$X_{O} = {}^{LC}X_{O} + \left({}^{WO}X_{O} - {}^{LC}X_{O}\right)\left(X_{W} - {}^{LC}X_{W}\right)/\left({}^{WO}X_{W} - {}^{LC}X_{W}\right). \tag{12.6}$$

The two essential lines (${}^{LC}X_{W}$, ${}^{LC}X_{O}\,{}^{LC}X_{S}$) to (0, 1, 0) and (${}^{LC}X_{W}$, ${}^{LC}X_{O}\,{}^{LC}X_{S}$) to (1, 0, 0) are obtained from Equation (12.6) by introducing numerical values for the coordinates in question.

The coordinates ${}^{J}X_{W}$ are obtained by a combination of Equations (12.5) and (12.6)

$$\begin{aligned}{}^{J}X_{W} = &\left({}^{P}X_{O} - {}^{LC}X_{O} + {}^{LC}X_{W}\left({}^{WO}X_{O} - {}^{LC}X_{O}\right)/\left({}^{WO}X_{W} - {}^{LC}X_{W}\right)\right)/\\ &\left({}^{P}X_{O} + \left({}^{WO}X_{O} - {}^{LC}X_{O}\right)/\left({}^{WO}X_{W} - {}^{LC}X_{W}\right)\right)\end{aligned} \tag{12.7}$$

with the special cases for (${}^{LC}X_{W}$, ${}^{LC}X_{O}\,{}^{LC}X_{S}$) to (0, 1, 0)

$${}^{I}X_{W} = \left({}^{P}X_{O} - {}^{LC}X_{O} - {}^{LC}X_{W}\left(1-{}^{LC}X_{O}\right)/{}^{LC}X_{W}\right)/\left({}^{P}X_{O} - \left(1-{}^{LC}X_{O}\right)/{}^{LC}X_{W}\right) \tag{12.8}$$

and (${}^{LC}X_{W}$, ${}^{LC}X_{O}\,{}^{LC}X_{S}$) to (1,0,0)

$${}^{LCW}X_{W} = \left(\left({}^{P}X_{O} - {}^{LC}X_{O} - {}^{LC}X_{W}\,{}^{LC}X_{O}\right)/\left(1-{}^{LC}X_{W}\right)\right)/\left({}^{P}X_{O} - {}^{LC}X_{O}\right)/\left(1-{}^{LC}X_{W}\right). \tag{12.9}$$

The weight fractions of the three phases are now attained

$$X_{LC} = \frac{{}^{WO}X_O - {}^{J}X_O}{{}^{WO}X_O - {}^{LC}X_O} \tag{12.10}$$

$$X_O = \frac{{}^{J}X_O - {}^{LC}X_O}{1 - {}^{LC}X_O} \tag{12.11}$$

$$X_W = \frac{{}^{J}X_W - {}^{I}X_W}{1 - {}^{I}X_W}. \tag{12.12}$$

Equation (12.12) is linear of first order in ${}^{J}X_W$, ${}^{J}X_O$ is also linear in ${}^{J}X_W$, and the weight fractions of both the aqueous and the oil weight fractions are linearly dependent on the total water fraction, ${}^{J}X_W$. Since the sum of the weight fractions of the three phases equals one, they are all linear of first order. Consequently, the ratio between the weight fractions of oil and liquid crystal at infinite dilution is proportional to the ratio for ${}^{J}X_W = {}^{I}X_W$, and the weight fraction $X_{LC}/(X_{LC}+X_O)$ is calculated for different values of $({}^{LC}X_W, {}^{LC}X_O\ {}^{LC}X_S)$ and $(0, {}^{P}X_O, {}^{P}X_S)$. A simplified Equation (12.10) directly gives the fraction liquid crystal, since the fraction $X_{Aq} = 0$

$$X_{LC} = \frac{1 - {}^{I}X_O}{1 - {}^{LC}X_O}. \tag{12.13}$$

Equation (12.13) first reveals the trivial fact that for ${}^{I}X_O = {}^{J}X_{LC}$ all the oil has been transferred to the liquid crystal. It may be tempting to interpret this as requiring an equal amount of surfactant to oil, but this is not true. The relationship is instead

$$\frac{{}^{I}X_S}{{}^{I}X_O} = \frac{{}^{P}X_S}{{}^{P}X_O}. \tag{12.14}$$

Since the ${}^{I}X_S/{}^{I}X_O$ is a measure of the solubilization of oil into the liquid crystal, this phenomenon stands out as the crucial factor, and the relation between this value and the final ratio of the two phases deserves a further analysis. At first, the analysis is made in general terms with the difference between ${}^{LC}X_O$ and ${}^{I}X_O$ with ΔX_O as the variable, Figure 12.16. Each curve represents a different location of ${}^{I}X_O$ from (0, 1, 0) (squares) to $({}^{LC}X_W, 0.001, {}^{LC}X_S)$ (*x*'s), and the ΔX_O scale signifies a gradual move of ${}^{LC}X_O$ toward ${}^{I}X_O$.

The results in Figure 12.16 reveal the fact that a combination of an extremely small fraction of surfactant in the original oil means that the solubilization of oil in the liquid crystal has to be unrealistically large, at the level of 0.95 in order for a substantial fraction of liquid crystalline phase to be present at infinite dilution. However, it has to be realized that the condition of ${}^{I}X_O = 0.99$ means a surfactant content on the order of one half of one percent in the original oil, which is not realistic. A numerical result from an example of a surfactant content of 0.3 in the oil gives a different view, Figure 12.17.

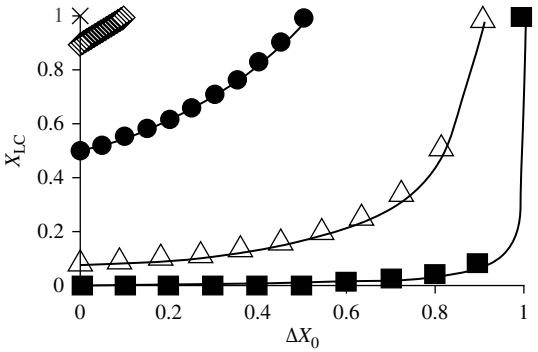

FIGURE 12.16 The fraction liquid crystal counted on liquid crystal and oil only. (The fraction aqueous phase equals zero for the conditions.). Symbol ${}^{l}X_{o}$ ■, 0.99; Δ, 0.9; ●, 0.5; ◊, 0.1; × 0.01.

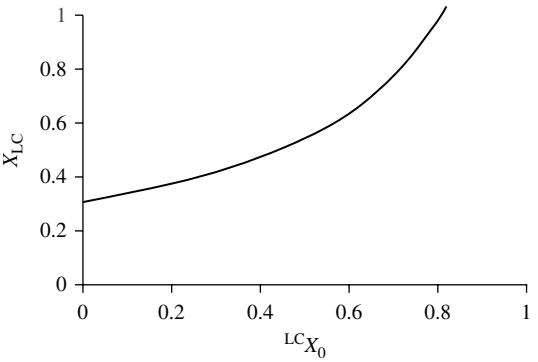

FIGURE 12.17 The weight fraction of a liquid crystal at the initiation of the three-phase range for an emulsion with an original oil phase with a 0.3 weight fraction surfactant.

The curve in Figure 12.17 shows that with reasonable weight fraction of surfactant in the oil, the fraction of liquid crystal is satisfactory, even with small or no solubilization of the oil in the liquid crystal. An illustrative example of the information that only the phase diagram approach can offer.

Finally, it is essential to emphasize that the liquid crystals referred to in this context are not by any means to be compared to the sophisticated variety used in display systems. The liquid crystals in question are formed by water and common surfactants, and it is useful to offer lecithin as an example. Lecithin is a low-price commodity, a by-product in the refining process of vegetable oils, and has the interesting feature of containing both phosphorous and nitrogen, essential elements for microbiological growth. Unfortunately, there seems not to be investigations available on this factor.

12.7 SOLID PARTICLES AND OIL FILM ON WATER

In principle, the interaction between solid surfaces and oil belongs to the area of cleaning of stranded oil, but one aspect in connection with an oil film on the sea surface is of interest to this chapter. The main events are covered in Figure 12.18, illustrating the particle falling toward the oil film, penetrating it, and descending into the sea.

This action would prevent the oil from reaching the shore and give the microbes an opportunity to digest the oil. The process depends on the fundamentals of three factors: surface free-energy balance, the kinetics of oil spreading on the particle, and the density of the particle covered by oil. The first factor, the well-known Young's equation, Figure 12.19, shows the three forces acting between a solid surface with an attached drop of media 2 in medium 1. These media may be gaseous or liquid.

Equilibrium requires

$$\gamma_{S/M_1} = \gamma_{S/M_2} + \gamma_{M_1/M_2} \cos a \tag{12.15}$$

and spreading of M_2 on S

$$\gamma_{S/M_1} > \gamma_{S/M_2} + \gamma_{M_1/M_2}. \tag{12.16}$$

Since the medium M_1 in this case is air, this condition is easily fulfilled by inorganic compounds with their polar surfaces of high surface free energy.

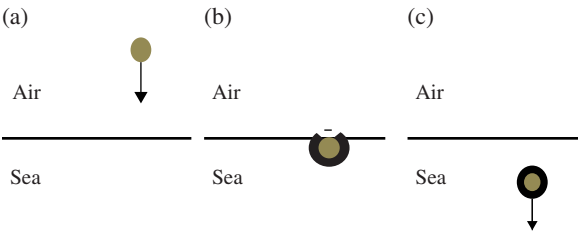

FIGURE 12.18 The development of a solid particle falling toward an oil film on the sea surface (**a**), penetrating the film (**b**), and sedimenting while covered with a layer of the film (**c**).

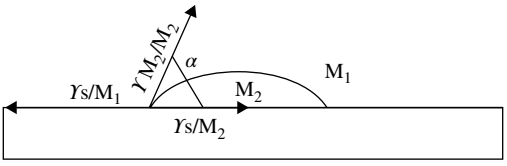

FIGURE 12.19 A drop of media 2, M_2, resting on a solid surface emerged in medium 1, M_1.

The next condition is that the drop density is sufficiently great to release it from the oil film and for it to descend through the seawater. The combined density of a sphere *s* of radius *r* covered by a layer of a liquid film *o* of thickness *d* is

$$\rho = \frac{4\pi r^3}{3}\rho_s + \left(\frac{(4\pi/3)\left((r+d)^3 - r^3\right)\rho_o/4\pi}{(r+d)^3/3} \right). \tag{12.17}$$

The density of petroleum varies between 0.79 and 0.95 g/cm^3, while the density of minerals that can be used also varies. In the same manner, the thickness of the oil film also varies highly from several micrometers to a fraction of this value. For the evaluation, 0.9 g/cm^3 was chosen for the oil and 3.0 g/cm^3 for the mineral as realistic values. The thickness of the oil film on the surface was chosen as 0.5 μm.

The first evaluation is concerning the sedimentation of the oil-covered particle. Equation (12.17) uses a value of the radius as 0.34 μm to give a density of 1.03 g/cm^3, and obviously, even rather small particles would be useful for the purpose. However, the sedimentation after release from the oil film may not be the decisive factor; the forces during the release may instead be the pivotal factor. An exact calculation of the forces during release is highly complex. For the present estimation, a simplified critical state in the process is assumed as the drop covered by an oil film, which also reaches in a hollow cylinder of the length of the particle to the surface. Such a film gives rise to an upward force from its surface tension toward air and toward water, approximated at 72.6 dynes/cm $\approx 456 r_p$ dynes. This buoyancy force acts against the gravity force $\approx g4\pi r^3(\rho_p - 1.03)/3 \approx 8.1 \times 10^3 r^3$. The results show the minimum size of the particle between 2 and 3 mm, a rather large size and a strongly limiting condition. However, since the particles are spread from a low-flying airplane or a boat through the spill, they arrive at the film with a certain velocity, and the retardation at the impact gives rise to a force. Assuming the distance of retardation is equal to the radius of the particle, one arrives at a simple expression for the deceleration force $\approx 4\pi r^2 v$. Approximate calculations show particles of a few micrometers to give rise to such a force at velocities of a few centimeters per second; and although field trials are necessary, the approach appears a promising process to remove oil films from the seawater surface.

12.8 MICROEMULSIONS

Microemulsions may at first glance appear extremely well suited for oil spill remediation since they are thermodynamically stable and form spontaneously; however, they require large concentrations of surfactant and they must be considered unpractical for an oil spill at sea. Nonionic surfactants of the ethylene oxide adduct kind will form microemulsions that allow "infinite dilution," but even so, these require surfactant–oil ratios in excess of one and are also sensitive to the hydrocarbon structure of the oil. Hence, they have been excluded from this chapter, in spite of their highly interesting colloidal structures (Corkery et al., 2010; Roger et al., 2011).

12.9 POTENTIAL FUTURE RESEARCH AREAS

This chapter has concentrated on traditional emulsions. Future fundamental problems to explore are primarily the features of microemulsions/nanoemulsions, the lesser known sponge phases, and oil solidification. Solutions in the form of solid three-dimensional oil continuous fractal structures corresponding to the aqueous sponge phases that can accommodate huge volumes with miniscule surfactant fractions should especially be explored. This area of research has not been focused on the complex mixture of compounds that is petroleum, but modern mathematical and physical theoretical framework has been established in three-dimensional minimal surfaces and successfully applied to bicontinuous microemulsions and minimal surface structures (from inorganic and metal crystals to cell membranes and biopolymers) (Andersson et al., 1988; Hyde et al., 1997). Such theoretical efforts are obviously outside the bounds of this chapter. In addition, the connection between evaporation from emulsions (Friberg, 2007, 2008) has not treated the phase behavior of nanoemulsions and their droplet size reduction by evaporative ripening or shear-induced disruption of dense nanoemulsion gels (Fryd and Mason, 2010, 2012; Wilking et al., 2011).

12.10 CONCLUSIONS

Some fundamental phenomena and structures of interest in oil spill remediation have been reviewed, and views have been given on a suitable surfactant structure for the purpose.

ACKNOWLEDGMENTS

The authors would like to thank our students A. Bozeya, I. A. Denisov, and K. A. Lukyanenko for their assistance. The authors are grateful to Ashland Consumer Markets for support.

REFERENCES

Andersson S, Hyde ST, Larsson K, Lidin S. Minimal surfaces and structures: from inorganic and metal crystals to cell membranes and biopolymers. Chem Rev 1988;88(1):221–242.

Binks PB. *Modern Aspects of Emulsion Science*. Cambridge, UK: Royal Society of Chemistry; 1998.

Corkery RW, Blute IA, Friberg SE, Guo R. Emulsion inversion in the PIT range: quantitative phase variations in a two-phase emulsion. J Chem Eng Data 2010;55(10):4471–4475.

Davies JT, Rideal EK. *Interfacial Phenomena*. New York: Academic Press; 1963.

Ekwall P, Brown GH. *Advanced Liquid Crystals*. New York: Academic Press; 1975.

Fanum M. *Microemulsions: Properties and Applications*. Boca Raton, FL: CRC Press; 2008.

Forgiarini A, Esquena J, González C, Solans C. Formation of nano-emulsions by low-energy emulsification methods at constant temperature. Langmuir 2001;17(7):2076–2083.

Friberg SE. Weight fractions in three-phase emulsions with an Lα phase. Colloids Surf A 2006;282/283:369–376.

Friberg SE. Evaporation from a three-phase emulsion. Can J Chem Eng 2007;85(5): 602–608.

Friberg SE. Constant vapor pressure evaporation from emulsions. Colloid Polym Sci 2008; 286(1):47–50.

Friberg SE, Al-Bawab A. Analytical expressions to calculate relative amounts of phases in a three-phase diagram. Langmuir 2005;21(22):9896–9900.

Friberg SE, Mandell L, Larsson M. Mesomorphous phases, a factor of importance for the properties of emulsions. J Colloid Interface Sci 1969;29:155–156.

Fryd MM, Mason TG. Time-dependent nanoemulsion droplet size reduction by evaporative ripening. J Phys Chem Lett 2010;1(23):3349–3353.

Fryd MM, Mason TG. Advanced nanoemulsions. Annu Rev Phys Chem 2012;63:493–518.

Gad J. Zur Lehre von der Fettresorption. Arch Anat Physiol 1878.

Granek R, Cates ME. Sponge phase of surfactant solutions: an unusual dynamic structure factor. Phys Rev A 1992;46(6):3319–3334.

Hyde ST, Andersson S, Larsson K, Blum Z, Landh T, Lidin S, Ninham BW. *The Language of Shape: The Role of Curvature in Condensed Matter: Physics, Chemistry and Biology*. Amsterdam: Elsevier; 1997.

Le TD, Olsson U, Wennerström H, Uhrmeister P, Rathke B, Strey R. Relaxation kinetics of an L3 (sponge) phase. J Phys Chem B 2002;106(36):9410–9417.

Leaf-Calderon F, Schmitt V, Bibette J. *Emulsion Science: Basic Principles*. New York: Springer; 2010.

Lee KY. Model to describe the binodal curve on a type 1 ternary phase diagram. J Environ Eng 2010;136(6):650–656.

Lee KY, Peters CA. UNIFAC modeling of cosolvent phase partitioning in nonaqueous phase liquids-water systems. J Environ Eng 2004;130(4):478–483.

Lindman B, Friberg SE. Microemulsions – a historical overview. In: Promod Kumar, Mittal KL, editors. *Handbook of Microemulsion Science and Technology*. New York: Marcel Dekker; 1999.

Lindman B, Kamenka N, Kathopoulis TM, Brun B, Nilsson PG. Translational diffusion and solution structure of microemulsions. J Phys Chem 1980;84(19):2485–2490.

Lopez-Montilla JC, Herrera-Morales PE, Pandey S, Shah DO. Spontaneous emulsification: mechanisms, physicochemical aspects, modeling, and applications. J Disper Sci Technol 2002;23(1–3):219–268.

Maldonado A, Urbach W, Ober R, Langevin D. Swelling behavior and local topology of an L3 (sponge) phase. Phys Rev E 1996;54(2):1774–1778.

Mason TG, Wilking JN, Meleson K, Chang CB, Graves SM. Nanoemulsions: formation, structure, and physical properties. J Phys Condens Matter 2006;18(41):R635–R666.

McClements DJ. *Food Emulsions: Principles, Practice and Techniques*. Boca Raton, FL: CRC Press; 2004.

Miller CA. Spontaneous emulsification produced by diffusion – a review. Colloids Surf 1988;29(1):89–102.

Miller CA, Raney KH. Solubilization–emulsification mechanisms of detergency. Colloids Surf A:Physicochem Eng Asp 1993;74(2–3):169–215.

Roger K, Cabane B, Olsson U. Emulsification through surfactant hydration: the PIC process revisited. Langmuir 2011;27(2):604–611.

Ruschak KJ, Miller CA. Spontaneous emulsification in ternary-systems with mass-transfer. Ind Eng Chem Fundam 1972;11(4):534–540.

Salager J, Forgiarini A, Lopez JC, Marfisis S, Alvarez G. Dynamics of near zero energy emulsification. CD Processings 6th World Surfactant Congress CESIO; 2004 Jun 21–23; Berlin, Germany; 2004, Paper #203.

Schelly ZA. Dynamics in water-in-oil microemulsions. Curr Opin Colloid Interface Sci 1997;2:37–41.

Scriven LE. Equilibrium bicontinuous structure. Nature 1976;263:123–125.

Sjöblom J. *Emulsions and Emulsion Stability*. New York: Taylor and Francis; 2006.

Solans C, Izquierdo P, Nolla J, Azaemar N, Garcia-Selma M-J. Nano-emulsions. Curr Opin Colloid Interface Sci 2005;10(3–4):102–110.

Tadros T, Izquierdo P, Esquena J, Solans C. Formation and stability of nano-emulsions. Adv Colloid Interface Sci 2004;108–109:303–318.

Talmon Y, Prager S. Statistical mechanics of microemulsions. Nature 1977;267:333–335.

Wilking JN, Chang CB, Fryd MM, Porcar L, Mason TG. Shear-induced disruption of dense nanoemulsion gels. Langmuir 2011;27(9):5204–5210.

13

PHYSICOCHEMICAL PROPERTIES OF HEAVY OIL–WATER INTERFACE IN THE CONTEXT OF OIL REMOVAL FROM SEAWATER BY FROTH FLOTATION

Louxiang Wang, Meghan Curran, Meijiao Deng, Qingxia Liu, Zhenghe Xu, and Jacob Masliyah

13.1 INTRODUCTION

In the past 50 years, 80% of the largest volume oil spills occurred offshore (Etkin, 1999). From April 20 to July 15, 2010, an approximate 4.9 million barrels (780,000 m^3) of crude oil was released into the Gulf of Mexico due to the explosion and subsequent collapse of the British Petroleum (BP) Deepwater Horizon exploration platform (Kerr, 2010; Lubchenco et al., 2010). This environmental disaster inflicted incalculable damage to the ecosystem of the gulf. The unified command response operations employed to deal with the oil spill include direct recovery of oil from the wellhead, *in situ* burning, skimming, and chemical dispersion of oil (Kerr, 2010).

Direct recovery of oil from the wellhead is estimated to account for 17% removal of the oil released from the BP Deepwater Horizon oil spill (Kerr, 2010). It was accomplished through the use of a riser pipe insertion tube and later a top hat system. *In situ* burning is estimated to account for 5% of the total oil spill, which reduces the spread of oil by deliberately burning crude oil on the sea surface. This method has the lowest cost involved for its implementation (Etkin and Tebeau, 2003) but raises

Oil Spill Remediation: Colloid Chemistry-Based Principles and Solutions, First Edition.
Edited by Ponisseril Somasundaran, Partha Patra, Raymond S. Farinato, and Kyriakos Papadopoulos.

questions about emissions and production of particulate matter (Schaum et al., 2010). It is estimated that 3% of the oil was recovered by skimming, which requires oil droplet size be sufficiently large for effective oil and water separation (Nordvik et al., 1996). This approach requires an advanced knowledge of the interfacial properties at seawater–crude oil interface, which determines the coalescence of oil droplets to sufficient size. In summary, it is estimated that direct recovery, burning, and skimming removed one quarter (25%) of the oil released from the wellhead, leaving the remaining 75% of the spill uncontained.

One quarter (25%) of the total oil naturally evaporated or dissolved, and 24% dispersed either naturally or as a result of chemical dispersion. The remaining amount (26%) washed up and was collected from the shore or was buried in sand and sediments (Kerr, 2010; Lubchenco et al., 2010). Oil in the residual and dispersed categories is in the process of being degraded. The emulsified small oil droplets form relatively low concentration as oil-in-water emulsion. Although the dispersed crude oil droplets are thermodynamically unstable, they are kinetically very stable due to the adsorption of natural surfactants (chemicals having a hydrophilic head and a hydrophobic tail), wax, and solids at the oil–water interface (Menon et al., 1988). We may not know the environmental consequences of these fugitive oils for years.

In an effort to minimize environmental consequences of the Gulf of Mexico oil spill, chemical dispersants were added to disperse 8% of the oil. Chemical dispersants consist of surfactants that attach to oil drop–water interface and reduce its interfacial tension. The decrease in interfacial tension promotes the breaking of the oil slicks into small droplets of diameter less than 100 μm and decreases the probability of oil droplet coalescence (Lubchenco et al., 2010). Dispersants Corexit 9527 and Corexit 9500A were reported to have been used both at the surface and at the wellhead in the amount of 2.1 million gallons (7950 m^3) (Kujawinski et al., 2011). This approach does not allow any recovery of the oil, and previous studies have shown detrimental effects of dispersants on wildlife and microbial colonies (Kujawinski et al., 2011; Milinkovitch et al., 2011). Furthermore, an adverse effect on the oxygen concentration due to increased microbial activity has also been illustrated (Kessler et al., 2011).

For the aforementioned reasons, it is of paramount importance to develop reliable, economical, and convenient methods to separate the relatively low concentration of crude oil from water, especially with regard to the small oil droplets. Based on the difference in the natural or induced hydrophobicity of particles or oil droplets, froth flotation has been widely used, for over a century, to quickly and efficiently separate valuable minerals from gangue minerals and for wastewater treatment. The attachment of particles to air bubbles is of fundamental importance for flotation, which includes many physiochemical and hydrodynamic phenomena in a dynamic system of solid particles, air bubbles, and aqueous solutions containing various chemicals. The goal of this chapter is to investigate the interfacial properties of heavy offshore oil by determining the coalescence time of oil droplets and the induction time of bubble–oil attachment in seawater using a novel induction timer (integrated thin film drainage apparatus or ITFDA). The intention is to lay a foundation for the removal of emulsified heavy oil such as that from the Gulf of Mexico oil spill by froth flotation in an economical and environmentally friendly manner.

TABLE 13.1 Properties and composition of crude oil and water used in this study

Crude oil properties (Simon et al., 2010)		Water properties		
			Brackish water	Tap water[a]
Density (g/cm^3) at 15°C	0.939	Density (g/cm^3) at 20°C	1.0166	1.00
TAN (mg/g)	2.15	Salinity (wt% of salt in water)	2.65	—
Wax content (wt%)	0.11	Na^+ (ppm)	6367	9.9
Saturates (wt%)	37	K^+ (ppm)	297	0.8
Aromatics (wt%)	44	Mg^{2+} (ppm)	997	13.5
Resins (wt%)	16	Ca^{2+} (ppm)	632	48
Asphaltenes, hexane insoluble (wt%)	2.5	Surface tension (mN/m)	72.6	72.3

[a]2010 Edmonton water and wastewater performance report.

13.2 MATERIALS AND METHODS

13.2.1 Materials and Sample Preparations

A Grane heavy crude oil from Statoil, Norway, was used in this study. The density, total acid number (TAN), water content (WC), and saturate, aromatic, resin and asphaltene (SARA) compositions of the oil are summarized in Table 13.1. Seawater was obtained from the west coast of Vancouver, British Columbia, Canada. The seawater was filtered with a 0.2 μm filter to remove fine solids. The seawater and tap water composition determined by atomic absorption spectroscopy (AAS) and salinity of the water are also listed in Table 13.1. It should be noted that the salinity of the seawater is a little bit less than the value normally reported. Hence, the seawater sample used in this work is more likely to be "brackish water". Petroleum naphtha (heavy reformate) was received from Champion Technologies. All the measurements were conducted at the ambient room temperature of 20 ± 0.5°C. The pH of the aqueous solutions was adjusted by reagent grade sodium hydroxide (NaOH) and hydrochloric acid (HCl) (Fisher Scientific) solutions.

Thirty drops of heavy oil were added into 100 mL of tap water or seawater at pH 9.0 and then homogenized by a PowerGen 125 (Fisher Scientific) operated at 6000 rpm for 10 min to prepare heavy oil-in-water emulsions. The emulsion was allowed to cream for about 30 min to equilibrate the oil–water interface. After 30 min, a thin layer of crude oil was observed at the top of the sample, and the sample underneath this oil layer was used for experiments. The size of the formed oil droplets was determined by focused beam reflectance method (Mettler-Toledo, Greifensee, Switzerland). The average diameter (measured as cord length) of the oil droplets prepared as such was determined to be approximately 10 μm and was stable for at least 2 h. The formed oil-in-water emulsion was used for zeta potential measurement and microflotation tests.

13.2.2 Measurement of Oil–Water Interfacial Properties

The oil–water interfacial tension and zeta potential of oil-in-water emulsions were determined. The oil–water interfacial tension was measured using a Processor Tensiometer K12 (Krüss, Hamburg, Germany) by the Du Noüy ring method. Prior to all the tests, the measurement chamber was filled with deionized water and the surface tension was measured. The chamber and the platinum ring were considered to be clean when the surface tension of deionized water was measured to be 72.8 ± 0.5 mN/m. After ensuring the cleanliness of the system, equal volumes of oil and seawater were added into the vessel. It has been well recognized that the presence of natural surfactants at the oil–water interface reduces the interfacial tension, and this interfacial tension reduces with aging time (Bhardwaj and Hartland, 1994). Hence, after positioning the ring into the seawater phase, the oil and water layers were left in contact for 30 min before measurements to allow the surface-active species to migrate from the oil phase to the oil–water interface. Zeta potentials of heavy oil droplets in seawater and tap water were determined using a ZetaPALS (Brookhaven Instruments Corp., New York). A dilute suspension of emulsified heavy oil was prepared by adding several drops of oil emulsions to 50 mL water of interest. The prepared suspensions were stirred with a magnetic mixer for 5 min before measurements. Five measurements were taken for each condition, and the average value together with the standard deviation was reported.

13.2.3 Measurement of Coalescence and Induction Times

The coalescence time of oil droplets and induction time of air bubble–oil attachment were determined by an ITFDA developed recently in our laboratories (Wang et al., 2013). Equipped with a bimorph force sensor, a computer-interfaced video capture device, and data acquisition system, this ITFDA was used to study the dynamic interactions between heavy oil droplets and between air bubbles and oil droplets.

As shown in Figure 13.1, a Teflon holder with a bowl-shaped top surface was clamped at the end of a bimorph beam. The bimorph beam was enclosed by a fluorinated ethylene propylene (FEP) sheath with one end being mounted on the wall of a small stainless steel chamber, which was placed on a 3-D translation stage. An air bubble (or a crude oil droplet) was generated at the end of a glass capillary tube that was connected to a speaker diaphragm. The movement of speaker diaphragm was controlled by an applied electrical voltage of desired wave form generated by a computer, which drives the bubble or oil droplet on the glass capillary tube to approach or retract from the lower surface at a well-controlled manner in terms of oil droplet displacement velocity, V. The extent (applied force) and duration of contact were also well controlled through this process. Two cameras were placed perpendicular to each other near the sample chamber for surface alignment, and control of bubble size and initial gap between the two surfaces. When the two surfaces approach each other, a deflection of the bimorph occurs due to the interaction force between

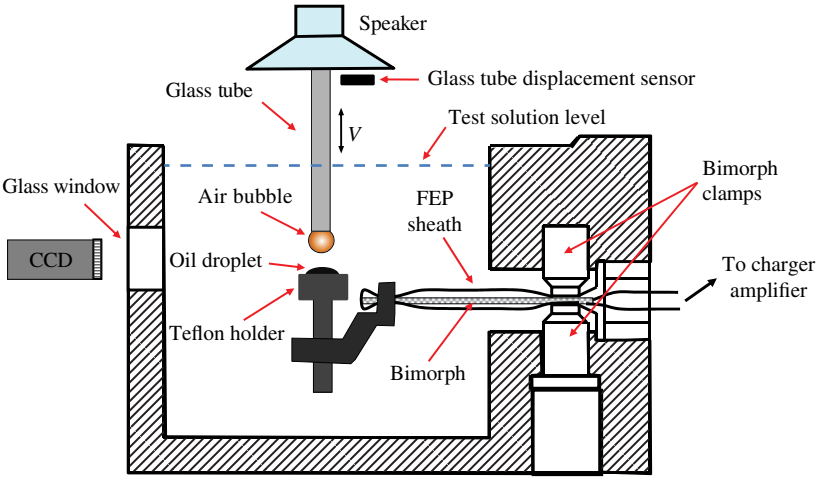

FIGURE 13.1 A cross-sectional view of the ITFDA for measuring the interaction between an air bubble and an oil droplet or between two droplets in a liquid.

the surfaces. This force was recorded by the bimorph charge amplifier in the form of bimorph electric charges. As a piezoelectric device, the charges generated on the bimorph are proportional to the deflection of the beam or the force applied at the end of the beam. A user-developed program, interfaced with LabVIEW 8.0, was used to monitor and investigate the entire dynamic process.

When the upper object (air bubble or oil droplet) is brought down to interact with the lower surface, a repulsive force causes the bimorph beam to deflect downward, producing a positive bimorph charge. In contrast, an attractive force between the two surfaces causes the bimorph beam to deflect upward, generating a negative charge on the bimorph. Figure 13.2 shows the bimorph signal recorded when an oil droplet A attached to the glass capillary tube approaches another oil droplet B, which is fixed on Teflon holder as shown in Figure 13.1 in seawater at pH 7.6. In this test, approach velocity is set to be 240 μm/s. At large separation distances, there is no detectable interaction force between the two oil droplets, represented by a zero bimorph signal with electrical noise. After the two droplets arrive at a distance where the hydrodynamic and/or surface forces begin to be detectable, a repulsive force is shown at point "a", represented by an increase in bimorph signal. The following sharp increase of bimorph signal until point "b" is a result of applied force by continued push of the upper oil droplet A down against the lower oil droplet B. At point "b", with the upper oil droplet being held stationary against the lower oil droplet, a constant bimorph signal is displayed. The constant bimorph signal over this "holding" period indicates a negligible leakage of electrical charges from the bimorph at the given sensitivity of the system. During the "holding" period, the thickness of the aqueous film continues to thin until the thickness of the film reaches a critical thickness whereby it ruptures. The break of the film is followed by the coalescence

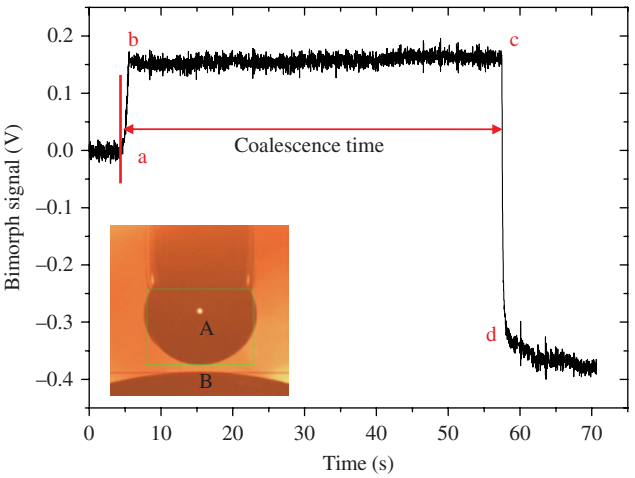

FIGURE 13.2 Bimorph signal profile for coalescence time determination of two oil droplets using ITFDA. The inset figure shows the two oil droplets of diameters 1.49 mm (**A**) and 8.52 mm (**B**). The measurement was conducted in seawater at pH 7.6 and an approach and retract velocity of 240 μm/s.

of the two oil droplets, which is characterized by a sharp drop of bimorph signal at point "c" to −0.34 V at point "d", indicating upward deflection of bimorph upon coalescence. The subsequent spreading of the coalescing oil droplets causes a slight lift of lower surface, as indicated by a continuous drop of bimorph signal beyond point "d". The drainage time of the aqueous film between the two oil droplets (or air bubble–oil droplet) is known as coalescence (induction) time (Hartland and Vohra, 1980; Yoon and Yordan, 1991). The coalescence time or induction time in this study is measured from point "a" to point "c", that is the time for film thinning. As shown in Figure 13.2, for example, the coalescence time of the two oil droplets in seawater at pH 7.6 is determined to be 52.9 s. The entire approaching and retracting processes are recorded in real time by one of the high-resolution digital video cameras interfaced with the computer that is used to drive the speaker diaphragm and record bimorph signal simultaneously.

Before each experiment, the chamber was filled with test solutions, followed by an oil droplet being placed on the Teflon sample holder. The glass capillary tube was filled with the heavy oil or fresh air before being brought into the solution. The system was then left for 2 h to stabilize the bimorph signal. Fresh air bubbles and heavy oil droplets were created for induction time and coalescence time measurements. In this study, the size of the upper and lower droplets was controlled to be 1.50 ± 0.02 and 8.50 ± 0.02 mm, respectively, and the initial separation distance between the two droplets was maintained at 0.12 ± 0.01 mm, unless otherwise indicated. Thirty measurements were taken at each condition and the average value was reported with the error being the standard deviation of these 30 measurements.

13.2.4 Microflotation Test

To demonstrate the feasibility of applying flotation to recover heavy oil from seawater, a microflotation test was employed. The pH of the homogenized oil-in-water emulsion was adjusted back to pH 7.6 before flotation. The emulsion was then transferred into the microflotation cell. The flotation was conducted for 20 min at an air flow rate of 25 mL/min. During flotation, a magnetic stir was placed on the fritted dish to better distribute the generated air bubbles. Due to the low concentration of oil in water and its sticky nature to glass, a quantitative analysis of oil from emulsion was not attempted. Instead, the subphase (the residual emulsion in the flotation cell) after the flotation test was collected to visually demonstrate the effectiveness of flotation.

13.3 RESULTS AND DISCUSSION

13.3.1 Interfacial Tension and Zeta Potentials

The interfacial tension and zeta potential of the heavy oil–water interface were measured as a function of pH to understand the surface properties of the heavy oil. For comparison, naphtha, a distillation product of crude oil, which is believed to have a much fewer surfactants, was used as a model oil. The naphtha–water interfacial tension was measured as a baseline. As shown in Figure 13.3, the interfacial tension of heavy oil–seawater interface decreased sharply with pH, from 22.7 mN/m at pH 6 to 8.9 mN/m at pH 10. The interfacial tension of naphtha–seawater was measured to be higher than heavy oil–seawater interface at most pH values studied, also decreasing

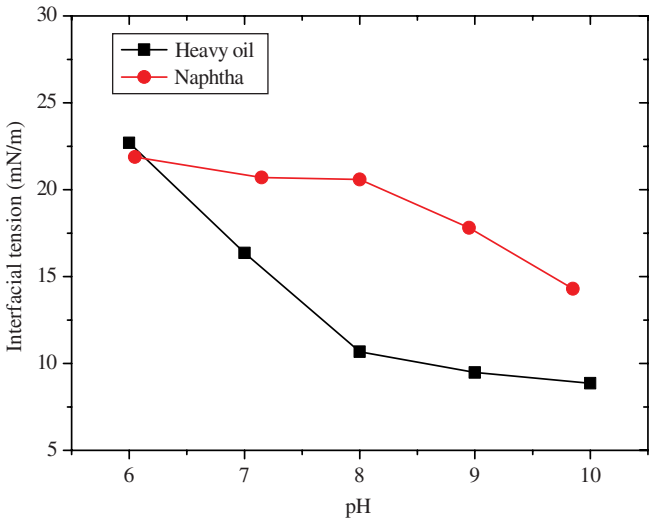

FIGURE 13.3 Interfacial tension of heavy oil–seawater and naphtha–seawater interface as a function of solution pH.

with pH but to a less extent. The effect of pH on the interfacial tension is explained by pH-dependent ionization of the surfactant present at heavy oil–water interface. Substantial amounts of amphiphile compounds such as asphaltenes, resins, and naphthenic acids were found in crude oil (Simon et al., 2010; Sjöblom et al., 2003). These indigenous compounds contain acidic and basic functional groups. A critical pH to reach a maximum interfacial tension value was observed (Bai et al., 2010; Nenningsland et al., 2010). Over the low pH range, the interfacial tension is mostly governed by the protonation of basic molecules, while over the high pH range, interfacial tension reduction is mainly attributed to extraction and dissociation of acidic surfactant molecules. It is therefore expected that the pH change of the aqueous solution will affect the ionization of the surfactant at the interface, causing a dramatic change in oil–water interfacial properties and solubility of surfactant in the water phase. The observed reduction of the heavy oil–seawater interfacial tension was mainly attributed to the increased concentration of surface-active molecules at heavy oil–water interface with contributions from increased dissociation of carboxylic acid groups, maximizing the accumulation of the indigenous surfactants at the heavy oil–water interface. The drop of the naphtha–seawater interfacial tension with pH also indicates the presence of surface-active components of acidic nature in naphtha at the interface. The amount of surfactants present in naphtha however was much less than in heavy oil, resulting in a higher interfacial tension of naphtha–water interface than that of the heavy oil–seawater interface.

Figure 13.4 shows the zeta potential of emulsified heavy oil as a function of pH in tap water and seawater. The zeta potentials of heavy oil droplets in these two types of water were negative, which indicates the presence of anionic surface groups at oil–water interfaces. The zeta potential became more negative with increasing pH and leveled off after pH 7 in tap water, indicating a dominant presence of a weak acid type of

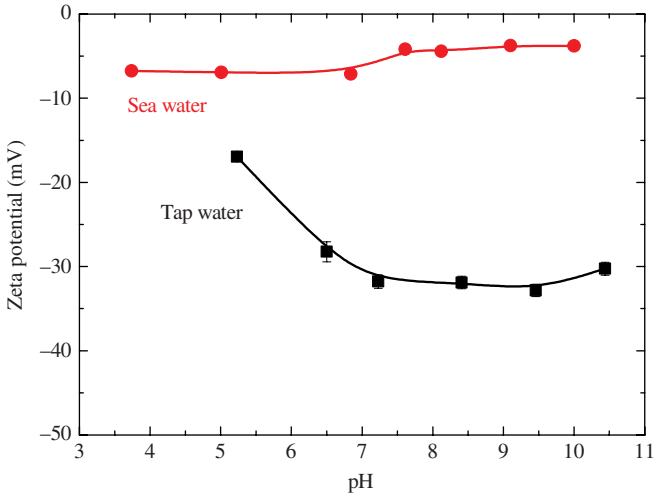

FIGURE 13.4 Zeta potential of oil droplets in tap water and seawater as a function of pH.

surfactant, most likely a carboxylic acid type at oil–water interface. Considering a typical pKa of 4–5, more carboxylic groups were dissociated at higher pH, resulting in a more negative surface charge of heavy oil droplets at higher pH. In contrast, in seawater, pH showed a marginal effect on the zeta potential of heavy oil droplets and the values were less negative. As shown in Table 13.1, the concentrations of simple electrolyte ions such as Na^+, Cl^-, and K^+ in seawater were considerably higher than that in tap water, which considerably compressed the electrical double layer of the heavy oil droplets, leading to a much smaller zeta potential value and less pH dependency. In addition, more divalent cations such as Mg^{2+} and Ca^{2+} were present in seawater. These ions can specifically adsorb at the oil–water interface through their binding with carboxylic groups, contributing to the reduction of negative zeta potential values.

13.3.2 Interactions between Oil Droplets

13.3.2.1 Effect of Solution pH

The coalescence time of two heavy oil droplets was measured using ITFDA in both tap water and seawater. The measurements were conducted at a constant droplet driving velocity of 240 μm/s and the results are shown in Figure 13.5. In tap water, no coalescence was observed even at a contact time of 300 s, showing a very stable water film between oil droplets in tap water. However, the oil droplets in seawater coalesced and the coalescence time increased dramatically with increasing seawater pH, from 8.7 s at pH 6.0 to 96.7 s at pH 9.0.

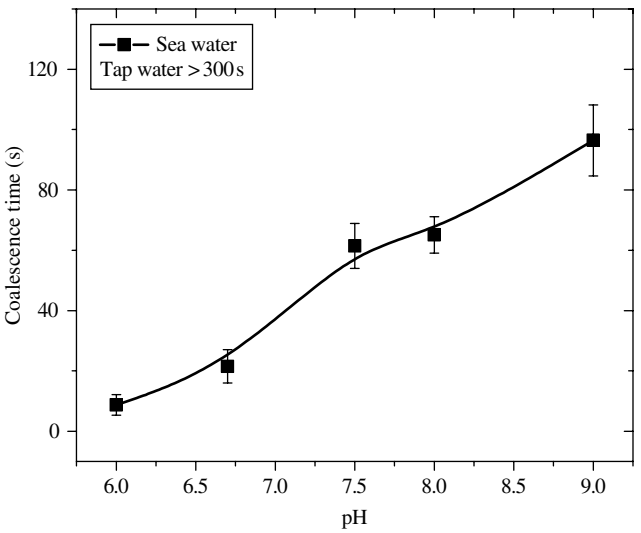

FIGURE 13.5 Coalescence time of heavy oil droplets in tap water and seawater as a function of solution pH at a driving velocity of 240 μm/s. In tap water, no coalescence was observed even at a contact time of 300 s at all studied pH values.

In tap water, the water film between two oil surfaces was very stable due to a positive disjoining pressure (a pressure used to describe the free energy change of the intervening liquid film) (Nguyen and Schulze, 2004), resulting in a very long coalescence time (larger than 300 s as illustrated in Figure 13.5). The coalescence of oil droplets in seawater indicates the water film ruptured during the interaction, suggesting a dramatic reduction of repulsive force or an increase of attractive force. Since the van der Waals force between two similar oil droplet surfaces in water is less sensitive to the change of solution chemistry, the observed change of the film stability is probably due to a reduction of repulsive electrical double layer force. From tap water to seawater, the repulsive electrical double layer force reduced dramatically with much less negatively charged oil surfaces and highly compressed electrical double layers. During the drainage process, the film became progressively thinner and thinner, when it reached a critical thickness, the attractive forces dominated the total force and the film ruptured.

The continuous increase in the coalescence time with increasing pH indicates a lower film drainage rate at higher pHs. According to Figure 13.4, the zeta potential of oil droplets in seawater remained almost the same over the pH range studied. Increasing pH would increase potential at the stern layer of oil droplets to a more negative value; however, the potential decays significantly with the distance due to a high electrolyte concentration, resulting in a very similar potential at the shear plan where the zeta potential value is measured. The calculation of the electrical double layer force between the two oil droplets (not presented here) indicates that the force changes little with the change of the stern potential. Little change of van der Waals force and electrical double layer force would render a similar property of drainage film between oil droplets. Therefore, the extended Derjaguin–Landau–Verwey–Overbeek (DLVO) theory needs to be used to analyze the interactions between two surfaces. In the extend DLVO theory, forces other than van der Waals force and electrical double layer force are considered, including attractive long-range hydrophobic force and repulsive short-range steric and/or hydration forces (Israelachvili, 1991). The increase in the coalescence time with pH may be contributed to the reduction in attractive hydrophobic force and/or increase in repulsive hydration force of hydrated carboxylate groups of natural surfactant accumulated at oil–water interface with increasing pH. As discussed previously, at high pH, more acidic groups of natural surfactant were dissociated at the oil–water interface as indicated by increased negative zeta potential values of the heavy oil droplets in tap water. A higher concentration of natural surfactants was also expected at oil–seawater interface; however, the high electrolytes concentration and the presence of divalent ions made the zeta potential measurement insensitive to the change of the oil–seawater interface. The increased adsorption and ionization of water-soluble surfactant would reduce the hydrophobicity of oil–water interface. The reduction of surface hydrophobicity reduced the attractive hydrophobic force between two oil surfaces. Moreover, the presence of more indigenous surfactants at the oil–water interface would incur a stronger hydration and steric repulsive force between hydrophilic head groups, contributing to the decreased film drainage rate and, hence, increased coalescence time with increasing pH of seawater.

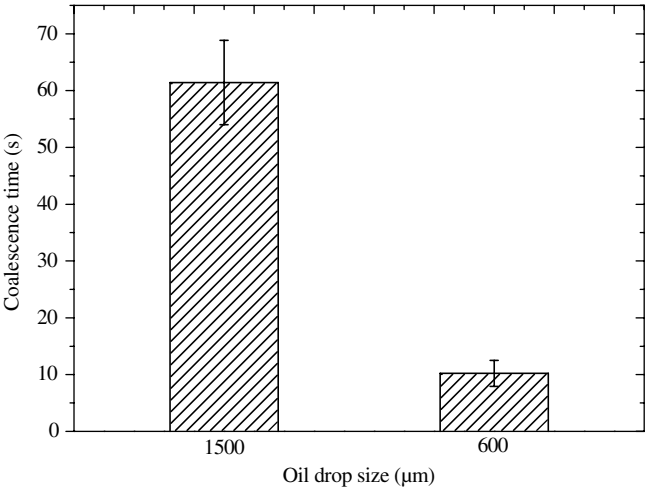

FIGURE 13.6 Effect of droplet size of upper heavy oil droplet on coalescence time in seawater at pH 7.6 with oil droplet driving velocity of 240 μm/s.

13.3.2.2 Effect of Oil Droplet Size and Driving Velocity

To study the effect of heavy oil droplet size on coalescence time, the diameter of the upper oil droplet was varied from 1500 to 600 μm, while the lower oil surface remained the same. As shown in Figure 13.6, the coalescence time dropped from 61.4 to 10.2 s by decreasing the size of upper oil droplet from 1500 to 600 μm. In this set of measurements, the applied force from the upper oil droplet to the lower oil droplet was kept the same during measurements as shown by the same voltage reading on the bimorph during the holding period. Consequently, a higher external pressure was applied on the lower oil droplet by the smaller upper oil droplet due to the reduced contact area. A higher pressure tends to drain the aqueous film faster, resulting in a decrease in coalescence time as observed.

Figure 13.7 shows the effect of upper oil droplet driving velocity on the coalescence time of heavy oil droplets in seawater at pH 6.0. As can be noted from the graph, the coalescence time changed little at low driving velocity and increased sharply when the driving velocity was larger than 240 μm/s. The thinning process of the liquid film is controlled by hydrodynamic force initially and by the surface forces at smaller separation distances. During the approaching, the water between two surfaces is repelled from the drainage film, which generates a hydrodynamic pressure. This hydrodynamic pressure deforms the oil–water interfaces and influences the whole drainage process. At a driving velocity smaller than 240 μm/s, the coalescence time remained similar due to limited differences in deformation of the interfaces. At higher driving velocities, the water film between two approaching oil droplets did not have sufficient time to be expelled sufficiently. The excess water volume trapped between the two oil droplets caused significant deformation of oil–water interfaces, forming a so-called dimple where the film thickness is higher at the center than at the barrier rim. In this case, the drainage of intervening liquid film was limited by water

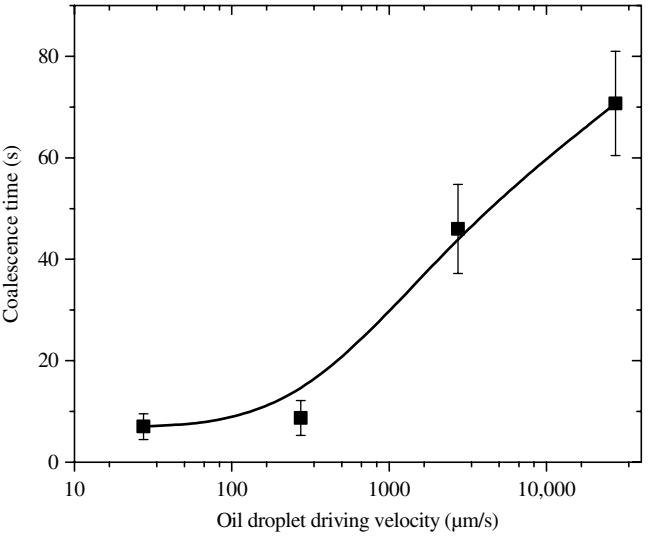

FIGURE 13.7 Coalescence time of heavy oil droplets in seawater at pH 6.0 as a function of oil droplet driving velocity.

flow through the rim between the two oil droplets. At a high driving velocity, therefore, the repulsive hydrodynamic force dominated the total force, thereby reducing the film drainage rate and increasing the coalescence time.

13.3.3 Air Bubble—Oil Droplet Interactions

Among all the subprocesses of successful mineral flotation, the attachment of the mineral particles to air bubbles is of fundamental importance. This process involves the thinning and rupture of the intervening liquid film, followed by the spreading of three-phase contact line on the mineral particle. The minimum contact time required for a successful air bubble–particle attachment is defined as induction time. The induction time was first described in the early 1930s and has been extensively used in flotation research and modeling (Gu et al., 2003; Sven-Nilsson, 1935; Yoon and Yordan, 1991). To determine the induction time in mineral flotation systems, a captive air bubble is usually moved toward and then away from a particle bed or a flat mineral surface. A shorter induction time leads to a higher recovery for both quartz flotation (Yoon and Yordan, 1991) and bitumen flotation (Wang et al., 2010). Since the induction time can reflect the kinetics and is linked with interfacial phenomena and the hydrodynamic effect in flotation, induction time between an approaching air bubble and heavy oil surface was investigated in this study.

Figure 13.8 shows the result of induction time measured between an air bubble and a heavy oil droplet in seawater as a function of bubble aging time. As can be seen from Figure 13.8, the induction time of fresh air bubble–heavy oil droplet attachment

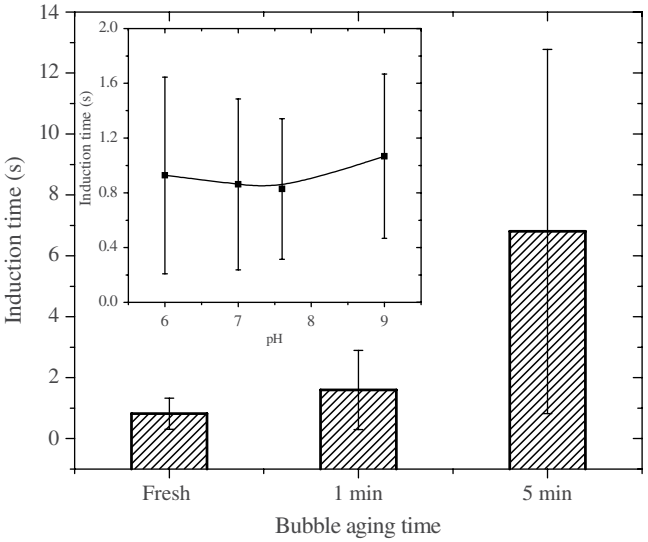

FIGURE 13.8 Aging of air bubble on induction time of air bubble–oil attachment in seawater at natural pH of 7.6 and bubble driving velocity of 240 μm/s; inset shows the effect of pH on induction time.

in natural pH was 0.83 s, much smaller than the coalescence time of oil droplets at the same condition (61.4 s). And the induction time of air bubble–oil attachment increased from 0.8 s for a fresh bubble to 1.6 and 6.8 s when the bubble was aged for 1 and 5 min, respectively. The increase of induction time with aging bubbles was mainly due to the accumulation of natural surface-active species at the air–water interface with time. When placing oil droplets into seawater, surfactants migrated from heavy oil to the oil–water interface and into aqueous solution. The accumulation of these surfactants at the oil–water interface not only reduced the interfacial tension (Fig. 13.3) but also made the oil surface more negatively charged in tap water (Fig. 13.4). When the air bubble was immersed in the aqueous solution, the adsorption of surfactant, originally from heavy oil, at the bubble–water interface was inevitable. Similar to the oil–water interface, the adsorption of surfactant at the bubble–water interface would not influence the zeta potential of bubble in an environment with a large ion concentration, hence the electrical double layer force. The marginal effect of water chemistry (i.e., solution pH) on the electrical double layer force between the air bubble and the oil surface was illustrated by the almost constant induction time of bubble–oil attachment at different pH in seawater. As shown in the inset of Figure 13.8, the induction time of fresh bubble–oil attachment remained around 0.9 s from pH 6 to 9 in seawater with a bubble driving velocity of 240 μm/s. Meanwhile, the adsorption of natural surfactants at the air–water interface decreased the air bubble hydrophobicity. The decreased attractive hydrophobic force and increased repulsive hydration force reduced the film drainage rate and hence increased the induction time of bubble attachment to heavy oil droplets in seawater with bubble aging time. This finding

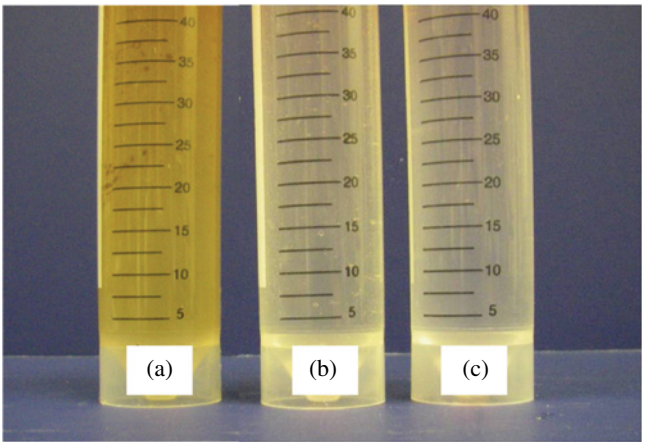

FIGURE 13.9 Photographs of samples: (**a**) heavy oil-in-seawater emulsion, (**b**) subphase of emulsion after 20 min of flotation, and (**c**) seawater.

suggests the use of fresh air bubbles to recover heavy oil from oil emulsions to maximize the flotation rate.

As discussed previously, it is evident that oil droplets are much easier to attach to air bubbles than to oil droplets themselves, as shown by a much shorter induction time (0.83 s) than coalescence time (61.4 s) at pH 7.6. This finding suggests that flotation of oil spill by induced air bubbles is more effective than by natural coalescence of spill oil droplets, even without considering more effective buoyancy force of air bubbles than oil for concentrating oils on water surface for effective removal and recovery.

13.3.4 Microflotation of Crude Oil

A microflotation test was conducted to recover heavy oil from seawater. The results are visually compared using photographs in Figure 13.9. Compared with the photograph of turbid oil emulsion after 12 h creaming without any treatment (a), the photograph (b) of subphase obtained after 20 min of microflotation using air bubbles is seen to be as clear as the seawater in photograph shown under c. The before-mentioned three photographs qualitatively illustrate the effectiveness of removing oil droplets from the emulsion by flotation, illustrating that flotation is an excellent method to remove oil from seawater.

13.4 CONCLUSIONS

The interfacial properties of heavy oil–water interface were studied in terms of interfacial tension and zeta potential as a function of seawater and tap water pH. The dissociation of surfactants at heavy oil–water interface not only reduced the interfacial

tension but also made the oil surface more negatively charged with increasing solution pH. The coalescence time of oil droplets and the induction time of air bubble–heavy oil attachment were determined by the ITFDA. In tap water, no coalescence was observed due to the presence of strong electrical double layer repulsive forces. In seawater, however, less negatively charged oil surfaces made the coalescence much easier to take place due to the high electrolyte concentration and presence of divalent cations. The coalescence time increased with increasing pH due to the increased adsorption and ionization of natural surfactants present in the heavy oil. Large size ratio of approaching to stationary oil droplets and low driving velocity were preferable for oil droplets coalescence. Fresh air bubbles were found to promote the attachment of air bubbles to oil droplets and the induction time increased with the aging of air bubbles. Flotation has been shown to be a convenient and efficient way to remove emulsified heavy oil from seawater.

ACKNOWLEDGMENTS

We would like to thank Dr. Sébastien Simon for providing us the heavy oil sample and Shiraz Merali for the AAS analysis of seawater. Financial support for this work from the NSERC Industrial Research Chair Program in Oil Sands Engineering is greatly appreciated.

REFERENCES

Bai JM, Fan WY, Nan GZ, Li SP, Yu,B. Influence of interaction between heavy oil components and petroleum sulfonate on the oil-water interfacial tension. J Disper Sci Technol 2010; 31(4):551–556.

Bhardwaj A, Hartland S. Dynamics of emulsification and demulsification of water-in-crude oil-emulsions. Ind Eng Chem Res 1994;33(5):1271–1279.

Etkin DS. Historical overview of oil spills from all sources (1960–1998). In: Proceedings of the 1999 International Oil Spill Conference; Mar 8–11, 1999. (Seattle, WA). API (Washington, DC), p 1097–1102.

Etkin DS Tebeau P. Assessing progress and benefits of oil spill response technology development since Exxon Valdez. In: Proceedings of the 2003 International Oil Spill Conference; Apr 6–10, 2003 (Vancouver, BC). API (Washington, DC), p 843–850.

Gu GX, Xu ZH, Nandakumar K, Masliyah J. Effects of physical environment on induction time of air-bitumen attachment. Int J Miner Process 2003;69(1–4):235–250.

Hartland S, Vohra DK. Effect of inter-drop forces on the coalescence of drops in close-packed dispersions. J Colloid Interface Sci 1980;77(2):295–316.

Israelachvili JN, editor. General Physical Chemistry. In: *Intermolecular and Surface Forces*. London: Academic Press; 1991. p 449.

Kerr RA. A lot of oil on the loose, not so much to be found. Science 2010;329(5993): 734–735.

Kessler JD, Valentine DL, Redmond MC, Du M, Chan EW, Mendes SD, Quiroz EW, Villanueva CJ, Shusta SS, Werra LM, Yvon-Lewis SA, Weber TC. A persistent oxygen anomaly reveals the fate of spilled methane in the deep Gulf of Mexico. Science 2011;331(6015):312–315.

Kujawinski EB, Kido Soule MC, Valentine DL, Boysen AK, Longnecker K, Redmond MC. Fate of dispersants associated with the deepwater horizon oil spill. Environ Sci Technol 2011;45(4):1298–1306.

Lubchenco J, McNutt M, Lehr B, Sogge M, Miller M, Hammond S, Conner W. BP Deepwater Horizon oil budget: what happened to the oil? 2010. http://www.usgs.gov/foia/budget/08-03-2010...Oil%20Budget%20description%20FINAL.pdf

Menon VB, Nikolov AD, Wasan DT. Interfacial effects in solids-stabilized emulsions – measurements of film tension and particle interaction energy. J Colloid Interface Sci 1988;124(1):317–327.

Milinkovitch T, Kanan R, Thomas-Guyon H, Le Floch S. Effects of dispersed oil exposure on the bioaccumulation of polycyclic aromatic hydrocarbons and the mortality of juvenile Liza ramada. Sci Total Environ 2011;409(9):1643–1650.

Nenningsland AL, Simon S, Sjöblom J. Surface properties of basic components extracted from petroleum crude oil. Energy Fuels 2010;24(12):6501–6505.

Nguyen A, Schulze HJ, editors. *Colloidal Science of Flotation*. Surfactant Science Series 118. New York: Marcel Dekker; 2004. p 850.

Nordvik AB, Simmons JL, Bitting KR, Lewis A, Strøm-Kristiansen T. Oil and water separation in marine oil spill clean-up operations. Spill Sci Technol Bull 1996;3(3):107–122.

Schaum J, Cohen M, Perry S, Artz R, Draxler R, Frithsen J. B, Heist D, Lorber M, Phillips L. Screening level assessment of risks due to dioxin emissions from burning oil from the BP deepwater horizon Gulf of Mexico spill. Environ Sci Technol 2010;44(24):9383–9389.

Simon S, Nenningstand AL, Herschbach E, Johan S. Extraction of basic components from petroleum crude oil. Energy Fuels 2010;24(2):1043–1050.

Sjöblom J, Aske N, Auflem IH, Sæther Ø, Westvik A, Johnsen EE, Kallevik H. Our current understanding of water-in-crude oil emulsions. Recent characterization techniques and high pressure performance. Adv Colloid Interface Sci 2003;100–102:399–473.

Sven-Nilsson I. Effect of contact time between mineral and air bubbles on flotation. Kolloid-Z 1935;69(2):230–232.

Wang L, Sharp D, Masliyah JH, Xu Z. Measurement of interactions between solid particles, liquid droplets, and/or gas bubbles in a liquid using an Integrated Thin Film Drainage Apparatus. Langmuir 2013;29:3504–6303.

Wang L, Dang-Vu T, Xu Z, Masliyah JH. Use of short-chain amine in processing of weathered/oxidized oil sands ores. Energy & Fuels 2010; 24(6): 3581–3588.

Yoon RH, Yordan JL. Induction time measurements for the quartz-amine flotation system. J Colloid Interface Sci 1991;141(2):374–383.

14

MEASUREMENT OF INTERFACIAL TENSION IN HYDROCARBON/ WATER/DISPERSANT SYSTEMS AT DEEPWATER CONDITIONS

Mohamed A. Abdelrahim and Dandina N. Rao

14.1 INTRODUCTION

Due to the unprecedented nature of the Deepwater Horizon oil spill, BP along with the U.S. Coast Guard and the Environmental Protection Agency decided to try the first subsea injection of chemical dispersants directly at the source. Over 700,000 gallons (http://www.noaa.gov; http://www.oilspillcommision.gov; http://www.uscg.mil) of chemical dispersants were sprayed directly onto the gushing oil at the wellhead located 5000 ft below the water level in an attempt to keep some of the oil under the water surface.

The purpose of an oil spill dispersant application is to lower the oil/water interfacial tension (IFT) to promote entrainment of small oil droplets into the water column (Clayton et al., 1993; Cormack et al., 1986–1987; Mackay and Hossain, 1982; Mackay et al., 1984). Entrainment of small oil droplets into the underlying water, by either physical (wind and/or wave turbulence) or chemical means (dispersant application), increases the oil–water interfacial area and requires some form of energy defined as the mixing energy (Equation 14.1) (Clayton et al., 1993):

$$W_k = \gamma_{o/w} A_{o/w} \tag{14.1}$$

Oil Spill Remediation: Colloid Chemistry-Based Principles and Solutions, First Edition.
Edited by Ponisseril Somasundaran, Partha Patra, Raymond S. Farinato, and Kyriakos Papadopoulos.

where W_k is the mixing energy, $\gamma_{o/w}$ is the oil–water IFT, and $A_{o/w}$ is the oil–water interfacial area. Thus, the reduction of the oil–water IFT will allow the formation of a greater interfacial area with a minimal amount of energy input to the system.

The effectiveness of a chemical dispersant can be defined by the magnitude of the decrease in the oil–water IFT to the critical micelle concentration (CMC) (Clayton et al., 1993; National Research Council (U.S.) Ocean Studies Board, 2005). The higher the magnitude of the oil–water IFT reduction to the CMC, the more effective the dispersing agent is. On the other hand, the efficiency of a chemical dispersant can be defined as the concentration of dispersant required to reach the CMC. Efficiency is greater when the CMC is attained at a lower dispersant concentration. A favorable dispersant will have a high degree of both effectiveness and efficiency. However, the two concepts are not the same and do not necessarily follow similar trends (i.e., an effective dispersant may not be efficient and vice versa).

Rewick et al. utilized the drop-weight test to estimate the oil–water IFT by measuring the weight of an oil drop before it detaches from a syringe equilibrated in a water–dispersant mixture (Rewick et al., 1984). In his work, he estimated the CMC of dispersant–water mixture and investigated the effects of water salinity and temperature on the measured IFT. From his data, he was able to show that as the temperature increased, the CMC decreased implying that the dispersant will perform more efficiently at higher temperatures. The dispersant sample used in his study was also observed to perform best when the water salinity was close to 25 ppt. This trend was attributed to the fact that the chemical dispersant included a complex blend of surfactants, and it was also noted that the interfacial interactions of any other dispersant/oil/water system would respond uniquely to the water salinity range tested.

Mackay and Hossain used the spinning drop technique to measure the oil–water IFT for systems of crude oils, distilled and saltwater, and chemical dispersants (Mackay and Hossain, 1982). They concluded that dispersion is more difficult at lower temperatures based on the fact that the experimentally measured oil–water interfacial values were higher at lower temperatures. Their results also indicated an increase in dispersant effectiveness with increasing water salinity based on noticeably higher measured oil–water IFT values than in distilled water.

Both IFT measurement techniques used by Rewick et al. and Mackay and Hossain have a good degree of reproducibility, but have not yet been adapted for high-pressure systems and therefore cannot account for the influence of pressure on the IFT. The scarcity of simultaneous low-temperature–high-pressure oil–water IFT data builds an impression of skepticism surrounding the effectiveness of chemical dispersion at conditions similar to that in deepwater. This could be attributed to the difficulty of simulating the complex marine environment in the laboratory or obtaining representative fluid samples from 5000 ft under water. The presence of salt in seawater further complicates the problem as well. Hence, this study was formulated to address the aforementioned issues by establishing a laboratory apparatus capable of replicating the Deepwater Horizon oil spill conditions of pressure, temperature, and fluids' compositions for both density and IFT measurements.

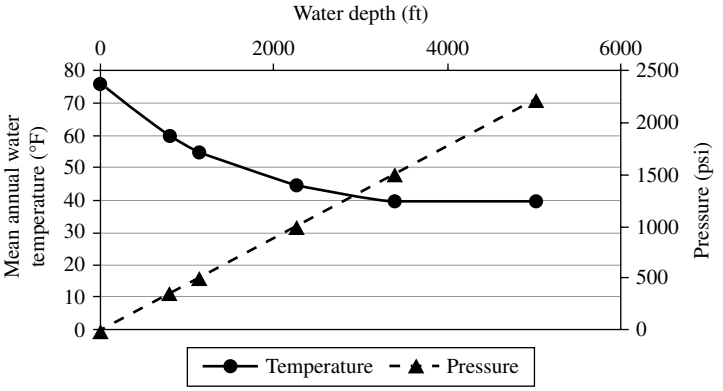

FIGURE 14.1 Representation of the conditions of pressure and temperature in the Gulf of Mexico waters (temperature and water depth data from http://www.nodc.noaa.gov).

14.2 EXPERIMENTAL METHODOLOGY

14.2.1 Design

The mean annual water temperature in the Gulf of Mexico as a function of water depth was acquired from the National Oceanographic Data Center (NODC) (http://www.nodc.noaa.gov). The pressure due to a hydrostatic column of seawater was then calculated using an average seawater density of 1.025 g/cc, typical of the Gulf of Mexico water (http://www.nodc.noaa.gov). Figure 14.1 shows the pressure and temperature variations along the water depth representing the conditions of the oil spill. Interfacial tension tests were conducted at conditions of pressure and temperature comprising the range of both variables shown in Figure 14.1. The effect of each variable was also studied independently while holding the other constant. Additionally, the influence of water salinity on the IFT and chemical dispersion was investigated as well.

14.2.2 Apparatus

An optical cell capable of withstanding high pressures and a wide range of temperatures (40°F–400°F) was specially built for this study. Made of titanium and hastelloy, the optical cell has a design rating of 20,000 psi at 400°F. The cell has four moveable arms of which the top arm and one of the side arms are used to hold solid surfaces (e.g., crystals) when conducting contact angle measurements and are therefore not utilized in this work. The other side arm is used to hold a calibration ball, while the bottom arm has a needle tip used to inject the oil in the form of pendant drops for IFT measurements.

The setup includes other accessories such as an air chiller used to attain the desired temperatures, an image-capturing system, and floating piston transfer vessels. The air chiller is connected to an ambient air supply at its inlet and pumps air at user-defined temperatures from its outlet. The image-capturing system consists of a

FIGURE 14.2 The low-temperature/high-pressure optical cell apparatus (**a**, optical cell; **b**, digital camera). *(See insert for color representation of the figure.)*

video recorder, a monitor, a light source, and a high-quality digital camera connected to a computer with an installed image analysis software. The floating piston transfer vessels were used to hold and transport experimental fluids. A digital water pump and a high-pressure hand pump were used to generate the required pressures. All wetted parts of the optical cell and its accessories such as valves, tubing, fittings, and floating piston transfer vessels are made of highly corrosion-resistant hastelloy metal (HC-276). An image of the low-temperature–high-pressure optical cell is shown in Figure 14.2 and a simplified sketch of the experimental setup is shown in Figure 14.3.

The cell, along with all wetted parts, was flushed with large amounts of toluene to dissolve any traces of hydrocarbons left after a previous experiment. Acetone was then used to remove toluene. Air from a compressed cylinder was then used to vaporize acetone. The cell was then flushed with large amounts of deionized water (DIW) and then dried with high-pressure nitrogen.

Density measurements were made using a high-quality density meter manufactured by Anton Paar. The DMA HP is a density-measuring cell designed to measure the densities of fluids at pressures ranging from 0 to 10,000 psi and temperatures ranging from +14°F to +392°F. The DMA HP works on the principle of measuring the period of harmonic oscillation of a built-in U-tube in which the fluid sample is contained. The cell electronically excites the U-tube, which acts as a tuning fork, at constant amplitude and a frequency meter measures the time corresponding to a fixed number of periods (Anton Paar Instruction Manual, 2005).

Before actual density measurements were made, the DMA HP was calibrated using two standard fluids with precisely known densities at each specific temperature

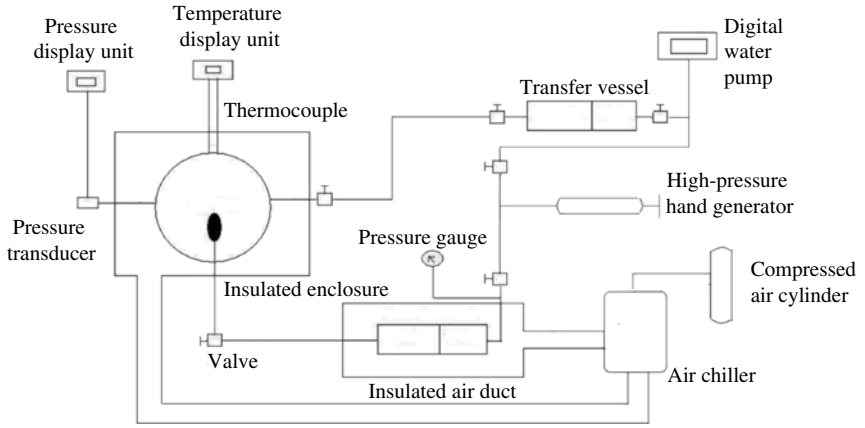

FIGURE 14.3 A schematic of the low-temperature/high-pressure experimental setup.

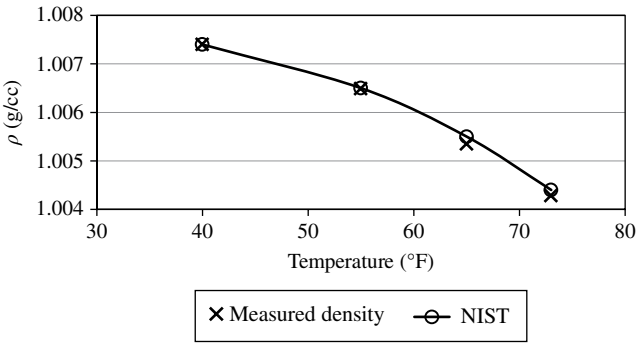

FIGURE 14.4 Measured water density compared to NIST values at 2225 psi and as a function of temperature.

and pressure. Decane and DIW were used as the standard fluids and their density values were obtained from the National Institute of Standards and Technology (NIST) website (http://webbook.nist.gov/chemistry/fluid). Since the densities of the fluids are the main user-defined inputs to the image analysis software heavily affecting the IFT calculation procedure, careful precision had to be taken during calibration. For validation purposes, the measured density of DIW was compared to values reported by the NIST following the calibration process. Figure 14.4 and Figure 14.5 show the deviation in measured water density values as a function of both temperature and pressure, respectively.

14.2.3 Procedure

The equilibrium shape of a hanging pendant drop (Fig. 14.6) is a balance between the forces acting on the drop, namely, net gravity or buoyancy, that pulls the drop upward by elongation and surface tension that acts to prevent the growth of surface area and

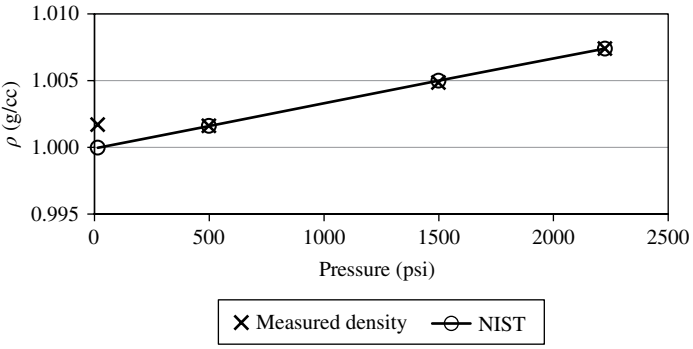

FIGURE 14.5 Measured water density compared to NIST values at 40°F and as a function of pressure.

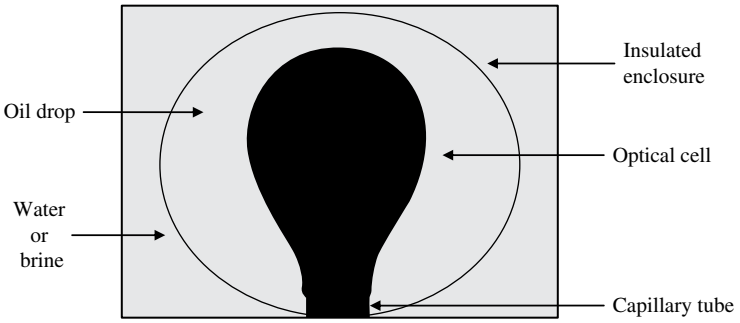

FIGURE 14.6 Illustration of the shape of a pendant drop.

pulls the drop into a spherical shape. The relationship between the oil–water IFT and the drop dimensions can be described as follows (Danesh, 1998):

$$\gamma = \frac{g\Delta\rho d_e^{\,2}}{S} \tag{14.2}$$

where g is the acceleration due to gravity, $\Delta\rho$ is the density difference between the two phases, d_e is the equatorial diameter or the maximum horizontal diameter, and S is the drop shape factor and is a function of both d_e and d_s, the latter being the diameter of the drop measured at a specific height above the bottom of the drop.

In hydromechanical equilibrium, the gravitational force that depends on the height of the drop corresponds to the Laplace pressure, resulting from the curvature of the drop contour at that point. The tendency of an interface between two immiscible phases is to create the smallest surface area, which gives rise to a pressure difference between the two fluids on either side of a curved interface. This pressure difference

is known as capillary (Laplace) pressure and is related to the IFT as defined by the Young–Laplace equation of capillarity:

$$\Delta P = \gamma \left(\frac{1}{R_1} + \frac{1}{R_2} \right) \tag{14.3}$$

where ΔP is the capillary pressure, γ is the IFT, and R_1 and R_2 are the principal radii of curvature.

In the laboratory, the low-temperature–high-pressure optical cell was first filled with the aqueous phase and pressurized to the desired pressure. A few drops of the hydrocarbon phase were introduced into the optical cell through a capillary tube and left to float to the top of the cell. The optical cell and the transfer vessel containing the oleic phase were then simultaneously cooled to the desired temperature. An aging period of 24 h, at which the desired pressure and temperature were constantly maintained, was allowed to attain equilibrium.

After equilibrium was reached, a drop of crude oil or *n*-octane was introduced through the capillary tube into the optical cell at a very slow rate (~2 min/drop). When the oil drop is just about to detach from the tip of the capillary tube, indicating that the buoyancy force is close to the IFT, an image of the drop was captured using a digital camera. The images were then transmitted to a computer for image analysis using a commercial software named Drop Shape Analysis (DSA) provided by Kruss, United States. This procedure was followed until the standard deviation between 10 consecutive drops, all introduced at approximately the same rate, was less than 0.25 mN/m. The average IFT among the 10 drops was then used as the reported value. Abdelrahim provided a detailed description of the experimental procedure carried out in this study (Abdelrahim, 2012).

Given the fluid densities, the software utilizes the axisymmetric drop shape analysis (ASDA) technique to analyze the shape of the pendant drop. The method constructs an objective function that expresses the error between the physically observed and a theoretical Laplacian curve that represents a solution of the Young–Laplace equation of capillarity (Equation 14.3). This objective function is then minimized using the method of incremental loading in conjunction with the Newton–Raphson method, which is the sum of the squares of the normal distances between measured points and the calculated curve (del Rio and Neumann, 1997; Rotenberg et al., 1983).

Rao has reported IFT values of *n*-octane/DIW system measured using the pendant drop method (Rao, 2001). The measurements were made at pressures up to 10,000 psi and 338°F. An increase in the IFT with increasing pressure was observed, while an opposite trend was observed with increasing temperature. The reproducibility and precision of the ASDA technique was also indicated by the low standard deviations associated with the reported IFT measurements. Rao also pointed out some of the advantages of analyzing pendant drop profiles using the ASDA technique, which include the following: (i) the drop shape can be measured from any convenient reference frame; (ii) no particular starting values are needed

TABLE 14.1 Salinities of the aqueous fluids used in this study

DIW:SSW ratio	Salinity, wt%
1:0	0
2:1	1.3
1:2	2.5
0:1	3.7

TABLE 14.2 Physical properties of MC252 crude oil

Property	Value
API gravity at 60°F (°API)	36.2
Kinematic viscosity at 104°F (cSt)	5.067
Sulfur content (wt%)	0.261
Water content (mg/Kg)	1680
Total light ends (wt%)	27.19
Nitrogen content (mg/Kg)	690
True vapor pressure (psi)	3.3
Corrected flashpoint (°F)	104
pH–water extract	6.4

for the IFT, radius of curvature at the apex, and the coordinates of the origin; and (iii) the procedure eliminates the need of a predetermined table of shape factors (Rao, 2001).

14.2.4 Fluids

Synthetic seawater (SSW) and DIW, both purchased from Cole-Parmer, were mixed in specific proportions resulting in the desired salinities. The dispersant used in this study was Corexit 9500 (EC9500A) and was provided by Nalco Holding Company. The dispersant was premixed with the aqueous fluid at the desired concentration for the IFT measurements. Table 14.1 provides the proportion of DIW and SSW in the prepared aqueous fluids and the resulting salinity as measured in the lab by a conductivity meter. All aqueous fluids were deaerated using a vacuum pump before the actual IFT tests or density measurements.

Originating from the Macondo prospect, in which the Deepwater Horizon rig was drilling, Mississippi Canyon Block 252 (MC252) crude oil was provided by BP. The sample was collected directly from the source on June 19, 2010, at ambient pressure and temperature and maintained at 45°F until analysis. Analysis has shown that the crude oil sample is "fresh" or uncontaminated and has not undergone any weathering or evaporation processes. Table 14.2 provides some typical physical properties of the MC252 crude oil sample. Reagent grade (99.8% purity) *n*-octane was also used as the oleic phase for comparison.

TABLE 14.3 Conditions of pressure and temperature specific to various water depths

Water depth (ft)	Pressure (psi)	Temperature (°F)
0	14.7	76
800	350	60
1125	500	55
2250	1000	45
3375	1500	40
5000	2225	40

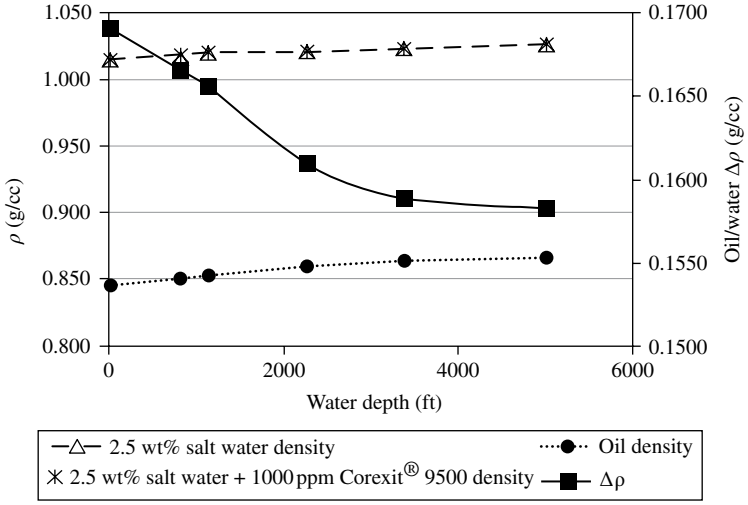

FIGURE 14.7 Oil and water densities at pressure and temperature conditions specific to various water depths.

14.3 RESULTS AND DISCUSSION

14.3.1 Water Depth Variation

The densities of oil and water were measured at conditions of pressure and temperature representative of specific water depths as shown in Figure 14.1. The density of *n*-octane was obtained from the NIST website (http://webbook.nist.gov/chemistry/fluid). A water salinity of 2.5 wt% was chosen since it is the closest to the average water salinity of the Gulf of Mexico waters (http://www.nodc.noaa.gov). The average oil–water and *n*-octane–water IFT were then measured at the same conditions, with and without the addition of the dispersant to the water phase. Table 14.3 specifies the pressure and temperature values at which the measurements were made and the corresponding water depths. Figure 14.7 shows the densities of the oil, the 2.5 wt% saltwater, and the same saltwater with 1000 ppm Corexit 9500 in solution, all plotted on the left vertical axis. The right vertical axis shows the density difference between the oil and the 2.5 wt% saltwater.

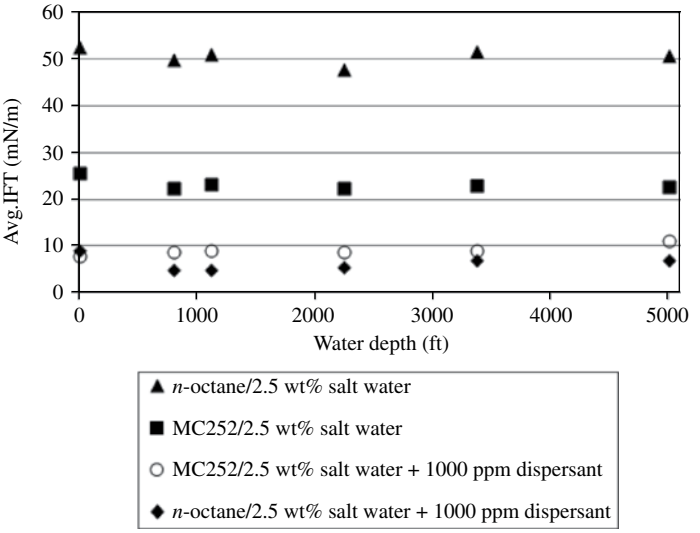

FIGURE 14.8 Average hydrocarbon/water IFT at pressure and temperature conditions specific to various water depths.

It can be noted from Figure 14.7 that the water phase density, with and without the addition of the dispersant, was less sensitive to changes in pressure and temperature than the MC252 crude oil. Addition of the dispersant to the saltwater had a negligible effect on its density, as it can be seen that the density data points of both are virtually overlapping each other. Both the oil and water densities were increasing as the pressure was increased, and temperature was decreased with water depth. However, the oil density was increasing at a much faster rate causing the density difference between the two phases to continuously decrease with increasing water depth.

The average hydrocarbon–water IFT is plotted against water depth in Figure 14.8. As can be seen from Figure 14.8, data with the 2.5 wt% saltwater did not show any specific trend; instead, the average IFT fluctuated between 22.0 and 26.0 mN/m for the crude oil–water system and between 47.0 mN/m and 53.0 mN/m for the *n*-octane/water system. With 1000 ppm dispersant in solution, the average oil–water IFT was much lower than that with the dispersant-free water but did not considerably change until 3000 ft, after which it slightly increased. For the *n*-octane/water/dispersant system, the average IFT slightly decreased once the pressure and temperature conditions were varied from room conditions and then continued to increase with increasing water depth.

The dispersant-induced reduction in the IFT is plotted in Figure 14.9 as a percentage of the dispersant-free IFT for both the oil/water and the *n*-octane/water systems. It is very evident from Figure 14.9 that the chemical dispersion process was much more effective in the *n*-octane/water system than in the crude oil–water system. The *n*-octane/water system experienced reductions in the IFT ranging from 85% to 90% decrease from the dispersant-free value. The magnitude of the reduction increased once the pressure and the temperature were changed from room conditions

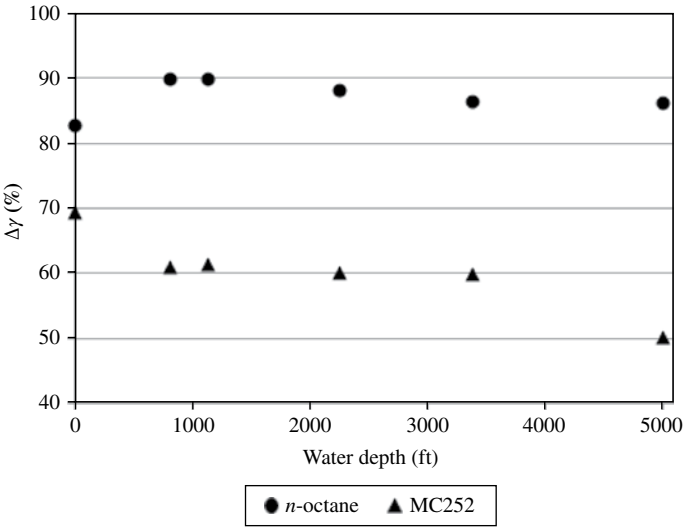

FIGURE 14.9 Dispersant-induced reduction in the hydrocarbon/water IFT as a percentage of the dispersant-free IFT at pressure and temperature conditions specific to various water depths.

and then slightly decreased as water depth increased. A 50–60% reduction in the IFT was observed in the crude oil–water system at the same conditions, with an observable decrease in the magnitude of reduction at the seafloor conditions.

14.3.2 Temperature Variation

Oil and 2.5 wt% saltwater densities were measured at a constant pressure of 2225 psi and temperatures ranging from room temperature 76°F to 40°F and are plotted in Figure 14.10. As expected, an increase in temperature caused the fluid densities to decrease, with the crude oil density being more responsive to the change in temperature. An increase in the temperature from seafloor conditions (40°F) to room temperature conditions (76°F) caused the saltwater density to decrease by only 0.3%. On the other hand, the crude oil density experienced a 1.5% decrease in density at the same conditions. The difference in density between the two phases can be seen to steadily increase as the temperature increases.

The average hydrocarbon–water IFT as a function of temperature is plotted in Figure 14.11, for both the crude oil/water and the *n*-octane–water systems. With no dispersant in solution, the crude oil–water IFT was observed to increase slightly with increasing temperatures. The *n*-octane–water IFT decreased to a minimum at 55°F, after which it also increased slightly with increasing temperature with no dispersant in solution. With a 1000 ppm Corexit 9500 in solution, the crude oil–water IFT decreased to a minimum at 65°F and then increased slightly upon further increase of the temperature. On the other hand, the *n*-octane–water IFT steadily decreased with increasing temperatures when the dispersant was dissolved in the saltwater.

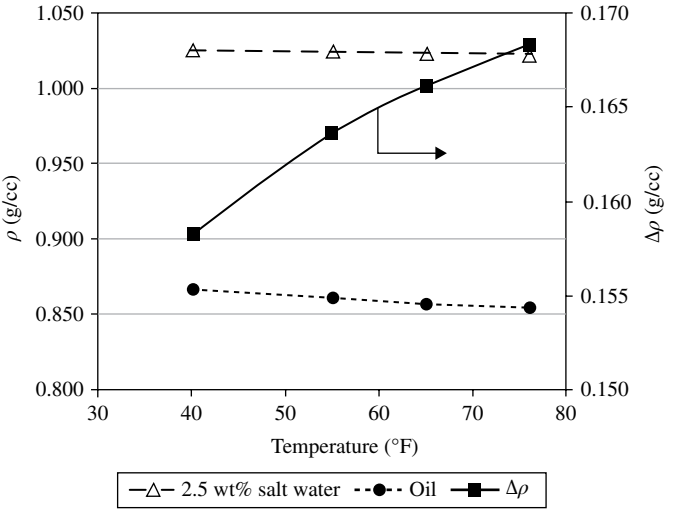

FIGURE 14.10 Oil and water densities at 2225 psi and various temperatures.

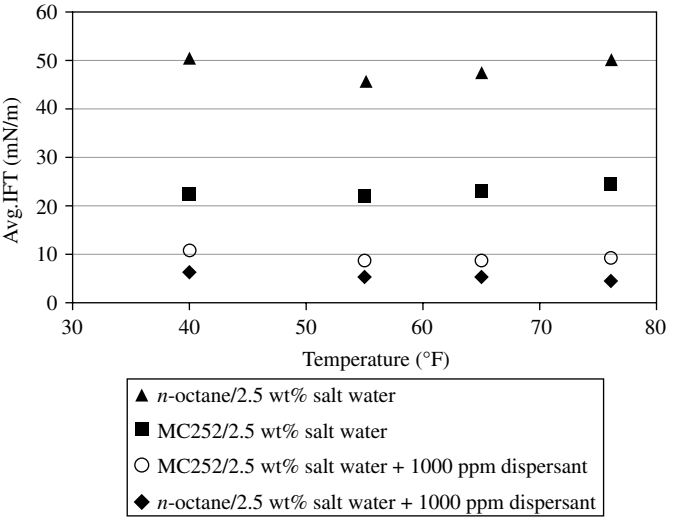

FIGURE 14.11 Average hydrocarbon/water IFT at 2225 psi and various temperatures.

The dispersant-induced reduction in the IFT is plotted in Figure 14.12 as a function of the temperature. The same distinction between the crude oil–water and the *n*-octane–water systems is seen in Figure 14.9 and Figure 14.12. However, both fluid systems exhibited the same trend when temperature was varied, with a decline in the magnitude of the IFT reduction as the temperature was lowered at a constant pressure (Figure 14.12) and at decreasing pressures (Figure 14.9).

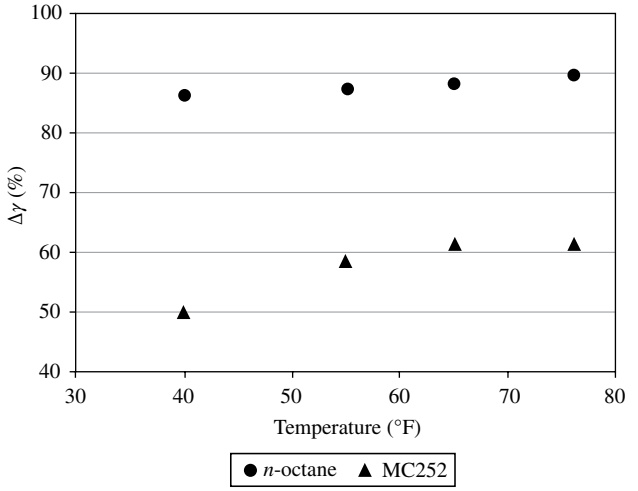

FIGURE 14.12 Dispersant-induced reduction in the hydrocarbon/water IFT as a percentage of the dispersant-free IFT at 2225 psi and various temperatures.

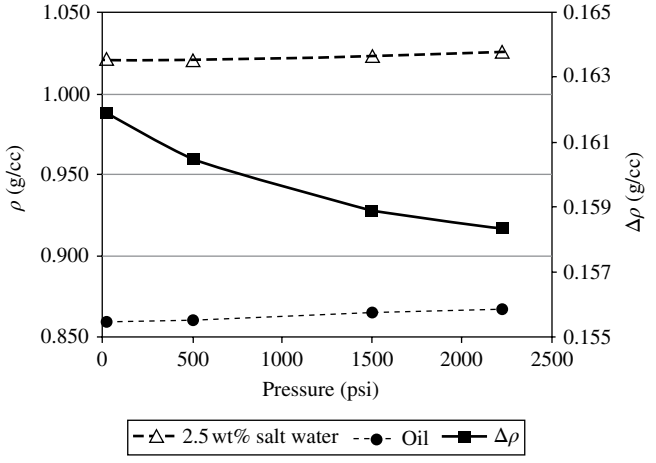

FIGURE 14.13 Oil and water densities at 40°F and various pressures.

14.3.3 Pressure Variation

Figure 14.13 shows oil and 2.5 wt% saltwater densities measured at a constant temperature representative of the seafloor conditions (40°F) and pressures ranging from atmospheric to 2225 psi (corresponding to 5000 ft water depth of seawater). An increase in pressure caused densities of both the phases to increase, with the crude oil experiencing a greater change than the 2.5 wt% saltwater. The decrease in the density difference between the two phases as the pressure is increased is attributed to the crude oil density being more responsive to changes in pressure.

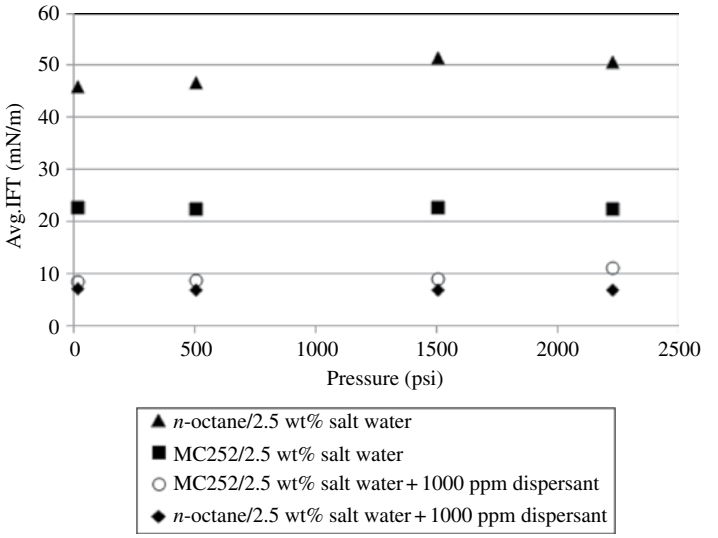

FIGURE 14.14 Average oil/water IFT at 40°F and various pressures.

The average oil–water IFT was measured at the same conditions and is shown in Figure 14.14. As can be seen from Figure 14.14, the 2.5 wt% saltwater data did not show any observable trend in the crude oil system; instead, the average crude oil–water IFT fluctuated between 22 and 23 mN/m. For the *n*-octane–water system, with no dispersant in solution, the average IFT increased with increasing pressures to a maximum at 1500 psi, after which it slightly decreased upon further increase of the pressure. This was the same behavior seen when the water depth conditions of pressure and temperature were varied (Fig. 14.8). With 1000 ppm of Corexit 9500 in solution with the 2.5 wt% saltwater, the average crude oil–water IFT increased slightly with increasing pressures. The *n*-octane/water/dispersant system did not show considerable sensitivity to pressure variations as the average IFT decreased by only 4% when the pressure was increased from 14.7 to 2225 psi.

Figure 14.15 shows the dispersant-induced reduction in the IFT as a function of pressure for both the crude oil–water and the *n*-octane–water systems. It is evident that the chemical dispersion process was more effective in reducing the IFT in the *n*-octane–water system. However, the magnitude in the reduction of *n*-octane–water IFT increased with increasing pressure as opposed to the behavior in the crude oil–water system. This can be attributed to the trend in Figure 14.14 where the crude oil/water/dispersant IFT increased slightly with increasing pressures.

14.3.4 Water Salinity Variation

The densities of water samples of different salinities were measured at seafloor conditions of pressure and temperature, namely, 2225 psi and 40°F, respectively, and are plotted on the left vertical axis of Figure 14.16. The crude oil density was measured at the same conditions and was found to be 0.8673 g/cc. The difference in

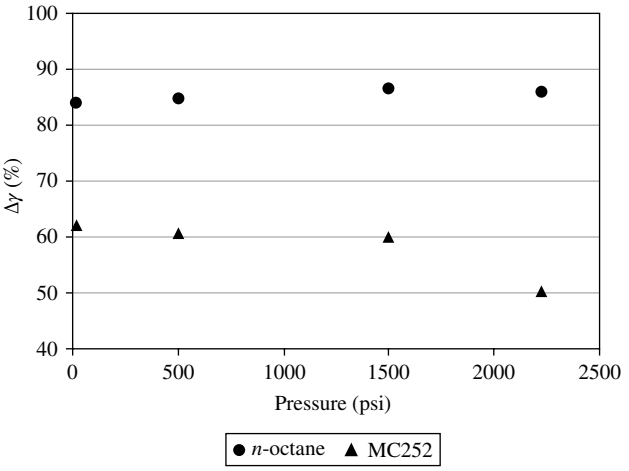

FIGURE 14.15 Dispersant-induced reduction in the hydrocarbon/water IFT as a percentage of the dispersant-free IFT at 40°F and various pressures.

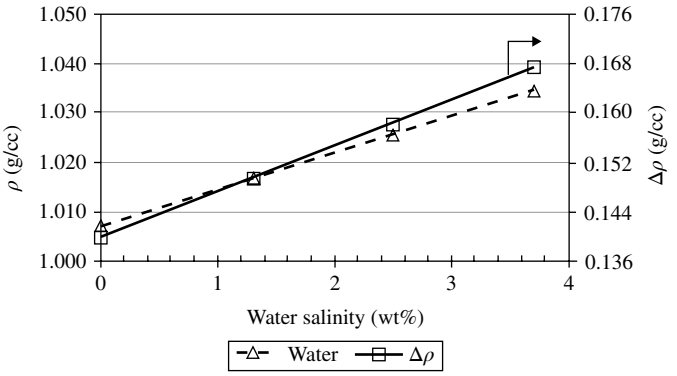

FIGURE 14.16 Water densities as a function of salinity at 2225 psi and 40°F.

density between the two phases is plotted on the right vertical axis of Figure 14.16. As expected, the density of water increased as the salinity was increased and consequently increased the difference in density between the two phases.

The average hydrocarbon–water IFT was measured at the seafloor conditions of pressure and temperature utilizing the variable water salinities. Interfacial tension measurements were also made with 1000 ppm Corexit 9500 in solution with the all water samples. The results are shown in Figure 14.17. For the dispersant-free water samples, the average oil–water IFT decreased to a minimum at 2.5 wt% and then increased again upon further increase of water salinity. A similar trend was seen with the 1000 ppm Corexit 9500 in solution except that the IFT minimum was observed at 1.3 wt% water salinity.

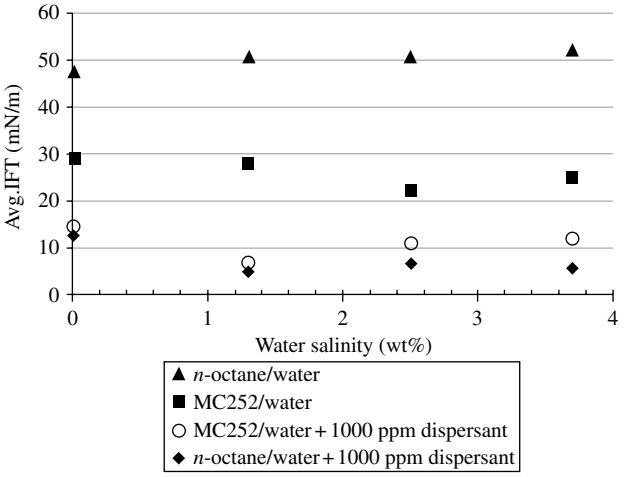

FIGURE 14.17 Average hydrocarbon/water IFT measured at 2225 psi and 40°F and as a function of water salinity.

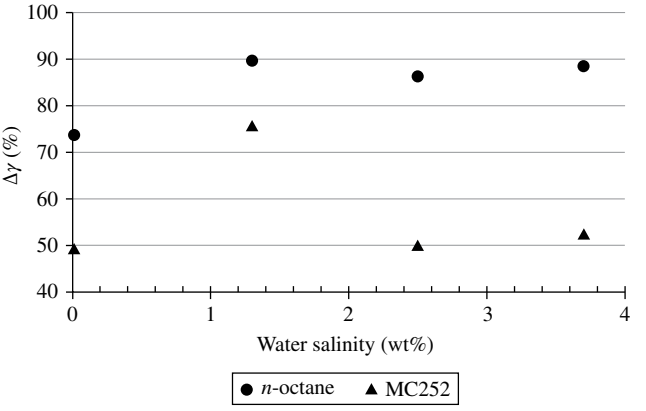

FIGURE 14.18 Dispersant-induced reduction in the hydrocarbon/water IFT as a percentage of the dispersant-free IFT at 2225 psi and 40°F.

The dispersant-induced reduction in the IFT is plotted in Figure 14.18 as a function of the water salinity for both the crude oil–water and *n*-octane–water systems. As can be seen in Figure 14.18, both systems showed significant fluctuations in the magnitude of the IFT reduction with a maximum IFT reduction at 1.3 wt%.

14.3.5 Dispersant-in-Oil Concentration Variation

The dispersant was also dissolved in the crude oil at different concentrations for two purposes. First, 1000 ppm was dissolved in the crude oil to examine how effective the dispersant would be in reducing the oil–water IFT as compared to when it was

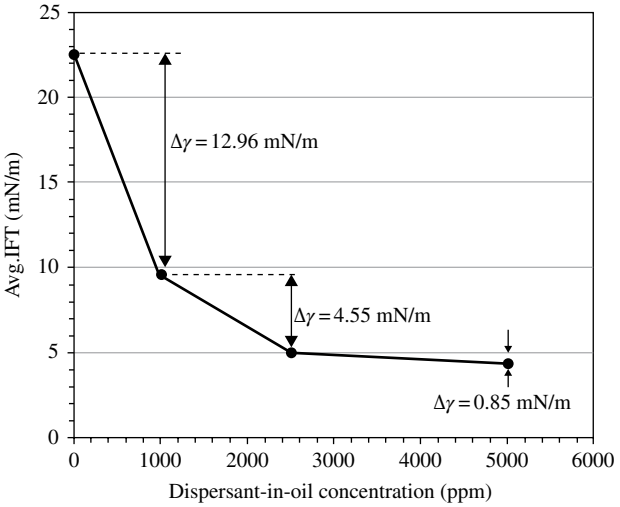

FIGURE 14.19 Average IFT between crude oil and 2.5 wt% saltwater at 2225 psi and 40°F and as a function of the dispersant concentration in the oil.

dissolved in the water phase. Second, the influence of the dispersant concentration was evaluated by increasing the amount dissolved in the crude oil in specific proportions. Experiments were conducted with a 2.5 wt% saltwater and at seafloor conditions of pressure (2225 psi) and temperature (40°F). Figure 14.19 shows the measured average IFT between the crude oil and the 2.5 wt% saltwater as a function of the dispersant concentration in the crude oil.

The average IFT can be observed to decrease greatly upon the addition of 1000 ppm of dispersant to the crude oil as is seen in Figure 14.19. The addition of more dispersant resulted in a progressively less pronounced reduction in the IFT, which is indicative of a CMC at or below 1000 ppm for this crude oil–water system.

It is also interesting to point out that more dispersant was dissolved in the crude oil, namely, 10,000 ppm, but attempts to introduce the crude oil into the water-filled optical cell at the same conditions in the form of a pendant drop were unsuccessful. Instead of breaking up into small droplets, the crude oil emerged from the tip of the capillary tube in the form of a continuous stream or jet. An actual photograph of the crude oil emerging from the tip of the capillary tube at seafloor conditions and 10,000 ppm concentration of dispersant dissolved in the crude oil is shown in Figure 14.20. The dispersant-induced reduction in the IFT is illustrated in Figure 14.21 as a percentage of the dispersant-free value.

It can be seen from Figure 14.21 that the IFT reduction at 1000 ppm of dispersant was greater when the dispersant was dissolved in the crude oil as compared to when it was dissolved in the 2.5 wt% saltwater. Accordingly, the dispersant effectiveness was higher when the dispersant agent was dissolved in the crude oil.

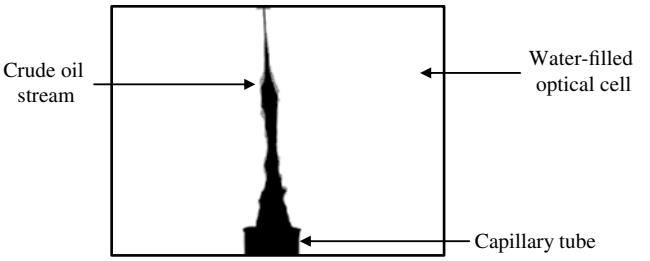

FIGURE 14.20 Photograph of the crude oil emerging from the tip of the capillary tube at 2225 psi, 40°F, and 10,000 ppm dispersant-in-oil concentration.

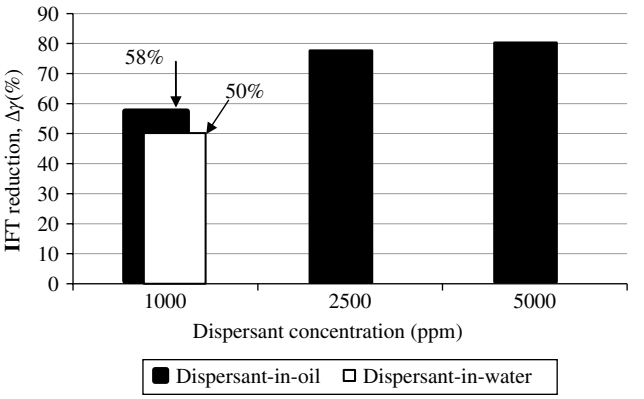

FIGURE 14.21 Dispersant-induced reduction in the crude oil/water IFT as a percentage of the dispersant-free IFT at 2225 psi and 40°F.

14.4 SUMMARY

A high-pressure optical cell was designed and fabricated to enable hydrocarbon/water/dispersant IFT measurements at deepwater conditions. The cell has a design rating of 20,000 psi and temperatures ranging from 40°F to 400°F. Crude oil samples were obtained from the Macondo well site in the Gulf of Mexico and used in the density and IFT measurements.

The magnitude of IFT reduction reached a maximum of 90% in the *n*-octane–water system, while a maximum of 70% reduction was observed in the crude oil–water system at the same conditions. The chemical complexity and the presence of indigenous surfactants in the crude oil may have led to a less effective dispersion process in the crude oil–water system than in the *n*-octane–water system.

The density of crude oil was much more sensitive to changes in pressure and temperature than the density of the 2.5 wt% saltwater. This difference in density change caused the density difference, $\Delta\rho$, between the two to decrease with increasing water depth or increasing pressure and decreasing temperature. The density difference, $\Delta\rho$, did not always follow the same trend as the measured IFT.

Based on the magnitude of the IFT reduction, the effectiveness of the dispersant decreased with increasing water depth and comes to a minimum at seafloor conditions. This was mainly due to the decrease in temperature at greater water depths as the increase in pressure had a relatively smaller effect on the IFT. An increase in temperature, at constant pressure, caused the density difference between oil and water to continuously increase. An unexpected effect of temperature was observed with the dispersant-free water at constant pressure, as the crude oil–water IFT increased from 22.57 mN/m at 40°F to 24.52 mN/m at 73°F. However, the dissolution of 1000 ppm of dispersant in water reversed that trend as the IFT decreased from 11.25 to 9.40 mN/m over the same temperature range. Consequently, the magnitude of IFT reduction decreased at lower temperatures, indicating a less effective dispersion process.

An increase in pressure, at constant temperature, caused the oil–water density difference to continuously decrease. Pressure had a negligible effect on the average crude oil–water IFT when the dispersant-free water solution was used. A considerable increase in the IFT was observed with increasing pressure when 1000 ppm Corexit 9500 in solution was used. This in turn resulted in lower magnitudes in the IFT reduction with increasing pressures and hence lower effectiveness at greater water depths.

The variation of water salinity showed that the average oil–water IFT decreased to a minimum at a specific salinity and then increased again upon addition of more salt for both the dispersant-free and the dispersant-in-solution systems. The Corexit 9500 dispersant was most effective when mixed with the 1.3 wt% saltwater inducing the greatest magnitude in the IFT reduction for both the crude oil–water and the *n*-octane–water systems.

When dissolved in the crude oil, an improvement in the effectiveness of the dispersant was observed as compared to the dissolution in the water phase. However, 1000 ppm was noted as a concentration value beyond the CMC, since the IFT reduction was less pronounced at higher concentrations. The reason behind this improvement in dispersant effectiveness is that the surfactant molecules responsible for reducing the IFT have a more efficient accumulation at the oil–water interface when the dispersant is dissolved in the crude oil. On the other hand, when the dispersant is dissolved in the water, a relatively larger amount of surfactant molecules are lost to the bulk water and, consequently, the IFT-reducing capabilities of the dispersant are significantly weakened.

The lowest measured oil–water IFT in this study was 4.46 mN/m and was recorded when 5000 ppm of dispersant was dissolved in the crude oil at deepwater conditions of pressure and temperature. It is noteworthy that even at such high concentrations of dispersant dissolved in oil, ultralow oil–water IFT (<1.0 mN/m) was not achieved. Furthermore, when the dispersant concentration was increased to 10,000 ppm at the same conditions of pressure and temperature, the oil emerged in the form of a jet from the tip of the capillary tube. These observations clearly demonstrate that the use of such high dispersant concentrations at deepwater conditions may not be an effective remedy to break up an oil plume into smaller droplets.

14.5 PRACTICAL IMPLICATIONS

Based on the experimentally measured oil–water IFT values, it is evident that the low temperature associated with the seafloor was the main factor responsible for worsening the IFT-reducing capabilities of the dispersant. Considering the conditions of the Deepwater Horizon oil spill, the seawater is at a much lower temperature than the oil gushing out of the failed wellhead. However, as the contact time between the two increases, the relatively smaller mass of oil will eventually reach a temperature as low as that of the seawater. Consequently, the oil viscosity increases and the penetration of the surfactant molecules into the oil is retarded. This in turn would result in a detrimental effect on the chemical dispersion of the spilled oil.

An effective design of a subsea dispersant injection system should therefore be able to counteract the effect of temperature and induce the greatest magnitude of IFT reduction possible. To do so, the wands spraying the dispersant onto the oil stream could be equipped with heaters, with consideration of power requirements, as to delay the decline in the temperature of the spilled oil. In addition, the thermal stability of the surfactant molecules within the dispersant formulation would have to be evaluated.

The nature and time of contact between the spilled oil and the dispersant are also important factors affecting the effectiveness of the dispersion process. One of the major requirements for the formation of small oil droplets, and hence the dispersion of spilled oil, is that the surfactant molecules within the dispersant must have enough time to penetrate and mix into the oil (National Research Council (U.S.) Ocean Studies Board, 2005). Moreover, the experimentally measured oil–water IFT in this study indicated that the effectiveness of the dispersant was higher when dissolved in oil than in water. It is also known that surfactant molecules within the dispersant are soluble in both oil and water and it is, therefore, important to minimize the loss of the dispersant to the surrounding water.

During the Deepwater Horizon spill, the oil was gushing out of the failed wellhead at such a fast rate that intimate contact between the oil and the sprayed dispersant was probably not achieved or at least the duration of contact could have been extended. Containing the spilled oil within a closed structure for a specific amount of time while simultaneously applying the dispersant would have enhanced the chemical dispersion process. There was an unsuccessful attempt to contain the spilled oil using a dome, also known as a cofferdam, placed over the leak to have the oil channeled to the water surface to be collected (http://www.oilspillcommision.gov). The failure was due to the fact that the methane gas escaping from the well formed slushy hydrates as it came in contact with the cold seawater and clogged the cofferdam.

The subsea application of dispersants could be improved by designing several domes that contain and inject dispersants into the spilled oil before releasing the oil back into the seawater for entrainment of the recently formed oil droplets into the water column. The period of time during which the oil is contained and the dispersant is applied could be predetermined by laboratory testing as to ensure sufficient mixing and penetration into the oil. Another potential benefit of such a design is that an adequate dispersant dosage can also be estimated since the volume of the contained oil can be approximated, given the fact that some seawater will inadvertently find its

way into the dome as well. As a result, both the efficiency and the effectiveness of the dispersant application process would be improved.

ACKNOWLEDGMENTS

This work was made possible by a grant from BP/the Gulf of Mexico Research Initiative. The authors are also grateful to Paul Rodriguez and Joe Bell of the Chemical Engineering Department at LSU for fabricating the high-pressure optical cell and to Dr. Kalliat Valsaraj for his valuable suggestions and recommendations.

REFERENCES

Abdelrahim MA. Measurement of interfacial tension in hydrocarbon/water/dispersant systems at deepwater conditions. Master's Thesis; Baton Rouge, LA: Louisiana State University; 2012.

Anton Paar Instruction Manual. *DMA HP Density Measuring Cell for High Pressure and High Temperatures*, GmbH, Graz, Austria; 2005.

Clayton JR, Payne JR, Farlow JS. *Oil Spill Dispersants: Mechanisms of Action and Laboratory Tests*, illustrated edition. Boca Raton, FL: CRC Press; 1993.

Cormack D, Lynch BWJ, Dowsett BD. Evaluation of dispersant effectiveness. Oil Chem Pollut 1986–1987;3(2):87–103.

Danesh A. *PVT and Phase behavior of Petroleum Reservoir Fluids*. London: Elsevier Science BV; 1998.

Lehtinen CM, Vesala A-M. Effectiveness of oil spill dispersants at low salinities and low temperatures. In: Allen TE, editor. *Oil Spill Chemical Dispersants: Research, Experience, and Recommendations, ASTM STP840*. Philadelphia, PA: American Society for Testing and Materials; 1984. p 108–121.

Mackay D, Hossain K. Interfacial tensions of oil, water, chemical dispersant systems. Can J Chem Eng 1982;60(4):546–550.

Mackay D, Chau A, Hossain K, Bobra M. Measurement and prediction of the effectiveness oil spill chemical dispersants. In: Allen TE, editor. *Oil Spill Chemical Dispersants: Research, Experience, and Recommendations*, ASTM STP840. Philadelphia, PA: American Society for Testing and Materials; 1984. p 38–54.

National Research Council (U.S.) Ocean Studies Board. *Oil Spill Dispersants: Efficacy and Effects*, illustrated edition. Washington, DC: The National Academic Press; 2005.

Rao DN. Fluid-fluid and solid-fluid interfacial interactions in petroleum reservoirs. Petrol Sci Technol 2001;19(1–2):157–188.

Rewick RT, Sabo KA, Smith JH. The drop-weight interfacial tension method for predicting dispersant performance. In: Allen TE, editor. *Oil Spill Chemical Dispersants: Research, Experience, and Recommendations, ASTM STP840*. Philadelphia, PA: American Society for Testing and Materials; 1984. p 94–107.

del Rio OI, Neumann AW. Axisymmetric drop shape analysis: computational methods for the measurement of interfacial properties from the shape and dimensions of pendant and sessile drops. J Colloid Interf Sci 1997;196(2):136–147..

Rotenberg Y, Boruvka L, Neumann AW. Determination of surface tension and contact angle from the shapes of axisymmetry fluid interfaces. J Colloid Interf Sci 1983;93(1):169–183.

15

SURFACTANT TECHNOLOGIES FOR REMEDIATION OF OIL SPILLS

Edgar J. Acosta and Suniya Quraishi

15.1 INTRODUCTION

In recent years, major oil spills have sparked the attention of the public and media alike, resulting in a global awareness of the risks and environmental damage associated with such events. These risks are likely to increase due to the increasingly larger volumes of fuels transported throughout the globe (Fingas, 2001). In the case of oil spills that occur in open waters, one of the concerns is that if these spills reach shorelines, cleanup becomes more difficult and expensive. The selection of the appropriate technology for oil spills that have reached the shoreline or for land-based oil spills depends on the chemistry of the spilled product, the degree of weathering before and after reaching the shoreline, the quantity of oil spilled, the type of soil (i.e., gravel, sand, silt, clay, humus, and water content), and the environmental conditions (Fingas, 2001). It can take 50 years or more to recover from oil spills on shorelines if the site is left untreated (Ornitz and Champ, 2002).

The most common remediation techniques used on spills that reach shorelines include manual and mechanical removal, the use of vacuums, flooding and washing, tilling and aeration, sediment reworking and surf washing, the use of sorbents and chemical agents, and enhanced bioremediation (Breuel, 1981; Fingas, 2001). Some less recommended yet employed cleanup techniques include high-pressure cold or hot water washing, steam cleaning and sand blasting, as well as *in situ* burning (Environment Canada, 1978; Fingas, 2001). From an applications perspective,

Oil Spill Remediation: Colloid Chemistry-Based Principles and Solutions, First Edition.
Edited by Ponisseril Somasundaran, Partha Patra, Raymond S. Farinato, and Kyriakos Papadopoulos.

mechanical treatment can be disadvantageous as there are risks of injuries to the personnel, large equipment is often required, and large amounts of material need to be removed and relocated (Environment Canada, 1978; Fingas, 2001). Techniques such as flooding, washing, tilling, and aeration can only be employed on sites with very specific characteristics (Fingas, 2001). Although bioremediation does not pose any major environmental damage, it is a slow process if it is not accelerated with special cultures and nutrients (Fingas, 2001).

Remediation of oil spills using soil washing technologies with chemical agents such as surfactants can be an advantageous alternative if they are properly designed to use low water and energy input, to minimize the transport and relocation of material, and if the process is designed to produce high processing throughputs with high oil removal efficiency. While the use of emulsifiers for oil spills in open waters is a common practice, the use of surfactant-based soil washing on land is still in development. A 1997 review by Taylor and Owens only mentions one surfactant-based soil washing technology in the remediation of the Morris J. Berman Spill in Puerto Rico (Taylor and Owens, 1997). In the same review, the authors recognize that soil washing techniques are the only ones capable of working with clays and silty soil and with a wide range of oil viscosities, except for semisolid materials.

There are a number of examples of successful attempts to use surfactant technologies for soil washing. For example, sand washing experiments conducted by Chang and coworkers for the removal of polycyclic aromatic hydrocarbons (PAHs) showed that 73.6–100% removal could be achieved using a sodium dodecyl sulfate (SDS) solution, in contrast to 30–80% removal using water alone (Chang et al., 2000). Another study on the removal of PAHs from contaminated soils showed that a microemulsion-based extraction process produced greater PAH removal compared to a hot toluene extraction process (Bragato and El Seoud, 2003). Studies performed on the cleaning of drill cuttings showed that concentrated surfactant solutions could remove up to 100% of the oil and that dilute surfactant solutions (≈ 0.1 wt%) were able to achieve sufficient cleaning for regulatory compliance (Childs et al., 2005). More recent studies performed on the washing of sands contaminated with diesel fuel showed that up to 98% fuel recovery could be achieved using SDS washing fluids, while water alone only removed 32% of diesel (Khalladi et al., 2009). Our group has extended surfactant washing technologies for the removal of solid-like bitumen from sand using a combination of solvent + surfactant washing technology, with more than 90% bitumen removal when using the appropriate washing conditions (Quraishi et al., 2009).

In addition to the examples of soil washing techniques used in the remediation of oil spills on shorelines and on land, surfactant-based technologies have been used in the remediation of subsurface oil spills (Sabatini et al., 1995). These spills are typically associated with leaks from underground fuel storage tanks or with improper disposal of chlorinated solvents.

There are two issues that need to be considered when developing and implementing surfactant-based technologies for the remediation of oil spills. First, the proper selection of the formulation and washing conditions must be made. The improper selection of these conditions can lead to difficult separations for oil–water–particle

emulsions, the loss of surfactant, and poor water quality. The second issue is the selection of the surfactant. There are many surfactants and additives that are toxic on their own, and therefore, selecting biocompatible and biodegradable surfactants is an important step in developing surfactant-based remediation technologies. One of the objectives of this chapter is to introduce the phase behavior of surfactant–oil–water (SOW) systems and an equation of state that describes this phase behavior and the properties of these SOW systems. A second objective is to connect the properties of SOW systems with the performance of surfactant-based remediation technologies (illustrated in Fig. 15.1) through the use of dimensionless numbers. A third objective is to illustrate the use of this integrated approach in designing remediation technologies that can incorporate biocompatible surfactants and improve the performance of these technologies.

15.2 PHASE BEHAVIOR OF SURFACTANT–OIL–WATER (SOW) SYSTEMS

15.2.1 Phase Diagrams

Figure 15.2 presents a generalized ternary phase diagram for SOW systems adapted from a review of Davis (1994). Spherical micelles and oil-swollen spherical micelles are obtained near the water vertex of the ternary phase diagram. As the oil and surfactant content increases, rodlike micelles and oil-swollen rodlike micelles are obtained. At even higher surfactant concentrations, lyotropic liquid crystal phases are typically obtained. There are several forms of liquid crystals, including hexagonal, cubic, lamellar, reverse cubic, and reverse hexagonal liquid crystals. The specific location of liquid crystalline regions in the ternary phase diagram depends on the molecular structure of the surfactant, the temperature of the system, the presence of electrolyte, and the presence of cosolvents or cosurfactants. For most remediation technologies, the presence of liquid crystalline phases is undesirable because the rate of surfactant and oil solubilization is slow and liquid crystals tend to adsorb at oil–water interfaces, thereby helping to stabilize emulsions. In most cases, the surfactant concentration is low enough to avoid the regions of liquid crystal formation. However, liquid crystals can be a problem if the surfactant is delivered from a concentrated solution. In some cases, surfactants are mixed with other cosurfactants or cosolvents to avoid forming liquid crystals and other gel phases.

At intermediate surfactant concentrations, one can form SOW systems with different configurations. Figure 15.2 shows that in some cases it is possible to find a single isotropic region where various surfactant assemblies can be found. In this isotropic region, as one increases the oil-to-water ratio, the surfactant assembly changes from oil-swollen micelles to oil-swollen rodlike micelles, to bicontinuous systems, to water-swollen rodlike reverse micelles, and finally to water-swollen reverse micelles suspended in oil. If the surfactant concentration is further reduced, then regions of two and three coexisting phases are observed.

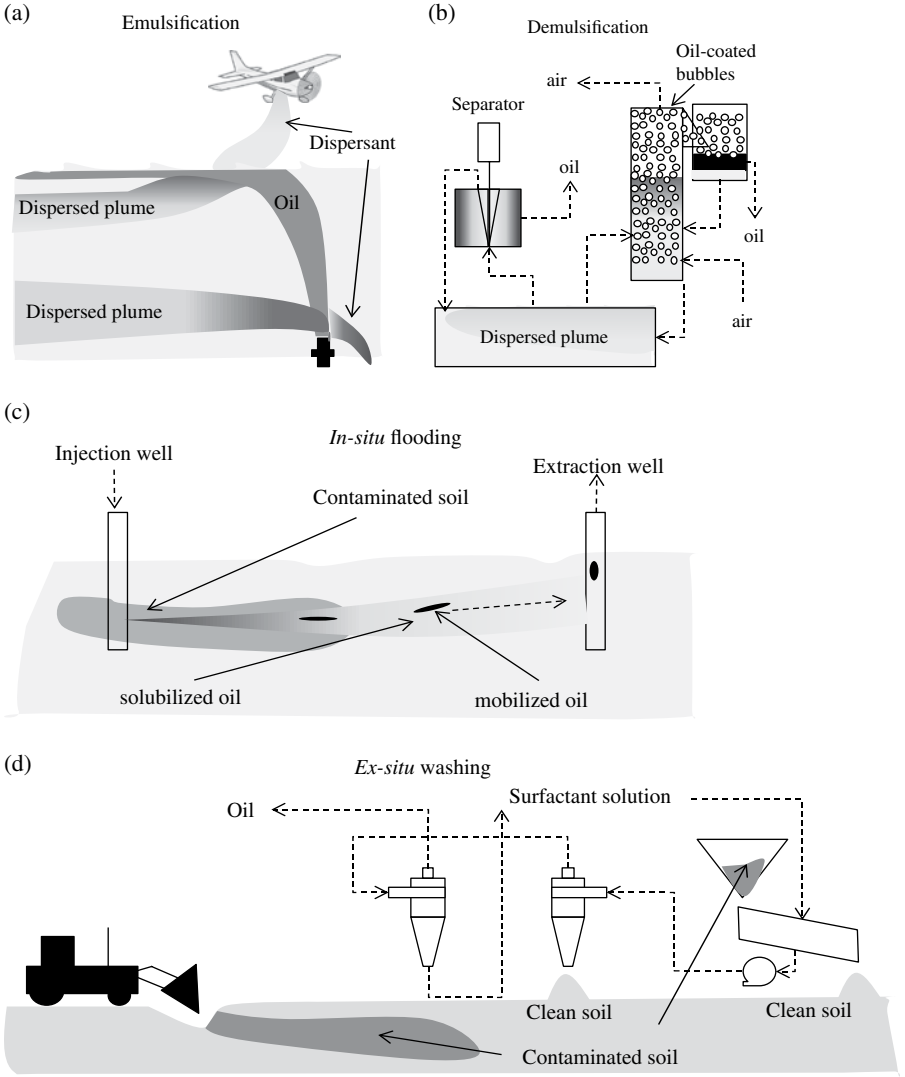

FIGURE 15.1 Surfactant-based technologies for oil spill remediation.

The isotropic region of Figure 15.2 is typically referred to as the microemulsion (μE) region. The word microemulsion is a misnomer for this region, first because μEs are thermodynamically stable systems, in contrast with the unstable nature of emulsions, and because the size of the oil and water domains in μEs is typically well below 100 nm (0.1 μm) (Bourrel and Schecter, 1988; Hoar and Schluman, 1943; Kumar and Mittal, 1999). During the 1970s and 1980s, μEs were evaluated for their use in surfactant-enhanced oil recovery (EOR). Later in the 1990s, the attention

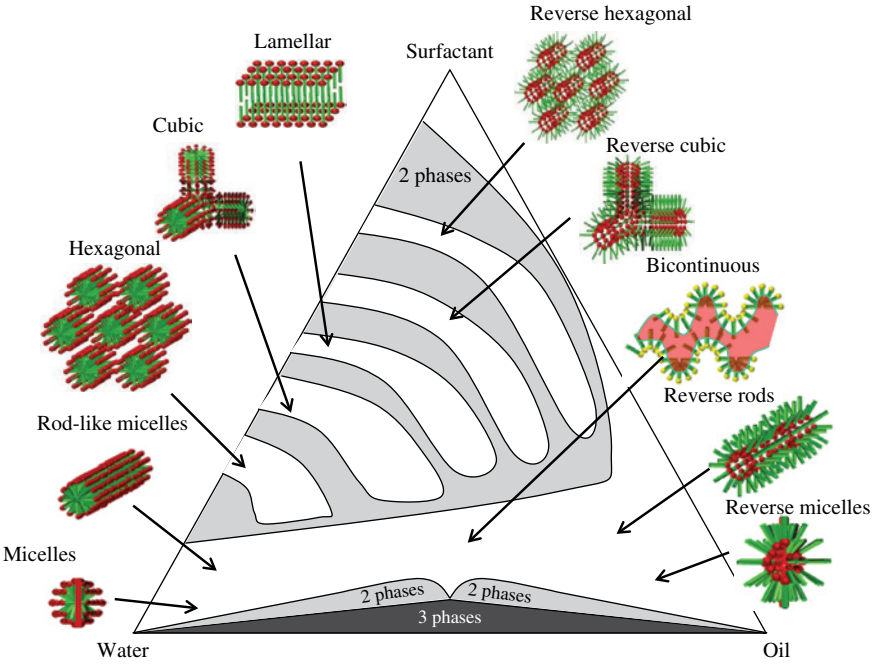

FIGURE 15.2 Schematic ternary phase diagram for an SOW system. Adapted from Davis (1994).

shifted toward their use in the remediation of aquifers contaminated by chlorinated solvents and for their use in the formulation of drug delivery systems. These research efforts have been summarized in numerous references (Bourrel and Schecter, 1988; Fanum, 2009; Kumar and Mittal, 1999; Solans and Kunieda, 1997).

Winsor introduced a classification system for μEs based on whether oil or water is the continuous phase, which is valid for systems prepared with oil-to-water ratios near 1 and with intermediate to low surfactant concentrations (Winsor, 1954). According to this nomenclature, there are four types of μEs. A Winsor Type I μE is composed of oil-swollen micelles in a continuous aqueous phase. Winsor Type II μEs are water-swollen reverse micelles suspended in the oil phase. Winsor Type III and Type IV μEs are bicontinuous systems that contain a network of oil and water channels. The difference between Type III and Type IV is that Type III systems coexist in equilibrium with excess oil and water phases and Type IV are single-phase μEs. The pictures of the test tubes in Figure 15.3 illustrate a phase scan of a system of toluene, sodium dihexyl sulfosuccinate (SDHS), and water. In phase scan experiments, the oil-to-water ratio is maintained at 1:1 with relatively low surfactant concentration (~5% of the total mass for the system of Fig. 15.3). The electrolyte concentration in the test tubes of Figure 15.3 increases from left to right, following a protocol known as the salinity scan. The bottom phase of the first three test tubes (from left to right) are Type I μEs. The intensity of the color of these bottom phases

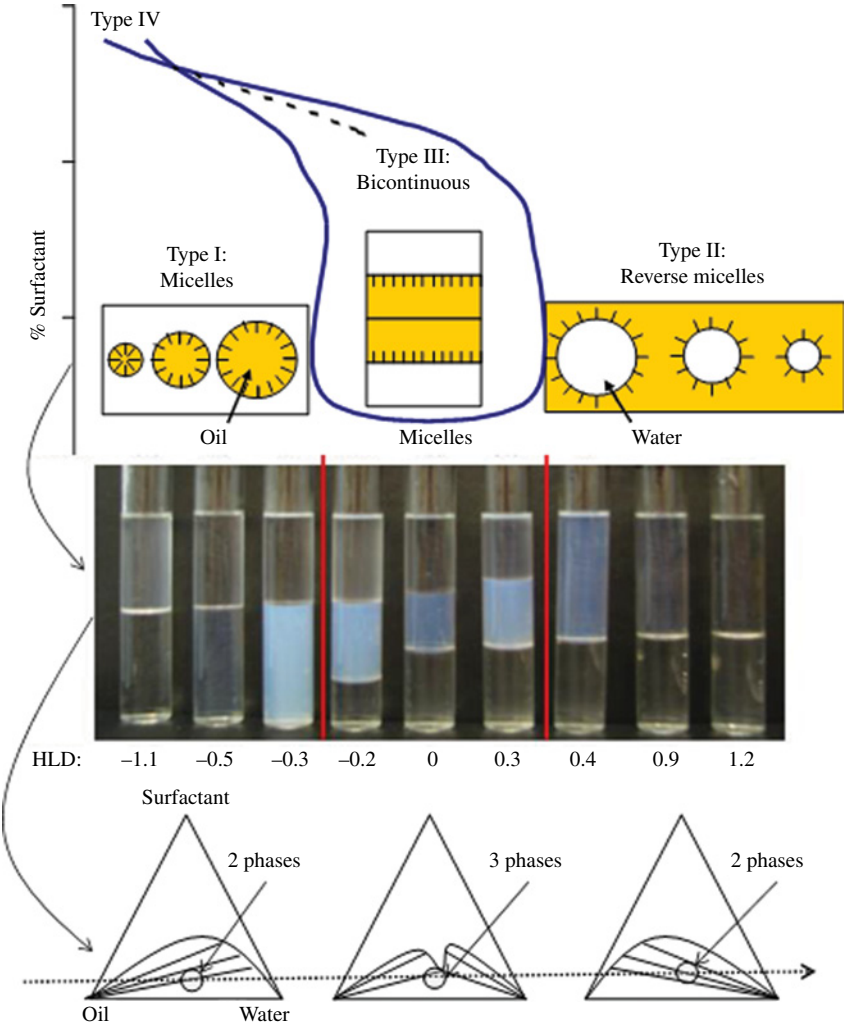

FIGURE 15.3 Phase diagrams for SOW systems. The top figure is a schematic of a "fish" phase diagram. The middle picture represents a salinity phase scan for SDHS–toluene–water. The bottom set of figures are schematics of the corresponding ternary phase diagrams for Type I, III, and II μEs.

increases from left to right as the micelles become swollen with toluene and their shape changes from spherical to rodlike micelles that scatter more light. The next three test tubes of the phase scan correspond to middle phase, Type III, μEs. The middle test tube contains approximately the same volume of oil and water solubilized in the middle phase. This specific condition is known as the optimal formulation. The last three test tubes of the phase scan correspond to water in oil, Type II, μEs.

Phase scan experiments can be undertaken at different surfactant concentrations. For each surfactant concentration, one registers the electrolyte concentration corresponding to the Type I–III and III–II phase transitions and the electrolyte concentration of the optimal formulation. This information can be used to graph these phase boundaries and optimal salinity as a function of surfactant concentration. The resulting diagram is known as the "fish" phase diagram (Bourrel and Schecter, 1988; Kahlweit, 1995; Kahlweit et al., 1983, 1990). A schematic of the fish phase diagram for the SDHS–toluene system is presented in the top panel of Figure 15.3 (Acosta et al., 2009). Similar phase diagrams can be constructed with nonionic surfactants using temperature, instead of electrolyte concentration, as the scanned variable. One important feature of the fish phase diagram is its bottom (lower boundary). The surfactant concentration of this lower boundary is known as the critical μE concentration or CμC. At the CμC, there is no middle-phase μE, but the interface retains the properties of bicontinuous μEs, particularly their ultralow interfacial tension (Acosta et al., 2004).

The three ternary phase diagrams presented at the bottom of Figure 15.3 illustrate the general shape of ternary diagrams obtained with Type I, III, and II μEs. As illustrated in these diagrams, the test tubes of the phase scan represent only one point in the phase diagram. However, the phase scan is a useful method to quickly examine the effect of formulation variables such as electrolyte concentration, surfactant hydrophobicity, oil hydrophobicity, temperature, and the addition of other additives to the SOW systems (Bourrel and Schecter, 1988; Kahlweit, 1995; Salager, 1999).

15.2.2 The Hydrophilic–Lipophilic Difference (HLD) and the Formulation of SOW Systems

As shown in the phase scan of Figure 15.3, the transition from Type I to Type III to Type II systems can be interpreted in terms of the hydrophilic–lipophilic difference or HLD. The HLD was originally developed as a set of empirical equations that correlated the optimal μE formulation conditions (Bourrel and Schecter, 1988; Márquez et al., 2002; Salager, 1999; Salager et al., 1979, 2000):

For ionic surfactants:

$$\mathrm{HLD} = \ln(S) - k \cdot \mathrm{EACN} + C_{\mathrm{c}} - \mathrm{a}_{\mathrm{T}}(T - 25°\mathrm{C}) + f(A); \tag{15.1}$$

for nonionic surfactants,

$$\mathrm{HLD} = b \cdot S - k \cdot \mathrm{EACN} + C_{\mathrm{cn}} + \mathrm{c}_{\mathrm{T}}(T - 25°\mathrm{C}) + f(A) \tag{15.2}$$

where S is the electrolyte concentration expressed as g NaCl/100 mL. The term $\ln(S)$ in Equation (15.1) represents the effect of electrolytes in reducing the Debye length around the head groups of ionic surfactants. The term $b \cdot S$ in Equation (15.2) represents the salting out of nonionic surfactants in the presence of electrolytes. The value of "b" is typically 0.13 for ethoxylated surfactants. The EACN is the equivalent alkane carbon number, a parameter that indicates the hydrophobicity of the oil phase as its equivalent normal alkanes with the given number of carbon atoms in the

molecule. The term $k \cdot \mathrm{EACN}$ reflects the balance of the surfactant–oil interaction, which contributes to the formation of the μE and the surfactant–surfactant and oil–oil interactions that oppose this process. The function $f(A)$ describes the effect of short- and medium-chain alcohols, and other aqueous cosolvents, on the HLD of the formulation. The parameters C_c and C_{cn} are the characteristic curvatures of the ionic and nonionic surfactants and represent the relative hydrophilic–lipophilic nature of the surfactant. The values of the constants k, a_T, and c_T depend on the structure of the surfactant head group.

For μEs formulated with ethoxylated surfactants, the Type I–III–II phase transition is induced by increasing the temperature (the term c_T $(T - 25°\mathrm{C})$ in Eq. 15.2. This increase in temperature weakens the hydrogen bonding between the ethylene oxide groups and the molecules of water, making the surfactant more hydrophobic. In the emulsion literature, the temperature that corresponds to the optimal system in the temperature scan (temperature for $\mathrm{HLD} = 0$) is called the phase inversion temperature (PIT).

Example applications of Equations (15.1) and (15.2) and typical values for the HLD variables and constants are available in literature (Bourrel and Schecter, 1988; Salager, 1999). Table 15.1 presents a summary of the surfactant parameters for selected systems. Table 15.2 presents a summary of EACN values for selected oils.

One of the uses of the HLD equations is to determine whether SOW systems produce oil-in-water (negative HLDs) or water-in-oil (positive HLDs) emulsions or

TABLE 15.1 HLD parameters for selected surfactants

Anionic surfactant	C_c	k	a_T (°C^{-1})	References
Sodium octanoate	−2.1	0.1	0.01	Acosta et al. (2008), Salager and Anton (1999)
Sodium oleate	−1.7	0.1	0.01	Acosta et al. (2008), Salager and Anton (1999)
Sodium dodecylbenzene sulfonate	−0.92	0.16	0.01	Acosta et al. (2008), Salager and Anton (1999)
Sodium dihexyl sulfosuccinate	−0.92	0.17	0.01	Acosta et al. (2008), Salager and Anton (1999)
Oleic acid	0	0.16	0.01	Acosta et al. (2008), Salager and Anton (1999)
Sodium dioctyl sulfosuccinate	+2.5	0.16	0.01	Acosta et al. (2008), Salager and Anton (1999)
$C_nH_{2n+1}(PO)_lSO_4Na$	$-3.8 + 0.1n + 0.16l$	0.08	−0.006	Hammond and Acosta (2012)
Nonionic surfactants	C_{cn}	k	c_T (°C^{-1})	References
$n>6$, $11>j>2$, $C_nH_{2n+1}(EO)_j$	$3.4 + 0.2n - j$	0.16	0.06	Acosta (2008)
Sorbitan monolaurate	3.5	0.16	N.D.	Abbot et al. (2012)
Soy lecithin	4	0.16	N.D.	Abbot et al. (2012)
Sucrose palmitate	−0.8	0.16	~0	Abbot et al. (2012)

Note: PO, propylene oxide; EO, ethylene oxide.

TABLE 15.2 Equivalent alkane number for selected oils

Oil	EACN	References	Oil	EACN	References
Normal C_nH_{2n+2}	For $n>5$, n		Asphaltenes	1	Kiran et al. (2009)
CH_2Cl_2	−13.8	Baran et al. (1994)	Bitumen	2.3	Kiran et al. (2009)
$CHCl_3$	−13.7	Baran et al. (1994)	C_2Cl_4	2.9	Baran et al. (1994)
C_2HCl_3	−3.8	Baran et al. (1994)	Maltenes	6.1	Kiran et al. (2009)
CCl_4	−0.1	Baran et al. (1994)	Dimethicone	13	Castellino et al. (2011)
Benzene	0	Baran et al. (1994)	Palm oil	14	Witthayapanyanon et al. (2006)
Toluene	1	Baran et al. (1994)	Canola oil	18	Witthayapanyanon et al. (2006)
Naphthalene	1	Kiran et al. (2009)	Soybean oil	18	Witthayapanyanon et al. (2006)

μEs at given formulation conditions. When formulating μE systems with HLD = 0, the formulation is optimal because at that point the largest cosolubilization of oil and water and the lowest interfacial tension are obtained.

It is important to clarify that HLD = 0 is only one of the necessary conditions for the formation of optimal bicontinuous μEs. There are SOW systems that fit the criteria of HLD = 0, but instead of producing bicontinuous μEs, these formulations produce precipitates, liquid crystals, or gels. In those cases, medium-chain alcohols or mixtures of long- and short-chain surfactants are used to reduce the surfactant–surfactant interactions that lead to the formation of those undesirable phases.

Based on the good correlation between HLD values and surfactant partition coefficients between oil and water, it has been proposed that the HLD represents the free energy change of transferring one surfactant molecule from the oil phase into the aqueous phase, normalized by $R \cdot T$ (R: gas constant) (Salager et al., 2000). The HLD concept has been used to understand the behavior of emulsifiers and demulsifiers (Goldszal and Bourrel, 2000; Rondón et al., 2006; Salager et al., 2003). The HLD has also been used in the design of methods of removing nonaqueous phase liquids (NAPLs) from subsurface spills (Baran et al., 1994; Sabatini et al., 1995). More recently, the HLD has been used to design a method of surfactant washing of beach sand contaminated with heavy oil (Quraishi et al., 2014).

Despite the usefulness of the HLD as a guideline for designing surfactant-based remediation technologies for oil spills, it does not predict the performance of the formulation. To this end, it is necessary to combine the HLD with the net-average curvature (NAC) model for SOW systems.

15.2.3 The Net-Average Curvature (NAC) Model and the Properties of SOW Systems

The initial hypothesis that drove the development of the NAC model was that if the HLD is a scale that defines the phase behavior of μEs, then it can be used to estimate the properties of those systems. This is a similar principle to that of the corresponding

states, which led to the formulation of equations of state for real fluids. According to the principle of the corresponding states, the property of a fluid (e.g., density) depends on its relative deviation from the critical point, as determined by the values of the reduced temperature (*T*/critical temperature) and pressure (*P*/critical pressure). Some elements of this principle have been used before in the scaling of the curvature ($H = 1$/radius of μE drops) of μEs formulated with ethoxylated surfactants with the difference between the temperature of the formulation and the PIT (Strey, 1994). This idea was extended in terms of HLD, such that $H = 1/R = \text{HLD}/L$, where R is the radius of the drop and L is a constant with a length dimension (Acosta et al., 2003c). However, the problem with this approach is that for systems near or at HLD = 0, the radius of solubilization (R) is significantly larger than the experimental value. This problem reflects the fact that near or at HLD = 0, the system is bicontinuous and cannot be represented as a drop in single continuous phase. To solve this inconsistency, bicontinuous μEs were represented, from a mathematical standpoint, as the average of two coexisting systems, one of drops of oils (with solubilization radius R_o) in water and a second system of drops of water (solubilization radius R_w) in oil. The net curvature (H_n) represents the difference between the curvatures of the coexisting systems and indicates if the interface is flat (net zero curvature), concave toward the oil (positive H_n), or concave toward the water (negative H_n):

$$H_n = \left(\frac{1}{R_o} - \frac{1}{R_w} \right) = \frac{-\text{HLD}}{L} \tag{15.3}$$

where L is a length scaling parameter proportional to the extended length of the surfactant tail (≈1.2 times) (Acosta et al., 2003c). A net zero curvature (HLD = 0) corresponds to a bicontinuous μE containing equal amounts of oil and water ($R_o \approx R_w$). A positive net curvature (HLD < 0) typically corresponds to Type I μEs ($R_w >> R_o$), and negative values (HLD > 0) to Type II μEs ($R_o >> R_w$).

The average curvature (H_a), on the other hand, establishes the surface area to solubilized volume ratio in μEs (~ inverse of the size of the μE domains):

$$H_a = \frac{1}{2}\left(\frac{1}{R_o} + \frac{1}{R_w} \right). \tag{15.4}$$

For a bicontinuous system, the characteristic size ($1/H_a$) should be equal to the characteristic length of the μE (ξ). This characteristic length corresponds to the maximum solubilization capacity of a μE system and is calculated from the phase volumes in middle-phase μEs:

$$\xi = \frac{6\phi_o \phi_w V_m}{A_s} \tag{15.5}$$

where ϕ_o and ϕ_w represent the volume fractions of oil and water, respectively; V_m is the volume of the μE; and A_s is the interfacial area introduced by the adsorption of the

surfactant at the oil–water interface. This interfacial area can be estimated assuming that all the surfactant adsorbs at the interface:

$$A_s = \sum n_{s,i} 6.02 \times 10^{23} a_{s,i} \tag{15.6}$$

where $n_{s,i}$ is the number of moles of surfactant "i" and $a_{s,i}$ is the area per molecule of surfactant "i." This value of A_s is also useful when calculating the apparent solubilization radius of water in Type I μEs (RW = 3 * volume of water/A_s), and the apparent solubilization radius of oil in Type II systems (RO = 3 * volume of oil/A_s).

The NAC model also includes the concept of interfacial rigidity to predict the interfacial tension in μE systems. The interfacial rigidity (E_r) can be understood as the energy of the μE assembly to counterbalance the surface excess free energy of the core of the micelle or reverse micelle (Acosta, 2008; Acosta et al., 2003c):

$$E_r = 4\pi R^2 \gamma \tag{15.7}$$

where R could be R_o or R_w as calculated by the HLD-NAC model and γ corresponds to the interfacial tension between the μE and the excess oil, or water, respectively. The interfacial tensions of systems that have been evaluated using the HLD-NAC model are typically fitted or predicted using a single value of E_r. This value of E_r is close to 1 $K_B T$ (K_B is the Boltzmann constant) for ionic surfactant systems and up to 5 $K_B T$ for nonionic surfactants (Acosta, 2008; Acosta et al., 2003c).

Figure 15.4a presents a comparison between the oil and water solubilization capacity obtained with the toluene–SDHS–water system of Figure 15.3 and the solubilization predicted using the HLD-NAC equations. Figure 15.4b presents a comparison between the interfacial tension obtained with the toluene–SDHS system (Kiran and Acosta, 2010) and the overall interfacial tension predicted with the HLD-NAC, calculated as the sum of the μE–oil and μE–water interfacial tensions. The details of the algorithm for calculating solubilization capacities and interfacial tension have been presented elsewhere (Acosta, 2008; Acosta et al., 2003c, 2008). Other properties that can be predicted using the HLD-NAC model includes the actual drop size and shape, viscosity, composition (density), μE phase volumes, and μE phase transition (Acosta, 2008; Acosta et al., 2003c, 2008; Kiran, 2013).

15.3 SURFACTANT REMEDIATION TECHNOLOGIES FOR SPILLS IN OPEN WATERS

The purpose of this section is to illustrate the use of HLD and HLD-NAC in the design of surfactant-based technologies to address oil spills in open waters. Here, the term open water refers to oceans, seas, lakes, rivers, wetlands, reservoirs, and tailing ponds. One of the technologies considered in this section is the use of dispersants to emulsify oil slicks formed on the surface of the water. The second methodology uses

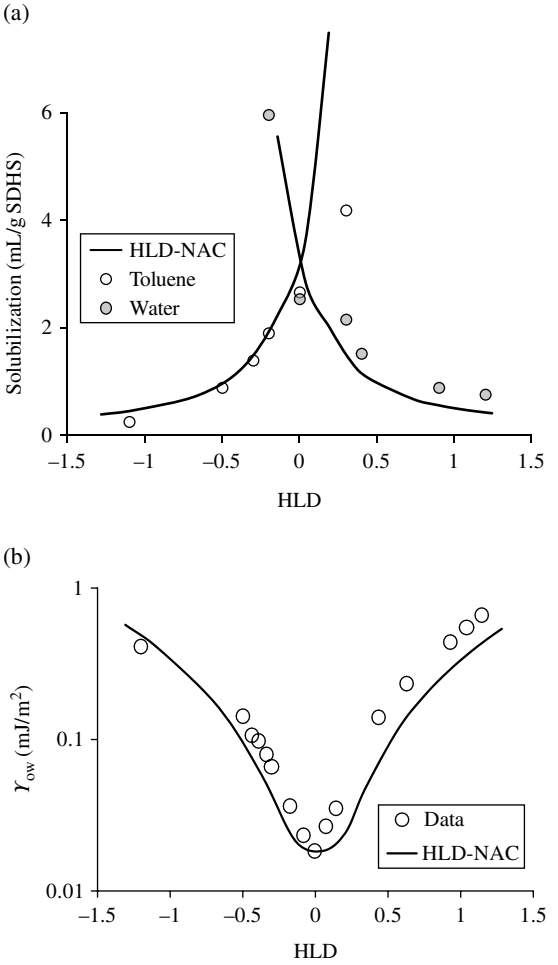

FIGURE 15.4 Solubilization capacity (**a**) and interfacial tension (**b**) for the SDHS–toluene–water system (system of Fig. 15.3) as a function of HLD. Interfacial tension and solubilization data obtained from Kiran and Acosta (2010).

the opposite phenomenon, emulsion destabilization, to liberate the oil via liquid–liquid separators or via froth flotation.

15.3.1 Emulsification and Dispersion

The reasons to disperse oil slicks formed after spills on surface waters have been discussed in other chapters of this book and in the literature (Fingas, 2001; Fingas and Banta, 2009; Kujawinski et al., 2011; Lewis et al., 2010; Ornitz and Champ, 2002). One of the most important objectives is to prevent the oil from reaching the shoreline where its impact on ecosystems is even greater and the costs of remediation

increase substantially. Dispersion methods are useful to treat large areas that have been covered by an oil slick because the emulsifier can be dosed from airplanes as illustrated in Figure 15.1. In the Deepwater Horizon oil spill, the technique of point of release injection of the dispersant (Fig. 15.1) was also introduced (Kujawinski et al., 2011). The objective of that technique was to reduce the amount of oil that reached the surface because once on the surface, the capacity to collect and dispose of the oil was limited.

There are several issues that affect the performance of a dispersant formulation, such as the chemical composition of the oil, viscosity of the oil, temperature, water chemistry, weather (particularly wind patterns), weathering time (before the application of dispersants), contact time (after application of dispersants), currents, and dispersant-to-oil ratio (DOR) (Blondina et al., 1997; Fingas and Banta, 2009; Lewis et al., 2010). The formulation of dispersants has evolved over the years, but it still remains a trial and error effort (Blondina et al., 1997). The goal for future dispersant formulations is to use more environmentally friendly additives that can promote the biodegradation of the dispersed oil (Fingas, 2001; Fingas and Banta, 2009).

The HLD-NAC can be used as a framework to understand the formulation of emulsifiers, their performance, and the potential reformulation strategies to incorporate more biocompatible surfactants. To illustrate the use of the framework, consider the formulation of a dispersant for a spill of light crude oil that occurred in seawater. Assume that the temperature of the seawater is close to 25°C. The electrolyte composition in seawater can be used to calculate its ionic strength, and using that value, it is possible to calculate the equivalent sodium chloride concentration with equivalent ionic strength. An electrolyte concentration of 3.5 g NaCl/100 mL will be used in this example. The EACN of the light crude oil can be determined using a protocol that involves producing phase scans with mixtures of toluene and the light crude oil (Kiran et al., 2009). If the oil is highly aliphatic, the value of EACN might be greater than that of maltenes (EACN = 6.1, see Table 15.1). For the purpose of this example, EACN = 8, consistent with the range of values used in literature for light crude oils (Bourrel and Schecter, 1988). Considering that one of the objectives of introducing emulsifiers is to lower the interfacial tension to facilitate emulsification, then one would target, according Figure 15.4, a value of HLD = 0. However, another important characteristic of the emulsifier is that it should partition in the oil phase (Lewis et al., 2010). Based on this premise, one should target positive values of HLD. Positive HLDs also produce Type II μEs that incorporate saline water into the emulsified oil, which increases the density of the emulsified oil-rich phase. If the formulation contains ionic surfactants, Equation (15.1) can be used to determine the appropriate surfactants (appropriate range of C_c) to produce positive HLD values, in which case

$$\ln(S) - k \cdot \mathrm{EACN} + C_c - a_T(T - 25°\mathrm{C}) + f(A) > 0. \tag{15.8}$$

According to Table 15.1, most surfactants have a value of $k = 0.16$. Considering that, as a first approximation, the formulation does not contain cosolvents, then $f(A) = 0$. Introducing all these considerations into Equation (15.8), then the value of C_c should

be greater than 0.03. The only ionic surfactant in the limited selection of Table 15.1 that complies with this condition is sodium dioctyl sulfosuccinate (Aerosol-OT or AOT). This finding is consistent with the fact that AOT is one of the surfactants used in commercial dispersants (Kujawinski et al., 2011; Lewis et al., 2010). However, AOT alone is too hydrophobic ($C_c = 2.5$), but it can be mixed with other more hydrophilic surfactants (negative C_c values) to obtain values of HLD ranging from 0 to +2.5. In fact, commercial dispersants are mixtures of AOT with more hydrophilic surfactants.

The HLD provides a range of compositions that would be useful in formulating dispersants, but does not predict the properties of the emulsion, particularly drop size and stability. The drop size produced during emulsification can be estimated if the interfacial tension and hydrodynamic conditions are known (Mukherjee et al., 2012). The Weber number helps describe this emulsification process:

$$\mathrm{We} = \frac{\rho v^2 d_p}{\gamma} \tag{15.9}$$

where ρ is the density of the fluid, v is the velocity of the fluid, d_p is the diameter of the drop, and γ is the interfacial tension between the oil and the aqueous phase. The Weber number represents the ratio between inertial forces that tend to stretch and break a drop and the interfacial tension forces that oppose drop stretching and breakup. When the Weber number is larger than a given critical value, the drops are unstable and break into smaller droplets. Walstra summarized various studies on the critical Weber number as a function of the ratio between the viscosity of the dispersed phase and the continuous phase (Walstra, 1993). In that review, Walstra indicates that for viscosity ratios between 0.01 and 10, the critical Weber number is approximately 1. For viscosity ratios larger than 10 or smaller than 0.01, the critical Weber is substantially larger, effectively preventing the emulsification of the oil. Commercial emulsifiers contain solvents, such as 2-buthoxyethanol, that help decrease the viscosity of the oil to be emulsified and prevent the surfactants from forming viscous liquid crystals or gels. Using a target viscosity ratio of 1:10, and the target DOR, the concentration of solvent in the formulation can be determined.

The value of We critical helps revisiting the question of how close to HLD = 0 should one operate. We critical can be used to estimate the drop size of the emulsion, using the interfacial tension predicted by the HLD-NAC model. To illustrate this principle, Figure 15.5 presents the emulsion drop sizes for the toluene–SDHS system of Figure 15.4 obtained by Kiran (2013) and the values predicted by the HLD-NAC model. The predicted drop sizes were obtained using $\mathrm{We}_{\mathrm{critical}} = 1$, the HLD-NAC interfacial tensions of Figure 15.4, and considering that the vortex-mixer configuration of Kiran and Acosta produced fluid velocities close to 0.3 m/s. Systems closer to HLD = 0 are easier to emulsify, and the drop size was very small, which would facilitate the dispersion of the oil. It has been observed in various studies that droplets smaller than 75 μm help ensure proper dispersion of the oil phase (Lewis et al., 2010). Setting 75 μm as target drop size and considering the average velocity of sea currents of 0.08 m/s (Kujawinski et al., 2011), the maximum acceptable

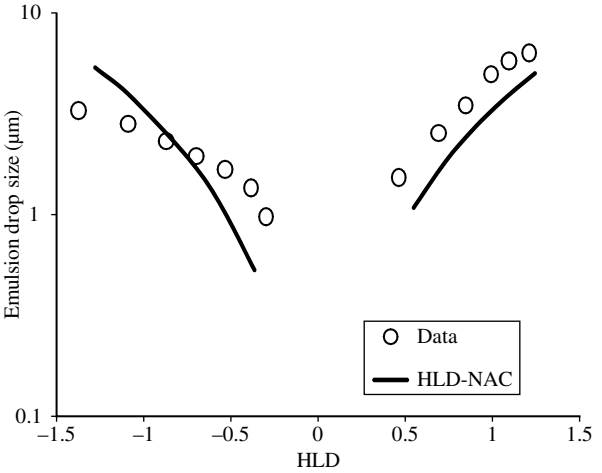

FIGURE 15.5 Emulsion drop diameter of SDHS–toluene–water emulsions as a function of HLD. The experimental data corresponds to the Sauter diameter (d_{32}) reported by Kiran (2003).

interfacial tension is approximately 0.5 mJ/m^2, which, in the case of Figure 15.4 can be obtained with systems with HLD between 0 and 1.2. Shaw produced a similar drop breakup analysis using energy dissipation rates, instead of the critical Weber number (Shaw, 2003).

Emulsion stability is another important property that influences the performance of the emulsifier. In standard bottle or bucket tests for dispersant efficiency for seawater applications, minimum settling times of 1 and 2 min are required (Blondina et al., 1997; Lewis et al., 2010). In pool tests, the process of emulsification lasts for about 30 min, and after that, the dispersion of the drops in the plume minimizes the chances of coalescence (Lewis et al., 2010). The settling time should be longer than those used in the standard tests if the oil to be dispersed has been spilled on calm waters.

Efforts to predict emulsion stability with the HLD-NAC framework are ongoing. It has been shown, however, that emulsion stability and other dynamic processes associated with μEs depend on the rigidity of the surfactant membrane adsorbed at the oil–water interface (Acosta et al., 2003b; Helfrich, 1973; Kozlov and Helfrich, 1992; Nazario et al., 2000). This rigidity can be expressed in terms of the interfacial rigidity (E_r) obtained from the HLD-NAC model (Acosta et al., 2003b).

Figure 15.6 summarizes the emulsion stability obtained with four SOW systems as a function of the HLD (Kabalnov and Weers, 1996; Rondón et al., 2006). According to Figure 15.6, the stability of the microemulsions reach a minimum at HLD = 0. As the HLD becomes more positive (or negative), the emulsion stability increases. It is important to note that two different SOW systems, SDS–kerosene–water and nonylphenol ethoxylates–lubricant oil–water, have almost equivalent stability curves. Both systems were produced with the same surfactant concentration (~1%). The system of

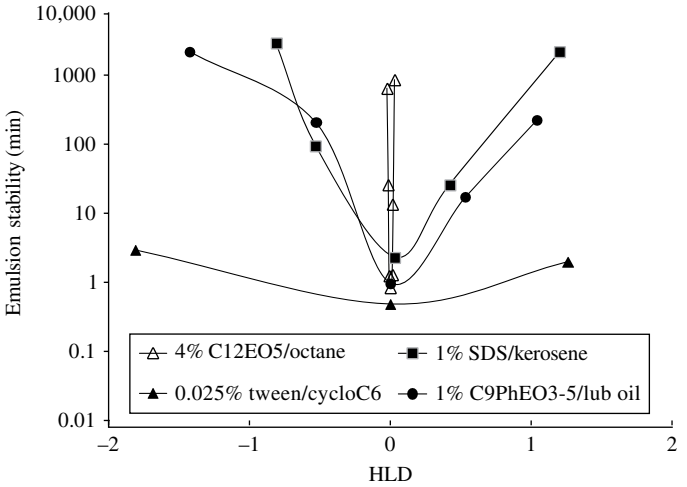

FIGURE 15.6 Emulsion stability as a function of HLD. The stability data for SDS–kerosene, Tween 20 + Span 80–cyclohexane, and nonylphenol ethoxylated–lubricating oil were obtained from Rondón et al. (2006). The data for the system of $C_{12}EO_5$–octane was obtained from Kabalnov and Weers (1996).

$C_{12}EO_5$–octane, on the other hand, was formulated with 4% surfactant and produced significantly larger emulsion stabilities. The system of Span 20 and Tween 80–cyclohexane–water was formulated with only 250 ppm of surfactant and produced the lowest emulsion stability. The data in Figure 15.4 highlights that, in addition to the HLD, the concentration of the emulsifier (at least during the first minutes of emulsification) has a tremendous influence on the stability of the emulsion. The same trend was observed by Kiran and Acosta with the SDHS–toluene–water system (Kiran, 2013). This evidence suggests that the best possible stability is obtained with the highest positive value of HLD that satisfies the interfacial tension required for the target drop size for the dispersed oil.

An ongoing issue with dispersants is their toxicity and their effect on biodegradability. A review by Fingas and Banta summarizes numerous publications concerning the effects of dispersants on the environment (Fingas and Banta, 2009). In that review, the authors indicate that although one of the objectives of introducing emulsifiers is to improve the biodegradation of the oil, biodegradation studies show that the emulsifiers used in current formulations do not improve the biodegradation of oil and that, in some cases, they might inhibit this process. A review by Cameotra and Makkar summarize numerous efforts in finding alternative biosurfactants that could contribute to improve the biodegradation of oils (Cameotra and Makkar, 2010). Biosurfactants are synthesized and released by microorganisms that are typically found in areas impacted by oil spills. These surfactants have a very low CMC, which contributes to make them effective even at low surfactant concentration. Although biosurfactants have been used for remediation of oil spills on shores and on land, their use in open waters has been limited perhaps in part due to their relatively high

cost and the fact that in some studies, some biosurfactants have been found to inhibit the degradation of polyaromatic hydrocarbons (Deschênes et al., 1996; Fingas and Banta, 2009; Shin et al., 2005).

Another problem with most biosurfactants and other "green" surfactants is that most of them, despite their low CMC, have negative characteristic curvatures, which would classify them as hydrophilic surfactants (Abbot et al., 2012). Thus far, only a few surfactants having positive characteristic curvatures have been identified. Table 15.1 suggests that sorbitan monolaurate and lecithin could be used as replacements for AOT. The problem with sorbitan monolaurate and lecithin is that they have an even greater tendency than AOT to produce viscous liquid crystal phases and gels. One potential strategy to introduce lecithin into dispersants is the use of the linker approach that combines lecithin with shorter chain surfactants (Acosta et al., 2005). This approach has been used in laboratory-scale studies for removal of viscous hydrophobic oils. Lecithin formulations will be discussed later in this chapter.

15.3.2 Demulsification and Separation

The approach of demulsification and separation is typically used in situations where the oil is in confined environments or in situations where the oil slick is thick enough to be collected by booms, skimmers, or liquid–liquid separators. The system depicted in Figure 15.1b illustrates the separation via liquid–liquid separators and froth flotation.

When using skimmers, one of the concerns is that the water emulsified with the collected oil occupies the storage space that could otherwise be used to capture more oil (Buist et al., 2005; Fingas, 2000; Fiocco et al., 2005). Another concern is that water–oil emulsions also affect the operation of pumps. Emulsions are also a concern for *in situ* burning as the emulsified water could extinguish the flame before all of the oil is burned, or it could prevent the oil from being ignited in the first place (McCourt et al., 2005).

Water-soluble demulsifiers are used to break the water-in-oil emulsions obtained during skimming and when implementing *in situ* burning operations (Fingas, 2000; McCourt et al., 2005). Typical target concentrations range from 100 to 1000 ppm (Fingas, 2000). These formulations have been produced with sulfosuccinates (e.g., SDHS and AOT), with block copolymer surfactants, with mixtures of surfactants and solvents, and with relatively hydrophilic nonionic surfactants (Fingas, 2000).

The data of emulsion stability presented in Figure 15.6 also helps in determining the conditions for best emulsion breaking, which correspond to values of HLD ~ 0 where the emulsion stability is at its minimum. However, because the objective is to leave the oil as free of water as possible, then one should formulate systems where surfactant partitions primarily in water (negative HLDs). Combining these two conditions, then formulations with slightly negative HLD values should be preferred for emulsion breakers. In this region, as indicated in Figure 15.4b, the interfacial tensions are low. Another formulation lead that can be extrapolated from Figure 15.6 is that one should use the lowest possible concentration of the surfactant. All these leads are consistent with the characteristics of some of the best performing formulas: they are

relatively hydrophilic, they are effective at reducing the interfacial tension, and they tend to be dosed at concentrations well below 1% (Buist et al., 2005).

If the formulation is too close to HLD = 0, then the oil will emulsify with little energy input, and this will cause the formation of small oil droplets with low creaming velocities that will be more difficult to separate in the absence of the higher *g*-forces of a liquid–liquid separator. This type of phenomena has been observed in the field, and it has been associated with poor oil separation (Buist et al., 2005). This is another reason for formulating away from HLD = 0 while maintaining low emulsion stability. The separation process can be helped by using gentle mixing to deliver the surfactant, followed by quiescent separation or by centrifuges. The use of centrifuges was evaluated, among other technologies, in the Deepwater Horizon spill (Dittrick, 2010).

Froth flotation is an emerging technology for removing oil from industrial wastewater and water contaminated with diesel, gasoline, and other hydrocarbons. As illustrated in Figure 15.1b, in froth flotation, air is bubbled through the aqueous solution containing the dispersed oil. This dispersed oil is collected as a film at the liquid–air interface and is carried by the froth to a separator where the froth breaks and where the final oil–water separation takes place (Chavadej et al., 2004a, b; Pondstabodee et al., 1998). In early studies, surfactant was added with the purpose of frothing the aqueous solution, but later, it was found that with increasing salt concentration the removal efficiency improved and it was maximum at HLD = 0 (Pondstabodee et al., 1998). Although a detailed mechanism of separation is not yet known, the improved oil removal in μE froth flotation correlated with the onset of ultralow interfacial tensions obtained with systems formulated near or at an HLD = 0 (Chavadej et al., 2004a). It was later determined that it is important to keep the surfactant concentration low, close to the CμC, to improve foam stability (Yanatatsaneejit et al., 2005). More recently, the first continuous pilot of this technology was reported (Watcharasing et al., 2008). In that pilot, 96% of diesel was removed from water with an electrolyte concentration close to that of seawater. The technology has several positive features such as the fact that it works with a wide range of oil-to-water ratios and that it has a relatively low energy demand (pumps and air compressor). The main problem thus far is the relatively large foam retention time required for the process (~1 h) that would make the footprint of the technology prohibitive at this time for offshore operations. This large retention time seemed to be associated with the large interfacial rigidity (E_r) of the extended surfactants used in that work, which slows down the process of coalescence and the overall separation process (Acosta et al., 2012; Watcharasing et al., 2008).

15.4 SURFACTANT REMEDIATION TECHNOLOGIES FOR SPILLS ON LAND

Remediation of oil spills on land presents additional challenges to those on sea because the presence of a solid surface provides an additional substrate where the oil can be deposited. Fundamentally, this also represents a new challenge because the design of the surfactant formulation not only has to account for the oil–water interface

but for the oil–solid and water–solid interfaces as well. Fortunately, the problem of oil removal from solid surfaces has been thoroughly investigated due to its relevance to detergency and hard surface cleaning. In the first part of this section, the mechanisms of oil removal from surfaces will be discussed, along with the relation between the HLD to the important parameters that control oil removal efficiency. Later, the use of surfactant-based technologies for *in situ* removal of underground oil spills and for *ex situ* soil washing of surface spills will be discussed.

15.4.1 Mechanisms of Oil Removal from Solid Surfaces

Figure 15.7 illustrates the three mechanisms of oil removal from solid surfaces: oil roll-up, oil snap-off, and oil solubilization (Acosta et al., 2012; Childs et al., 2005; Dillan et al., 1979; Thompson, 1994).

The roll-up mechanism for oil removal can be used in situations when the oil does not wet the surface; this is when the contact angle of the oil is substantially larger than 180°. In those situations, it is important to break the oil film in order to form a three-phase line (solid–water–oil). This contact line tends to retract given the affinity

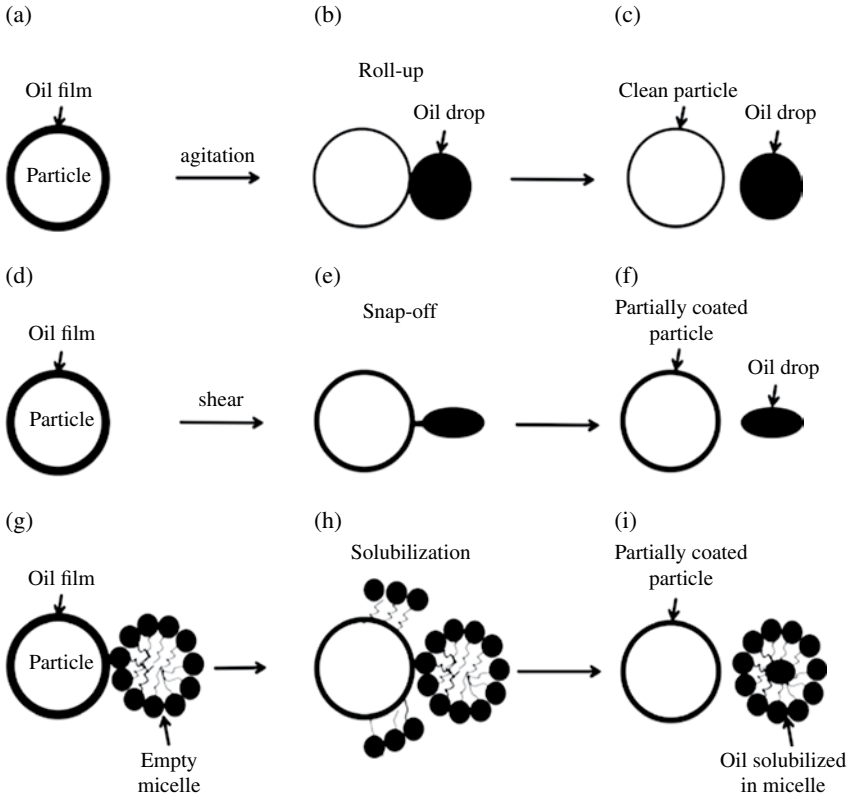

FIGURE 15.7 Mechanisms of oil removal from solid surfaces. Images are not to scale.

of the surface for the aqueous solution, producing an oil drop that eventually detaches. Unfortunately, the roll up does not happen in most cases associated with oil spill events. Dudášová et al. (2009) determined that asphaltenes found in crude oils, particularly heavy crude oils, adsorb on mineral surfaces and turn them hydrophobic (i.e., oil contact angles lower than 90°). For example, they determined that the contact angle of water on a kaolin surface exposed to air was 12°, which suggests that the surface of kaolin is highly hydrophilic. After exposure to asphaltenes, the contact angle of water on kaolin increased to 100°.

The snap-off mechanism requires a substantial reduction in the interfacial tension between oil and water because it involves stretching the film of oil into the continuous aqueous phase under the action of shear and eventually breaking up the film under the action of the same capillary instabilities that controlled the breakup of drops in emulsions. The mechanism of snap-off is important for systems formulated around HLD = 0. The only problem with the snap-off mechanism is that it leaves a residue of oil, as illustrated in Figure 15.7 (Childs et al., 2005). Some methods of oil removal used in detergency applications involve a first cleaning step with a formulation at HLD = 0, followed by a rinsing solution that changes the wettability of the oil and promotes the roll-up mechanism (Tanthakit et al., 2008; Tongcumpou et al., 2003, 2005).

The solubilization mechanism involves the dissolution of oil molecules into the hydrophobic core of surfactant micelles. Solubilization mechanisms can produce 100% oil removal (Childs et al., 2005). However, it is better used as a polishing methodology because, otherwise, high surfactant concentrations are required, which lead to high surfactant costs, potential issues of surfactant toxicity, and issues of potential particle destabilization (formation of stable suspensions) (Childs et al., 2005). Solubilization schemes can be used with high surfactant concentrations (~5 wt%) if there is a surfactant recovery in place and if the site is rinsed at the end of the extraction period to reduce the residual surfactant concentration (Krebbs-Yuill et al., 1995; Sabatini et al., 1995). Solubilization with biosurfactants is yet another remediation approach that is gaining some attention, particularly in combination with microorganisms that can degrade the oil once it is solubilized in the aqueous solution (Cameotra and Makkar, 2010; Laha et al., 2009).

While understanding these mechanisms is a useful guideline, it is important to translate these ideas into equations and measurable parameters that can be used to design the appropriate remediation processes. Having this objective in mind, Thompson evaluated the removal of hexadecane from polyester using *n*-dodecyl pentaethylene glycol ($C_{12}EO_5$) solutions (among other systems) (Thompson, 1994). Figure 15.8 presents selected data from that work, renormalized in terms of the HLD scale. Figure 15.8a presents the interfacial tension data for this system along with the HLD-NAC prediction. Figure 15.8a also includes the contact angle of hexadecane on polyester in the surfactant solution. It is interesting to note that the contact angle changes sharply around HLD = 0 and that the surface is preferentially hexadecane-rich Type II μEs at HLD > 0. Similar trends in contact angle changes around HLD = 0 have been observed by Reed and Healy for μEs on various surfaces, including minerals (Reed and Healy, 1984).

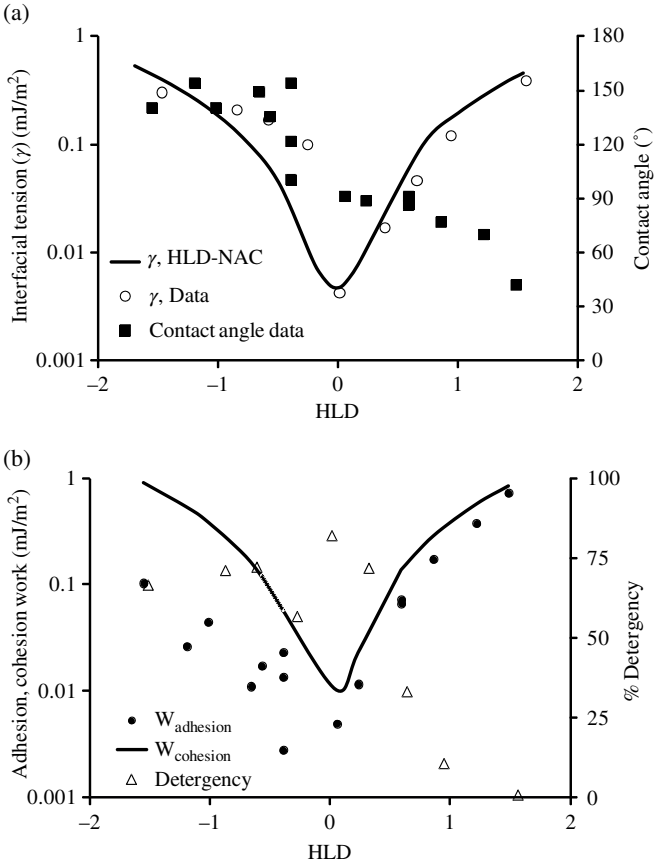

FIGURE 15.8 Properties of the system $C_{12}EO_5$–hexadecane–water (0.5% NaCl) as a function of HLD (Thompson, 1994). (**a**) Includes the interfacial tension and the contact angle of hexane on polyester. (**b**) Includes the work of adhesion and cohesion and the fraction of hexadecane removed (detergency).

Thompson used the concepts of work of adhesion and work of cohesion to explain the removal of hexadecane from polyester fabric (Thompson, 1994):

$$W_{\text{adhesion}} = \gamma(1 + \cos\alpha) \tag{15.10}$$

$$W_{\text{cohesion}} = 2\gamma \tag{15.11}$$

where γ is the interfacial tension between oil and water and α is the contact angle of hexadecane on polyester in the presence of the surfactant solution. Figure 15.8b presents the work of adhesion and cohesion for the $C_{12}EO_5$–hexadecane–water–polyester system as a function of the HLD. Systems with negative HLD, close to HLD = 0,

produced the lowest work of adhesion. According to Figure 15.8b, these systems with low work of adhesion also produced the largest detergency (hexadecane removal). The low oil removal obtained with positive HLDs has been linked to the wettability of Type II μEs at HLD > 0 (Thompson, 1994).

15.4.2 *In Situ* Surfactant Flooding

There are numerous oil spills that can occur on land such as pipeline ruptures, accidents during the transportation of oily substances via railcars or tankers, leaks from aboveground and underground storage tanks, and oil spills during fuel transfer operations. Perhaps one of the most notorious (and expensive to remediate) oil spill involves the inappropriate disposal of chlorinated solvents. Spills of chlorinated solvents are particularly a problem because these oils have low viscosity, high density, low volatility, and relatively low surface tension, all of which facilitate their penetration through the vadose zone of the soil, especially in sandy soils. Once the chlorinated solvents reach the water table, they continue their downward migration to zones of low permeability within the aquifer. Once there, their solubility in water is high enough to pose serious health risks (they are carcinogens) but low enough to keep the pool of chlorinated solvents almost unchanged for decades.

There have been several technologies introduced to remove oils, also known as NAPLs, from aquifers and from the vadose zone. Among these technologies, surfactant-enhanced aquifer remediation (SEAR) has been shown to be capable of removing chlorinated solvents (dense NAPLs or DNAPLs) and light hydrocarbon contaminants (light NAPLs or LNAPLs) (Abriola et al., 1993; Palmer and Fish, 1992; Paria, 2008; Pennell et al., 1993, 1994; Pope and Wade, 1995; Shiau et al., 1994).

Figure 15.1c presents a schematic of the SEAR technology. There are several configurations for SEAR, but the configuration illustrated in Figure 15.1c corresponds to the more conventional "line drive." In this configuration, the surfactant solution is injected into one well, typically close to the pool of NAPL, and the oil that is solubilized in micelles or mobilized as oil plugs (capillary displacement) is then captured by one or more collection wells.

Pitts et al. reported the use of SEAR to remove 84% of creosote from a contaminated aquifer (Pitts et al., 1993). Fountain et al. also reported 84% removal of PCE spilled at a controlled test site in Borden, Ontario (Fountain et al., 1996). The SEAR technology was also tested at Hill Air Force Base (AFB), Utah, for the removal of LNAPLs and DNAPLs (Brown et al., 1999; Hirasaki et al., 1997; Jawitz et al., 1998; Knox et al., 1999; Londergan et al., 2001). Two of these studies reported removal efficiencies of 90% and 98% (Brown et al., 1999; Hirasaki et al., 1997).

A recent review compared several technologies for NAPL removal, including solvent extraction, cyclodextrin complexation, surfactant solubilization (away from HLD = 0), supersolubilization in μEs (negative HLD, closer to zero), surfactant mobilization (HLD = 0), and air sparging (McCray et al., 2011). In that review, it was identified that systems formulated with HLD = 0 or closer to zero are the systems that produce the largest oil removal. However, for DNAPLs, those systems with HLD = 0 pose a risk of downward mobilization of the oil plume. On the other hand, systems

that rely on only solubilization were not as efficient, but did not pose the risk of downward mobilization (Hasegawa et al., 2000; Sabatini et al., 2000). To improve the performance of the solubilization, it is important to optimize the flow pattern (flow rate, well configuration) to maximize the solubilization rate (Jawitz et al., 2000; Pope and Wade, 1995; Sabatini et al., 2000).

The optimization of flow patterns for solubilization and mobilization scenarios has been undertaken with multiphase flow models used in reservoir engineering that couple the properties of the surfactant formulation (solubilization capacity, interfacial tension, viscosity, density) with mass and momentum transport equations (Brown et al., 1999; Londergan et al., 2001). While the existing reservoir simulators have provided useful guidance for the implementation of SEAR technologies, their accuracy in predicting the phase behavior of SOW systems requires improvement.

At the moment, these simulators use empirical correlations to estimate important properties of SOW systems, such as interfacial tension solubilization capacity and viscosity. The HLD-NAC framework could be incorporated into reservoir simulators to predict the changes in SOW properties (γ, ρ, μ, solubilization capacity) as the surfactant solution moves through the reservoir, encountering different temperatures and electrolyte concentrations. Another limitation of current simulators is that the mass transfer equations used to represent solubilization in surfactant solutions are too simple to reflect the complexity of oil and surfactant transport across interfaces.

Miller et al. proposed that the solubilization of oil in micelles takes place through the formation of intermediate lamellar phases at the oil–water interface (Miller, 1996; Nishimi and Miller, 2000; Rang and Miller, 1999). A similar "direct contact" mechanism has been proposed by Kralchevsky et al. (Christov et al., 2002; Kralchevsky et al., 2002), but in this case, the adsorption of micelles on the oil surface controls the rate of solubilization. Carroll et al. (Carroll, 1981; Carroll et al., 1982; O'Rourke et al., 1987) proposed a similar model to that of Kralchevsky et al. but indicated that for oils that are partially soluble in water, the solute could diffuse through the aqueous phase until it finds a micelle.

Figure 15.9 presents a schematic of the "direct contact" solubilization mechanism corresponding to Type I systems along with experimental data on the rate of limonene solubilization in SDHS using a flow-thru dialyzer (Acosta et al., 2007). Direct contact solubilization involves the transport of the micelle from the bulk solution to the oil–water interface (depicted in this case as a surfactant monolayer). Once there, the micelle needs to adsorb on the interface and exchange matter with the oil and surfactants at the interface; then, the oil-swollen micelles desorb from the interface; and finally, these swollen micelles are transported back into the bulk solution. The challenge of predicting the rate of solubilization in surfactant systems is that any of these steps can limit the rate of solubilization. In the case of the SDHS–limonene system of Figure 15.9 (HLD ~ -0.9), there are two distinct regions, one controlled by surfactant adsorption at low surfactant concentrations and a region controlled by surfactant desorption at high SDHS concentrations. The mass transfer in the adsorption-limited region is strongly influenced by the surfactant concentration, and the flow rate (superficial velocity) of the solution passing over the membrane plays a minor role in the overall transport. On the other hand, in the desorption-limited

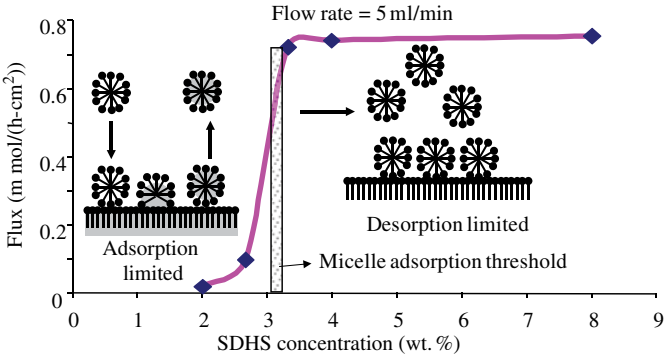

FIGURE 15.9 Effect of surfactant concentration on the solubilization flux of limonene into SDHS formulations formulated with 3 wt% NaCl (Acosta et al., 2007). The micelles (not to scale) illustrate the "direct contact" mechanism of solubilization.

region, the concentration of SDHS plays only a minor role, and the rate of solubilization is highly dependent on the flow rate of the surfactant solution (data not shown). Similar behavior has been observed for the transport of hydrophilic and lipophilic solutes with Type I and Type II μEs (Plucinski and Nitsch, 1993; Yuan et al., 2010). Another study on the kinetics of alkane solubilization in micelles suggests that the limiting step is the uptake of the oil by micelles adsorbed at the interface (Luning-Prak et al., 2000).

While the details on the effect of flow rate and surfactant concentration on the effective mass transfer coefficient are yet to be further elucidated, most of these studies agree that the rate of solubilization is proportional to the oil solubilization capacity in micelles. As indicated by Figure 15.4a, this is accomplished at negative HLD values that are closer to zero. The region of the phase scan at the boundary of Type I and Type III μE is also known as the supersolubilization region (Acosta et al., 2003c).

The SEAR-solubilization technology was used at Dover AFB with the objective of removing 0.08 m^3 of tetrachloroethylene (C_2Cl_4 or PCE) (Childs et al., 2006; McCray et al., 2011) from a test cell with 12 m^3 of pore volume. In that work, 68% of the target PCE was removed after flushing 140 m^3 of a 3.3% SDHS solution (HLD ~ −1.4), followed by 80 m^3 of rinse water. The researchers injected 4.3 tons of surfactants into the aquifer and recovered 3.9 tons after the surfactant flush. Fortunately, the surfactant was reused by introducing a stripping unit to remove PCE from the surfactant solution. The surfactant was recycled nine times before disposal, which saved 82% in surfactant costs and reduced waste disposal by 91%. If one extrapolates the data of Figure 15.9 for the SDHS system, then the surfactant flooding system used at Dover AFB was properly designed to work on the region of desorption-limited solubilization. However, from the solubilization point of view (extrapolating the data of Fig. 15.4a), the system was not properly designed as the solubilization capacity was relatively low. However, the chosen formulation (HLD)

provided the largest possible solubilization while minimizing the chances of downward mobilization (Childs et al., 2004, 2006). Another limitation of the solubilization approach is that a large mass of surfactant had to be used to remove a relatively small mass of contaminant. This is an issue that cannot be helped given the configuration of the test cell. One way to minimize the volume of surfactant is to restrict the flow to an area near the contaminant site via close configuration of injection and extraction wells or via single well injection/extraction in push–pull configurations (Field et al., 1999).

The removal of LNAPLs with surfactant solutions is often accomplished by targeting negative HLD values close to zero where the interfacial tension is typically ultralow (Fig. 15.4b) and where the work of adhesion is the lowest (Fig. 15.8b) (Knox et al., 1997; Pope and Wade, 1995; Sabatini et al., 1997, 1998, 2000). In this approach, low surfactant concentrations (near CμC) are desirable to minimize surfactant costs and the formation of highly viscous and stable emulsions (Fig. 15.6).

Once low interfacial tensions are achieved, the oil is easily displaced from the porous media by viscous forces associated with the flow of the surfactant solution through the porous media. Gravitational (buoyancy) forces can also contribute to the displacement of oil from the porous media (Shiau et al., 2003).

The HLD-NAC framework can be used to calculate the interfacial tension, viscosity, and density of the surfactant formulation. These formulation properties can be integrated with capillary curves (Pope and Wade, 1995), trapping curves (Pennell et al., 1996), and gradient curves (Childs et al., 2004) to predict the performance of a given NAPL mobilization strategy. The capillary curve indicates fraction of total fluid volume in the aquifer occupied by NAPL (NAPL saturation or Sn) for a given capillary number (Ca). The capillary number indicates the ratio between the viscous or shear forces that tend to stretch or spread the oil and the interfacial forces that tend to keep the oil trapped in small pores:

$$\mathrm{Ca} = \frac{\mu \cdot v}{\gamma} \tag{15.12}$$

where μ is the viscosity of the surfactant solution, v is the velocity of the solution in the pore, and γ is the interfacial tension between the surfactant solution and the NAPL phase.

Another important dimensionless number is the Bond number (Bo) that reflects the ratio between gravity (buoyancy) forces that contribute to NAPL mobilization and the interfacial tension forces that oppose this mobilization:

$$\mathrm{Bo} = \frac{\Delta\rho \cdot g \cdot r^2}{\gamma} \tag{15.13}$$

where $\Delta\rho$ is the difference between the density of the surfactant solution and the density of the NAPL, g is acceleration due to gravity, and r is a length scale appropriate for the system.

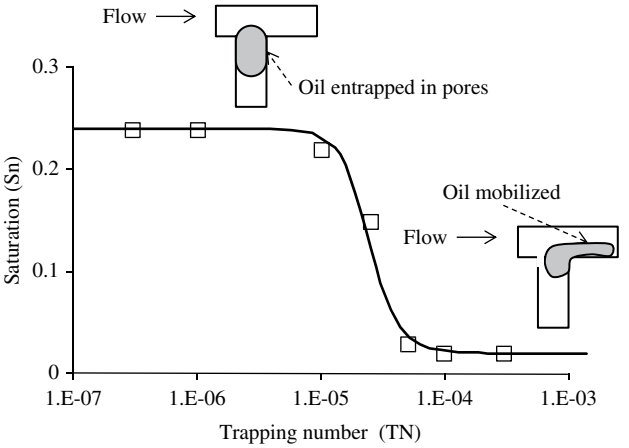

FIGURE 15.10 Trapping curve for tetrachloroethylene (C_2Cl_4, PCE) on a sand (mesh 40–270) column. Data obtained from the work of Pennell et al. (1996). Solid line obtained by fitting the data with the generalized Van Genuchten equation.

In reality, shear forces and gravity forces act at the same time. In some cases, they can work together if they point in the same direction such as the upflow mobilization of a LNAPL. The combined process can be described by the trapping number (TN) (Pennell et al., 1996):

$$\mathrm{TN\,(trapping\ \ number)} = (\mathrm{Ca}^2 + 2\mathrm{Ca}\cdot\mathrm{Bo}\cdot\sin\theta + \mathrm{Bo}^2)^{0.5} \qquad (15.14)$$

where θ is the angle between the buoyancy and the shear forces. When the two forces are orthogonal, $\theta = 0°$, when both forces point in the same direction, $\theta = 90°$. Pennell et al. introduced the trapping curve (Pennell et al., 1996) to correlate the NAPL saturation with the corresponding TN. Figure 15.10 presents an example of a PCE trapping curve obtained by Pennell et al. for a 40–270 mesh Ottawa sand (Pennell et al., 1996). To interpret the significance of Figure 15.10, it is important to keep in mind, after combining Equations (15.12), (15.13), and (15.14), that TN $\propto 1/\gamma$. The HLD-NAC framework can be used to determine the appropriate formulation (HLD value) that would lead to an interfacial tension (γ) that is low enough to produce a TN of 10^{-4}. Larger TN values do not result in additional oil removal. Another important feature of Figure 15.4 is that even at large TN values, not all of the oil is removed, which is consistent with the snap-off mechanism discussed earlier.

Capillary curves, as well as trapping curves, can be fitted using a generalized form of the Van Genuchten equation (Quraishi et al., 2012; Van Genuchten, 1980):

$$\varphi = \varphi_{\mathrm{residual}} + \frac{(\varphi_{\mathrm{saturation}} - \varphi_{\mathrm{residual}})}{\left[1 + \left(\mathrm{TN}/\mathrm{TN}_{\mathrm{critical}}\right)^n\right]^{1-(1/n)}} \qquad (15.15)$$

where ϕ is the volume fraction or Sn of NAPL in the aquifer, $\varphi_{residual}$ is the residual volume fraction or Sn obtained at high TN values, and $\varphi_{saturation}$ is the volume fraction or Sn obtained at low TN values. The value of $TN_{critical}$ represents the transition point in the curve. It has a similar meaning to that of Wecritial used to predict the drop size during emulsification. For the system of Figure 15.10, $TN_{critical} = 2.2 \times 10^{-5}$, and the scaling exponent $n = 4$.

It is important to note that the capillary curve, or a trapping curve, is characteristic for a given soil, with a given contaminant and a given surfactant formulation. Changes in the viscosity of the oil or the surfactant solution or heterogeneities in the permeability of the aquifer could change these curves. Proper characterization of the formation is very important in order to design surfactant flooding (SEAR) systems. The compatibility between the formation and the surfactant solution is also important. Anionic surfactants, for example, tend to adsorb on calcite and on clays with high calcium and aluminum content. If the aquifer contains relatively high concentrations of multivalent cations or if the temperature of the aquifer is below the Krafft temperature of the surfactant, this could cause surfactant precipitation. Surfactant–soil and surfactant–water screening tests should be undertaken when formulating a SEAR system (Hasegawa et al., 2000; Pope and Wade, 1995; Sabatini et al., 1997, 2000). Sulfosuccinate surfactants, alkyl naphthalene sulfonates, alkyl ether sulfates, and mono- and dialkyl diphenyl oxide disulfonate, used alone or in combinations with nonionic surfactants and/or alcohols, are often used in SEAR and soil washing technologies (Sabatini et al., 1997, 2000).

The selection of the surfactant also has an impact on the solubilization and interfacial tension, as predicted by the HLD-NAC model. Surfactants with longer alkyl groups (larger L parameter in Eq. 15.3) are desirable to increase the solubilization capacity of the formulation and produce lower interfacial tensions. Unfortunately, surfactants with long alkyl groups tend to have higher Krafft temperatures and form liquid crystals or gel phases. These undesirable effects can be avoided with linker additives. Graciaa et al., introduced lipophilic linkers as weak amphiphiles such as long-chain alcohols (Graciaa et al., 1993a, b; Salager et al., 1998). These molecules segregate near the surfactant tail, which effectively links the surfactant tail with oil molecules located into the hydrophobic core of the μE. To enhance the effect of lipophilic linkers, Uchiyama et al. introduced hydrophilic linkers as surfactant-like molecules with short hydrophobic tails (typically six to nine carbons per head group) that adsorb with the surfactant at the oil–water interface (Acosta et al., 2002; Uchiyama et al., 2000). The combination of hydrophilic and lipophilic linkers produces a pseudosurfactant that further improves the solubilization capacity of μEs (Acosta et al., 2004, 2005).

Figure 15.11 illustrates a schematic of the combined linker approach using lecithin as the main surfactant, sorbitan monooleate as the lipophilic linker, and hexyl glucoside as the hydrophilic linker. Figure 15.11 also presents the optimal solubilization capacity (expressed as characteristic length, ξ, at HLD = 0) of three linker formulations as a function of the EACN of the oils solubilized. One of the linker formulations corresponds to the lecithin-linker μE described in section 15.3.1 and the other two formulations used a combination of oleyl alcohol as the lipophilic linker, sodium

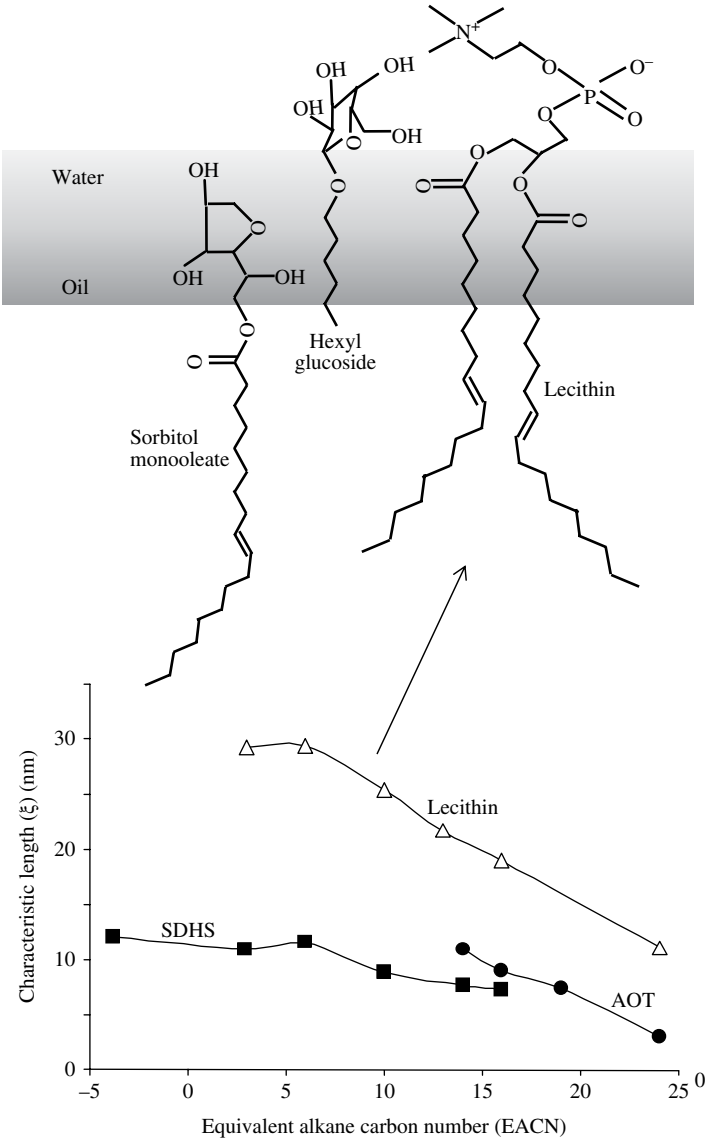

FIGURE 15.11 Schematic of the linker effect and solubilization capacity (expressed as characteristic length, ξ) of linker μEs formulation as a function of the EACN of the solubilized oil. Adapted from Acosta et al. (2005).

mono- and dimethyl naphthalene sulfonate (SMDNS) as the hydrophilic linker, and SDHS and AOT as the surfactants. It is important to mention that without the introduction of linkers, it would not have been possible for these surfactants to produce μEs with all these oils (Acosta et al., 2005). The data in Figure 15.11 also provides an opportunity to reflect on alternatives to address the issue of surfactant biocompatibility

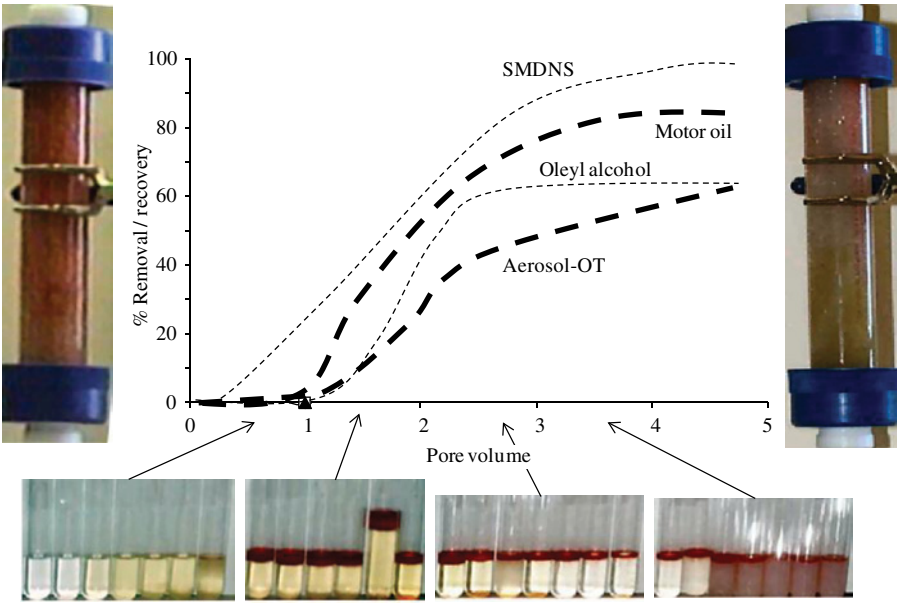

FIGURE 15.12 Recovery of surfactant (AOT), linkers (SMDNS, oleyl alcohol), and oil (motor oil) from a column packed with 40 mesh glass beads. Pore volume (PV), 35 mL; flow rate, 1 mL/min; surfactant injection (2 PV), 4% AOT, 0.09 M oleyl alcohol, 0.18 M SMDNS, 5% NaCl. Adapted from Acosta et al. (2003a).

when formulating solutions for remediating oil spills. Lecithin-linker μEs have been shown to be biocompatible and, as Figure 15.11 indicates, very efficient in producing μEs with a wide range of oils (Acosta et al., 2005; Yuan et al., 2010).

To evaluate the linker approach in formulating μEs for the removal of hydrophobic oils (high EACN values), a column study was conducted (Acosta et al., 2003a). The column filled with 0.5 mm glass beads was contaminated with SAE-30 motor oil. Two pore volumes of a 4% AOT, oleyl alcohol, and SMDNS formulation were flushed through the column. Figure 15.12 illustrates the column before and after wash, a picture of the vials collected during the first four pore volumes, and the fractions of oil, surfactant, and linkers recovered (Acosta et al., 2003a). Nearly 80% of motor oil was removed from the column, and SMDNS was recovered within three pore volumes. Almost one third of AOT and oleyl alcohol could not be recovered in the aqueous phase, and it is likely that they might have been lost to the oil phase. The picture of the vials collected help illustrate that although the surfactant concentration was relatively high, most of the motor oil was removed as a free oil phase (top dark phases in the vials), and only a small fraction was solubilized (darker bottom phases in the last five vials). In similar experiments conducted using hexadecane, nearly all of the hexadecane, surfactant, and linkers were removed within three pore volumes (Acosta et al., 2003a).

The fact that most of the oil removed was mobilized is consistent with earlier discussions that when remediating subsurface spills, mobilization is a far more

efficient approach than solubilization since more oil can be removed within a shorter time frame and using lower surfactant concentrations. One limitation with the linker approach, however, is that if the surfactant concentration is too low (near or below the CμC), then the hydrophilic linker simply remains dissolved in water and the lipophilic linker partitions into the oil phase (Sabatini et al., 2003). This limitation can be surmounted using extended surfactants (Miñana-Pérez et al., 1995a, b; Scorzza et al., 2002a, b). These surfactants have an alkyl (tail) group chemically bound to a number of propylene oxide units (which play a similar role to that of lipophilic linkers) that are also bound to a number of ethylene oxide groups (which have a role similar to hydrophilic linkers). The surfactant is finally capped by a hydrophilic group that may be a sulfate or other hydrophilic group. These surfactants have several interesting features including solubilization capacities four to ten times larger than other anionic surfactants, they have very low CμCs, and they are among the few surfactants that produce μEs with triglycerides (Acosta et al., 2012; Hammond and Acosta, 2012; Huang et al., 2004; Miñana-Pérez et al., 1995b; Witthayapanyanon et al., 2006).

15.4.3 *Ex Situ* Soil Washing

Surfactant solutions can be used as *ex situ* washing fluids to remove oil from drill cuttings and other oil-contaminated soils (Ahn et al., 2008; Bragato and El Seoud, 2003; Bragato et al., 2002; Childs et al., 2005; Daniels 2004; Deshpande et al., 1999; Gotlieb et al., 1993; Han et al., 2009; Kalali et al., 2011; Monig et al., 1998; Urum et al., 2004; Weaver and Kremer, 2001). Figure 15.1d illustrates an example of a soil washing process (Envirosupply and Services, Inc., 2012; US Environmental Protection Agency (EPA), 2012; Vertase FLI Ltd., 2012). In this example, the contaminated soil is excavated and processed through a first cleaning stage on a sieving–washing unit. The fines and oil suspended in the aqueous solution are introduced into the settling units (e.g., inclined plate settlers, not shown) and/or hydrocylones to separate the clean fine particles. A second hydrocyclone is used to separate the oil from the aqueous solution. The aqueous solution is reconditioned (e.g., addition of makeup water and/or surfactant) and reinjected into the washing process. A similar process is also used for soil washing for removing heavy metals from soils (US EPA, 2012).

There are various approaches to surfactant washing. One approach involves oil solubilization in micelles and subsequent removal using activated carbon (Ahn et al., 2008; Deshpande et al., 1999). Another method is to promote the detachment (mobilization) of oil from the particles via a substantial reduction in the interfacial tension of the system (Childs et al., 2005; Quraishi et al., 2012). In most cases, however, there is a third mechanism at play where the oil is transferred from larger particles to small hydrophobic particles or oil–particle agglomerates. This oil transfer occurs when the interfacial tension is low enough and under sufficient mixing conditions. The oil–particle agglomerates have lower densities than the rest of the particles and are separated using settling units, fluidized beds, or hydrocyclones (Niven and Khalili, 2002; Niven et al., 2000). In other cases, froth flotation and gas

aphrons are also used to concentrate the fraction of the soil (typically clays) that has the greatest oil content (Niven and Khalili, 1998).

The cost of surfactant is close to $15 per ton of soil washed for technologies that use surfactant concentrations close to 0.1 wt% (Childs et al., 2005; Envirosupply and Services, Inc. 2012), and the entire cost of the process is close to $100 (1993 USD)/ton of soil processed (Gotlieb et al., 1993). This cost can increase substantially for the removal of viscous oils. The removal of heavy oils or weathered oils via solubilization or mobilization is particularly difficult (Quraishi et al., 2012; Urum et al., 2004). Several technologies use organic solvents presolubilized in micelles that after reaching the surface of the particles, the solvent is delivered, facilitating the solubilization and mobilization of the oil (Bragato and El Seoud, 2003; Daniels 2004; Deshpande et al., 1999; Gotlieb et al., 1993; Monig et al., 1998; Weaver and Kremer, 2001).

Childs et al. (2005) compared the effectiveness of solubilization and mobilization approaches to remove diesel and alpha olefins from drill cuttings. The solubilization approach was capable of removing all the oil (no oil detected after solvent extraction), but the process produced a wastewater containing 4% surfactant and the solubilized oil. In that work, a high surfactant concentration was required because the drill cuttings had elevated oil content (10%). However, for initial oil contents of 1% (~10,000 ppm), the solubilization approach would only require a 0.4% surfactant solution, which would have been a reasonable alternative to explore. For the mobilization approach, Childs et al. used a 0.1 wt% extended surfactant solution (just above its CμC) that produced interfacial tensions in the order of 10^{-3} mJ/m^2. This surfactant solution on its own was not capable of removing the oil because the surfactant adsorbed on the cuttings due to the high calcium content in the cuttings. Alkyl sulfobetaines were introduced to prevent the extended surfactant from adsorbing on the drill cuttings, thus maintaining ultralow interfacial tensions throughout the washing process. This reformulated solution was able to remove 80% of the oil in the drill cuttings. Similar to other oil mobilization scenarios, this mobilization strategy cannot remove all the oil from the solids. A combination of mobilization and solubilization could be the best strategy for complete oil removal. However, this combined strategy has not been reported in literature.

The detachment of oil from the surfaces of particles can be described by dimensionless numbers. Smith and Van de Ven described the detachment of oil from oil-coated particles submerged in water as a result of the balance of buoyancy and gravity forces (Smith and Van de Ven, 1985). The authors correlated the maximum volume of oil that can be retained by a particle of radius r and the contact angle of the oil (α) for different Bond numbers using the radius of the particle as the characteristic dimension in Equation (15.13). Figure 15.13 presents the fraction of oil retained, evaluated from the article of Smith and Van de Ven, as a function of the "adhesive" Bond number that includes the contact angle of the oil. Similar to the trapping curve of Figure 15.11, Figure 15.13 shows a transition around a critical adhesive Bond number. The simplified Van Genuchten equation (Eq. 15.15) can be used to describe this transition using a critical adhesive Bond number of 0.7 and a scaling exponent $n = 2.4$. Fan et al. reproduced the findings of Van de Ven using a CFD code that solved the continuity, and Navier–Stokes equations that included inertia, shear, gravity, and

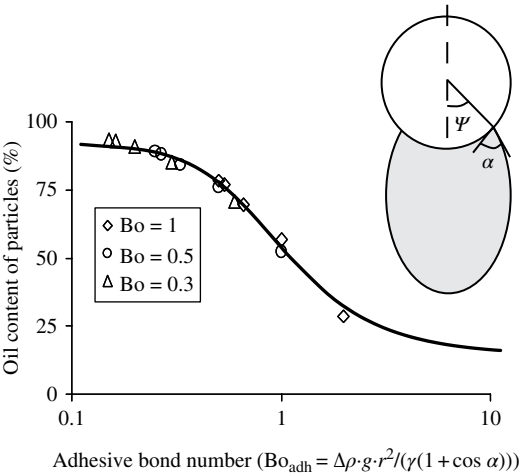

FIGURE 15.13 Maximum oil content of particles subject to a gravitational field as a function of the adhesive Bond number. Data obtained from the work of Smith and Van de Ven (1985).

surface tension forces apply to axisymmetric flow in spherical coordinates (Fan et al., 2011). The model of Fan et al. was also used to predict the detachment of oil from particles under shear. To correlate the onset of oil detachment with different interfacial tensions and flow conditions, Fan et al. determined filling angle ψ (Fig. 15.13) as a function of the capillary number as presented in Equation (15.12) (Fan et al., 2011). The authors determined that the filling angle also tends to 0 (oil detachment) as the capillary number approaches a critical capillary number that was close to 1 for typical soil washing conditions.

Quraishi et al. conducted a set of washing experiments to remove bitumen from bitumen-coated beach sand (Quraishi et al., 2012). In these experiments, the authors added toluene to the contaminated sand with the objective of reducing the viscosity of the oil. A solution of SDHS formulated at HLD = 0 was added using different concentrations between its CMC and its CμC (0.3 wt% SDHS). These different surfactant solutions produced a wide range of interfacial tensions. After mixing for 3 min at 3200 rpm and settling over night, the liberated oil floated on the surface of the vial. Additional toluene was gently added on the surface of the washing solution to dilute and measure the extracted oil (see Fig. 15.14). Figure 15.14 presents the fraction of oil retained on the sand versus a Weber number calculated using Equation (15.9) and the diameter of the particle (Quraishi et al., 2012).

The solid line of Figure 15.14 represents the fit of the generalized Van Genuchten equation (Eq. 15.15) using a critical Weber number of 36 and a scaling exponent $n = 1.4$. The critical Weber number was lower for systems where more toluene was used to pretreat the soil, further reducing the viscosity of the oil (Quraishi et al., 2012). This observation is consistent with the fact that the critical Weber number, for emulsification purposes, is at its minimum when the viscosity ratio between the dispersed and continuous phase is closer to 1.

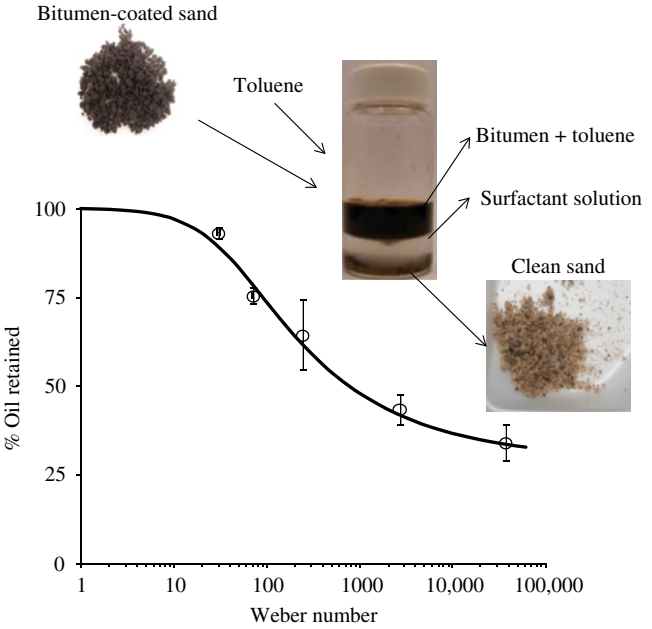

FIGURE 15.14 Fraction of oil retained by sand particles coated with bitumen as a function of the particle-based Weber number. Adapted from Quraishi et al. (2014).

15.5 SUMMARY AND OUTLOOK

Increasing fuel demands, along with the aging of the infrastructure associated with its production and distribution, suggests that in the future there could be greater risks of oil spill events. Fortunately, technologies used to prevent these events and remediate their consequences are also improving. In the case of dispersants, although their use continues to be discouraged, they are still the most effective method to address the fraction of oil that escapes the primary methods of containment. Current dispersant formulations are less toxic than formulations used in the past, but they are yet to enhance the biodegradation of the emulsified oil. Future reformulation efforts to incorporate biocompatible surfactants, such as lecithin, cannot be undertaken as a simple trial and error exercise. The HLD-NAC framework, combined with the appropriate dimensionless numbers that describe the hydrodynamic conditions, can be used to engineer the design of a new generation of dispersant formulations. In the future, the HLD-NAC could be incorporated into transport equations to determine the fate of these emulsified oils. The HLD-NAC could also offer insights on the influence of formulation properties on the biodegradation of the emulsified oils.

One of the important messages of this chapter is that one should not focus on the suitability of a surfactant for a specific remediation technology, but instead on the suitability of the entire formulation. A surfactant like AOT has a very poor performance on its own, but if used in the appropriate formulation, it can produce the desired

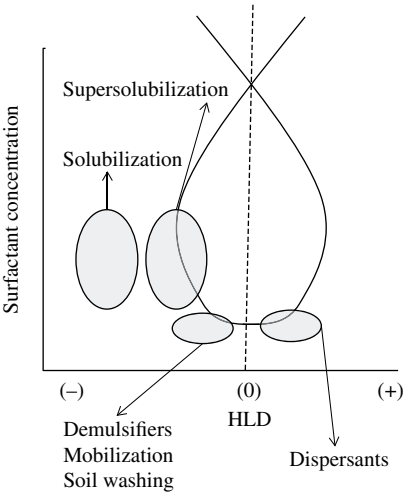

FIGURE 15.15 Concentration–HLD map of optimal formulations for surfactant-based technologies for oil spill remediation.

effects. The HLD scale, which reflects the hydrophilic–lipophilic nature of the entire formulation, can serve as a guidance to select the appropriate formulations for different oil spill remediation technologies. Figure 15.15 summarizes the different ranges of HLD and surfactant concentrations discussed for the remediation technologies considered in this chapter. In the case of dispersants, positive HLD facilitates the incorporation of surfactant and water in oil, increasing the density of the oil phase. For emulsion breakers, they should remain in the aqueous phase (negative HLDs) to avoid the incorporation of water into the oil phase, which would reduce the effectiveness of skimming and *in situ* burning operations. Solubilization methods used for remediation of oil spills on land could be effective when used as a polishing step after a method of oil displacement (mobilization) has been used to remove the largest fraction of oil. Whenever possible, supersolubilization conditions (negative HLDs closer to zero) should be used instead of simple solubilization given that the rate of solubilization is proportional to the solubilization capacity. For remediation technologies on land, critical capillary numbers, critical Bond numbers, and critical particle-based Weber numbers are useful to determine the appropriate combination of hydrodynamic conditions and formulation properties (interfacial tension) required to remove NAPLs from porous media or from suspended particles.

ACKNOWLEDGMENTS

The authors would like to acknowledge the support from the Petroleum Research Fund program of the American Chemical Society and from the Natural Sciences and Engineering Research Council of Canada (NSERC).

REFERENCES

Abbot S, Acosta E, Callaghan I, Donoghue G, Gregory S, Van Loon S. 2012. The 30-day formulation challenge. Available at http://www.stevenabbott.co.uk/GreenSurfactant30DaySummary.pdf. Accessed April 30, 2012.

Abriola LM, Dekker TJ, Pennell KD. Surfactant-enhanced solubilization of residual dodecane in soil columns. 2. Mathematical modeling. Environ Sci Technol 1993;27:2341–2351.

Acosta EJ. The HLD-NAC equation of state for microemulsions formulated with nonionic alcohol ethoxylate and alkylphenol ethoxylate surfactants. Colloids Surf A 2008;320:193–204.

Acosta E, Uchiyama H, Sabatini DA, Harwell JH. The role of hydrophilic linkers. J Surfactants Deterg 2002;5:151–157.

Acosta E, Do Ph, Harwell JH, Sabatini DA. Linker-modified microemulsions for a variety of oils and surfactants. J Surfactants Deterg 2003a;6:353–363.

Acosta EJ, Le MA, Harwell JH, Sabatini DA. Coalescence and solubilization kinetics in linker-modified microemulsions and related systems. Langmuir 2003b;19:566–574.

Acosta E, Szekeres E, Sabatini DA, Harwell JH. Net-average curvature model for solubilization and supersolubilization in surfactant microemulsions. Langmuir 2003c;19:186–195.

Acosta EJ, Harwell JH, Sabatini DA. Self-assembly in linker-modified microemulsions. J Colloid Interface Sci 2004;274:652–664.

Acosta EJ, Nguyen T, Witthayapanyanon A, Harwell JH, Sabatini DA. Linker-based biocompatible microemulsions. Environ Sci Technol 2005;39:1275–1282.

Acosta E, Yuan Sh, Yip A, Gerber M. Rate of solubilization and mass transfer phenomena in microemulsion systems. 98th AOCS National Meeting; 2007 May 13–16; Québec City, Canada.

Acosta EJ, Yuan JS, Bhakta AS. The characteristic curvature of ionic surfactants. J Surfactants Deterg 2008;11:145–158.

Acosta EJ, Szekeres E, Harwell JH, Grady BP, Sabatini DA. Morphology of ionic microemulsions: comparison of SANS studies and the net-average curvature (NAC) model. Soft Matter 2009;5:551–561.

Acosta EJ, Kiran SK, Hammond CE. The HLD-NAC model for extended surfactant microemulsions. J Surfactants Deterg 2012;15:495–504.

Ahn CK, Kim YM, Woo SH, Park JM. Soil washing using various nonionic surfactants and their recovery by selective adsorption with activated carbon. J Hazard Mater 2008;154:153–160.

Baran Jr JR, Pope GA, Wade WH, Weerasooriya V, Yapa A. Microemulsion formation with mixed chlorinated hydrocarbon liquids. J Colloid Interface Sci 1994;168:67–72.

Blondina GJ, Sowby ML, Ouanot MT, Singer MM, Tjeerdema RS. A modified swirling flask efficacy test for oil spill dispersants. Spill Sci Technol Bull 1997;4:177–185.

Bourrel M, Schecter R. *Microemulsions and Related Systems*. New York: Marcel Dekker; 1988. p 420.

Bragato M, El Seoud OA. Formation, properties, and “ex situ” soil decontamination by vegetable oil-based microemulsions. J Surfactants Deterg 2003;6:143–150.

Bragato M, Subklew G, Schwuger MJ, El-Seoud OA. Vegetable oils-based microemulsions: formation, properties, and application for “ex-situ” soil decontamination. Colloid Polym Sci 2002;280:973–983.

Breuel A. *Oil Spill Cleanup and Protection Techniques for Shorelines and Marshlands*. Park Ridge, NJ: Noyes Data Corporation; 1981. p 404.

Brown CL, Deshald M, Dwarakanath V, Jackson RE, Londergan JT, Meinardus HW, McKinney DC, Oolman T, Pope GA, Wade WH. Demonstration of surfactant flooding of an alluvial aquifer contaminated with DNAPL. In: Brusseau M, Sabatini D, Gierke J, editors. *Innovative Subsurface Remediation: Field Testing of Physical, Chemical and Characterization Technologies*. ACS Symposium Series 725. Washington, DC: American Chemical Society; 1999. p 64–85.

Buist I, Lewis A, Guarino A, Mullin J. Examining the fate of emulsion breakers used for decanting. 2005 International Oil Spill Conference; 2005. p 11456–11460.

Cameotra SS, Makkar RS. Biosurfactant-enhanced bioremediation of hydrophobic pollutants. Pure Appl Chem 2010;82:97–116.

Carroll BJ. The kinetics of solubilization of nonpolar oils by nonionic surfactant solutions. J Colloid Interface Sci 1981;79:126–135.

Carroll BJ, O'Rourke BGC, Ward AJI. The kinetics of solubilization of single component non-polar oils by a nonionic surfactant. J Pharm Pharmacol 1982;34:287–292.

Castellino V, Cheng Y-L, Acosta E. The hydrophobicity of silicone-based oils and surfactants and their use in reactive microemulsions. J Colloid Interface Sci 2011;353:196–205.

Chang MC, Huang CR, Shu HY. Effects of surfactants on extraction of phenanthrene in spiked sand. Chemosphere 2000;41:1295–1300.

Chavadej S, Phoochinda W, Yanatatsaneejit U, Scamehorn JF. Clean-up of oily wastewater by froth flotation: effect of microemulsion formation III: use of anionic/nonionic surfactant mixtures and effect of relative volumes of dissimilar phases. Separ Sci Technol 2004a;39:3097–3112.

Chavadej S, Ratanarojanatam P, Phoochinda W, Yanatatsaneejit U, Scamehorn JF. Clean-up of oily wastewater by froth flotation: effect of microemulsion formation II: use of anionic/nonionic surfactant mixtures. Separ Sci Technol 2004b;39:3079–3096.

Childs JD, Acosta E, Knox R, Harwell RJH, Sabatini DA. Improving the extraction of tetrachloroethylene from soil columns using surfactant gradient systems. J Contam Hydrol 2004;71:27–45.

Childs JD, Acosta E, Scamehorn JF, Sabatini DA. Surfactant-enhanced treatment of drill cuttings. J Energy Resour Technol 2005;127:153–162.

Childs J, Acosta E, Annable MD, Brooks MC, Enfield CG, Harwell JH, Hasegawa M, Knox RC, Rao PSC, Sabatini DA, Shiau B, Szekeres E, Wood AL. Field demonstration of surfactant-enhanced solubilization of DNAPL at Dover Air Force Base, Delaware. J Contam Hydrol 2006;82:1–22.

Christov NC, Denkov ND, Kralchevsky PA, Broze G, Mehreteab A. Kinetics of triglyceride solubilization by micellar solutions of nonionic surfactant and triblock copolymer. 1. Empty and swollen micelles. Langmuir 2002;18:7880–7886.

Daniels A, (Herbal Apothecary Limited). Hydrocarbon wetting and separation agent. European Patent Application 1380630. Jan 28, 2004.

Davis HT. Factors determining emulsion type: hydrophile–lipophile balance and beyond. Colloids Surf A 1994;91:9–24.

Deschênes L, Lafrance P, Villeneuve JP, Samson R. Adding sodium dodecyl sulfate and *Pseudomonas aeruginosa* UG2 biosurfactants inhibits polycyclic aromatic hydrocarbon biodegradation in a weathered creosote-contaminated soil. Appl Microbiol Biotechnol 1996;46:638–646.

Deshpande S, Shiau BJ, Wade D, Sabatini DA, Harwell JH. Surfactant selection for enhancing ex situ soil washing. Water Res 1999;33:351–360.

Dillan KW, Goddard ED, McKenzie DA. Oily soil removal from a polyester substrate by aqueous nonionic surfactant systems. J Am Oil Chem Soc 1979;56:59–70.

Dittrick P. Journally speaking: cleaning oil, sand & water. Oil Gas J 2010;108:14.

Dudášová D, Flåten GR, Sjöblom J, Øye G. Study of asphaltenes adsorption onto different minerals and clays. Part 2. Particle characterization and suspension stability. Colloids Surf A 2009;335:62–72.

Environment Canada. *The Impact and Cleanup of Oil Spill on Canadian Shorelines: A Summary*. Ottawa: Environment Canada; 1978. p 44.

Envirosupply and Services, Inc. 2012. Ivey-sol® surfactant enhanced soil washing technology overview and project experience. Available online at http://www.iveyinternational.com/pdfs/Surfactant_SoilWashing_Case_Study_100408.pdf. Accessed January 7, 2014.

Fan ESC, Bussmann M, Acosta E. Equilibrium configurations of drops attached to spheres immersed in a uniform laminar flow. Can J Chem Eng 2011;89:707–716.

Fanum M, editor. *Microemulsions: Properties and Applications*. New York: CRC Press; 2009. p 533.

Field JA, Istok JD, Schroth MH, Sawyer TE, Humphrey MD. Laboratory investigation of surfactant-enhanced trichloroethene solubilization using single-well, 'push-pull' tests. Ground Water 1999;37:581–588.

Fingas M. Use of surfactants for environmental applications. In: Shramm L, editor. *Surfactants: Fundamentals and Applications in the Petroleum Industry*. Cambridge, UK: Cambridge University Press; 2000. p 461–540.

Fingas M. *The Basics of Oil Spill Cleanup*. New York: Lewis Publishers; 2001. p 233.

Fingas M, Banta J. Review of literature related to oil spill dispersants. Proceedings of the 32nd AMOP Technical Seminar on Environmental Contamination and Response; 2009; Ottawa. 2, p 869–920.

Fiocco RJ, Becker KW, Walsh MA, Hokstad JN, Daling PS, Lewis A. Improved laboratory demulsification tests for oil spill response. 2005 International Oil Spill Conference; 2005. p 3740–3753.

Fountain JC, Starr RC, Middleton T, Beikrich M, Taylor C, Hodge DA. Controlled field test of surfactant-enhanced aquifer remediation. Ground Water 1996;34:910–916.

Goldszal A, Bourrel M. Demulsification of crude oil emulsions: correlation to microemulsion phase behavior. Ind Eng Chem Res 2000;39:2746–2751.

Gotlieb I, Bozzelli JW, Gotlieb E. Soil and water decontamination by extraction with surfactants. Separ Sci Technol 1993;28:793–804.

Graciaa A, Lachaise J, Cucuphat C, Bourrel M, Salager JL. Improving solubilization in microemulsions with additives. 1. The lipophilic linker role. Langmuir 1993a;9:669–672.

Graciaa A, Lachaise J, Cucuphat C, Bourrel M, Salager JL. Improving solubilization in microemulsions with additives. 2. Long chain alcohols as lipophilic linkers. Langmuir 1993b;9:3371–3374.

Hammond CE, Acosta EJ. On the characteristic curvature of alkyl-polypropylene oxide sulfate extended surfactants. J Surfactants Deterg 2012;15:157–165.

Han M, Ji G, Ni J. Washing of field weathered crude oil contaminated soil with an environmentally compatible surfactant, alkyl polyglucoside. Chemosphere 2009;76:579–586.

Hasegawa MH, Shiau B-J, Sabatini DA, Knox RC, Harwell JH, Lago R, Yeh L. Proceedings of the 2nd International Conference on Remediation of Chlorinated and Recalcitrant Compounds; 2000 May 22–25; Monterey, Battelle Press, Columbus, Ohio. CA p 219–226.

Helfrich W. Elastic properties of lipid bilayers. Z Naturforsch 1973;28c:693–703.

Hirasaki GJ, Miller CA, Szafranski R, Tanzil D, Lawson JB, Meinardus HW, Jin M, Londergan JT, Jackson RE, Pope GA, Wade WH. Field demonstration of the surfactant foam process for aquifer remediation. Proceedings of Society of Petroleum Engineers 72nd Annual Technical Conference; Richardson, TX: SPE 39292; 1997.

Hoar TP, Schulman JH. Transparent water-in-oil dispersions: the oleopathic hydro-micelle. Nature 1943;152:102–103.

Huang L, Lips A, Co C. Microemulsification of triglyceride sebum and the role of interfacial structure on bicontinuous phase behavior. Langmuir 2004;20:3559–3563.

Jawitz JW, Annable MD, Rao PSC, Rhue RD. Field implementation of a Winsor type I surfactant/alcohol mixture for in situ solubilization of LNAPL as a single-phase microemulsion. Environ Sci Technol 1998;32:523–530.

Jawitz JW, Sillan RK, Annable MD, Rao PSC, Warner K. In-situ alcohol flushing of a DNAPL source zone at a dry cleaner site. Environ Sci Technol 2000;34:3722–3729.

Kabalnov A, Weers J. Macroemulsion stability within the Winsor III region: theory versus experiment. Langmuir 1996;12:1931–1935.

Kahlweit M. How to prepare microemulsions at prescribed temperature, oil, and brine. J Phys Chem 1995;99:1281–1284.

Kahlweit M, Lessner E, Strey R. Influence of the properties of the oil and surfactant on the phase behavior of systems of the type H_2O-oil-nonionic surfactant. J Phys Chem 1983;87:5032–5040.

Kahlweit M, Strey R, Busse G. Microemulsions: a quantitative thermodynamic approach. J Phys Chem 1990;94:3881–3894.

Kalali A, Ebadi T, Rabbani A, Moghaddam SS. Response surface methodology approach to the optimization of oil hydrocarbon polluted soil remediation using enhanced soil washing. Int J Environ Sci Technol 2011;8:389–400.

Khalladi R, Benhabiles O, Bentahar F, Moulai-Mostefa N. Surfactant remediation of diesel fuel polluted soil. J Hazard Mater 2009;164:1179–1184.

Kiran SM, Acosta EJ. Predicting the morphology and viscosity of microemulsions using the HLD-NAC model. Ind Eng Chem Res 2010;49:3424–3432.

Kiran S. APPLICATION OF THE HLD AND NAC MODELS TO THE FORMATION AND STABILITY OF EMULSIONS. PhD. Dissertation. University of Toronto, 2013.

Kiran SK, Acosta EJ, Moran K. Evaluating the hydrophilic-lipophilic nature of asphaltenic oils and naphthenic amphiphiles using microemulsion models. J Colloid Interface Sci 2009;336:304–313.

Knox RC, Sabatini DA, Harwell JH, Brown RE, West C, Blaha F, Griffin S. Surfactant remediation field demonstration using a vertical circulation well. Ground Water 1997; 35:948–953.

Knox RC, Shiau BJ, Sabatini DA, Harwell JH. Field demonstration of surfactant enhanced solubilization and mobilization at Hill Air Force Base, UT. In: Brusseau M, Sabatini D, Gierke J, editors. *Innovative Subsurface Remediation: Field Testing of Physical, Chemical and Characterization Technologies*. ACS Symposium Series 725. Washington, DC: American Chemical Society; 1999. p 49–63.

Kozlov MM, Helfrich W. Effects of a cosurfactant on the stretching and bending elasticities of a surfactant monolayer. Langmuir 1992;8:2792–2797.

Kralchevsky PA, Denkov ND, Todorov PD, Marinov GS, Broze G, Mehreteab A. Kinetics of triglyceride solubilization by micellar solutions of nonionic surfactant and triblock copolymer. 2. Theoretical model. Langmuir 2002;18:7887–7895.

Krebbs-Yuill B, Harwell JH, Sabatini DA, Knox RC. Economic considerations in surfactant-enhanced pump-and-treat. In: *Surfactant Enhanced Subsurface Remediation: Emerging Technologies*. ACS Symposium Series 594. Washington, DC: American Chemical Society; 1995. p 265–278.

Kujawinski EB, Kido Soule MC, Valentine DL, Boysen AK, Longnecker K, Redmond MC. Fate of dispersants associated with the Deepwater Horizon oil spill. Environ Sci Technol 2011;45:1298–1306.

Kumar P, Mittal K, editors. *Handbook of Microemulsion Science and Technology*. New York: Marcel Dekker; 1999. p 849.

Laha S, Tansel B, Ussawarujikulchai A. Surfactant-soil interactions during surfactant-amended remediation of contaminated soils by hydrophobic organic compounds: a review. J Environ Manage 2009;90:95–100.

Lewis A, Ken-Trudel B, Belore RC, Mullin JV. Large-scale dispersant leaching and effectiveness experiments with oils on calm water. Mar Pollut Bull 2010;60:244–254.

Londergan JT, Meinardus HW, Mariner PE, Jackson RE, Brown CL, Dwarakantah V, Pope GA, Ginn JS, Taffinder S. DNAPL removal from a heterogeneous alluvial aquifer by surfactant-enhanced aquifer remediation. Ground Water Monit R 2001;21:57–67.

Luning-Prak DJ, Abriola LM, Weber Jr WJ, Bocskay KA, Pennell KD. Solubilization rates of n-alkanes in micellar solutions of nonionic surfactants. Environ Sci Technol 2000;34: 476–482.

Márquez N, Graciaa A, Lachaise J, Salager JL. Partitioning of ethoxylated alkylphenol surfactants in microemulsion-oil–water systems: influence of physicochemical formulation variables. Langmuir 2002;18:6021–6024.

McCourt J, Buist L, Mullin J. Operational parameters for in situ burning of six U.S. outer continental shelf crude oils. 2005 International Oil Spill Conference; 2005. p 5935–5938.

McCray JE, Tick GR, Jawitz JW, Gierke JS, Brusseau ML, Falta RW, Knox RC, Sabatini DA, Annable MD, Harwell JH, Wood AL. Remediation of NAPL source zones: lessons learned from field studies at Hill and Dover AFB. Ground Water 2011;49:727–744.

Miller CA. Solubilization and intermediate phase formation in oil–water-surfactant systems. TENSIDE SURFACT DET. 1996;33:191–196.

Miller CA, Raney KH. Solubilization-emulsification mechanisms of detergency. Colloids Surf A 1993;74:169–215.

Miñana-Pérez M, Antón RE, Graciaa A, Lachaise J, Salager JL. Solubilization of polar oils with extended surfactants. Colloids Surf A 1995a;100:217–224.

Miñana-Pérez M, Graciaa A, Lachaise J, Salager JL. Solubilization of polar oils in microemulsion systems. Prog Colloid Polym Sci 1995b;98:177–179.

Monig K, Clemens W, Haegel F-H, Schwuger MJ. Application of microemulsions in soil remediation. In: Shah DO, editor. *Micelles, Microemulsions, and Monolayers: Science and Technology*. New York: Marcel Dekker; 1998. p 215–231.

Mukherjee B, Wrenn BA, Ramachandran P. Relationship between size of oil droplet generated during chemical dispersion of crude oil and energy dissipation rate: dimensionless, scaling, and experimental analysis. Chem Eng Sci 2012;68:432–442.

Nazario LMM, Crespo JPSG, Holzwarth JF, Hatton TA. Dynamics of AOT and AOT/nonionic cosurfactant microemulsions. an iodine-laser temperature jump study. Langmuir 2000;16: 5892–5899.

Nishimi T, Miller CA. Spontaneous emulsification of oil in aerosol-OT/water/hydrocarbon systems. Langmuir 2000:16:9233–9241.

Niven RK, Khalili N. Gas–liquid upflow washing for in situ remediation of diesel-contaminated soils. Can Geotech J 1998;35:938–960.

Niven RK, Khalili N. In situ fluidization for peat bed rupture, and preliminary economic analysis. J Contam Hydrol 2002;59:67–85.

Niven RK, Khalili N, Hibbert DB. Mixed solid/disperse phase particles in multiphase fluidized beds. I: Gibbs free energy of stability due to interfacial tension. Chem Eng Sci 2000;55: 3013–3032.

Ornitz BE, Champ MA. *Oil Spills First Principles: Prevention and Best Response*. New York: Elsevier; 2002. p 333.

O'Rourke BGC, Carroll BJ, Ward AJI. Investigations of the solubilization kinetics of binary mixtures of nonpolar oils by nonionic surfactants. J Pharm Pharmacol 1987;39:865–870.

Palmer CD, Fish W. Chemical enhancements to pump-and-treat remediation, groundwater issue. United States Environmental Protection Office, Center for Environmental Research Information, Cincinnati, OH 1992. p 22. EPA/540/S-92/001. Order No. PB92-180074.

Paria S. Surfactant-enhanced remediation of organic contaminated soil and water. Adv Colloid Interface Sci 2008;138:24–58.

Pennell KD, Abriola LM, Weber Jr WJ. Surfactant-enhanced solubilization of residual dodecane in soil columns. 1. Experimental investigation. Environ Sci Technol 1993;27: 2332–2340.

Pennell KD, Jin M, Abriola LM, Pope GA. Surfactant enhanced remediation of soil columns contaminated by residual tetrachloroethylene. J Contam Hydrol 1994;16:35–53.

Pennell KD, Pope GA, Abriola LM. Influence of viscous and buoyancy forces on the mobilization of residual tetrachloroethylene during surfactant flushing. Environ Sci Technol 1996;30:1328–1335.

Pitts M, Wyatt K, Sale TC, Piontek KR. Utilization of chemically-enhanced oil recovery technology to remove hazardous oily waste from alluvium. The Society of Petroleum Engineers International Symposium on Oilfield Chemistry; 1993; Richardson, TX. p 33–44.

Plucinski P, Nitsch W. Kinetics of interfacial phenylalanine solubilization in a liquid/liquid microemulsion system. J Phys Chem 1993;97:8983–8988.

Pondstabodee S, Scamehorn JF, Chavedej S, Harwell JH. Cleanup of oily wastewater by froth flotation: effect of microemulsion formation. Separ Sci Technol 1998;33(4):591–609.

Pope GA, Wade WH. Lessons from enhanced oil recovery research for surfactant-enhanced aquifer remediation. In: Surfactant enhanced subsurface remediation: emerging technologies. ACS Symposium Series 594; Washington, DC: American Chemical Society; 1995. p 142–160.

Quraishi S, Acosta E. Flow dynamics around oil-coated particles defining strategies for oil-water-particle separation. 8th World Congress of Chemical Engineering, Canada, 2009, p. 520e. Available at http://archivos.labcontrol.cl/wcce8/offline/techsched/manuscripts/1mib6p.pdf. Accessed January 22, 2014.

Quraishi S, Busmann M, Acosta E. Capillary curves for ex-situ washing of oil-coated particles. J Surfactants Deterg 2014.

Rang MJ, Miller CA. Spontaneous emulsification of oils containing hydrocarbon, nonionic surfactant, and oleyl alcohol. J Colloid Interface Sci 1999;209:179–192.

Reed RL, Healy RN. Contact angles for equilibrated microemulsion system. Soc Pet Eng J 1984;24:342–350.

Rondón M, Bouriat P, Lachaise J, Salager J-L. Breaking of water-in-crude oil emulsions. 1. Physicochemical phenomenology of demulsifier action. Energy Fuels 2006;20:1600–1604.

Sabatini DA, Knox RC, Harwell JH, editors. Surfactant-enhanced subsurface remediation. ACS Symposium Series 594. Washington, DC: American Chemical Society; 1995.

Sabatini DA, Knox RC, Harwell JH, Soerens TS, Chen L, Brown RE, West C. Design of a surfactant remediation field demonstration based on laboratory and modeling studies. Ground Water 1997;35, 954–963.

Sabatini DA, Harwell JH, Hasegawa M, Knox RC. Membrane processes and surfactant-enhanced subsurface remediation: results of a field demonstration. J Membr Sci 1998, 151, 89–100.

Sabatini DA, Knox RC, Harwell JH. Integrated design of surfactant enhanced DNAPL remediation: efficient supersolubilization and gradient systems. J Contam Hydrol 2000;45, 99–121.

Sabatini DA, Acosta EJ, Harwell JH. Linker molecules in surfactant mixtures. Curr Opin Colloid Interface Sci 2003;8(4,5):316–326.

Salager JL. Microemulsions. In: Broze G, editor. *Handbook of Detergents – Part A: Properties*. New York: Marcel Dekker; 1999. p 253–302.

Salager JL, Anton RE. Ionic microemulsions. In: Kumar P, Mittal KL, editors. *Handbook of Microemulsion Science and Technology*. New York: Marcel Dekker; 1999. p 247–280.

Salager JL, Morgan J, Schechter RS, Wade WH, Vasquez E. Optimum formulation of surfactant-oil–water systems for minimum tension and phase behavior. Soc Pet Eng J 1979;19:107–115.

Salager JL, Graciaa A, Lachaise J. Improving solubilization in microemulsions with additives. Part III: lipophilic linker optimization. J Surfactants Deterg 1998;1:403–406.

Salager JL, Márquez N, Graciaa A, Lachaise J. Partitioning of ethoxylated octylphenol surfactants in microemulsion-oil–water systems: influence of temperature and relation between partitioning coefficient and physicochemical formulation. Langmuir 2000;16:5534–5539.

Scorzza C, Godé P, Goethals G, Martin P, Miñana-Pérez M, Salager JL, Usubillaga A, Villa P. Another new family of "extended" glucidoamphiphiles. Synthesis and surfactant properties for different sugar head groups and spacer arm lengths. J Surfactants Deterg 2002a;5: 337–343.

Scorzza C, Godé P, Martin P, Miñana-Pérez M, Salager JL, Villa P. Synthesis and surfactant properties of a new "extended" glucidoamphiphile made from D-glucose. J Surfactants Deterg 2002b;5:331–335.

Salager JL, Antón RE, Briceno MI, Choplin L, Márquez L, Pizzino A, Rodriguez MP. The emergence of formulation engineering in emulsion making – transferring know-how from research laboratory to plant. Polym Int 2003;52:471–478.

Shaw JM. A microscopic view of oil slick break-up and emulsion formation in breaking waves. Spill Sci Technol Bull 2003;8:491–501.

Shiau BJ, Sabatini DA, Harwell JH. Solubilization and mobilization of DNAPLS using direct food additive (edible) surfactants. Ground Water 1994;32:561–569.

Shiau BJ, Hasegawa MA, Brammer JM, Carter T, Goodspeed M, Harwell JH, Sabatini DA, Knox RC, Szekeres E. Field demonstration of surfactant-enhanced DNAPL remediation: two case studies. In: *Chlorinated Solvent and DNAPL Remediation: Innovative Strategies for Subsurface Cleanup*. (eds. Susan M. Henry, Scott D. Warner). Washington, DC: American Chemical Society; 2003. p 51–72.

Shin K-H, Ahn Y, Kim K-W. Toxic effect of biosurfactant addition on the biodegradation of phenanthrene. Environ Toxicol Chem 2005;24:2768–2774.

Smith PG, Van de Ven TGM. The separation of a liquid drop from a stationary solid sphere in a gravitational field. J Colloid Interface Sci 1985;105:7–20.

Solans C, Kunieda H, editors. *Industrial Applications of Microemulsions*. New York: Marcel Dekker; 1997. p 404.

Strey R. Microemulsion microstructure and interfacial curvature. Colloid Polym Sci 1994;272:1005–1019.

Tanthakit P, Chavadej S, Scamehorn JF, Sabatini DA, Tongcumpou C. Microemulsion formation and detergency with oily soil: IV. Effect of rinse cycle design. J Surfactants Deterg 2008;11:117–128.

Taylor E, Owens EH. Specialized mechanical equipment for shoreline cleanup. International Oil Spill Conference; 1997. p 79–87.

Thompson L. The role of oil detachment mechanism in determining optimum detergency conditions. J Colloid Interface Sci 1994;163:61–73.

Tongcumpou C, Acosta EJ, Quencer LB, Joseph AF, Scamehorn JF, Sabatini DA, Chavadej S, Yanumet N. Microemulsion formation and detergency with oily soils: II. detergency formulation and performance. J Surfactants Deterg 2003;6:205–214.

Tongcumpou C, Acosta EJ, Quencer LB, Joseph AF, Scamehorn JF, Sabatini DA, Yanumet N, Chavadej S. Microemulsion formation and detergency with oily soils: III. Performance and mechanisms J Surfactants Deterg 2005;8:147–156.

Uchiyama H, Acosta E, Tran S, Sabatini DA, Harwell JH. Supersolubilization in chlorinated hydrocarbon microemulsions: solubilization enhancement by lipophilic and hydrophilic linkers. Ind Eng Chem Res 2000;39:2704–2708.

Urum K, Pekdemir T, Çopur M. Surfactants treatment of crude oil contaminated soils. J Colloid Interface Sci 2004;276:456–464.

US Environmental Protection Agency (EPA). 2012. Cost and performance report: soil washing at the King of Prussia technical corporation superfund site. Available at http://www.clu-in.org/products/costperf/SOILWASH/Kop.htm. Accessed March 26, 2012.

Van Genuchten MTh. A closed form equation for predicting hydraulic conductivity in unsaturated soils. Soil Sci Soc Am J 1980;44, 892–898.

Vertase FLI Ltd. 2012. Soil washing (Scrubbing). Available at http://www.vertasefli.co.uk/soil-washing-c53.html. Accessed March 26, 2012.

Walstra P. Principles of emulsion formation. Chem Eng Sci 1993;48:333–349.

Watcharasing S, Chavadej S, Scamehorn JF. Diesel oil removal by froth flotation under low interfacial tension conditions II: continuous mode of operation. Separ Sci Technol 2008;43:2048–2071.

Weaver CE, Kremer LN. (Baker Hughes). Oil-in water microemulsion cleaning compositions. International Patent Application WO 2001034760. May 17, 2001.

Winsor P. *Solvent Properties of Amphiphilic Compounds*. London: Butterworth; 1954. p 207.

Witthayapanyanon A, Acosta EJ, Harwell JH, Sabatini DA. Formulation of ultralow interfacial tension systems using extended surfactants. J Surfactants Deterg 2006;9:331–339.

Yanatatsaneejit U, Witthayapanyanon A, Rangsunvigit P, Acosta EJ, Sabatini DA, Scamehorn JF, Chavadej S. Ethylbenzene removal by froth flotation under conditions of middle-phase microemulsion formation I: Interfacial tension, foamability, and foam stability. Separ Sci Technol 2005;40:1537–1553.

Yuan JS, Yip A, Nguyen N, Chu J, Wen X-Y, Acosta EJ. Effect of surfactant concentration on transdermal lidocaine delivery with linker microemulsions. Int J Pharm 2010;392:274–284.

16

ROLE OF STRUCTURAL FORCES IN CLEANING SOILED SURFACES

Darsh Wasan, Alex Nikolov, and Gopi Sethumadhavan

16.1 INTRODUCTION

Surfactants or surface active agents are widely used in the oil industry in cleaning oil spills as well as in enhancing oil recovery from petroleum reservoirs. Surfactant flooding is also an *in situ* remediation technique that is used to remove contaminants from soil. "Roll-up," "emulsification," and the solubilization of oil in surfactant micelles are some of the generally accepted pollutant or oil removal mechanisms. Roll-up and emulsification are generally treated as alternate processes, but they are interdependent and probably occur simultaneously. Moreover, they have different surface chemical requirements, so that the relationship between the overall removal and the various physiochemical factors may be expected to shift depending on the nature of the dominant process and the extent of the domination (Thompson, 1994).

According to the "roll-up" mechanism, first described by Adams (1937), the driving force causes the pollutant to separate from the soil surface and roll-up results from the unbalanced tensions at the interface between the pollutant, solution, and soil. In an ideal case (Fig. 16.1), the apparent contact angle θ of the pollutant on the soil increases from 0° to 180°, and the pollutant rolls up when the resultant interface tension force f is positive:

$$f = \sigma_{SP} - \sigma_{SW} + \sigma_{PW} \cos\theta \tag{16.1}$$

where σ_{SP} denotes the interfacial tension between the soil and the pollutant, σ_{SW} is the interfacial tension between the soil and the solution, σ_{PW} denotes the interfacial

Oil Spill Remediation: Colloid Chemistry-Based Principles and Solutions, First Edition.
Edited by Ponisseril Somasundaran, Partha Patra, Raymond S. Farinato, and Kyriakos Papadopoulos.

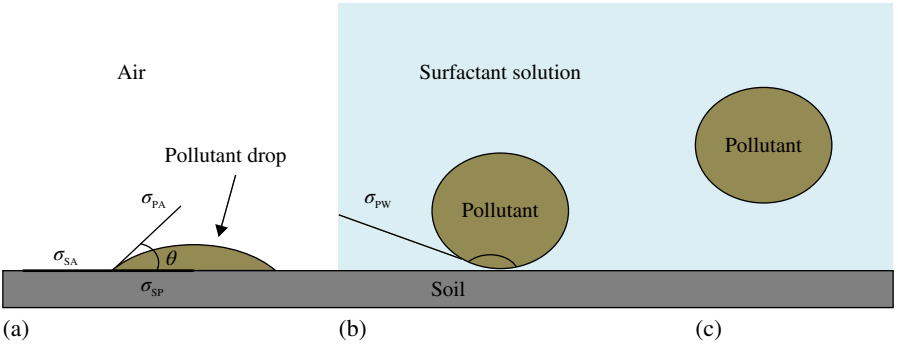

FIGURE 16.1 Rolling-up mechanism.

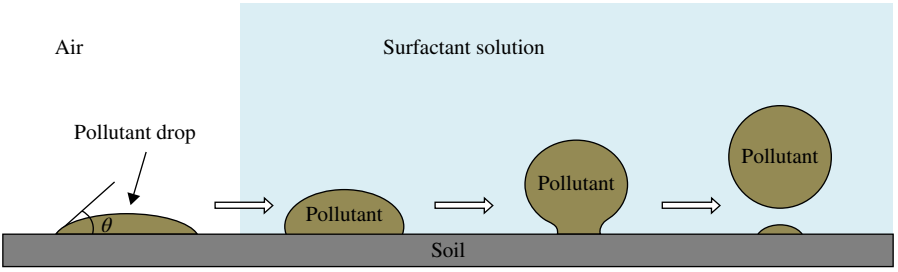

FIGURE 16.2 Marginal roll-up and incomplete removal of pollutant.

tension between the pollutant and the solution, and θ is the contact angle of the pollutant on the soil.

However, a positive resultant interfacial tension force f is not a sufficient condition for the separation of the pollutant from the soil surface. The roll-up rate of the pollutant is opposed by the frictional force between the soil and the pollutant, which depends on the cohesive energy of the pollutant and the soil. If the frictional force is high, the interfacial tension force may not be sufficient for rolling up the pollutant and an external force may be needed to dislodge the soil.

In real systems, the roll-up of pollutants does not usually occur by the ideal sequence shown in Figure 16.1. The balance between the buoyancy, capillary, and adhesion forces can cause the necking and drawing of the oil or pollutant droplet (Fig. 16.2). Partial drop detachment, or emulsification, occurs when the surface tension and capillary forces holding the drop together are exceeded by the buoyancy force pulling the droplet apart. Complete pollutant removal may involve the necking of several droplets before the roll-up.

Once again, the pollutant–solution interfacial tension, the three-phase contact angle, or/and the capillary force (drop size) are involved in determining the ease with which the pollutant drop breaks up or rolls up (detaches). The contact angle

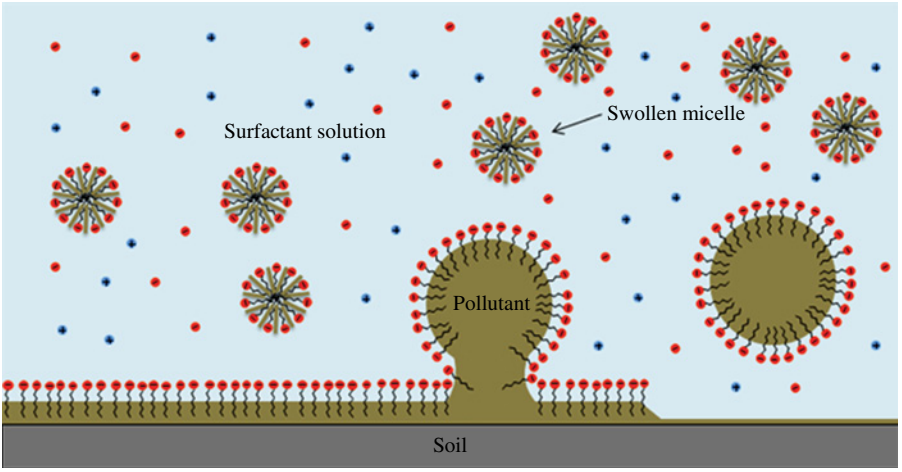

FIGURE 16.3 Micellar solubilization and microemulsification of pollutant.

demonstrates that roll-up is an integral part of the emulsification process, occurring as a precursor mechanism to the detachment step and controlling, in part, the efficiency and mechanism by which it occurs (Cutler and Kissa, 1987). Roll-up is one of the possible mechanisms when the pollutant exists as drops in the soil matrix. When the pollutant is coated as a thin layer, then the mechanism of pollutant removal is due to the film rupture on the soil surface by instability. The lower the interfacial tension between the surrounding medium and the pollutant, the higher the probability of the surface waves (instability) forming in the pollutant film due to thermal or mechanical disturbances. There could be points where the film thickness is less than the critical thickness (h_{cr}) needed for instability (e.g., $d\Pi/dh>0$) (the disjoining pressure vs. film thickness is positive) and in those areas, the film becomes unstable and ruptures, forming smaller isolated drops that can be rolled up or solubilized.

"Micellar solubilization" is a term that describes the process of dissolving an otherwise insoluble substance and incorporating it into the micelles of a surfactant solution. A surfactant is an amphiphile consisting of a hydrophilic polar segment and an oleophilic tail. In solution beyond the critical micelle concentration (CMC), surfactants associate to form micelles in which the hydrophilic segment of the surfactant is oriented toward water. The solubilized segment is located in the interior of the micelle or, when the substance is polar, between the surfactant molecules forming the micelle.

Micellar solubilization is an irreversible pollutant removal process that can be described by a four-step mechanism (Fig. 16.3):

1. The surfactant adsorbs on the pollutant–water interface, causing a reduction in the interfacial tension.
2. Thermal and mechanical instabilities cause surface or capillary waves on the pollutant water interface.

3. In the perturbed state, where $d\Pi/dh > 0$, a part of the pollutant from a wave peak could "neck" away from the bulk of the pollutant, forming a small pollutant globule with the surfactant absorbed at the interface. This is a micelle with a swollen core of the pollutant, free to move in the aqueous phase.
4. The micelle containing the solubilized pollutant diffuses into the bulk water.

In this work, a new mechanism based on the research performed by Wasan, Nikolov, and their co-workers is presented for the removal of contaminants from solid surfaces (Chengara et al., 2004; Kondiparty et al., 2011; Nikolov et al., 2010; Wasan and Nikolov, 2003; Wasan et al., 2011). Wasan and Nikolov published a paper in *Nature* (Wasan and Nikolov, 2003) in which they presented experimental observations and theoretical calculations using nanoparticle dispersions (like aqueous solutions of surfactant micelles) and showed that the surfactant micelles (or nanoparticles) form two-dimensional (2-D) layered structures (caused by the entropic affect) in the three-phase contact region of a liquid wedge film (Chaudhury, 2003) formed between an oily soil (pollutant) and substrate (Fig. 16.4).

The nanoparticle structuring phenomenon gives rise to the structural disjoining pressure (a pressure normal to the interfaces in the wetting film) and is an osmotic pressure component contributing near the tip of the wedge of the wetting film (Fig. 16.5). As a result of the normal pressure increase, the oil–nanofluid interface moves forward and the nanofluid spreads over the solid surface, detaching the oil drop.

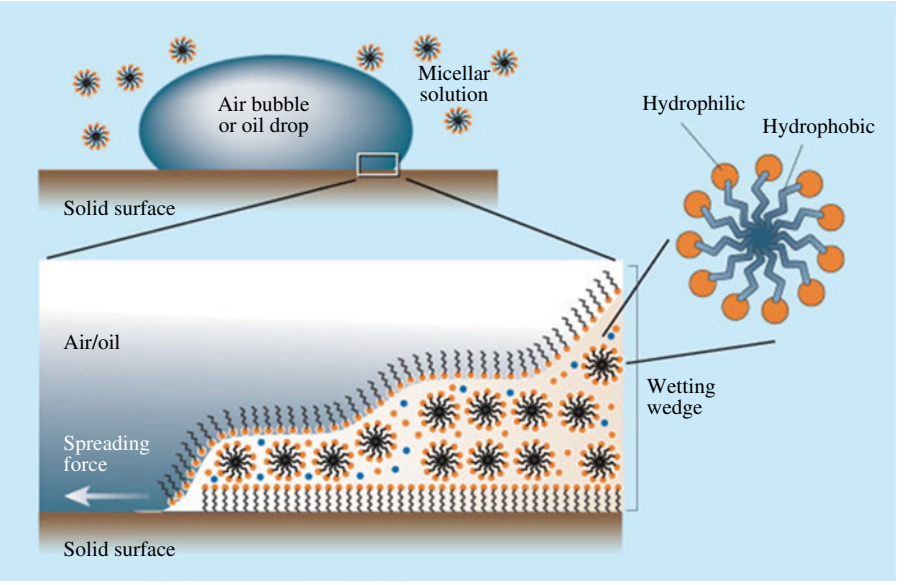

FIGURE 16.4 Micelle structuring in the wedge film resulting in structural disjoining pressure gradient (spreading force) at the wedge vertex (Chaudhury, 2003). Reprinted with permission from Nature Publishing Group.

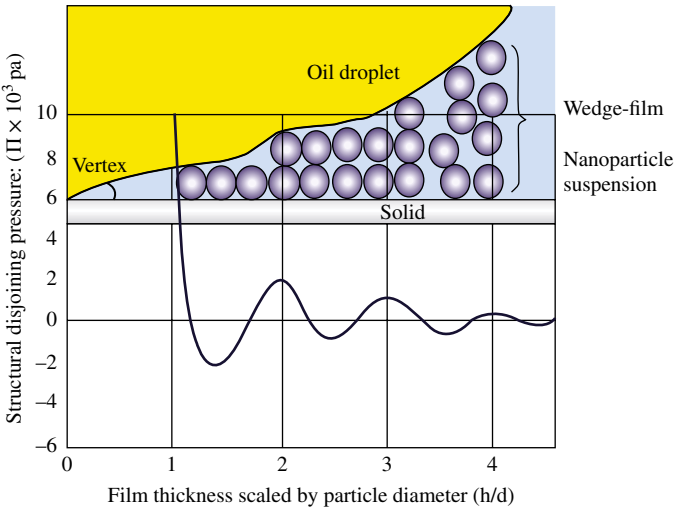

FIGURE 16.5 Pressure on the walls of wedge for 0.5° contact angle at the vertex as a function of radial distance (Kondiparty et al., 2011). Reprinted with permission from Elsevier Limited.

The magnitude of the structural disjoining pressure depends on the effective particle or micelle volume fraction, particle diameter (D), particle polydispersity, and contact angle. The film structural energy W_{st} is an oscillatory exponentially decaying curve versus film thickness (h) given by the following equation (Trokhymchuk et al., 2001):

$$W_{st}(h) = \int_{h}^{\infty} \Pi_{st} \mathrm{d}h = A\cos\left(\frac{2\pi h}{D}\right)\exp\left(-\frac{h}{D}\right) \tag{16.2}$$

where A is a parameter that accounts for the osmotic pressure contribution. The contribution of the resultant film tension force f_{st} due to the particle structuring is given by the equation

$$f_{st} \approx \int_{h_{eq}}^{\infty} \Pi_{st}(h)\,\mathrm{d}h. \tag{16.3}$$

It should be noted that all the current explanations for cleaning (detergency) mechanisms focus on the tangential (interface tension) force. However, the new mechanism proposed by Wasan and Nikolov for the role of structural forces arising due to nanoparticle (or surfactant micelles) structuring in the wetting film can be exploited in the detergents used to remediate soils contaminated by oil spills. In this chapter, we summarize the results of our recent experiments using this new mechanism based on the structural disjoining pressure to remove a coated organic pollutant such as pyrene and an oil drop from a solid surface using surfactant micellar solutions.

TABLE 16.1 Surfactants used in the study

WITCONOL-2722 (sorbitan + Oleate; CMC = 0.0062% w/w)	WITCAMIDE-5085 (CMC = 0.0006%W/W)
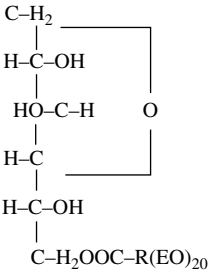	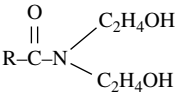

R = C_{18}

16.2 ORGANIC POLLUTANT REMOVAL FROM A SOLID SURFACE

The ability of micellar solutions to dislodge an organic pollutant such as pyrene from a glass surface was investigated in the present study. A mixture of two nonionic surfactants manufactured by Witco Corp., Houston (now a subsidiary of AkzoNobel), were used: (i) Witconol 2722 sorbate (abbreviated to W2722, CMC in 15% EOH of 0.08% (w/w) or 0.06 mM) and (ii) Witcamide-5085 (abbreviated to W85, CMC in 15% EOH of 0.0008% (w/w) or 0.02 mM). The chemical structures of these surfactants are shown in Table 16.1.

Several solutions of various ratios of the two nonionic surfactants were prepared and equilibrated for 2 days before use in all experiments. The final solution contained 4.78% (w/w) surfactants and 15% (w/w) ethanol, and the remaining percentage was water. The total surfactant concentration (W85 + W2722) was kept constant, and the ratio of W85:W2722 was varied in all the experiments. Five surfactant compositions were studied: (i) W85 = 0% (0 mM), W2722 = 4.78% (37.2 mM); (ii) W85 = 1.2% (31.2 mM), W2722 = 3.6% (28.1 mM); (iii) W85 = 2.4% (62.5 mM), W2722 = 2.4% (18.7 mM); (iv) W85 = 3.6% (93.8 mM), W2722 = 1.2% (9.3 mM); and (v) W85 = 4.78% (124.5 mM), W2722 = 0% (0 mM).

Static light scattering was used to investigate the effects of the change in the surfactant composition on the intermicellar interaction (Sethumadhavan et al., 2003). Light from a monochromatic source (green light, 541 nm) was passed through a sample and its intensity measured at 90° to the incident light. The turbidity of the sample was obtained from the measured intensity using the Hach model 2100A turbidimeter. The instrument was calibrated using the known turbidity values of pure solutions of benzene, carbon tetrachloride, and water. The second virial coefficients were calculated from the slopes of the Debye plot. Table 16.2 lists the values of the second virial coefficient, which is an indicator of the intermicellar interaction (positive values signify repulsion) and osmotic pressure.

Experiments were conducted to study the effect of the surfactant concentration on the removal of an organic pollutant (pyrene) from a silica (e.g., glass) surface.

TABLE 16.2 Summary of light scattering experiments

Sample	Second virial coefficient	Intermicellar interaction
W2722: 4.78%, W5780: 0%	2.3×10^{-4}	Intermediate repulsion
W2722: 2.4%, W5780: 2.4%	14×10^{-4}	Most repulsion
W2722: 2.4%, W5780: 2.4%	-4.3×10^{-4}	Most attraction

TABLE 16.3 Efficiency of pyrene removal for different surfactant formulations

Surfactant composition	Efficiency of pyrene removal (ethanol = 15% (w/w))	Surface tension (dynes/cm)
W85 = 0%, W2722 = 4.78%	53.3%	33.7
W85 = 1.2%, W2722 = 3.6%	57.6%	32.1
W85 = 2.4%, W2722 = 2.4%	70.3%	30.6
W85 = 3.6%, W2722 = 1.2%	67%	30.1
W85 = 4.78%, W2722 = 0%	60%	29.5
Ethanol	15.6%	42.3
Water	0%	72

Removal of pyrene from a flat hydrophilic glass surface was studied by immersing a coated glass slide in a micellar surfactant solution. The glass surface was first left overnight in chromic acid to remove all traces of impurities from the glass surface, rinsed with deionized water, and dried. The pyrene was deposited on the glass by evaporating a solution of pentanol containing 10,000 ppm pyrene. This left a crystalline layer deposit of pyrene on the glass surface. The coated glass slide was immersed in 17 mL of the surfactant micellar solution with a different composition ratio for 1 h. A control experiment was carried out in parallel with water or ethanol instead of the surfactant solution.

Different amounts of pyrene coating were stripped off the glass surface by exposing it for 1 h to the micellar surfactant solution and water or ethanol; the results are presented in Table 16.3. The observations conducted using a microscope revealed that over time, the micellar surfactant solution slowly penetrated between the glass surface and the pyrene crystalline (coated) layer, leading to its removal.

The removed pyrene was present as flakes in the bottom of the experimental vial, suggesting a mechanism of pollutant removal from a solid surface other than roll-up. One can expect that, in general, a lower surface tension in the solution will result in a greater imbalance in the forces. Even though the pollutant removal efficiency goes through a maximum, the surface tension decreases monotonically as the amide increases (Table 16.3). This indicates that the detergency maximum is not caused by variations in the surface tension of the different formulations.

This study finds that the more repulsive the intermicellar interactions, the higher the structural disjoining pressure pulling the film surfaces apart, resulting in pollutant removal. The lower intermicellar repulsion in the study was believed to be caused by the higher micelle polydispersity as the mixed surfactant composition was changed.

It should be noted that all the surfactant formulations used in the present study have nearly the same effective micellar volume function of about 0.43, as determined by the number of micelle layers in the film (Sethumadhavan et al., 2003). However, the film formed from a surfactant solution at an optimum concentration was much more stable and it remained at a high thickness; the micelles showed a higher tendency to stay inside the film. This is typical of surfactant formulations that display a good micellar in-layer structure in the film (Chu et al., 1994). Our previous studies have shown that the structural disjoining pressure (i.e., the pressure exerted by the micelles on the film surface) is high for a monodisperse surfactant formulation, as compared to a polydisperse system (Chu et al., 1996). The micellar solutions' ability to dislodge organics from a solid surface is highest when the system is monodispersed with the highest intermicellar and structural forces.

16.3 OIL REMOVAL FROM A SOLID SURFACE

The second application of the mechanism of the structural disjoining pressure involves the removal of oil from a solid surface. Kao et al. (1988) were the first to examine the crude oil–solid interactions in the presence of a micellar solution using a reflected light differential interference microscope. They placed a crude oil droplet below the horizontal glass slide in the presence of 1 wt% C_{16} alpha olefin sulfonate and 1 wt% NaCl. They used the differential interference method (DI) to determine the meniscus profile and the meniscus–film contact line of the oil droplet at the solid–air surface but common reflected light interferometry to measure the profile of the mobile oil droplet at the solid–micellar solution surface. The micellar solution penetrates between the oil and the glass surface, forming the micellar film. In effect, two contact lines were established. The microscopic photograph depicting the inner and outer contact lines is shown in Figure 16.6. The outer line is formed

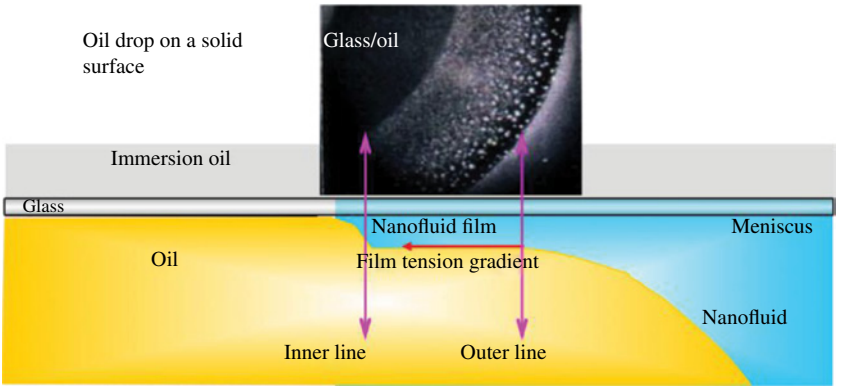

FIGURE 16.6 Microscopic photograph taken using reflected light interferometry depicting the inner and outer contact lines and the nanofluid film region (Kao et al., 1988). *(See insert for color representation of the figure.)*

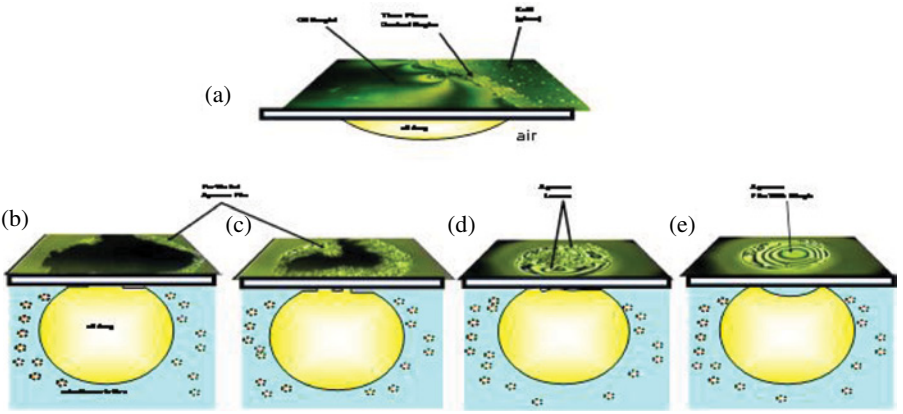

FIGURE 16.7 Dynamics of the three-phase contact region. (**a**) Photomicrograph showing the oil drop placed on a glass surface and differential interference patterns formed at the three-phase (solid–liquid–air) contact region. (**b–e**) Photomicrographs taken at increasing times after addition of the aqueous micellar solution: (**b**) 30 s, (**c**) 2 min, (**d**) 4 min, and (**e**) 6 min. (**b**) The beginning of the formation of the prewetting aqueous film between the glass surface and the oil droplet. (**c**) The spreading of the prewetting film. (**d**) The prewetted film now covers the whole area, and small water lenses are formed. (**e**) The separation of the oil droplet from the glass surface by a thick aqueous film with a dimple (Wasan and Nikolov, 2003). Reprinted with permission from Nature Publishing Group.

between the oil drop, the solid surface, and the aqueous micellar solution film that is the boundary between the meniscus and the micellar film; the inner line is between the oil drop, the solid surface, and the aqueous film that is the boundary between the micellar film and the oil–glass interface. The formation of the micellar (nanofluid) film is seen as a bright region in the reflected light interferometry (as seen in Fig. 16.6).

More recently, Wasan and Nikolov (2003) have reported results of additional experiments depicting the various steps of oil droplet removal from a glass surface in the presence of an aqueous micellar solution. They used hexadecane and a solution consisting of an anionic sodium dodecyl sulfate (SDS) surfactant of an effective micelle diameter of 8 nm, at a concentration equal to ten times the CMC, which is an effective volume fraction of 0.4, or concentration of 0.1 M. Figure 16.7 shows that the micellar solution penetrates between the oil and the glass surface and forms a micellar film. Over time, the micellar film increases in thickness and the white spots encircled by dark fringes are formed between the inner and outer contact regions. The thickness of the speckled band increases with the lapse of time, because the inner contact line recedes more rapidly than the outer contact line (Fig. 16.7d). Eventually, the oil droplet is separated completely from the solid surface by a thick aqueous film with a dimple (Fig. 16.7e).

The effect of an electrolyte (such as sodium chloride) on the oil detachment phenomenon was also studied by Wasan and Nikolov (2003). In their experiments

using 0.1 M SDS, they noticed that the oil droplet shrank due to the reduction in the interfacial tension between the oil and the aqueous micellar solution at a higher salt concentration (0.1 M NaCl), but the formation of the wedge film was not seen in this case and the micellar fluid did not spread over the solid surface. At high salt concentrations, the effective micellar diameter (and thereby the micellar volume fraction) decreases owing to the shrinkage of the electrical double layer around each micelle. Therefore, the magnitude of the disjoining pressure diminishes, reducing the driving force for the detachment of the drop. The drop does not detach from the solid surface.

16.4 OUTLOOK

The previous examples of soil remediation and oily soil removal (i.e., detergency) illustrate the practical importance of the phenomenon of nanoparticle structure formations in the film giving rise to the film structural force. However, all the current explanations of detergency mechanisms focus on the interfacial tension force and ignore this nanoparticle structuring effect (Kolve et al., 2004; Kralchevsky et al., 2005).

The study of the ordering of nanofluids (i.e., the suspension of nanoparticles dispersed in liquids) in confined environments is highly relevant to many technological applications. For example, films of nanoparticle dispersions are spread on solid surfaces to build magnetic, light-sensitive tapes and disks. Nanostructured materials such as color inks, solar cells, light emitting displays, and biochemical sensors are other examples. Microfluidic devices offer yet another example of the effect of confinement on the behavior of nanofluids. Therefore, we need to have a better understanding of the role of the structural forces (arising from the self-organization of nanoparticles) involved in a variety of technological contexts. Specifically, we are presently applying this structural force mechanism to develop "green cleaners," which are environmentally benign nanofluids for cleaning soiled surfaces, and the first "smart fluids" that accelerate the recovery of hydrocarbon and stimulation fluids from oil and gas reservoirs (Kondiparty, 2011). Currently, most detergents are surfactant micellar formulations derived from expensive and environmentally unfriendly petroleum products; they are used in detergency applications and in oil spills, as well as oil and gas recovery from petroleum reservoirs. High petroleum costs make it vital to explore other alternatives for these detergents.

REFERENCES

Adam NK. Detergent action and its relation to wetting and emulsification. J Soc Dyers Colour 1937;53(4):121–129.

Chaudhury MK. Complex fluids: spread the word about nanofluids. Nature 2003;423: 131–132.

Chengara A, Nikolov AD, Wasan DT, Trokhymchuk A, Henderson D. Spreading of nanofluids driven by the structural disjoining pressure gradient. J Colloid Interface Sci 2004;280(1): 192–201.

Chu XL, Nikolov AD, Wasan DT. Monte Carlo simulation of inlayer structure formation in thin liquid films. Langmuir 1994;10(12):4403–4408.

Chu XL, Nikolov AD, Wasan DT. Effects of particle size and polydispersity on the depletion and structural forces in colloidal dispersions. Langmuir 1996;12(21):5004–5010.

Cutler WG, Kissa E, editors. *Kinetics and Mechanism of Soiling and Detergency: Theory and Technology*. Surface Science Series. New York: Marcel Dekker; 1987. p 20.

Kao RL, Wasan DT, Nikolov AD, Edwards DA. Mechanisms of oil removal from a solid surface in the presence of anionic micellar solutions. Colloids Surf 1988;34(4):389–398.

Kolve VL, Kochijashky II, Danov KD, Kralchevsky PA, Broze G, Mehreteab A. Spontaneous detachment of oil drops from solid substrates: governing factors. J Colloid Interface Sci 2004;257(2):357–363.

Kondiparty K. Spreading of nanofluids on solids driven by structural disjoining pressure [unpublished PhD dissertation]. Chicago, IL: Illinois Institute of Technology; 2011.

Kondiparty K, Nikolov AD, Wu S, Wasan DT. Wetting and spreading of nanofluids on solid surfaces driven by the structural disjoining pressure: statics analysis and experiments. Langmuir 2011;27(7):3324–3334.

Kralchevsky PA, Danov KD, Kolev VL, Gurkov TD, Temelska MI, Brenn G. Detachment of oil drops from solid surfaces in surfactant solutions: molecular mechanisms at a moving contact line. Ind Eng Chem Res 2005;44(5):1309–1321.

Nikolov AD, Kondiparty K, Wasan DT. Nanoparticle self-structuring in a nanofluid film spreading on a solid surface. Langmuir 2010;26(11):7665–7670.

Sethumadhavan GN, Nikolov AD, Wasan DT. Ethanol-based foam stability as probed by foam lamella thinning. Ind Eng Chem Res 2003;42(12):2634–2638.

Thompson L. The role of oil detachment mechanisms in determining optimum detergency conditions. J Colloid Interface Sci 1994;163(1):61–73.

Trokhymchuk A, Herderson D, Nikolov AD, Wasan DT. A simple calculation of structural and depletion forces for fluids/suspensions confined in a film. Langmuir 2001;17(16): 4940–4947.

Wasan DT, Nikolov AD. Spreading of nanofluids on solids. Nature 2003;423:156–159.

Wasan DT, Nikolov AD, Kondiparty K. The wetting and spreading of nanofluids on solids: role of the structural disjoining pressure. Curr Opin Colloid Interface Sci 2011;16(16):334–349.

INDEX

Oil Spill Remediation: Colloid Chemistry-Based Principles and Solutions, First Edition.
Edited by Ponisseril Somasundaran, Partha Patra, Raymond S. Farinato, and Kyriakos Papadopoulos.

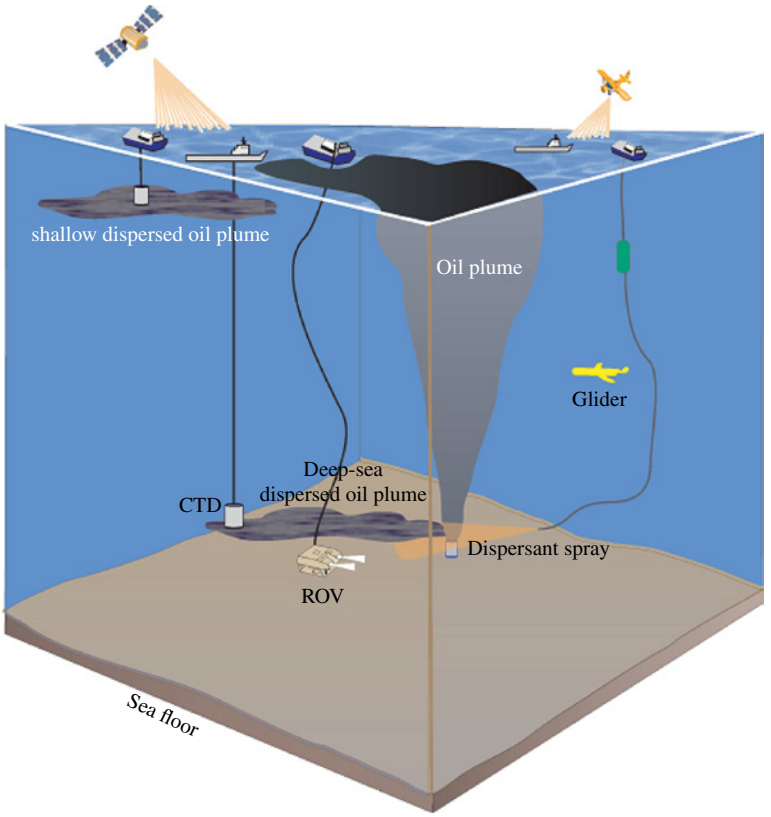

FIGURE 1.1 Conceptual diagram of monitoring efforts on the surface and in the deep sea.

Oil Spill Remediation: Colloid Chemistry-Based Principles and Solutions, First Edition.
Edited by Ponisseril Somasundaran, Partha Patra, Raymond S. Farinato, and Kyriakos Papadopoulos.

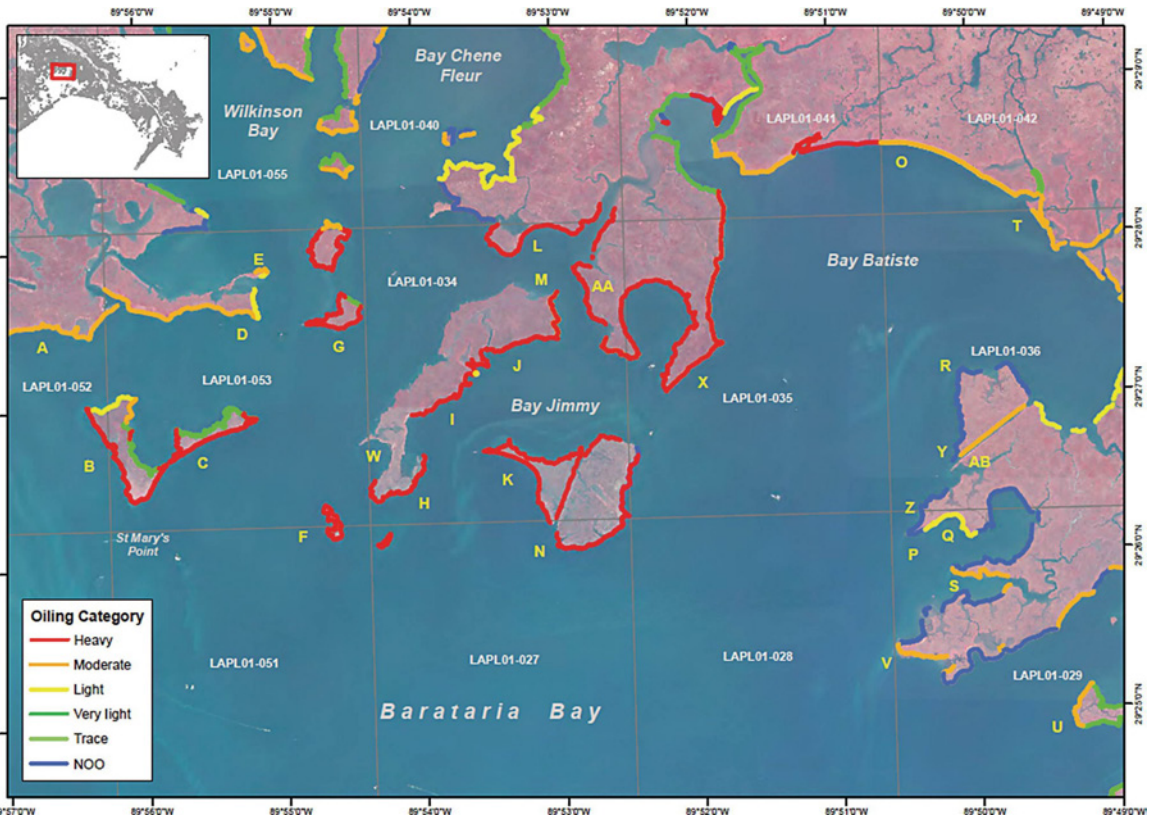

FIGURE 3.2 The distribution and intensity of oiling in northeastern Barataria Bay, Louisiana. Shoreline was categorized and identified for remediation according to the extent of oiling. Shoreline "K" in Bay Jimmy is host to ongoing studies of shoreline remediation and recovery. Map from Zengel and Michel (2013).

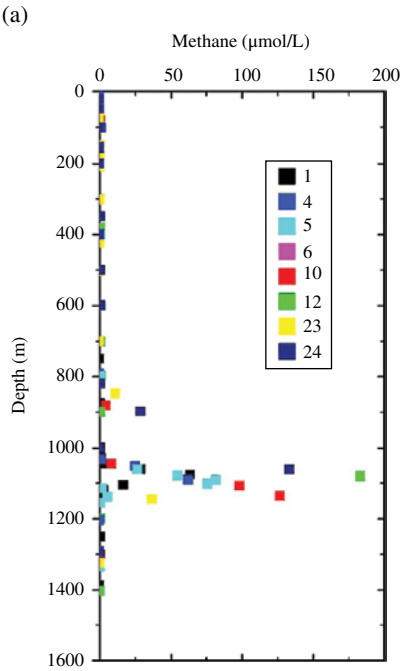

FIGURE 4.3 Methane concentration with depth at various areal locations around the wellhead.

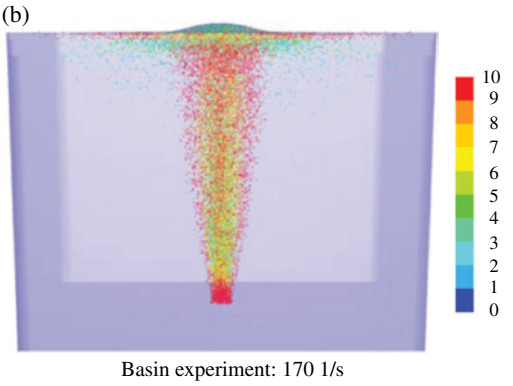

FIGURE 4.6 Shows the results from a CFD-based simulation of bubbles tracked in the Lagrangian framework (Cloete et al., 2009). The color map indicates the bubble size in millimeters. Source: Cloete et al., 2009. Reproduced with permission of Elsevier.

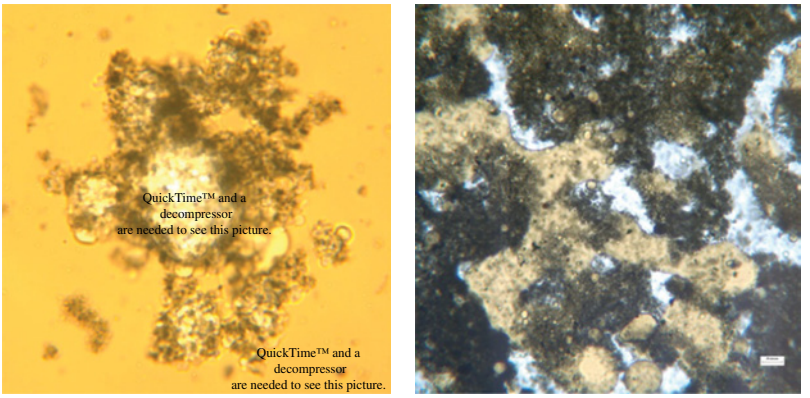

FIGURE 6.2 Photomicrographs of oil–water systems stabilized by biwettable particles located at the oil–water interface. Cluster of water droplets in oil prevented from coalescence by solids adsorbed at the oil–water interface. Scale bar is 20 μm (left). Crud phase from poorly separated slop oil. Light blue regions are aqueous, tan regions are oil, and black material is composed of bi-wettable solids. Scale bar is 20 μm (right).

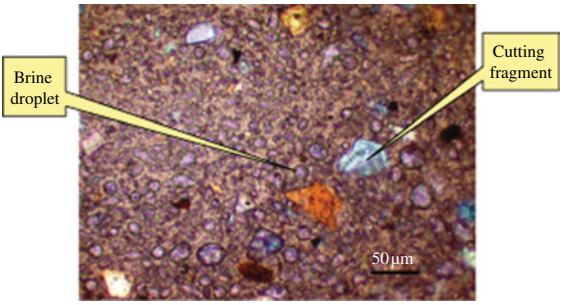

FIGURE 6.3 Optical micrograph of used oil-based drilling mud; polarized light with quarter-wave plate; scale bar is 50 μm.

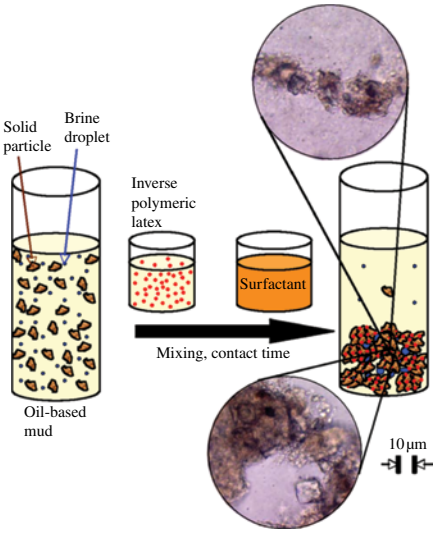

FIGURE 6.4 Direct use of polymeric inverse emulsions to aggregate hydrophilic solids in a used oil-based drilling mud in order to recover oil phase. Bright-field optical micrograph scale bar is 10 μm.

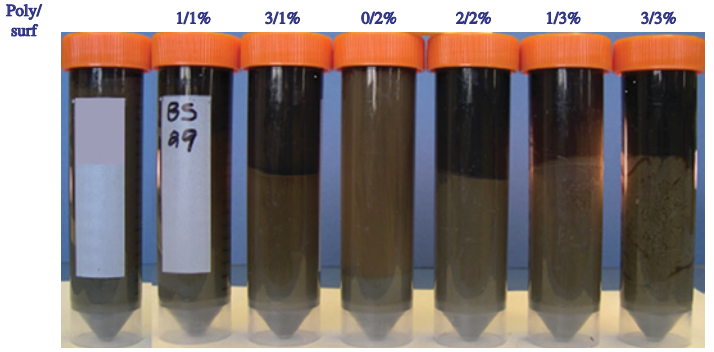

FIGURE 6.5 Lab testing of chemical treatment of used oil-based drilling fluid; samples shown after centrifugation.

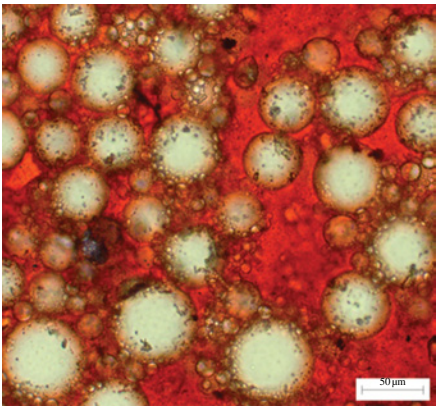

FIGURE 6.6 Optical micrograph of oil-continuous slop; scale bar is 50 µm.

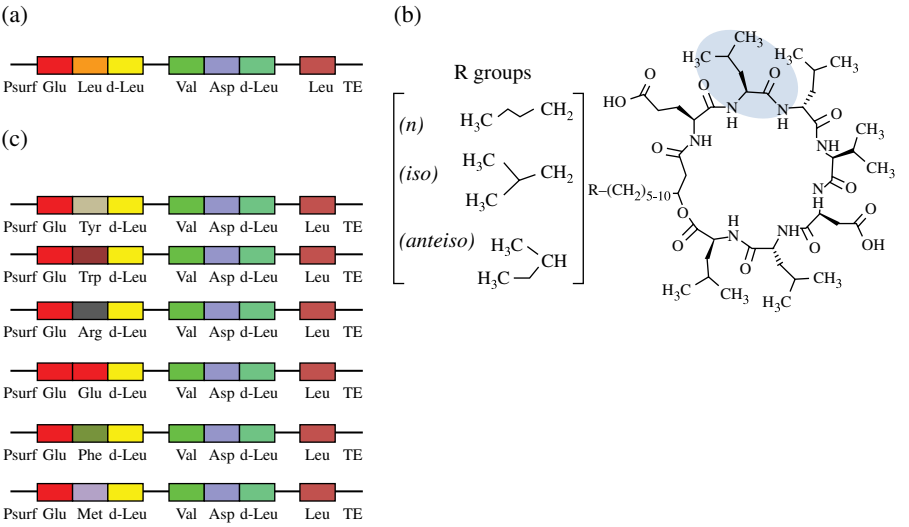

FIGURE 7.10 (**a**) Wild-type surfactin synthetase operon. (**b**) Chemical structure of wild-type surfactin. (**c**) Six of the surfactin analogs in Modular's collection have substitutions at position 2 of the cyclic amino acid.

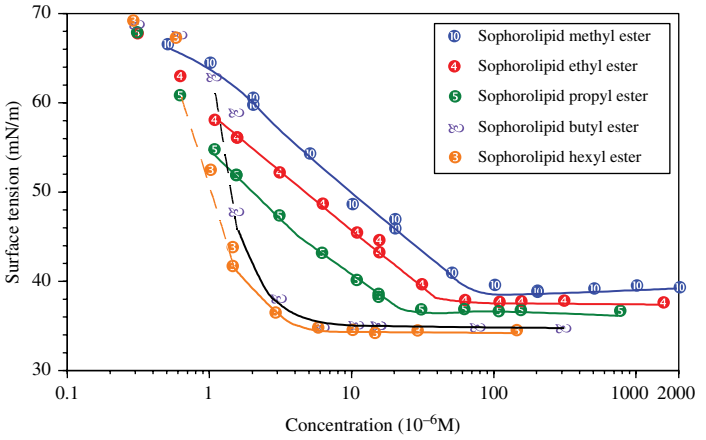

FIGURE 7.11 Surface tension of esters of sophorolipids. Reproduced with permission from Somasundaran et al. (2004). © Elsevier.

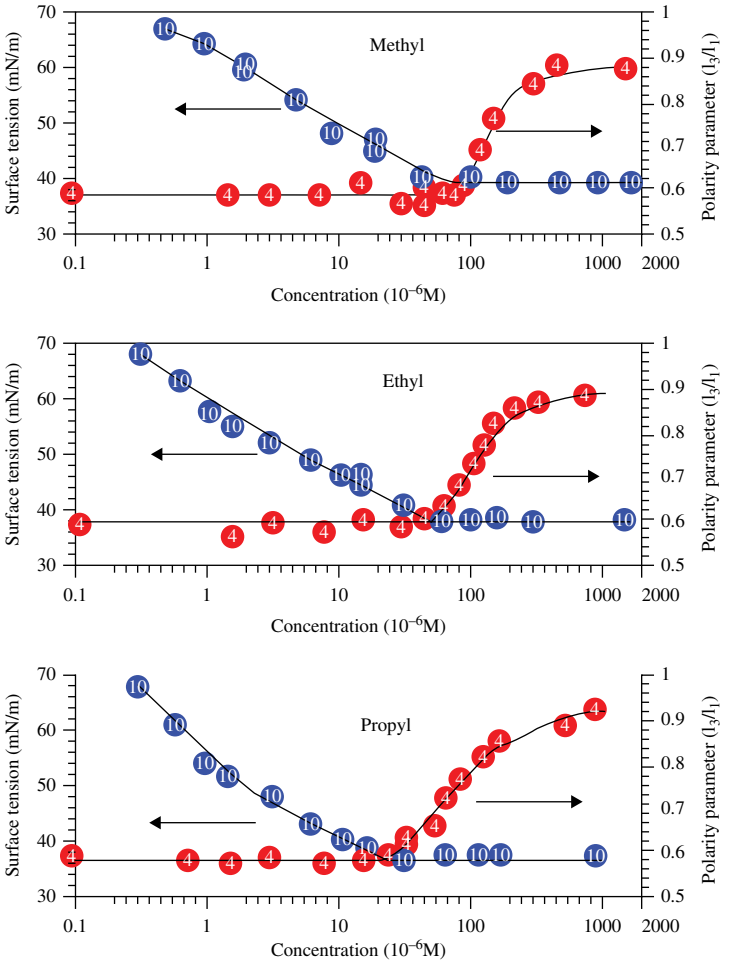

FIGURE 7.12 Surface tension and polarity parameters of sophorolipid methyl, ethyl, and propyl esters in solutions. Reproduced with permission from Somasundaran et al. (2004). © Elsevier.

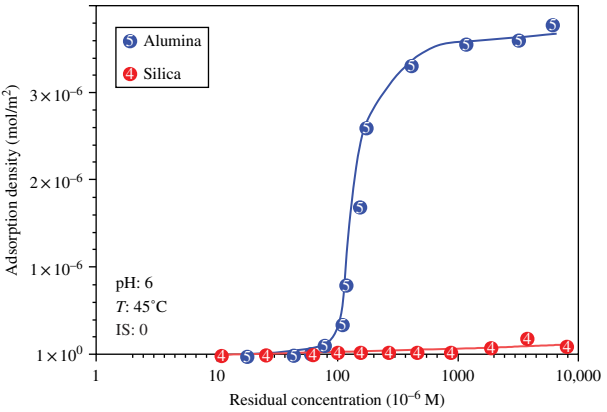

FIGURE 7.13 Adsorption isotherms of sophorolipid methyl ester on alumina and silica. Reproduced with permission from Somasundaran et al. (2004). © Elsevier.

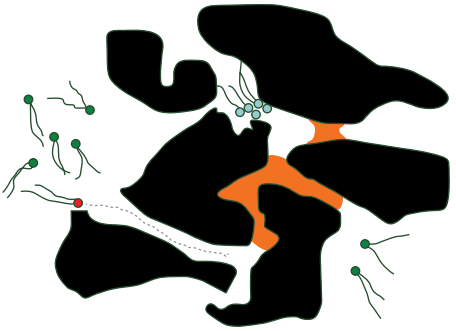

FIGURE 8.1 Schematic of trapped oil (orange) in porous media (black).

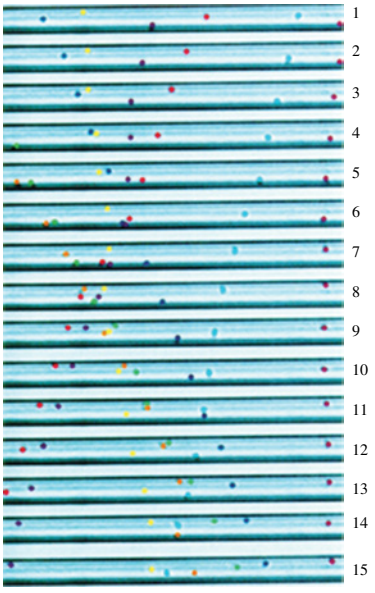

FIGURE 8.11 Sequence of 15 photographic stills shows the swimming of eight E. *coli* cells in a 6 μm capillary. Each still is taken at the time interval of 0.33 s. Bacteria were artificially colored so as to track their path in time. Reprinted from Liu and Papadopoulos (1995) with permission of the American Society of Microbiology.

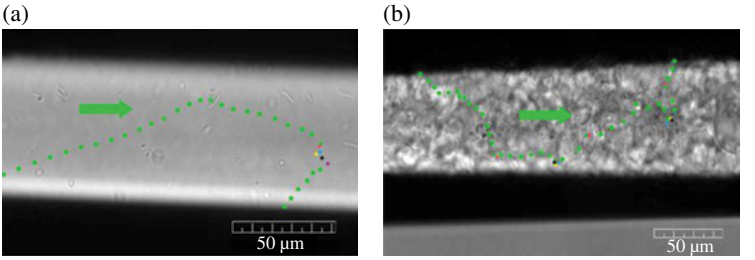

FIGURE 8.19 The movement pathways of B. *subtilis* in bulk growth medium (**a**) and random porous medium (**b**), which are shown by dots drawn at time increment of 0.4 s. Green arrows indicate the swimming direction of the bacterium followed. In the case of tumbles, they are indicated by a dot-color change from green to one or more different colors and by resuming the use of green dots once the tumbling has ceased.

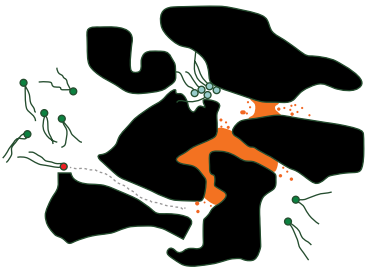

FIGURE 8.21 A schematic of how bacteria get access to oil (orange) trapped in the porous medium (black). The steric hindrance of pore space can assist bacteria (red) to travel through pore channels unidirectionally.

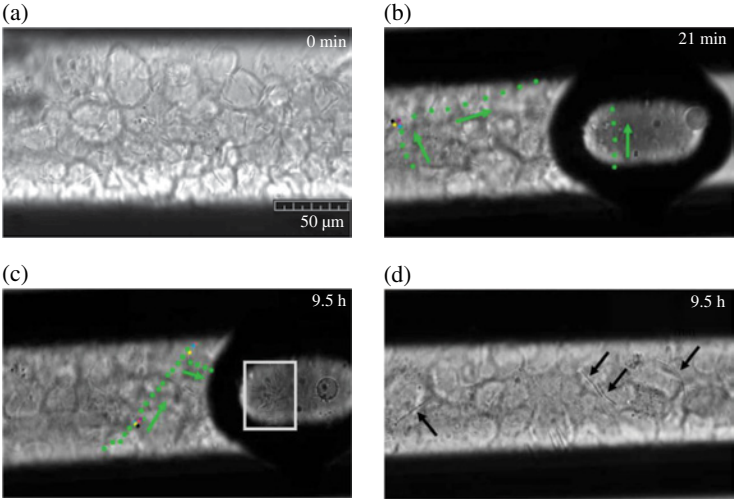

FIGURE 8.22 The movement of *B. subtilis* in the random porous medium with the presence of a Horizon-BP-crude oil droplet. (**a**) Initial injection of *B. subtilis*; (**b**) bacteria reaching the oil droplet after approximately 21 min; (**c**) bacteria have formed a colony around oil droplet ataproximately 9.5 h; (**d**) the porous medium at a location of approximately 7.35 mm from thepoint of injection (~9.5 h). In (**b**) and (**c**), the trajectories of *B. subtilis* are indicated by dots separated by time increments of 0.4 s; green arrows indicate the swimming direction of the bacterium followed. To facilitate the observation of bacterial movement, instances of tumbling are indicated by a dot-color change from green to different colors with the order of red, blue, yellow, black, and purple and by resuming the use of green dots once the tumbling has ceased. The scale bar in (**a**) is applicable for all other images.

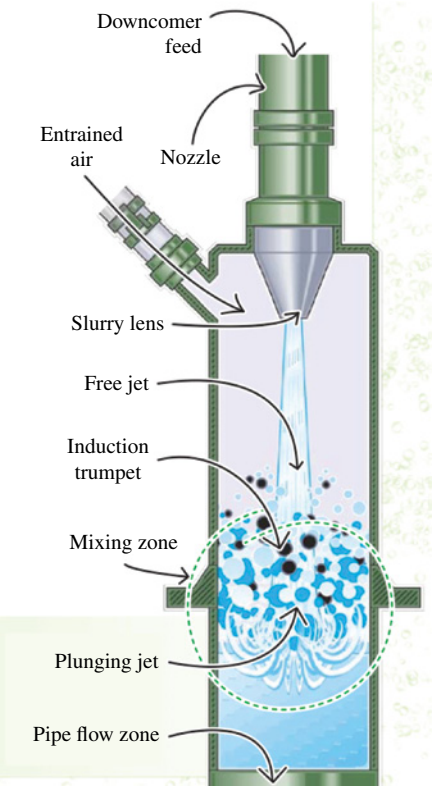

FIGURE 9.2 Expanded view of the injection nozzle and slurry lens.

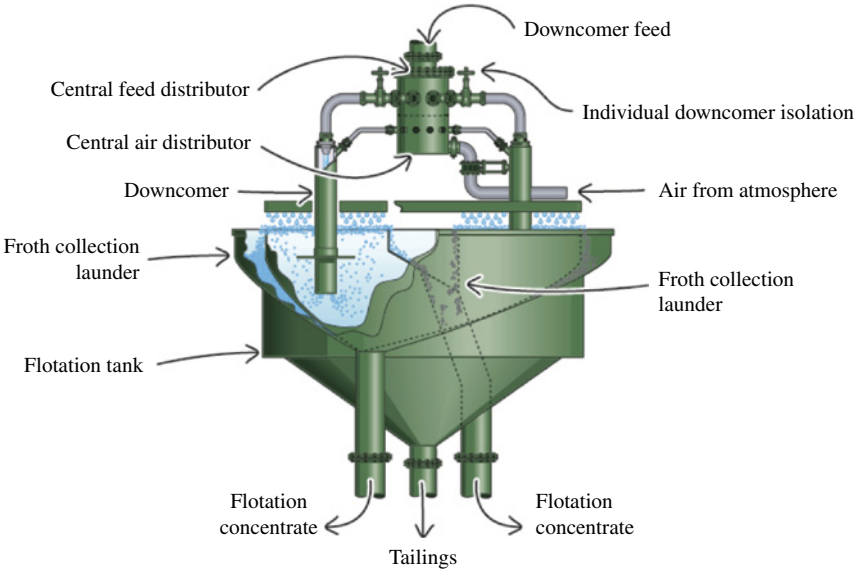

FIGURE 9.3 A full-size Jameson Cell.

FIGURE 9.5 Patches of recovered oil are seen floating on top of the blue copper sulfate solution prior to electrolysis.

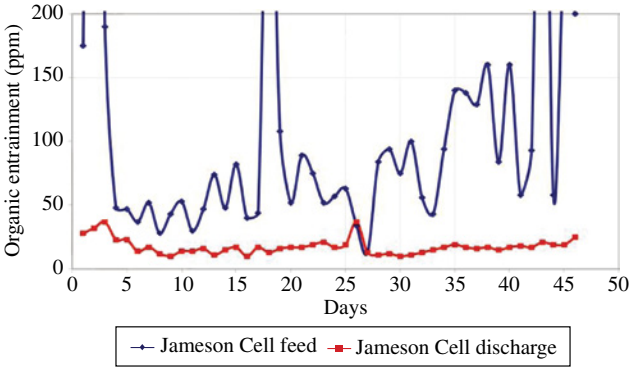

FIGURE 9.7 Measured value of the hydrocarbon before and after flotation.

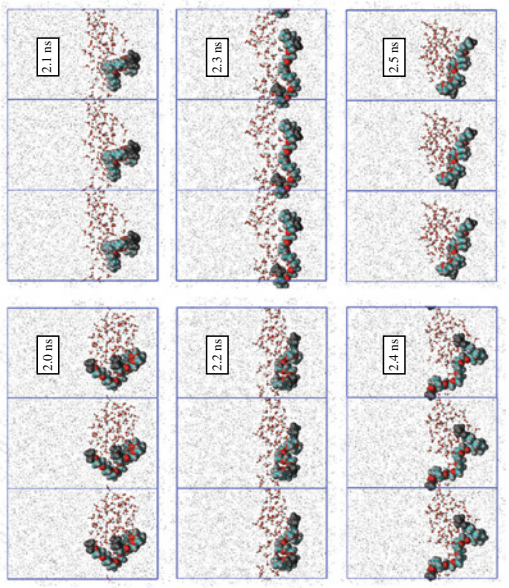

FIGURE 11.1 Formation and then breakup of a fluid column by reconnection across periodic boundary conditions. (See text for full caption.)

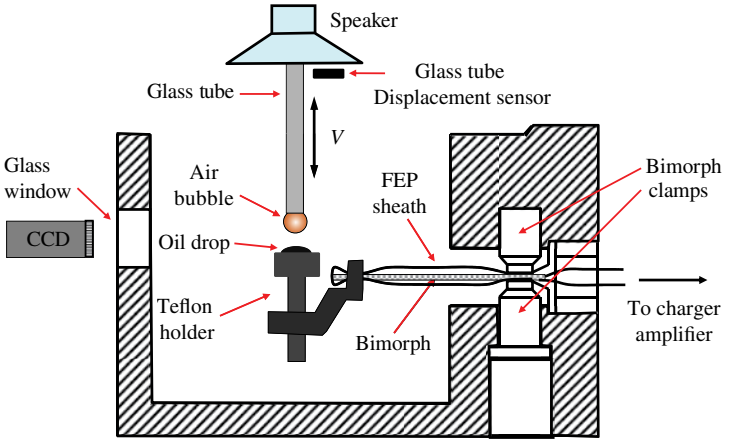

FIGURE 13.1 A cross-sectional view of the ITFDA for measuring the interaction between an air bubble and an oil droplet in a liquid.

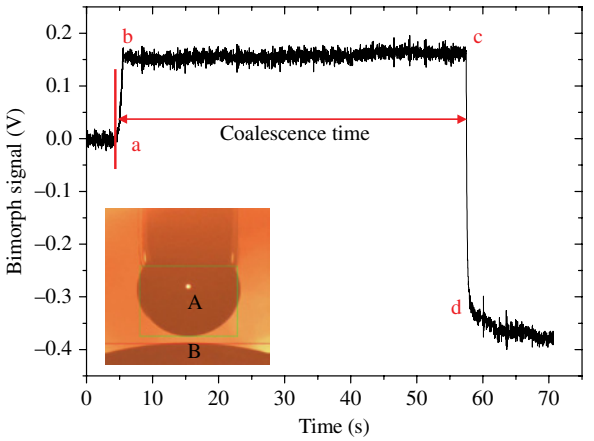

FIGURE 13.2 Bimorph signal profile for coalescence time determination of two oil drops using ITFDA. The inset figure shows the two oil droplets of diameters 1.49 mm (**a**) and 8.52 mm (**b**). The measurement was conducted in seawater at pH 7.6 and an approach and retract velocity of 240 μm/s.

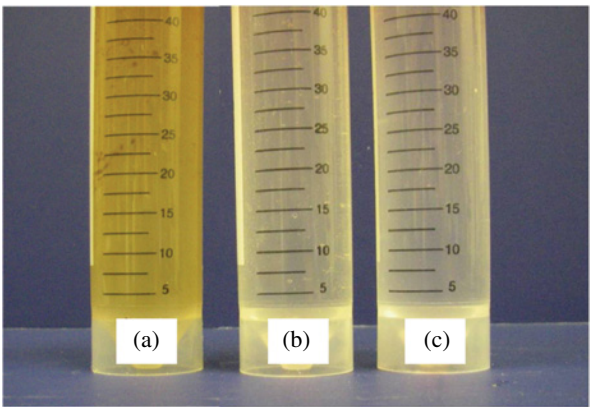

FIGURE 13.9 Photographs of samples: (**a**) heavy oil-in-seawater emulsion, (**b**) subphase of emulsion after 20 min of flotation, and (**c**) seawater.

FIGURE 14.2 The low-temperature/high-pressure optical cell apparatus (**a**, optical cell; **b**, digital camera).

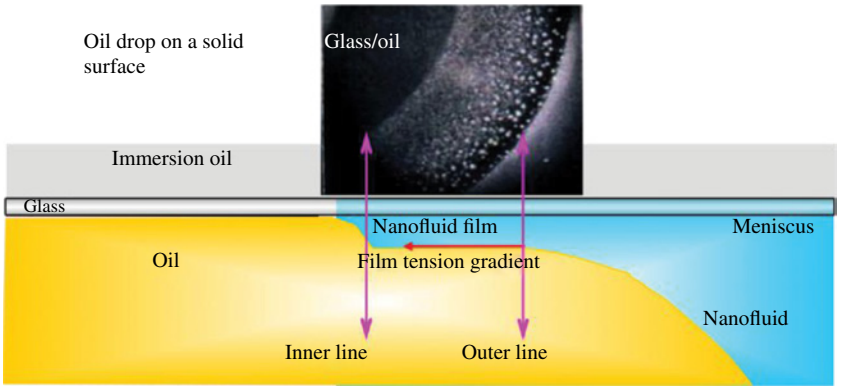

FIGURE 16.6 Microscopic photograph taken using reflected light interferometry depicting the inner and outer contact lines and the nanofluid film region (Kao et al., 1988).